DYNAMIC CHLORINATION OF KRAFT PULP

by

Omar F. Ali, B.Eng., M.Eng.

A thesis submitted to the Faculty of Graduate Studies and Research in partial fulfillment of the requirements for the degree Doctor of Philosophy.

Department of Chemical Engineering
McGill University
Montreal, Canada
© Omar F. Ali, 1989

February 1989

ABSTRACT

Chlorination of kraft black spruce pulp was studied in a fixed bed reactor. Breakthrough curves of the reactant chlorine and the products TOC, chloride and methanol were measured. The flow residence time distribution was determined by performing a stimulus response tracer experiment preceding chlorination of each pulp pad. The chlorine and methanol breakthrough curves were well described by a parallel plug flow model and instantaneous chlorine-lignin and first order chlorine-carbohydrates reactions. The representation of the residence time distribution by plug flow through segregated channels rather than by axial dispersed plug flow was confirmed by the effect of operating variables on the residence time distribution and by comparison with theory and numerical predictions. The good representation of the actual flow by the parallel plug flow model can be explained by poor radial mixing and a relatively large scale of variation in radial velocity. The latter is a direct consequence of the large aspect ratio of pulp fibers and their associated tendency to flocculate. This also explains why the dispersion in pulp pads is larger than in beds of regular shaped particles which have the same equivalent diameter as pulp fibers.

Chlorine-lignin and methanol-lignin stoichiometries were determined as a function of operating conditions. The chlorine-lignin stoichiometry is a function of mean residence time and temperature, but not of chlorine feed concentration. The values of the chlorine-lignin stoichiometry are lower than found for corresponding batch chlorination of softwood

pulps. The methanol–lignin stoichiometry is not influenced by any of the operating variables. The methanol concentration in the effluent can be used as an indicator for the completion of the chlorine–lignin reaction. Pulp properties such as lignin content, kappa number and viscosity were measured at the end of an experiment. Maximum delignification in any channel is obtained at chlorine breakthrough. Recycling of reconcentrated spent filtrate did not hinder delignification rates. The reciprocal intrinsic viscosity is proportional to the chlorine charge on pulp. Higher pulp viscosities are obtained at lower temperatures and mean residence times and at higher chlorine feed concentrations for the same chlorine charge on pulp. Viscosity protection agents like chlorine dioxide are effective in dynamic chlorination.

RESUME

En nous servant d'un réacteur à lit compacté, nous avons étudié le processus de chloration des pâtes kraft faites d'épinette noire. Nous avons mesuré les courbes de rupture du chlore réagissant et des produits de carbone organique total, de mêmes que celles du chlorure et du méthanol. La répartition du temps de résidence de l'écoulement a été calculée à l'aide d'une expérience de décèlement des réponses aux stimulus effectuée avant la chloration de chaque matelas de pâte. Les courbes de rupture du chlore et du méthanol ont été fort bien tracées au moyen d'un modèle d'écoulement idéal parallèle et des réactions instantanées chlore-lignine et des réactions de premier ordre chlore-carbohydrates. La representation de la répartition du temps de résidence par écoulement idéal à cheminements séparés plutôt que par écoulement idéal à dispersement axial s'est vue confirmée par les effets des variables d'exploitation sur la répartition du temps de résidence et par les comparaisons établies avec les données théoriques et les prévisions numériques. La bonne représentation de l'écoulemlent effectif par le modèle d'écoulement idéal parallèle s'explique par un mélange radial assez pauvre et une large plage de variation dans la vitesse radiale. Ce dernier facteur est la conséquence directe du rapport d'allongement élevé des fibres de la pâte et de leur tendance associée à la floculation. Cela explique également pourquoi la dispersion dans les matelas de pâte est plus importante que dans les couches de particules de forme régulière qui ont un diamètre équivalent aux fibres de la pâte.

Nous avons pu établir que les stoechiométries de chlore-lignine et

méthanol-lignine sont l'une de fonctions de conditions d'exploitation. La stoechiométrie chlore-lignine est une fonction du temps moyen de résidence et de la température, mais non pas de la concentration du chlore de chargement.

Les valeurs de stoechiométries chlore-lignine sont plus faibles que dans le cas de la chloration correspondante en discontinu de pâtes de bois résineux. La stoechiométrie méthanol-lignine n'est pas influencée par les variables d'exploitation. La concentration de méthanol dans les effluents peut servir d'indicateur de l'achèvement de la réaction chlore-lignin. Les propriétés des pâtes telles que la teneur en lignine, l'indice kappa et la viscosité ont été mesurées à la fin de l'expérience. La délignification maximale dans n'importe quel type de cheminement se produit au point de rupture du chlore. Le recyclage du filtrat résiduel reconcentré n'a pas entravé le taux de délignification. La viscosité intrinsèque réciproque est proportionnelle à la charge de chlore sur la pâte. L'on obtient des pâtes de viscosités plus élevées à des températures et un temps moyen de résidence plus bas et aussi à des concentrations de chlore de chargement plus élevées, tout en conservant la même charge de chlore sur la pâte. Les agents de protection de la viscosité tels que le dioxyde de chlore sont efficaces dans la chloration dynamique.

ACKNOWLEDGEMENTS

I extend my sincerest appreciation and thanks to my thesis supervisor, Dr. A.R.P. van Heiningen, for all his help, guidance and enthusiasm throughout the course of this study. It was a great learning experience!

The financial support from PAPRICAN over the duration of the study is gratefully acknowledged.

Special thanks to Mr. J. Ing and the chemical testing section of PAPRICAN and to Mr. R. Collins for their help with some of the analytical work.

My sincerest thanks to the many people whose assistance in various forms allowed completion of this work. The names are too numerous to mention, but you know who you are. Thanks!

I also appreciate the efforts of Miss A. McGuinness who assisted me in typing parts of this document.

To my friends at 3420 University - thanks! You are a great bunch. Special thanks to Roberto, the "boy from Brazil". It was a pleasure sharing the same laboratory with you.

The sacrifices of my parents in the past years allowed me the opportunity to pursue my studies and to embark on this thesis. My sincerest thanks to Mom and Dad for everything.

My greatest thanks go to my wife, Rani, who was there through many difficult times. Thank you for all your love, support and encouragement, and thanks for helping to make the completion of this work possible. Thanks also to my little son, Tariq, who did not see much of his daddy during the first year of his life.

To my wife, Rani, and my little son, Tariq.

TABLE OF CONTENTS

Page

1. GENERAL INTRODUCTION

1.1 Background and objectives 1

1.2 Outline of thesis 3

References 5

2. LITERATURE REVIEW

2.1 Introduction 6

2.2 Commercial pulp chlorination 7

2.2.1 Batch chlorination 7

2.2.2 Displacement chlorination 8

2.3 Experimental chlorination studies 10

2.3.1 Chlorination reactions 10

2.3.1.1 Chlorine-water reaction 10

2.3.1.2 Chlorine-lignin reaction 10

2.3.1.3 Chlorine carbohydrates reaction 12

2.3.2 Kinetic studies 13

2.3.3 Rate limiting steps 16

2.3.3.1 General 16

2.3.3.2 External limitations 16

2.3.3.3 Internal limitations 17

2.3.3.4 Chemical limitations 18

2.4 Modelling of packed beds 18

2.4.1 Introduction 18

2.4.2 Without reaction 19

Page

2.4.3 With reaction 21

2.4.4 Parameter estimation 24

2.5 Conclusions 25

References 27

3. EXPERIMENTAL APPARATUS AND PROCEDURES

3.1 Introduction 32

3.2 Experimental facility 34

3.3 Experimental procedures 38

3.3.1 Preliminary preparations 38

3.3.1.1 Chlorine water preparation 38

3.3.1.2 Sample tray preparations 38

3.3.2 Pulp pad formation 41

3.3.3 Experimental method 42

3.4 Analytical techniques 44

3.4.1 Sugar analysis 44

3.4.2 Chloride analysis 45

3.4.3 Chlorine analysis 46

3.4.4 Total organic carbon analysis 48

3.4.5 Other analyses 50

3.4.5.1 Kappa number 50

3.4.5.2 U.V. and Klason lignin 50

3.4.5.3 Pulp viscosity 50

3.4.5.4 Chloride content 50

3.4.5.5 Methanol 50

Page

3.5 Safety precautions 51

References 52

4. RESIDENCE TIME DISTRIBUTION IN A PACKED BED OF PULP FIBERS

4.1 Introduction 53

4.2 Experimental and data reduction techniques 55

4.2.1 Experimental 55

4.2.2 Data reduction techniques 57

4.2.2.1 Experimental breakthrough curves 57

4.2.2.2 Parameter estimation 59

4.3 Reproducibility 64

4.4 Tracer characterization 69

4.4.1 Introduction 69

4.4.2 Molecular size of tracer 71

4.4.3 Concentration 74

4.4.4 pH 78

4.5 Influence of pad formation and operating conditions 78

4.5.1 Pad formation 78

4.5.2 Superficial velocity 82

4.5.3 Pad height 87

4.5.4 Temperature 89

4.5.5 Mobility ratio 91

4.6 General discussion 97

4.7 Conclusions 110

References 112

Page

5. KINETICS OF CARBOHYDRATE-CHLORINE REACTION

5.1 Introduction 114

5.2 Experimental 119

5.3 Characterization of breakthrough curves 121

5.4 Data reduction techniques 124

5.5 Initial carbohydrates-chlorine kinetics 128

5.5.1 Influence of pulp types 128

5.5.2 Influence of chlorine concentration 130

5.5.3 Influence of temperature 132

5.6 General discussion 137

5.7 Conclusions 138

References 140

6. DYNAMIC CHLORINATION OF KRAFT PULP: EXPERIMENTAL RESULTS

6.1 Introduction 141

6.2 Experimental and data reduction techniques 143

6.2.1 Experimental 143

6.2.2 Data reduction 145

6.3 Overall mass balances 150

6.3.1 Chlorine 150

6.3.2 Lignin 150

6.4 Reproducibility 151

6.5 Results and discussion 153

6.5.1 Chlorine breakthrough curves 153

Page

6.5.1.1 Effect of mean residence time 153

6.5.1.2 Effect of residence time distribution 168

6.5.1.3 Effect of chlorine concentration 172

6.5.1.4 Effect of temperature 181

6.5.1.5 Effect of consistency 184

6.5.1.6 Effect of recycle 189

6.5.2 TOC breakthrough curves 189

6.5.2.1 Effect of mean residence time 189

6.5.2.2 Effect of residence time distribution 200

6.5.2.3 Effect of chlorine concentration 202

6.5.2.4 Effect of temperature 207

6.5.2.5 Effect of consistency 207

6.5.3 Total inorganic chloride breakthrough curves 210

6.5.3.1 Effect of mean residence time 210

6.5.3.2 Effect of temperature 219

6.5.3.3 Effect of chlorine concentration 219

6.5.4 Methanol breakthrough curves 219

6.5.5 Pulp properties 233

6.5.5.1 Effect of charge factor 233

6.5.5.2 Effect of chlorine concentration 252

6.5.5.3 Effect of temperature 254

6.5.5.4 Effect of consistency 257

6.5.5.5 Effect of recycle 262

Page

6.5.5.6 Effect of viscosity protection agents 262

6.6 Conclusions 264

References 269

7. MODELLING OF DYNAMIC PULP CHLORINATION

7.1 Introduction 271

7.2 Axial dispersed plug flow model 272

7.2.1 Mathematical description 272

7.2.2 Numerical solution 277

7.2.3 Model verification 283

7.2.3.1 Effect of the number of nodes and time step size 283

7.2.3.2 Comparison with exact solution 286

7.2.3.4 Prediction of experimental breakthrough curve .. 291

7.3 Parallel plug flow model 298

7.3.1 Prediction of chlorine breakthrough curve 298

7.3.1.1 Introduction 298

7.3.1.2 Mathematical description 302

7.3.1.3 Results 304

7.3.2 Prediction of methanol breakthrough curve 311

7.3.2.1 Mathematical formulation 311

7.3.2.2 Results 313

7.4 General discussion 318

7.5 Conclusions 326

References 327

Page

8. CONTRIBUTIONS TO KNOWLEDGE 329

APPENDICIES

Appendix 3-1: Physical and chemical properties of pulp used in this experimental study. 335

Appendix 4-1: Derivation of dimensionless axial dispersion equation. 338

Appendix 4-2: Computer program to calculate mean residence time and Peclet number from tracer breakthrough curve. . 340

Appendix 4-3: Dimensions of water swollen fiber. 350

Appendix 4-4: Equivalent diameter of fibers in pulp pad. 351

Appendix 4-5: Calculation of radial dispersion coefficient, D_R. . 353

Appendix 6-1: Calculation of hydrodynamic diameters of chlorine and glucose. 354

Appendix 6-2: Derivation of equations to evaluate SL_o. 355

Appendix 6-3: Derivation of slope of the axial dispersion model combined with a single instantaneous reaction. 358

Appendix 6-4: Derivation of equations to evaluate S. 365

Appendix 6-5: Derivation of equations to evaluate R. 369

Appendix 6-6: Consumption of chlorine by carbohydrates. 372

Appendix 7-1: Computer program for both versions of model 1. 377

Appendix 7-2: Application of axial dispersion to "constant pattern" behavior in a fixed bed of pulp fibers. .. 393

Appendix 7-3: Dispersion calculations in radial direction for fixed pulp fiber beds. 394

LIST OF FIGURES

Page

Figure 2.1 Mechanism of displacement bleaching. 9

Figure 2.2 Effect of pH on composition of chlorine water, Giertz (7). 11

Figure 3.1 Schematic of reactor. 35

Figure 3.2 Schematic of experimental facility. 37

Figure 3.3 Preparation of chlorine water. 39

Figure 3.4 Preparation of pulp pad. 43

Figure 3.5 Flow Injector Analyzer (FIA) system. 47

Figure 3.6 Technicon AutoAnalyzer system. 49

Figure 4.1 Schematic of experimental facility. 56

Figure 4.2 Typical glucose and dextran T-2000 breakthrough curves. 60

Figure 4.3 Typical non-dimensional glucose and dextran T-2000 breakthrough curves. 61

Figure 4.4a Comparison of experimental and modelled glucose breakthrough curves. 65

Figure 4.4b Comparison of experimental and modelled dextran T-2000 breakthrough curves. 66

Figure 4.5 Duplicate glucose breakthrough curves. 67

Figure 4.6 Duplicate dextran T-2000 breakthrough curves. 68

Figure 4.7 Cumulative pore volume, cm /g, versus molecular diameter; from Stone and Scallan (12). 70

Page

Figure 4.8 Influence of type of tracer on breakthrough curves. 73

Figure 4.9 Inaccessible volumes obtained with different tracers - comparison with Stone and Scallan (13). 77

Figure 4.10a Effect of glucose concentration on breakthrough curves. 79

Figure 4.10b Effect of dextran T-2000 concentration on breakthrough curves. 80

Figure 4.11 Effect of pH on glucose breakthrough curves. 81

Figure 4.12 Effect of pad formation on glucose breakthrough curves. 83

Figure 4.13 Effect of pad formation on dextran T-2000 breakthrough curves. 84

Figure 4.14 Effect of superficial velocity on glucose breakthrough curves. 85

Figure 4.15 Effect of superficial velocity on dextran T-2000 break through curves. 86

Figure 4.16 Effect of temperature on glucose breakthrough curves. .. 90

Figure 4.17 Effect of mobility ratio on glucose breakthrough curves. 94

Figure 4.18 Effect of mobility ratio on dextran T-2000 breakthrough curves. 95

Figure 4.19 Influence of mobility ratio on Peclet number. 96

Figure 4.20 Pressure drop at different flowrates. 101

Figure 4.21 Comparison of glucose axial dispersion results of this study with those of other studies: based on equivalent diameter. 105

Page

Figure 4.22 Comparison of glucose axial dispersion results of this study with those of other studies: based on fiber or particle length. 107

Figure 5.1 Mechanism for the ionic oxidation at glycosidic bonds with chlorine, Fredricks et al. (1). 116

Figure 5.2 Mechanism for hydrogen abstraction at a glycosidic bond, Fredricks et al. (1) 117

Figure 5.3 Characterization of chlorine breakthrough curves. 122

Figure 5.4 Characterization of total organic carbon breakthrough curves. 123

Figure 5.5 Chlorine breakthrough curves at high temperature and low superficial velocity. 125

Figure 5.6 Total organic carbon breakthrough curves at high temperature and low superficial velocity. 126

Figure 5.7 Comparison of chlorine breakthrough curves from chlorite treated and fully bleached pulp under similar operating conditions. 129

Figure 5.8 Comparison of total organic carbon breakthrough curves from chlorite treated and fully bleached pulp under similar operating conditions. 131

Figure 5.9 Influence of residence time and chlorine concentration on the initial chlorine-carbohydrates reaction. 133

Page

Figure 5.10 Dependence of the first order chlorine-carbohydrates reaction on temperature. 134

Figure 5.11 Arrhenius dependence of the first order chlorine-carbohydrates reaction. 136

Figure 6.1 Schematic of chlorination reactor. 144

Figure 6.2 Chlorine, total inorganic chloride and TOC breakthrough curves of a typical experiment. 146

Figure 6.3 Dimensionless chlorine, total inorganic chloride and TOC breakthrough curves of a typical experiment. 148

Figure 6.4 General dimensionless breakthrough curves of a typical experiment. 149

Figure 6.5 Duplicate glucose breakthrough curves. 154

Figure 6.6 Duplicate chlorine breakthrough curves. 155

Figure 6.7 Duplicate TOC breakthrough curves. 156

Figure 6.8 Duplicate total inorganic chloride breakthrough curves. 157

Figure 6.9 Effect of mean residence time, $\bar{t}_r$, on chlorine breakthrough curves; variable u_o at fixed H. 159

Figure 6.10 Effect of mean residence time, $\bar{t}_r$, on generalized chlorine breakthrough curves, variable u_o at fixed H. .. 162

Figure 6.11 Effect of mean residence time, $\bar{t}_r$, on SL_o calculated over the duration of the experiment. 165

Figure 6.12 Effect of mean residence time, $\bar{t}_r$, on average SL_o. 167

Page

Figure 6.13 RTD's of poorly and well formed pad obtained with glucose tracer tests. 169

Figure 6.14 Chlorine breakthrough curves of poorly and well formed pads. 170

Figure 6.15 Applicability of axial dispersion model to represent chlorine breakthrough curves. 173

Figure 6.16 Applicability of parallel plug model to represent chlorine breakthrough curves. 174

Figure 6.17 Effect of chlorine concentration on dimensionless chlorine breakthrough curves. 175

Figure 6.18 Effect of chlorine concentration on generalized chlorine breakthrough curves. 177

Figure 6.19 Effect of chlorine concentration on SL_o versus $[(T_c - 1)C_o\varepsilon_a]/[L_oC_f]$. 178

Figure 6.20 Effect of chlorine concentration on SL_o at complete breakthrough. 179

Figure 6.21 Applicability of parallel plug flow model to represent chlorine breakthrough curves: effect of chlorine concentration. 180

Figure 6.22 Effect of temperature on generaiized chlorine breakthrough curves. 182

Figure 6.23 Effect of temperature on SL_o versus $[(T_c - 1)C_o\varepsilon_a]/[L_oC_f]$ of the experiment. 183

Page

Figure 6.24 Effect of temperature on average SL_o at complete breakthrough. 185

Figure 6.25 Applicability of parallel plug flow model to represent chlorine breakthrough curves: effect of temperature. ... 186

Figure 6.26 Effect of consistency on dimensionless chlorine breakthrough curves. 187

Figure 6.27 Effect of consistency on generalized chlorine breakthrough curves. 188

Figure 6.28 Applicability of parallel plug flow model to represent chlorine breakthrough curves: effect of consistency. ... 190

Figure 6.29 Effect of recycle on chlorine breakthrough curves. 191

Figure 6.30 Effect of mean residence time, $\bar{t}_r$, on generalized TOC breakthrough curves; variable u_o at fixed H. 193

Figure 6.31 Effect of mean residence time, $\bar{t}_r$, on generalized TOC breakthrough curves; variable H at fixed u_o. 194

Figure 6.32 Effect of mean residence time, $\bar{t}_r$, on TOC_m/C_o. 199

Figure 6.33 TOC breakthrough curves of poorly formed and well formed pads. 201

Figure 6.34 Effect of chlorine concentration on TOC breakthrough curves. 203

Figure 6.35 Effect of chlorine concentration on generalized TOC breakthrough curves. 204

Figure 6.36 Effect of chlorine concentration on TOC_m. 205

Page

Figure 6.37 Effect of temperature on generalized TOC breakthrough curves. 208

Figure 6.38 Effect of temperature on TOC_m. 209

Figure 6.39 Effect of consistency on generalized TOC breakthrough curves. 211

Figure 6.40 Effect of mean residence time, $\bar{t}_r$, on total inorganic chloride breakthrough curves; variable u_o at fixed H. .. 212

Figure 6.41 Effect of mean residence time, $\bar{t}_r$, on total inorganic chloride breakthrough curves; variable H at fixed u_o. .. 214

Figure 6.42 Effect of mean residence time, $\bar{t}_r$, on S; variable u_o at fixed H. 217

Figure 6.43 Effect of mean residence time, $\bar{t}_r$, on S; variable H at fixed u_o. 218

Figure 6.44 Effect of temperature on S. 220

Figure 6.45 Effect of chlorine concentration on S. 221

Figure 6.46 Typical methanol breakthrough curve. 223

Figure 6.47 Comparison of chlorine, TOC and methanol breakthrough curves. 224

Figure 6.48 TOC breakthrough curves with or without correction for methanol. 225

Figure 6.49 Effect of temperature on methanol breakthrough curves. . 227

Figure 6.50 Profile of R versus $(T_c - 1)C_o\varepsilon_a/(L_oC_f)$. 230

Figure 6.51 Effect of chlorine concentration and superficial velocity on the methanol breakthrough curves. 231

Page

Figure 6.52 Effect of chlorine concentration and superficial velocity on generalized methanol breakthrough curves. 232

Figure 6.53 Final dimensionless chlorine concentration at different chlorine charges. 235

Figure 6.54 CW (Klason + UV) lignin as a function of chlorine charge based on the whole pad. 236

Figure 6.55 CW (Klason + UV) lignin as a function of chlorine charge based on pulp pad under consideration. 237

Figure 6.56 CWE (Klason + UV) lignin as a function of chlorine charge based on the whole pad. 239

Figure 6.57 CWE (Klason + UV) lignin as a function of chlorine charge based on sections of the pad. 240

Figure 6.58 CWE Kappa number as a function of chlorine charge based on sections of the pad. 241

Figure 6.59 CWE cuene viscosities as a function of chlorine charge based on the whole pad. 243

Figure 6.60 Nomogram relating cuene to intrinsic viscosities, from Gloor and Klug (20). 245

Figure 6.61 Intrinsic CWE viscosities as a function of chlorine charge based on the pulp pad under consideration. 246

Figure 6.62 Reciprocal intrinsic CWE viscosities versus chlorine charge based on the pulp pad under consideration. 251

Page

Figure 6.63 Effect of chlorine concentration on CW (Klason + UV) lignin as a function of chlorine charge based on the pulp pad under consideration. 253

Figure 6.64 Effect of chlorine concentration on reciprocal intrinsic CWE viscosities versus chlorine charge based on the pulp pad under consideration. 255

Figure 6.65 Effect of temperature on CW (Klason + UV) lignin. 256

Figure 6.66 Effect of temperature on CWE kappa number. 258

Figure 6.67 Effect of temperature on reciprocal intrinsic viscosities versus chlorine charge based on the pulp pad under consideration. 259

Figure 6.68 Effect of consistency on CW (Klason + UV) lignin as a function of chlorine charge based on the pulp pad under consideration. 260

Figure 6.69 Effect of consistency on CWE (Klason + UV) lignin as a function of chlorine charge based on the pulp pad under consideration. 261

Figure 6.70 Effect of consistency on reciprocal intrinsic viscosities versus chlorine charge based on the pulp pad under consideration. 263

Figure 6.71 Effect of viscosity protection agent, ClO_2, on cuene viscosities. 265

Figure 6.72 Effect of viscosity protection agent, sulfamic acid, on cueme viscosities. 266

		Page
Figure 7.1	Representation of pulp pad by nodes and control volumes.	278
Figure 7.2	Stepwise profile assumption.	281
Figure 7.3	Piecewise linear profile.	282
Figure 7.4	Algorithm for version 1 of axial dispersed plug flow model.	284
Figure 7.5	Algorithm for version 2 of axial dispersed plug flow model.	285
Figure 7.6	Effect of number of nodes on numerical solution of version 2.	287
Figure 7.7	Effect of number of nodes on numerical solution of version 2 - expanded scale.	288
Figure 7.8	Effect of time step on numerical solution of version 2. .	289
Figure 7.9	Comparison of numerical solution, without source terms, to exact analytical solution.	290
Figure 7.10	Prediction of chlorine breakthrough curve for fully bleached pulp; version 1 of axial dispersed plug flow model.	292
Figure 7.11	Prediction of chlorine breakthrough curve with axial dispersed plug flow model; C_o = 0.55 g/l.	293
Figure 7.12	Prediction of chlorine breakthrough curve with axial dispersed plug flow model; C_o = 1.10 g/l.	294

Page

Figure 7.13 Prediction of chlorine breakthrough curve with axial dispersed plug flow model; C_o = 2.20 g/l. 295

Figure 7.14 Prediction of chlorine breakthrough curve with version 1 of axial dispersed plug flow model; reaction rate constants artifically changed. 297

Figure 7.15 Schematic representation of the pulp pad according to the parallel plug flow model. 300

Figure 7.16 Comparison of normalized chlorine BTC and glucose tracer curve. 303

Figure 7.17 Prediction of chlorine BTC with parallel plug flow model; C_o = 0.55 g/l, $\bar{t}_r$ = 186 s, T = 35°C, P = 27, SL_o = 0.95. 305

Figure 7.18 Prediction of chlorine BTC with parallel plug flow model; C_o = 1.10 g/l, $\bar{t}_r$ = 46 s, T = 35°C, P = 27, SL_o = 0.92. 306

Figure 7.19 Prediction of chlorine BTC with parallel plug flow model; C_o = 2.20 g/l, $\bar{t}_r$ = 68 s, T = 35°C, P = 38, SL_o = 0.99. 307

Figure 7.20 Prediction of chlorine BTC with parallel plug flow model; C_o = 1.10 g/l, $\bar{t}_r$ = 68 s, T = 50°C, P = 30, SL_o = 1.27. 308

Figure 7.21 Prediction of chlorine BTC with parallel plug flow C_o = 2.20 g/l, $\bar{t}_r$ = 34 s, T = 35°C, P = 32, SL_o = 0.80. .. 309

Page

Figure 7.22 Prediction of chlorine BTC with parallel plug flow model; C_o = 1.10 g/l, $\bar{t}_r$ = 68 s, T = 35°C, P = 2.31 SL_o = 1.20. 310

Figure 7.23 Prediction of methanol BTC with parallel plug flow model; C_o = 1.10 g/l, $\bar{t}_r$ = 136 s, T = 35°C, P = 49 SL_o = 1.20. 314

Figure 7.24 Prediction of methanol BTC with parallel plug flow model; C_o = 0.55 g/l, $\bar{t}_r$ = 297 s, T = 35°C, P = 61 SL_o = 1.21. 315

Figure 7.25 Prediction of methanol BTC with parallel plug flow model; C_o = 1.10 g/l, $\bar{t}_r$ = 136 s, T = 19°C, P = 38 SL_o = 1.01. 316

Figure 7.26 Prediction of methanol BTC with parallel plug flow model; C_o = 1.10 g/l, $\bar{t}_r$ = 136 s, T = 50°C, P = 34 SL_o = 1.27. 317

LIST OF TABLES

		Page
Table 4 1	Range of operating conditions.	58
Table 4.2	Molecular weights and diameter of sugar tracers.	72
Table 4.3	Peclet number and porosities obtained with different tracers.	75
Table 4.4	Inaccessible volumes obtained with different tracers: comparison of static and dynamic tests.	76
Table 4.5	Mean and standard deviation of Peclet numbers at different pad heights.	88
Table 4.6	Viscosities and mobility ratios of glucose and dextran tracers at different concentrations.	93
Table 4.7	Peclet number versus superficial velocities: Western Red cedar and Douglas fir pulp.	103
Table 5.1	Experimental conditions and analysis of chlorine BTC.	120
Table 5.2	Determination of chlorine losses in experimental set-up without pulp.	127
Table 5.3	Influence of temperature on rate constant: initial chlorine-carbohydrate reaction.	135
Table 6.1	Lignin mass balance.	152
Table 6.2	Pulp properties of duplicate experiment.	158
Table 6.3	Comparison of C_m/C_o with C/C_o calculated from kinetics of the reaction between chlorine and carbohydrates (equation 5.8).	160

Page

Table 6.4 Characteristic parameters of TOC breakthrough curves; effect of mean residence time $\bar{t}_r$. 196

Table 6.5 TOC_f of unbleached and fully bleached pulp. 198

Table 6.6 Effect of chlorine concentration on cumulative TOC removal. 206

NOMENCLATURE

t	- reaction time, s.
t_c	- reaction time corrected for "dead volume" of reactor, s.
t_r	- residence time of a single channel, s.
$\bar{t}_r$	- mean residence time of all channels, s.
t_b	- breakthrough time of a single channel, s.
$\bar{t}_b$	- mean breakthrough time of all channels, s.
t_{rc}	- critical time at which breakthrough occurs for a single channel, s.
t_{cf}	- total reaction time, s.
T	- dimensionless time.
T_c	- dimensionless time corrected for "dead volume" of reactor.
T_{cf}	- total dimensionless reaction time.
T_b	- dimensionless breakthrough time of a single channel.
$\bar{T}_b$	- mean dimensionless breakthrough time of all channels.
C	- exit chlorine concentration at any time, g/l.
C_o	- inlet chlorine water concentration, g/l.
C_m	- maximum chlorine concentration, g/l.
C_a	- concentration of methanol, g/l.
$[Cl^-]_f$	- free chloride concentration, g/l.
$[Cl]^-_{RL}$	- chloride concentration from chlorine-lignin reaction, g/l.
$[Cl^-]_{RC}$	- chloride concentration from chlorine-carbohydrate reaction, g/l.
u_o	- liquid velocity based on empty reactor, cm/s.
u_a	- liquid velocity based on accessible volume, cm/s.
u_i	- liquid velocity based on inter-fiber volume, cm/s.

u_p - pit pore velocity, cm/s.

ε_a - accessible porosity, cm^3 accessible liquid volume/cm^3 bed.

ε_t - total porosity in pulp pad, cm^3 pore volume/cm^3 bed.

ε_i - external porosity, cm^3 inter-fiber volume/cm^3 bed.

ε_w - fiber wall porosity, cm^3 pore volume of fiber wall/cm^3 fiber.

L_o - initial lignin content of pulp, g lignin/g pulp.

L_1 - initial lignin content for "fast" reaction, g lignin/g pulp.

L_2 - initial lignin content for "slow" reaction, g lignin/g pulp.

L_3 - initial lignin content unavailable for reaction, g lignin/g pulp.

L_1^* - dimensionless lignin content for "fast" reaction.

L_2^* - dimensionless lignin content for "slow" reaction.

k_1 - reaction rate constant for "fast" chlorine-lignin reaction, l•s/g.

k_2 - reaction rate constant for "slow" chlorine-lignin reaction, l•s/g.

k_c - reaction rate constant for chlorine-carbohydrate reaction, s^{-1}.

C_f - pulp pad consistency, g pulp/l suspension.

C_p - pulp pad consistency, g pulp/(100 g pulp water suspension).

C_h - carbohydrate content of pulp, g carbohydrate/g pulp.

SL_o - average chlorine-lignin stoichiometry, g chlorine consumed/g original lignin.

$SL_{o,1}$ - average chlorine-lignin stoichiometry of "fast" reaction, g chlorine consumed/g lignin reacted.

$SL_{o,2}$ - average chlorine-lignin stoichiometry of "slow" reaction, g chlorine consumed/g lignin reacted.

e,f,g,h - reaction orders of chlorine-lignin reactions.

x - distance from inlet of reactor, cm.

x_f - distance of front from inlet of reactor, cm.

X - dimensionless distance from inlet of reactor.

H - pad height, cm.

A - cross-sectional area of reactor, cm^2.

R_p - radius of pit pore, cm.

L_p - length of pit pore, cm.

d_p - fiber diameter, cm.

d_e - equivalent fiber diameter, cm.

r_e - equivalent fiber radius, cm.

D_e - effective diffusivity, cm^2/s.

D - free diffusion coefficient of chlorine or inert tracer, cm^2/s.

D_R - radial diffusion coefficient, cm^2/s.

D_L - axial diffusion coefficient.

D'_R - turbulent contribution to radial dispersion coefficient, cm^2/s.

P - axial Peclet number based on pad height and interstitial velocity, $u_i H/D_L$.

P_p - pit pore Peclet number based on length of pit pore, $u_p L_p/D$.

Pe_L - axial Peclet number based on particle diameter.

Pe_R - radial Peclet number based on particle diameter.

S - substitution reaction as fraction of chlorination.

R - methanol stoichiometry, g methanol produced/g original lignin.

D_{pw} - degree of polymerization of carbohydrate chains.

$[PS]$ - concentration of carbohydrate chains, g/l.

$[PS]_o$ - initial concentration of carbohydrdate chains, g/l.

$dF(t_r)$ - fraction of channels in pad having same residence time.

Q - flow rate of liquid through pulp pad, cm^3/min.

ΔP - pressure drop, Pa.

J - ratio of $C_x/C_xH_yO_z$.

ρ_f - fiber density, g/cm^3.

η - fluid viscosity, kg/m·s.

n - solute concentration in fibers, g/l.

Re - Reynolds number.

Sc - Schmidt number.

CHAPTER 1

GENERAL INTRODUCTION

1.1 Background and Objectives

The bleaching sequence which follows the pulping operation serves to remove the remaining lignin from pulp. Removal of the residual lignin leads to large increases in whiteness and brightness of the pulp. Chlorination and extraction are usually the first steps in the bleaching sequence and are responsible for removal of most of the residual lignin. Subsequent stages in the bleaching sequence are primarily for brightening. Chlorination normally consists of contacting the pulp suspension with chlorine gas in a mixer in order to achieve uniform distribution and dissolution of chlorine in the pulp suspension. The pulp suspension then flows through a chlorination tower having a mean residence time of 45 minutes to allow chlorination to go to completion. There is no relative motion between the chlorine-water and pulp fibers.

In 1962 Rapson (1) introduced the concept of "displacement" or "dynamic" bleaching whereby a bleaching solution was forced through a bed of pulp fibers. Increased bleaching rates were observed. This type of contacting is also used in pulp washing and displacement bleaching of pulp. Reactants and products are transported to and from the fibers by relative motion between the continuous phase and the fibers. In any other mixing or continuous process, including the recent medium consistency mixer (2), the relative motion between fibers and continuous phase is small compared to the absolute velocity of the fiber or fluid phases. Since only the relative motion contributes to transport to and from fibers, flow through a fiber bed is a very efficient contacting process in terms of energy requirements. However more fundamental study is required

in terms of residence time distribution and inter- and intra-fiber mass transfer processes for better use and further development of contacting devices or reactors employing flow through fiber mats. For example, the most efficient use of wash water or chemicals and minimum production of effluent volumes are achieved when the residence time distribution approaches plug flow. Understanding which physical phenomena are responsible for dispersion of the continuous phase might lead to the development of new or improved contacting devices or reactors.

In the present study, dynamic chlorination was selected for the study of the interaction between mass transfer and chemical reaction in flow through fiber mats because of the relative ease of chemical analysis and handling of chlorine and its reaction products. Breakthrough curves of chlorine, chloride, TOC and methanol are measured as a function of residence time distribution, mean residence time, chlorine feed concentration, temperature, pulp consistency and viscosity protection agents. Pulp properties such as kappa number, lignin content and viscosity were determined at the end of the experiment.

The shape of the breakthrough curves obtained during dynamic pulp chlorination is determined by the flow residence time distribution, kinetics of the different chlorine-pulp reactions and mass transfer resistances external to and within the pulp fibers. In order to predict the breakthrough curves from first principles and with the least number of adjustable parameters, the kinetics of the chlorine-pulp reactions must be known. Therefore in the present study the kinetics of the chlorine-lignin and chlorine-carbohydrates reactions are, respectively, obtained from literature or measured. Also, most importantly, the residence time distri-

bution for each pulp pad used for dynamic chlorination is determined separately.

There is no concensus in the literature as to whether flow through a pulp pad is governed by channelling flow (3) or by axial dispersion (4). A detailed residence time distribution study is undertaken in the present investigation to resolve this question. The residence time distribution is determined with step-up and step-down stimulus-response experiments with glucose and higher molecular weight dextrans as inert tracer. Based on this study an appropriate flow model is chosen for theoretical analysis and numerical modelling. The residence time distribution characteristics for flow through pulp pads are also compared with general packed bed literature. The differences are attributed to the unique dimensions of softwood pulp fibers of about 30 micron diameter and a length of about 3 mm.

Analysis of the experimental breakthrough curves also allows determination of chemical characteristics for dynamic pulp chlorination. These include TOC production and the chlorine-lignin and methanol-lignin stoichiometries, as well as lignin content and carbohydrates degradation of the chlorinated pulp. The influence of operating variables on these characteristics are discussed in terms of the different reactions and reaction kinetics.

1.2 Outline of Thesis

The overall objective of this thesis is to obtain a fundamental understanding of the dynamic chlorination process. The results are presented in 8 chapters. Relevant literature on pulp bleaching and flow through fixed beds are discussed in Chapter 2. The experimental apparatus

and techniques employed are presented in Chapter 3. Chapter 4 includes the effect of several operating variables on the residence time distribution and elucidation of the governing mechanism for flow through a packed bed of pulp fibers. The chlorine-carbohydrates reaction kinetics are presented in Chapter 5. The experimental breakthrough curves and pulp properties are discussed in detail in Chapter 6. Predictions of the experimental breakthrough curves obtained with two flow models are given in Chapter 7. Finally, Chapter 8 summarizes the contributions to knowledge from this study.

References

1. Rapson, W.H., and Anderson, C.B., Tappi, Vol. 49, No. 8 (1966).

2. Gullichsen, J., Harkonen, E., and Nishaneni, T., Tappi, Vol 64, No. 9 (1981).

3. Lee, P.F., Tappi, Vol. 67, No. 11 (1984).

4. Poirier, N.A., M.Eng. Thesis, McGill University (1986).

CHAPTER 2

LITERATURE REVIEW

2.1 Introduction

The major objective in bleaching of pulp is to make the pulp whiter and brighter without significantly decreasing its strength. Colour arises from light absorption by conjugated double bond systems present in lignin and extractives. The colour of unbleached pulp varies with both the pulping process and the wood species used. Kraft pulp is always darker in colour than the original wood and has a brightness level of 20 to 30%. Sulphite pulp is brighter at about 55 to 60% and is off-white in colour. In all cases, however, chemical pulping introduces chromophoric groups in lignin leading to darkening of the pulp.

The lignin content of unbleached kraft and sulfite pulps are rather low, between 3 to 5%. These colour causing substances are easily and economically removed by 1) delignification - dissolution of the lignin and resinous components of the pulp 2) brightening - conversion of the remaining lignin and resin into substances capable of light reflectance. An effective bleaching agent must then be selective, only attacking lignin and resin, must produce a stable white bright pulp and be inexpensive. Chlorine has satisfied these requirements for many decades and is still widely used today.

Pulp is conventionally bleached to the desired brightness in many stages. A typical stage consists of 1) equipment to bring the stock to the desired consistency 2) a mixer to blend fibers, steam and chemicals 3) retention vessel to provide time for reaction and 4) a washer to separate the treated fibers from the spent chemicals. As many as eight stages are

sometimes used in a batch bleaching sequence. The CEDED (C=chlorination, E=extraction, D=chlorine dioxide) sequence is very common. In addition to the conventional batch bleaching process, other processes like gas phase bleaching and displacement bleaching have also received attention. Many displacement bleach plants are in existence around the world today. In these plants the entire bleaching sequence, with the exception of the chlorination stage, is located in a single tower. Chlorination occurs in medium consistency mixers or in conventional chlorination towers.

It was the objective of this work to investigate the displacement or dynamic chlorination of kraft pulp in a fixed bed reactor system. The relevant literature dealing with bleaching of pulp and with flow, transport and reaction phenomena in packed beds will be reviewed in this chapter.

2.2 Commercial pulp chlorination

2.2.1 Batch chlorination

Many combinations of chemicals have been used in the conventional batch bleaching process over the years. The most common sequence, CEDED, has been modified in many ways. Chlorine dioxide addition to the first stage, typically 4 to 15% (1), leads to improved pulp strength and hence allows higher operating temperatures. Addition of an oxygen stage before the chlorination stage and also in the extraction stage, OCE_oD, produces pulp of high brightness (2,3). Hypochlorite and hydrogen peroxide are also used in some bleaching sequences.

The bleaching times of batch sequences are in the order of several hours and large equipment sizes are needed for each stage since the pulp consistency is about 3%. The water and energy consumption of these plants

are also enormous. The need to bleach pulp more rapidly and economically has led to the development of displacement bleaching.

2.2.2 Displacement bleaching

Displacement or dynamic bleaching was first proposed by Rapson and Anderson (4) and since then was investigated extensively leading to the first commercial scale process in late 1975 at Temple-Eastex Inc. kraft pulp mill in Evadale Texas. Since then many displacement bleach plants have come on stream (1). Displacement bleaching differs from batch bleaching in that initially there is relative motion between fibers and solution. It is, however, similar to batch bleaching in the variability of stages that make up a sequence. Three separate steps can be distinguished from one displacement bleaching stage as seen in Figure 2.1. An initial dynamic period where the chemical is displaced into the pulp suspension, a static period where the fiber suspension travels up to the following displacement zone and finally another dynamic period where the liquid is displaced.

The chlorination stage is performed external to the tower since complete chlorination cannot be achieved with displacement of a single padvolume of solution. This is because of the nature of the chlorine-lignin reaction and the limited solubility of chlorine in water. A significant advantage of displacement bleaching over batch bleaching is that there is no washing between stages. The capital and operating costs savings are significant and the bleaching times are in the order of minutes (5). The reasons cited for this increased bleaching rate were an increase in mass transfer rate of active chemicals to the fiber surface due to the reduction in thickness of the water film surrounding the fibers and also

Figure 2.1 Mechanism of displacement bleaching.

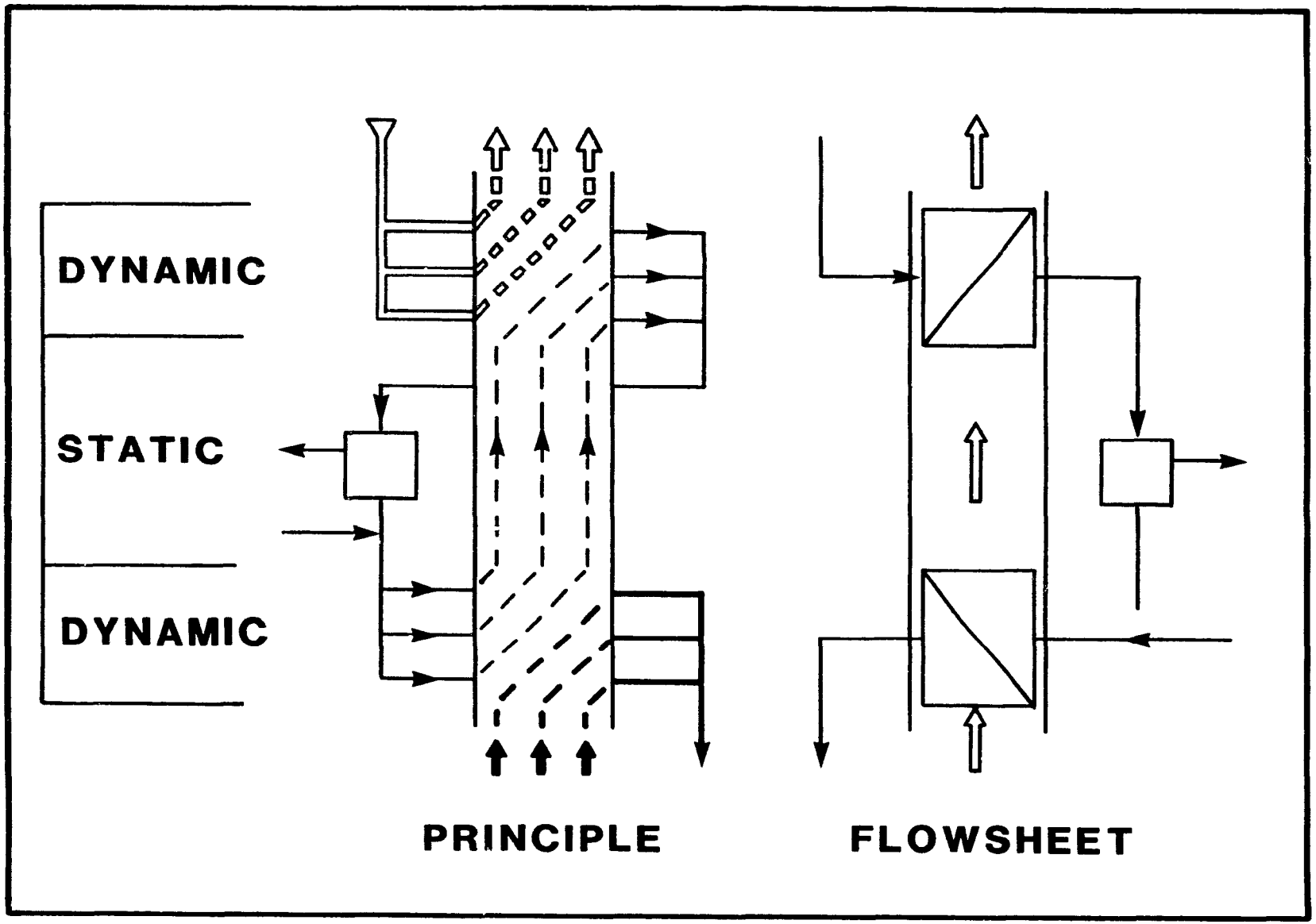
DYNAMIC
STATIC
DYNAMIC
PRINCIPLE
FLOWSHEET

to the continuous removal of reaction products around the fiber (4,6). The location of the rate limiting step in chlorination has always been controversial and will be addressed in a later section.

2.3 Experimental chlorination studies

2.3.1 Chlorination reactions

2.3.1.1 Chlorine-water reaction

Chlorine is not very soluble in water. At a partial pressure of 1 atmosphere and at 50°C the solubility is 4 g/l. Chlorine undergoes a reversible hydrolysis in water to form hypochlorous and hydrochloric acids.

$$Cl_2 + H_2O \rightarrow HOCL + H^+ + Cl^- \qquad [2.1]$$

$$HOCl \rightarrow H^+ + OCl^- \qquad [2.2]$$

Hydrochloric acid dissociates completely in water whereas hypochlorous only dissociates at pH 7. The effect of pH on the composition of the chlorine water system is profound (7) as seen in Figure 2.2. Chlorination is conducted at pH 2 where 20% of the oxidizing power is in the form of elemental chlorine and 80% as hypochlorous acid.

2.3.1.2 Chlorine lignin reactions

Because of the difficulty in isolating pure lignin from wood the reaction mechanism between lignin and chlorine was inferred from lignin model compound studies (8). These studies agree with the many documented reports on pulp chlorination that de-lignification occurs initially by a fast substitution reaction followed by a much slower oxidation reaction.

Figure 2.2 Effect of pH on composition of chlorine water, Giertz (7).

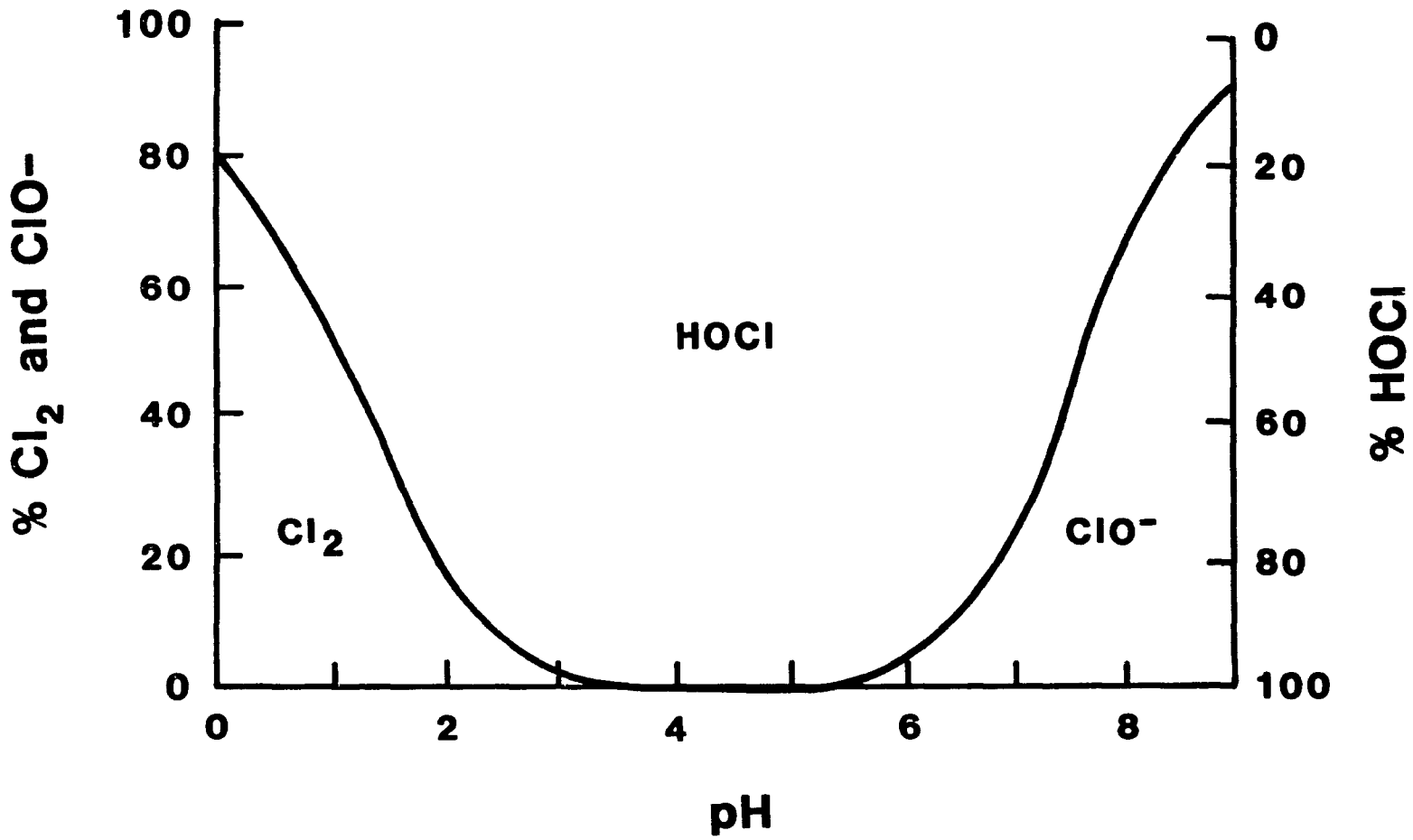
% Cl_2 and ClO-
100
80
60
40
20
0
0
2
4
6
8
pH
Cl_2
HOCl
ClO^-
0
20
40
60
80
100
% HOCl

The chlorine consumption within the first two minutes has been reported by many authors to be between 60 to 80% of the total consumption. The substitution chlorination reaction results in aromatically attached chlorine atoms on to the phenyl propane lignin monomer units. The number of chlorine atoms/C_9 unit has been reported to be between 0.75 and 2.00 (9,10, 11). These substituted lignin monomers are alkali labile. Perhaps, the oxidation of the methoxyl group of the phenyl propane unit to form methanol (12,13,14) is the fastest of the oxidation reactions. Other oxidation reactions result in ring opening and fragmentation and hence to increased water solubility. The kinetics of the chlorine-lignin reactions will be discussed subsequently.

2.3.1.3 Chlorine-carbohydrate reaction

Chlorine is not entirely selective in its reaction with lignin during pulp chlorination. It also oxidises and de-polymerises the carbohydrate fraction resulting in a loss in pulp strength and yield. It is beleived that degradation occurs by a free radical mechanism. Chlorine dioxide, a free radical scavenger, is applied in bleach plants to protect the carbohydrate fraction.

In this study chlorination was generally carried out without a viscosity protecting agent. Since modelling was a main part of this study, the reaction kinetics between carbohydrates and chlorine had to be known. Much of the present knowledge of the oxidation of carbohydrates by chlorine has been obtained through model compound studies (15,16,17,18, 19,20). The oxidation is believed to be governed by both a free radical and an ionic mechanism (19,20) with the free radical mechanism predominate

ing at pH 1 to 3. Due to the complexity of the reaction products and its dependence on pH, a description of the kinetics is difficult. In spite of these difficulties Fredricks et al (20) proposed an ionic reaction mechanism that involves hydride or proton transfer and suggested a rate expression that was first order in substrate concentration and that also included Cl_2 and HOCl. The free radical mechanism was represented by a rate expression first order in chlorine and was beleived to involve hydrogen atom abstraction. However no values of rate constants or activation energies were presented.

The need to study the kinetics of the carbohydrate-chlorine reaction is thus apparent. In the present work such a study was done on lignin free samples of wood pulp.

2.3.2 Kinetic studies

The kinetics of the reaction between chlorine and lignin has been the subject of numerous studies. Chapnerkar (21) showed that 85% of the bleaching action of chlorine water on kraft pulp was completed within five minutes, the time of his first data point. He modelled the system by assuming an instantaneous reaction followed by two reactions that were first order in lignin. Russell (22) studied the chlorination of kraft pulp meal in a tubular reactor, at reaction times of less than one minute, in an effort to elucidate the initial phase of the reaction. His results were described by the following rate expression:

$$-dL/dt = k' L^a \qquad [2.3]$$

$$k' = k f'' [C] \qquad [2.4]$$

where k' is the pseudo rate constant and reaction orders (a) were between 1.6 and 2.0. The pseudo rate constant was found to have a strong dependence on chlorine concentration over the first 25% of delignificaton.

Karter (23) considered the initial 2.5 minutes of pulp fiber chlorination in a tubular reactor system in terms of heterogeneous reaction kinetics. The unreacted shrinking core model that considered either film diffusion, internal diffusion or chemical reaction as the rate limiting step was used to model the resulting kinetic data. The internal diffusion model was found to describe the rate behaviour over the first 60 seconds of chlorination when the effective non-Fickian diffusion coefficient (D_e) was described in terms of the fiber radius (R), reference diffusion coefficient (D), arbitrary fiber radius (r) and a reaction order (n) between 7 and 10.

$$D_e = D\,(r/R)^n \qquad [2.5]$$

When applied to Russels tubular reactor data (22) chemical reaction was found to be limiting at short times and internal diffusion at longer times.

Koch (24) investigated the chlorination of kraft pulp pads in a differential reactor. He reported that delignification rates increase at higher flowrates and consequently a finite external mass transfer resistance to chlorine exists.

Ackert (25) also investigated the chlorination of kraft pulp pads in a differential reactor. He applied both homogeneous and heterogeneous reaction kinetics to his experimental data. Three heterogeneous models

that take various physical resistances into account gave poor fits. Of the four homogeneous models considered, the two that incorporated series or parallel reactions gave the best fits. The one chosen by Ackert was the two parallel reactions model since this is more in accordance with traditional pulp chlorination studies.

$$-dL_1/dt = f\ k_1\ [L_1]\ [C] \qquad [2.6]$$

$$-dL_2/dt = f\ k_2\ [L_2]\ [C] \qquad [2.7]$$

$$dL_1/dt + dL_2/dt = dL/dt \qquad [2.8]$$

Germgard and Karlsson (26) also studied the batch chlorination kinetics of pulp. Their rate expressions, however, have not been published to date.

The most recent chlorination kinetics study was done by MacKinnon (27). He also neglected physical effects and represented the chlorination kinetics by two parallel non-linear reactions. Mackinnon suggested different stiochiometries (g chlorine/g lignin) for the "fast" and "slow" reactions.

$$-dL_1/dt = k_1[L_1]^e[C]^f \qquad [2.9]$$

$$-dL_2/dt = k_2[L_2]^g[C]^h \qquad [2.10]$$

$$dL_1/dt + dL_2/dt = dL/dt \qquad [2.11]$$

$$L_1^0 + L_2^0 + L_f = L_o \qquad [2.12]$$

2.3.3 Rate limiting step

2.3.3.1 General

The rate limiting step in pulp chlorination could be physical or chemical in nature. Physical limitations could be due to diffusion of chlorine through the bulk phase and through the thin film surrounding the fiber (external) or through the fiber wall to the reactant sites (internal). The influence of outward diffusion of products is important for an irreversible heterogeneous reaction. Chemical reaction becomes limiting at slow reaction rates. No consensus exists concerning the rate limiting step as was shown in the previous section. However this has to be known in order to properly model pulp chlorination. Consequently in the following sections, these studies and others will be assessed in an attempt to identify the controlling resistance.

2.3.3.2 External limitations

In conventional chlorination the diffusion of chlorine gas through the bulk could contribute to external mass transfer resistance if proper mixing is lacking (28,29). In dynamic bleaching, contributions to the external resistance could be due only to diffusion through the thin film surrounding the fibers since chlorine is already in solution. Proponents of to the external film resistance theory include Koch (24) and Rapson and Andersen (4). Kochs' claim was refuted by Ackert (25) who used the same experimental system and found no increase in reaction rate with increased flowrates. Ackert further showed that the mass transfer rates were several orders of magnitude faster than the reaction rates. Rapson and

Andersens' assertion was based on the high bleaching rates obtained in displacement bleaching. They contended that the thin film was constantly being eroded leading to a reduction in film resistance and hence increase in reaction rates. Mackinnon (27) presented a dimensional analysis to quantify the significance of film resistance. Using typical conventional batch chlorination conditions, he showed that this film resistance could be neglected after 10 seconds of reaction.

Much of the evidence in the literature supports neglecting film resistance. Such a rate limiting step also cannot explain the transition from fast to slow rates and the formation of a limiting CE Kappa number. Furthermore, increased bleaching rates were not observed by Ackert (25) when he increased the flowrate. The high bleaching rates obtained in displacement chlorination (4) could be due to another phenomenon like rapid product removal from the immediate vicinity of the pulp fibers. This will allow the chlorinated products to diffuse out faster from the fibers and consequently the chlorine to react with unreacted lignin rather than chlorinated products.

2.3.3.3 Internal limitations

Many authors (21,22,23,30,31) contend that the rate limiting step in pulp chlorination is the diffusion of chlorine through the fiber wall. The barrier formed by the reaction products causes an increase in the internal diffusion resistance and hence a reduction in the reaction rates. The limiting CE Kappa number is due to chlorine never reaching unreacted lignin beyond this barrier. This internal limitation theory was rejected by Berry and Fleming (11) and Kuang et al (32) who showed the

presence of chlorine in the unreacted CE lignin. Berry and Fleming (11) further contended that if diffusion was rate limiting then extended chlorination times should eliminate the limiting CE Kappa number. This was not observed. Mackinnon (27) presented a dimensional analysis using typical conventional batch chlorination conditions and concluded that diffusion of chlorine is not rate limiting after 10 seconds of reaction. Ackert (25) obtained a poor fit to his data when he considered internal diffusion as the rate limiting step.

2.3.3.4 Chemical limitations

Ackert (25) and Mackinnon (27) modelled pulp chlorination in terms of homogeneous reaction kinetics. Berry and Fleming (11) concluded that chemical reaction is rate limiting and substantiated this with a "blocking group" theory. They contended that during pulp chlorination alkali labile "blocking groups", possibly chloroquinones and chlorocarboxylic acids, are formed and these allow residual lignin to react very slowly with chlorine. Removal of these groups with alkali restores the rapid chlorination rate. The "blocking group" theory can explain the existance of a limiting CE Kappa number. Recent work by Ni et al. (70) strongly supported the "blocking group" theory. They identified guaiacyl monomer units with three chlorine atoms substituted in the benzene nucleus as the so-called "blocking groups".

2.4 Modelling of packed beds

2.4.1 Introduction

For a description of the concentration of a reactant at the exit of the reactor the reaction kinetics, the residence time distribution and the degree of segregation has to be known. If the reaction are linear then

knowledge of the residence time distribution is sufficient to predict the reactor performance. For non-linear kinetics, flow models that closely approximate the real flow have to be used (33).

Many types of models can be used to characterize non-ideal flow patterns within process vessels. They can be broadly classified as Fickian or non-Fickian. The Fickian or dispersion models draw on the analogy between actual flow and diffusion and is well suited for packed beds or tubular reactors. The non Fickian models, mixing cell and cross-flow models (34,35), overcome some of the shortcomings of the dispersion models but are more complicated. The solutions are, however, very similar and consequently the simplicity of the dispersion model favors its selection. In the following sections, some of the vast literature in this area will be reviewed both for the cases of non-chemical and chemical modification of the fluid as it passes through the process vessel. The former is addressed since part of this study also involved inert tracer studies.

2.4.2 Without reaction

The axial dispersion model is a simplification of the general dispersion model and assummes no radial variations in concentrations, constant axial dispersion coefficient and constant mean velocity and has the following form:

$$\frac{\partial (C/C_o)}{\partial T} = \frac{1}{P} \frac{\partial^2 (C/C_o)}{\partial X^2} - \frac{\partial (C/C_o)}{\partial X} \qquad [2.13]$$

where P is the Peclet number based on the interstitial velocity.

Solution of the above equation can be obtained with the Danckwerts' (36) boundary conditions. An analytical solution to equation [2.13] is available (37).

This one dimensional model was applied to laminar flow in a tubular reactor (38) and was found to adequately describe the two dimensional flow behaviour provided that the residence time of the system, H/u, was significantly greater than radial diffusive transport times, $0.138a^2/D$ (i.e. $Pe = 48DH/a^2 u > 6.65$) where a is the the tube radius. When radial diffusion occurs rapidly the concentration gradients at any cross section diminish and the dispersion model which assumes a lumped concentration value at each cross section becomes physically more realistic. Extensions of this dispersion equation to account for other physical phenomena by addition of a source term are readily available in the literature. Sherman (39) assumed a linear adsorption isotherm to account for adsorbed solute. Pellet (40) accounted for both internal and external mass transfer resistances and also a linear adsorption isotherm. Both of these studies were conducted on beds of uniform cylindrical porous fibers. Rasmuson (41) presented an exact solution that involved longitudinal dispersion, external and internal mass transfer resistances and linear adsorption.

Many studies have been concerned with the effects of experimental variables on the longitudinal dispersion coefficient (42,43,44,45,46,47, 48) for uniformly shaped packing materials. Peclet numbers are correlated with Reynolds and Schmidt numbers. Fewer studies are available on the

mixing characteristics of pulp fiber beds. Rabergeau (49) modelled displacement washing of a fiber bed with a pure plug flow model and accounted for internal diffusion resistance. A poor fit was obtained in the initial breakthrough region. Poirier (50) modelled displacement washing for both high and low initial pad liquor concentrations. The axial dispersion model without source term was found to be adequate for high solute concentrations. Inclusion of a sorption isotherm was needed at low solute concentrations. The Peclet number increased with increasing pad height and decreasing consistency. Increasing superficial velocities resulted in an increase in Peclet number at low consistency and a decrease at high consistency. Temperature changes on the Peclet number were found to be insignificant by Poirier (50) and important by Lee (51).

The effect of operating variables on a fixed bed of pulp fibers was also investigated in this work. Sugar solutions of glucose and dextrans were used as the displacing fluid. Operating variables were studied on the same pad, unlike the other pulp fiber studies cited above, and consequently variation in pulp pad formation were unimportant. Also these sugars do not adsorb onto the pulp fibers (52).

2.4.3 With reaction

The axial dispersion model has been used extensively to represent mixing effects in chemical reactors (53). The suitability of this model was discussed by many authors (54,55,56,57,58). Unlike the inert case discussed above where the concentration driving force only comes from an injected species at the tube entrance and is distributed with respect to position and time, the reaction case also involves concentration differ-

ences due to generation or consumption. Bischoff and Levenspiel (54) showed qualitatively that the steady state axial dispersion model and associated reaction term accurately represents a slow first order reaction occuring in a long tube. This was verified numerically by Bischoff (55) who compared the predictions of the axial dispersion model with the two dimensional mass balance equation representing symmetric laminar flow and first order reaction in a round tube. Wan and Ziegler (56) extended this analysis and stated that in reactive systems a reaction time compared to a radial diffusion time is needed to determine the suitability of the axial dispersion model. They concluded that for both first and second order reactions the conversion in a steady flow laminar reactor may be accurately simulated with the axial dispersion model and a generalized value of Taylors' (38) Peclet number. Consequently Taylors' definition of the Peclet number for inert cases ($Pe = 48DL/a^2 u$) is replaced by ($Pe = 48\alpha X$ with $\alpha > 0.5$) for the reactive case, where α is the ratio of a reaction rate to a radial diffusion rate. Thus if the radial diffusion rate is greater than twice the reaction rate, the axial dispersion equation can be used with confidence. Wissler (57) confirmed these findings.

Subramanian et al. (58) extended the testing of the axial dispersion equation for laminar flow and first order homogeneous kinetics in tubular reactors by comparing exact solutions of the governing equations to the axial dispersion model solutions for both the steady state and transient cases. Good agreement between exact and dispersion model solutions were obtained for slow reactions at positions far from the reactors' inlet for the transient case. The agreement became progressively worse

for more rapid reactions.

Corrigan et al. (59) compared the predictions of the axial dispersion and plug flow models when applied to steady state packed bed reactors. The effect of axial dispersion on first and second order reactions were predicted from transient response with no reactions. They concluded that for both first and second order reactions, at high conversion levels, the predicted conversions of the axial dispersion model was significantly different from that of the plug flow model. Both models represented the experimental data very well at low conversion levels but the axial dispersion model was better at high conversion levels. Applicability of the axial dispersion equation to represent the more flat velocity profile in fixed bed reactor system is more readily obtainable than for tubular reactors. The criterion of much faster radial diffusion rates, however, continue to apply.

Fan and Bailie (60) presented numerical solutions for the steady state axial dispersion equation with a single reaction having orders other than zero and first in fixed bed reactors. Burghardt and Zaleski (61) presented approximate analytical solutions to the steady state axial dispersion equation having a general reaction kinetics for a single reaction also in fixed bed reactors.

The analytical solution to the transient axial dispersion model with linear rate term in fixed bed reactors was presented by Danckwerts (62), Crank (63), Bird et al. (64), Lightfoot (65) and Vrentas et al. (66). They proposed that solution of this problem could be derived from the solution of the corresponding diffusion problem without chemical reaction. A more practically useful solution to this problem, and that in-

cluded Danckwerts' boundary conditions, was presented by Deckwer and Langemann (67) and Iyer and Vasudeva (68). These solutions were very good in the range of Peclet number 0.04 to 10 but gave physically unrealistic values at Peclet number greater than 10.

Many studies applying the axial dispersion equation in fixed bed chemical reactors have been restricted to the steady state cases with a single reaction. The packings in these reactors are of regular shape. Requirements of this work will entail numerical solution of the unsteady state axial dispersion equation and three associated reactions, one of which is relatively fast, for the case of a fixed bed reactor system made up of pulp fibers of complicated geometry and characteristics. Because of this fast reaction good predictions are not guaranteed since the bounds of this one dimensional approximation of the two dimensional convection-diffusion problem may be violated.

2.4.4 Parameter estimation

The axial dispersion model is governed by a single parameter, the Peclet number. Evaluation of this parameter can be done with several methods: moments, weighted moments, fourier analysis, transfer function fitting and time domain analysis (69).

The moments method is popular and quite simple. The axial dispersion equation is solved in the Laplace domain and the moments of the equations are compared to the corresponding moments of the experimental response curve to elucidate the parameters. The moments method has the shortcoming that a large weight is placed on the tail ends of the response curve. Since this is generally the least accurate portion of the curve, errors can be quite severe especially if higher moments, fourth and fifth,

are used. In cases where mass transfer resistances are negligible, the tail of the response curve is short and the accuracy of the moments technique is very good. Such is the case with the sugar tracers in this work. The second moment allows calculation of the Peclet number and is the highest moment used in this study.

2.5 Conclusions

The technique of displacement or dynamic bleaching is of commercial importance and bleaching times are significantly shorter than conventional batch bleaching methods. The chlorination stage, however, is still external to the tower. Ackert's (25) investigation of displacement chlorination was limited to very thin pads and restricted to kappa number and residual chlorine measurements at the end of the reaction period. More detailed experimental and theoretical analysis is needed for a proper understanding of this method of chlorination. Such knowledge will also assist in a better understanding of the other stages of displacement bleaching. Review of the literature indicates that many studies on the reaction between chlorine and pulp have been done. It seems that the reaction kinetics can best be represented by ignoring physical resistances and considering only homogeneous reaction kinetics. The rate expressions proposed by Ackert (25) and Mackinnon (27) are applied in this study.

The axial dispersion model has been used extensively to model tubular and packed bed reactors. These studies were mainly restricted to the steady state case and with a single rate equation. Applicability of the axial dispersion model with a single very fast rate equation (54, 55, 56, 57, 58) were less successful. Modelling of the chlorine breakthrough curve is attempted with the axial dispersion model: physical resistances

are neglected and kinetics governing the reactions between chlorine and pulp included. The suitability of the axial dispersion model cannot be guaranteed though because of the rapid chlorine- lignin reaction. Modelling of the inert sugar tracer, however, is amenable to the axial dispersion model and parameter estimation by the moments technique is used.

References

1. Ducey, M.J., Pulp and Paper, (1984)
2. Schleinkofer, R.W., CPPA 68th Annual meeting PrePrints, 211, (1982)
3. Munroe, F.C., Bleach Plant Operations, TAPPI PRESS, Atlanta, 45, (1984)
4. Rapson, W.H., and Andersen, C.B., Tappi, Vol.49, No. 8, (1966)
5. Torregrossa, L.O., Bleach Plant Operations, (1983)
6. Gullichsen, J., "The bleaching of pulp", Chapter 10, 3rd edition, Tappi Press (1979).
7. Giertz, H.W., "Chemistry in wood", E. Hägglund, Academic, New York, N.Y., 1951, p.508.
8. Dence, C.W., and Annergren, C.E., The Bleaching of Pulp, 3rd Edition, TAPPI Press, 29 (1979)
9. van Buren, J.B., and Dence, C.W., TAPPI, Vol.53, No.12, 2246 (1970)
10. Heuser, E., and Sieber, R., Agnew. Chem., Vol.26, 801 (1913)
11. Berry, R.M., and Fleming, B.I., Preprints, Int'l Symp. in Wood and Pulp Chem., (1985)
12. Sarkanen, K.V., and Strauss, R.W., TAPPI, Vol.44, No.7, 459 (1969)
13. Dence, C.W., Meyer, J.A., Unger, K., and Sadowski, J., TAPPI, Vol.48, No.3, 148 (1965)
14. van Buren, J.B., and Dence, C.W., TAPPI, Vol.53, No.12, 2246 (1970)
15. Alfredsson, B., and Samuelson, O., Svensk Papperstid, nr.12, (1974)

16. Theander, O., Tappi, Vol.48, No.2, (1965)

17. Fredricks, P.S., Lindgren, B.O., and Theander, O., Tappi, Vol 54, No.1 (1971)

18. Theander, O., Svensk Papperstid, Nr.18, (1958)

19. Fredricks, P.S., Lindgren, B.O., and Theander, O., Cellulose Chem. Technol. Vol.4,533-547 (1970)

20. Fredricks, P.S., Lindgren, B.O., and Theander, O., Svensk Papperstid, Nr. 15, (1971)

21. Chapnerkar, V.D., Ph.D Thesis, University of Florida (1961)

22. Russel, N.A., Ph.D Thesis, IPC (1966)

23. Karter, E.M., Ph.D Thesis, University of Maine, Orono, (1968)

24. Koch, D.D., Ph.D Thesis, University of Idaho (1971)

25. Ackert, J.E., Ph.D Thesis, University of Idaho (1973)

26. Germgard, U., and Karlsson, R., Svensk Papperstid., nr.18, 146 (1985)

27. Mackinnon, J., M.Eng Thesis, Mc Gill University (1987)

28. Paterson, A.H., and Kerekes, R.J., PGRL, PPRIC, (1983)

29. Paterson, A.H., and Kerekes, R.J., PrePrints, 1985 Int'l Pulp Bleach. Conf.

30. Pugliese, S.C., and McDonough, J.J., "Kraft pulp chlorination: A new mechanistic description", 1988 Pulp Bleaching Conference, Florida.

31. Giertz, H.W., Tappi, Vol.34, No.5, 209 (1951)

32. Kuang, S.J., Saka, S., and Goring, D.A., J. Wood Chem. Technol. 4,(2),163, (1984)

33. Levenspiel, O., and Bischoff, K.B., Adv. Chem. Eng.,4, 95-197, (1963)

34. Sundaresean, S., Amundson, N.R., and Aris, R., AIChE J., 529- 36, (1980)

35. Hinduja, M.J., Sundaresean, S., and Jackson, R., AIChE J., 26(2), (1980)

36. Danckwerts, P.V., Chem. Eng. Sci., 2(1), 1-13, (1953)

37. Brenner, H., Chem. Eng. Sci., vol.17, 229-243, (1962)

38. Taylor, G.I., Proc. Roy. Soc., A219, 186-203, (1953)

39. Sherman, W.R., AIChE J., 10(6), 855-860, (1964)

40. Pellet, G.L., Tappi, 49(2), 75-82, (1966)

41. Rasmuson, A., AIChE J., 31, No.3, (1985)

42. Han, N., Bhakta, J., and Carbonell, R.G., AIChE J., 31, No. 2, (1985)

43. Chung, S.F., and Wen, C.Y., AIChE J., 14, No. 6, (1968)

44. Carberry, J.J., and Bretton, R.H., AIChE J., 4(3), 367-375, (1958)

45. Rafai, M.N.E., Ph.D. Dissertation, University Calif., Berkeley, (1956)

46. Kramers, H., and Alberda, G., Chem. Eng. Sci., 2, 173, (1953) 47, Danckwerts, P.V.,

48. Klikenburgh, A., and Sjenitzer, F., Chem. Eng. Sci., 5(6), 258, (1956)

49. Rabergeau, G., Etude du lavage en lit fixe de pates cellulosiques, D.E.A. de Genie Chimique, Ecole Francaise de Papeterie, Institut National Polytechnique de Grenoble, (1982-83)

50. Poirier, N.A., M.Eng. Thesis, Mc Gill University, (1986)

51. Lee, P.F., Tappi, 62 (9), 75-78, (1979)

52. Stone, J.E., and Scallan, A.M., "A structural model of the cell wall of water swollen pulp fibers based on their accessibility to macromolecules", Cellulose Chem. and Tech., 2, 343-358, 1968.

53. Bischoff, K.B., Ind. Eng. Chem., No.11, 58, 18, (1966)

54. Bischoff, K.B., and Levenspiel, O., Chem. Eng. Sci., 17, 257, (1962)

55. Bischoff, K.B., AIChE J., 14, No.5, (1968)

56. Wan, C., and Ziegler, E.N., Chem. Eng. Sci., 25, 723-727, (1970)

57. Wissler, E.H., Chem. Eng. Sci., 24, (1969).

58. Subramanian, R.S., Gill, W.N., and Marra, R.A., Can. J. of Chem.Eng., 52, 563-568, (1971)

59. Corrigan, T.E., Bauer, J.L., and Dean, M.J., Can. J. of Chem. Eng., 48, (1970)

60. Fan, L., and Bailie, C., Chem. Eng. Sci., 13, 63-68, (1960)

61. Burghardt, A., and Zaleski, T., Chem. Eng. Sci., 23, 575-591, (1968)

62. Danckwerts, P.V., Trans. Faraday Soc., 47, 1014, (1951)

63. Crank, J., The Mathematics of diffusion, Oxford, London, 124, (1956)

64. Bird, R.B., Stewart, W.E., and Lightfoot, N.E., Transport Phenomena, Wiley, New York, 621 (1960)

65. Lightfoot, E.N., AIChE J., 10, 278, (1964)

66. Vrentas, J.S., and Vrentas, C.M., AIChE J., 1, 167, (1987)

67. Deckwer, W.D., and Langemann, H., Chem.-Ing-Techn., 44, 1318, (1972)

68. Vasudeva, K., and Iyer, R.N., Chem. Eng. Sci., 33, 1299-1300, (1978)

69. Fahim, M.A., and Wakao, N., "Parameter estimation from tracer response measurements", Chem. Eng. Journal, 25 (1982).

70. Ni, Y., Kubes, G.J., and Van Heiningen, A.R.P., Preprints 75th Annual Meeting Tech. Section, CPPA, Montreal, A101-109 (1989).

CHAPTER 3

EXPERIMENTAL APPARATUS AND PROCEDURES

3.1 Introduction

In dynamic pulp chlorination, a chlorine-water solution is constantly being forced through a pad of pulp fibers. The chlorine in the displacing fluid reacts preferentially with lignin in the pulp. Some of the resulting chlorolignin is water soluble and is removed from the pad together with spent solution. Due to this constant flow of fresh chlorine water solution, a lignin reaction front is formed. The pulp pad preceding this front is depleted in lignin and chlorine consumption here is due to both the residual lignin and carbohydrates. Beyond the reaction front is unreacted pulp. This front moves away from the inlet of the pad at a speed determined by the superficial velocity and concentration of the chlorine water solution, temperature and pulp pad consistency.

The shape of the reaction front is governed by the flow distribution through the pad. For plug flow, the reaction front is flat. Real systems are characterized by varying degrees of mixing and this results in a reaction zone that is correspondingly diffuse. Chlorine appears at the exit when any part of the reaction front has travelled through the complete length of the pad. With time, the entire reaction front would have reached the pad exit and chlorine consumption by the pulp pad would be due only to residual lignin and carbohydrates. Measurement of the chlorine concentration at the exit of the pad at different times gives rise to a breakthrough curve (BTC). The area above this BTC represents the amount of chlorine consumed. In addition to residual chlorine, chloride, methanol and total organic carbon (TOC) in the effluent stream area are also measured.

The purpose of this experimental study was to investigate the chlorination of pulp in a fixed bed reactor system with the chlorine water solution being the mobile phase. The resulting experimental data would form a base for testing a suitable model describing the relevant physical and chemical phenomenon of the process. The variables investigated were flow rate, chlorine concentration and temperature of chlorine water solution, pad height and reaction time. The consistency of the pulp pad and effect of recycle of spent chlorination liquor were also studied.

As mentioned above, chlorine reacts with both lignin and carbohydrates. Thus in order to adequately model the system, the kinetics of the reaction between chlorine and lignin and chlorine and carbohydrates has to be known. Many authors (1,2,3,4,5,6) have studied the chlorine-lignin reactions and several rate expressions are available in the literature. The chlorine-carbohydrates reaction has, however, received less attention and no rate expression is currently available. Elucidation of the kinetics of this reaction was then included in the experimental program of this study.

The changes in the flow characteristics of the chlorine water solution during its passage through the pulp pad also has to be known so as to facilitate modelling of the dynamic chlorination process. Stimulus response experiments were performed with suitable inert tracers (glucose and dextran) to obtain a description of the mixing characteristics of the fixed bed system.

The experimental facility, techniques and procedures used to study the dynamic chlorination of kraft pulp is described in the subsequent

sections. The chemical and physical properties of the black spruce kraft pulp used in this experimental study are given in Appendix 3-1.

3.2 Experimental facility

The stainless steel reactor system used to study the dynamic chlorination of kraft pulp is illustrated in Figure 3.1. A pulp pad is formed in the hollow cylindrical region, 7.5 cm diameter and 20 cm high, and held between a stationary lower plate and a moveable upper piston. The plate and piston are each perforated by 16 holes, of 3.5 mm diameter, and situated evenly on the periphery of a 6.5 cm diameter circle.

The lower plate is connected to an exit line and this facilitates the flow of effluent out of the reactor system. The dead volume between the bottom of the pulp pad and the end of the exit line is approximately 20 cm^3. The upper moveable piston serves to fix the height of the pulp pad and, in addition, allows solution to enter into the reactor system. Also attached to the piston is a bleed line that serves as another exit line of the reactor system. This is of value in pad formation and at the beginning and end of an experimental run and will be addressed subsequently. Attached to both the lower plate and the piston are 200 mesh screens that serves to minimize the loss of fines or fibers from the pulp pad.

The bleed and outlet lines of the reactor are equipped with solenoid valves that are connected to a common two way switch. These two lines are both never open or closed at the same time. Consequently when the bleed line is closed the outlet line is open and solution can flow through the pulp pad. The other option that closes the outlet line and opens the bleed line allows the piston to be filled with solution and prevents flow through the pulp pad. Hence, the exact start of the contact time between the solution (chlorine or inert tracer) and pulp pad is very well defined.

Figure 3.1 Schematic of reactor.

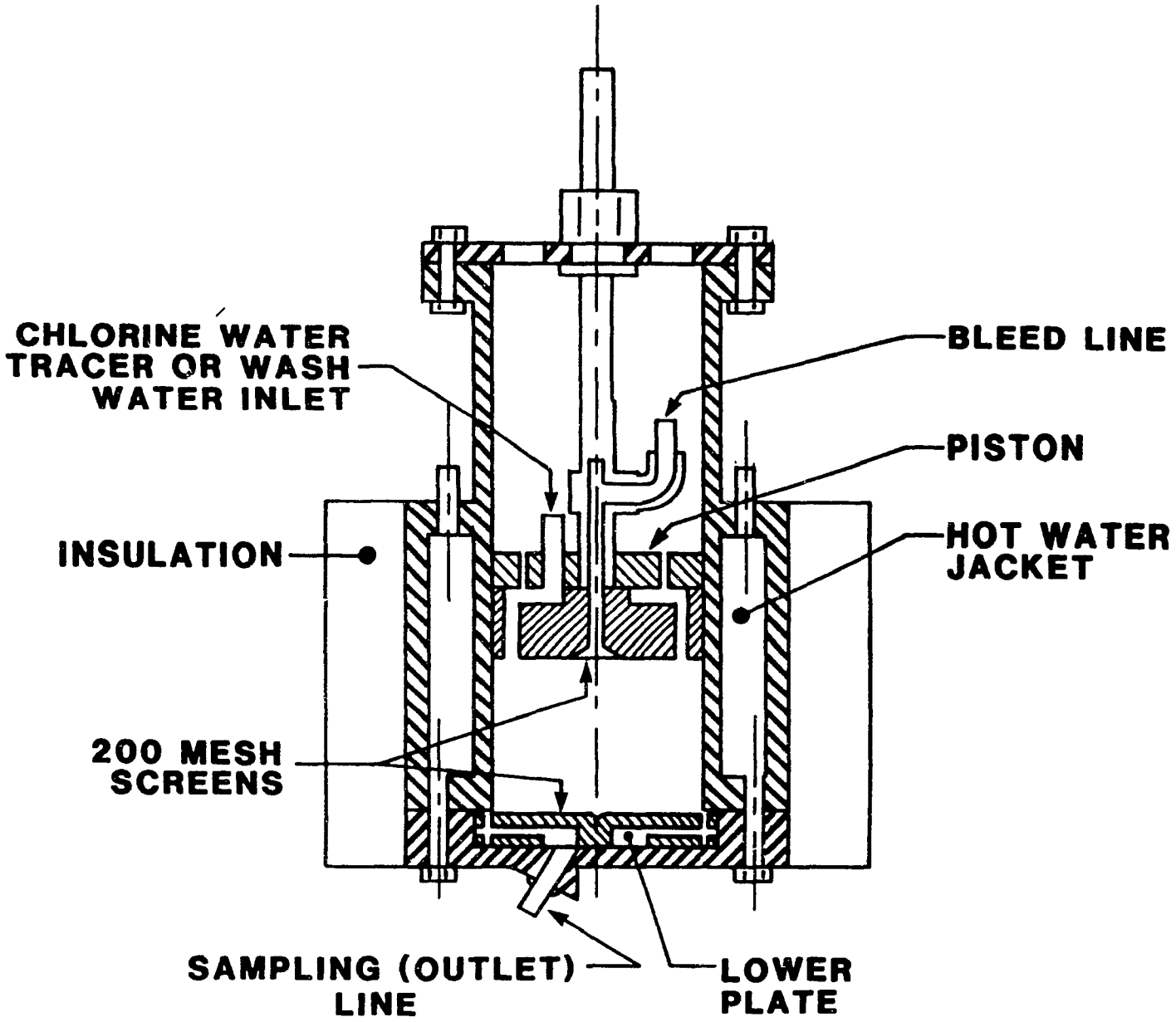
CHLORINE WATER
TRACER OR WASH
WATER INLET
BLEED LINE
PISTON
INSULATION
HOT WATER
JACKET
200 MESH
SCREENS
SAMPLING (OUTLET)
LINE
LOWER
PLATE

This arrangement reduces the dead volume at the top of the pulp pad to effectively zero. The pulp pad temperature was controlled by a heating jacket to the required temperature. This heating was supplemented with heating tapes at higher temperatures. The temperatures of the jacket, pulp pad and solution were monitored by thermocouples.

A schematic of the reactor and auxillary equipment is shown in Figure 3.2. Chlorine water is made and stored in a large (50 cm * 50 cm * 50 cm) tank. This is essential in order to keep the change in static pressure head of the chlorine water during an experiment to a minimum and consequently minimize variations in inlet chlorine concentration and flow-rate. The chlorine water is pumped by a peristaltic pump (Masterflex R-7523) to a three neck flask that is immersed in a constant temperature bath. The air in the flask is removed through a bleed line. The chlorine water solution is then directed through a two way valve, V_1, leading either back to the tank or towards the reactor. Another two way valve, V_2, allows either chlorine water or wash water to flow to the reactor. The wash water is pumped by another head of the same peristaltic pump through a two way valve, V_3, that gives the option of recycle back to the wash water tank or leads to valve V_2. Just before the reactor is another two way valve, V_4. One port of this valve allows sampling of the chlorine water solution just before it enters the reactor while the other port leads to the piston of the reactor. The wash water line is used for pulp washing after chlorination and for the stimulus response experiments with glucose and dextran before chlorination. The water for the heating jacket is pumped by another peristaltic pump (Masterflex R-7553) through coils immersed in a heating bath and finally to the reactor. The reactor and all lines leading to the reactor are well insulated.

Figure 3.2 Schematic of experimental facility.

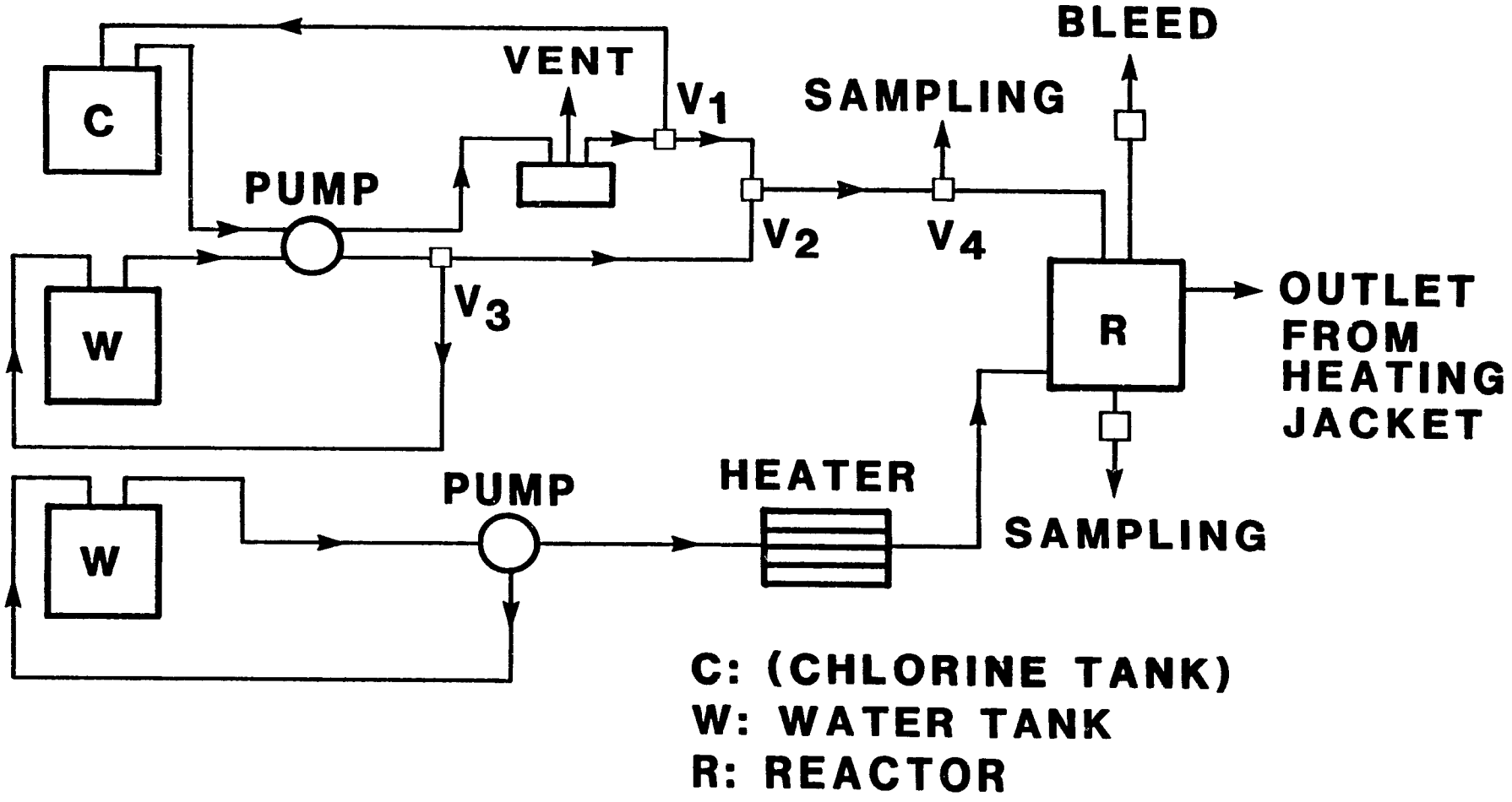
BLEED
VENT
V_1
SAMPLING
C
PUMP
V_2
V_4
V_3
R
OUTLET
FROM
HEATING
JACKET
W
PUMP
HEATER
W
SAMPLING
C: (CHLORINE TANK)
W: WATER TANK
R: REACTOR

3.3 Experimental procedures

Several preliminary and preparative steps are necessary prior to the actual dynamic chlorination process. In this section the preliminaries like chlorine water and sample tray preparations as well as the pulp pad formation techniques are discussed. Finally the experimental procedures for a typical run are outlined.

3.3.1 Preliminary preparations

3.3.1.1 Chlorine water preparation

Preparation of chlorine water to the desired concentration was done the day prior to the experiment. A schematic of the system is shown in Figure 3.3. Chlorine gas is continuously bubbled through a dispersion tube located about one inch from the bottom of the tank. Mixing of the gas through the liquid bulk was facilitated with a mechanical stirrer. A mechanical seal around the rod of the stirrer prevented escape of chlorine gas. A purge system was connected to the tank and all displaced air was bubbled through a caustic solution to remove entrained chlorine gas. Samples were taken from an outlet port of the tank at regular intervals and analysed for chlorine concentration.

3.3.1.2 Sample tray preparation

The effluent stream is analysed for chlorine, chloride, total organic carbon and lignin and in some cases for methanol during a dynamic chlorination experiment. Chlorination is traditionally characterized by a fast reaction between chlorine and lignin, within the first few minutes of chlorination, followed by a much slower chlorine consumption by both residual lignin and carbohydrates. Consequently the highest concentration

Figure 3.3 Preparation of chlorine water.

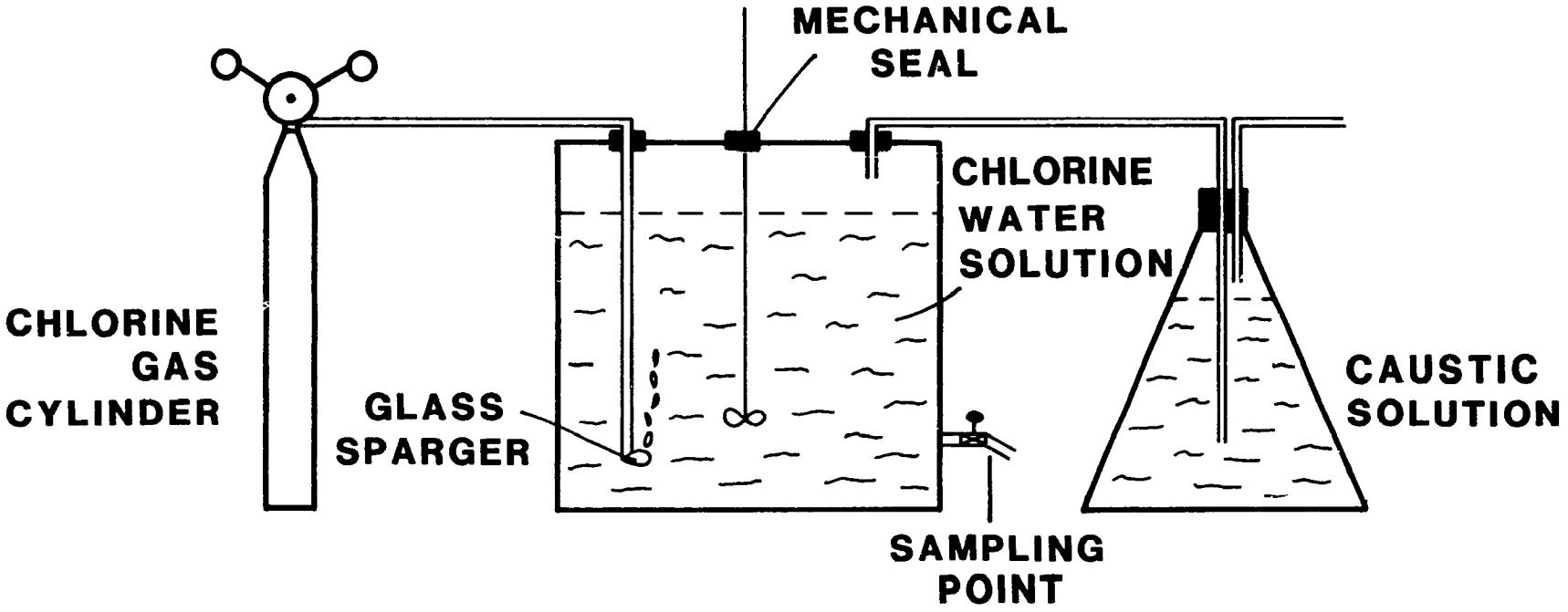
MECHANICAL
SEAL
CHLORINE
WATER
SOLUTION
CHLORINE
GAS
CYLINDER
GLASS
SPARGER
CAUSTIC
SOLUTION
SAMPLING
POINT

of total organic carbon, lignin and generated chloride will be in the first few padvolumes of effluent leaving the reactor. The chlorine concentration during this time span is very low. The sampling techniques were then structured to suit these conditions. Samplings were done continuously over the time span encompassing the first few displaced padvolumes with the time span and the sample collection times determined from operating conditions like pulp pad consistency and height and the superficial velocity of the chlorine water solution. Generally the sample collection times for individual samples ranged from 5 to 20 seconds. During this initial continuous sampling period chlorine samples were collected after two sets of samples were collected for the other analyses. Subsequently the sampling rates became equal and the time between sample collection was extended. Sample trays were prepared to satisfy these needs. In addition suitable reagents were added to the sample bottles. A mixture of acid and potassium iodide solution of known volume was added to the chlorine sample bottles to determine all residual chlorine. The chloride concentration was determined from another sample. The residual chlorine was converted to chloride after reaction with a known volume and strength of sodium metabisulfite in the sample bottles. Samples for total organic carbon and lignin analysis were collected in empty bottles. The technique of analyses will be discussed in a subsequent section. Sampling during inert tracer experiments were done continuously at sample collection times dependent on the pad height and superficial velocity. The sugar solutions were kept overnight to allow the solutions to stabilize before starting an experiment.

3.3.2 Pulp pad preparation

Extreme care is necessary to form a pulp pad that will allow a displacing fluid to exhibit a flow distribution that is close to plug flow. Such a flow distribution assures uniform distribution of the displacing fluid over the pulp. The presence of channelling and other non-ideal flow behaviour results in unbleached regions in the pulp pad if the displacing fluid is chlorine water. It is known that no two pulp pads can be made the same because of the geometry and characteristics of the pulp fibers. The best that can be done from an experimental standpoint is to exercise care and to quantify the flow characteristics of the resulting pad. After repeated trials a technique was developed that resulted in pads that exhibited fairly sharp residence time distributions. The residence time distribution was quantified by stimulus-response experiments on each pad.

A softwood kraft pulp was used in all chlorination experiments. The weight of pulp needed to form a pulp pad of a certain consistency depends on the pad height and cross-sectional area of the reactor and could be calculated from the following equation.

$$X = \frac{A \cdot H}{(1/\rho_f - 1) + 100/C_p} \qquad [3.1]$$

where H is the pad height, A the cross-sectional area (45.05 cm^2), X the mass of O.D. pulp required, ρ_f the density of fibers (1.5 g/cm^3), and C_p the consistency of pulp pad, g pulp/ 100 g pulp suspension.

The pulp was disintegrated for about two minutes with a high speed stirrer and then de-aerated for about 40 to 45 minutes so as to remove the trapped air bubbles. The pulp water suspension was then diluted to about 0.5% consistency and poured carefully into the reactor that was modified as shown in Figure 3.4. The function of the added section was to allow complete addition of the pulp water slurry. The water was allowed to drain through the exit line of the reactor at an accelerated rate due to the applied vacuum. Drainage was continued until the level of the slurry was just above the desired final pad height. The added section was then removed and the piston was placed into the cylindrical section and slowly depressed to the final preset height. During this operation the bleed line from the plunger was opened to allow removal of excess water while the exit line from the lower plate was closed. The plunger was then bolted on to the body of the reactor.

3.3.3 Experimental method

After completion of the preliminaries, the heaters were turned on and all flow lines to and from the reactor installed. The peristaltic pump was calibrated by passing water through the "chlorine line" and through the pulp pad. Glucose and dextran T-2000 tracer tests were conducted at the same flowrate to be used in chlorination. The pulp pad was thoroughly washed with water after each tracer test to prevent solution carryover. Mixing cup samples were collected at the exit of the reactor over the duration of both tests. Samples of the original solution were taken both at the beginning and at the end of the tracer experiment. The analytical technique used to determine the sugar concentration in these samples will be discussed subsequently.

Figure 3.4 Preparation of pulp pad.

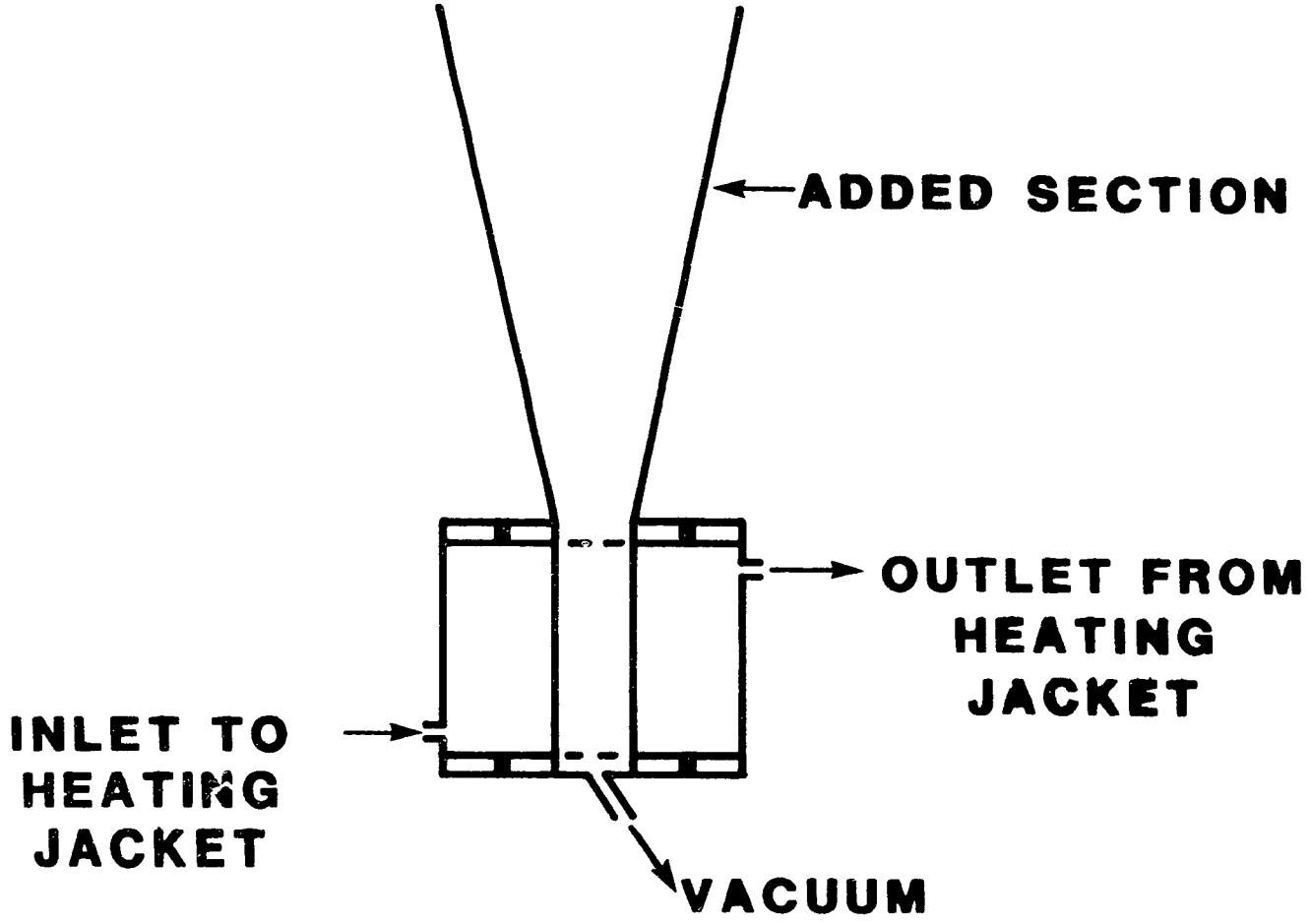
ADDED SECTION
OUTLET FROM HEATING JACKET
INLET TO HEATING JACKET
VACUUM

The system was then allowed to reach the desired operating temperature. Chlorine water solution was continuously recycled back to the tank during this time interval so that both the temperature and the concentration will be stable. The wash water flow was also directed back to the wash water tank. After temperature stability was achieved the solenoid valve at the exit line of the bottom plate of the reactor was closed and the bleed line of the piston opened. Chlorine water was then directed towards the reactor and allowed to circulate through the piston and out through the bleed line. Chlorination was allowed to commence by closing the bleed line and opening the exit line of the bottom plate. Samples were collected at the exit of the reactor at pre-determined times throughout the chlorination period. The inlet chlorine water was also regularly sampled. At the end of the chlorination period the chlorine water solution was directed back to the tank and the wash water was directed to the reactor. The pulp pad was thoroughly washed and the chlorination reaction terminated. The pulp pad was then removed from the reactor and a portion of it was caustic extracted under the following conditions:

consistency = 10%

charge = 3% on pulp

time = one hour

temperature = 70°C

Handsheets were made from both the chlorinated-washed pulp and the chlorinated-washed-extracted pulp.

3.4 Analytical techniques

3.4.1 Sugar analysis

The samples collected during the tracer tests were analysed by

polarimetry. The rotation exhibited by these optically active samples depended only on concentration since the temperature, wavelength and path length were kept constant during all analyses. The ratio of the sample rotation to the rotation of the initial solution is then a dimensionless measure of the exit concentration. A plot of this fraction as a function of time give rise to a breakthrough curve for the sugar tracer.

The polarimeter used (model # AUTOPOL 111-589-10) was purchased from RUDOLPH RESEARCH in New Jersey. The precision was 0.001 degrees, the wavelength 589 nm and the bandwith 10 nm. A 10 cm sample tube (model # 14-8.5-100-6.0) was found to be adequate. All measurements were done at room temperature. The main components of the polarimeter are the light source, polarizer, sample tube, analyzer and a measuring device. The output from a high intensity halogen cycle tungsten light source is focussed into a 6 mm diameter beam of unpolarized white light and passes through a Glan- Thompson polarizer and then to the sample tube. After transmission through the sample chamber the linear rotated polarized light passes through a rotatable analyser prism and then to a photomultiplier tube. The analyser is driven through an angle equal to the sample rotation and polarimetric balance is re-established i.e. the analyser and polarizer transmission axes are precisely perpendicular. This rotation is digitally displayed.

3.4.2 Chloride analysis

Hydrochloric acid is generated from both substitution and oxidation reactions during chlorination. In addition, chloride from residual chlorine is also present in solution in an amount depending on the equilibrium reaction between chlorine and water. Addition of sodium metabisul-

phite converts all residual chlorine in the sample to chloride. Hence determination of the total chloride and residual chlorine concentration will allow calculation of the amount of chloride produced by reactions.

The chloride concentration was measured by a flow injection analyser (model FIAstar 5020) in conjunction with a spectrophotometer (model FIAstar 5023) that consists of a detector controller (model #5023) and spectrophotometer optical unit (model # 5023-011). Flow injection analysis is based on introduction of a defined volume of sample into a carrier stream. This results in a sample plug bracketed by the carrier. The sample stream is merged with a reagent stream in a chemifold to obtain a chemical reaction between the sample and the reagent. More than one reagent stream can be mixed with the sample plug. The sample becomes progressively dispersed as the stream moves towards the detector. The degree of dispersion of the sample can be controlled by varying a number of factors such as sample volume, length and diameter of mixing coils and flow rates. When the sample stream reaches the detector, neither chemical reaction nor the dispersion process has reached a steady state. Since experimental conditions are held identical for both samples and standards, the samples can be evaluated against appropriate standards injected in the same manner. A schematic of the system is shown in Figure 3.5. The reagent used for chloride determination contained mercury thiocynate, iron (111) nitrate, nitric acid, methanol and water in fixed proportions. The chloride ions in the sample or standard reacts with this reagent to form a red thiocynate complex that is detected at a wavelength of 470 nm by the spectrophotometer.

3.4.3 Chlorine analysis

A continuous method to monitor the concentration of chlorine was

Figure 3.5 Flow Injector Analyzer (FIA) system.

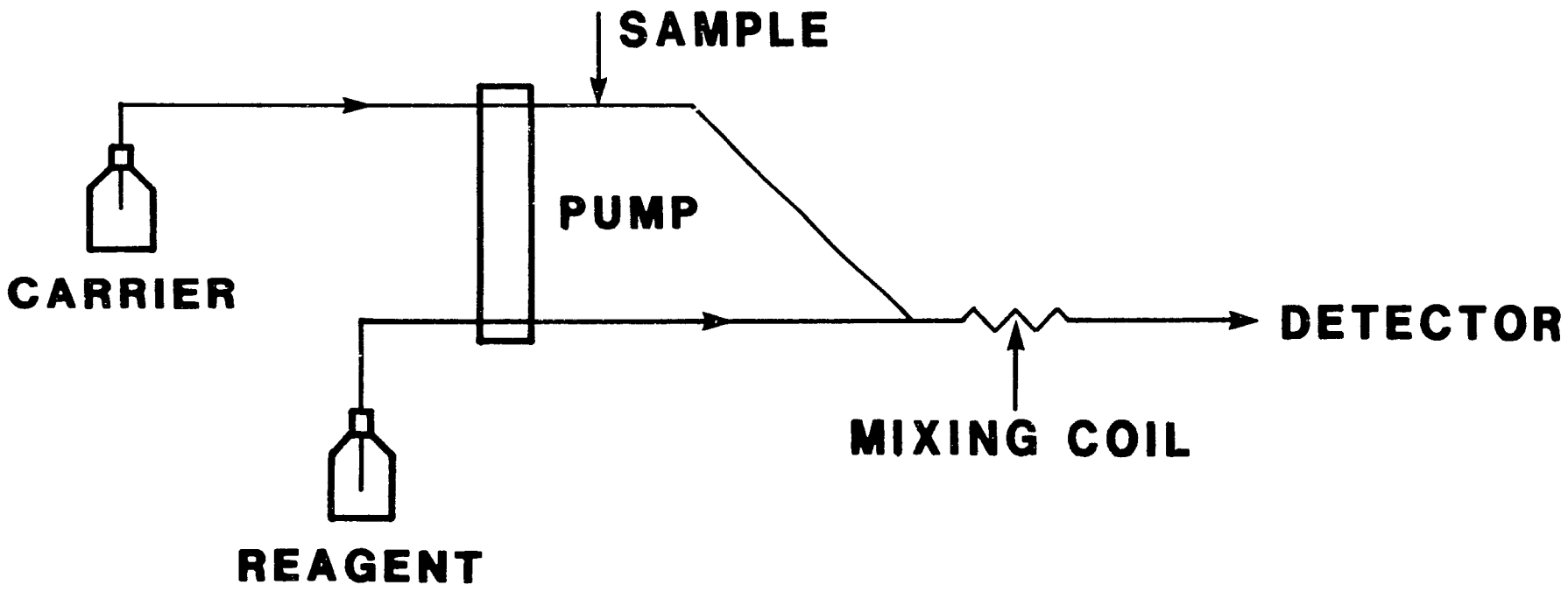
SAMPLE
PUMP
CARRIER
DETECTOR
MIXING COIL
REAGENT

worked out with the flow injection apparatus described above. Samples were aspirated from the exit line of the reactor after preset time intervals and mixed first with acid then potassium iodide in the chemifolds. The resulting iodine concentration was detected at a wavelength of 400 nm and converted to chlorine concentration from a predetermined calibration curve. This method was attractive in that the effluent samples were never exposed to air, but it was used sparingly in this work because of the long times that were needed to carefully and accurately prepare standards. A batch process was adopted whereby samples were collected in an acid-potassium iodide solution. This sampling technique was found to be very reliable. The resulting iodine solution was titrated against sodium thiosulphate solution of known strength.

3.4.4 Total organic carbon analysis

Total organic carbon (TOC) in the effluent arises from both reacted solubilized lignin and degraded carbohydrates. In the initial stages of chlorination the major fraction of this TOC is due to degraded lignin. Determination of the TOC concentrations was carried out with a Technicon AutoAnalyser System. A schematic of the system is shown in Figure 3.6. The basic components of the system are a peristaltic sampling pump, chemistry modules for reactant addition, spectrophotometer and a strip chart recorder. The method outlined by Trinh and Crotogino (7) was followed. Samples were analysed for both total carbon and inorganic carbon. Total carbon was analysed by mixing the sample with potassium persulphate and a phosphate buffer and exposing it to ultra-violet radiation. The carbon dioxide generated was dialyzed into a phenolphthalein indicator solution and the colour intensity decrease was detected by a

Figure 3.6 Technicon AutoAnalyzer system.

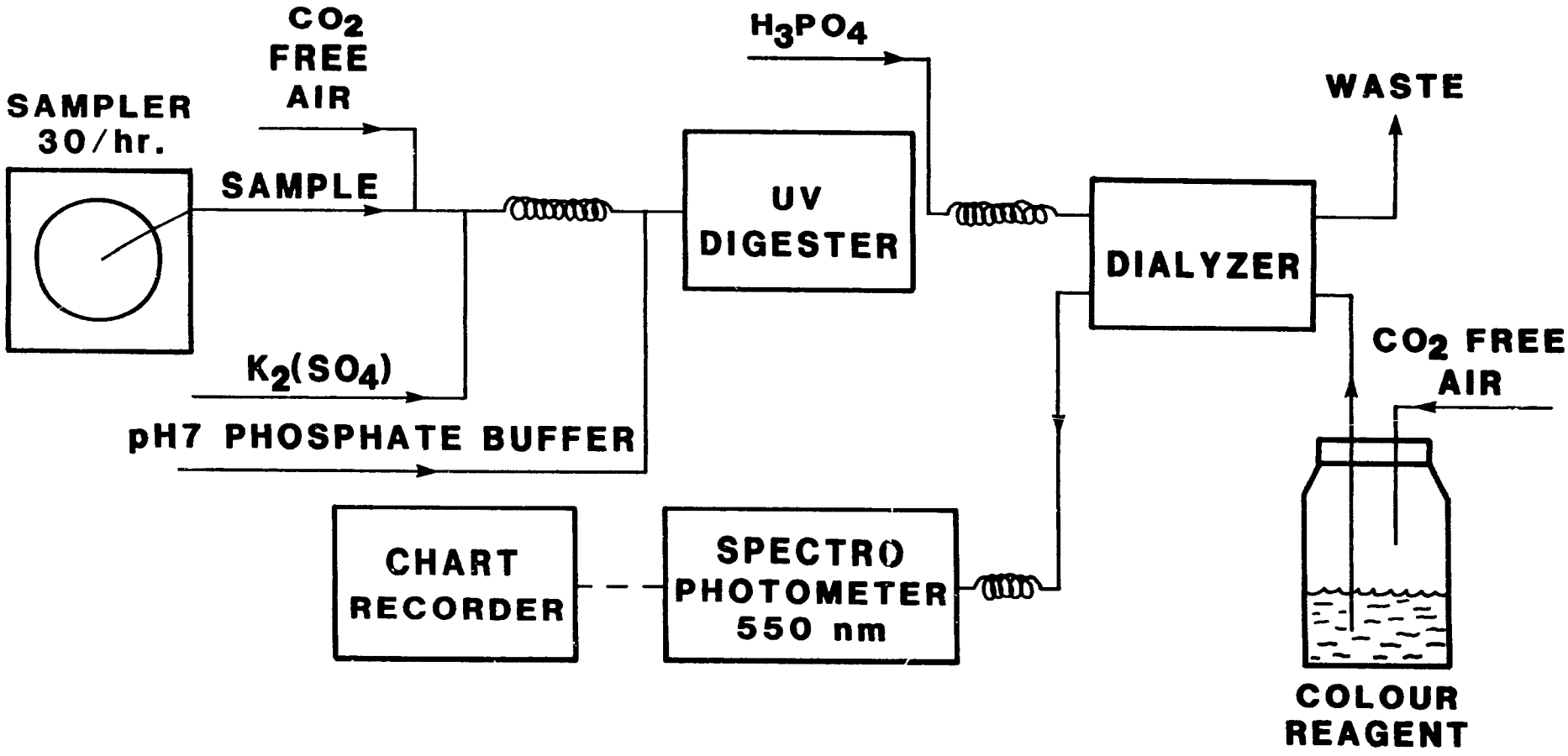
CO_2 FREE AIR
H_3PO_4
WASTE
SAMPLER 30/hr.
SAMPLE
UV DIGESTER
DIALYZER
CO_2 FREE AIR
$K_2(SO_4)$
pH7 PHOSPHATE BUFFER
CHART RECORDER
SPECTRO PHOTOMETER 550 nm
COLOUR REAGENT

spectrophotometer. Determination of inorganic carbon was carried out in the same way, however only phosphoric acid was added and the ultra-violet radiation was omitted. Only inorganic carbon in the sample is converted to carbon dioxide for analysis. The total organic carbon was found by difference.

3.4.5 Other analyses

3.4.5.1 Kappa number

Kappa number determinations were carried out according to TAPPI standard methods, test G 18. Micro kappa numbers were done as outlined by Berzins (8) and described in TAPPI useful methods 246.

3.4.5.2 U.V. and Klason lignin

These absolute lignin determinations were carried out as specified by TAPPI standard test G.9.

3.4.5.3 Pulp viscosity

Pulp viscosity determinations were carried out as specified by TAPPI G.24.

3.4.5.4 Chloride content

Known weights of oven dried pulp were wrapped in filter paper and combusted in a Schröniger combustion flask containing 10 ml of a 0.1 molar KOH solution to absorb combustion gases. The chloride content of the solution was analysed with the Flow Injection Analyser. Blanks done exactly as described above, but without pulp, allowed the chloride results to be suitably corrected.

3.4.5.5 Methanol

Methanol concentration in the effluent samples was determined with a Gas Chromatograph (model # HP 5890A) equipped with a packed column

(chromosorb # 102). The following operating conditions gave very good separation of the methanol peak:

sample volume = 0.4 ml

oven temperature = 140°C

detector temperature = 200°C

injection temperature = 150°C.

3.5 Safety precautions

Prolonged exposure to low concentrations (1 ppm) of chlorine causes nose, throat and eye irritations. Exposure to higher concentrations can be fatal. Extreme care was taken at all times in handling both chlorine gas and water.

References

1. Chapnerkar, V.D., Ph.D. Thesis, University of Florida (1961).
2. Russell, N.A., Ph.D. Thesis, IPC (1966).
3. Karter, E.M., Ph.D. Thesis, University of Main, Orono (1968).
4. Koch, D.D., Ph.D. Thesis, University of Idaho (1971).
5. Ackert, J.E., Ph.D. Thesis, University of Idaho (1973).
6. Mackinnon, J. M.Eng. Thesis, McGill University (1987).
7. Trinh, D.T., and Crotogino, R.H., The analysis of carbon in pulping liquors using an automataic colormetric method. PAPRICAN internal report, PPR512, January 1985.
8. Berzins, V., Micro Kappa numbers, Pulp & Paper Magazine of Canada, T206-T208, March 1966.

CHAPTER 4

RESIDENCE TIME DISTRIBUTION IN A PACKED BED OF PULP FIBERS

4.1 Introduction

Flow through a packed bed of pulp fibers is used in industrial applications such as pulp washing and displacement bleaching of pulp. In these processes the reactants and products are transported to and from the fibers by the relative motion between the continuous phase and the fibers. In any other mixing or contacting device used for pulp processing, including the recent medium consistency mixer, the relative motion between the fibers and continuous phase is small compared to the absolute velocity of the fibers and fluid phases. Since only the relative motion contributes to the transport to and from the fibers, flow through a fiber bed is the most efficient contacting process in terms of energy requirement. A fundamental study is required of the residence time distribution and inter- and intra-fiber mass transfer processes in fiber beds for better use and further development of such contacting devices or reactors. Most efficient use of wash water or chemicals, and minimum production of effluent volumes is achieved when the residence time distribution approaches plug flow. This provides the economic incentive to understand which physical phenomena are responsible for the dispersion of the continuous phase.

Relevant literature dealing with the residence time distribution for flow through pulp fiber beds are the pulp washing studies. However, in none of these studies by Lee (1,16), Grähs (2), Gren and Ström (3), and Poirier (4) was the flow residence time distribution measured separately. Since these investigators used a new pulp pad for each experiment when studying the effect of operating variables, the pulp pad structure and thus the residence time distribution, is an unknown parameter in their washing results. This might explain the opposing trends found by Gren and

Ström (3) and Grähs (2) for the effect of superficial velocity, while no effect was observed by Lee (1). Similarly, Lee (1) found a marked increase in washing efficiency with temperature, compared to no effect measured by Poirier (4). The excellent washing studies of Sherman (5) and Pellett (6) on non-porous Dacron fibers and porous viscose fibers do not suffer from this deficiency. They showed that axial dispersion gave a good description of the flow behavior for the two types of fiber beds. The inter- and intra-fiber mass transfer resistances in the porous fiber beds could be neglected for small diameter fibers (< 30 μm) and low molecular weight solutes. For larger diameter viscose fibers (> 60 μm) Pellett (6) used a solute to which viscose fibers were essentially impermeable. Sherman's data also confirm the importance of fiber bed formation since experiments on duplicate Dacron beds gave axial dispersion coefficients which differed by a factor 3. Pellett (6) and Sherman (5) also pointed out that the axial dispersion coefficient is up to 100 times larger than for beds of spherical particles of the same size as the fiber diameter. For the range of fiber length to diameter ratio of 50-400 their data show that the axial dispersion effect is determined not by the fiber diameter but by the fiber length.

Finally, although the residence time distribution in pulp beds is well represented by the axial dispersion model, as was recently shown by Poirier(4), Lee (16) reported that the actual flow is better described by "fingering" rather than by longitudinal dispersion. The residence time distributions in the present study were obtained by employing non-adsorbing sugars of different molecular size as tracers in step-up and step-down experiments.

The initial goal of the present study was to characterize the flow in a fiber bed before performing a dynamic chlorination experiment on the same pad (Chapter 6). However, on further analysis, the study was extended to resolve the contradiction between actual "fingering" flow and the use of the axial dispersed plug flow model for its description. Also, the fiber bed system was further analyzed to characterize the phenomena which are responsible for the high dispersion in fiber beds compared to more conventional beds. By using the same pulp pad as was done by Sherman (5) and Pellett (6) for viscose beds, the deficiency of a variable bed structure in the earlier pulp washing studies was eliminated. Finally, following the solute exclusion-technique developed by Stone and Scallan (7), it was possible with the use of different tracers to determine the pore structure of the wood pulp fibers under dynamic conditions.

4.2 Experimental and data reductions techniques

4.2.1 Experimental

The same reactor as employed for the dynamic pulp chlorination experiments (Chapter 6) was used in the present study. A schematic of the stainless steel reactor and auxillary equipment is shown in Figure 4.1. A detailed description of the equipment and pulp pad formation techniques is given in Chapter 3.

The residence time distribution of fluid flowing through the pulp pad was determined with the stimulus-response technique. Optically active tracers such as glucose and dextrans of varying molecular weights and hence varying molecular size were used. A step change in the input tracer concentration was generated by simultaneously opening and closing the

Figure 4.1: Schematic of experimental facility.

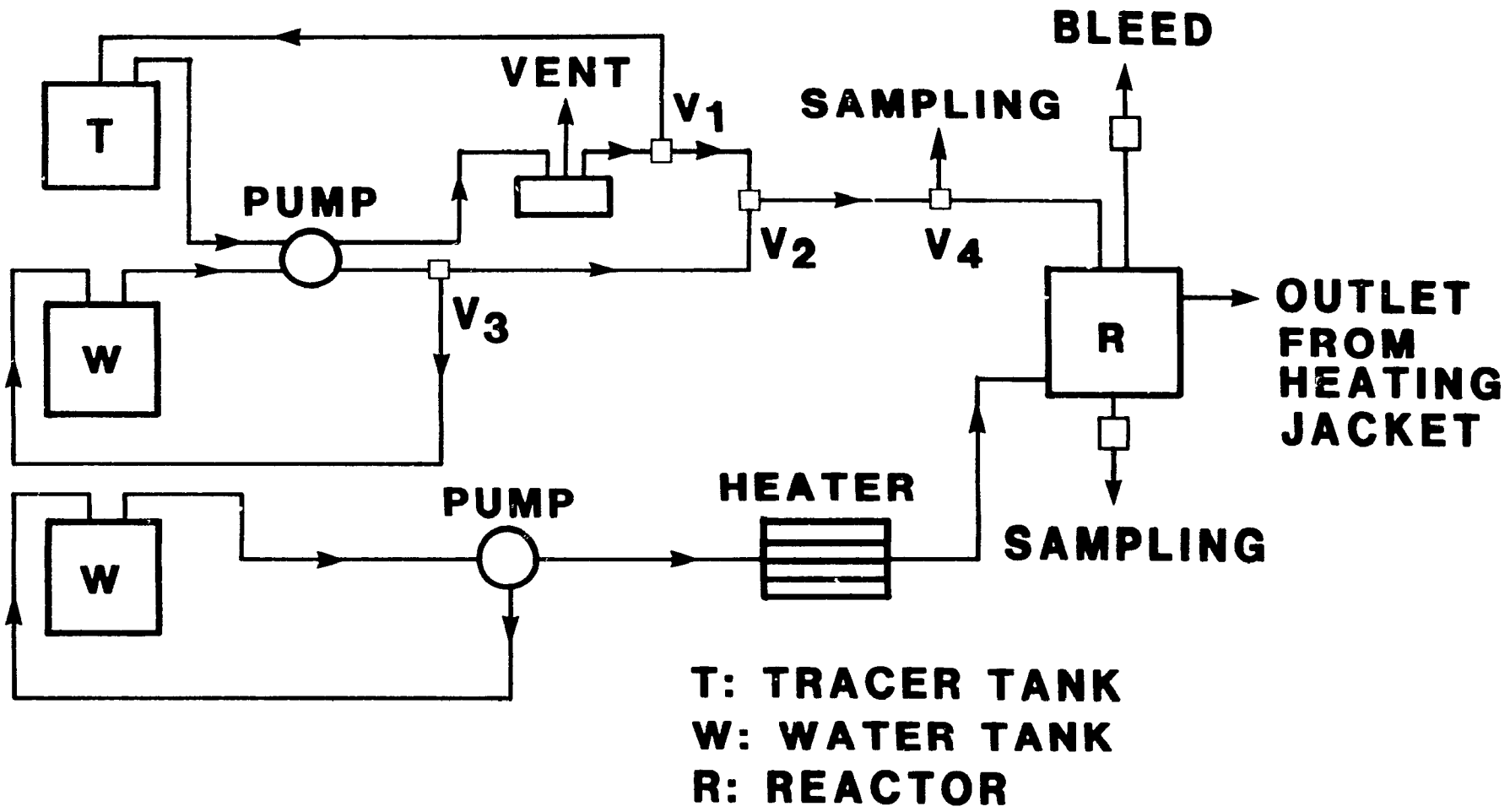
BLEED
VENT
V_1
SAMPLING
T
PUMP
V_2
V_4
V_3
W
R
OUTLET
FROM
HEATING
JACKET
PUMP
HEATER
W
SAMPLING
T: TRACER TANK
W: WATER TANK
R: REACTOR

solenoid valves in respectively the exit and bleed lines. As a result, the tracer solution flowing through the plunger was suddenly introduced at the top of the pulp pad. "Mixing cup" samples were collected at the exit of the reactor over regular time intervals. These samples along with several taken from the inlet were later analyzed with a polarimeter. The optical rotation is directly proportional to the weight concentration of the sugars in solution.

Never dried kraft Black Spruce pulp (kappa number 29.5) was used in all experiments. The pulp properties are given in Appendix 3-1. The range of experimental parameters investigated are summarized in Table 4.1.

4.2.2 Data reduction techniques

4.2.2.1 Experimental breakthrough curves

The effluent concentration, C, was normalized by the inlet concentration, C_o, and plotted as a function of sample time, t. Because of the "mixing cup" sampling technique, the sample time is taken to be the average time over the sampling interval. The sample time, t, is corrected by subtracting the "dead time", t_d, resulting from the 20 cm^3 volume, V_c, between the bottom of the pad and the sampling point. The time t_d is equal to V_c/Q_v where Q_v is the flow rate.

The flow rate Q_v is equal to $u_a \varepsilon_a A$, where u_a is the velocity based on the accessible liquid volume in the pad, A is the cross-sectional area of the pulp pad and ε_a represents the volume fraction of the bed accessible to the tracer. The value of ε_a is larger for glucose than dextran T-2000 because contrary to dextran T-2000 the smaller glucose molecule can

TABLE 4.1

Range of operating conditions

Parameter	level
Pad height, H	2, 4 and 6 cm
Sup. vel., u_o	0.020, 0.041 and 0.082 cm/s
Temperature, T	20, 35 and 48°C
Glucose conc.	10, 30 and 50 g/l
Dextran conc.	2 and 15 g/l
pH	2.61, 6.50 and 11.20

enter into the porous structure of the fiber wall. The larger accessible volume leads to later breakthrough for glucose. This can be seen from Figure 4.2 which shows typical breakthrough curves for glucose and dextran T-2000 for the same pulp pad and operating conditions. The corrected time, t_c, is non-dimensionalized by the mean residence time $\bar{t}_r = H/u_a$ as $T_c = t_c u_a/H$. Plots of dimensionless concentration, C/C_o, versus corrected dimensionless time, T_c, for the tracer curves of Figure 4.2 are presented in Figure 4.3. The mean residence time, $\bar{t}_r$, and thus also u_a and ε_a for each tracer experiment is obtained from the relationship:

$$\int_0^\infty (1 - C/C_o)\, dT_c = 1.0 \qquad [4.1]$$

ε_a for the glucose and dextran T-2000 breakthrough curves in Figure 4.3 are, respectively, 0.93 and 0.77.

4.2.2.2 Parameter estimation

As discussed in Chapter 2, various models have been proposed to characterize the flow in vessels. Levenspiel (9) states that one parameter models adequately represent flow in packed beds and tubular reactors. Poirier (4) has shown that the axial dispersed plug flow model gives a good description of the removal of solute during displacement washing of a pulp pad for high initial solute concentrations when desorption from the fiber wall can be neglected. Under these conditions the solute behaved like an inert tracer. Since the experimental system of Poirier (4) was essentially the same as the present, the axial dispersed plug flow model was adopted to represent the residence time distributions.

Figure 4.2: Typical glucose and dextran T-2000 breakthrough curves.

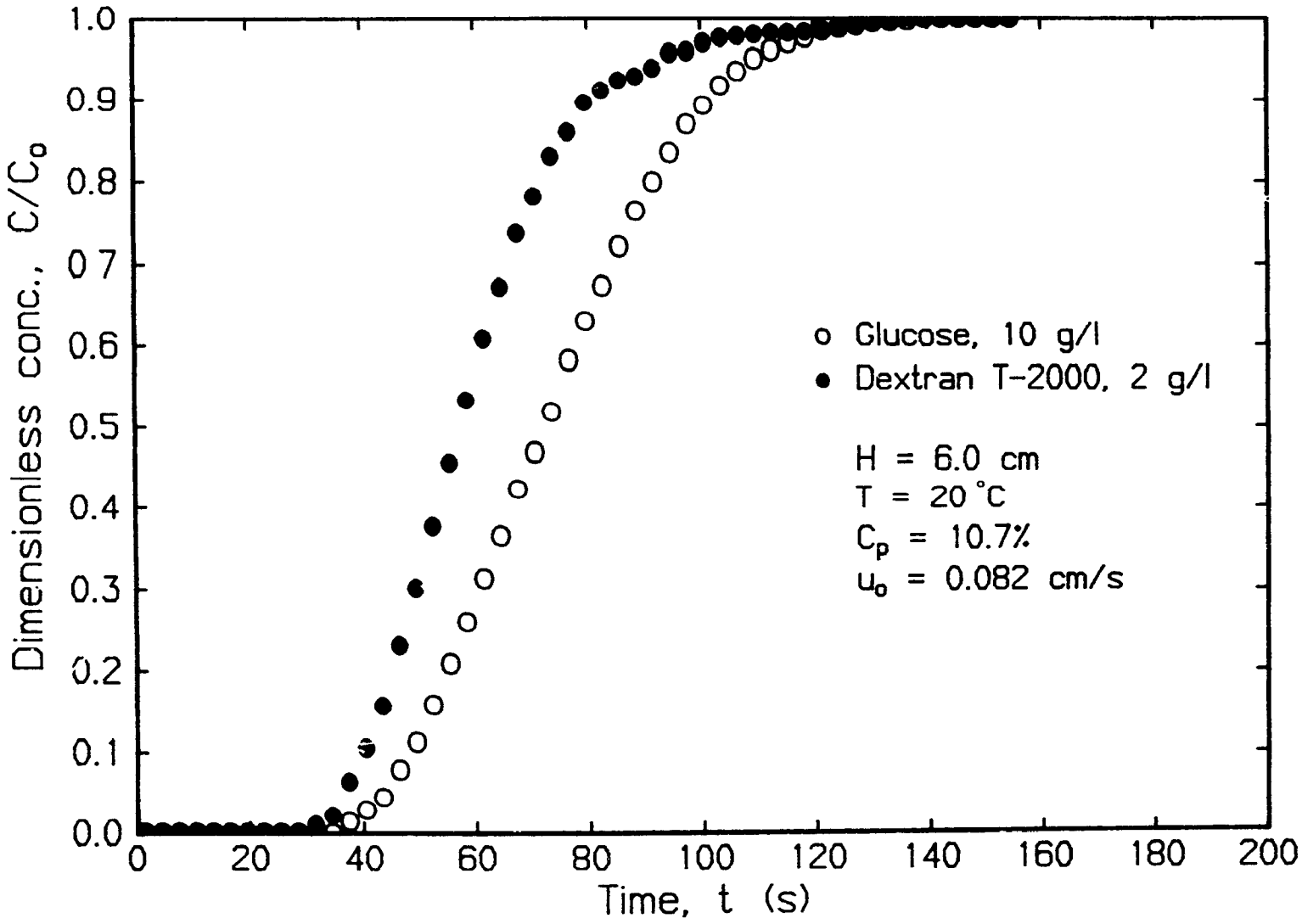
Dimensionless conc., C/C$_o$
1.0
0.9
0.8
0.7
0.6
0.5
0.4
0.3
0.2
0.1
0.0
0
20
40
60
80
100
120
140
160
180
200
Time, t (s)
o Glucose, 10 g/l
• Dextran T-2000, 2 g/l
H = 6.0 cm
T = 20 °C
C$_p$ = 10.7%
u$_o$ = 0.082 cm/s

Figure 4.3: Typical non-dimensional glucose and dextran T-2000 breakthrough curves.

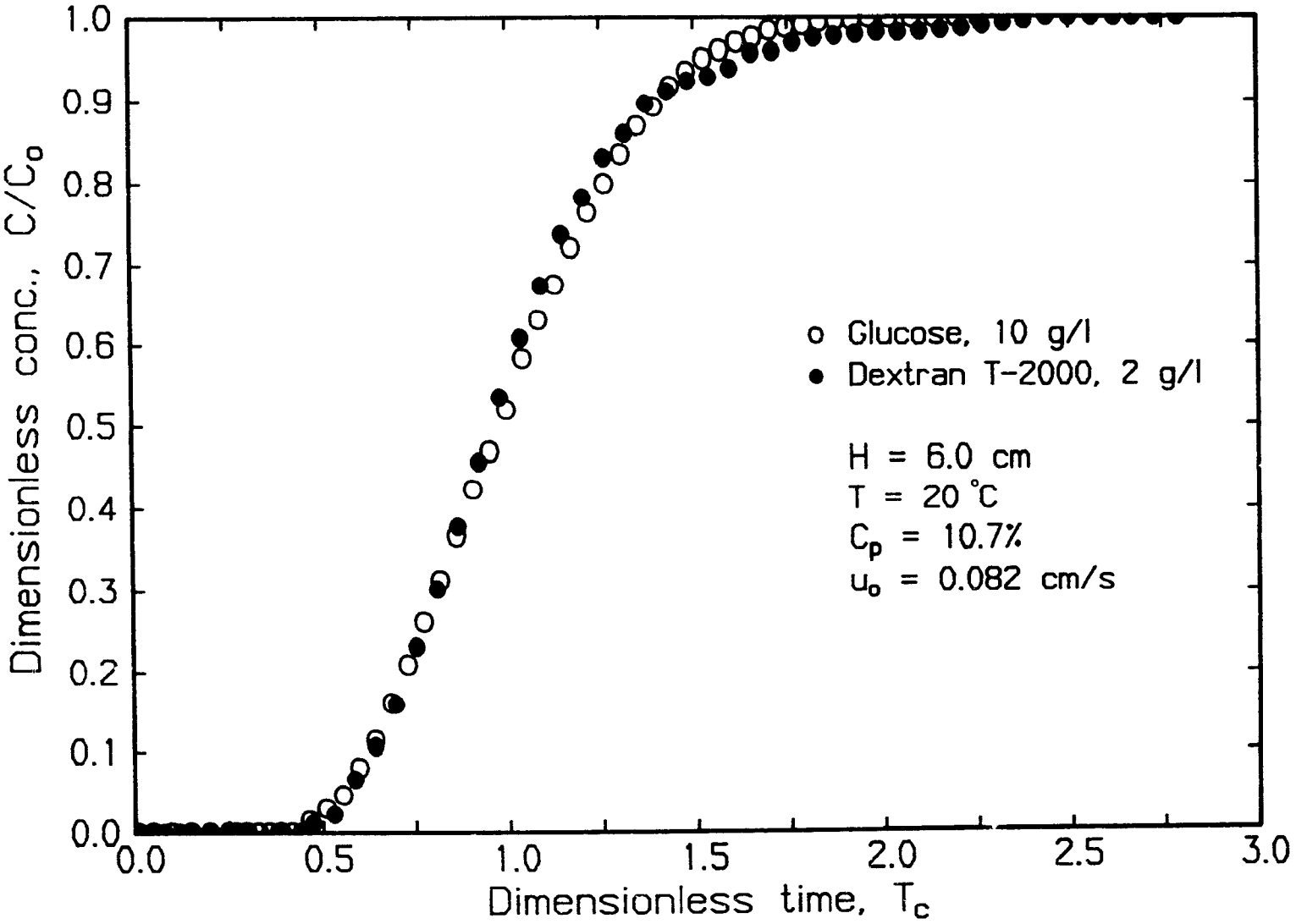
Dimensionless conc., C/C$_o$
Dimensionless time, T$_c$
o Glucose, 10 g/l
• Dextran T-2000, 2 g/l
H = 6.0 cm
T = 20 °C
C$_p$ = 10.7%
u$_o$ = 0.082 cm/s
0.0
0.1
0.2
0.3
0.4
0.5
0.6
0.7
0.8
0.9
1.0
0.0
0.5
1.0
1.5
2.0
2.5
3.0

Besides the standard assumptions associated with the axial dispersed plug flow model (9), the following conditions are added to account for the porous nature of the fibers:

- Flow inside the fibers can be neglected with respect to flow outside the fibers.

- The tracer concentrations in the fluid phase inside and outside the fibers are the same.

- The axial dispersion coefficient is based on the fluid external to the fibers.

The first two conditions, as well as the absence of adsorption of the tracer on the fiber wall, will be further analyzed later in this chapter. For this modified flow model a tracer mass balance over an incremental slice of the pulp pad gives (see Appendix 4-1)

$$\frac{\partial(C/C_o)}{\partial T} = \frac{1}{P}\frac{\partial^2(C/C_o)}{\partial X^2} - \frac{\partial(C/C_o)}{\partial X} \qquad [4.2]$$

The single parameter in this model is the Peclet number, $P = u_i H/D_L$, where u_i is the interstitial velocity based on the bed volume fraction external to the fibers. It should be noticed that T and P are based on different velocities, respectively u_a and u_i.

The initial and Danckwerts type boundary conditions (10) for a "step-up" change in inlet concentration are:

$$C/C_o = 0 \quad \text{for} \quad 0 < X < 1 \quad \text{at} \quad T = 0 \qquad [4.3]$$

$$C/C_o = 1 + \frac{1}{P}\frac{\partial(C/C_o)}{\partial X} \quad \text{at} \quad X = 0 \quad \text{for} \quad T > 0 \qquad [4.4]$$

and

$$\frac{\partial(C/C_o)}{\partial X} = 0 \text{ at } X = 1 \text{ for } T > 0 \qquad [4.5]$$

An asymptotic solution of the above equations can be obtained from Brenner (11). The expression for the exit concentration is

$$\begin{aligned} C/C_o = {} & [0.5 \text{ erfc}[(Pe/T)^{0.5}(1-T)]] + \\ & [(4\ PeT/\pi)^{0.5}[3+2Pe(1+T)]\ \exp[-Pe(1-T)^2/T]] \\ & - [[0.5 + 2Pe(3+4T) + 4Pe^2(1+T)^2] * \\ & \exp(4Pe)\ \text{erf}[(Pe/T)^{0.5}\ (1+T)]] \end{aligned} \qquad [4.6]$$

where Pe = P/4.

The Peclet number is obtained from the experimental breakthrough curve by means of the moment technique. The n^{th} moment is defined as

$$\mu_n = \int_o^\infty (1 - C/C_o)t^n dt \qquad [4.7]$$

The normalized first moment is related to the Peclet number of the axial dispersed plug flow model as:

$$\mu_1' = \frac{\mu_1}{(\mu_o)^2} = \frac{1}{2} + \frac{1}{P} - \frac{1}{P^2}\ (1 - e^{-P}) \qquad [4.8]$$

The zeroth moment, μ_o, is equal to the mean residence time, $\bar{t}_r$, by definition. A computer code to calculate the zeroth and first moments and subsequently the mean residence time, porosity ε_a and the Peclet number is given in Appendix 4-2.

The accuracy of the moment technique and the ability of the axial dispersion model to reproduce the residence time distribution was tested by comparing the breakthrough curves with equation [4.6]. Excellent agreement is obtained between the experimental glucose and calculated breakthrough curves as can be seen in Figure 4.4a. A similar comparison for dextran T-2000 tracer is shown in Figure 4.4b. The axial dispersion model does not represent the dextran T-2000 breakthrough curve as well. The extended tail of the dextran curve results in a too low calculated Peclet number. Proper representation of the dextran breakthrough curve by the axial dispersion model can be obtained by addition of a source term, as was done by Poirier (4), to account for the slow transport of dextran T-2000 from pulp fibres. This will be further discussed later in this chapter.

The glucose Peclet number derived by the moments technique can be used for accurate description of the residence time distribution in a pulp pad. The difference between the glucose and dextran T-2000 Peclet numbers gives an indication of the tailing which can be expected for large size molecules.

4.3 Reproducibility

The accuracy of the experimental techniques was tested by conducting duplicate tracer tests. Pulp pad formation effects are eliminated by using the same pulp pad. Duplicate glucose tracer tests are shown in Figure 4.5. The excellent agreement between the breakthrough curves is evident. The calculated Peclet numbers were 43.9 and 43 while the corresponding porosity ε_a was 0.934 in both cases. Duplicate dextran tracer tests are shown in Figure 4.6. Again, very good agreement between the

Figure 4.4a: Comparison of experimental and modelled glucose breakthrough curves.

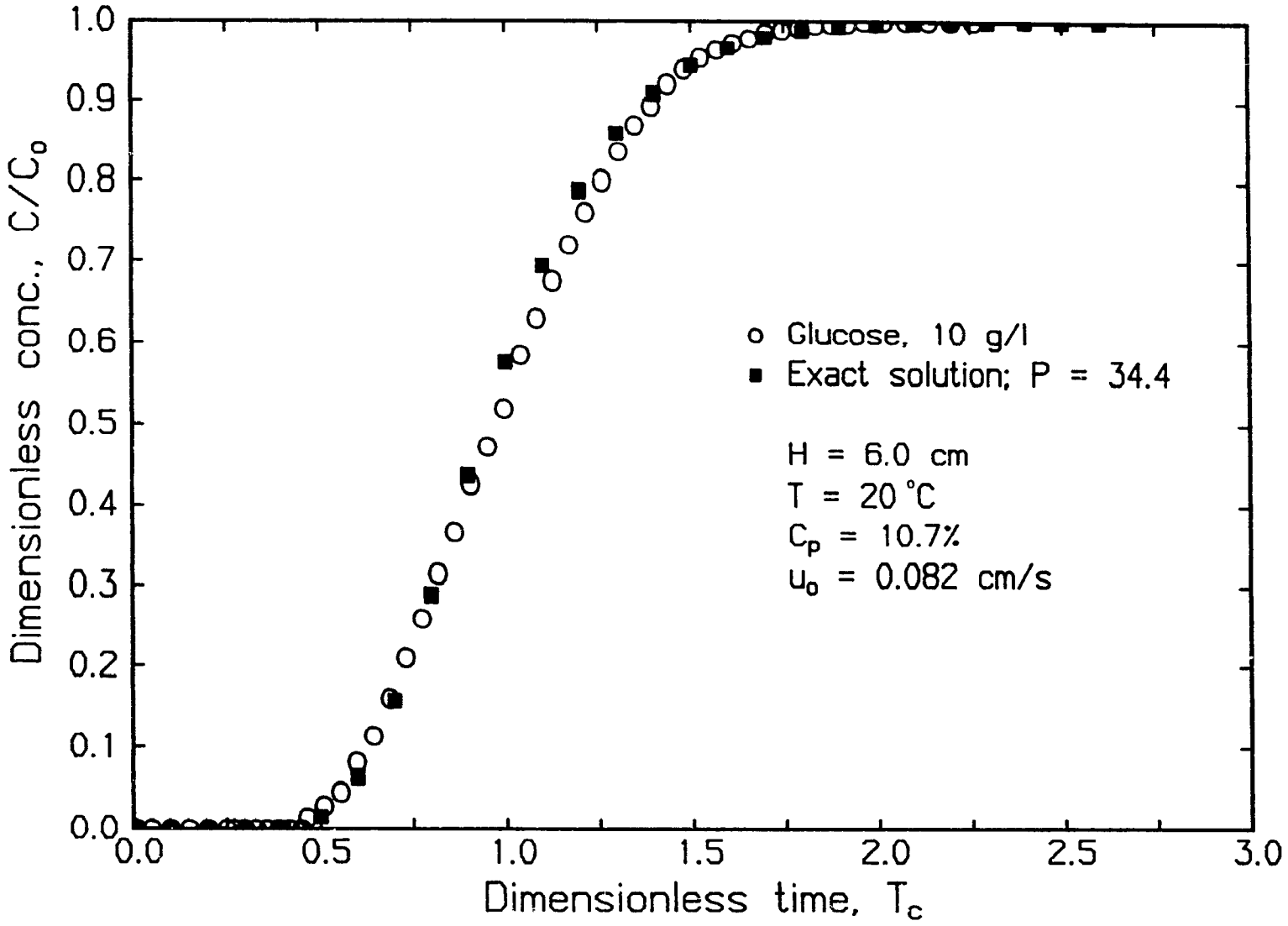
Dimensionless conc., C/C$_o$
1.0
0.9
0.8
0.7
0.6
0.5
0.4
0.3
0.2
0.1
0.0
0.0
0.5
1.0
1.5
2.0
2.5
3.0
Dimensionless time, T$_c$
o Glucose, 10 g/l
■ Exact solution; P = 34.4
H = 6.0 cm
T = 20 °C
C$_p$ = 10.7%
u$_o$ = 0.082 cm/s

Figure 4.4b: Comparison of experimental and modelled dextran T-2000 breakthrough curves.

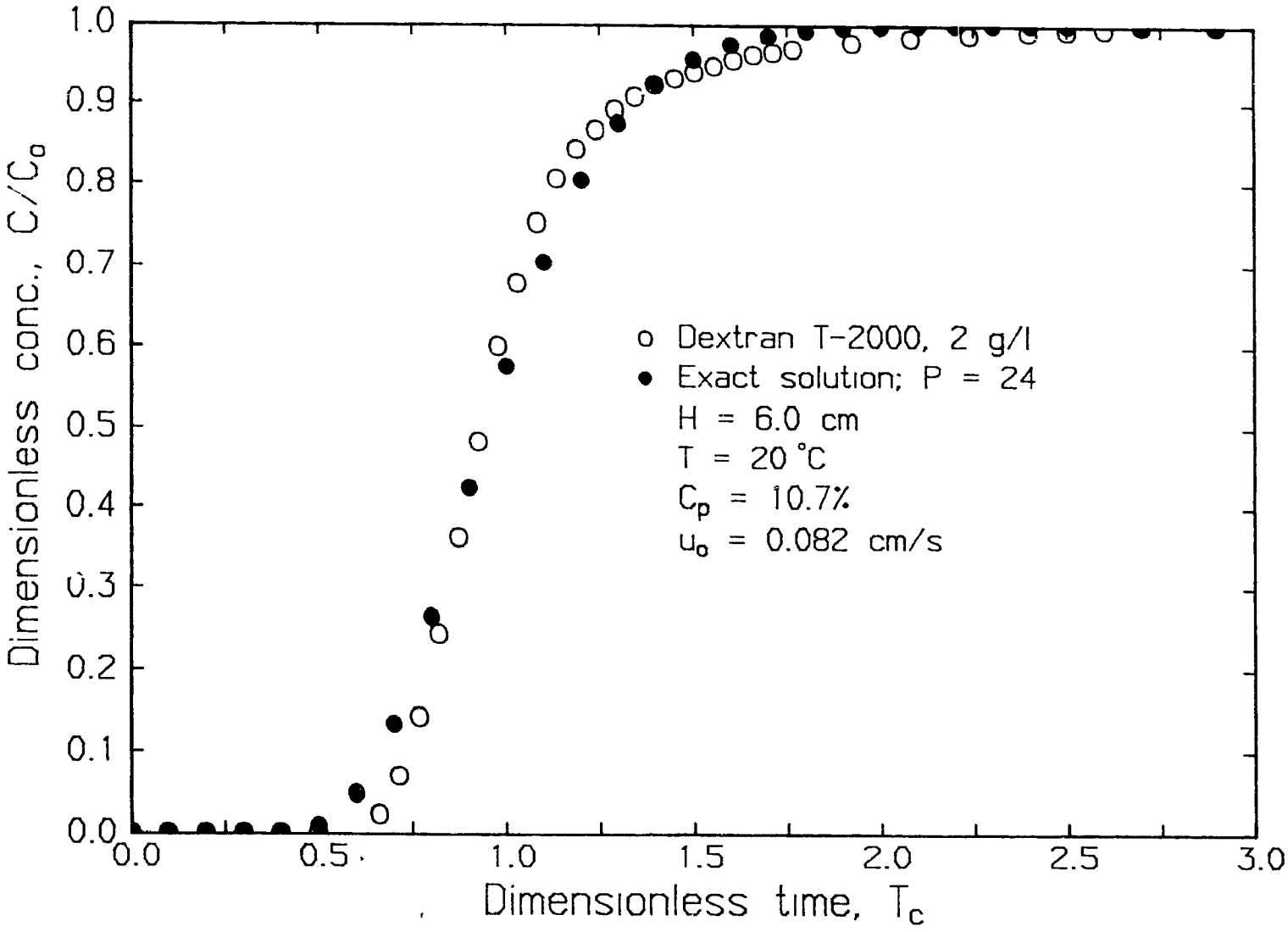
Dimensionless conc., C/C₀
Dimensionless time, T_c
1.0
0.9
0.8
0.7
0.6
0.5
0.4
0.3
0.2
0.1
0.0
0.0
0.5
1.0
1.5
2.0
2.5
3.0
o Dextran T-2000, 2 g/l
• Exact solution; P = 24
H = 6.0 cm
T = 20 °C
C_p = 10.7%
u_o = 0.082 cm/s

Figure 4.5 Duplicate glucose breakthrough curves.

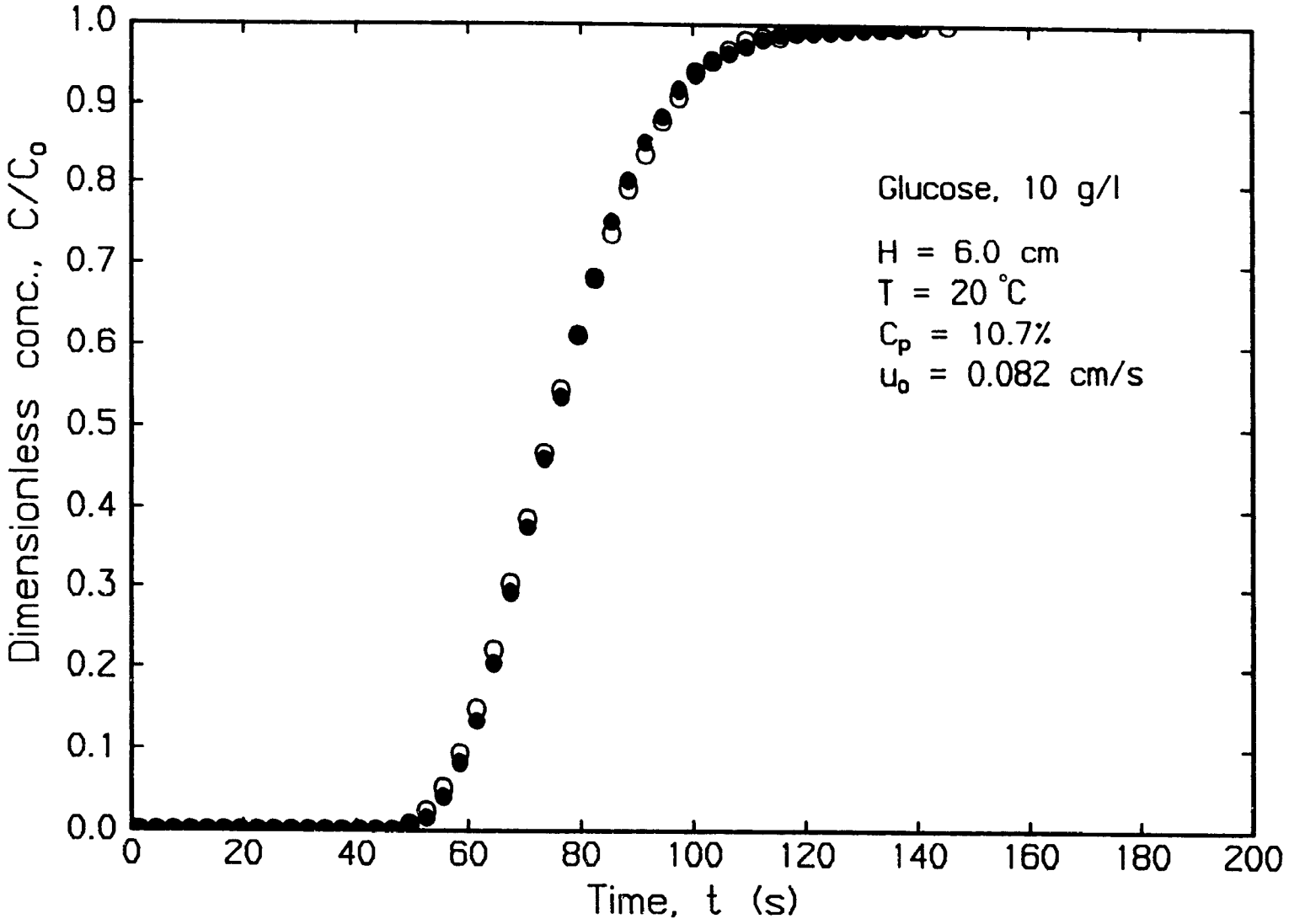
Dimensionless conc., C/C$_o$
1.0
0.9
0.8
0.7
0.6
0.5
0.4
0.3
0.2
0.1
0.0
0
20
40
60
80
100
120
140
160
180
200
Time, t (s)
Glucose, 10 g/l
H = 6.0 cm
T = 20 °C
C$_p$ = 10.7%
u$_o$ = 0.082 cm/s

Figure 4.6: Duplicate dextran T-2000 breakthrough curves.

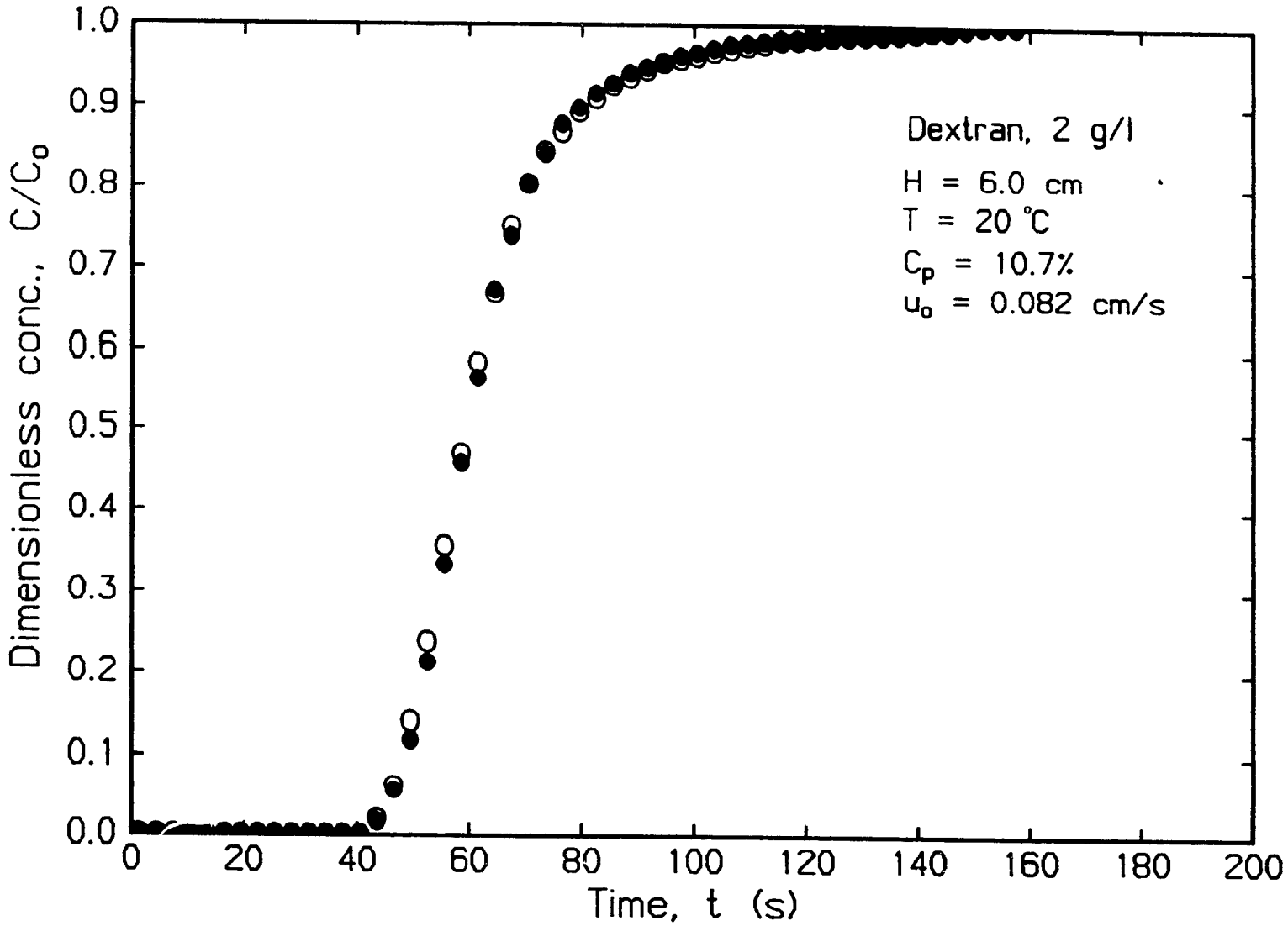
Dextran, 2 g/l
H = 6.0 cm
T = 20 °C
C_p = 10.7%
u_o = 0.082 cm/s
Dimensionless conc., C/C_o
Time, t (s)
0.0
0.1
0.2
0.3
0.4
0.5
0.6
0.7
0.8
0.9
1.0
0
20
40
60
80
100
120
140
160
180
200

runs is evident. The Peclet number in these cases were 30.7 and 32.3 and the corresponding porosities, ε_a, 0.767 and 0.769 respectively.

4.4 Tracer characterization

4.4.1 Introduction

As shown by Stone and Scallan (7) the pore structure of fibers in the wet state can be determined by the solute - exclusion technique. Non-ionic solutes such as glucose and dextrans of different molecular weights are used to establish the pore volume distribution in the fiber wall. The inaccessible pore volume increases with molecular size of the tracer. At very high molecular weights, the solute is completely excluded from the pore structure of the fibre wall and has access only to the central cavity of the fibre, the lumen. Shown in Figure 4.7 is the cumulative pore volume distribution obtained with this technique for an unbleached kraft pulp similar to that used in the present study. The figure, reproduced from Scallan (7), shows that a small molecule like glucose has access to essentially the complete water-filled pore structure of the fibre wall while a large molecule like dextran T-2000 is completely excluded. The large molecules enter the lumen via the pit openings which connect the lumen with the fluid external to the fibers. There are pit openings much larger than the molecular size of the largest sugars as can be inferred from the fact that TiO_2 particles of 200 nm in diameter can enter the lumen via the pits (13). The water inaccessible to the high molecular weight sugars is equivalent to the water contained by the fibers at the so-called fiber saturation point. All previous studies with these sugars, including the removal of water from fibers under compressive loading (8), were done under static conditions.

Figure 4.7: Cumulative pore volume, cm^3/g, versus molecular diameter; from Stone and Scallan (7).

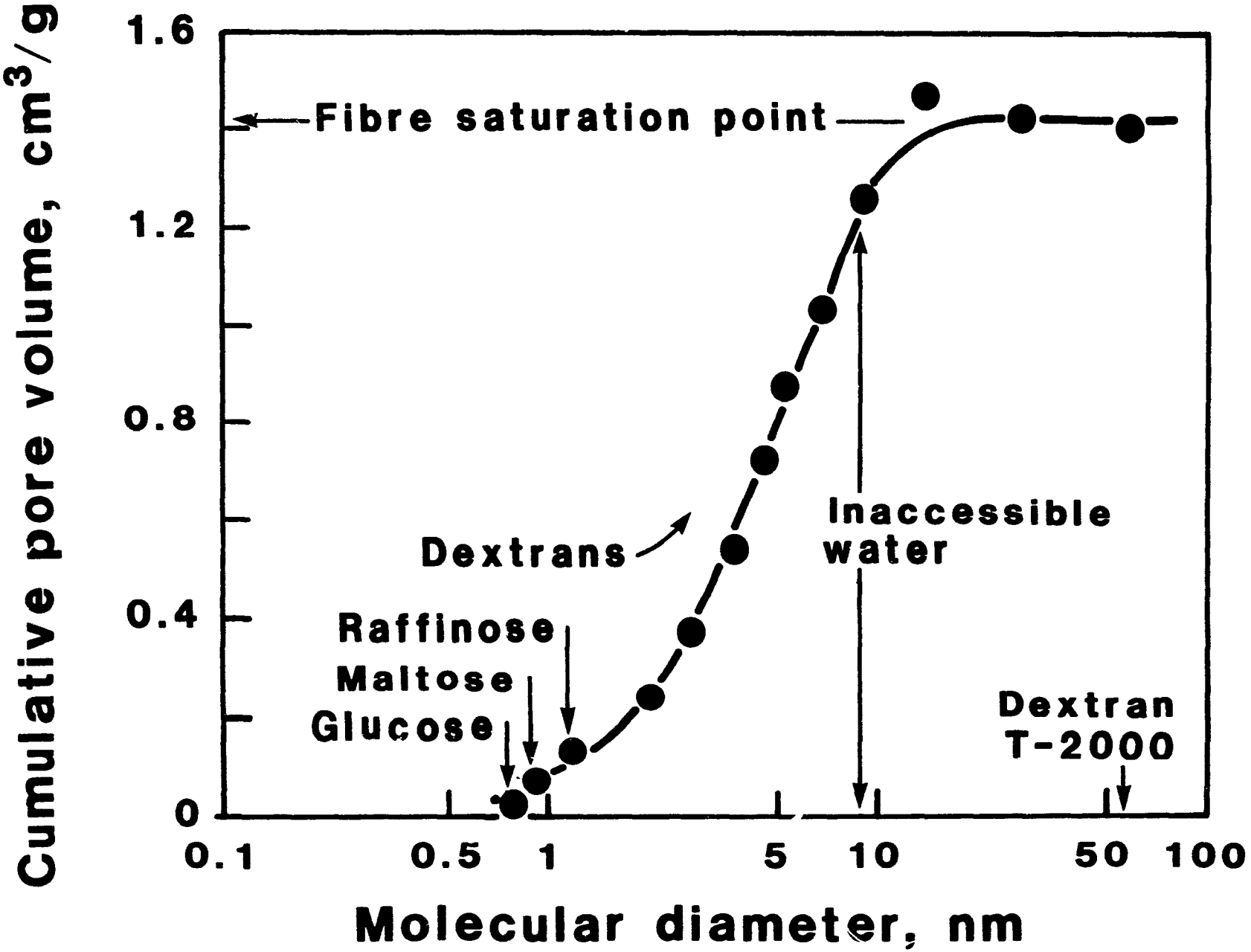
Cumulative pore volume, cm³/g
1.6
1.2
0.8
0.4
0
Fibre saturation point
Dextrans
Raffinose
Maltose
Glucose
Inaccessible water
Dextran T-2000
0.1
0.5
1
5
10
50
100
Molecular diameter, nm

In order to make a selection and establish the suitability of the sugars as inert tracers for dynamic RTD studies on a packed bed of pulp fibers, a series of characterization tests were performed. The variables were molecular size, concentration of the sugars and the pH of the tracer solution. All tracer characterization tests discussed in this section were conducted on the same pulp pad. This is important since it is impossible to form two pulp pads with the same packing structure and hence flow characteristics.

4.4.2 Molecular size of tracer

The tracers used to establish the influence of molecular size of the tracer on the residence time distribution curves are listed in Table 4.2. The molecular sizes of the sugars are obtained from Stone and Scallan (7) who calculated the hydrodynamic diameters from the diffusion coefficients and the Stokes-Einstein relationship. Grotte (15) has reviewed evidence to show that predominantly linear dextran molecules behave in solution as hydrodynamic spheres.

All runs were done at 20°C, a superficial velocity based on the empty reactor, u_o, of 0.082 cm/s, a bed height, H, of 6.1 cm and a consistency, C_p, of 10.7%. A plot of dimensionless exit concentration, C/C_o, versus uncorrected sampling time, t, is shown in Figure 4.8 for the five different tracers. It can readily be observed that with glucose, the smallest tracer molecule, a much larger mean residence time is obtained than with the dextrans. The mean residence times of dextran T-2000 and dextran T-500 are identical and slightly smaller than that of dextran T-40. Dextran T-10, the smallest of the dextran molecules studied, has a mean residence time that is larger than any of the dextrans studied but

TABLE 4.2

Molecular weights and diameters of sugar tracers.

Tracer	Molecular weight	Molecular diameter, A
glucose	180	8
dextran T-10	10,000	51
dextran T-40	40,000	90
dextran T-500	500,000	270
dextran T-2000	2 * 106	560

@ dextrans obtained from Pharmacia Inc.

@ range of molecular diameters within a dextran fraction is very small.

Figure 4.8: Influence of type of tracer on breakthrough curves.

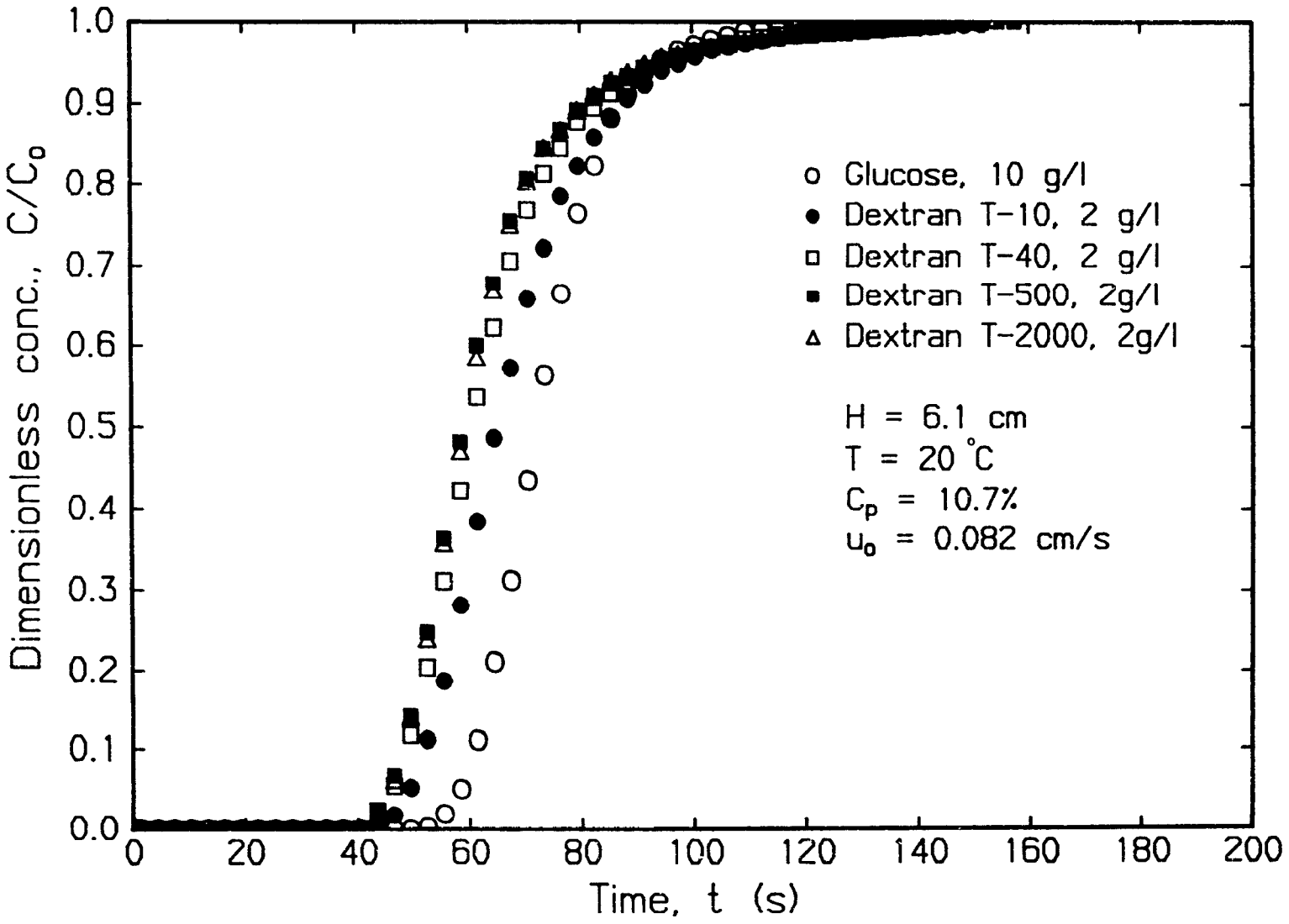
Dimensionless conc., C/C$_o$
1.0
0.9
0.8
0.7
0.6
0.5
0.4
0.3
0.2
0.1
0.0
0
20
40
60
80
100
120
140
160
180
200
Time, t (s)
o Glucose, 10 g/l
• Dextran T-10, 2 g/l
□ Dextran T-40, 2 g/l
■ Dextran T-500, 2g/l
△ Dextran T-2000, 2g/l
H = 6.1 cm
T = 20 °C
C$_p$ = 10.7%
u$_o$ = 0.082 cm/s

smaller than that of glucose.

The Peclet numbers and accessible porosities, ε_a, calculated from these RTD's are listed in Table 4.3. The total porosity, ε_t, represents the volume occupied by the lumen, the inter fiber regions and the fluid volume in the cell wall. It is obtained from the oven dried weight of pulp, 29.3 g, the pad volume, 44.05*6.1 cm^3, and the density of the non-porous fibre wall, (1.5 g/cm^3 (independent of wood species or degree of pulping (12)) as

$$\varepsilon_t = [44.05*6.1 - 29.3/1.50]/[44.05*6.1] = 0.927 \qquad [4.9]$$

The inaccessible water volume per gram of oven dried fibre wall is calculated as $(\varepsilon_t - \varepsilon_a)(44.05*6.1)/29.3$. Listed in Table 4.4 is the inaccessible volume calculated for the different tracers. Also reported are the inaccessible volumes determined with the static solute exclusion technique (12) measured on the same pulp. The good agreement between the two types of experiments shows that the dynamic characterization of the pulp pad is accurate and that very slow transients are absent.

The present data are compared with inaccessible volumes measured by Stone and Scallan (12) for unbleached kraft Black Spruce pulp of two different yields in Figure 4.9. The intermediate inaccessible volumes obtained in this work is in agreement with the corresponding intermediate yield of 48.9 % for the present pulp. The data also shows that the present pulp has a fibre saturation point of about 1.46 cm^3/g.

4.4.3 Concentration

The effect of tracer concentration on the breakthrough curves was

TABLE 4.3

Peclet number and porosities obtained with different tracers.

Tracer	Peclet No. P	porosity ε_a
glucose	82.9	0.933
dextran T-10	33.0	0.840
dextran T-40	34.8	0.784
dextran T-500	28.2	0.768
dextran T-2000	31.4	0.767

TABLE 4.4

Inaccessible volumes obtained with different tracers.

Comparison of static and dynamic tests.

Tracer	Inaccessible volume, cm^3/g pulp	
	Dynamic	Static
dextran T-10	0.82	0.84
dextran T-40	1.37	1.32
dextran T-500	1.46	1.47
dextran T-2000	1.46	1.45

Figure 4.9: Inaccessible volumes obtained with different tracers - comparison with Stone and Scallan (12).

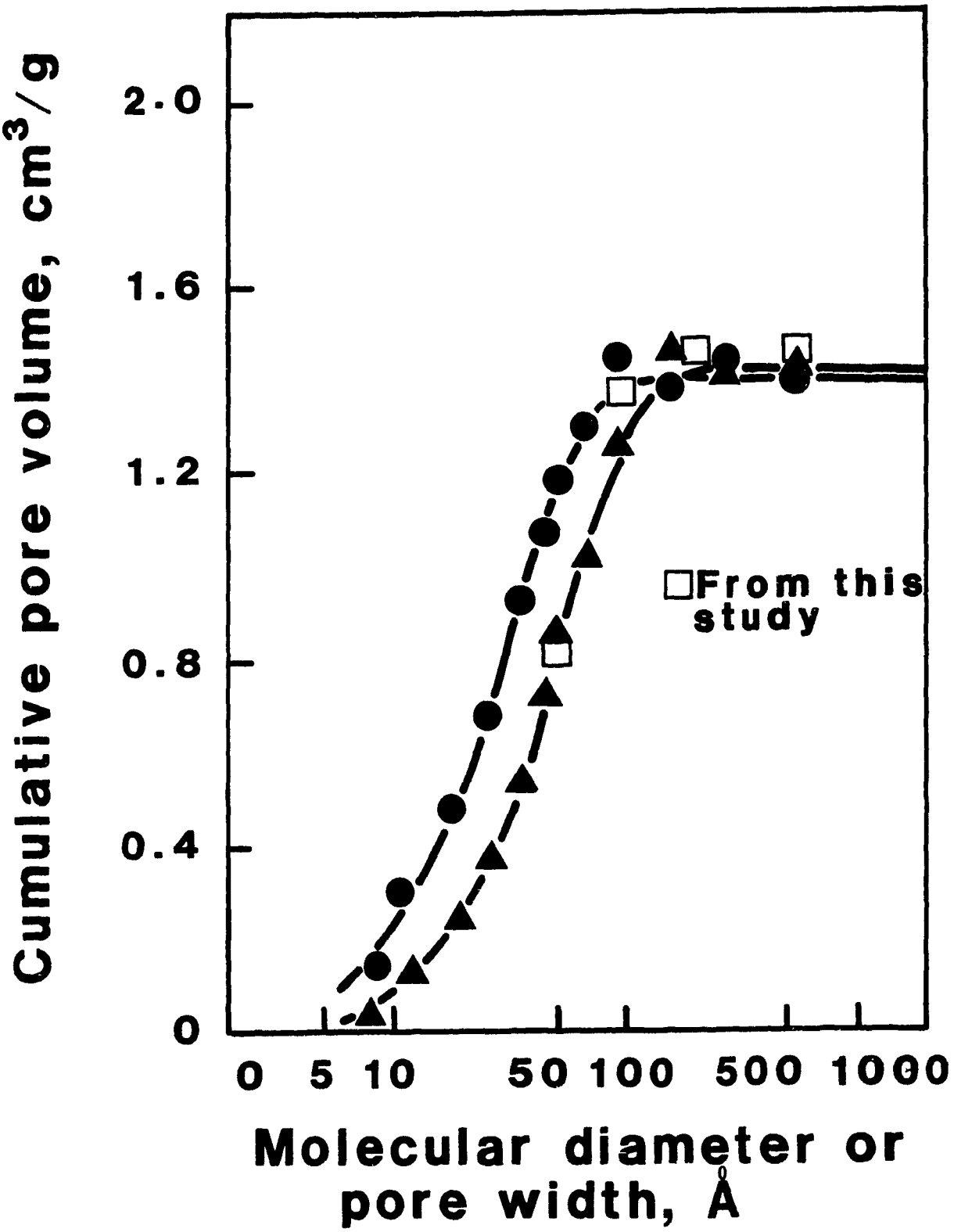
Cumulative pore volume, cm³/g
2.0
1.6
1.2
0.8
0.4
0
0 5 10 50 100 500 1000
Molecular diameter or pore width, Å
From this study

studied for glucose and dextran T-2000. One pulp pad was used for glucose and another for dextran T-2000. The glucose concentrations were 10, 30 and 50 g/l while the dextran T-2000 concentrations were a factor 5 lower. Identical breakthrough curves are obtained for glucose as can be seen in Figure 4.10a. The non-dimensional dextran T-2000 breakthrough curves shown in Figure 4.10b are almost identical. These results confirm that sugar adsorption on the pulp fibers can be neglected.

The remaining glucose and dextran tracer experiments were conducted at a concentration level of 10 g/l and 2 g/l respectively.

4.4.4 pH

Breakthrough curves were obtained under acid, neutral and alkaline conditions. The plots of C/C_o versus t for a pH of 2.61, 6.50 and 11.20 are shown in Figure 4.11. The breakthrough curves at pH 6.50 and 2.61 are identical. The importance of this result is that the tracer tests performed under neutral conditions can be used to characterize the flow in subsequent pulp chlorination experiments done at a pH of about 2.1 (Chapters 6 and 7). The upper region of the breakthrough curve at alkaline conditions is different from those at the two lower pH levels. The values at C/C_o greater than unity are thought to be caused by degradation and/or dissolution of carbohydrates in the fibers since fiber fragments were visually evident in the effluent samples. All further tracer tests were conducted under neutral conditions.

4.5 Influence of pad formation and operating conditions

4.5.1 Pad formation

The extreme difficulty in forming pulp pads of identical packing characteristics is apparent when Peclet numbers for different pulp pads

Figure 4.10a: Effect of glucose concentration on breakthrough curves.

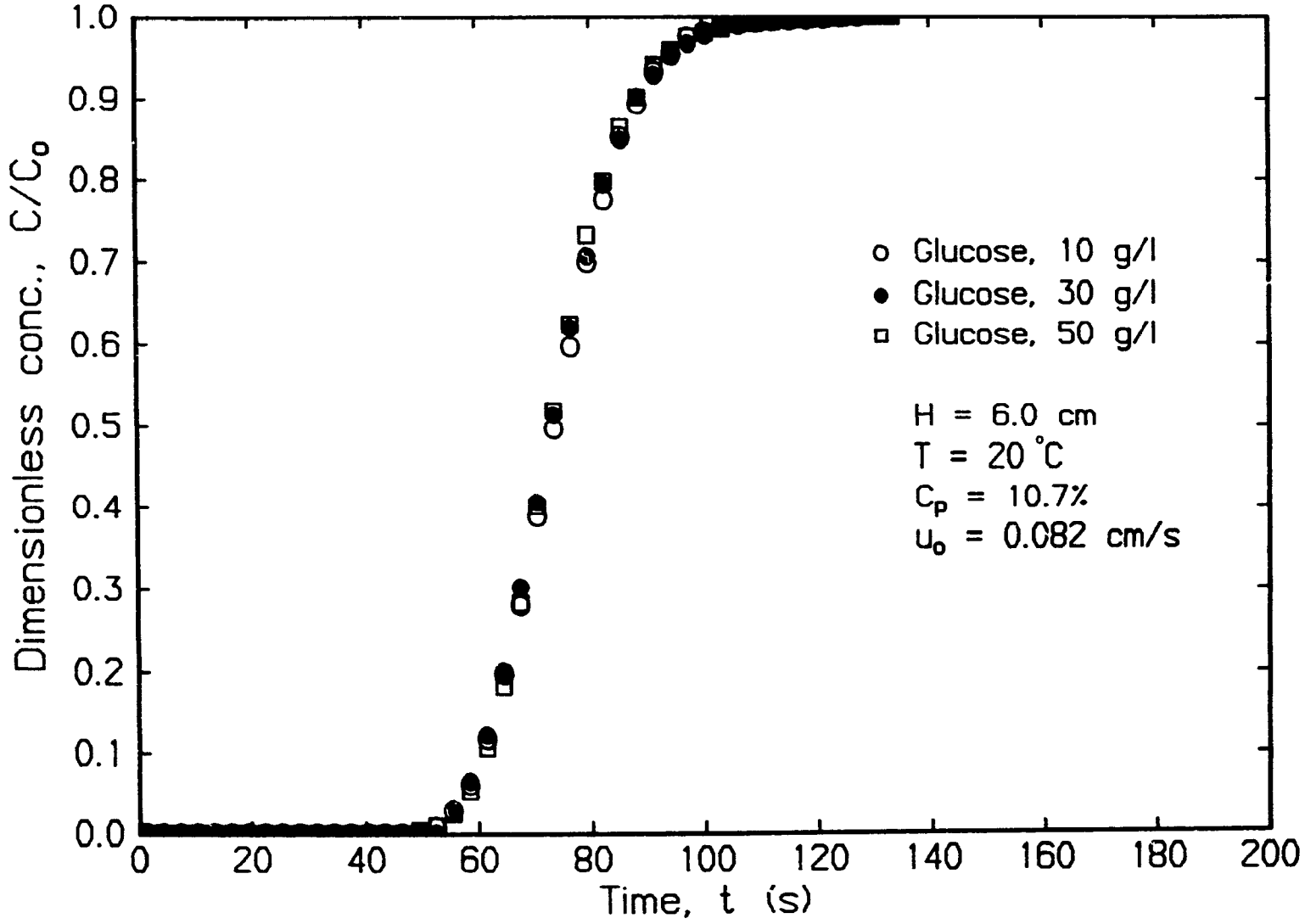
Dimensionless conc., C/C$_o$
1.0
0.9
0.8
0.7
0.6
0.5
0.4
0.3
0.2
0.1
0.0
0
20
40
60
80
100
120
140
160
180
200
Time, t (s)
o Glucose, 10 g/l
● Glucose, 30 g/l
□ Glucose, 50 g/l
H = 6.0 cm
T = 20 °C
C$_p$ = 10.7%
u$_o$ = 0.082 cm/s

Figure 4.10b: Effect of dextran T-2000 concentration on breakthrough curves.

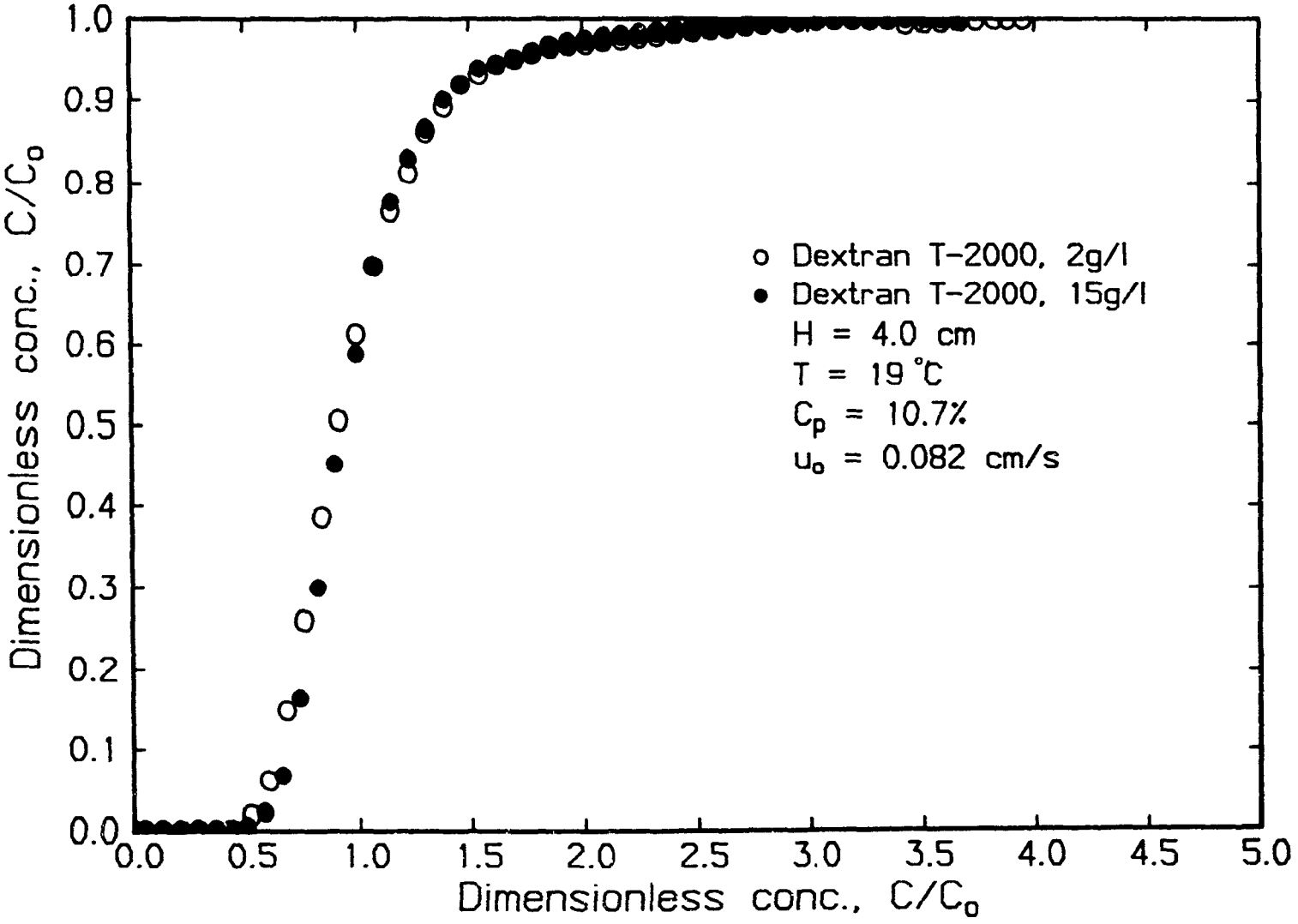
Dimensionless conc., C/C$_o$
Dimensionless conc., C/C$_o$
o Dextran T-2000, 2g/l
• Dextran T-2000, 15g/l
H = 4.0 cm
T = 19 °C
C$_p$ = 10.7%
u$_o$ = 0.082 cm/s
0.0
0.1
0.2
0.3
0.4
0.5
0.6
0.7
0.8
0.9
1.0
0.0
0.5
1.0
1.5
2.0
2.5
3.0
3.5
4.0
4.5
5.0

Figure 4.11: Effect of pH on glucose breakthrough curves.

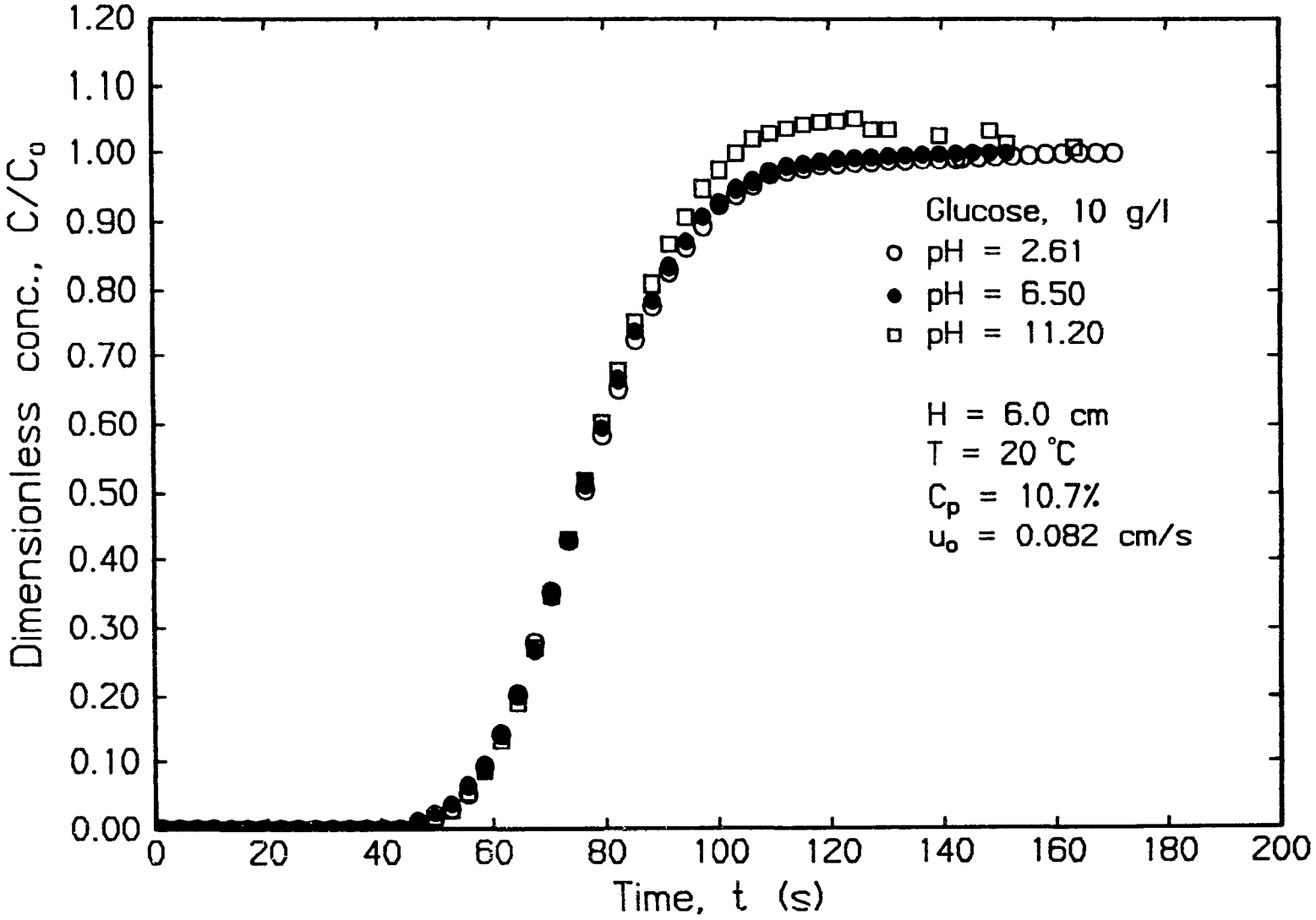
Dimensionless conc., C/C$_o$
1.20
1.10
1.00
0.90
0.80
0.70
0.60
0.50
0.40
0.30
0.20
0.10
0.00
0
20
40
60
80
100
120
140
160
180
200
Time, t (s)
Glucose, 10 g/l
o pH = 2.61
● pH = 6.50
□ pH = 11.20
H = 6.0 cm
T = 20 °C
C$_p$ = 10.7%
u$_o$ = 0.082 cm/s

but identical operating conditions are compared.

Shown in Figures 4.12 and 4.13 are the various Peclet numbers obtained for glucose and dextran T-2000 respectively as a function of superficial velocity. The scatter in the Peclet numbers obtained from the glucose and dextran T-2000 tracer tests emphasize the need to use the same pulp pad when studying the influence of any operating variable. The relatively high Peclet numbers in Figures 4.12 and 4.13 are indicative of the good pad formation technique employed.

4.5.2 Superficial velocity

The effect of superficial velocity was studied on the same pulp pad. The close match between the dimensionless breakthrough curves for glucose in Figure 4.14 shows that the Peclet number is independent of the superficial velocity or that the axial dispersion coefficient is proportional to the interstitial velocity. Similar results are shown in Figure 4.15 for dextran T-2000. These results are in agreement with those of Sherman (5) and Pellett (6) who also found that the axial dispersion coefficient was proportional to the interstitial velocity for a bed of porous viscose fibers. However for displacement washing of a packed bed of wood pulp fibers Lee (1), Grahs (2) and Gren and Strom (3) found no or a small influence of superficial velocity on the displacement efficiency of the solute in the pulp pad. Poirier (2) found that the Peclet number increased with increasing velocity at low consistencies (3%) and that the reverse trend occurred at high consistencies (15%). As noted earlier, a different pulp pad was used for each experiment in the pulp washing studies.

These results therefore confirm that pulp pad formation is an

Figure 4.12: Effect of pad formation on glucose breakthrough curves.

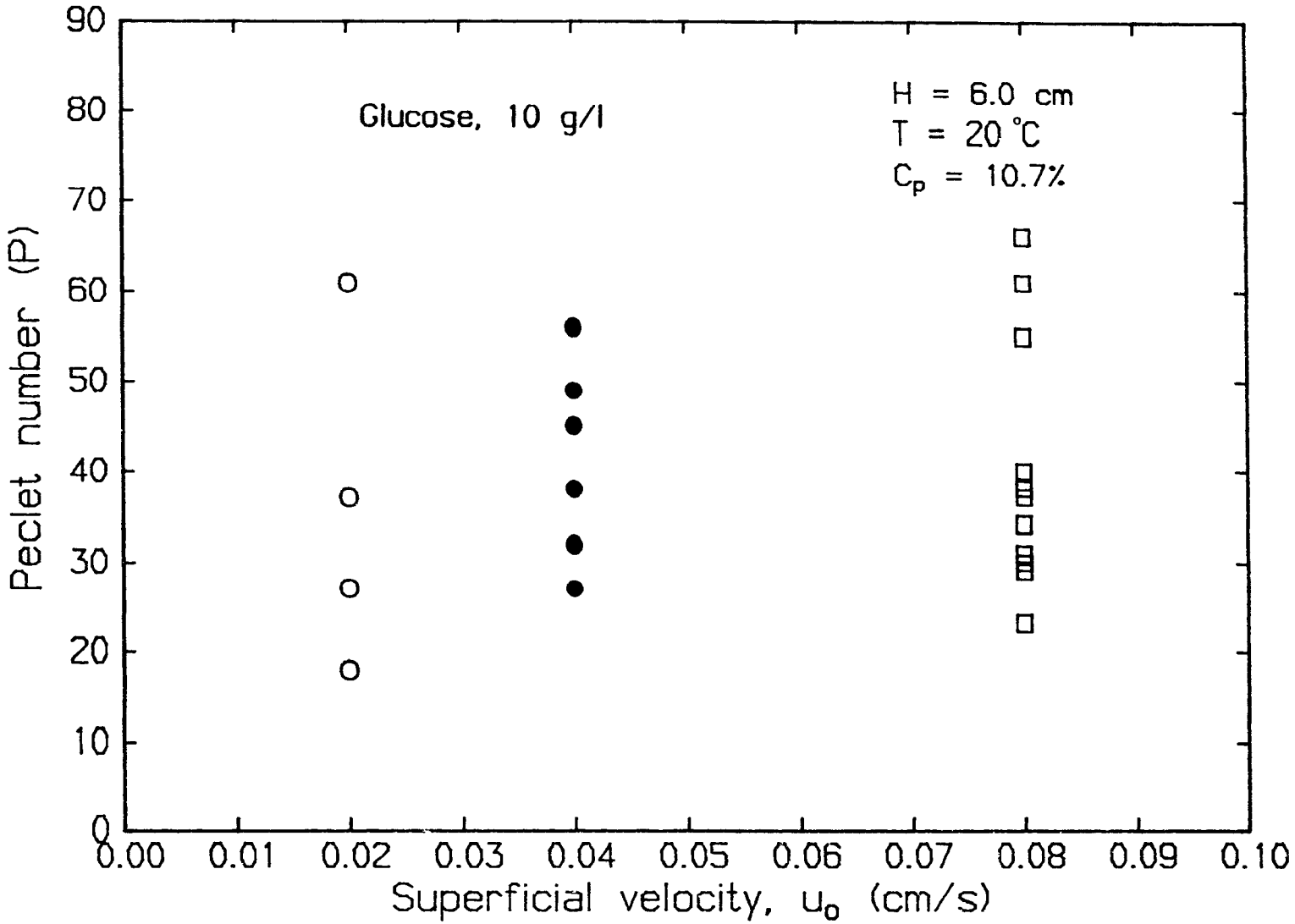
Glucose, 10 g/l
H = 6.0 cm
T = 20 °C
C_p = 10.7%
Peclet number (P)
Superficial velocity, u_o (cm/s)
0
10
20
30
40
50
60
70
80
90
0.00
0.01
0.02
0.03
0.04
0.05
0.06
0.07
0.08
0.09
0.10

Figure 4.13: Effect of pad formation on dextran T-2000 breakthrough curves.

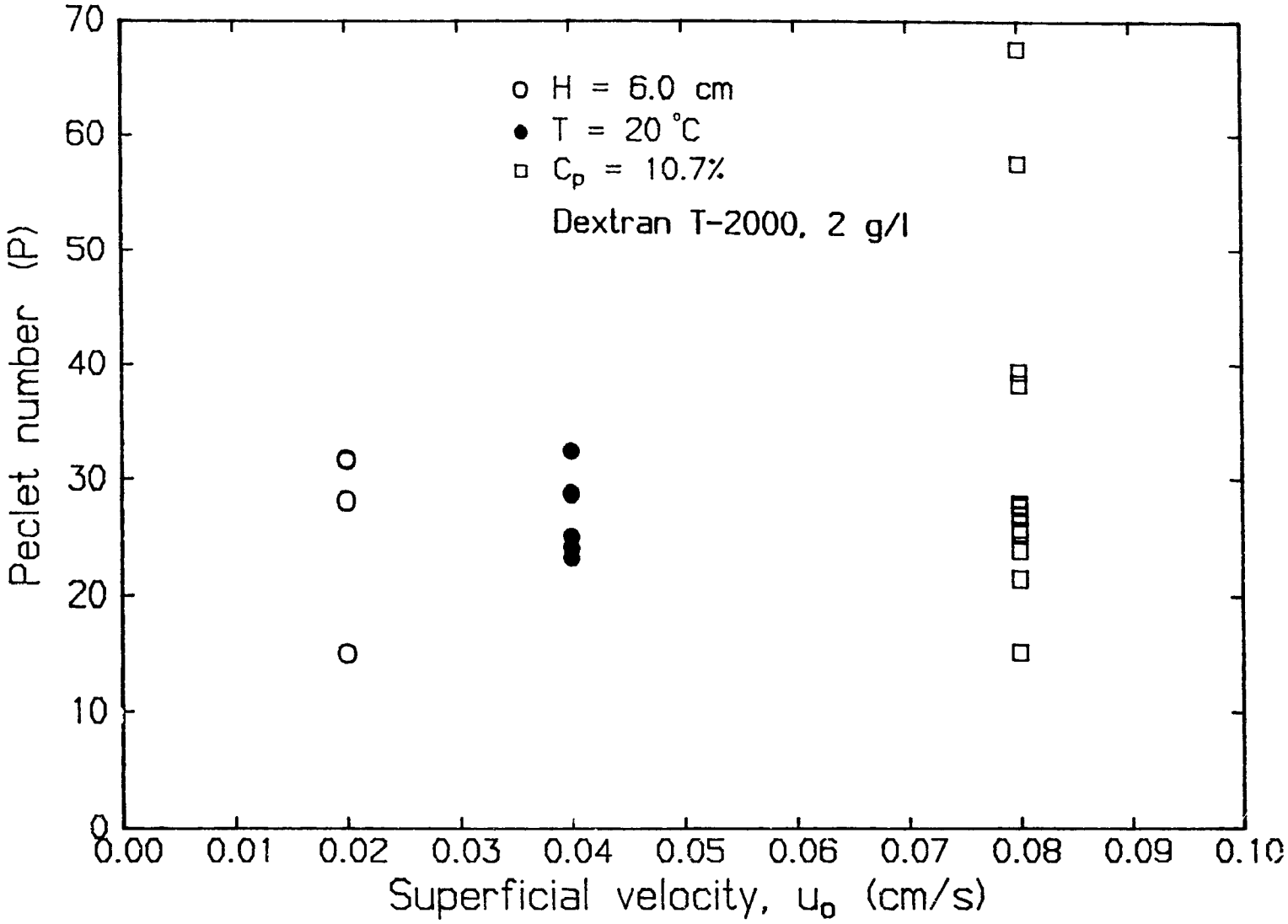
o H = 6.0 cm
• T = 20 °C
□ C_p = 10.7%
Dextran T-2000, 2 g/l
Peclet number (P)
Superficial velocity, u_o (cm/s)
0
10
20
30
40
50
60
70
0.00
0.01
0.02
0.03
0.04
0.05
0.06
0.07
0.08
0.09
0.10

Figure 4.14: Effect of superficial velocity on glucose breakthrough curves.

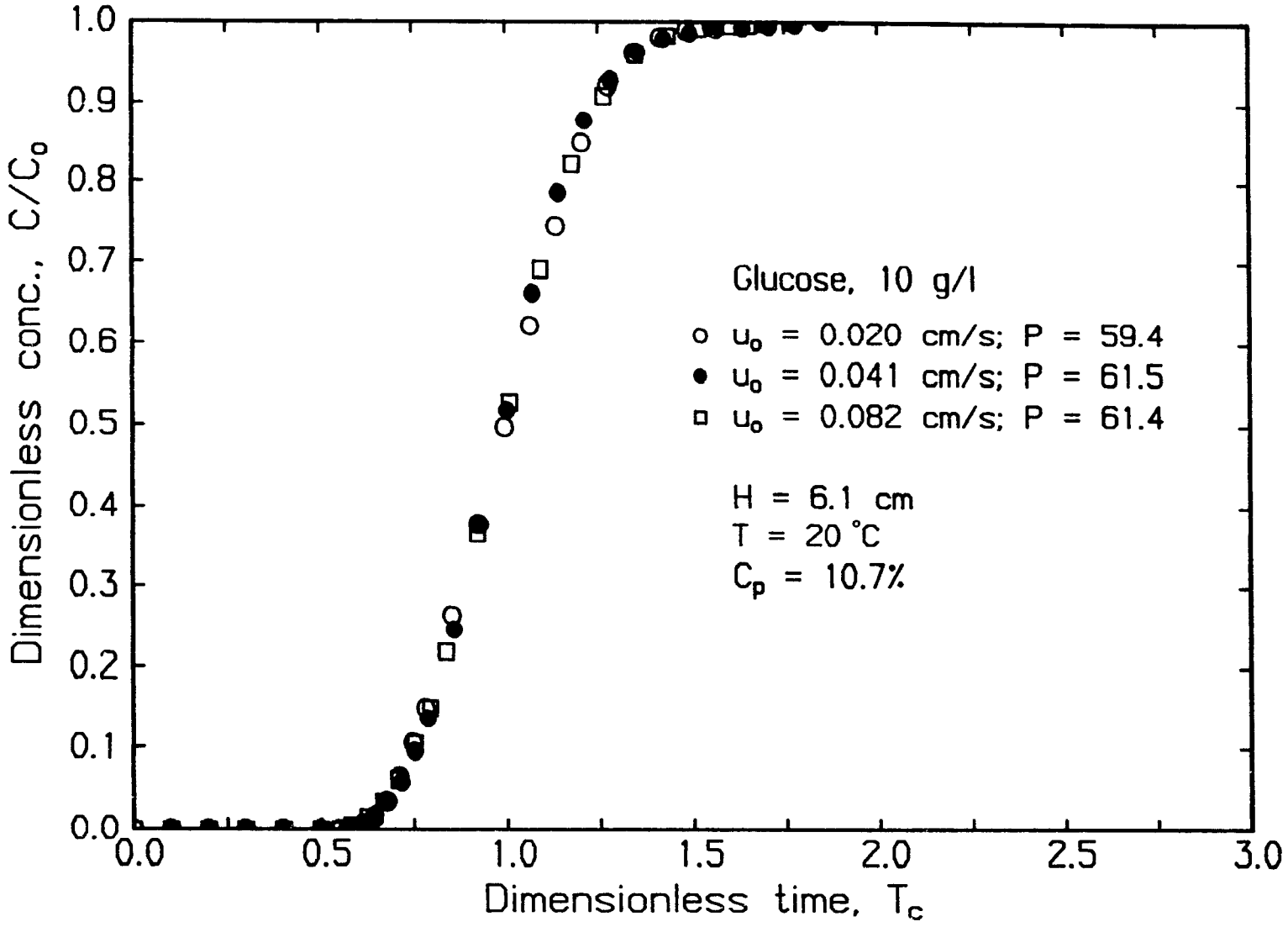
Dimensionless conc., C/C$_o$
Dimensionless time, T$_c$
Glucose, 10 g/l
u$_o$ = 0.020 cm/s; P = 59.4
u$_o$ = 0.041 cm/s; P = 61.5
u$_o$ = 0.082 cm/s; P = 61.4
H = 6.1 cm
T = 20 °C
C$_p$ = 10.7%
0.0
0.1
0.2
0.3
0.4
0.5
0.6
0.7
0.8
0.9
1.0
0.0
0.5
1.0
1.5
2.0
2.5
3.0

Figure 4.15: Effect of superficial velocity on dextran T-2000 breakthrough curves.

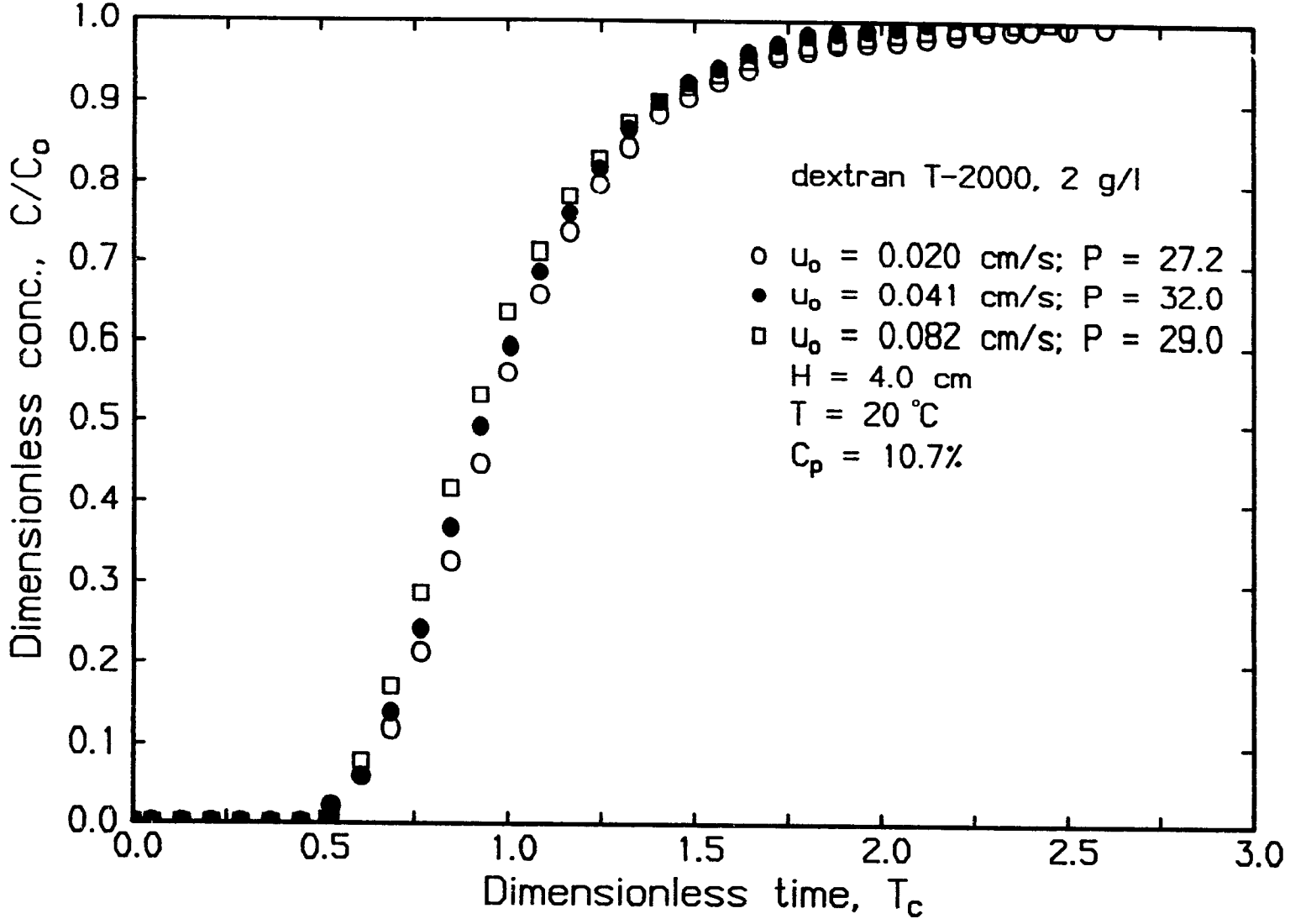
Dimensionless conc., C/C$_o$
Dimensionless time, T$_c$
dextran T-2000, 2 g/l
o u$_o$ = 0.020 cm/s; P = 27.2
• u$_o$ = 0.041 cm/s; P = 32.0
□ u$_o$ = 0.082 cm/s; P = 29.0
H = 4.0 cm
T = 20 °C
C$_p$ = 10.7%
0.0
0.1
0.2
0.3
0.4
0.5
0.6
0.7
0.8
0.9
1.0
0.0
0.5
1.0
1.5
2.0
2.5
3.0

unknown variable in all pulp washing studies, and that the effect of operating variables on the flow through unconsolidated fiber beds should be performed without changing the packing.

Another important conclusion from the present results is that the intra- and inter-fiber mass transfer resistances can either be neglected or that these resistances vary proportional to the superficial velocity. If this was not the case, smaller Peclet numbers would be obtained at higher velocities. Negligible intra- and inter-fiber mass transfer resistances are in agreement with the assumption of local equilibrium in the fiber bed used for the derivation of equation 4.2. Local equilibrium was also found by Sherman (5) and Poirier (4) for washing of, respectively, 16 and 30 μm diameter viscose fiber beds and for sodium from beds of unbleached kraft softwood fibers. The mass transfer resistances could not be neglected when viscose fibers of 60 or 122 μm or a slow difusing tracer were used. However, it is interesting to note that Poirier (4) also did not need a source term in the axial dispersed plug flow model for good representation of the removal of slow diffusing soluble lignin fragments from a bed of kraft softwood fibers.

4.5.3 Pad height

For obvious reasons, the effect of pad height cannot be studied without changing the packing of the pulp pad. Therefore, a statistical analysis was made for the Peclet numbers of a large number of tracer experiments conducted at three pad heights (2, 4 and 6 cm).

The mean and standard deviation of the Peclet numbers for both the glucose and dextran experiments are shown in Table 4.5. The standard deviation of the glucose Peclet numbers is larger than the corresponding

TABLE 4.5

Mean and standard deviations of Peclet numbers at different pad heights

Pad height cm	Glucose	Dextran
2	$\bar{X}$ = 35.7	$\bar{X}$ = 15.1
	s = 16.9	s = 4.5
4	$\bar{X}$ = 34.9	$\bar{X}$ = 22.1
	s = 11.8	s = 5.3
6	$\bar{X}$ = 38.5	$\bar{X}$ = 25.3
	s = 13.3	s = 10.3

@ $\bar{X}$: mean value

@ s : standard deviation

@ C_p : 10.7%

@ T : 20°C

dextran Peclet numbers. The glucose Peclet numbers show no significant trend with increasing bed height. The dextran Peclet numbers show an increasing trend with increasing pad height. This trend was checked at the 95% probability level by testing the null hypothesis that there is no difference between the mean values of the Peclet number at any two pad heights. The analysis showed that the mean Peclet number at pad heights of 4 and 6 cm were significantly higher than at 2 cm. The difference between the mean values at pad heights 4 and 6 cm, however, was found to be insignificant at the 95% probability level. The dextran T-2000 data are in agreement with Poirier (4) who also measured an increase in the Peclet number at 10% consistency when the bed height was increased from 2.5 to 5.0 cm. A small decrease was, however, obtained from 5.0 to 8.5 cm. Gren and Strom (3) found that the washing efficiency increased with bed height.

It should be noted that the axial dispersion studies by Pellet (6) on viscose fibers showed that $D_L/u\varepsilon_i$ is independent of bed height when bed height is changed by compression of the original bed.

4.5.4 Temperature

The effect of temperature on the glucose residence time distribution curves for the same pulp pad was investigated at 20, 35 and 48°C. The displacing tracer solution and pulp pad were maintained at the same temperature. The close agreement between the three dimensionless breakthrough curves in Figure 4.16 show that the temperature has no significant effect on the glucose Peclet number. This result shows that the temperature dependent diffusion of glucose into the fibers is not a rate determining step in the displacement process, and supports the local equili-

Figure 4.16: Effect of temperature on glucose breakthrough curves.

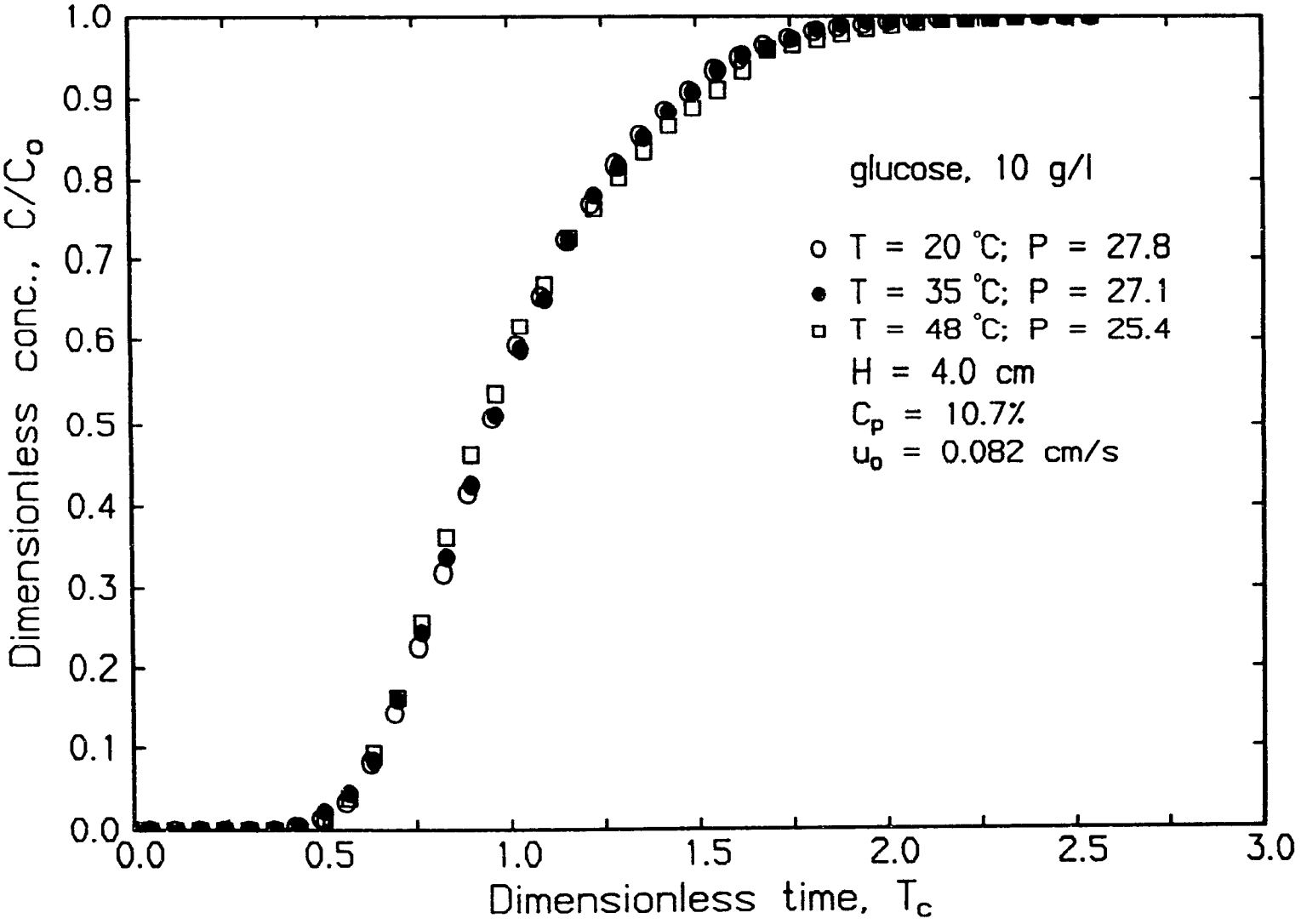
glucose, 10 g/l
o T = 20 °C; P = 27.8
• T = 35 °C; P = 27.1
□ T = 48 °C; P = 25.4
H = 4.0 cm
C_p = 10.7%
u_o = 0.082 cm/s
Dimensionless conc., C/C_o
Dimensionless time, T_c
0.0
0.1
0.2
0.3
0.4
0.5
0.6
0.7
0.8
0.9
1.0
0.0
0.5
1.0
1.5
2.0
2.5
3.0

brium assumption.

Poirier (4) reported no effect of temperature on the washing efficiency of sodium or lignin of 10% consistency pulp pads in the range of 60 to 90°C. The data of Lee (1), however, show a significant increase in the displacement washing efficiencies for 10% consistency pulp pads when the temperature was increased from 20 to 55°C.

4.5.5 Mobility ratio

Lee (1) reported that trace quantities of a high molecular weight polymer added to the wash liquor resulted in improved displacement pulp washing efficiencies. This was attributed to a decrease in the mobility of the wash liquor relative to the displaced liquor and hence a decrease in the growth of "fingers" at the interface of the two fluids. The mobility is defined as the ratio of the permeability and fluid viscosity, k/η, where k is obtained from Darcy's law so that

$$k/\eta = Q_v/(\Delta p/H) \qquad [4.10]$$

where Δp and Q_v are respectively the pressure drop over the bed and the liquid flowrate. Bringham, Reed and Dew (17) reported that even a slightly lower mobility of the wash liquor relative to that of the displacing liquor (mobility ratio of 0.998) resulted in the suppression of "fingering". Increased "fingering" was reported at mobility ratios greater than 1.002.

The effect of mobility ratio was invectigated in the present study by displacing the water in the pad by a tracer solution (step-up BTC) and then displacing the tracer solution by wash water (step-down BTC).

Glucose solutions of 10 and 50 g/l and dextran T-2000 solution of 2 and 15 g/l were used. Since the same pulp pad was used for all four pairs of step-up and step-down experiments, the permeability is unchanged and the mobility ratio becomes a ratio of the viscosity of the displaced to wash liquor, η_d/η_w. The viscosities and mobility ratios for the step-up and step-down experiments are listed in Table 4.6.

The step-up and step-down tracer curves can easily be compared when the step-up breakthrough curve is plotted as C/C_o versus T_c and the step-down as $(1-C/C_o)$ versus T_c. This is shown in Figure 4.17 for the 50 g/l glucose experiments. The Peclet number for the step-up experiment (P = 26.0) is larger than for the step-down test (P = 21.3) although the increase is smaller than reported for other systems (16,17) where the mobility ratio was varied. The difference between the Peclet numbers is not very significant for 10 g/l glucose with P of 22.0 and 20.0 for respectively the step-up and step-down experiments.

The differences between the corresponding breakthrough curves increased substantially for 15 g/l dextran T-2000 shown in Figure 4.18, with the Peclet number of the step-down and step-up BTC being respectively 7.5 and 21.4. The Peclet number of the 2 g/l dextran T-2000 experiments are in between those of the 15 g/l dextran T-2000 results.

The Peclet number from these experiments are plotted versus mobility ratio in Figure 4.19. The decreasing trend of Peclet number with increasing mobility ratio is readily apparent for dextran T-2000. A similar trend over a narrower range of mobility ratio can be seen for the glucose tracer. It is interesting to note also that the dextran T-2000 Peclet numbers are lower than for glucose, even with a favourable mobility

TABLE 4.6

Viscosities and mobility ratios of glucose and dextran tracers at different concentrations

Tracer	Conc.	η	Mobility ratio	
	g/l	cP	Step-up	Step-down
glucose	0	1.002	1.000	1.000
glucose	10	1.021	0.981	1.019
glucose	50	1.145	0.875	1.143
dextran T-2000	2	1.060	0.945	1.058
dextran T-2000	15	2.450	0.409	2.445

Figure 4.17: Effect of mobility ratio on glucose breakthrough curves.

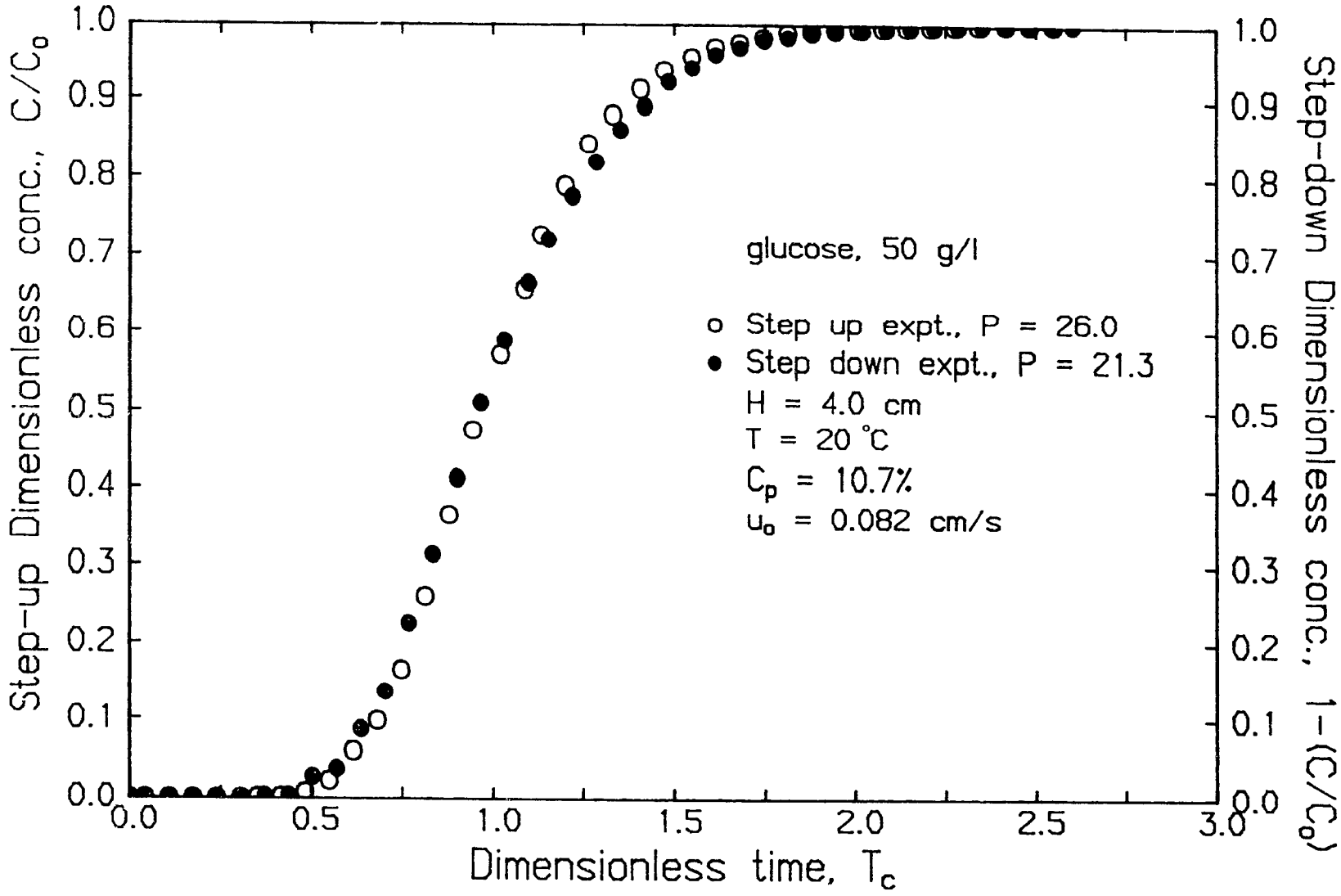
Step-up Dimensionless conc., C/C$_o$
Step-down Dimensionless conc., 1-(C/C$_o$)
Dimensionless time, T$_c$
glucose, 50 g/l
o Step up expt., P = 26.0
• Step down expt., P = 21.3
H = 4.0 cm
T = 20 °C
C$_p$ = 10.7%
u$_o$ = 0.082 cm/s
0.0
0.1
0.2
0.3
0.4
0.5
0.6
0.7
0.8
0.9
1.0
0.0
0.5
1.0
1.5
2.0
2.5
3.0

Figure 4.18: Effect of mobility ratio on dextran T-2000 breakthrough curves.

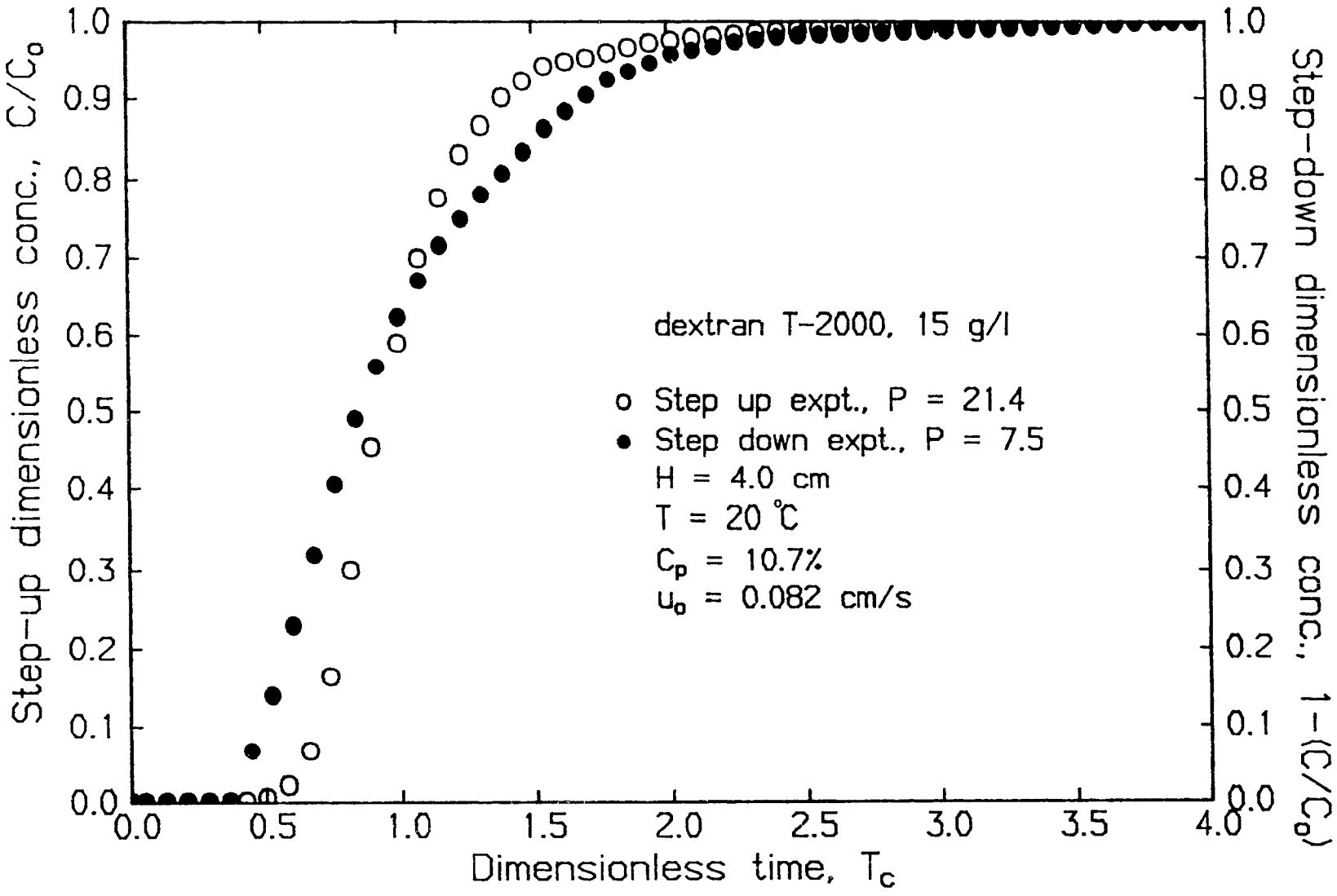
Step-up dimensionless conc., C/C$_o$
Step-down dimensionless conc., 1-(C/C$_o$)
Dimensionless time, T$_c$
dextran T-2000, 15 g/l
o Step up expt., P = 21.4
• Step down expt., P = 7.5
H = 4.0 cm
T = 20 °C
C$_p$ = 10.7%
u$_o$ = 0.082 cm/s
0.0
0.1
0.2
0.3
0.4
0.5
0.6
0.7
0.8
0.9
1.0
0.0
0.5
1.0
1.5
2.0
2.5
3.0
3.5
4.0

Figure 4.19: Influence of mobility ratio on Peclet number.

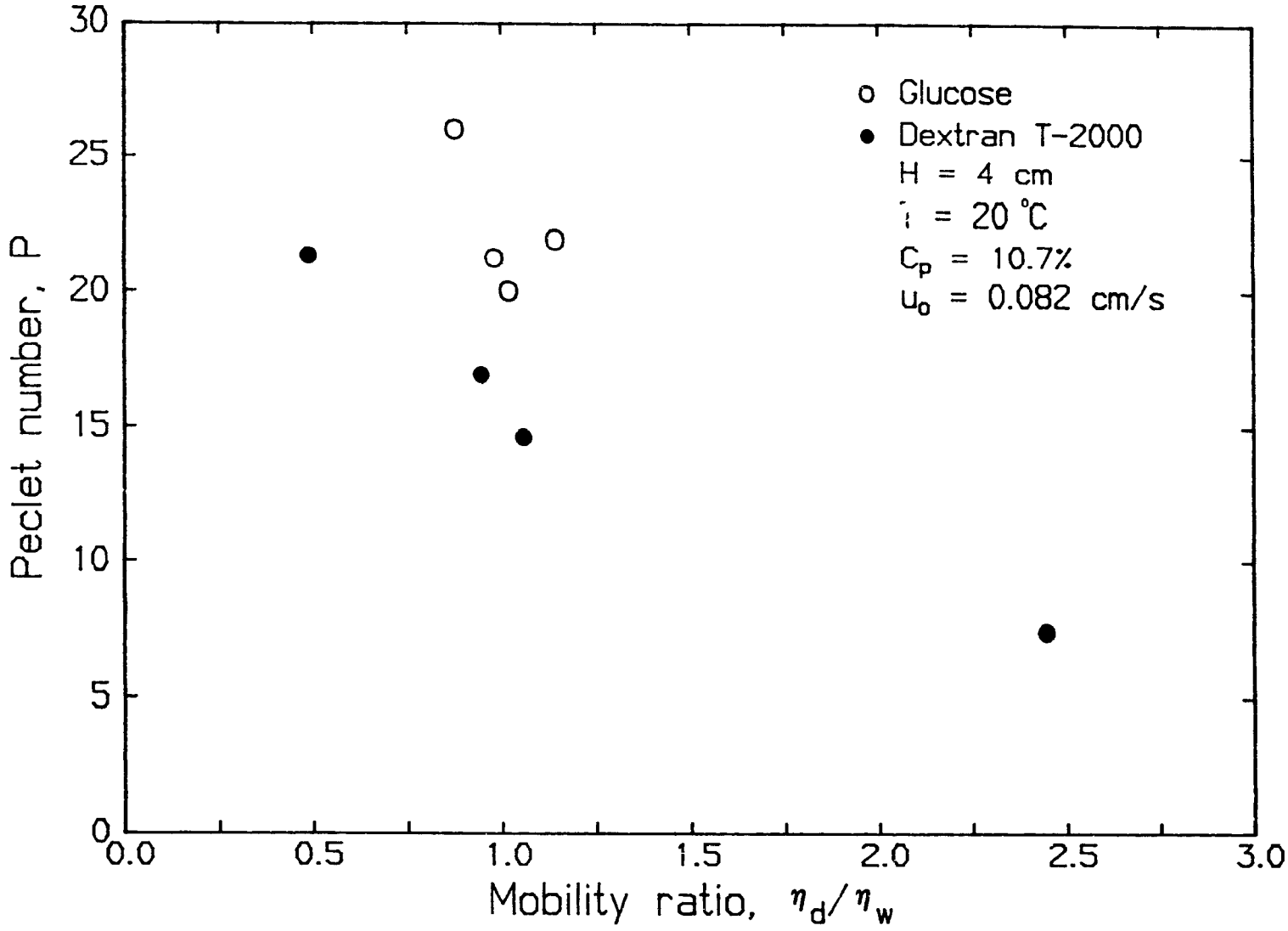
o Glucose
• Dextran T-2000
H = 4 cm
T = 20 °C
C_p = 10.7%
u_o = 0.082 cm/s
Peclet number, P
Mobility ratio, η_d/η_w
0
5
10
15
20
25
30
0.0
0.5
1.0
1.5
2.0
2.5
3.0

ratio.

4.6 General discussion

The glucose BTC's were adequately described by the axial dispersed plug flow model and the assumption of local equilibrium between the inter- and intrafiber voids. The assumption of local equilibrium was supported by the insensitivity of the Peclet number to large variations in flowrate and temperature. Furthermore, the finding that the Peclet number (or u_i/D_L at constant H) is not dependent on the flowrate is also in agreement with axial dispersion theory (15).

However, there is strong evidence that the actual flow behavior is not governed by axial dispersion, even though the RTD is well represented by the axial dispersed plug flow model. For example, the Peclet number obtained with glucose was found to be independent of the pad height in contradiction with the axial dispersion model which requires the Peclet number to vary proportionally to the pad height. The pulp washing experiments of Poirier (4) show the same behavior. The result that the Peclet numbers obtained with high concentrations of dextran T-2000 are higher for a step-up than a step-down experiment is also in disagreement with the axial dispersed plug flow model.

The two previous results which are in disagreement with the dispersion model can be explained by chanelling. As shown in section 4.5.5 the differences in Peclet number with the step-up and step-down tests with dextran T-2000 were related to the different mobility ratios. A mobility ratio lower than one suppresses "fingering" and thus increases the Peclet number, while the opposite occurs at mobility ratios greater than one. Also the proportional increase in dispersion (D_L/u_i) with bed height H (or

P independent of H) in section 4.5.3 is in agreement with a linear growth of the fluctuations in the displacement front profile with bed height. Further evidence that the actual flow through the pulp pad is better represented by chanelling rather than axial dispersion is:

- The presence of well bleached and dark regions at an axial cross-section when a dynamic chlorination experiment is broken off early (Chapter 6).
- The chlorine breakthrough curves are much better modelled by parallel plug flow through multiple channels than axial dispersion (Chapter 7).

In all cases it was found that the Peclet number obtained with dextran T-2000 was smaller than with glucose as tracer. Also the dextran T-2000 step-up BTC's showed in general more tailing than predicted by the axial dispersed plug flow model. This suggests that the slower diffusion of the large dextran T-2000 molecule out of the lumen might be responsible for these phenomena. However it was also shown that the dextran T-2000 BTC's were essentially independent of flowrate (section 4.5.2) in contradiction with a diffusion limited process. Because of these apparent inconsistencies the transport processes on the fiber scale were analysed in more detail.

A water swollen, delignified softwood fiber can be visualized as a long hollow round tube. The cell wall is porous and has larger holes called pits which provide a direct path for tracers to enter the central cavity or lumen. The lumen diameter of a black spruce fiber is about 18.4 microns and the swollen fiber wall thickness is about 4.2 microns giving a total diameter of 26.8 microns (see Appendix 4-3). The unsteady diffusion of tracer into a fiber can be approximated by diffusion into an infinite

water filled cylinder with a modified cylinder radius. When there is no external mass transfer resistance and the cylinder is initially free of tracer then the unsteady diffusion into the fiber is 95% complete when

$$Dt_{0.95}/r^2 = 0.45 \qquad [4.11]$$

where r is the modified cylinder radius and D the molecular diffusion coefficient of the tracer. The modified cylinder radius is defined as

$$r = r_i + \left((D\varepsilon_w/D_e)^{0.5}\right)(r_o - r_i) \qquad [4.12]$$

where r_i and r_o are the inner and outer fiber wall radius and D_e and ε_w, respectively, the effective diffusion coefficient and porosity in the fiber wall. The effective diffusion coefficient can be estimated as $\varepsilon_w D/\tau$ where τ is the tortuosity. With $\varepsilon_w = 0.687$ (Appendix 4-3), $\tau = 2.5$ and D = 0.6*10-9 m^2/s for glucose at 20°C, one obtains $D_e = 0.17*10^{-9}$ m^2/s, r = $15.8*10^{-6}$ m and $t_{0.95} = 0.19$ s. The ratio of diffusion time $t_{0.95}$ to the mean residence time $\bar{t}_r$ is:

$$t_{0.95}/\bar{t}_r = 0.45r^2/D\bar{t}_r = 0.45r^2u_a/DH \qquad [4.13]$$

Even for the highest flowrate of 216 cm^3/min and bed height of 6 cm (or $\bar{t}_r$ = 68.3 s), the ratio $t_{0.95}/\bar{t}_r$ is more than two orders of magnitude smaller than 1 for glucose.

From the above analysis it is clear that the assumption of local

equilibrum is easily achieved for glucose even at the highest flowrates and lowest temperatures. Repeating the same analysis for dextran T-2000 with D = $0.008*10^{-9}$ m^2/s one obtains $t_{0.95}/\bar{t}_r$ = 0.21. However, since dextran T-2000 has only access to the lumen via the pit openings which occupy about 1.1% (18) of the external surface of the fiber, the assumption of pure radial diffusion in the lumen is not valid anymore. Therefore the value of $t_{0.95}/\bar{t}_r$ could be many times larger than calculated above. This could explain the tailing found for the dextran BTC's but not the insensitivity of the tailing to the wide range of flowrates shown in Figure 4.15. Because of this inadequacy of the diffusional mechanism for dextran T-2000, an order of magnitude analysis was undertaken to estimate whether flow or diffusion of dextran T-2000 through the pit openings is the dominant transport mechanism.

From Poiseuille's equation it may be shown (22) that the equivalent diffusivity in a pit pore is

$$D_p = P_d R_p^2/(8\eta) \qquad [4.14]$$

where R_p is the radius of a pit pore opening, $1*10^{-6}$ m, and P_d is the pressure drop through a pit pore opening. The pressure drop measured across a 6 cm high and 10.7% consistency pulp pad at different flowrates is shown in Figure 4.20. The pressure drop across a 6 cm pad at a flowrate of 216 cm^3/min (u_o = 0.082 cm/s) is about $1.2*10^4$ Pa. The pressure drop across a horizontal fiber of 26.8 μm diameter is then estimated to be 5 Pa. If two pit pores are assumed to be on opposite sides of the horizontal fiber then the pressure drop across one pit, P_d, is 2.5 Pa. The

Figure 4.20: Pressure drop at different flowrates.

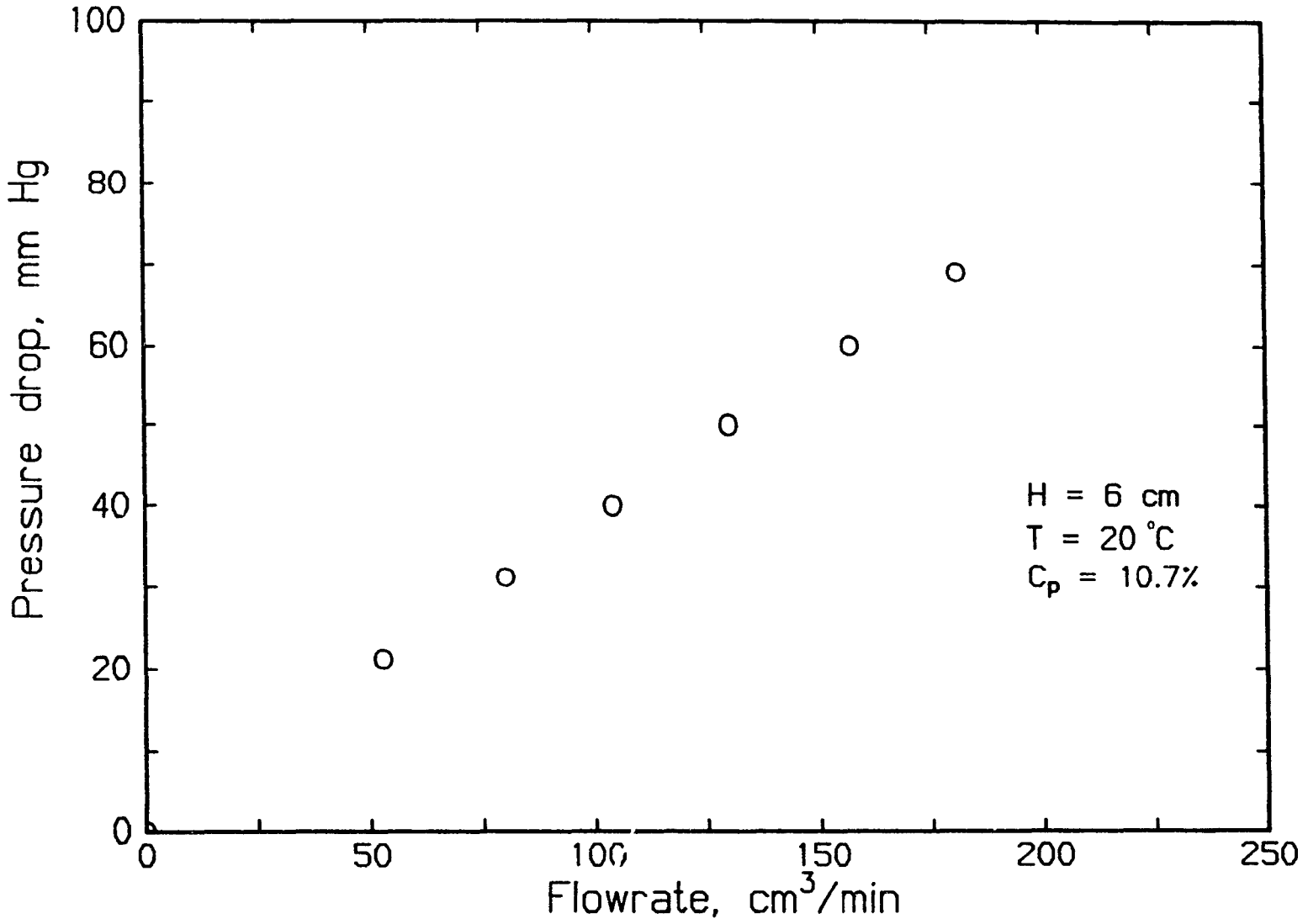
Pressure drop, mm Hg
100
80
60
40
20
0
0
50
100
150
200
250
Flowrate, cm3/min
H = 6 cm
T = 20 °C
Cp = 10.7%

equivalent diffusivity is then 3.1×10^{-10} m^2/s. This is 2 times smaller and 39 times larger than the diffusion coefficients of, respectively, glucose and dextran T-2000. This indicates that flow rather than diffusion is the dominant mechanism for the transport of dextran T-2000 through the pit openings into the lumen. Since both the velocity through the pits and the interstitial fiber bed velocity vary linearly with the pressure gradient over the bed, the intra- and inter-fiber transport of dextran T-2000 are proportional to each other. This would explain why the tailing with dextran T-2000 is not a function of flowrate. However tailing will still be present because the flowrate through the pits is very small compared to the flowrate through the external fiber voids since the average radius of the external voids is one order of magnitude larger than the pit pores and the flowrate is proportional to radius^4.

To confirm the importance of the size and number of pit openings on the tailing of the dextran T-2000 breakthrough curves, two other kraft wood fiber types were tested. The wood types were Western Red Cedar and Douglas Fir characterised respectively by larger and smaller pit openings than Black Spruce. The Peclet numbers should then be closer to that of glucose for the Western Red Cedar pulp pad and farther for the Douglas Fir pulp pad. Such results are obtained as shown in Table 4.7.

The effect of superficial velocity on the residence time distribution in packed beds of regularly shaped packings was studied by many researchers. Levenspiel and Bischoff (15) presented a comprehensive review and showed that for liquid systems the experimental axial dispersion coefficient can be represented by a Peclet number, based on particle diameter,

TABLE 4.7

Peclet number versus superficial velocity: Western red cedar and Douglas fir pulps

Pulp type	Tracer	u_o, cm/s	P
WRC	glucose	0.082	29.6
WRC	dextran T-2000	0.082	24.1
WRC	dextran T-2000	0.041	27.9
WRC	dextran T-2000	0.020	25.5
D•fir	glucose	0.082	37.7
D•fir	dextran T-2000	0.082	20.2
D•fir	dextran T-2000	0.041	25.7
D•fir	dextran T-2000	0.020	25.3

Conditions: H = 6 cm, T = 20°C, C_p = 10.7%.

of about 2 in the laminar flow region for 0.1 $Re_e = u_o d_e/\eta$ 50, where d_e is the effective diameter (see later). At even lower flowrates, the axial dispersion coefficient becomes independent of the superficial velocity and is equal to the molecular diffusion coefficient divided by the tortuosity (19). The tortuosity accounts for the longer paths in packed beds. Different authors have obtained different values of the tortuosity at low velocities. Suzuki and Smith (23) obtained values of 1.03 and 1.27, respectively, for fine porous particles and non-porous glass beads, while Edwards and Richardson (24) obtained a value of 1.27. This behavior was recently verified by Chen and Fan (20) for gas flow through a long (50 cm) and narrow (0.4 cm) bed of 15 μm mean diameter carbon fibers. However there is also evidence by Kehinde et al. (21) that at low velocities and very small particle sizes, the non-homogenities in the bed packing lead to channelling and call into question the validity of the axial dispersed plug flow model. There is virtually no literature on liquid phase axial dispersion in unconsolidated packed beds at very low Reynolds number (Re_e 0.1) except for the few studies on viscose and softwood pulp fiber beds. The glucose axial dispersion coefficients from this study are compared to the fiber bed studies and the data of Bischoff and Levenspiel (15) in Figures 4.21 and 4.22. The Reynolds number, Re_e, is based on the equivalent diameter, d_e, calculated from pressure drop measurements (Appendix 4-4). The equivalent fiber diameter for the present softwood pulp fiber bed at 10.7% consistency is calculated as 26.5 microns. This is close to the mean fiber diameter. The equivalent diameter for the other studies on fiber beds is taken to be the fiber diameter since no pressure drop data were reported.

Figure 4.21: Comparison of glucose axial dispersion results of this study with those of other studies: based on equivalent diameter.

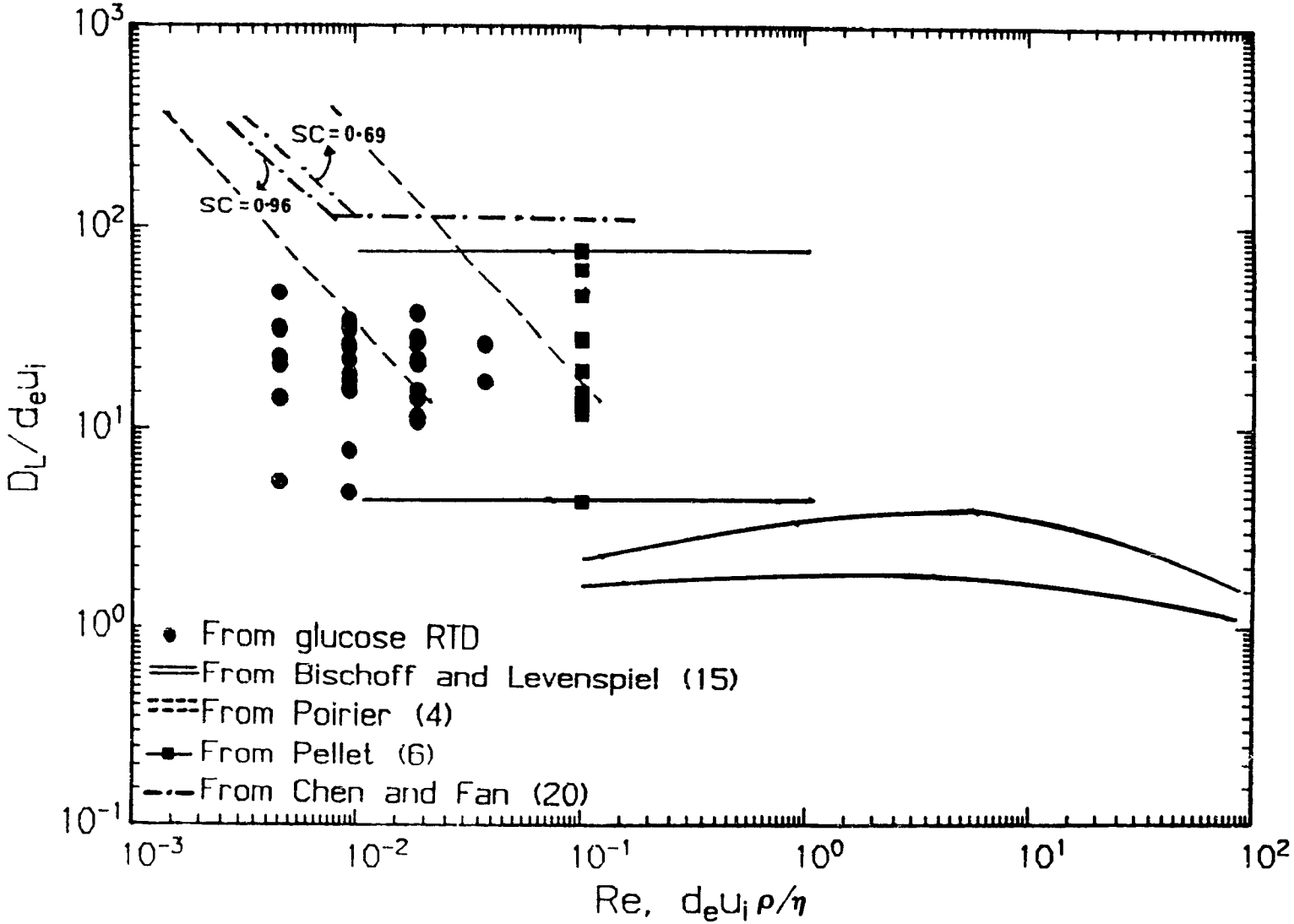
10^3
10^2
10^1
10^0
10^{-1}
D_L/d_eu_i
SC = 0·69
SC = 0·96
From glucose RTD
From Bischoff and Levenspiel (15)
From Poirier (4)
From Pellet (6)
From Chen and Fan (20)
10^{-3}
10^{-2}
10^{-1}
10^0
10^1
10^2
Re, $d_eu_i\rho/\eta$

Figure 4.22: Comparison of glucose axial dispersion results of this study with those of other studies based on fiber or particle length.

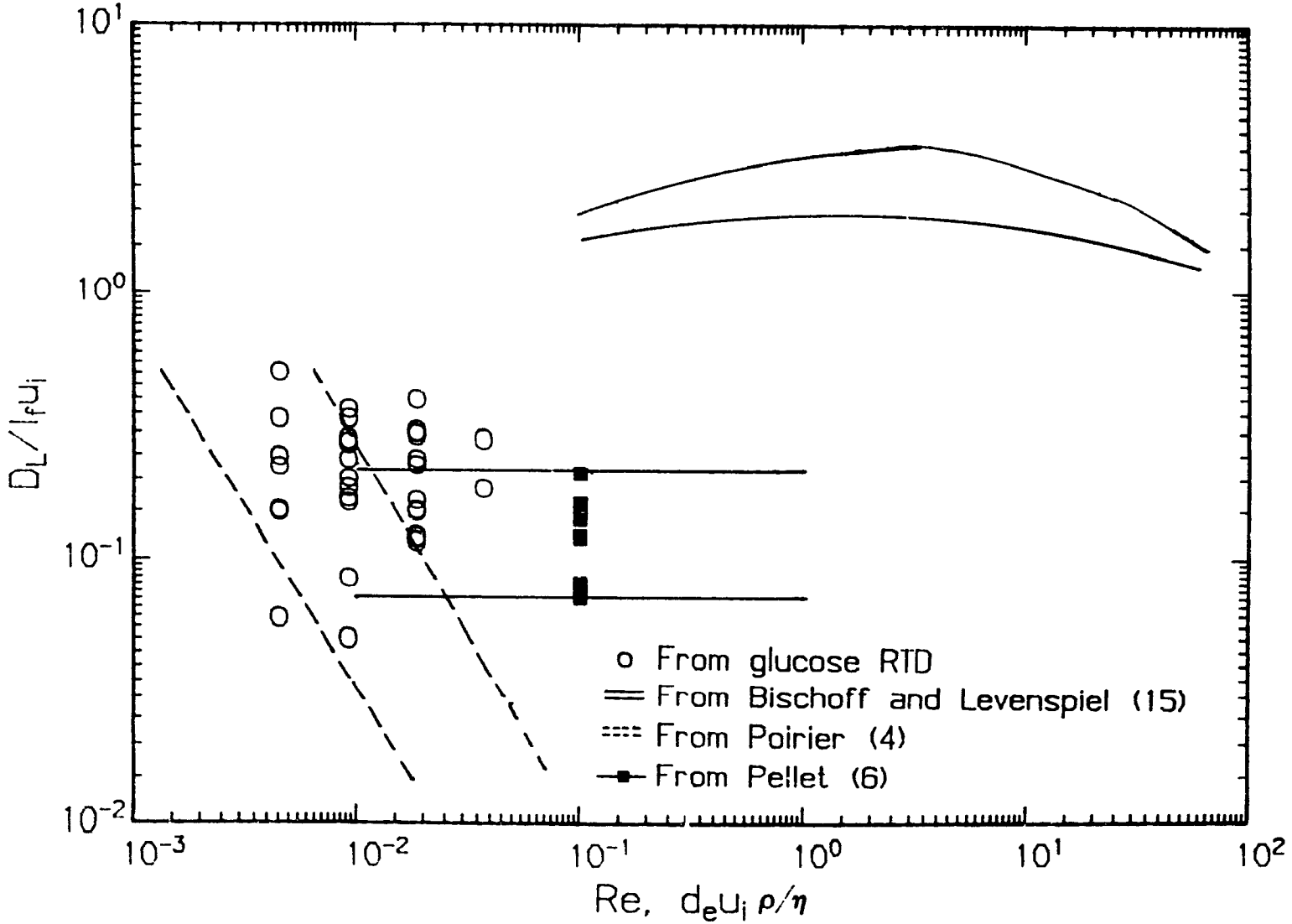
10^1
10^0
10^{-1}
10^{-2}
$D_L/l_f u_i$
10^{-3}
10^{-2}
10^{-1}
10^0
10^1
10^2
Re, $d_e u_i \rho/\eta$
o From glucose RTD
From Bischoff and Levenspiel (15)
From Poirier (4)
From Pellet (6)

The last two figures show that $D_L/u_i d_e$ for fiber beds is 1-2 orders of magnitude larger than for beds of regular shaped particles. Also the fiber length rather than the fiber diameter is a more appropriate characteristic dimension to unify the Peclet numbers of different types of fibers. Before further discussing these results, an order of magnitude analysis will be presented to show that the unique geometric characteristics of fibers favour the formation of channelling flow.

Particles with a large length/diameter ratio such as wood pulp fibers have a tendency to flocculate, Kerekes et al. (25). It is likely that flocs of fibers are formed in the present experiments after stirring and during subsequent sedimentation of the fiber suspension. The flocs represent a fiber network of higher mass concentration in the pulp suspension. The size of flocs is approximately two times the fiber length (Kerekes et al. (25)) or with the present length/diameter ratio of about 100, approximately 200 times the fiber diameter. It is also likely that the fiber mass concentration is higher in the middle of these flocs than near the edges. A pulp pad can then be visualized as a packed bed of axially compacted flocs. As a result, the inter-fiber porosity will fluctuate in the transverse direction with a periodicity of about 200 fiber diameters or about 6 mm. The governing condition for channelling flow is that the extent of transverse mixing is small compared to the periodicity in the transverse direction of the axial velocity fluctuations. The transverse mixing depth at the exit of the fiber bed, δ_D, defined as the distance where the concentration is reduced by a factor 10 is given by

$$\delta_D = 1.35\sqrt{D_R t_r} = 1.35\sqrt{D_R \varepsilon_a H/u_o} \qquad [4.15]$$

where D_R is the radial dispersion coefficient. For a typical experiment with the present equipment, T = 20°C, u_o = 0.082 cm/s, ε_a = 0.93, H = 6 cm and $D_R = 3.11*10^{-9}$ m^2/s (Appendix 4-5), one obtains δ_D ≈ 0.6 mm. This is one order of magnitude smaller than the size of the transverse periodicity in axial velocity fluctuations. The analysis shows that transverse mixing is too small to smooth the concentration gradients formed as a result of the axial velocity distribution in the transverse plane. This condition is equivalent to "channelling" flow. Similarly the analysis shows that the axial dispersed plug flow model is invalid because the model assumes no gradients in the transverse direction at each axial position.

In a packed bed of particles with a length/diameter ratio close to 1, the radial dispersion is also determined by convective mechanisms. As a result the radial Peclet number is approximately 10 (Doraiswamy and Sharma (26)) and the radial diffusion coefficient is 0.1 $d_e u_i$. For typical packed beds, the bed height H is of the order 100 d_e so that a transverse penetration depth of a few particle diameters is obtained. Since the axial velocity is also expected to fluctuate on a scale of one or a few particle diameters, the transverse gradients will be relatively small in a typical packed bed.

With the above analysis, it is easier to explain the difference in Figure 4.21 between fiber beds and regular packed beds. For example, if $D_L/u_i d_e \approx 2$ for fiber beds, then $P = (u_i d_e/D_L)\cdot(H/d_e)$ would be $O(10^3)$, which is essentially equivalent to plug flow. It has just been shown, however, that flow through a fiber bed is best represented by segregated flow through a series of channels of different inter-fiber porosity. Liquid flow through fiber beds is described by the Kozeny equation (Robertson and Mason (27))

$$u_o = \frac{\varepsilon_i^3}{5.55\ nS_v^2(1-\varepsilon_i)^2}\ \frac{\Delta P}{H} \qquad [4.16]$$

where ε_i is the inter-fiber void fraction, S_v the external fiber surface area per unit volume (m^2/m^3), and ΔP the pressure drop over the bed. The form of equation 4.16 is such that small variations in ε_i lead to rather large differences in u_o. For example a change of ε_i from 0.55 to 0.60 gives an increase of u_o of 64% (note that $\varepsilon_i = 0.565$ for the present fiber beds at 10.7% consistency). Therefore significant fluctuations are expected as a result of the inevitable variation in ε_i in the pulp pad and $u_i d_e/D_L$ for fiber beds must be considerably smaller than for regular packed beds. At present there is no theory to predict a priori the value of $u_i d_e/D_L$ for fiber beds. Considering the sensitivity of $u_i d_e/D_L$ to the pad formation technique, the development of a good predictive theory based on network structure principles will be difficult.

The results in Figure 4.22 show that the fiber length rather than the fiber diameter is better at unifying the Peclet number from beds of different fiber types. The data of Chen and Fan (20) could not be added to Figure 4.22 because fiber lengths were not given. The stronger dependence on fiber length rather than on fiber diameter was earlier noted by Sherman (5) who found that 15 μm and 120 μm viscose fibers, both 6.35 mm long, gave the same value of D_L/u_i. The data of Pellet (6) also show that D_L/u_i increases almost linearly with increasing fiber length and is independent of the fiber diameter. As mentioned earlier, the fiber density in the compressed flocs in the pulp pad decreases from the center of a floc to its edges. Since the size of the flocs is proportional to the fiber

length one would also expect that the fiber density variation is larger for longer fibers. Therefore it also seems plausible that the variations in inter-fiber porosity and thus superficial velocities via equation 4.16 are larger for longer fibers. This would explain the increase in dispersion with increasing fiber length measured by Pellet (6) and the fact that $D_L/u_i l_f$ is better than $D_L/u_i d_e$ in unifying the dispersion data of fiber beds. The increase in dispersion with fiber length might also partly explain (besides other factors like foam formation) why softwood pulps ($l_f \approx 3$mm) require more washwater than hardwood pulps ($l_f \approx 1$ mm) in drum washers.

4.7 Conclusions

The RTD of flow through a pad of pulp fibers can be adequately characterized with glucose as inert tracer. Although these RTD's are well represented by the axial dispersed plug flow model, the actual flow phenomenon is channelling flow. The different flow types for fiber and packed beds of regular particles is attributed to the large aspect ratio of fibers and their tendency to form flocs. Theoretical considerations demonstrated that the size of these flocs are of sufficient size that transverse velocity fluctuations cannot be eliminated by radial mixing This explains the existance of channelling flow in fiber beds. Further evidence of channelling flow is the significant difference in the step-up and step-down RTD's for the same pulp pad when dextran T-2000 at a high concentration is used as tracer, and the independence of Peclet number on pad height. It was also shown that the transport of glucose into fibers is governed by diffusion while transport of dextran T-2000 is governed by flow. The intra-fiber pore distribution was also characterized for the

first time with a "dynamic" version of the solute-exclusive technique. The results are very similar to those obtained with the "static" technique.

References

1. Lee, P.F., Tappi, 62(9), 75-78, 1979.
2. Grahs, L.G., Svensk Papperstidning, Vol. 79, 84, 1976.
3. Gren, U.B. and Strom, K.H.U., Pulp and Paper Canada, 86, 9, 1985
4. Poirier, N.A., M Eng. Thesis, McGill University, 1986.
5. Sherman, W.R., AIChE., 10(6), 855-860, 1964.
6. Pellet, G.L., Tappi,k 49(2), 75-82, 1986.
7. Stone, J.E. and Scallan A.M., "A structural model of the cell wall of water swollen pulp fibers based on their accessibility to macromolecules", Cellulose Chem. and Tech., 2, 343-358, 1968.
8. Carlsson, G., Lindstrom, T., and Floren, T., "Permeability to water of compressed pulp fibre mats", Svensk Papperstidning, R128-134, 1983.
9. Levenspiel, O., "Chemical Reaction Engineering", John Wiley and Sons Inc., U.S.A., 1972.
10. Danckwerts, P.V., Chem.Eng.Sci., 2(1), 1-13, 1953.
11. Brenner, H., Chem. Eng. Sci., Vol.17, 229-243, 1962.
12. Stone, J.E. and Scallan, A.M., "The effect of component removal upon the porous structure of the cell wall of wood", 69, R288, 1968.
13. Green, H.V., Fox, T.J., and Scallan, A.M., Pulp and Paper Can., 83 (7), 1982.
14. Grotte, G., Acta Chim. Scand., 211, 1-84, 1956
15. Bischoff, K.B., and Levenspiel, O., Adv. Chem. Eng., 4, 1963.
16. Lee, P.F., Tappi, 67(11), 100-103, 1984.

17. Bringham, W.E., Reed, P.W. and Dew, J.W., Soc. Petrol. Eng. J.,1:1, 1961.

18. Stamm, A.J., Passage of liquids, vapours and dissolved materials through softwoods, U.S.D.A. Tech. Bulletin No. 929, 1946.

19. Bischoff, K.B. and Levenspiel, O., Chem. Eng. Sci., 17, 257-264, 1962.

20. Chen, S. and Fan, Y., "Axial dispersion of a gas in a fibre bed", Int. Chem. Eng., 26, 1, 149-154, 1986.

21. Khenide, A.J., Hudgins, R.R., and Silveston, P.L., J. Chem. Eng. of Japapn, Vol.16, No.5, 1983.

22. Ruthven, D.M., Principles of adsorption and adsorption processes, John Wiley & Sons, 1984.

23. Suzuki, M., and Smith, J.M., Chem. Eng. J., 3, 256, 1972.

24. Edwards, M.F., and Richardson, J.F., Chem. Eng. Sci., 23, 109, 1968.

25. Kerekes, R.J., Soszynski, R.M., and Tam Doo, P.A., Transactions of the 8th Fundamental Research Symposium, Vol. 1, 265, Oxford, London, 1985.

26. Doraiswamy, L.K., and Sharma, M.M., Heterogeneous Reactions: Analysis, Examples and Reactor Design, John Wiley and Sons, 1984.

27. Robertson, A.A., and Mason, S.G., Pulp and Paper Mag. Can., 50(3), 1949.

CHAPTER 5

KINETICS OF CARBOHYDRATES-CHLORINE REACTION

5.1 Introduction

In dynamic chlorination, chlorine water is forced through a pad of pulp fibers. In the pulp pad chlorine reacts with lignin and carbohydrates. Due to the dominant and fast reaction with lignin, a chlorine concentration front is formed that moves through the pad at a speed governed by operating variables and pulp lignin content. Chlorine appears at the exit of the reactor when any part of the front reaches the end of the pad. A measurement of the chlorine concentration at the exit of the reactor as a function of time is called a breakthrough curve (BTC). The area above this curve represents the consumption of chlorine by both lignin and carbohydrates.

The reaction of chlorine with carbohydrates is much slower than with lignin. However the consumption of chlorine by carbohydrates can be significant in dynamic chlorination because of the high chlorine concentration in the pulp pad before the lignin reaction front and the low concentration of dissolved lignin which acts as free radical scavenger. Therefore the kinetics of the chlorine-carbohydrate reaction must be known for analysis of the BTC

A review of the literature presented in Chapter 2 showed that no kinetic expression is available for the carbohydrate fraction in bleached or unbleached pulp. All previous chlorine-carbohydrate kinetic studies were conducted on either model compounds or cellulose powder (1,2,3,4). Only in the study by Fredricks et al. (1) was a rate expression presented. They conclude that chlorination proceeds by both an ionic and a free radical mechanism. The ionic reaction kinetics at 50°C for a pH of 1-4 was represented by

$$- d[Cl_2]/dt = 10^{-3} [Me] (1.69 [Cl_2] + 0.0324 [HOCl] + 12.0 [HOCl]^2) \quad [5.1]$$

where [Me] is the concentration of the model compound methyl D-glucopyranoside. It shows that the rate of disappearance of chlorine is first order in the model carbohydrate concentration and proportional to a complex combination of the chlorine species in solution. All concentrations are in moles/l and t is the time in seconds. It was proposed that the ionic reaction mechanism involved hydride or proton transfer reactions as shown in Figure 5.1. The free radical mechanism was proposed to occur via hydrogen abstraction by a free radical as shown in Figure 5.2 for pH less than 4. Thus the proposed mechanism for carbohydrate oxidation by aqueous chlorine after formation of the free radical $X^{\bullet}$ is

$$RH + X^{\bullet} \rightarrow R^{\bullet} + HX \quad [5.2]$$

$$R^{\bullet} + XCl \rightarrow RCl + X^{\bullet} \quad [5.3]$$

followed by the hydrolysis of RCl whereby HCl is formed. The free radical $X^{\bullet}$ represents $Cl^{\bullet}$, $OH^{\bullet}$ or $ClO^{\bullet}$. No initiation reaction was suggested by Fredricks et al. (1) because the usual formation of a radical

$$RH + XCl \rightarrow R^{\bullet} + X^{\bullet} + HCl \quad [5.4]$$

is incompatible with the experimental result that the reaction is independent of the carbohydrate concentration (1).

Figure 5.1 Mechanism for the ionic oxidation at glycosidic bonds with chlorine, Fredricks et al. (1).

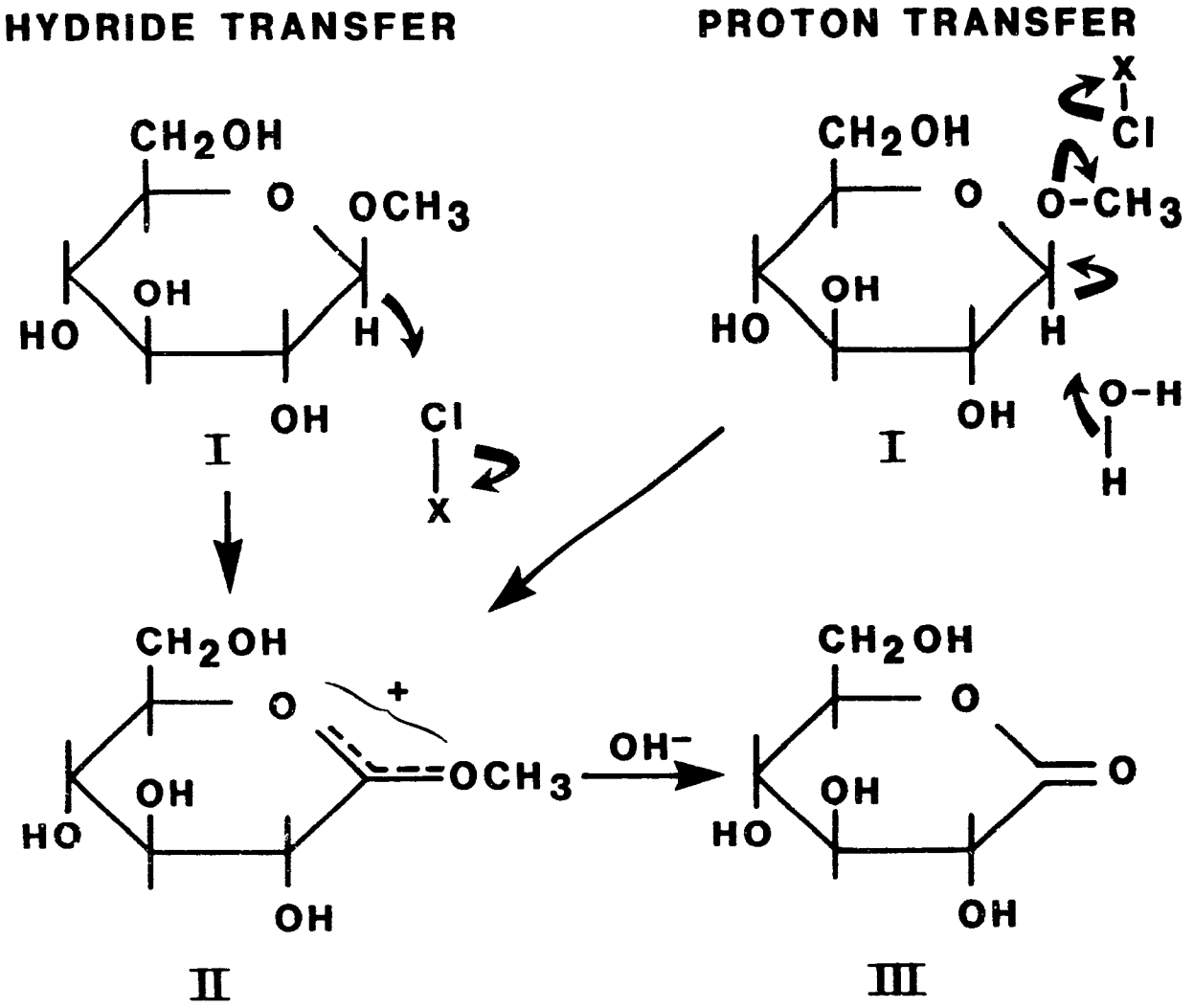
HYDRIDE TRANSFER
PROTON TRANSFER
CH2OH
O
OCH3
OH
HO
H
OH
I
Cl
X
CH2OH
O
O-CH3
OH
HO
H
OH
X
Cl
O-H
H
I
CH2OH
O
+
OCH3
OH
HO
OH
II
OH−
CH2OH
O
O
OH
HO
OH
III

Figure 5.2 Mechanism for hydrogen abstraction at a glycosidic bond, Fredricks et al. (1)

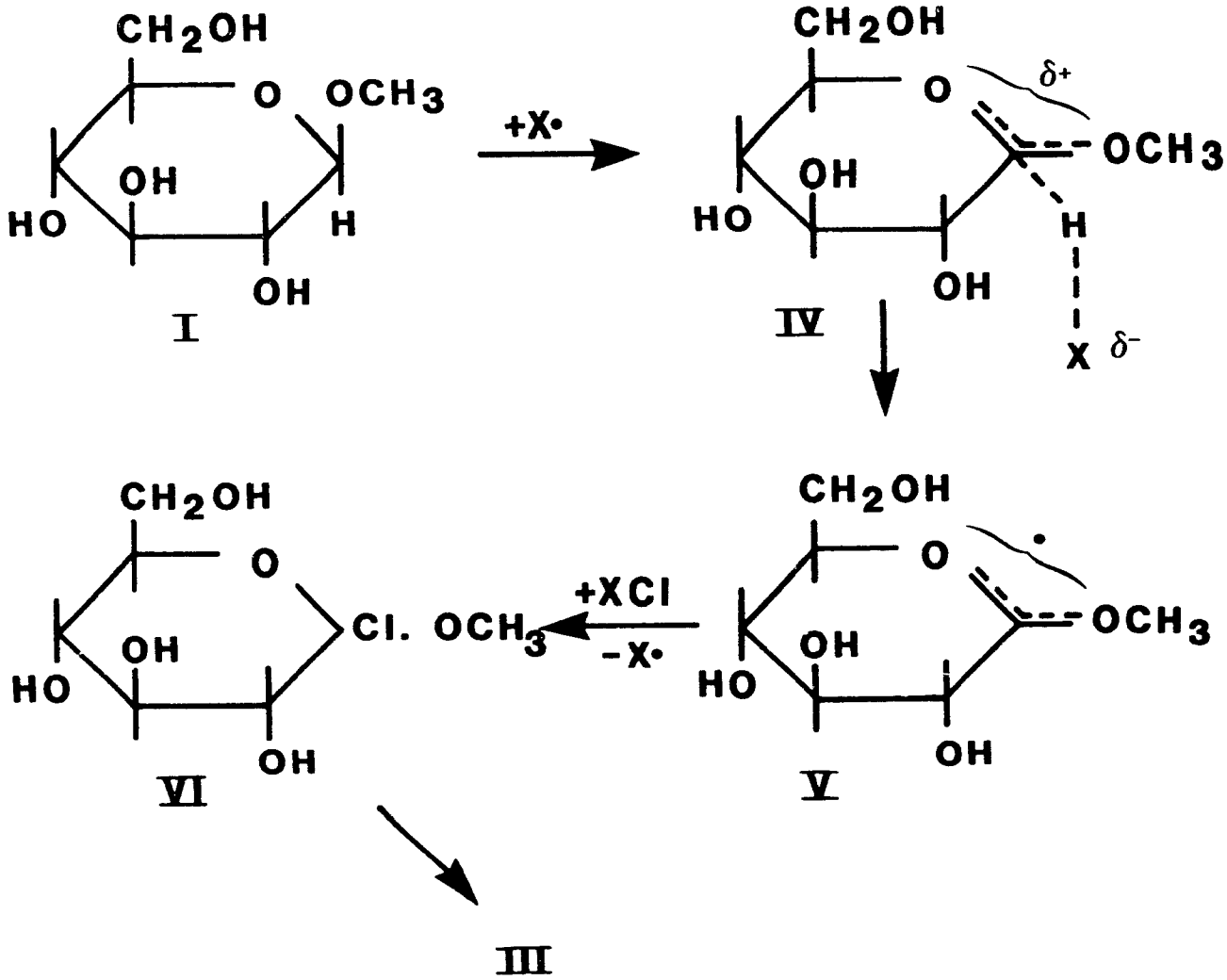
CH2OH
O
OCH3
OH
HO
H
OH
I
+X•
CH2OH
O
δ+
OCH3
OH
HO
H
OH
X δ−
IV
CH2OH
O
•
OCH3
OH
HO
OH
V
+XCl
-X•
CH2OH
O
Cl. OCH3
OH
HO
OH
VI
III

Over the pH range of 1 to 3, where there is a drastic change in Cl_2 to HOCl concentration ratio, the free radical component of the rate of disappearance of chlorine was found to be proportional to the total chlorine concentration, i.e.

$$d[Cl_2]/dt = k_c[Cl_2] \qquad [5.5]$$

The reaction constant k_c calculated from the data of Fredricks et al. (1) is about $2.2*10^{-5}$ s^{-1} at 50°C. The influence of temperature for both the ionic and radical reaction was not investigated. An interesting consequence of the two rate expressions is that the radical reaction increases in importance at low carbohydrate concentrations. In another paper, Fredricks et al. (3) report on the influence of inhibitors on the cellulose degradation by chlorine. The data showed a decrease in the chlorine consumption at pH 1-3 of one order of magnitude when chlorine dioxide, a free radical scavenger, is added to a suspension of cellulose powder. Therefore it is suggested (2) that the radical reaction predominates over the ionic reaction in the chlorination of cellulose.

In the present study most experiments were performed with a chlorite delignified pulp. The chlorite treatment removes almost all remaining lignin from unbleached kraft pulp without significant degradation of the carbohydrate fraction. The chlorination experiments with chlorite treated pulp allowed investigation of the chlorine-carbohydrate reaction without interference from the chlorine-lignin reaction.

5.2 Experimental

The kinetics of the chlorine-carbohydrate reaction was studied in the same experimental system as used for dynamic chlorination of unbleached kraft pulp. A detailed description of the equipment was presented in Chapter 3.

Chlorine breakthrough curves (C/C_o vs T_c) were obtained for various combinations of initial chlorine concentrations (0.55, 1.10 and 2.20 g/l : ± 0.04%), temperature (19, 35 and 50°C : ± 1°C) and superficial velocity (0.020, 0.041, 0.082, 0.123 and 0.164 cm/s). In all cases the pad height of chlorite treated pulp was 6 cm and the consistency, C_p, was 10.7%.

Before the start of each chlorination experiment, a glucose tracer test was conducted to characterize the flow through the pulp pad. The residence time distribution obtained from the tracer test could be described by the axial dispersed plug flow model with the Peclet number determined by the moments technique. The computer code to obtain the Peclet number from the BTC is given in Appendix (4-2).

The chlorination effluent was analyzed for residual chlorine concentration, C, and total organic carbon (TOC). The non-dimensional effluent concentration, C/C_o, was plotted versus non-dimensional time, $T_c = t/\bar{t}_r$, with the mean residence time, $\bar{t}_r$, obtained from the preceding tracer experiment. A listing of all the runs along with operating conditions, Peclet number, maximum and final dimensionless chlorine concentrations are given in Table 5.1.

TABLE 5.1

Experimental conditions and analysis of chlorine BTC

Run	$[C_o]$ g/l	u_o (cm/s)	T °C	P	$(C/C_o)_m$	$(C/C_o)_f$
C1	0.55	0.020	19	78.9	0.94	0.90
C14	0.54	0.082	20	23.8	0.99	0.99
C12	0.57	0.020	35	116.5	0.74	0.55
C2	0.55	0.041	35	34.6	0.87	0.76
C3	0.55	0.041	35	68.2	0.86	0.73
C10	0.55	0.082	35	27.6	0.94	0.93
C11	0.55	0.164	35	31.6	0.97	0.96
C4	0.55	0.082	49	27.6	0.81	0.50
C13	0.56	0.164	49	39.5	0.90	0.82
C9	1.08	0.041	19	64.2	0.96	0.96
C6	1.10	0.020	35	63.2	0.78	0.60
C7	1.06	0.041	34	59.3	0.87	0.82
C5	1.10	0.082	34	20.7	0.95	0.95
C8	1.06	0.164	35	26.7	0.95	0.95
C16	2.20	0.041	34	34.6	0.87	0.85
C15	2.25	0.082	35	31.6	0.95	0.94

5.3 Characterization of breakthrough curves

Two typical dimensionless chlorine breakthrough curves are shown in Figure 5.3. During displacement of the water in the pulp pad by chlorine water, the non-dimensional chlorine concentration at the reactor outlet increases from zero to a maximum value less than one due to the consumption of chlorine by carbohydrates. Subsequently, C/C_o remains constant for high superficial velocity (u_o = 0.164 cm/s) or decreases after reaching a maximum for the low velocity (u_o = 0.020 cm/s) experiment. The former experiment corresponds to a steady chlorine consumption while in the latter the consumption increases with time. A constant C/C_o after complete breakthrough was obtained for superficial velocities of 0.082 cm/s or at a temperature of 35°C or lower. At room temperature, a constant value C/C_o was obtained at a superficial velocity of 0.041 cm/s. Lower superficial velocities and/or higher temperatures resulted in a gradual decrease of C/C_o after complete breakthrough.

The corresponding total organic carbon breakthrough curves are shown in Figure 5.4. After an initial sharp peak, the low superficial velocity shows a gradual increase in TOC with time, while the TOC stabilizes at a constant value in the high velocity run. The initial TOC peak is caused by reaction of chlorine with a small amount of lignin present in the chlorite treated pulp as will be shown later. The TOC behavior is in agreement with the increased or constant consumption of chlorine after breakthrough in Figure 5.3 after respectively the slow and fast superficial velocity experiments. An increased consumption of chlorine by carbohydrates leads to the formation of more degradation products and hence more total organic carbon in the effluent stream. This effect was more pro-

Figure 5.3 Characterization of chlorine breakthrough curves.

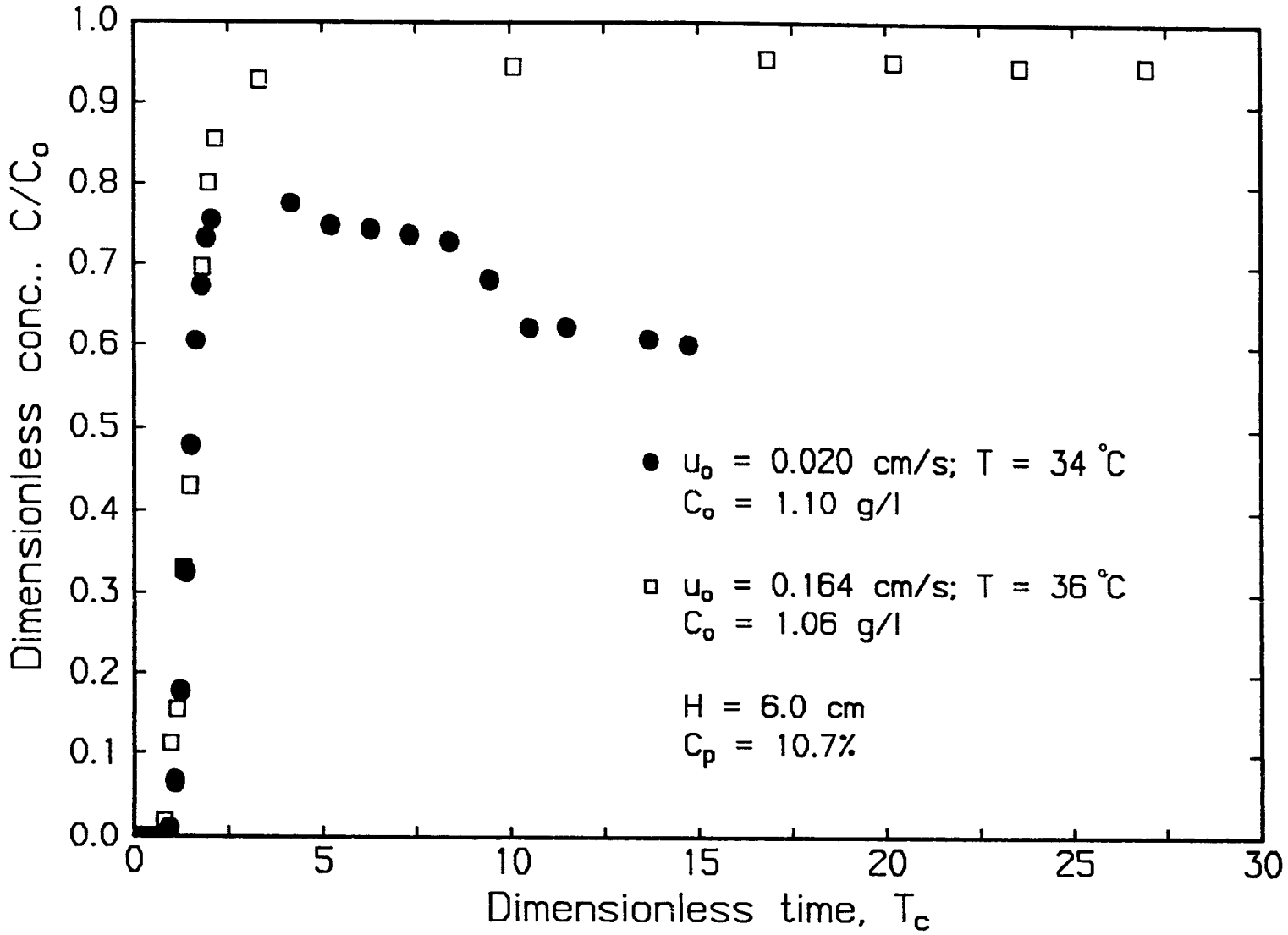
1.0
0.9
0.8
0.7
0.6
0.5
0.4
0.3
0.2
0.1
0.0
Dimensionless conc., C/C$_o$
0
5
10
15
20
25
30
Dimensionless time, T$_c$
u$_o$ = 0.020 cm/s; T = 34 °C
C$_o$ = 1.10 g/l
u$_o$ = 0.164 cm/s; T = 36 °C
C$_o$ = 1.06 g/l
H = 6.0 cm
C$_p$ = 10.7%

Figure 5.4 Characterization of total organic carbon breakthrough curves.

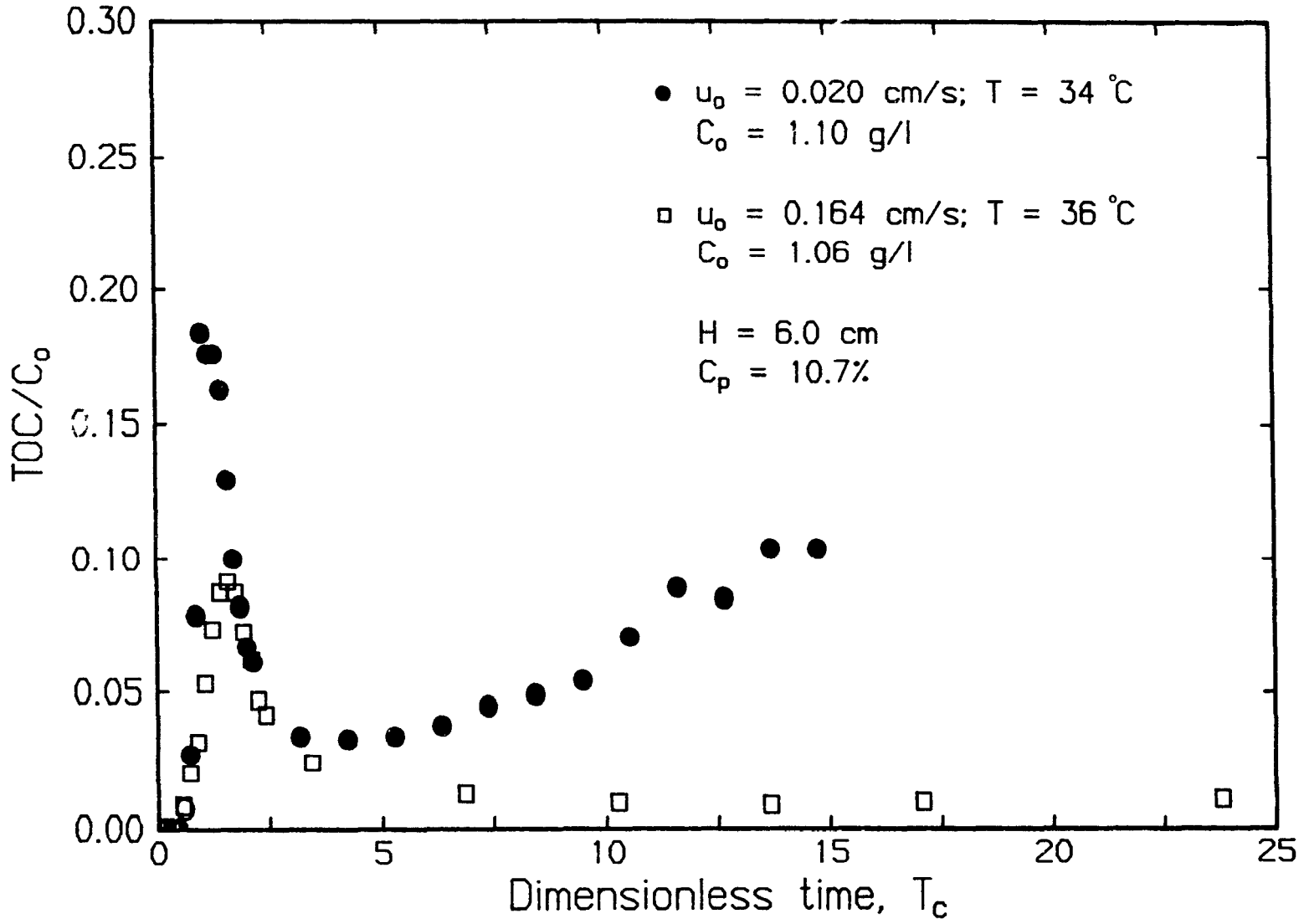
0.30
0.25
0.20
0.15
0.10
0.05
0.00
TOC/C$_o$
0
5
10
15
20
25
Dimensionless time, T$_c$
● u$_o$ = 0.020 cm/s; T = 34 °C
C$_o$ = 1.10 g/l
□ u$_o$ = 0.164 cm/s; T = 36 °C
C$_o$ = 1.06 g/l
H = 6.0 cm
C$_p$ = 10.7%

nounced at the lowest superficial velocity and highest temperature as can be seen in Figure 5.5 for the chlorine breakthrough curve and in Figure 5.6 for the corresponding total organic carbon breakthrough curve. It can also be noted that the onset of the gradual TOC increase coincided with the beginning of the maximum in the chlorine breakthrough curve.

The increasing reactivity between chlorine and carbohydrates, under conditions which favor excessive degradation of carbohydrates, can be explained by the increased chlorine consumption by the increasing number of reducing end groups formed by scission of the cellulose chains. This will be further elaborated on in section 5.6.

5.4 Data reduction techniques

Since the exit chlorine concentration after the initial transient is not always constant, the reaction kinetics were determined using the maximum value of C/C_o, i.e. $(C/C_o)_m$. Because $(C/C_o)_m$ occurs immediately after the initial transient, the derived rate expressions are representative of the initial reaction between chlorine and carbohydrates, i.e. when degradation of the carbohydrates is still modest. In all cases, $(C/C_o)_m$ was corrected for a small chlorine loss due to reaction of chlorine with the walls and piping. This loss was determined by measuring C/C_o at the outlet of the reactor in the absence of a pulp pad. A listing of the average values of C/C_o and standard deviation for different experimental conditions is given in Table 5.2. It shows that the experimental set-up and techniques lead to a decrease in C/C_o of about 0.01 independent of operating conditions. This decrease is accounted for to obtain the chlorine consumption by carbohydrates only.

Figure 5.5 Chlorine breakthrough curves at high temperature and low superficial velocity.

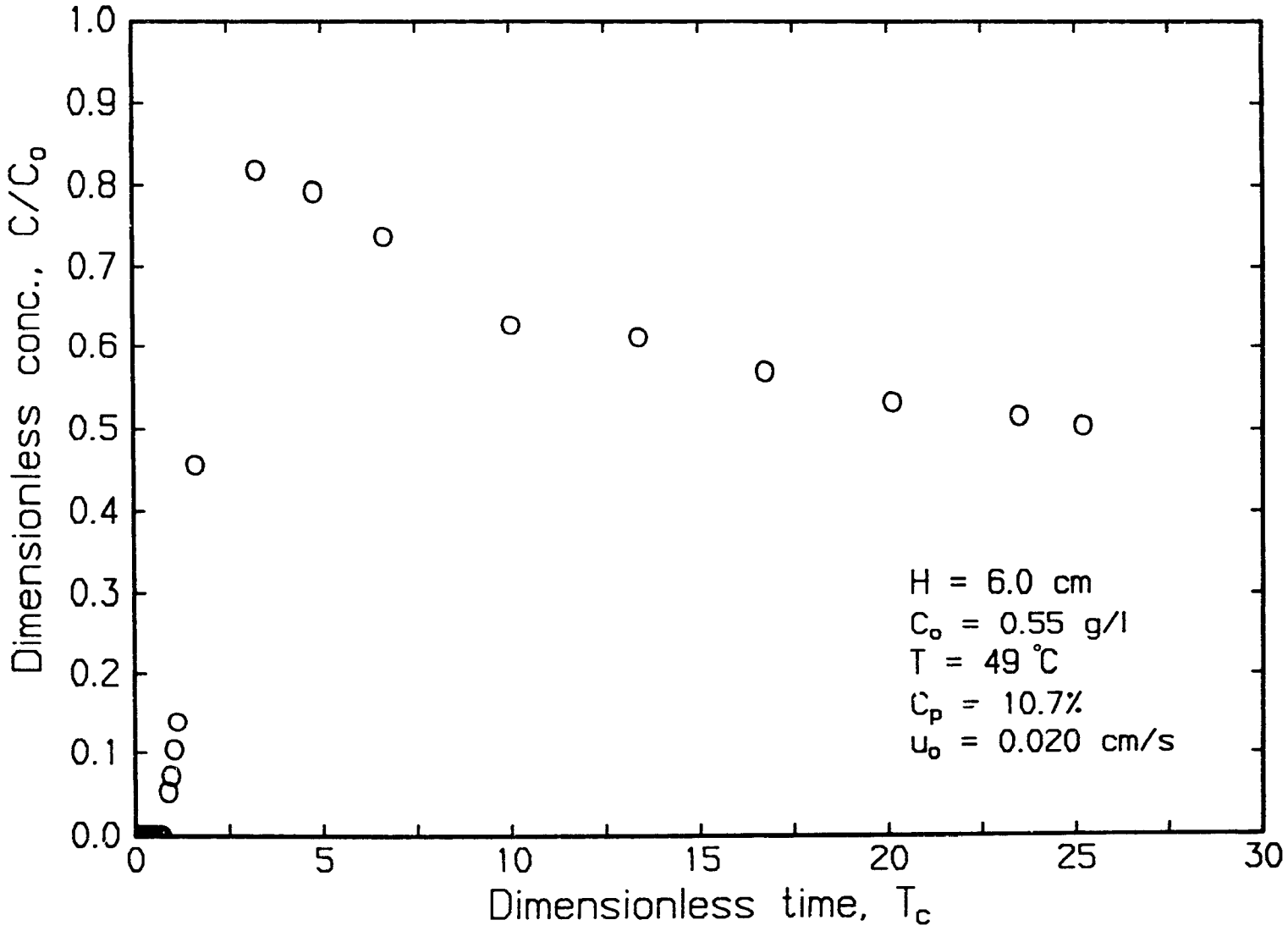
1.0
0.9
0.8
0.7
0.6
0.5
0.4
0.3
0.2
0.1
0.0
Dimensionless conc., C/C$_o$
0
5
10
15
20
25
30
Dimensionless time, T$_c$
H = 6.0 cm
C$_o$ = 0.55 g/l
T = 49 ℃
C$_p$ = 10.7%
u$_o$ = 0.020 cm/s

Figure 5.6 Total organic carbon breakthrough curves at high temperature and low superficial velocity.

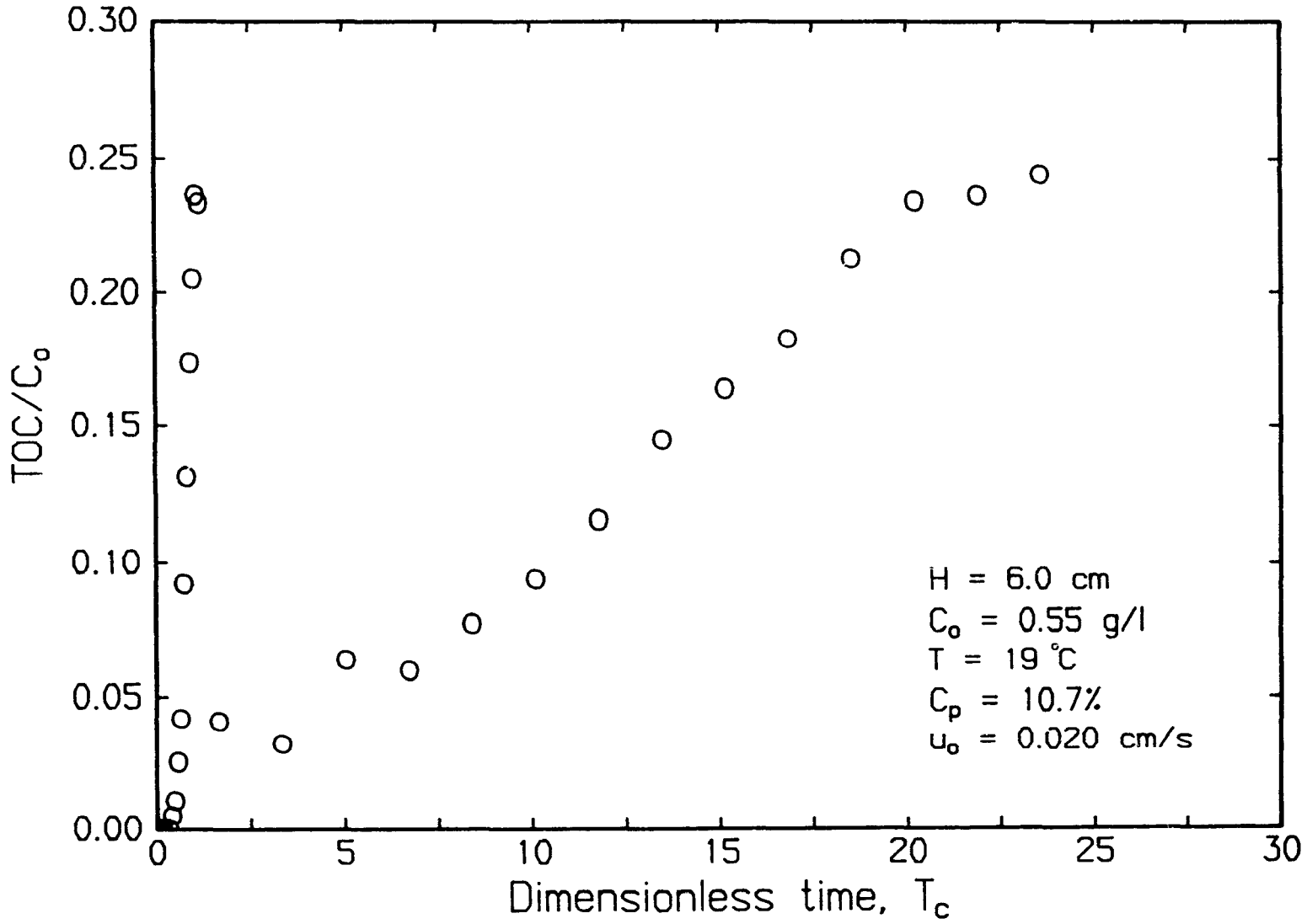
0.30
0.25
0.20
0.15
0.10
0.05
0.00
TOC/C$_o$
0
5
10
15
20
25
30
Dimensionless time, T$_c$
H = 6.0 cm
C$_o$ = 0.55 g/l
T = 19 °C
C$_p$ = 10.7%
u$_o$ = 0.020 cm/s

TABLE 5.2

Determination of chlorine losses in experimental set-up without pulp

u_o (cm/s)	T °C	$[C_o]$ (g/l)	C/C_o Mean	C/C_o Std.Dev.
0.082	19	1.550	0.989	0.0062
0.041	35	0.970	0.991	0.0070
0.041	50	1.200	0.987	0.0071

Assuming plug flow and first order reaction kinetics in chlorine, the relation between the exit chlorine concentration and mean residence time, $\bar{t}_r = H/u_a$, for steady state conditions is given by Levenspiel (5) as

$$k_c \bar{t}_r = \ln(C_o/C) \qquad [5.6]$$

with k_c being the first order reaction constant. Since the changes in exit chlorine concentration after the initial transient are relatively small, the assumption of pseudo steady state is valid in this region of the breakthrough curve.

The assumption of plug flow is also good for the present analysis because the residence time distribution in the pulp pad was characterized by large Peclet numbers, $u_i H/D_L$, ranging from 20.7 to 116.5.

From the slope of $\ln(C_o/C)$ versus $\bar{t}_r$ the reaction constant, k_c, can be determined. For first order reaction kinetics, a single straight line fit should be obtained independent of the inlet chlorine concentration.

5.5 Initial carbohydrates-chlorine kinetics

5.5.1 Influence of pulp types

The chlorination of carbohydrates was studied with two types of pulp to establish the influence of degree of degradation on the reaction kinetics. The majority of experiments were done with unbleached kraft pulp that was subsequently treated with chlorite to remove the residual lignin. The remaining experiments were done with fully bleached CEDED kraft pulp. The carbohydrates in the fully bleached kraft pulp are more degraded than in the chlorite treated kraft pulp.

The chlorine breakthrough curves obtained with the two pulps for the same operating conditions are compared in Figure 5.7. The breakthrough curve of the chlorite treated pulp is shifted slightly to the right of the fully bleached pulp. The associated extra consumption of chlorine can be attributed to reaction with a small amount of lignin still remaining after chlorite treatment. This is confirmed in Figure 5.8 by the sharp initial total organic carbon peak caused by the lignin degradation products when chlorinating chlorite treated pulp.

Further inspection of Figure 5.7 shows $(C/C_o)_m$ of both pulps are very similar. The consumption of chlorine by the fully bleached pulp was however slightly greater than that of the chlorite treated pulp at longer times. This increased chlorine consumption corresponds with a higher total organic carbon in the fully bleached pulp effluent as can be seen from Figure 5.8.

A possible reason for the increased chlorine consumption with fully bleached pulp is that the level of reducing end groups is higher than for chlorite pulp as a result of more severe cellulose chain scission with the former pulp. However, the similar values of $(C/C_o)_m$ obtained for both pulp types under identical operating conditions show that the degree of cellulose degradation associated with conventional pulp bleaching does not significantly influence the kinetics of the initial chlorine-carbohydrates reaction. Therefore $(C/C_o)_m$ obtained with both pulp types will be used in the kinetic analysis.

5.5.2 Influence of chlorine concentration

Continuous chlorination experiments were done for all combinations of two chlorine concentrations (0.55 and 1.10 g/l : ± 0.04%) and four

Figure 5.7 Comparison of chlorine breakthrough curves from chlorite treated and fully bleached pulp under similar operating conditions.

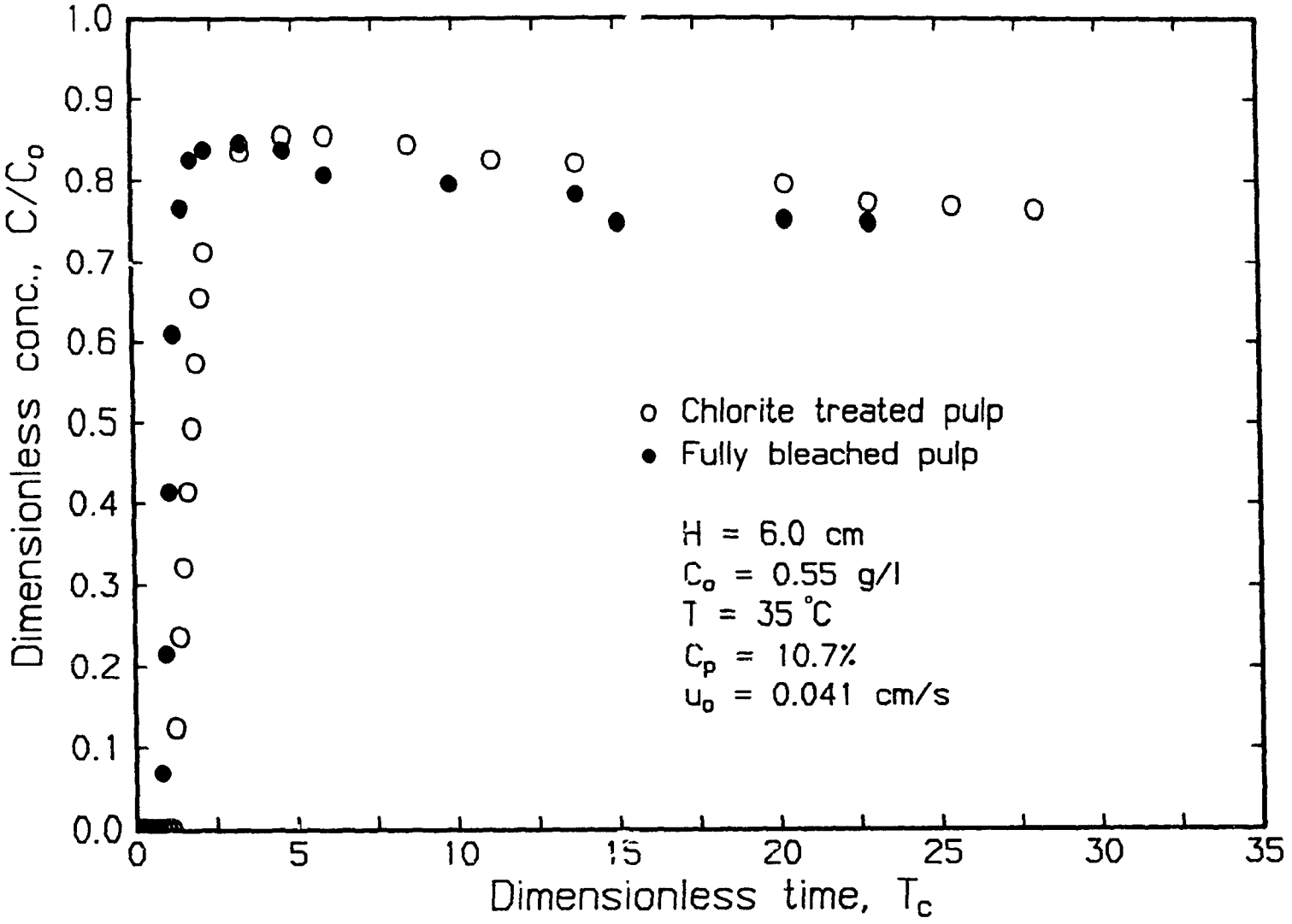
Dimensionless conc., C/C$_o$
Dimensionless time, T$_c$
o Chlorite treated pulp
• Fully bleached pulp
H = 6.0 cm
C$_o$ = 0.55 g/l
T = 35 °C
C$_p$ = 10.7%
u$_o$ = 0.041 cm/s
0.0
0.1
0.2
0.3
0.4
0.5
0.6
0.7
0.8
0.9
1.0
0
5
10
15
20
25
30
35

Figure 5.8 Comparison of total organic carbon breakthrough curves from chlorite treated and fully bleached pulp under similar operating conditions.

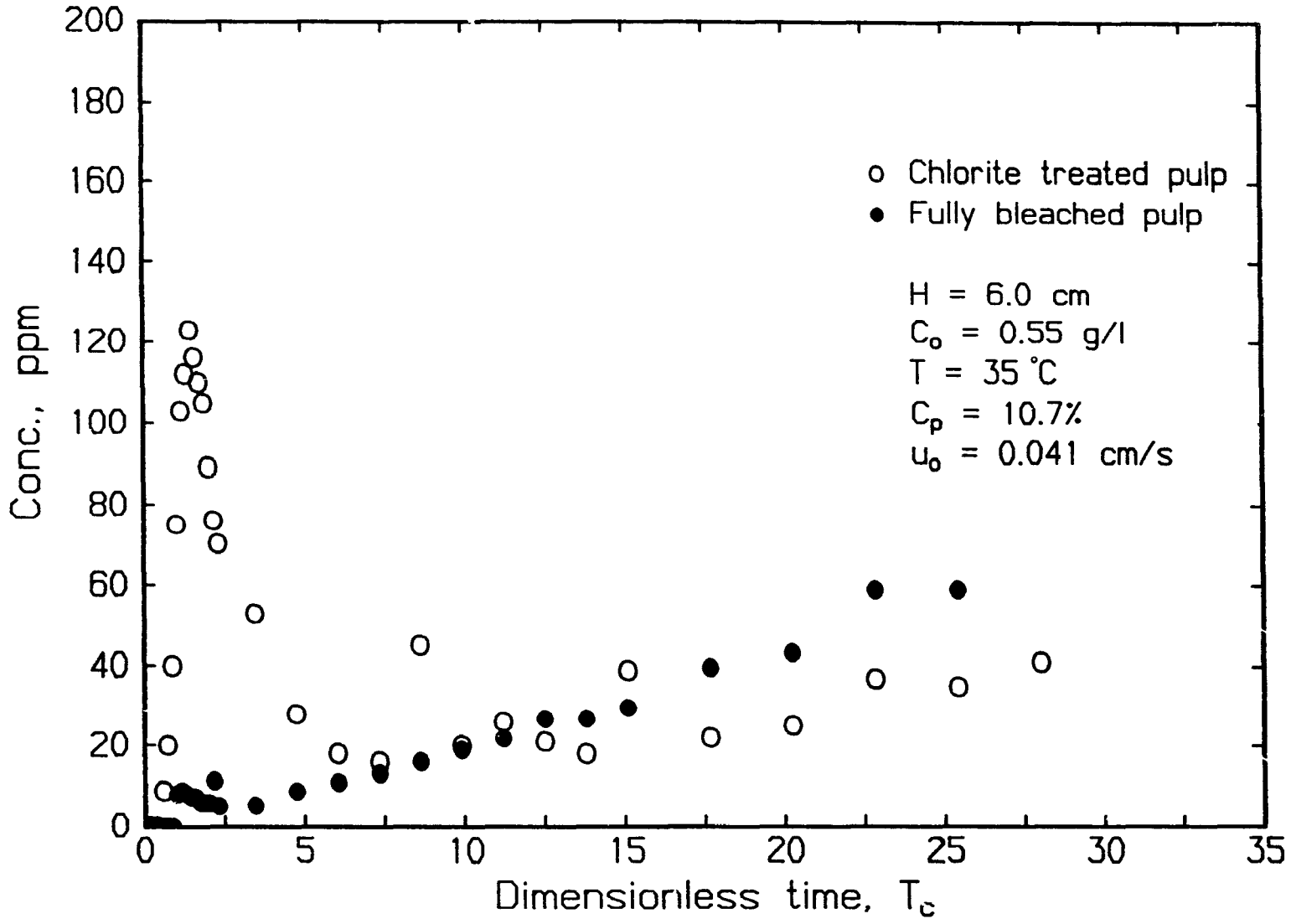
Conc., ppm
Dimensionless time, T_c
o Chlorite treated pulp
• Fully bleached pulp
H = 6.0 cm
C_o = 0.55 g/l
T = 35 °C
C_p = 10.7%
u_o = 0.041 cm/s
0
20
40
60
80
100
120
140
160
180
200
0
5
10
15
20
25
30
35

superficial velocities (u_o = 0.020, 0.041, 0.082 and 0.164 cm/s). In addition, two experiments were done at the high chlorine concentration of 2.20 g/l and superficial velocities 0.041 and 0.082 cm/s. The temperature was maintained at 35°C in all cases.

First order kinetics in chlorine was tested by plotting $\ln(C_o/C)_m$ versus mean residence time, H/u_a, as shown in Figure 5.9. The data points were fitted to the following linear regression equation:

$$\ln[C_o/C] = 0.001214\ \bar{t}_r \qquad [5.7]$$

The good single straight line fit to the data obtained for different values of C_o proves that the chlorine-carbohydrates reaction is first order in chlorine, with the rate constant, k_c, being 0.001214 s^{-1} at 35°C.

5.5.3 Influence of temperature

The dependence of the initial chlorination rate on temperature was investigated by performing additional experiments at 19 and 50°C. Shown in Figure 5.10 is a graph similar to Figure 5.9 for the three temperature levels. The rate constants obtained from linear regression at the three temperature levels studied are shown in Table 5.3. The activation energy was determined by an Arrhenius plot of ln (k_c) versus ln(1/T) as shown in Figure 5.11. From the slope of a straight line fitted through the data points an activation energy of 57 kJ/mole was obtained.

Thus the rate expression for the initial chlorine-carbohydrates reaction can be represented as:

$$-d[Cl_2]/dt = (5.948*10^6)\cdot\exp(-57{,}136/RT)\cdot [CL_2] \qquad [5.8]$$

Figure 5.9 Influence of residence time and chlorine concentration on initial chlorine-carbohydrates reaction.

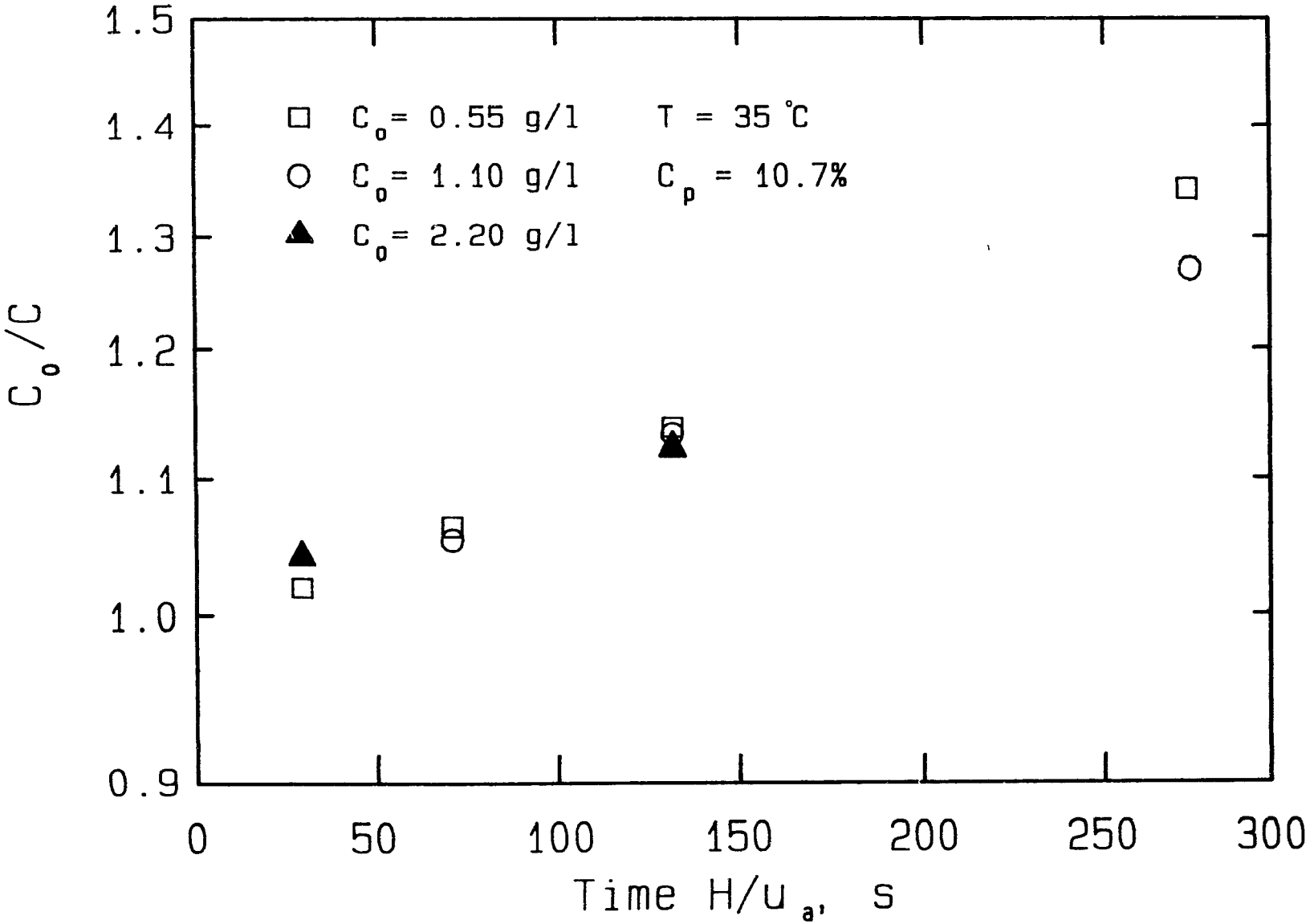
1.5
1.4
1.3
1.2
1.1
1.0
0.9
C_o/C
C_o= 0.55 g/l
C_o= 1.10 g/l
C_o= 2.20 g/l
T = 35 °C
C_p = 10.7%
0
50
100
150
200
250
300
Time H/u_a, s

Figure 5.10 Dependence of the first order chlorine-carbohydrates reaction on temperature.

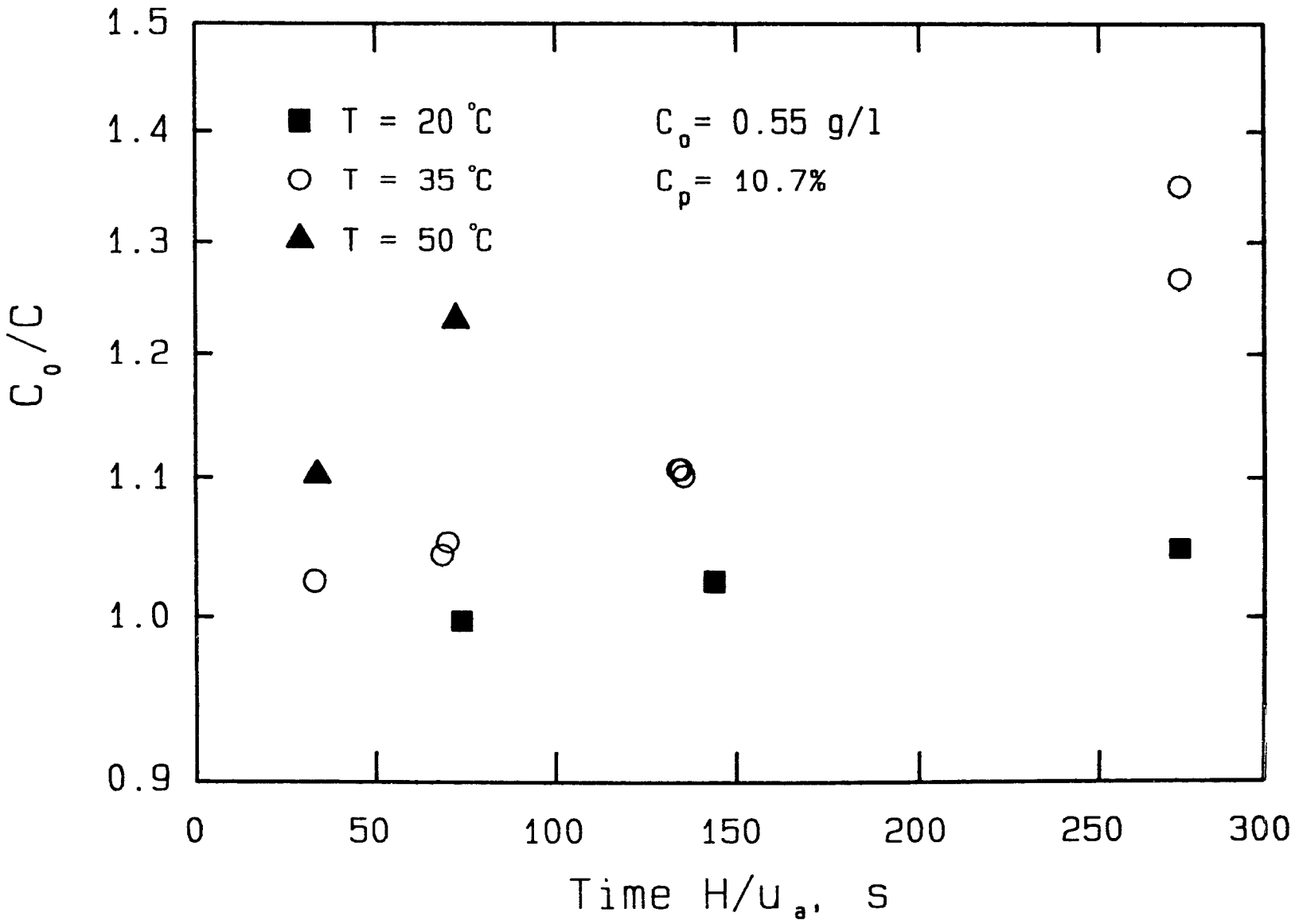
1.5
1.4
1.3
1.2
1.1
1.0
0.9
C_o/C
T = 20 °C
T = 35 °C
T = 50 °C
C_o = 0.55 g/l
C_p = 10.7%
0
50
100
150
200
250
300
Time H/u_a, s

TABLE 5.3

Influence of temperature on rate constant of initial chlorine carbohydrate reaction

T (°C)	k_c (s^{-1})
19	0.000314
35	0.001214
50	0.003130

Figure 5.11 Arrhenius dependence of the first order chlorine-carbohydrates reaction.

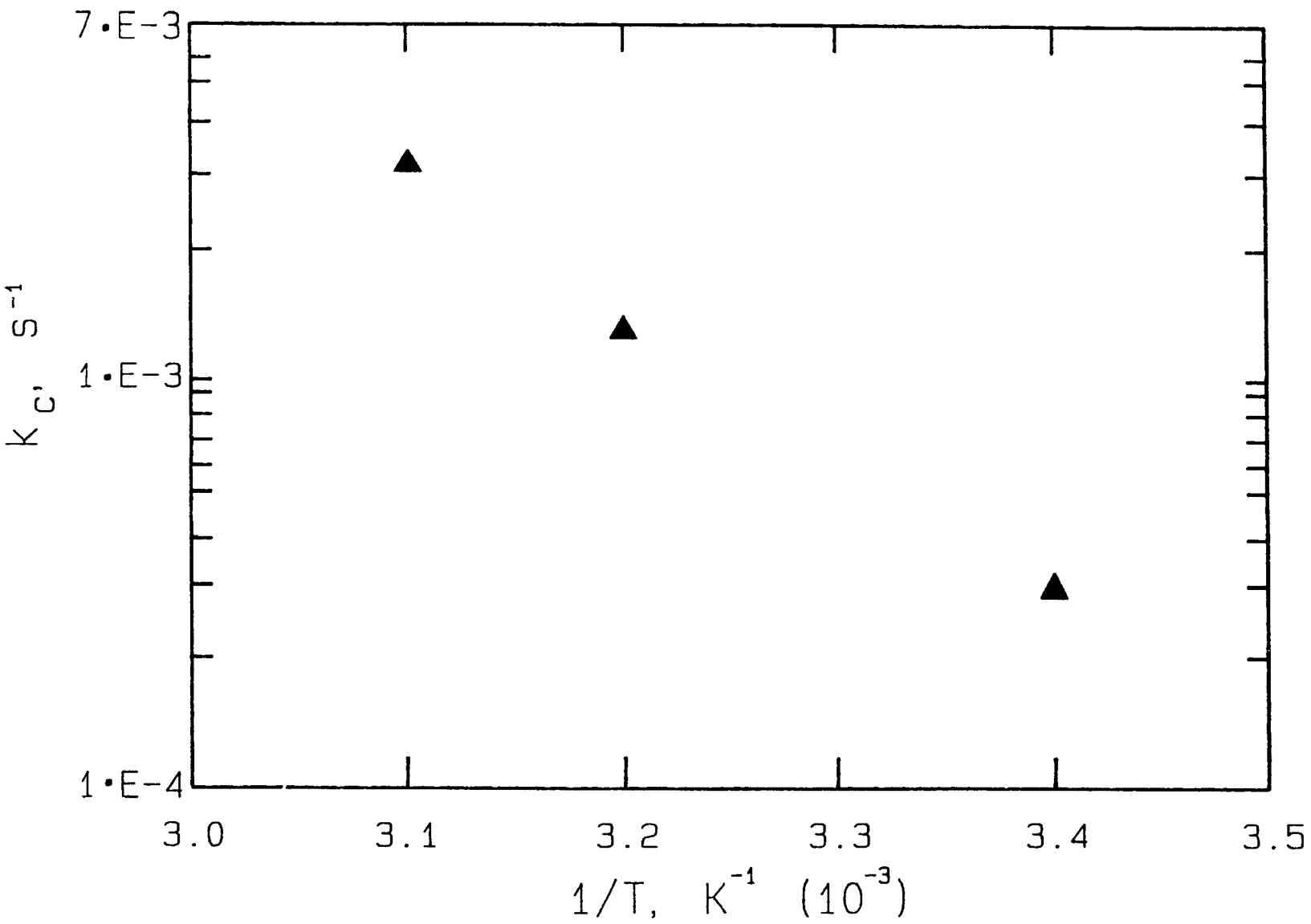
7•E-3
1•E-3
1•E-4
$K_{C'}$, S^{-1}
3.0
3.1
3.2
3.3
3.4
3.5
1/T, K^{-1} (10^{-3})

with R = 8.324 J/mole and t and T expressed in seconds and degrees Kelvin, respectively.

5.6 General discussion

It was shown that the kinetics of the initial reaction between chlorine and bleached pulp are first order in chlorine. A review of the literature showed no previously published studies between chlorine and bleached pulp. Fredricks et al. (1), however, also proposed a first order reaction kinetics for the radical reaction between chlorine and a model cellulose compound. This radical reaction was shown (2) to be the dominant chlorination reaction for cellulose powder. Therefore it is likely that the initial reaction between chlorine and fully bleached pulp also proceeds via a free radical mechanism.

The chlorine consumption by fully bleached pulp increases considerably after this initial period when the mean residence time and reaction temperature are high. This behavior could be explained by assuming that two reactions between chlorine and carbohydrates occur. The dominant reaction during the initial period is chain scission of the polysaccharide polymers due to attack on glycosidic bonds by chlorine. The dominant reaction during the final period is between chlorine and the reducing end of the polysaccharide chains. Initially the degree of polymerization of the polysaccharide chains is very large so that the number of reducing ends is very small compared to the number of glycosidic bonds. As a result the reaction between chlorine and the reducing ends can initially be neglected. However after considerable carbohydrate degradation this reaction eventually becomes more important than the chain scission reaction. This explains the substantial increase in chlorine consumption in

the final period under conditions which favor excessive degradation of the carbohydrates. The proposed reactions could also explain the increase in TOC (Figure 5.4) in the final period when the mean residence time and temperature are relatively high. Under these conditions the carbohydrates are severely degraded so that carbohydrate chains of a relatively small degree of polymerization become soluble and are detected in TOC. Finally, the chain scission reaction can explain that the rate of chlorine consumption by carbohydrates under relatively mild conditions remains constant over the entire chlorination experiment. In this case the number of glycosidic bonds is approximately constant because the degree of polymerization remains large, even through the degree of polymerization might be reduced considerably over the course of the reaction. This mechanism forms the basis for analysis in Chapter 6 of the pulp viscosity data obtained after continuous chlorination of kraft pulp.

The initial chlorine-carbohydrates reaction kinetics will be used for analysis and prediction of the breakthrough curves obtained during dynamic chlorination of kraft pulp in Chapters 6 and 7, respectively. The present kinetics cannot be used for regular batch chlorination of kraft pulp because of the presence in the batch process of dissolved lignin, which acts as a free radical scavenger. This also explains why carbohydrate degradation in continuous chlorination of kraft pulp is much more severe than in batch chlorination.

5.6 Conclusions

1. The kinetics of the initial reaction between chlorine and carbohydrates in dynamic chlorination are first order in chlorine. The activation energy of the reaction is 57k J/mol. It is likely that the

dominant reaction during the initial period is chain scission due to attack on glycosidic bonds by chlorine and proceeds via a free radical mechanism.

2. When the residence time and reaction temperature are high in dynamic chlorination, the rate of reaction of chlorine with carbohydrates increases considerably after the initial period. It is suggested that the increased chlorine consumption is due to the increasing importance of a proposed reaction between chlorine and the reducing end of polysaccharide chains.

REFERENCES

1. Fredricks, P.S., Lindgren, B.O. and Theander, O., Svensk Papperstidning, 74 (19), 597, (1971).

2. Fredricks, P.S., Cellulose Chem. Technol., 4 (5), 533, (1971)

3. Fredricks, P.S., Tappi, 54 (1), 87, (1971)

4. Theander, O., Tappi, 48 (2), 105, (1965)

5. Levenspiel, O., "Chemical Reaction Engineering", John Wiley and Sons Inc., 1972.

CHAPTER 6

DYNAMIC CHLORINATION OF KRAFT PULP: EXPERIMENTAL RESULTS.

6.1 Introduction

The bleaching sequence which follows the pulping operation serves to remove the remaining lignin from the pulp. Removal of the residual lignin leads to large increases in whiteness and brightness of the pulp. Chlorination is usually the first step in the bleaching sequence and is responsible for removal of most of the residual lignin. The subsequent stages in the bleaching sequence are primarily for brightening. The first step in chlorination normally consist of contacting the pulp suspension with chlorine gas in a mixer in order to achieve dissolution in and uniform distribution of chlorine within the pulp suspension. The pulp suspension then flows through a chlorination tower with mean residence time of 45 minutes to allow the chlorination process to be completed. There is no relative motion between the chlorine-water and the pulp fibers.

In 1962 Rapson (1) introduced the concept of "displacement" or "dynamic" bleaching whereby a bleaching solution was forced through a fixed bed of pulp fibers. Increased bleaching rates were observed. Subsequent studies primarily by Kamyr and Gullichsen (2) led to the development of a compact bleach plant with a medium consistency chlorination step followed by displacement extraction and bleaching steps. In medium consistency chlorination, a 11-14% consistency pulp suspension is mixed with chlorine and some chlorine dioxide in a medium consistency mixer external to a single or two bleaching tower(s). The contact time between chlorine and the pulp suspension is generally 3-7 minutes, Gullichsen (3). The following displacement steps i.e. caustic extraction and chlorine dioxide treatments are performed in one displacement bleach tower. Displacement of one chemical by the next eliminates the intermediate washing stage that

is characteristic of conventional bleaching.

A fundamental chemical reaction engineering study of dynamic bleaching has never been reported. The few studies in the literature (2,4) were limited to important practical aspects like pulp properties, chemical consumption and contact time. However a breakthrough curve of bleaching chemical has never been published except in a numerical study by Baldus and Edwards (5). An understanding of the bleaching chemical breakthrough curve in terms of bleaching reaction kinetics, fluid flow and transport processes might lead to improved operation and design of the present processes. Also determination of the still controversial location of the rate determining steps (Pugliese and McDonough (6), Berry and Fleming (7), Anderson and Rapson (1) Russel (8), Koch (9) and Ackert (4)) may result in identification of more efficient bleaching reactors or sequences.

In the present study, dynamic chlorination rather than dynamic bleaching with chlorine dioxide is investigated because of the relative ease of chemical analysis and handling of chlorine and its reaction products. A chlorine-water solution was forced through a packed bed of kraft Black Spruce fibers. Breakthrough curves of chlorine, total inorganic chloride (chlorine plus chloride), TOC and methanol are measured as a function of mean residence time, residence time distribution (RTD) of the flow, chlorine feed concentration, temperature, pulp consistency and addition of viscosity protection agents. Pulp properties such as kappa number, lignin content and viscosity were determined at the end of an experiment. The results are analysed in terms of residence time distribution measured for each pulp pad (Chapter 4), and kinetics and stoichiome-

try of the chlorine-lignin and chlorine carbohydrates (Chapter 5) reactions.

The effect of varying experimental conditions will be presented separately for the chlorine, total inorganic chloride, TOC and methanol breakthrough curves and for the pulp properties. This order allows uninterrupted development of the theories and discussion of the results for each of the four variables.

6.2 Experimental and data reduction techniques

6.2.1 Experimental

The dynamic chlorination reactor is shown in Figure 6.1. A pulp pad is formed between the stationary lower plate and the adjustable upper plunger of the reactor. Chlorine water is forced through the pulp pad at pre-determined flowrates, concentration and temperatures. In all cases step-up stimulus response experiments with glucose as inert tracer preceded the actual chlorination runs to determine the RTD for each pulp pad.

Samples were collected throughout the chlorination experiment at the exit of the reactor and analysed for chlorine, total inorganic chloride, TOC, and in some cases lignin, carbohydrates and methanol. Handsheets were made of the chlorinated and subsequently thoroughly water washed (or CW) pulp. A portion of the handsheets was analysed for its Klason and UV lignin content and in some cases for chloride content. The remainder of the CW pulp handsheets was extracted with sodium hydroxide and the resulting CWE pulp analysed for UV and Klason lignin content, kappa number, viscosity and chloride content. A detailed description of the complete experimental facility and experimental procedures can be found in chapter 3.

Figure 6.1 Schematic of chlorination reactor.

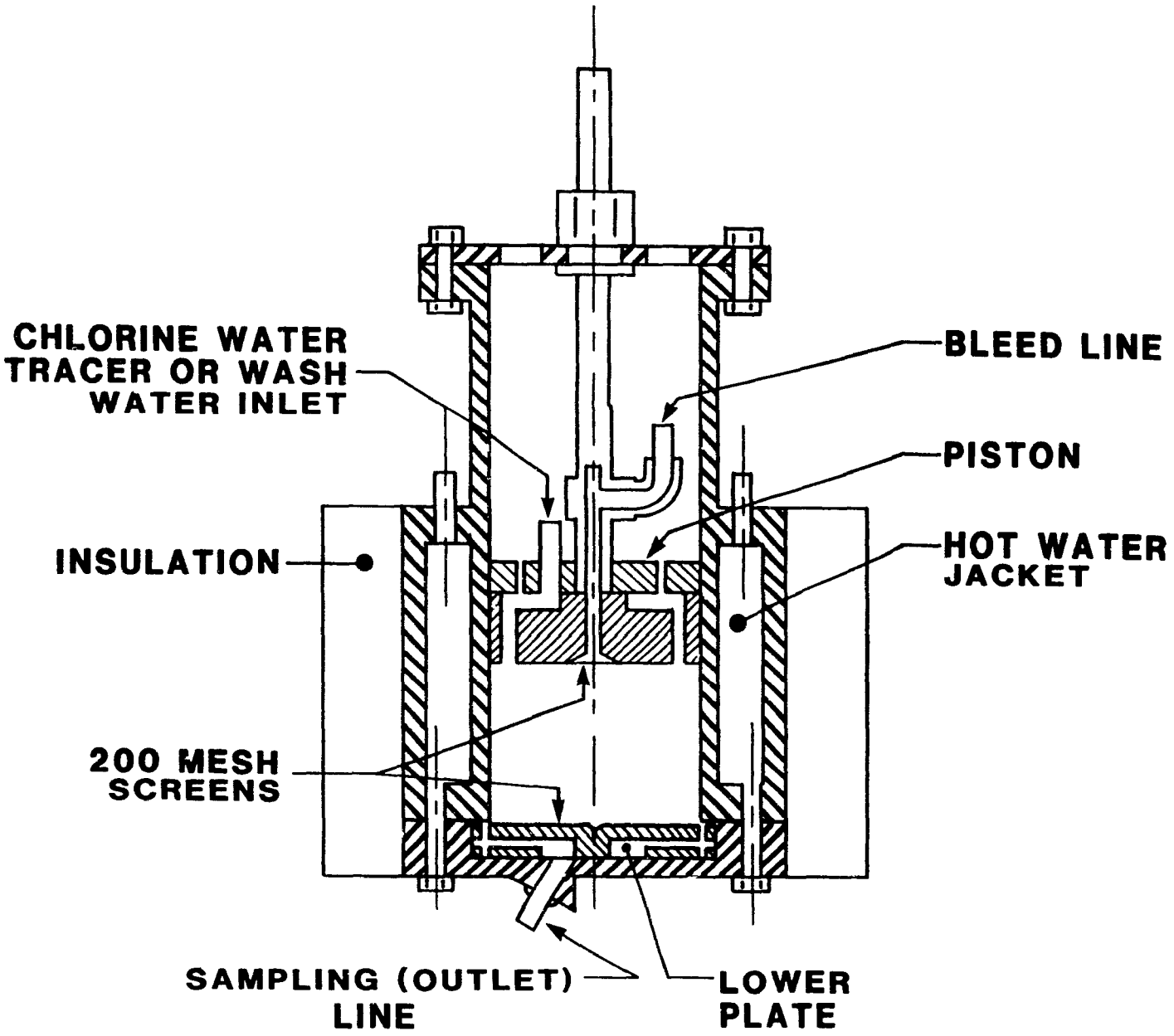
CHLORINE WATER
TRACER OR WASH
WATER INLET
BLEED LINE
PISTON
INSULATION
HOT WATER
JACKET
200 MESH
SCREENS
SAMPLING (OUTLET)
LINE
LOWER
PLATE

The kappa number and viscosity of the unbleached Black Spruce kraft pulp used in this study were 29.5 and 38 mPa.s respectively. A complete summary of the properties of the pulp is given in Appendix 3-1.

6.2.2 Data reduction

The residence time distribution (RTD) of each pulp pad was well characterised by the average residence time, $\bar{t}_r$, and the Peclet number, P, of the axial dispersed plug flow model (11). The moment technique used to determine these flow parameters is described in detail in Chapter 4.

The chlorine, total inorganic chloride and TOC concentration versus time for a typical experiment are shown in Figure 6.2. The time t is the time at the midpoint of the sampling interval while t_c is defined as t minus the "dead time" resulting from the volume, V_c, of 20 cm^3 between the bottom of the pulp pad and the sampling point. The average residence time is defined as

$$\bar{t}_r = H/u_a = H\varepsilon_a/u_o \qquad [6.1]$$

where u_a and u_o are, respectively, the superficial velocities based on the accessible liquid volume and the total empty volume of the reactor. The accessible bed porosity, ε_a, is obtained from $\bar{t}_r$ using equation 6.1. Implicit in the calculation of ε_a is the assumption that chlorine and glucose have access to the same inter and intra fiber pore volume. Evidence for the latter assumption is given in Chapters 4 and 7. In Chapter 4 it is shown by the solute-exclusion technique that glucose has access to the total intra-fiber pore volume. In Chapter 7 it is shown that the chlorine breakthrough curve for fully bleached pulp is well predicted when chlorine has access to the same pore volume as glucose. Finally, it

Figure 6.2 Chlorine, total inorganic chloride and TOC breakthrough curves of a typical experiment.

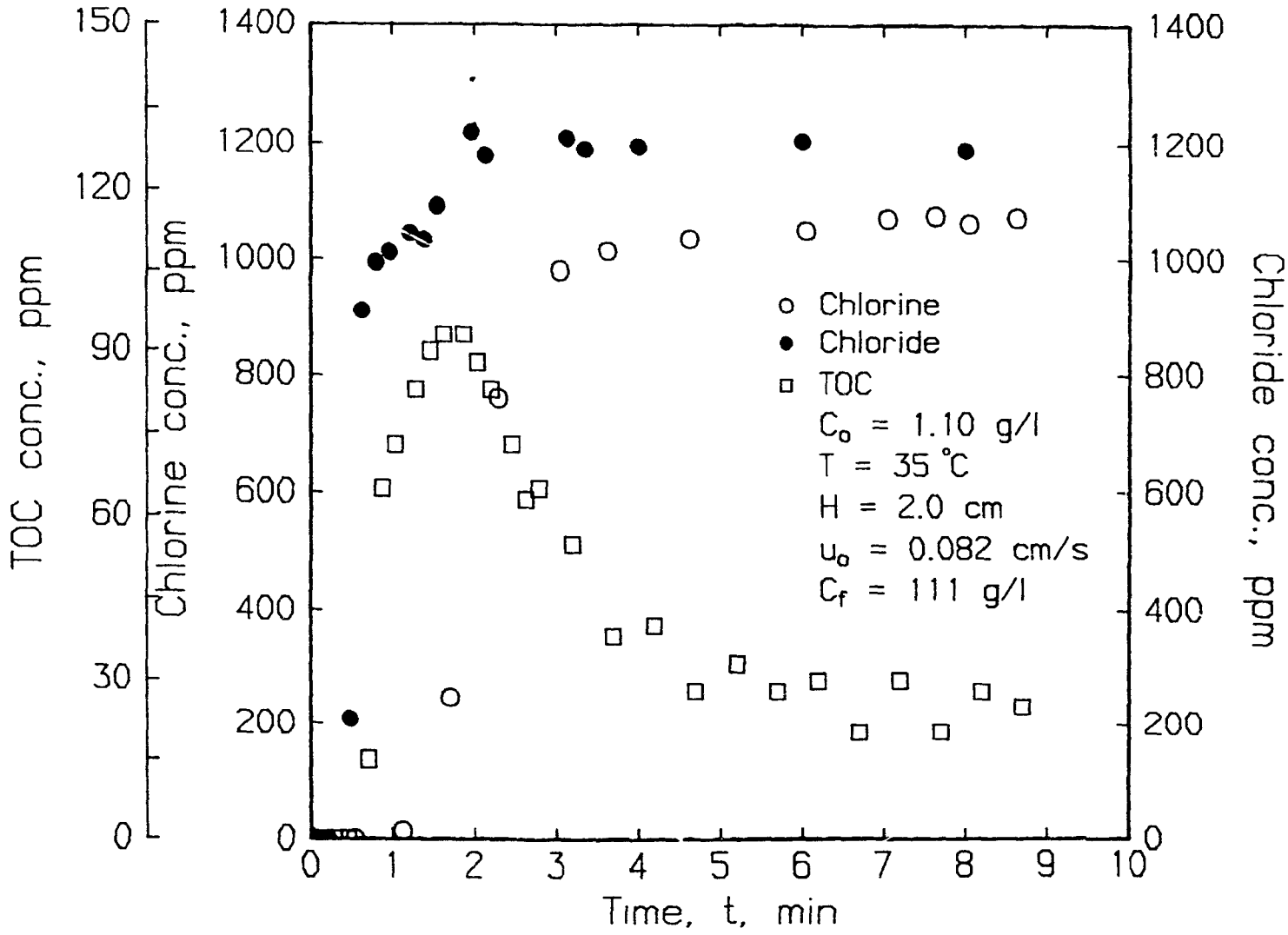
TOC conc., ppm
Chlorine conc., ppm
Chloride conc., ppm
Time, t, min
Chlorine
Chloride
TOC
C_o = 1.10 g/l
T = 35 °C
H = 2.0 cm
u_o = 0.082 cm/s
C_f = 111 g/l

should be noticed that the hydrodynamic diameters of chlorine and glucose are of the same order, 2.9 and 6.5 Å, respectively, (Appendix 6-1).

The concentrations in Figure 6.2 are non-dimensionalized by the inlet chlorine concentration, C_o, and plotted versus dimensionless time $T_c = t_c/\bar{t}_r = t_c u_a/H$ in Figure 6.3. The C/C_o values of the total inorganic chloride breakthrough curve are greater than 1 due to the presence of excess chloride in the feed. A more general form of the dimensionless breakthrough curves is obtained when T_c is replaced by the ratio of grams of chlorine emerging from the bed per gram of lignin initially present in the bed, or $(T_c-1)C_o\varepsilon_a/(L_oC_f)$, where L_o is the initial lignin content (g/g pulp) and C_f is the pulp concentration (g pulp/liter suspension). The corrected dimensionless time is reduced by 1 since changes at the inlet are only felt at the exit of the reactor after displacement of water initially present in the pulp pad. This correction may result in breakthrough at negative values of $(T_c-1)C_o\varepsilon_a/L_oC_f$ when the dispersion is high and the chlorine feed concentration is large. The data in Figure 6.3 is plotted against $(T_c-1)C_o\varepsilon_a/(L_oC_f)$ in Figure 6.4.

Additional data reduction procedures will be presented separately for each type of breakthrough curve later in this chapter. For example the calculation method for the chlorine-lignin stoichiometric ratio, SL_o, the fraction of chlorine in the lignin-chlorine reaction used for substitution, S, and the methanol-lignin stoichiometric ratio, R, will be outlined when discussing, respectively, the chlorine, total inorganic chloride and methanol breakthrough curves. In all cases these calculations are based on representation of the pulp pad by a series of parallel plug flow

Figure 6.3 Dimensionless chlorine, total inorganic chloride and TOC breakthrough curves of a typical experiment.

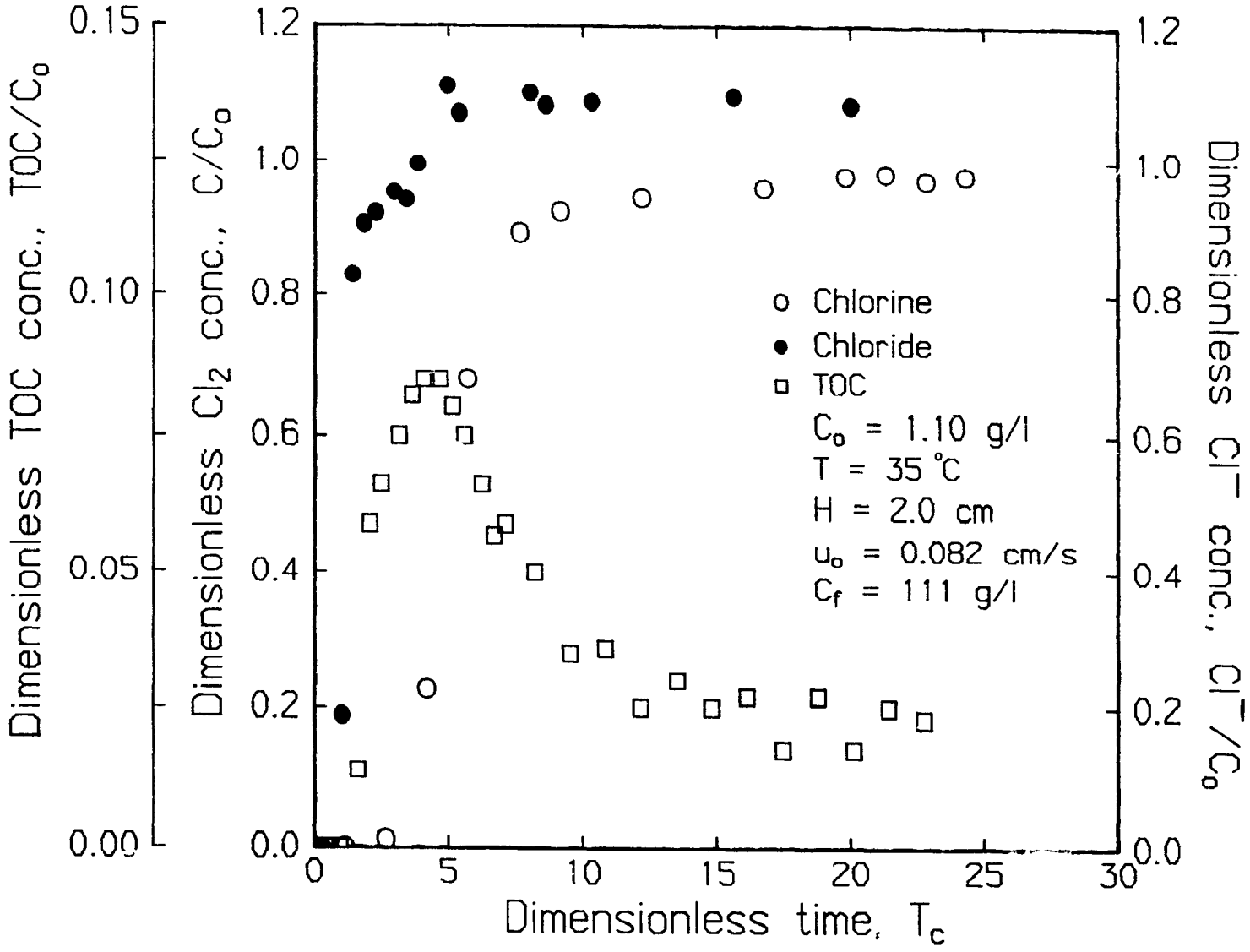
Dimensionless TOC conc., TOC/C$_o$
Dimensionless Cl$_2$ conc., C/C$_o$
Dimensionless Cl$^-$ conc., Cl$^-$/C$_o$
Dimensionless time, T$_c$
0.15
0.10
0.05
0.00
1.2
1.0
0.8
0.6
0.4
0.2
0.0
0
5
10
15
20
25
30
Chlorine
Chloride
TOC
C$_o$ = 1.10 g/l
T = 35 °C
H = 2.0 cm
u$_o$ = 0.082 cm/s
C$_f$ = 111 g/l

Figure 6.4 General dimensionless breakthrough curves of a typical experiment.

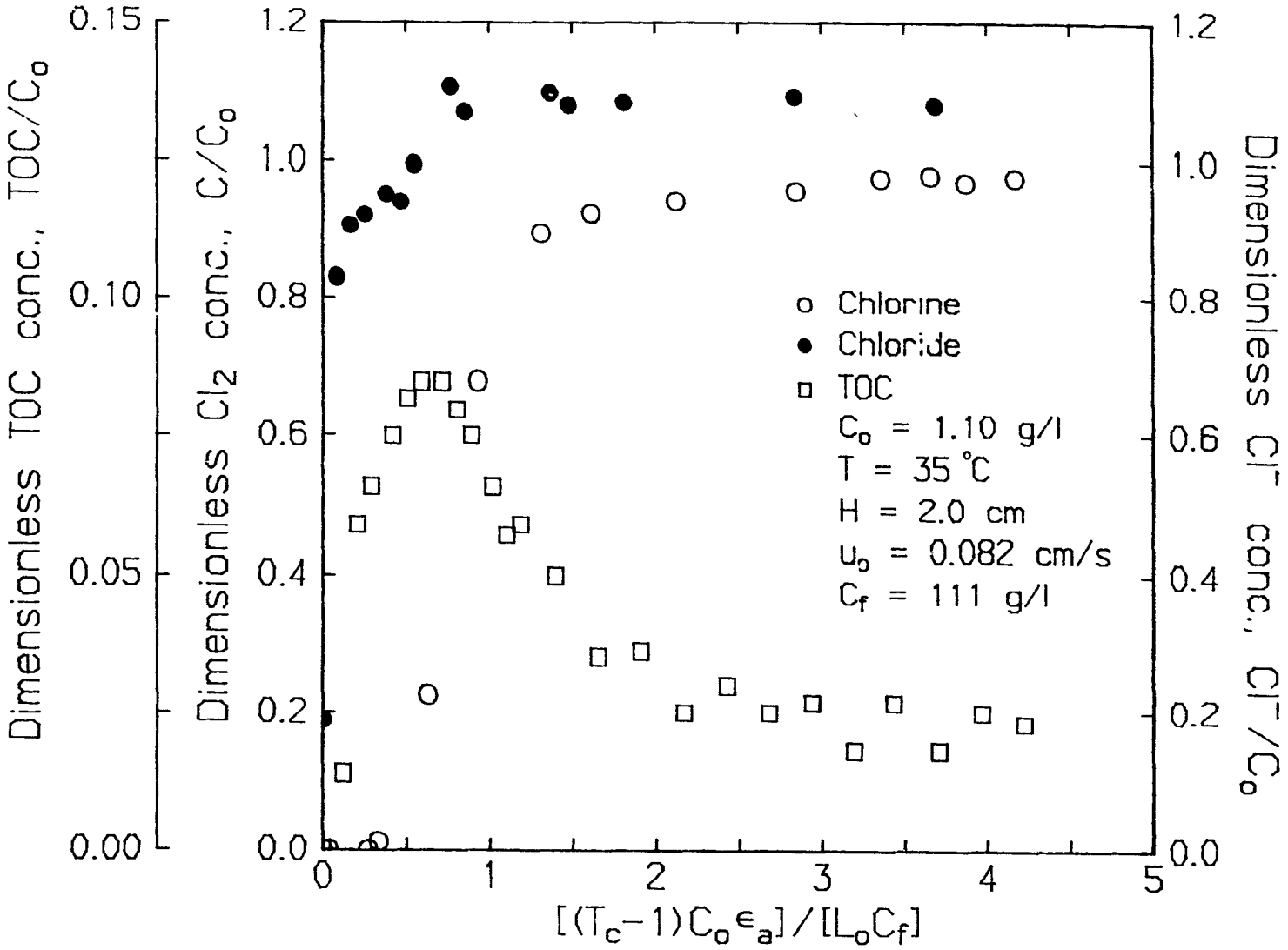
Dimensionless TOC conc., TOC/C$_o$
Dimensionless Cl$_2$ conc., C/C$_o$
Dimensionless Cl$^-$ conc., Cl$^-$/C$_o$
[(T$_c$−1)C$_o$ε$_a$]/[L$_o$C$_f$]
0.15
0.10
0.05
0.00
1.2
1.0
0.8
0.6
0.4
0.2
0.0
0
1
2
3
4
5
Chlorine
Chloride
TOC
C$_o$ = 1.10 g/l
T = 35 °C
H = 2.0 cm
u$_o$ = 0.082 cm/s
C$_f$ = 111 g/l

channels (chapter 4).

6.3 Overall mass balances

6.3.1 Chlorine

During a chlorination experiment, the chlorine concentration in the effluent stream increases while the chloride concentration decreases. In addition some chlorine is chemically bound to lignin remaining in the pulp and to water soluble lignin fragments removed during chlorination. The weight percent of chlorine in the CW pulp was determined by the Schöniger combustion flask method. The chloride removed with the water soluble lignin was calculated from the TOC removed assuming a Cl/C_9 ratio of 1.0. Finally, the total inorganic chloride (sum of chlorine and chloride) in the inter and intra fiber voids in the pulp pad was calculated assuming a linear variation in total inorganic chloride concentration between the inlet and exit of the bed.

The sum of the weight of chlorine in the various forms discussed above were compared to the total amount of inorganic chloride fed to the reactor. The difference between these values were generally less than 5%.

6.3.2 Lignin

The lignin mass balance can be checked by comparing the lignin in the unbleached pulp with the lignin remaining in the CW pulp and dissolved in the bleach effluent. The lignin content in the CW pulp was determined as UV and Klason lignin by standard methods. Soluble lignin in wash liquor after pulping has been quantitatively determined by colorimetry with a Technicon AutoAnalyser (11). Attempts to use this technique for the present bleaching liquor were not successful due to difficulties in

finding a reliable calibration standard. Therefore the lignin content in the effluent stream was determined indirectly from the TOC measurements. The TOC consists of solubilized fragments and degradation products of the chlorine-lignin and chlorine-carbohydrates reactions. The contribution of the carbohydrates fraction to the TOC is very small for chlorination experiments at room temperature and short residence times, as will be shown later. For these operating conditions the carbohydrates contribution can be neglected and TOC can be converted to lignin concentration in mg/l as

$$\text{lignin} = [\text{TOC}/J] \qquad [6.2]$$

where J is the weight fraction of carbon in the original kraft lignin. According to Kempf and Dence (16) the structural formula of milled Kraft lignin is:

$$C_{8.86}\,H_{8.06}\,O_{2.88}\,S_{0.05}\,(OCH_3)_{0.96}\,(CO)_{0.13} \qquad [6.3]$$

The fraction J calculated from the above formula was 0.615. With this indirect method the closure of the lignin balance is shown in Table 6.1 for a wide range of experimental conditions. The lower exit lignin content could be attributed to the J value being too high i.e. if J is assumed to be 0.5 the lignin balance will be much closer.

6.4 Reproducibility

The reproducibility was checked for a number of duplicate experiments. Differences in Peclet number are inevitable since each experiment required the formation of a new pulp pad. To minimize the influence of

TABLE 6.1

Lignin mass balance

H,cm	u_o,cm/s	T,°C	C_o,g/l	C_p,%	in,mg	out,mg	% diff.
2	0.041	35	0.55	10.7	460	426	-7.4
4	0.041	35	0.55	10.7	918	982	+6.9
6	0.082	35	0.55	10.7	1378	1070	-22.4
4	0.082	35	1.10	10.7	918	875	+4.7
2	0.082	35	1.10	10.7	465	350	-24.7
6	0.082	17	1.10	10.7	1390	1154	-17.0
6	0.082	17	0.55	10.7	1385	1144	-17.4

pad formation on reproducibility, a pair of duplicate experiments was selected with similar RTD's as can be seen in Figure 6.5.

The chlorine, total inorganic chloride and TOC breakthrough curves for the duplicate experiments are shown in Figures 6.6, 6.7 and 6.8 respectively. The CW and CWE pulp properties for the two experiments are listed in Table 6.2. The close agreement between the breakthrough curves and pulp properties demonstrate the good reproducibility of the experimental techniques and procedures.

6.5 Results and Discussion

6.5.1 Chlorine breakthrough curves

6.5.1.1 Effect of mean residence time

The mean residence time, $\bar{t}_r = H/u_a$, was varied from 23 to 279 seconds by changing the pad height, H, from 2, 4 to 6 cm and the superficial velocity, u_o, from 0.020, 0.041 to 0.082 cm/s. Shown in Figure 6.9 are typical real time chlorine breakthrough curves for variable $\bar{t}_r$ of 23, 45 and 93 seconds at fixed pad height of 2 cm, T = 35°C and C_o = 1.10 g/l. The accessible pad porosity, ε_a was 0.93 for all three experiments. As expected chlorine breakthrough occurs earlier for smaller $\bar{t}_r$. Also higher mean residence times result in lower dimensionless chlorine concentrations at complete breakthrough, C_m/C_o. These C_m/C_o values are in good agreement with the chlorine-carbohydrates kinetics given by equation 5.8 as can be seen from the broken lines in the top right hand corner of Figure 6.9. This is further confirmed in Table 6.3 where C_m/C_o is compared with C/C_o calculated with equation 5.8 for a wide range of mean residence times. The good agreement establishes that all reactive lignin is consumed at complete breakthrough or that further reaction between remaining lignin

Figure 6.5 Duplicate glucose breakthrough curves.

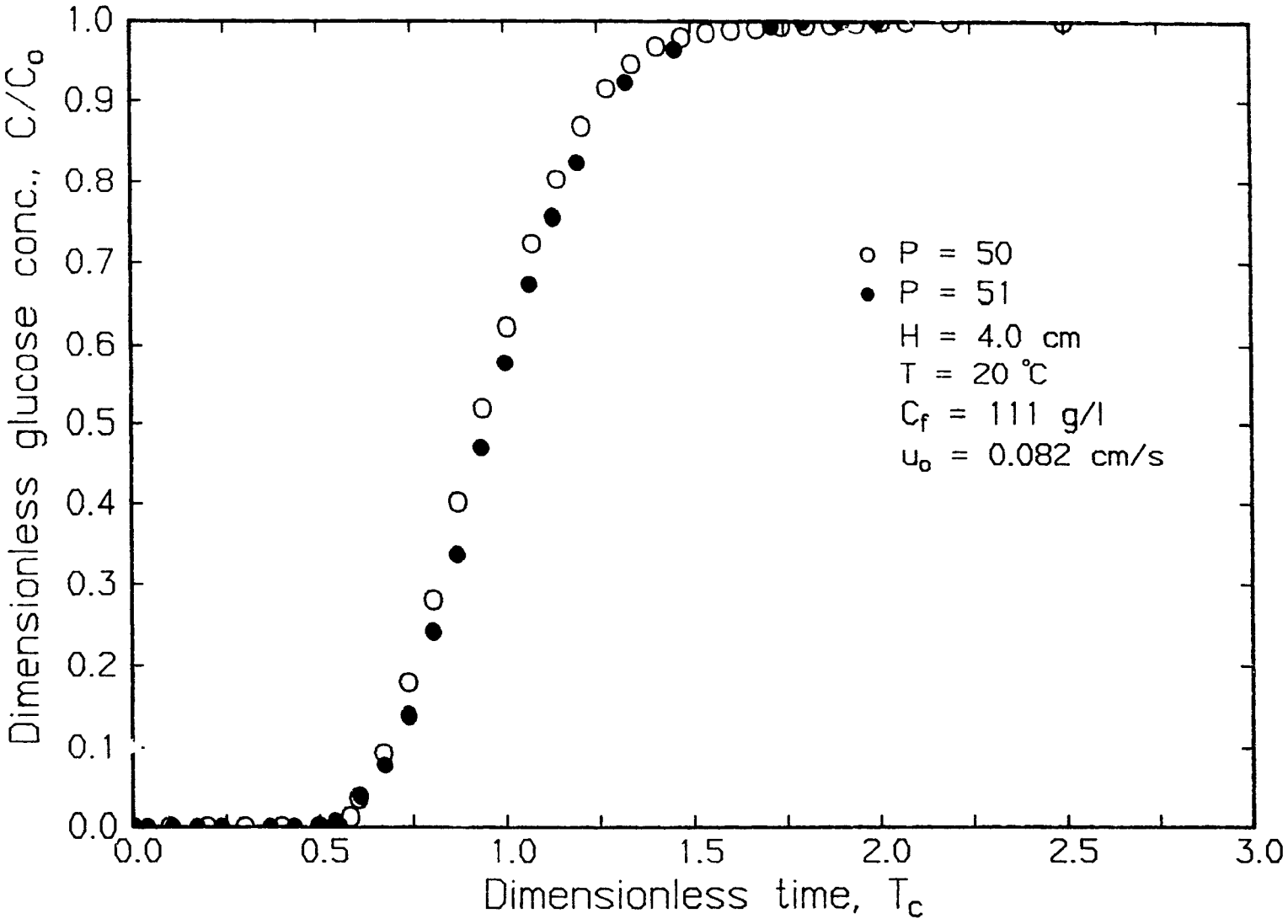
Dimensionless glucose conc., C/C$_o$
1.0
0.9
0.8
0.7
0.6
0.5
0.4
0.3
0.2
0.1
0.0
0.0
0.5
1.0
1.5
2.0
2.5
3.0
Dimensionless time, T$_c$
o P = 50
• P = 51
H = 4.0 cm
T = 20 ℃
C$_f$ = 111 g/l
u$_o$ = 0.082 cm/s

Figure 6.6 Duplicate chlorine breakthrough curves.

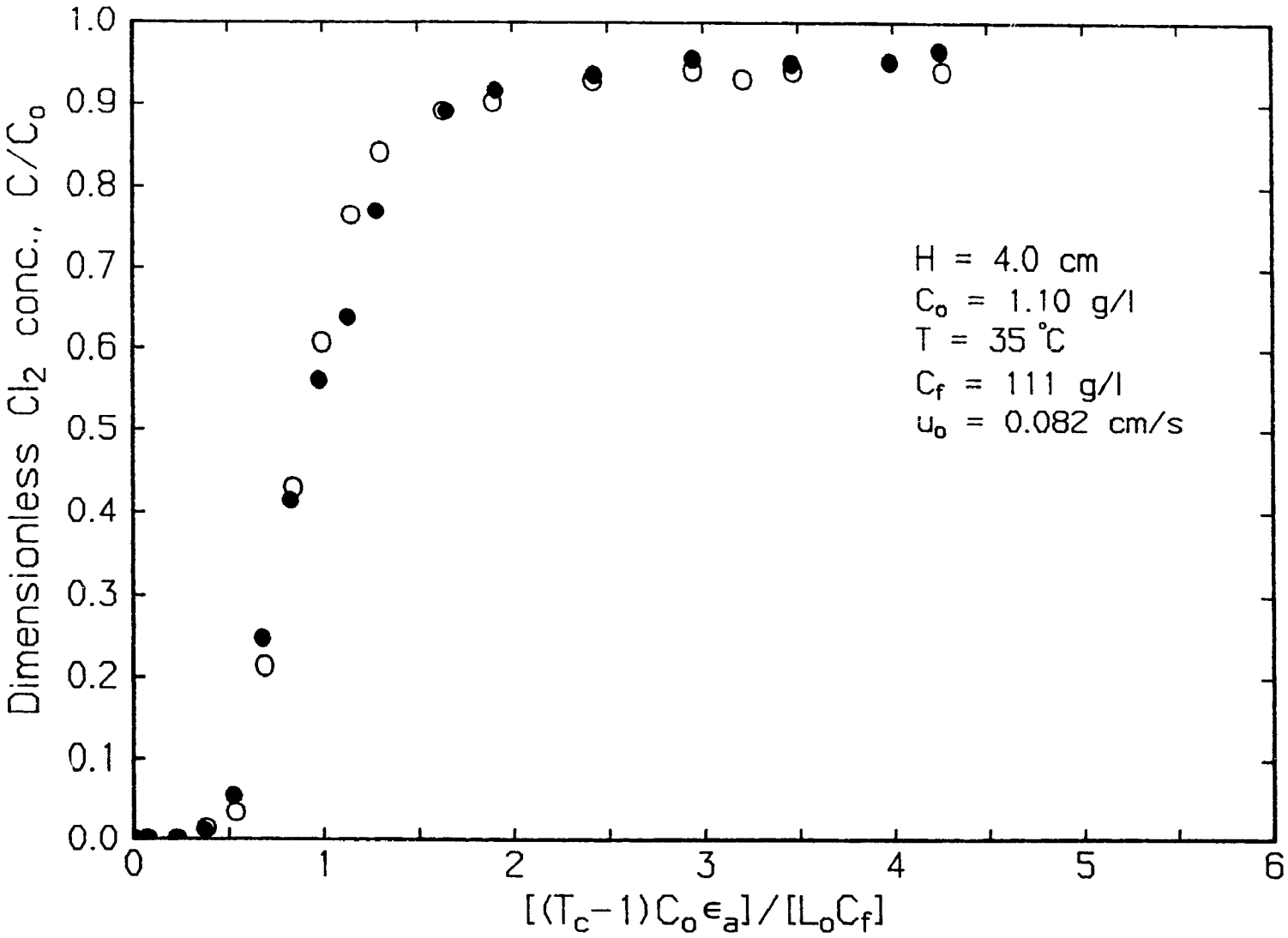
Dimensionless Cl_2 conc., C/C_o
1.0
0.9
0.8
0.7
0.6
0.5
0.4
0.3
0.2
0.1
0.0
0
1
2
3
4
5
6
$[(T_c-1)C_o\epsilon_a]/[L_oC_f]$
H = 4.0 cm
C_o = 1.10 g/l
T = 35 °C
C_f = 111 g/l
u_o = 0.082 cm/s

Figure 6.7 Duplicate TOC breakthrough curves.

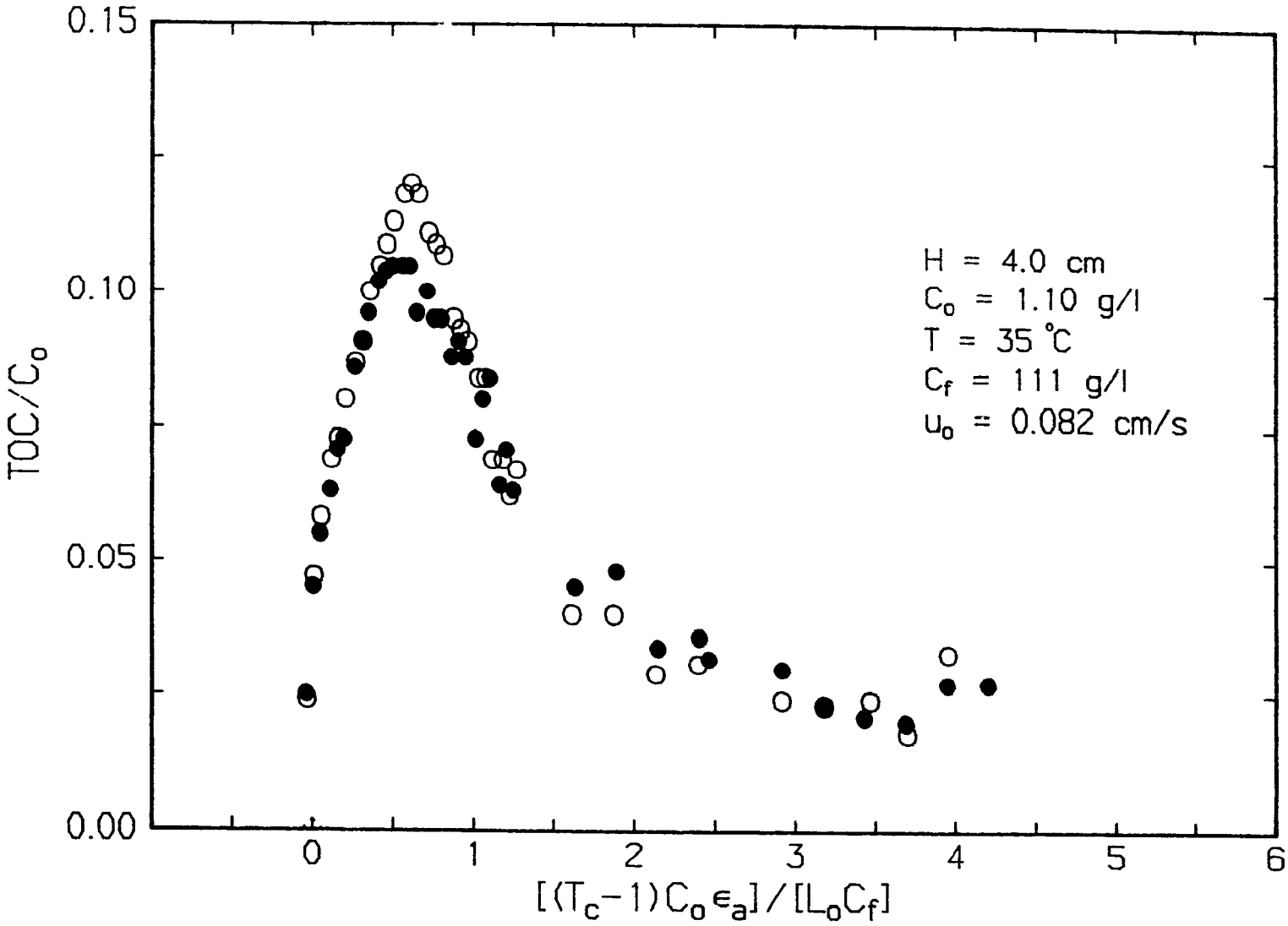
0.15
0.10
0.05
0.00
TOC/C$_o$
0
1
2
3
4
5
6
[(T$_c$−1)C$_o$ε$_a$]/[L$_o$C$_f$]
H = 4.0 cm
C$_o$ = 1.10 g/l
T = 35 °C
C$_f$ = 111 g/l
u$_o$ = 0.082 cm/s

Figure 6.8 Duplicate total inorganic chloride breakthrough curves.

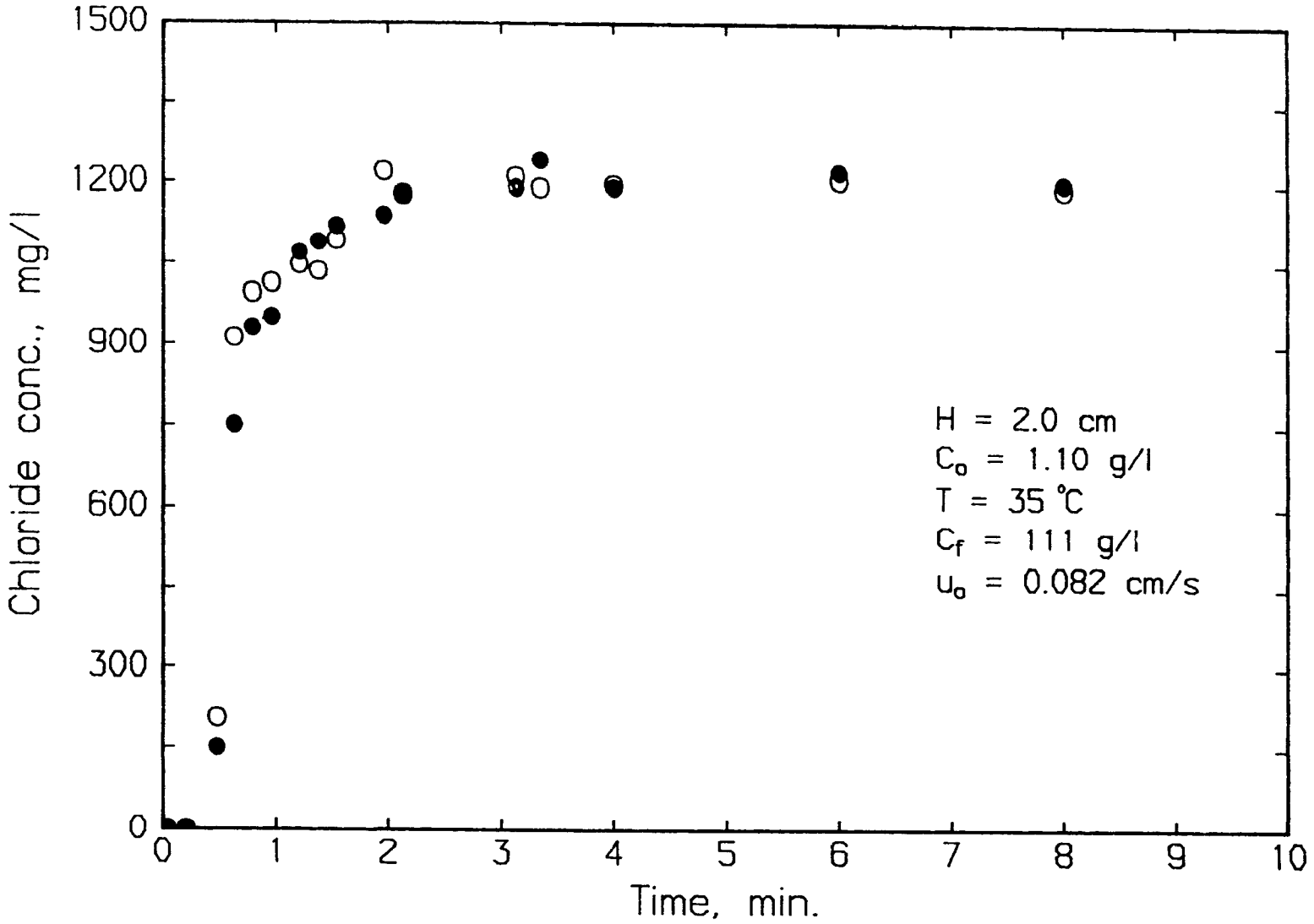
1500
1200
900
600
300
0
Chloride conc., mg/l
0
1
2
3
4
5
6
7
8
9
10
Time, min.
H = 2.0 cm
C_o = 1.10 g/l
T = 35 °C
C_f = 111 g/l
u_o = 0.082 cm/s

TABLE 6.2

Pulp properties of duplicate experiments

expt.	CW pulp		CWE pulp		
	Lignin %	Klason Lignin %	Lignin %	Klason Lignin %	Kappa
1	1.15	1.91	0,49	0.34	2.90
2	1.02	1.80	0.46	0.37	3.49

Figure 6.9 Effect of mean residence time, $\bar{t}_r$, on chlorine breakthrough curves; variable u_o at fixed H.

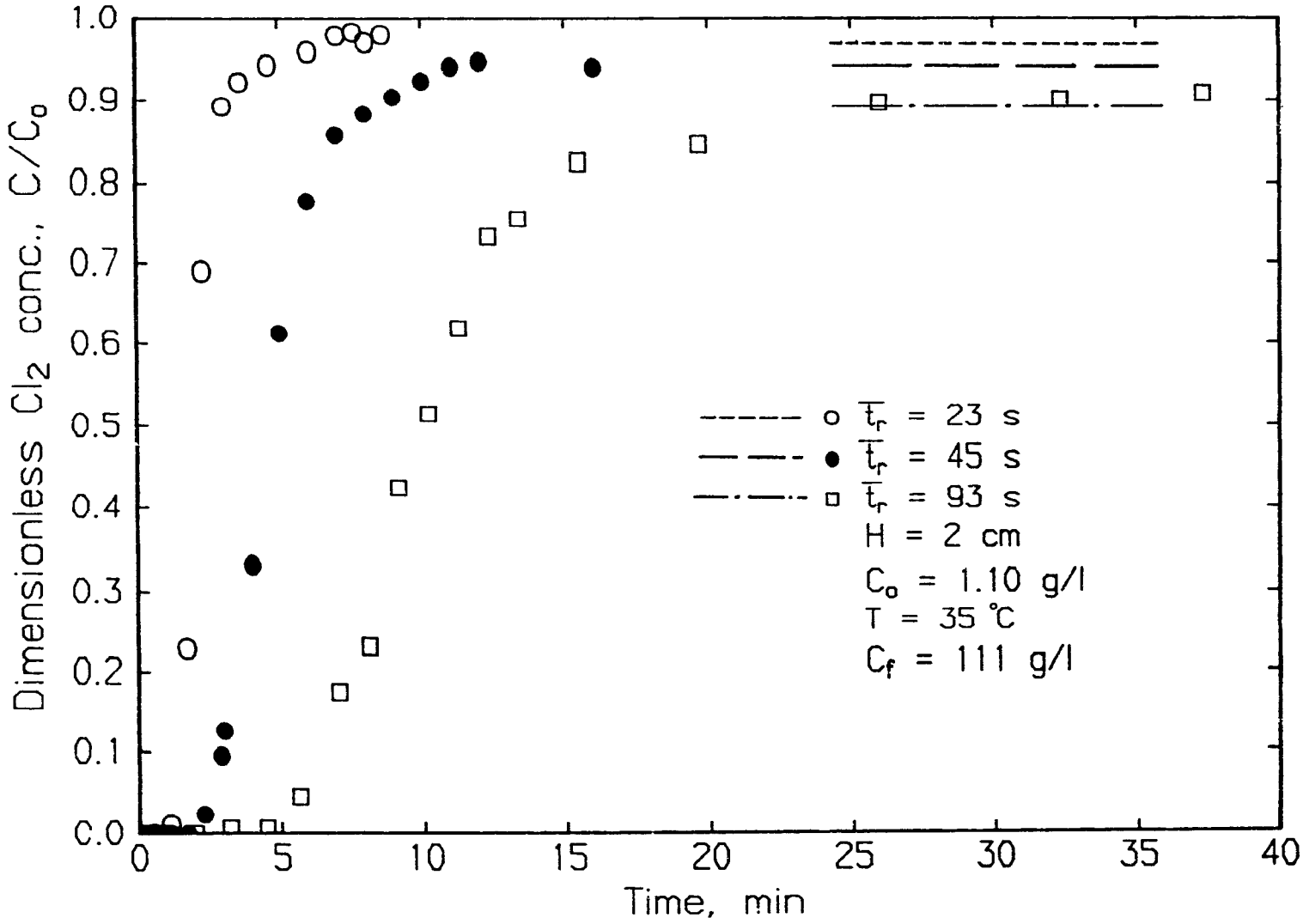
Dimensionless Cl_2 conc., C/C_o
1.0
0.9
0.8
0.7
0.6
0.5
0.4
0.3
0.2
0.1
0.0
0
5
10
15
20
25
30
35
40
Time, min
o $\bar{t}_r$ = 23 s
● $\bar{t}_r$ = 45 s
□ $\bar{t}_r$ = 93 s
H = 2 cm
C_o = 1.10 g/l
T = 35 °C
C_f = 111 g/l

TABLE 6.3

Comparison of C_m/C_o with C/C_o calculated from kinetics of the reaction between chlorine and carbohydrates (equation 5.8)

C_o (g/l)	T (°C)	C_p (%)	$\bar{t}_r$ (s)	(C_m/C_o)expt.	(C/C_o)theor.
0.55	35	10.7	93	0.90	0.89
0.55	35	10.7	45	0.93	0.95
0.55	35	10.7	23	0.96	0.97
0.55	35	10.7	186	0.82	0.80
0.55	35	10.7	90	0.91	0.90
0.55	35	10.7	46	0.92	0.95
0.55	35	10.7	279	0.73	0.71
0.55	35	10.7	136	0.86	0.85
0.55	35	10.7	68	0.91	0.92
1.10	35	10.7	93	0.91	0.89
1.10	35	10.7	45	0.95	0.95
1.10	35	10.7	23	0.97	0.97
1.10	35	10.7	186	0.84	0.80
1.10	35	10.7	90	0.92	0.90
1.10	35	10.7	46	0.96	0.95
1.10	35	10.7	279	0.72	0.71
1.10	35	10.7	136	0.85	0.85
1.10	35	10.7	68	0.93	0.92

and chlorine is slow compared to the chlorine-carbohydrates reaction.

The chlorine breakthrough curves of Figure 6.9 are reduced to dimensionless plots in Figure 6.10. Although the differences between the three breakthrough curves are now much smaller, the experiments with the larger average residence times are still slightly shifted to the right. This can be partly explained by the relative larger consumption of chlorine by carbohydrates at higher $\bar{t}_r$.

For the effect of mean residence time on the consumption of chlorine by lignin alone the results must be corrected for the chlorine-carbohydrates reaction. This was done by representing the pulp pad by a series of parallel plug flow channels, with the distribution of the total flow over the channels given by the RTD obtained from a glucose tracer experiment. Strong evidence for this representation was presented in Chapter 4. Also it is assumed that the reaction between chlorine and lignin is instantaneous while the chlorine-carbohydrate reactions are described by the kinetics given in Chapter 5.

The reason for selecting an instantaneous reaction is that the initial reaction rate between chlorine and lignin is very high. For example at room temperature and otherwise commercial bleaching conditions about 70% of the chlorine is consumed in 12 seconds (Liebergott et al (12)), while at higher temperatures 90-98% of the reaction occurs within 30 seconds (Singh (13)). Since these times are small compared to the present chlorine breakthrough times which are in the order of several minutes the assumption of an instantaneous reaction between chlorine and lignin seems reasonable. It is noteworthy that this assumption was also successfully used by Patterson and Kerekes (14) to predict the progression

Figure 6.10 Effect of mean residence time $\bar{t}_r$ on generalized chlorine breakthrough curves, variable u_o at fixed H.

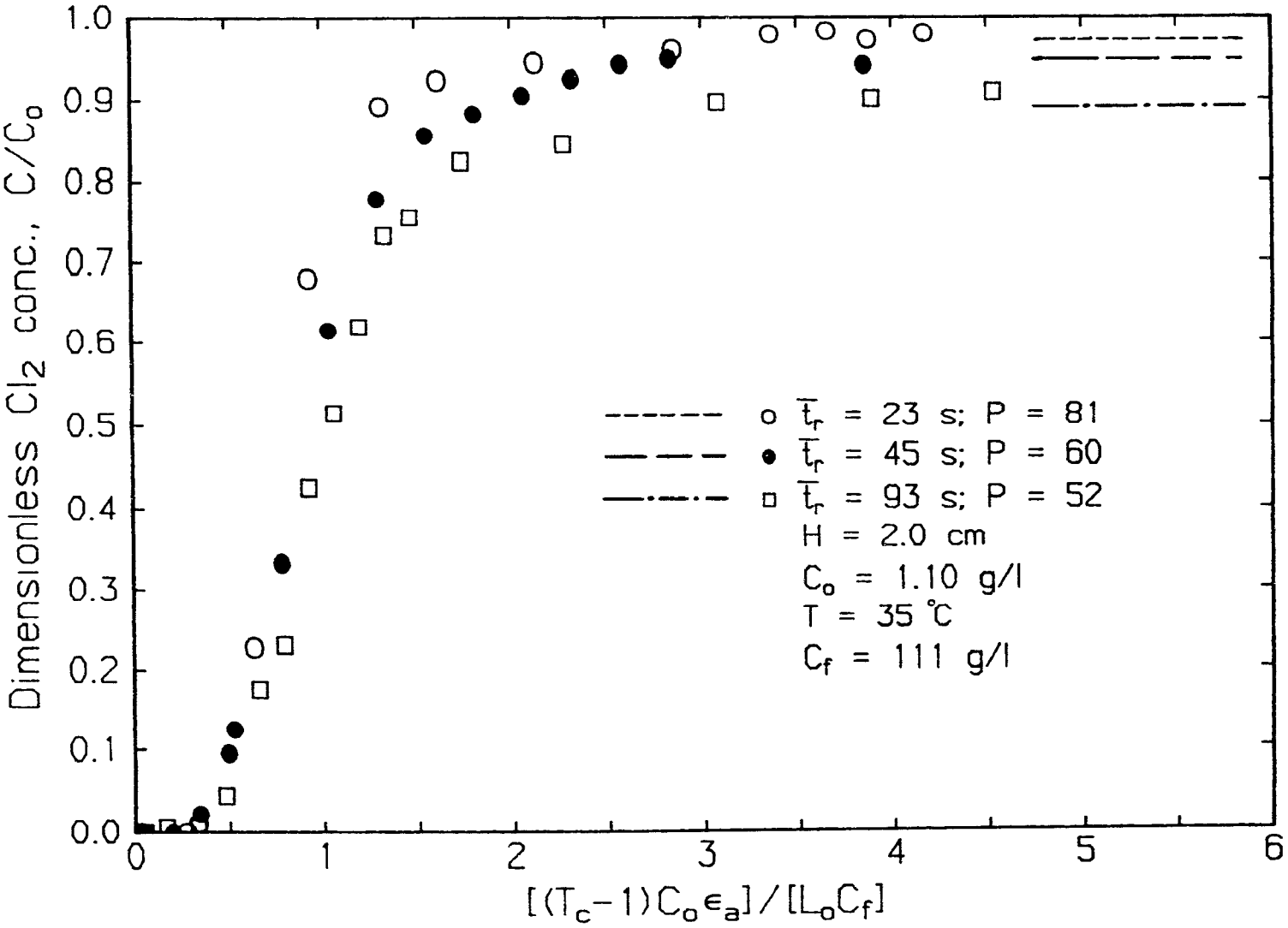
Dimensionless Cl_2 conc., C/C_o
1.0
0.9
0.8
0.7
0.6
0.5
0.4
0.3
0.2
0.1
0.0
0
1
2
3
4
5
6
$[(T_c-1)C_o\epsilon_a]/[L_oC_f]$
o $\bar{t}_r$ = 23 s; P = 81
● $\bar{t}_r$ = 45 s; P = 60
□ $\bar{t}_r$ = 93 s; P = 52
H = 2.0 cm
C_o = 1.10 g/l
T = 35 °C
C_f = 111 g/l

of the chlorine front in a stationary pulp suspension.

With these assumptions a sharp reaction front exists in each channel. The chlorine concentration upstream of a front is solely determined by the chlorine-carbohydrates reaction kinetics. Similarly the chlorine concentration at the exit of a channel is either zero or determined by the chlorine-carbohydrates reaction kinetics depending on whether or not the front has reached the exit of the channel. With these conditions the net inflow (inflow minus outflow) of chlorine to the bed can be represented by (Appendix 6-2):

$$AH\varepsilon_a C_o \left[T_c - \int_o^{F(t_{rc})} (T_c - T_b)\, e^{-k_c t_r}\, dF \right] \qquad [6.4]$$

with

$$T_b = \frac{t_b}{\bar{t}_r} = \frac{SL_o L_o C_f}{\varepsilon_a k_c C_o \bar{t}_r} \left(e^{k_c t_r} - 1 \right) + \frac{t_r}{\bar{t}_r} \qquad [6.4a]$$

and $F(t_{rc})$ is the value of the step-up response function (F-curve) at t_{rc} obtained from

$$t_c = \frac{SL_o L_o C_f}{\varepsilon_a k_c C_o} \left(e^{k_c t_{rc}} - 1 \right) + t_{rc} \qquad [6.4b]$$

In equation [6.4], dF represents the fraction of flow with a residence time between t_r and $t_r + dt_r$. T_b and t_b are, respectively, the non-dimensional and dimensional breakthrough time for fluid in a channel with a residence time of t_r. SL_o and k_c are, respectively, the chlorine-

lignin apparent stoichiometric ratio (g Cl_2/g initial lignin) and the chlorine-carbohydrates reaction constant. The net inflow of chlorine obtained experimentally is:

$$u_a \varepsilon_a A \int_o^{T_c} (C_o - C)\, dT_c \qquad [6.5]$$

By equating [6.4] and [6.5], and using $F(t_r)$ obtained from the preceeding tracer experiment, it is possible to determine the only unknown parameter SL_o as a function of t_c. This was done for the three experiments shown in Figure 6.10.

The SL_o values presented in Figure 6.11 increase with $[(T_c - 1)C_o\varepsilon_a]/[L_oC_f]$ until a constant value is reached at complete chlorine breakthrough. This trend was observed irrespective of mean residence time. The increase in SL_o could be attributed to additional chlorine consumption by reacted lignin in the growing zone upstream of the reaction front. This explanation is in contradiction with the assumption of an instantaneous chlorine-lignin reaction. However the result of this assumption, the movement of a sharp lignin and chlorine reaction front, is still valid because these non-linear kinetics lead to a "constant pattern" behavior of the reaction front (Chapter 7). Thus in the parallel plug flow model, chlorine consumed by lignin at the reaction front and upstream of the front is represented by an instantaneous reaction between chlorine and lignin at the reaction front only.

The rate of chlorine consumption at the reaction front increases almost proportionally with the chlorine feed rate, independent of the location of the front. On the other hand, the rate of consumption by

Figure 6.11 Effect of mean residence time, $\bar{t}_r$, on SL_o calculated over the duration of the experiment.

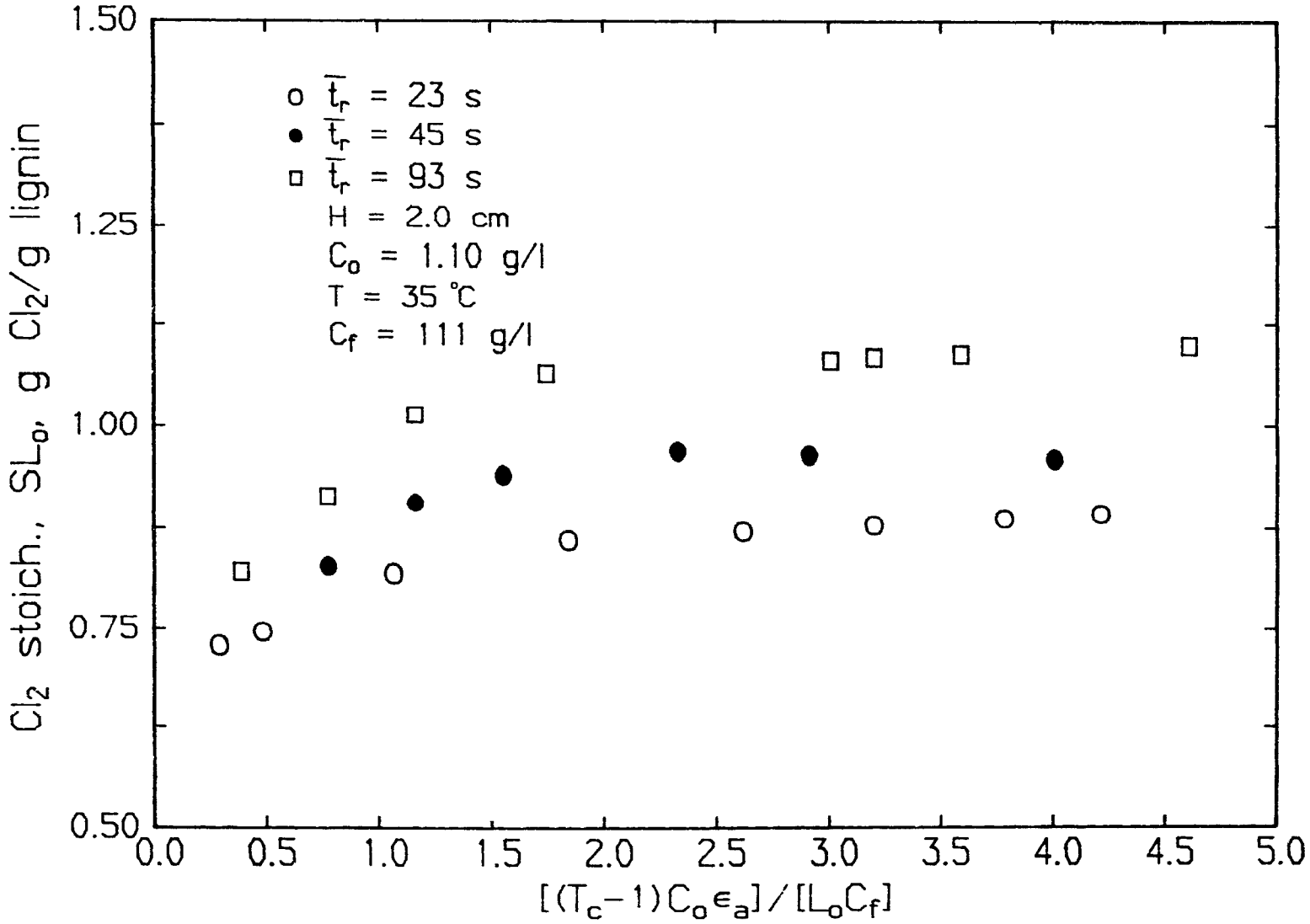
o $\bar{t}_r$ = 23 s
● $\bar{t}_r$ = 45 s
□ $\bar{t}_r$ = 93 s
H = 2.0 cm
C_o = 1.10 g/l
T = 35 °C
C_f = 111 g/l
Cl_2 stoich., SL_o, g Cl_2/g lignin
1.50
1.25
1.00
0.75
0.50
0.0
0.5
1.0
1.5
2.0
2.5
3.0
3.5
4.0
4.5
5.0
$[(T_c-1)C_o\epsilon_a]/[L_oC_f]$

reacted lignin upstream of the front is much less dependent on the chlorine feed rate but increases with further downstream position of the front. As a result the relative contribution to SL_o by lignin upstream of the reaction front should decrease with increasing chlorine feed rate. This is confirmed in Figure 6.11 which shows that SL_o decreases with decreasing mean residence time (or increasing chlorine feed rate) at each value of $[(T_c - 1)C_o\varepsilon_a]/[L_oC_f]$. A value of SL_o of 0.70-0.75 g Cl_2/g lignin obtained by extrapolation to $[(T_c - 1)C_o\varepsilon_a]/[L_oC_f] = 0$ could be considered to represent the contribution of the fast chlorine-lignin reaction only. This is equivalent to the consumption of 2 chlorine molecules per monomer unit (M = 196) of the kraft lignin polymer. In comparison, a chlorine charge of 1.50 g Cl_2/g lignin (or a so-called charge factor of 0.22% Cl_2/ kappa unit) is customary in industrial practice.

The apparent stoichiometry SL_o is almost independent of $(T_c - 1)C_o\varepsilon_a/(L_oC_f)$ after complete chlorine breakthrough, or when $(T_c - 1)C_o\varepsilon_a)/L_oC_f) > 3$. This is expected since SL_o is derived from the integrated RTC (equation 6.3), and very little chlorine is consumed by lignin after complete chlorine breakthrough, as evidenced by the agreement between measured and predicted C_m/C_o in Table 6.3. SL_o after complete breakthrough is shown in Figure 6.12 as a function of $\bar{t}_r$ obtained by varying both H and u_a. The results show that SL_o increases with $\bar{t}_r$ irrespective of whether H or u_a was changed. This means that the relative contribution to SL_o of lignin at the front and upstream of the front remains the same when u_a and H are changed proportionally. In other words, since the contribution to SL_o due to lignin at the reaction front increases almost linearly with u_a, the contribution to SL_o of lignin upstream of the front must increase

Figure 6.12 Effect of mean residence time, $\bar{t}_r$, on average SL_o.

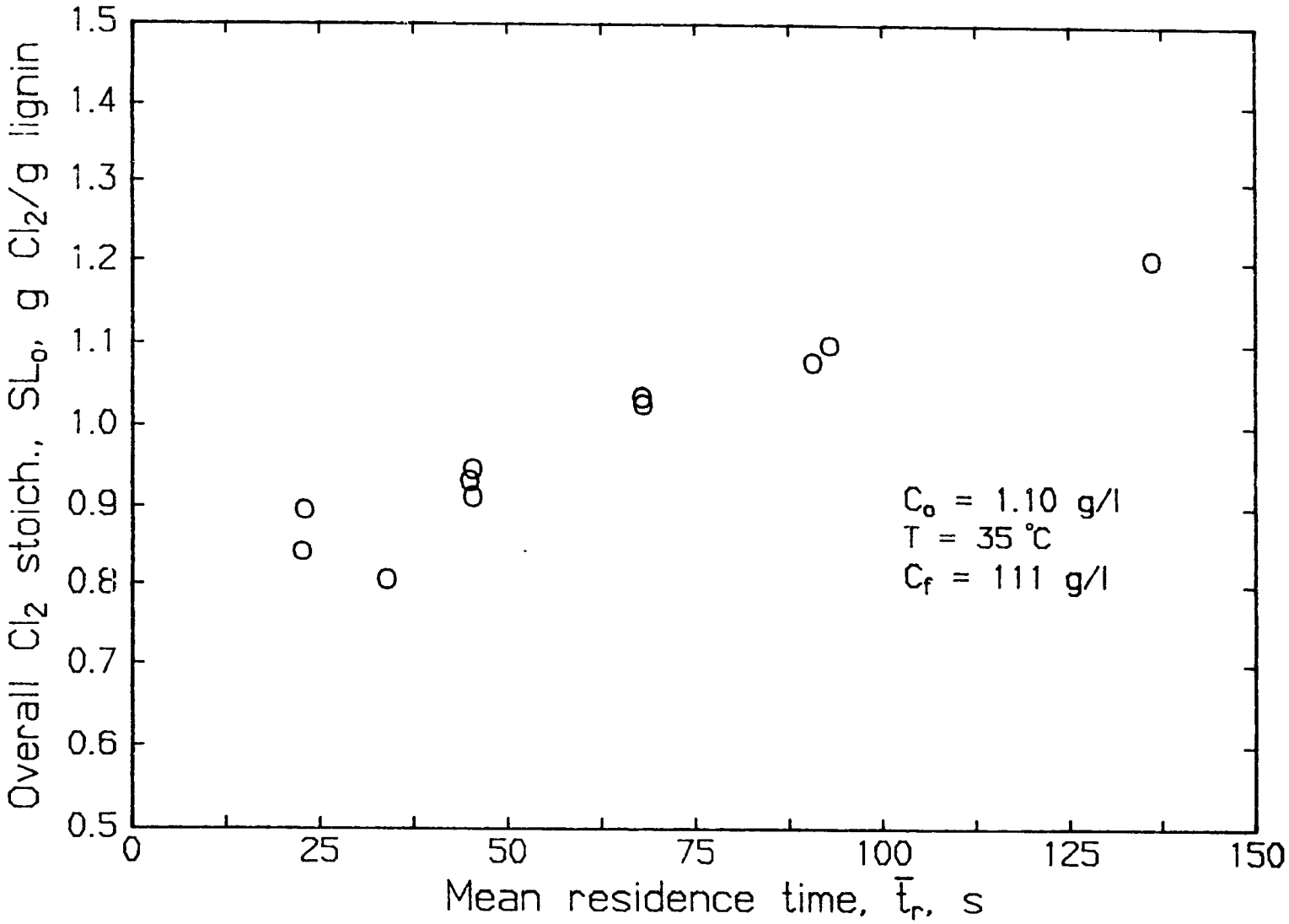
Overall Cl_2 stoich., SL_o, g Cl_2/g lignin
1.5
1.4
1.3
1.2
1.1
1.0
0.9
0.8
0.7
0.6
0.5
0
25
50
75
100
125
150
Mean residence time, $\bar{t}_r$, s
C_o = 1.10 g/l
T = 35 °C
C_f = 111 g/l

almost linearly with increasing H.

6.5.1.2 Effect of residence time distribution

To establish the influence of the RTD on the breakthrough curves, experiments were performed on a well formed and a poorly formed pad at otherwise the same operating conditions. The glucose tracer curves for the two cases are shown in Figure 6.13. The poorly formed pad is characterised by early appearance of the tracer at the exit and gradually increasing concentrations at longer times similar to the RTD for a CSTR. In contrast, the well formed pad displays a behaviour close to plug flow. The Peclet number, P, for the well formed and poorly formed pads are 31 and 2.3, respectively.

The chlorine breakthrough curves of the well formed and the poorly formed pads are shown in Figure 6.14. Except for a lower final C/C_o level due to reaction between chlorine and carbohydrates, the shape of the chlorine breakthrough curves are similar to the corresponding RTD's. This suggests that the flow behaviour determines the characteristics of the chlorine breakthrough curve and that the chlorine-pulp reactions merely act as a scaling factor. The previously described model of a series of parallel plug flow elements with a single instantaneous reaction and no inter element mass exchange has these characteristics.

In chapter 7 it will be shown that for $P \gg 1$ and/or $k_c t_r \ll 1$ this model requires that the chlorine breakthrough curve is identical to the RTD when the time axis of the former is divided by T_c and the vertical axis by C_m/C_o. For $P \gg 1$, the slope of the RTD at $C/C_o = 0.5$ can be approximated (Kramers and Westerterp (15)) as

Figure 6.13 RTD's of poorly and well formed pad obtained with glucose tracer tests.

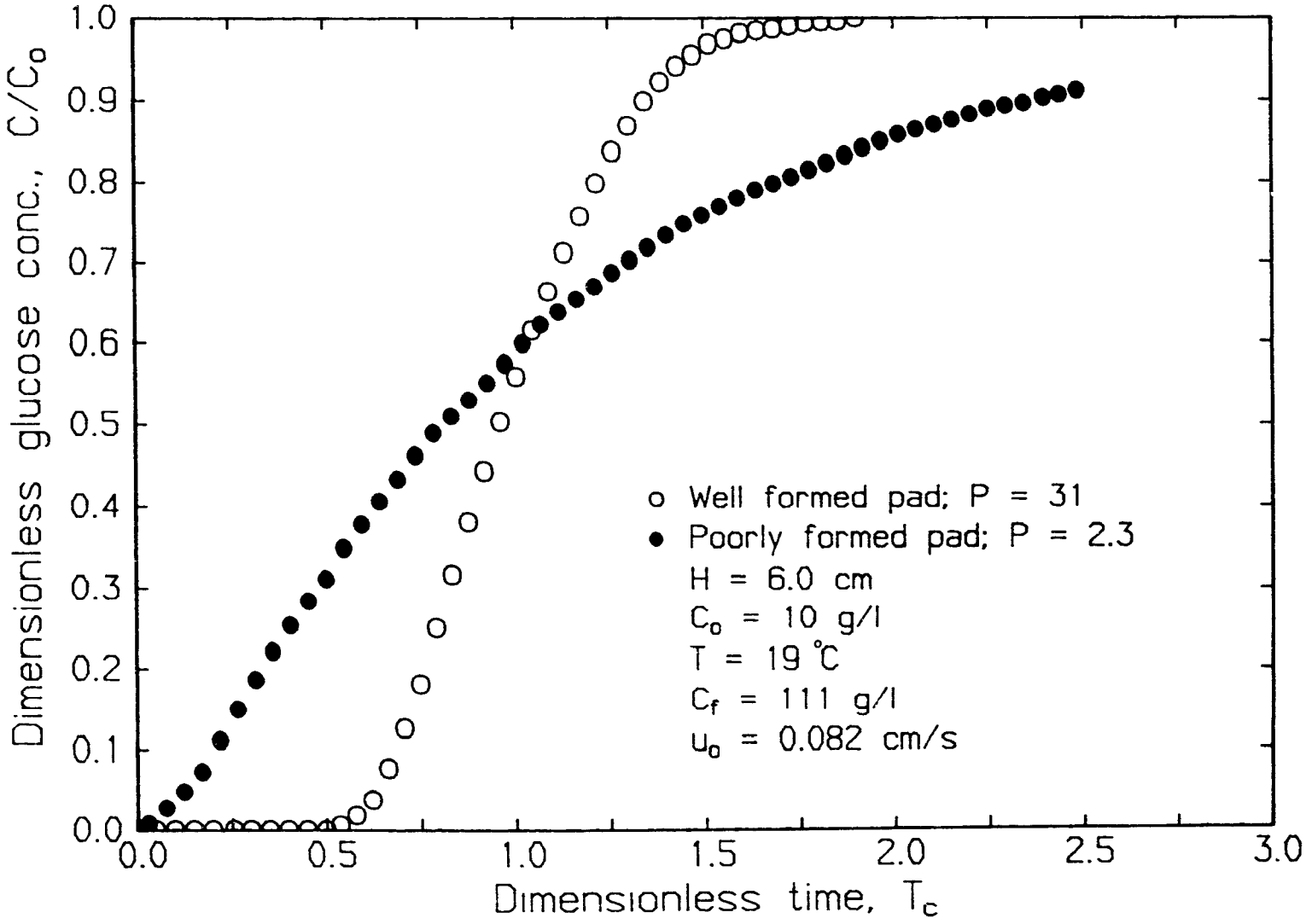
Dimensionless glucose conc., C/C$_o$
1.0
0.9
0.8
0.7
0.6
0.5
0.4
0.3
0.2
0.1
0.0
0.0
0.5
1.0
1.5
2.0
2.5
3.0
Dimensionless time, T$_c$
o Well formed pad; P = 31
• Poorly formed pad; P = 2.3
H = 6.0 cm
C$_o$ = 10 g/l
T = 19 °C
C$_f$ = 111 g/l
u$_o$ = 0.082 cm/s

Figure 6.14 Chlorine breakthrough curves of poorly and well formed pads.

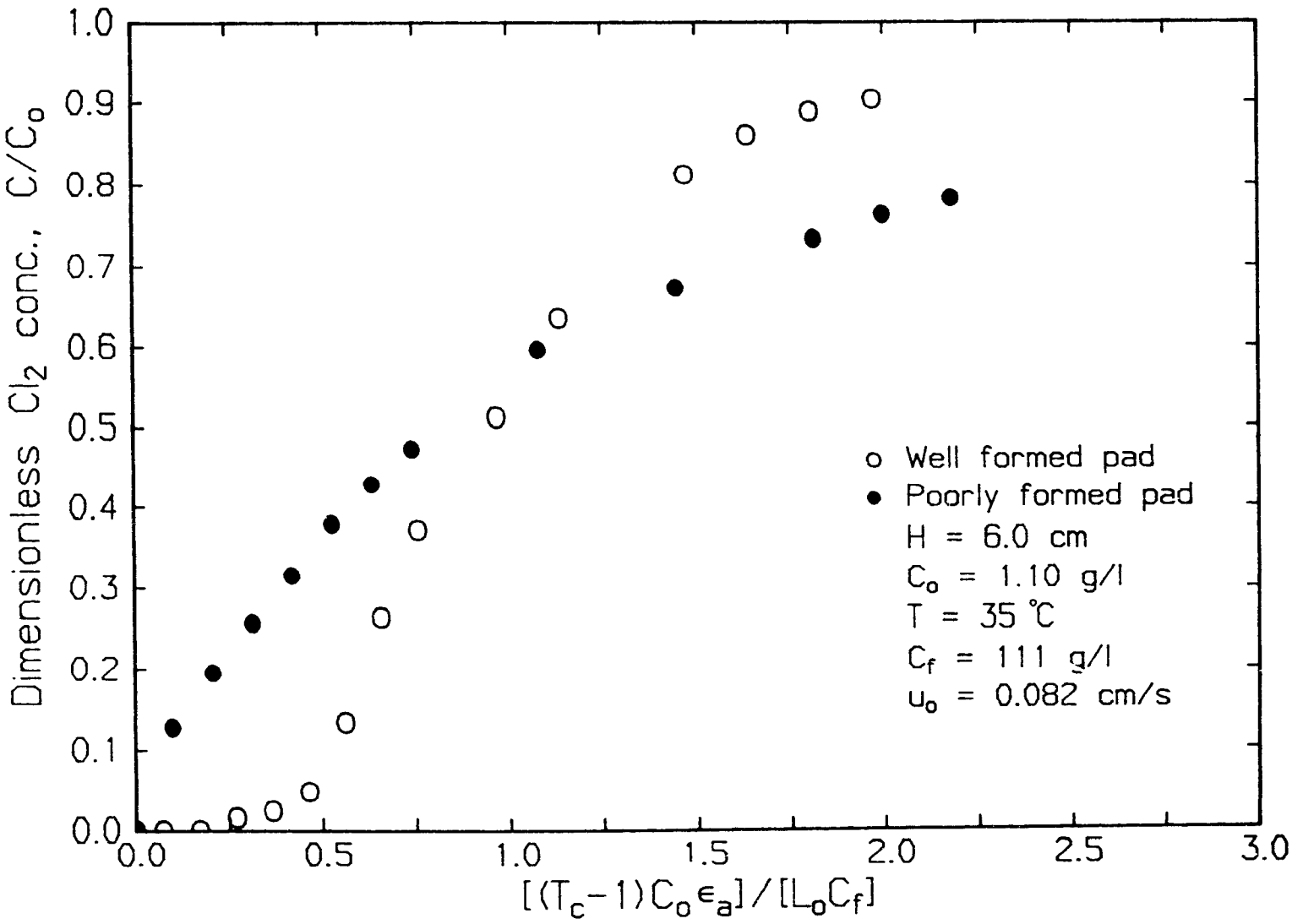
Dimensionless Cl_2 conc., C/C_o
1.0
0.9
0.8
0.7
0.6
0.5
0.4
0.3
0.2
0.1
0.0
0.0
0.5
1.0
1.5
2.0
2.5
3.0
$[(T_c-1)C_o\epsilon_a]/[L_oC_f]$
o Well formed pad
• Poorly formed pad
H = 6.0 cm
C_o = 1.10 g/l
T = 35 °C
C_f = 111 g/l
u_o = 0.082 cm/s

$$\left(\frac{d(C/C_o)}{dT_c}\right)_{C/C_o = 0.5} = 0.5\ (P/\pi)^{0.5} \qquad [6.6]$$

Thus if the parallel plug flow model is appropriate for dynamic bleaching, the normalized slope of the chlorine breakthrough curve at $C/C_m = 0.5$ is related to P of the RTD as

$$G = \left(T_c \frac{d(C/C_o)}{dT_c}\right)_{C/C_m = 0.5} \cdot \frac{C_o}{C_m} = 0.5\ \left(\frac{P}{\pi}\right)^{0.5} = 0.282(P)^{0.5} \qquad [6.7]$$

Higher order effects due to the chlorine-carbohydrate reaction on equation 6.7 can be neglected when $P \gg 1$ and/or $k_c t_r \ll 1$ (chapter 7).

It is interesting to compare equation 6.7 with the theoretical solution for the axial dispersed plug flow model combined with a single instantaneous reaction. In Appendix (6-3) it is derived that this model leads to the expression

$$\left(T_c \frac{d(C/C_o)}{dT_c}\right)_{C/C_o = 0.5} = 0.5P \frac{\bar{T}_b}{(\bar{T}_b - 1)}\left(1 - \frac{1}{\varepsilon_a(\bar{T}_b - 1)}\right) - 0.1534 \qquad [6.8]$$

where $\bar{T}_b$ is the average non-dimensional breakthrough time. When P and $\bar{T}_b$ are much larger than 1, equation 6.8 can be approximated by

$$\left(T_c \frac{d(C/C_o)}{dT_c}\right)_{C/C_o = 0.5} = 0.5P \qquad [6.9]$$

The applicability of the two models was tested by comparing the normalised slope of the chlorine breakthrough curve, G, with equations 6.9 and 6.7, respectively, valid for axial dispersed plug flow with instantaneous reaction and parallel plug flow with instantaneous reaction. Shown in Figure 6.15 is the normalised slope, G, as a function of Peclet number, P, measured by the preceeding glucose tracer test for the two experiments of Figure 6.13. Also included in this figure are values obtained at the various mean residence times discussed in the previous section. It can be seen that the equation $G = 0.5P$ drastically over predicts the experimental data and represents a too high dependence on P. On the contrary in Figure 6.16 equation $G = 0.282(P)^{0.5}$ for parallel plug flow agrees quite well with the measured normalised slopes for the different experiments. The good agreement confirms that for the operating conditions of Figure 6.13, "fingering" flow determines the RTD and that the chlorine consumption by lignin simply leads to a uniform retardation of the chlorine front. The somewhat lower values for G than predicted by equation 6.7 are probably due to the slow chlorine consumption by lignin upstream of the reaction fronts. This will lead to "tailing" after breakthrough for each channel.

6.5.1.3 Effect of chlorine concentration

The effect of varying chlorine concentration on the chlorine breakthrough curves was investigated at three levels - 0.55, 1.10 and 2.20 g/l. Dimensionless plots of C/C_o versus T_c at a pad height and consistency of 6 cm and 10.7%, respectively, and a reaction temperature of 35°C are shown in Figure 6.17. Complete breakthrough is achieved at much smaller values of T_c with increasing chlorine concentration. This is expected as the rate of chlorine supply increases proportionally with increasing

Figure 6.15 Applicability of axial dispersion model to represent chlorine breakthrough curves.

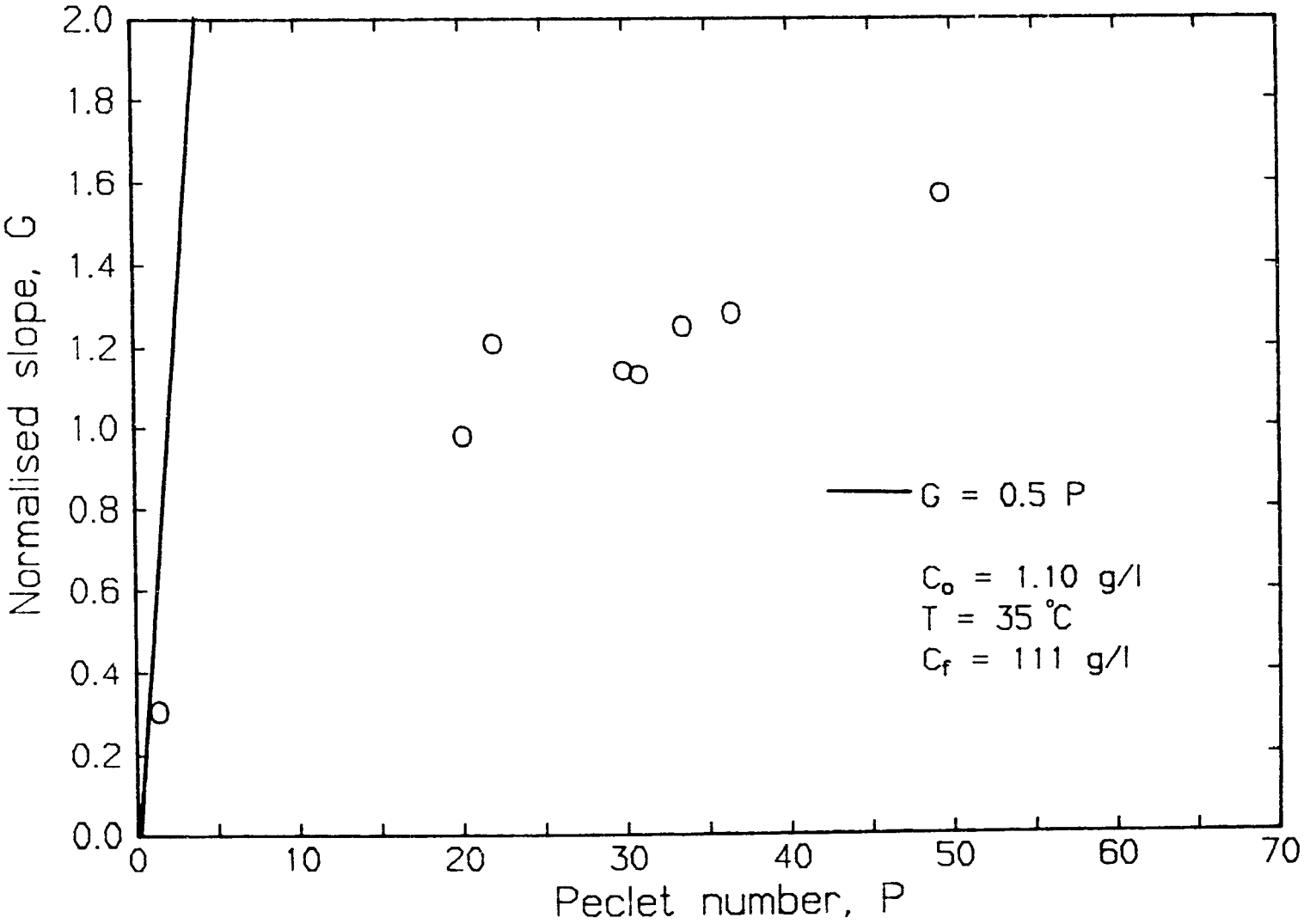
Normalised slope, G
Peclet number, P
G = 0.5 P
C_o = 1.10 g/l
T = 35 °C
C_f = 111 g/l
0.0
0.2
0.4
0.6
0.8
1.0
1.2
1.4
1.6
1.8
2.0
0
10
20
30
40
50
60
70

Figure 6.16 Applicability of parallel plug model to represent chlorine breakthrough curves.

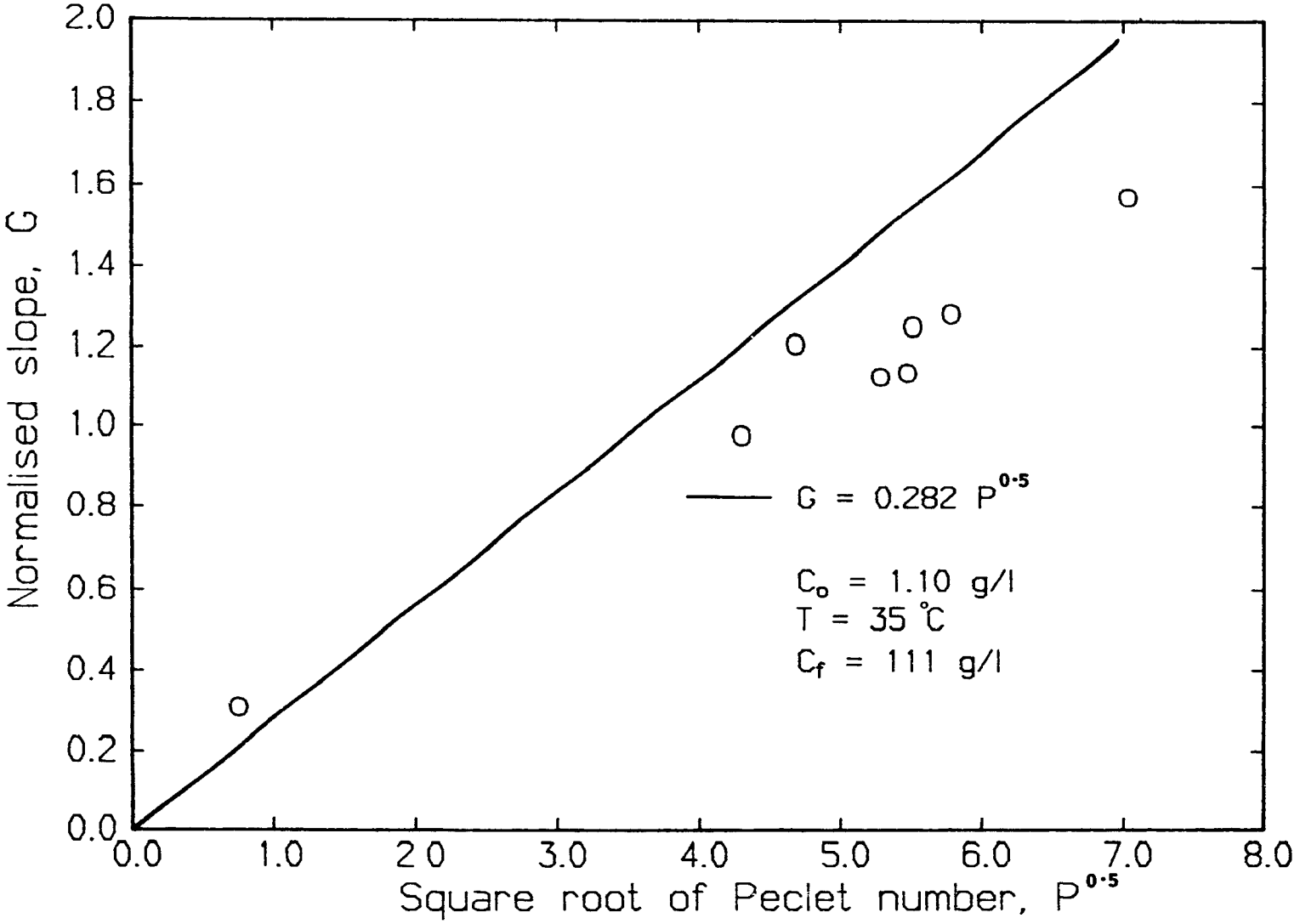
Normalised slope, G
2.0
1.8
1.6
1.4
1.2
1.0
0.8
0.6
0.4
0.2
0.0
0.0
1.0
2.0
3.0
4.0
5.0
6.0
7.0
8.0
Square root of Peclet number, P^0.5
G = 0.282 P^0.5
C_o = 1.10 g/l
T = 35 °C
C_f = 111 g/l

Figure 6.17 Effect of chlorine concentration on dimensionless chlorine breakthrough curves.

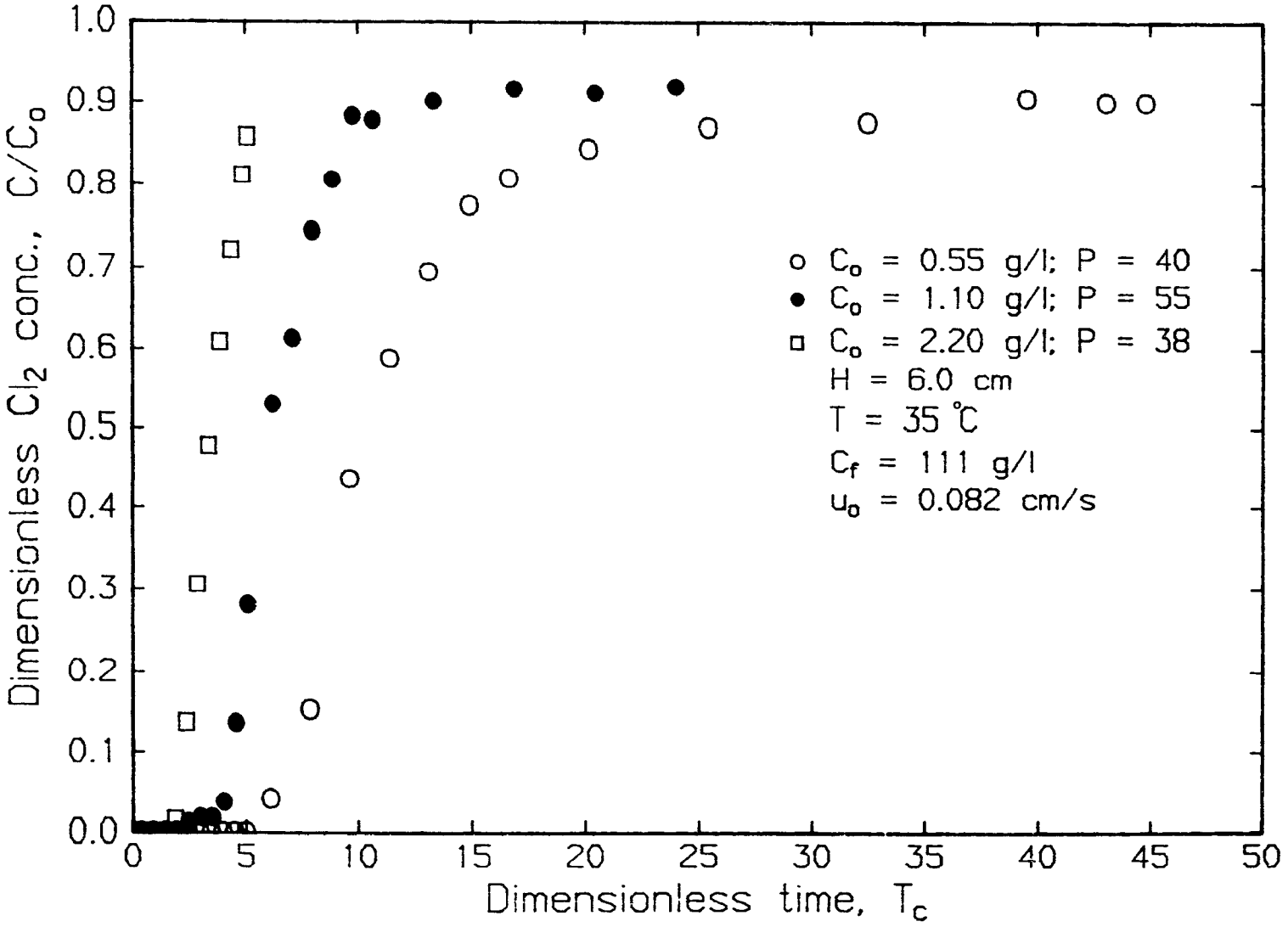
Dimensionless Cl_2 conc., C/C_o
1.0
0.9
0.8
0.7
0.6
0.5
0.4
0.3
0.2
0.1
0.0
0
5
10
15
20
25
30
35
40
45
50
Dimensionless time, T_c
C_o = 0.55 g/l; P = 40
C_o = 1.10 g/l; P = 55
C_o = 2.20 g/l; P = 38
H = 6.0 cm
T = 35 ℃
C_f = 111 g/l
u_o = 0.082 cm/s

chlorine concentration. The influence of the rate of supply of chlorine on the breakthrough curves can be eliminated by plotting against the normalized variable $(T_c-1)C_o\varepsilon_a/L_oC_f$. In this manner the three curves of Figure 6.17 essentially collapses to a single curve as shown in Figure 6.18. The value of C/C_o after complete breakthrough is independent of the inlet concentration since the carbohydrates-chlorine reaction is first order in chlorine and the mean residence time is the same for the three experiments. It also follows from the close agreement between the three breakthrough curves in Figure 6.18 that the consumption of chlorine per initial weight of lignin, SL_o, is independent of C_o. This is confirmed when SL_o is calculated as a function of the three chlorine concentrations for the duration of the experiments as shown in Figure 6.19. Similar to Figure 6.11, SL_o increases as breakthrough progresses and eventually reaches a plateau level. The small differences in SL_o before complete breakthrough are related to P. As expected, SL_o is slightly higher before complete breakthrough for higher P, and the plateau level is reached at a smaller value of $(T_c - 1)C_o\varepsilon_a/[L_oC_f]$. The effect of chlorine concentration on SL_o after complete breakthrough shown in Figure 6.20 further confirms the independence of the chlorine-lignin stoichiometry on chlorine concentration.

The steepness of the chlorine breakthrough curves is shown in Figure 6.21 where the normalised slope G is plotted against $0.282(P)^{0.5}$ with chlorine concentration as parameter. Reproduced in Figure 6.21 are all the data presented in Figure 6.16 obtained at C_o = 1.10 g/l and variable mean residence times $\bar{t}_r$. The unique linear relationship between the steepness of the breakthrough curve and $P^{0.5}$, independent of C_o and

Figure 6.18 Effect of chlorine concentration on generalized chlorine breakthrough curves.

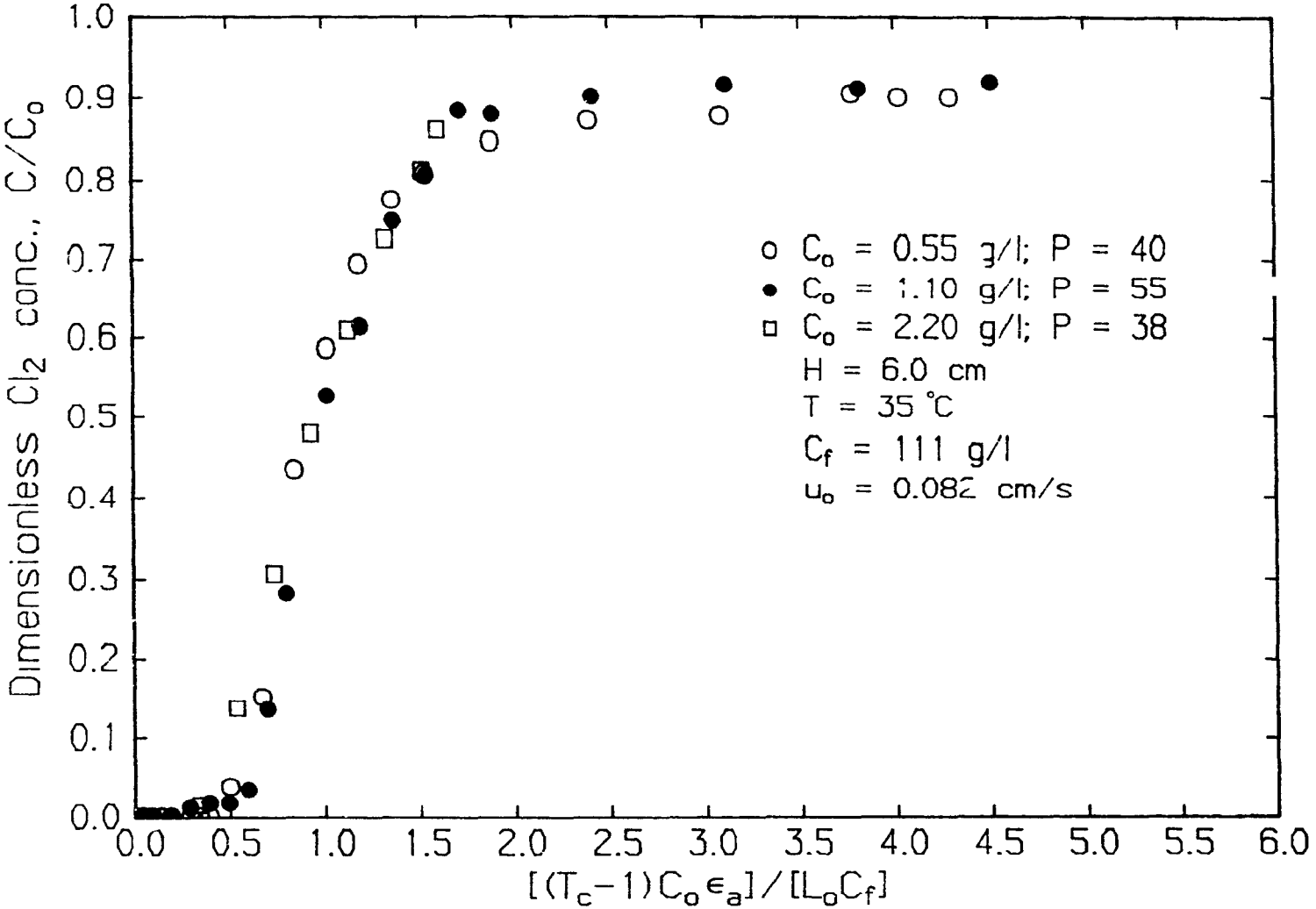
Dimensionless Cl_2 conc., C/C_o
1.0
0.9
0.8
0.7
0.6
0.5
0.4
0.3
0.2
0.1
0.0
0.0 0.5 1.0 1.5 2.0 2.5 3.0 3.5 4.0 4.5 5.0 5.5 6.0
$[(T_c-1)C_o\epsilon_a]/[L_oC_f]$
o C_o = 0.55 g/l; P = 40
• C_o = 1.10 g/l; P = 55
□ C_o = 2.20 g/l; P = 38
H = 6.0 cm
T = 35 °C
C_f = 111 g/l
u_o = 0.082 cm/s

Figure 6.19 Effect of chlorine concentration on SL_o verus $(T_c - 1)C_o\varepsilon_a / [L_oC_f]$.

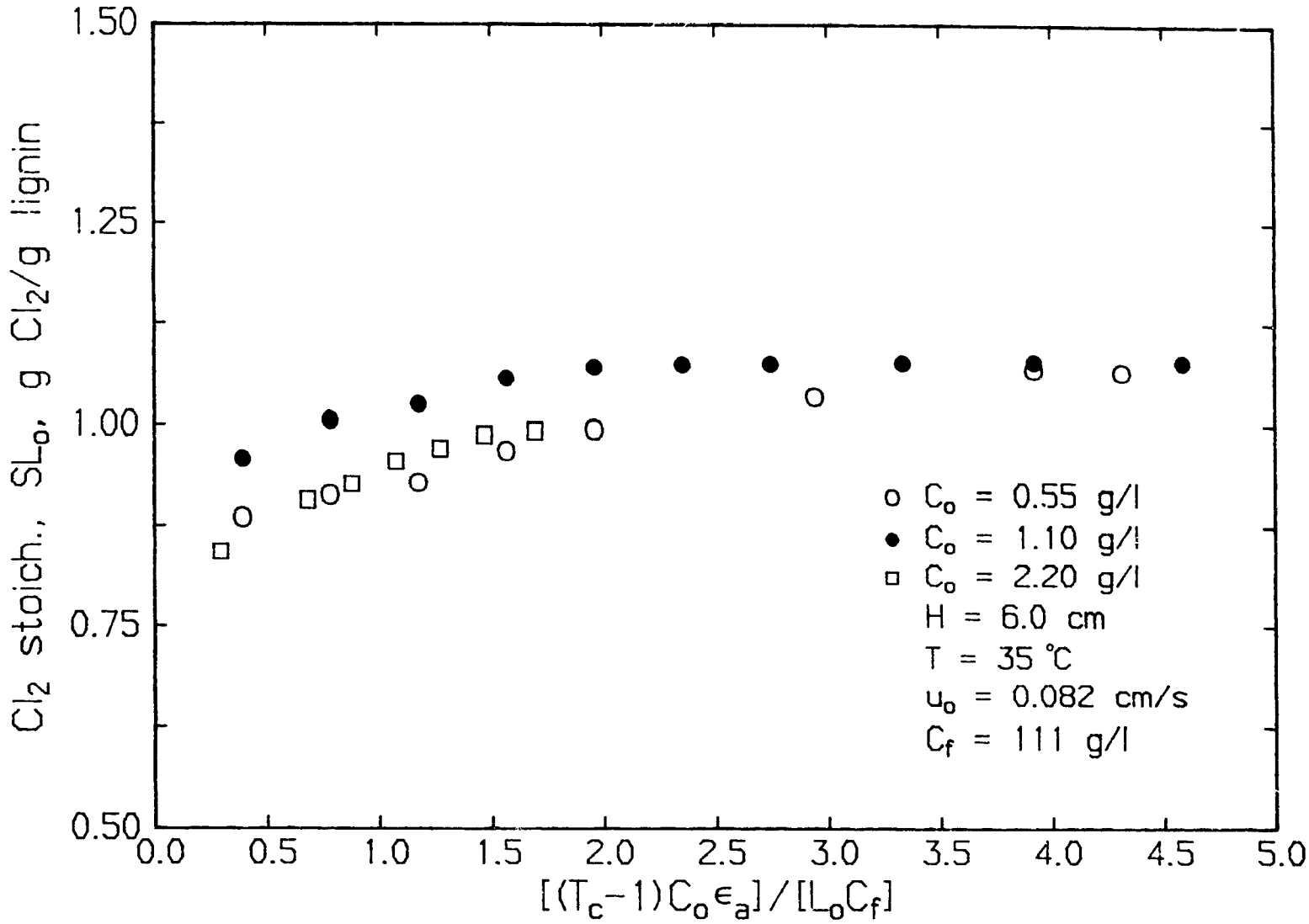
1.50
1.25
1.00
0.75
0.50
0.0
0.5
1.0
1.5
2.0
2.5
3.0
3.5
4.0
4.5
5.0
Cl2 stoich., SLo, g Cl2/g lignin
[(Tc−1)Co∈a]/[LoCf]
o Co = 0.55 g/l
• Co = 1.10 g/l
□ Co = 2.20 g/l
H = 6.0 cm
T = 35 °C
uo = 0.082 cm/s
Cf = 111 g/l

Figure 6.20 Effect of chlorine concentration on SL_o at complete breakthrough.

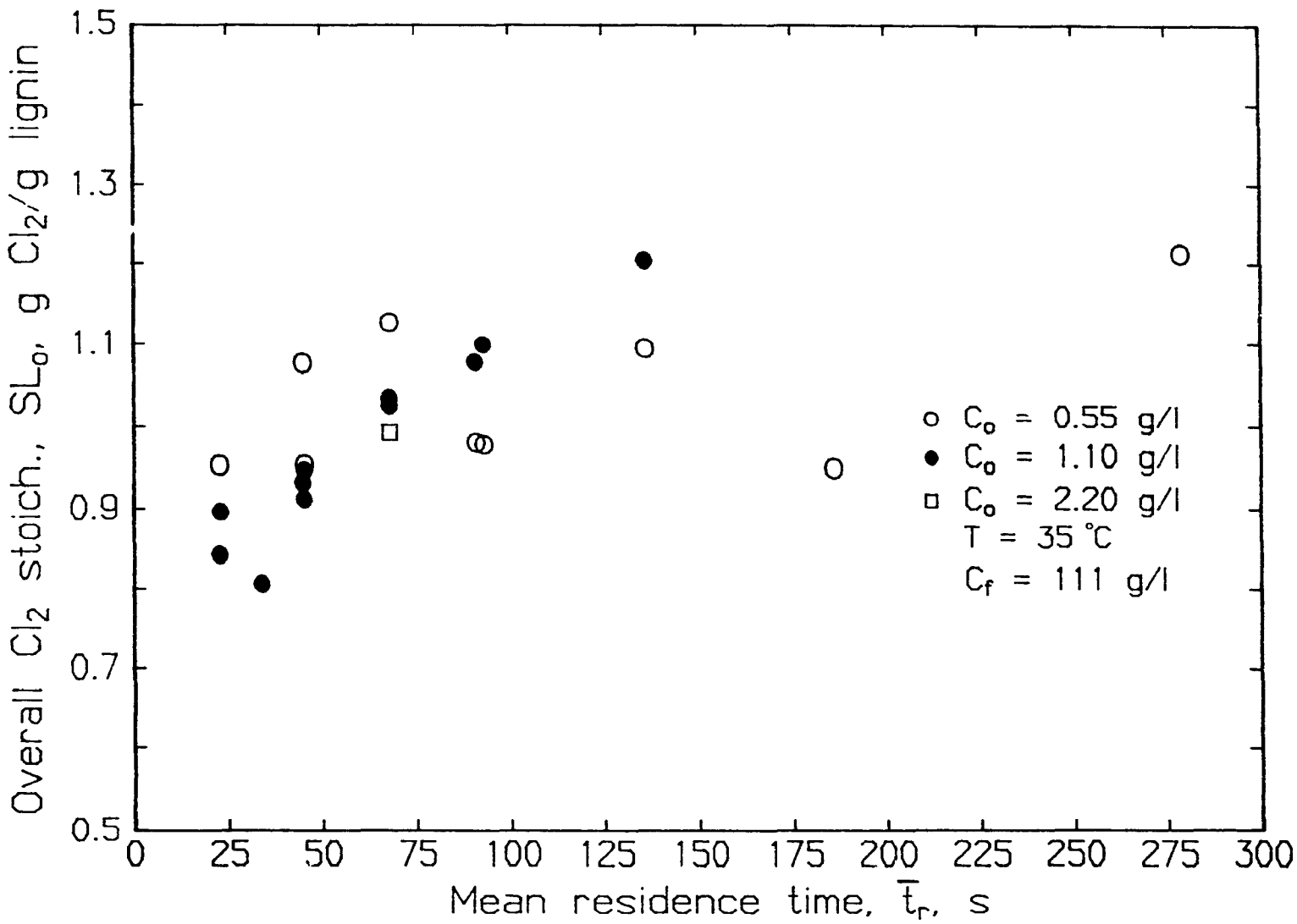
Overall Cl_2 stoich., SL_o, g Cl_2/g lignin
1.5
1.3
1.1
0.9
0.7
0.5
0
25
50
75
100
125
150
175
200
225
250
275
300
Mean residence time, $\bar{t}_r$, s
C_o = 0.55 g/l
C_o = 1.10 g/l
C_o = 2.20 g/l
T = 35 °C
C_f = 111 g/l

Figure 6.21 Applicability of parallel plug flow model to represent chlorine breakthrough curves: effect of chlorine concentration.

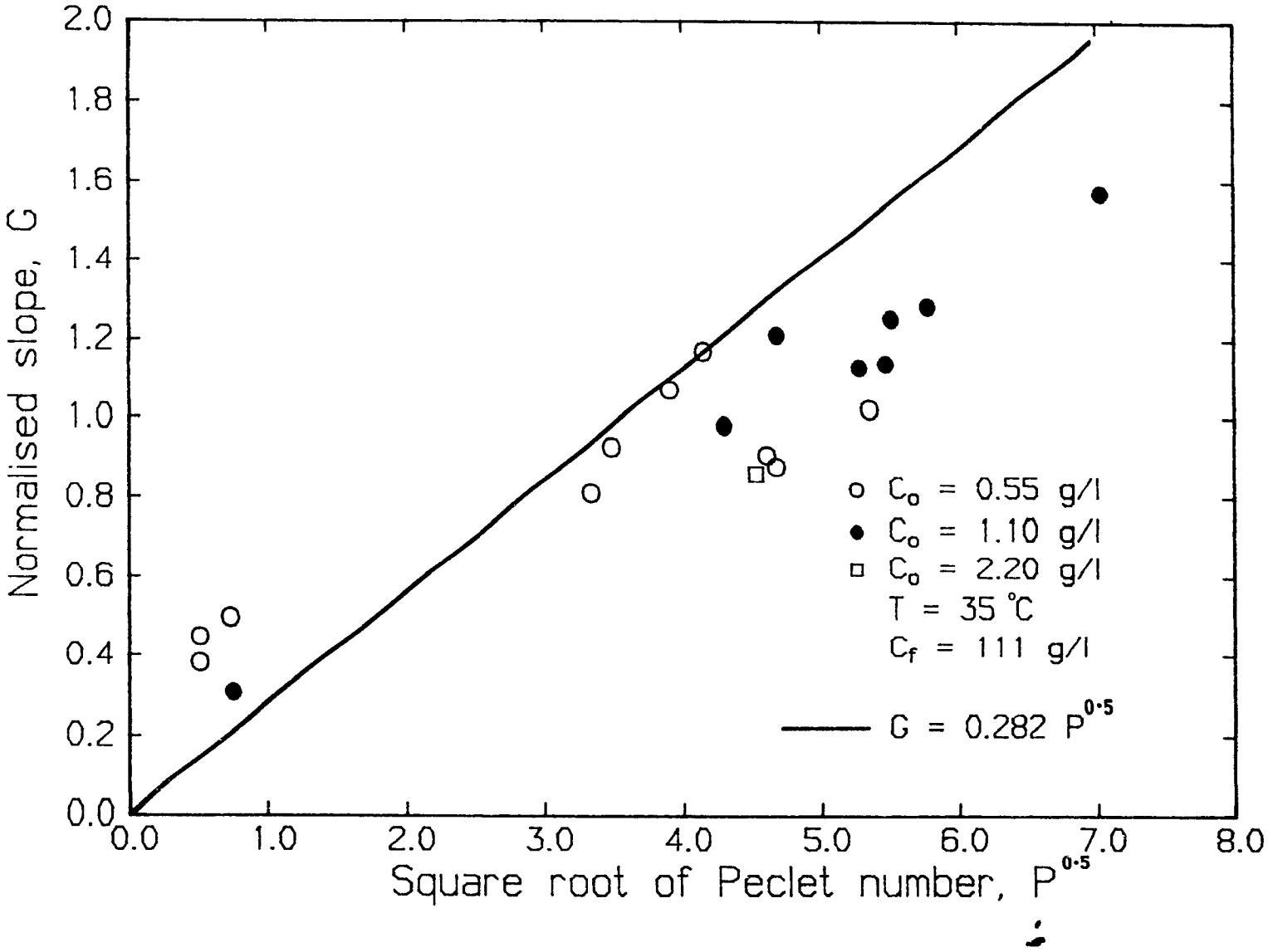
Normalised slope, G
Square root of Peclet number, $P^{0.5}$
2.0
1.8
1.6
1.4
1.2
1.0
0.8
0.6
0.4
0.2
0.0
0.0
1.0
2.0
3.0
4.0
5.0
6.0
7.0
8.0
C_o = 0.55 g/l
C_o = 1.10 g/l
C_o = 2.20 g/l
T = 35 °C
C_f = 111 g/l
G = 0.282 $P^{0.5}$

and $\bar{t}_r$, further confirms that the actual flow is best described by parallel plug flow.

6.5.1.4 Effect of temperature

The effect of temperature on dynamic pulp chlorination was investigated at three levels: 19, 35 and 50°C. The effect of temperature will be demonstrated for C_o = 2.20 g/l, H = 6 cm, u_o = 0.082 cm/s and C_p = 10.7% The chlorine breakthrough curves are presented in Figure 6.22. The curves are shifted to the right at higher temperatures. As will be shown subsequently, this increased consumption of chlorine is caused both by reactions with lignin and carbohydrates. The increased chlorine consumption by carbohydrates at higher temperatures is indicated by the decreasing value of C_m/C_o calculated theoretically with equation 5.8 and represented by the lines in the top right hand corner of Figure 6.22. The earlier breakthrough at 50°C compared to 35°C in Figure 6.22 can be attributed to the lower Peclet number, 28.8 compared to 37.9, respectively.

The variation of SL_o during the three experiments is seen in Figure 6.23. Again the SL_o values increase until a plateau value is reached. Following the phenomenological description presented earlier, the extrapolation of SL_o to $(T_c - 1)C_o\varepsilon_a/[L_oC_f] = 0$ suggests that the chlorine-lignin stoichiometry of the fast reaction at the front increases strongly with increasing temperature. The stoichiometry for the slow reaction upstream of the front, characterized by the difference between the plateau value of SL_o and SL_o extrapolated to $(T_c - 1)C_o\varepsilon_a = 0$, also increases with increasing temperature. Previously it was shown that SL_o at $(T_c-1)C_o\varepsilon_a/L_oC_f = 4.0$, i.e. at complete breakthrough, was only a function of $\bar{t}_r$ and not C_o. Therefore all experimental values of SL_o at 10.7% consistency are plotted

Figure 6.22 Effect of temperature on generalized chlorine breakthrough curves.

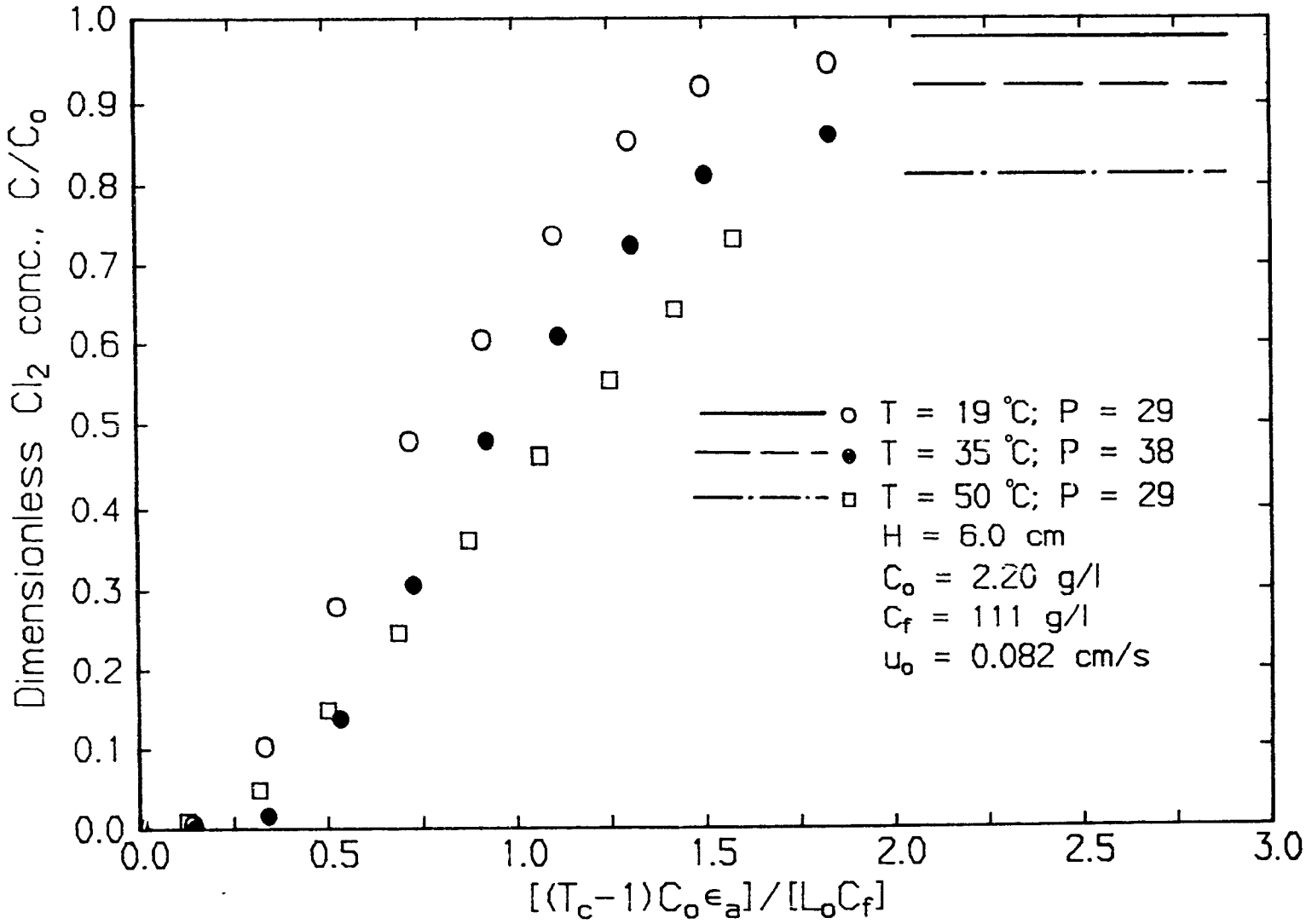
Dimensionless Cl_2 conc., C/C_o
1.0
0.9
0.8
0.7
0.6
0.5
0.4
0.3
0.2
0.1
0.0
0.0
0.5
1.0
1.5
2.0
2.5
3.0
$[(T_c-1)C_o\epsilon_a]/[L_oC_f]$
T = 19 °C; P = 29
T = 35 °C; P = 38
T = 50 °C; P = 29
H = 6.0 cm
C_o = 2.20 g/l
C_f = 111 g/l
u_o = 0.082 cm/s

Figure 6.23 Effect of temperature on SL_o versus $(T_c - 1)C_o\varepsilon_a/[L_oC_f]$.

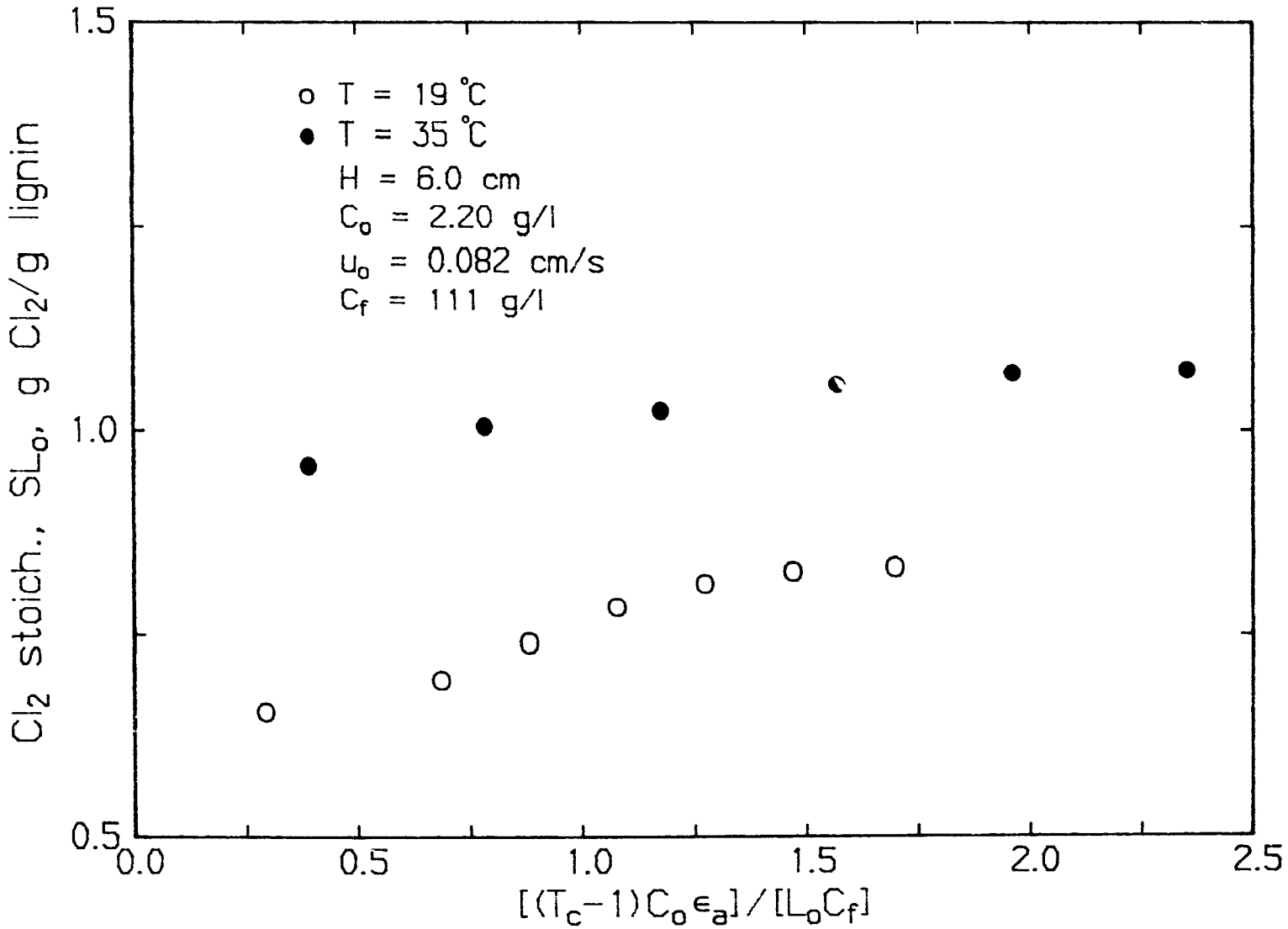
o T = 19 °C
• T = 35 °C
H = 6.0 cm
C_o = 2.20 g/l
u_o = 0.082 cm/s
C_f = 111 g/l
Cl_2 stoich., SL_o, g Cl_2/g lignin
1.5
1.0
0.5
0.0
0.5
1.0
1.5
2.0
2.5
$[(T_c-1)C_o\epsilon_a]/[L_oC_f]$

in Figure 6.24 with the temperature as parameter. This figure summarises the chlorine consumption by lignin at complete breakthrough of the present 29.5 kappa number kraft pulp for the two important operating variables T and $\bar{t}_r$.

Similarly, as was shown for varying mean residence times and varying chlorine concentrations, the normalised slope G of the chlorine breakthrough curve plotted versus the square root of the Peclet number is independent of temperature. This is shown in Figure 6.25 where the present experiments at 19°C and 50°C are within the scatter of all previously reported values at 35°C. It also shows that the decrease in the slope of the non-dimensional breakthrough curve at higher temperatures, due to the higher chlorine consumption, is accounted for in G by multiplying the slope by T_c at $C/C_m = 0.5$.

6.5.1.5 Effect of consistency

The effect of pulp pad consistency was investigated at three levels - 8.0, 10.7 and 12.8% corresponding to pulp concentrations of 83, 111 and 133 g/l, respectively. The dimensionless chlorine concentration versus T_c breakthrough curves for H = 6 cm, C_o = 1.10 g/l, u_o = 0.082 cm/s and T = 35°C are shown in Figure 6.26. The curves are shifted to the right at higher consistencies because more lignin is contained within the same bed volume. The difference between these breakthrough curves are smaller in the generalized plots of Figure 6.27. The earlier than expected breakthrough of chlorine at 10.7% consistency can be attributed to its lower Peclet number of 23 compared to 66 and 55 for the 8 and 10.7% consistency experiments.

The normalised slope G of the chlorine breakthrough curves is

Figure 6.24 Effect of temperature on SL_o at complete breakthrough.

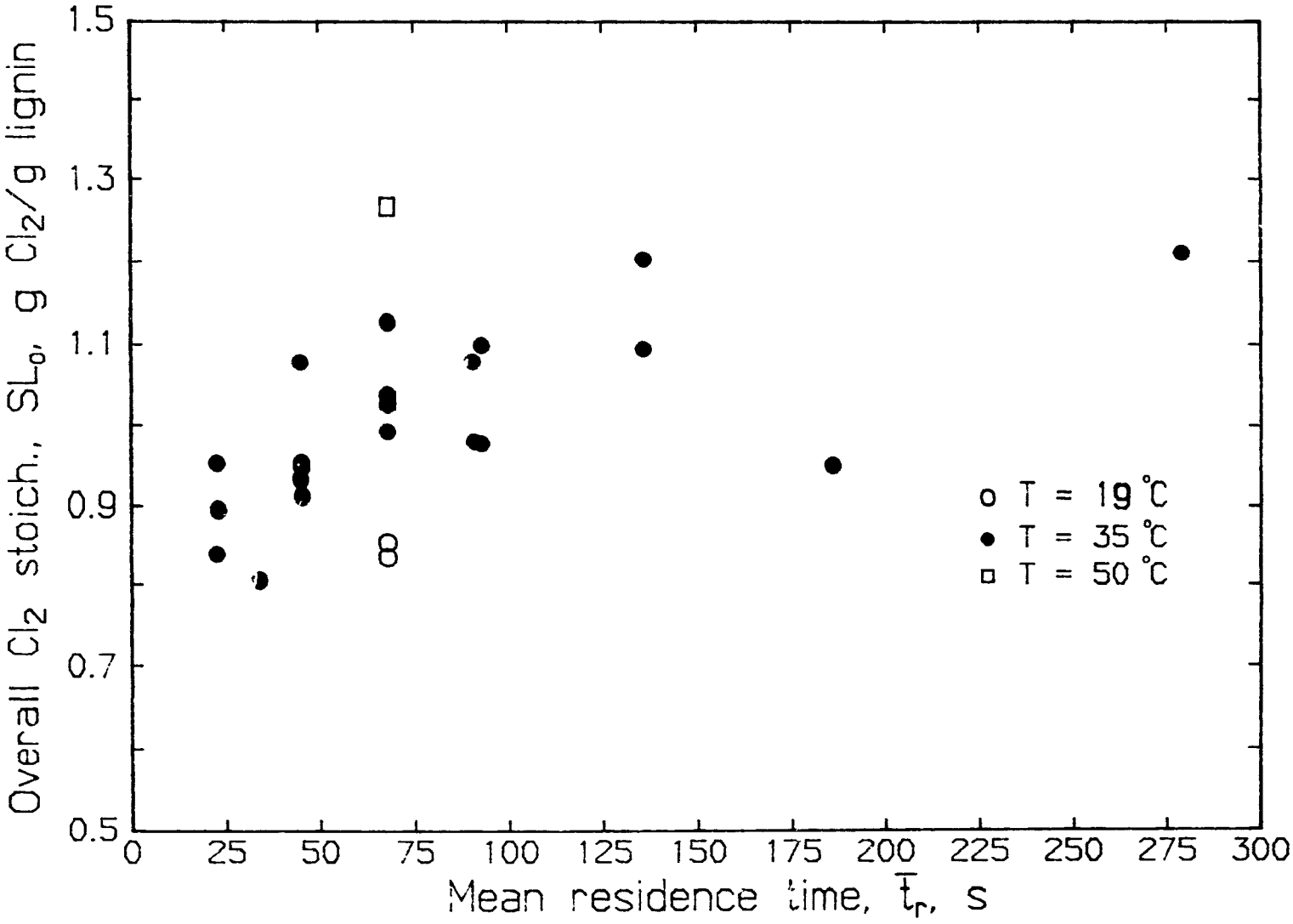
Overall Cl_2 stoich., SL_o, g Cl_2/g lignin
1.5
1.3
1.1
0.9
0.7
0.5
0
25
50
75
100
125
150
175
200
225
250
275
300
Mean residence time, $\bar{t}_r$, s
T = 19 °C
T = 35 °C
T = 50 °C

Figure 6.25 Applicability of parallel plug flow model to represent chlorine breakthrough curves: effect of temperature.

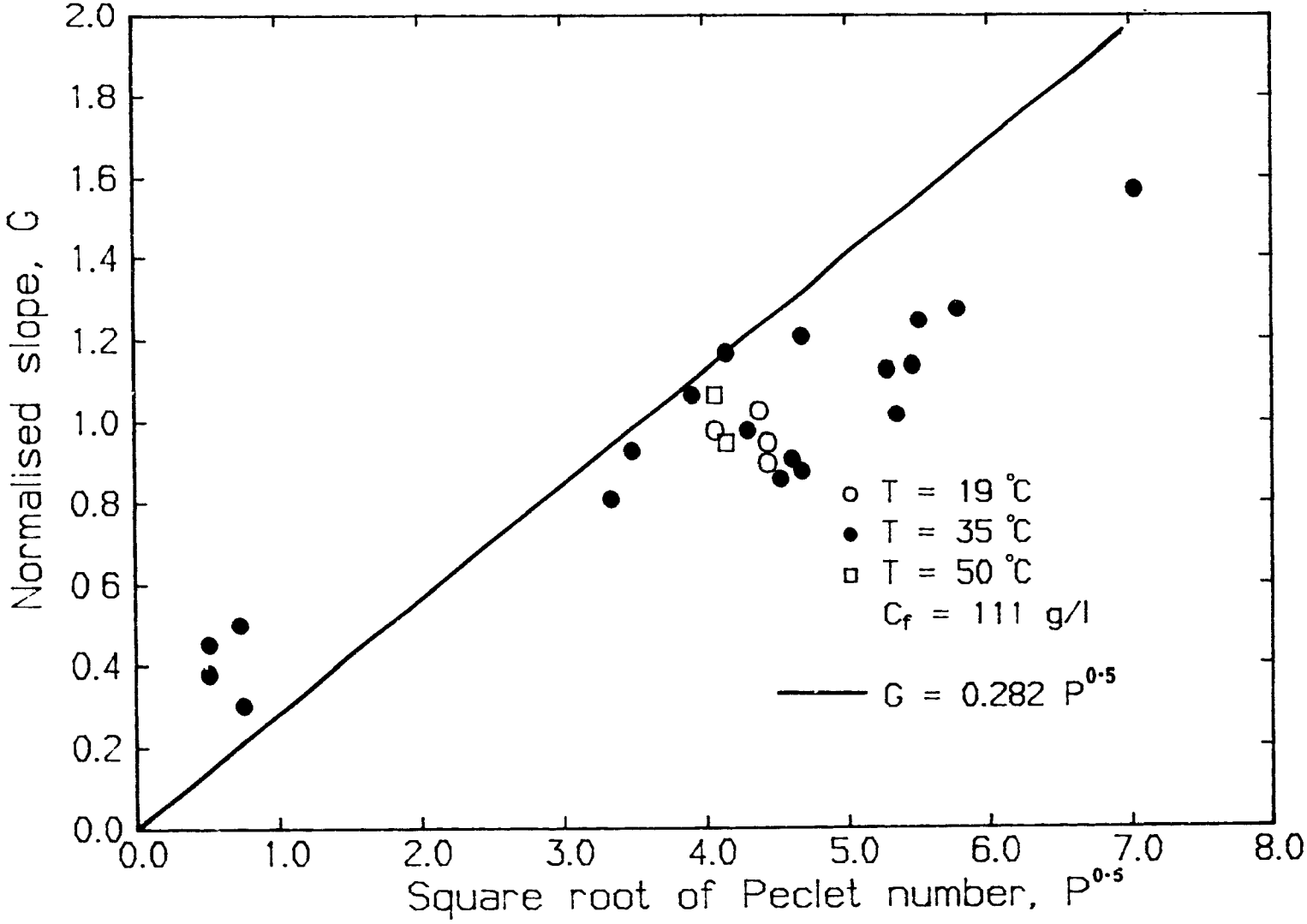
Normalised slope, G
Square root of Peclet number, $P^{0.5}$
2.0
1.8
1.6
1.4
1.2
1.0
0.8
0.6
0.4
0.2
0.0
0.0
1.0
2.0
3.0
4.0
5.0
6.0
7.0
8.0
o T = 19 °C
• T = 35 °C
□ T = 50 °C
C_f = 111 g/l
G = 0.282 $P^{0.5}$

Figure 6.26 Effect of consistency on dimensionless chlorine breakthrough curves.

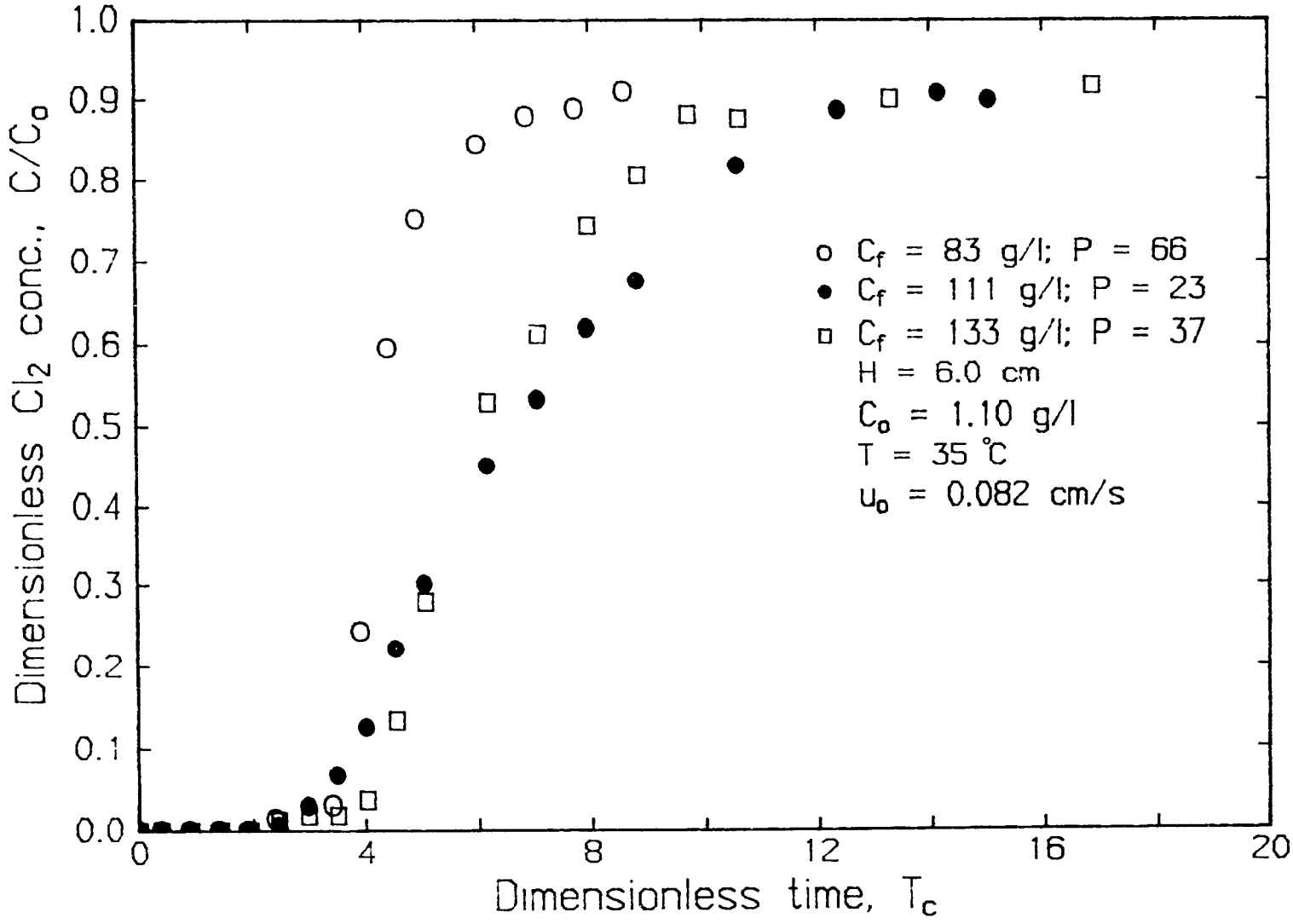
1.0
0.9
0.8
0.7
0.6
0.5
0.4
0.3
0.2
0.1
0.0
0
4
8
12
16
20
Dimensionless Cl_2 conc., C/C_o
Dimensionless time, T_c
o C_f = 83 g/l; P = 66
• C_f = 111 g/l; P = 23
□ C_f = 133 g/l; P = 37
H = 6.0 cm
C_o = 1.10 g/l
T = 35 °C
u_o = 0.082 cm/s

Figure 6.27 Effect of consistency on generalized chlorine breakthrough curves.

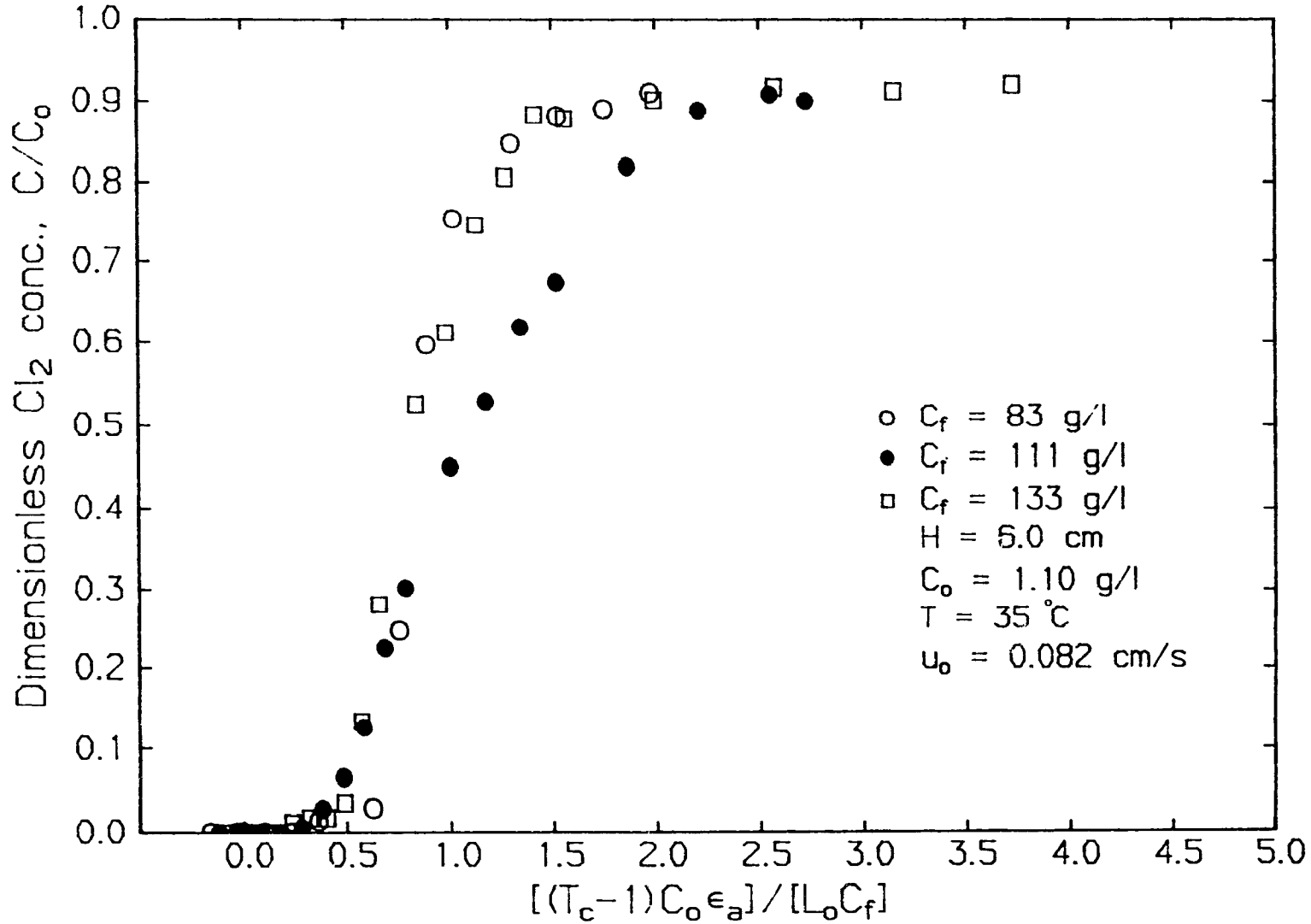
Dimensionless Cl_2 conc., C/C_o
1.0
0.9
0.8
0.7
0.6
0.5
0.4
0.3
0.2
0.1
0.0
0.0
0.5
1.0
1.5
2.0
2.5
3.0
3.5
4.0
4.5
5.0
$[(T_c-1)C_o\epsilon_a]/[L_oC_f]$
o C_f = 83 g/l
● C_f = 111 g/l
□ C_f = 133 g/l
H = 5.0 cm
C_o = 1.10 g/l
T = 35 °C
u_o = 0.082 cm/s

plotted versus the square of the Peclet number in Figure 6.28. The close agreement of the results at consistencies 8 and 12.8% with the general trend shows that the normalised slope is not a function of consistency, nor of any of the other operating variables, but strictly determined by the Peclet number.

6.5.1.6 Effect of recycle

The effect of recycling the chlorination effluent was investigated in a series of two experiments. The effluent from an experiment conducted on a 6 cm pulp pad, a reaction temperature of 19°C, a superficial velocity of 0.164 cm/s and a concentration of 2.10 g/l was contacted with chlorine gas to a concentration of 1.10 g/l. Chlorination was then carried out with this undiluted spent liquor on a 2 cm pad at 35°C and at a superficial velocity of 0.041 cm/s. Since the volume of this chlorine water containing spent liquor was small only a chlorine application of 0.068 g chlorine/ g pulp was possible.

The resulting dimensionless chlorine breakthrough curve is compared in Figure 6.29 with an experiment conducted under similar operating conditions but with fresh chlorine water. The Peclet numbers in both experiments were, 52 and 57, respectively, so that the flow conditions can be considered similar. The close agreement in Figure 6.29 shows that the dissolved organics present in the recycled liquor have negligible effect on the chlorine breakthrough curve.

6.5.2 Total organic carbon breakthrough curves

6.5.2.1 Efect of mean residence time

The mean residence time, $\bar{t}_r = H/u_a$, was varied from 23 to 279 seconds by changing the pad height, H, from 2, 4 to 6 cm and the superfi-

Figure 6.28 Applicability of parallel plug flow model to represent chlorine breakthrough curves: effect of consistency.

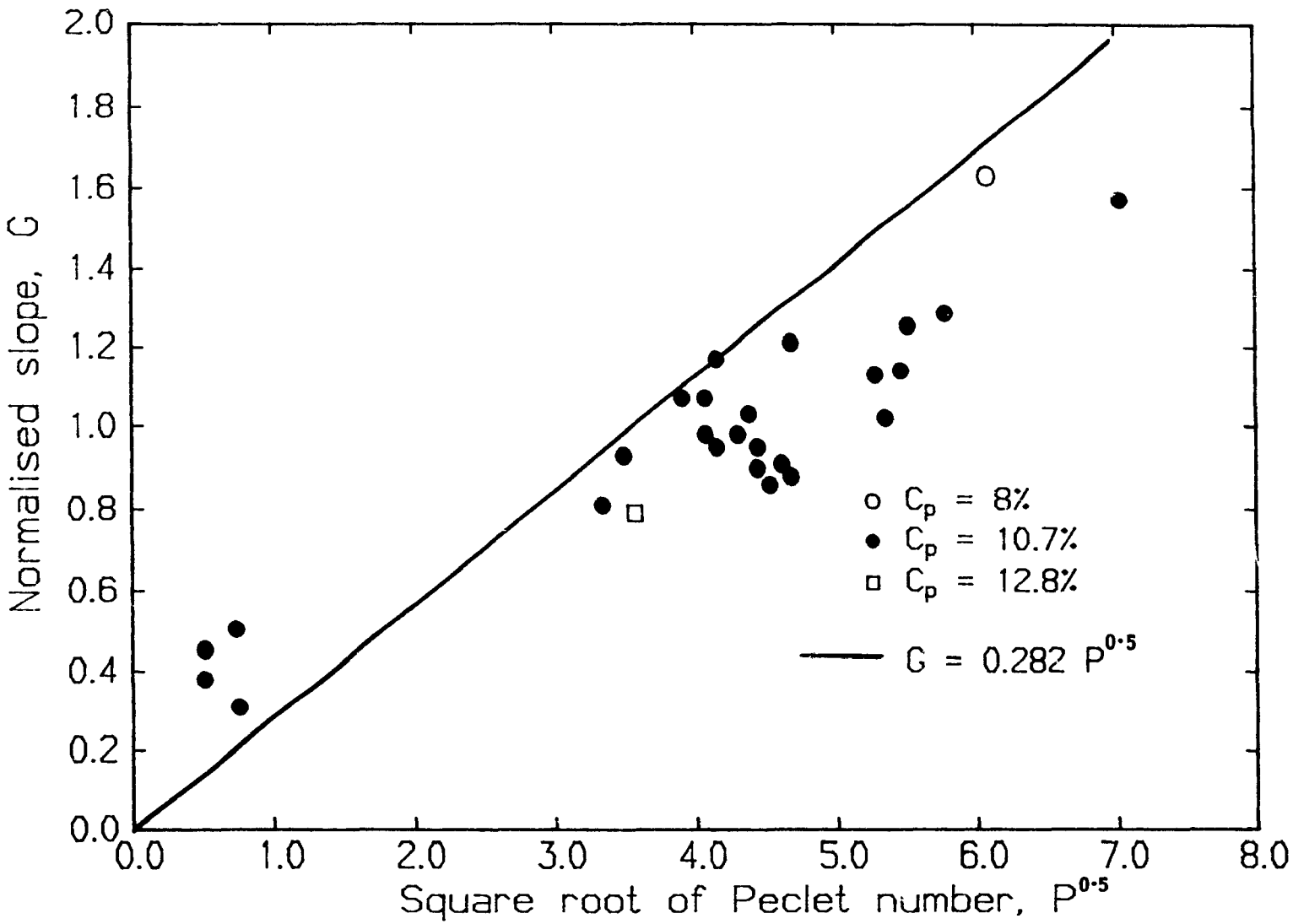
Normalised slope, G
Square root of Peclet number, $P^{0.5}$
2.0
1.8
1.6
1.4
1.2
1.0
0.8
0.6
0.4
0.2
0.0
0.0
1.0
2.0
3.0
4.0
5.0
6.0
7.0
8.0
C_p = 8%
C_p = 10.7%
C_p = 12.8%
G = 0.282 $P^{0.5}$

Figure 6.29 Effect of recycle on chlorine breakthrough curves.

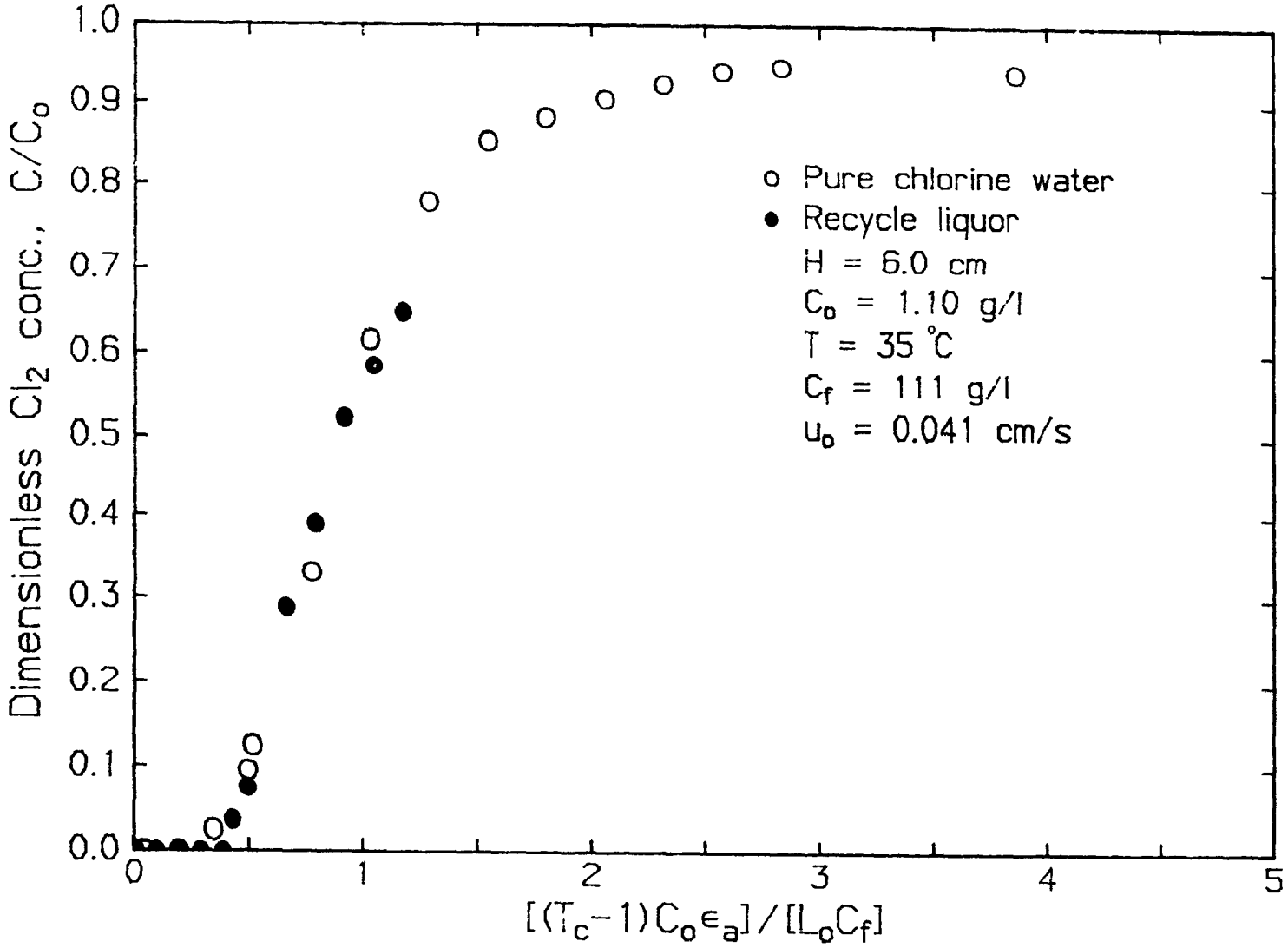
Dimensionless Cl_2 conc., C/C_o
1.0
0.9
0.8
0.7
0.6
0.5
0.4
0.3
0.2
0.1
0.0
0
1
2
3
4
5
$[(T_c-1)C_o\epsilon_a]/[L_oC_f]$
o Pure chlorine water
• Recycle liquor
H = 6.0 cm
C_o = 1.10 g/l
T = 35 °C
C_f = 111 g/l
u_o = 0.041 cm/s

cial velocity, u_o, from 0.020, 0.041 and 0.082 cm/s. Shown in Figure 6.30 are total organic carbon breakthrough curves for variable superficial velocities at a fixed pad height of 2 cm or for $\bar{t}_r$ of 23, 45 and 93 seconds at T = 35°C and C_o = 1.10 g/l. The TOC curves for variable bed heights at a fixed superficial velocity of 0.082 cm/s or for $\bar{t}_r$ of 23, 45 and 68 seconds at T = 35°C and C_o = 1.10 g/l are shown in Figure 6.31. The accessible pad porosity was 0.93 in all cases. Both figures show that the TOC concentration increases with $\bar{t}_r$ at the same value of $(T_c-1)C_o \varepsilon_a/L_o C_f$, although the increases are larger when the increase in $\bar{t}_r$ is caused by an increase in H rather than a decrease in u_o. A small amount of TOC is measured for $(T_c-1)C_o\varepsilon_a/L_oC_f < 0$, because of TOC produced in bed sections with residence times less than $\bar{t}_r$.

The contribution of all sections of the bed to the TOC concentration at the exit results in a rapid increase in TOC/C_o for $(T_c-1)C_o\varepsilon_a/L_oC_f \geq 0$ in Figures 6.30 and 6.31. TOC/C_o reaches a maximum, TOC_m/C_o, at or shortly after breakthrough of chlorine as can be seen in the typical experiment shown in Figure 6.4 (the experiment in Figure 6.4 is the same as one of the experiment in Figure 6.30). Subsequently a gradual decrease in TOC/C_o is observed until (in most cases) a low value, TOC_f/C_o, is reached asymptotically approximately at the same time when complete chlorine breakthrough is obtained at $(T_c-1)C_o\varepsilon_a/L_oC_f \sim 4$. The latter can be confirmed in Figure 6.4. The close agreement between the times which characterise the chlorine and TOC breakthrough curves implies that most of the TOC is generated at the sharp lignin reaction front. However since the effect of $\bar{t}_r$ on TOC production is more pronounced when H rather than u_o is changed and because the TOC production remains finite at complete chlorine

Figure 6.30 Effect of mean residence time, $\bar{t}_r$, on generalized TOC breakthrough curves; variable u_o at fixed H.

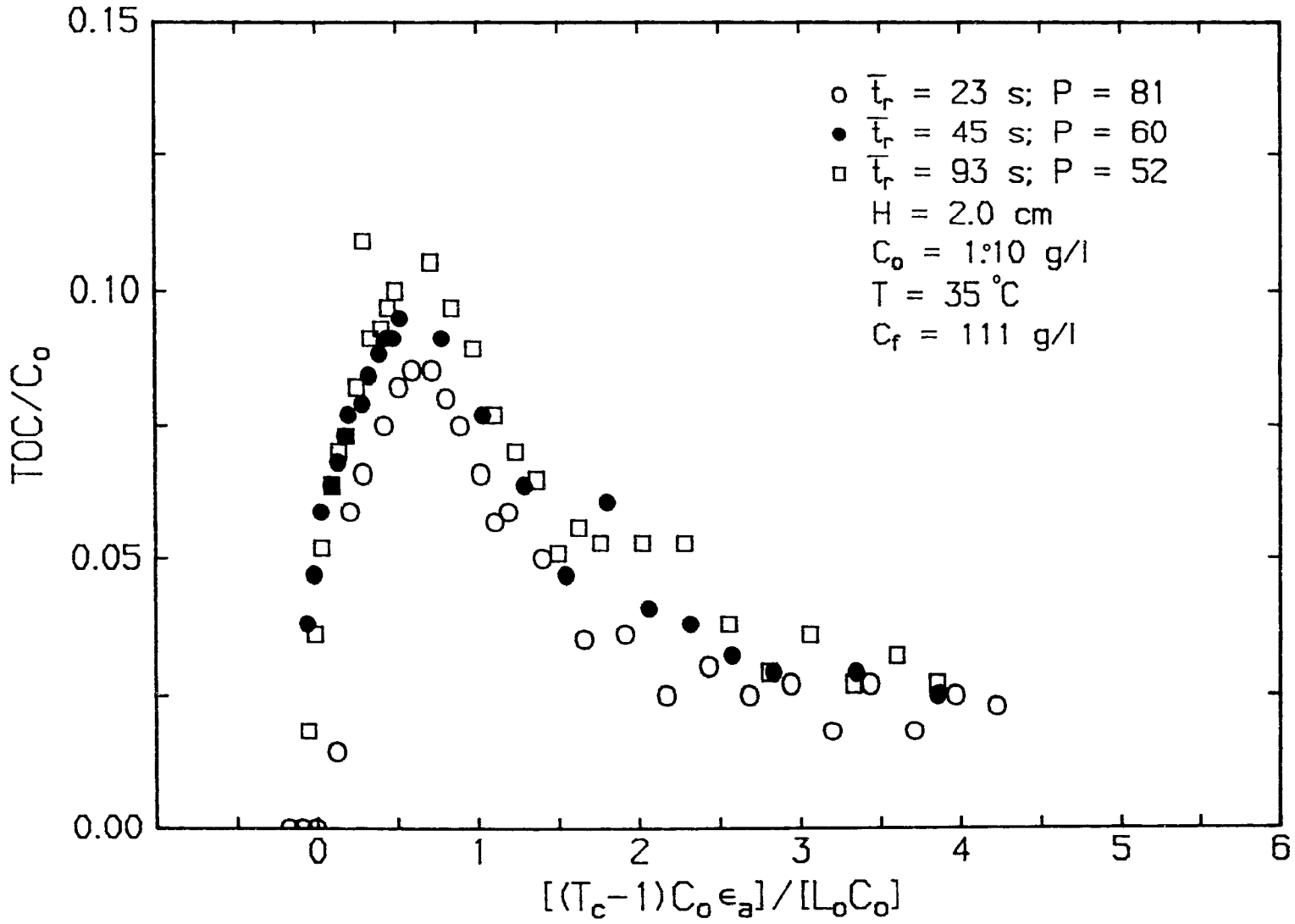
0.15
0.10
0.05
0.00
TOC/C$_o$
0
1
2
3
4
5
6
[(T$_c$−1)C$_o$ ∈$_a$] / [L$_o$C$_o$]
o $\bar{t}_r$ = 23 s; P = 81
● $\bar{t}_r$ = 45 s; P = 60
□ $\bar{t}_r$ = 93 s; P = 52
H = 2.0 cm
C$_o$ = 1.10 g/l
T = 35 °C
C$_f$ = 111 g/l

Figure 6.31 Effect of mean residence time, $\bar{t}_r$, on generalized TOC breakthrough curves; variable H at fixed u_o.

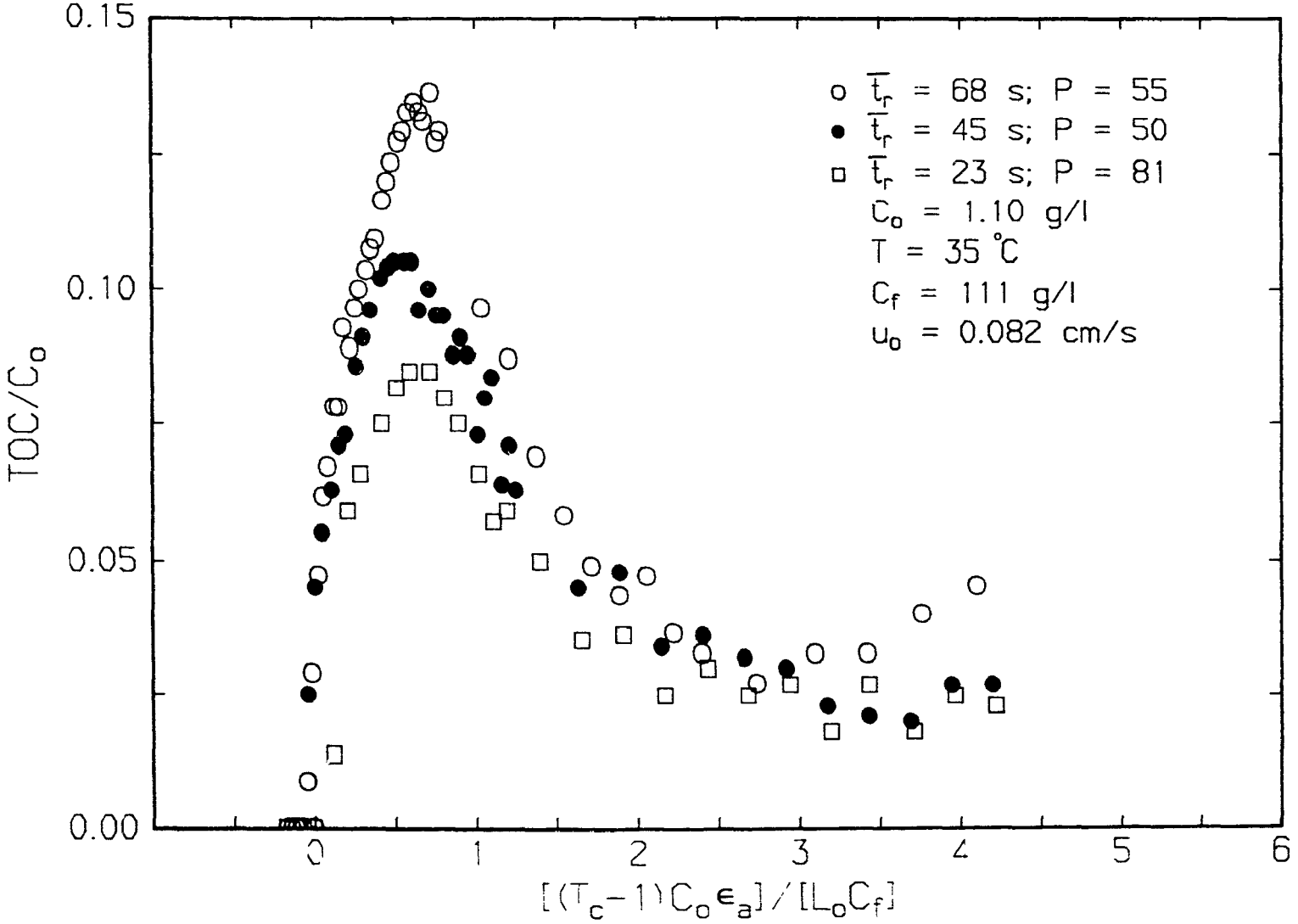
0.15
0.10
0.05
0.00
TOC/C$_o$
0
1
2
3
4
5
6
[(T$_c$−1)C$_o$ε$_a$]/[L$_o$C$_f$]
o $\bar{t}_r$ = 68 s; P = 55
● $\bar{t}_r$ = 45 s; P = 50
□ $\bar{t}_r$ = 23 s; P = 81
C$_o$ = 1.10 g/l
T = 35 °C
C$_f$ = 111 g/l
u$_o$ = 0.082 cm/s

breakthrough, a smaller fraction of TOC must be formed by another process than fast reaction between lignin and chlorine. This aspect will be further addressed later in this section. The TOC curves can further be characterized by the maximum TOC, TOC_m, the final TOC, TOC_f, and the total amount of TOC removed during chlorination, TOC_r (g/g pulp). Therefore the effect of residence time on the TOC curves will now be discussed in terms of these three parameters.

Previously it was shown that the chlorine-carbohydrates reaction is the dominant reaction responsible for the chlorine consumption after complete chlorine breakthrough. From equation 5.8 it follows that a four fold increase of $\bar{t}_r$ from 23 to 93 s at 35°C leads to an increase in chlorine consumption by a factor of 3.9. Also, it can be seen from Figure 6.9 and Table 6.3 that these conditions result in an experimental increase in chlorine consumption of approximately a factor 3. Therefore if the TOC after complete chlorine breakthrough is mainly produced by the carbohydrates reaction one would expect a significant increase in TOC with increasing $\bar{t}_r$ in Figure 6.30 when $(T_c - 1)\, C_o \varepsilon_a / L_o C_f \approx 3.4\text{-}4.0$. Since only a small increase is observed it seems unlikely that most of the TOC emerging from the pad after complete chlorine breakthrough originates from carbohydrates.

The cumulative TOC removed per weight of pulp, $TOC_r/(HAC_f)$, of the experiments of Figure 6.30 and 6.31 are listed in Table 6.4. Also given in Table 6.4 is the $TOC_r/(HAC_f)$ calculated from the decrease in UV + Klason lignin on a chlorine free basis between initial and CW pulp assuming that the ratio $J = C/CH_xO_y$ for lignin is 0.615 g/g and that the CW lignin contains 15.8 % by weight of chlorine (Kempf and Dence (16)).

TABLE 6.4

Characteristic parameters of TOC breakthrough curves;

effect of mean residence time, $\bar{t}_r$

H	u_o	$\bar{t}_r$	P	$\frac{TOC_m}{C_o}$	$\frac{TOC_f}{C_o}$	$\frac{TOC_r}{HAC_f}$	$\frac{1-C}{C_o}$	UV+Kl. lignin in CW pulp	$\frac{TOC_r}{HAC_f}$ Calc.
(cm)	(cm/s)	(s)		(g/g)	(g/g)	(g/g)		(g/gpulp)	(g/gpulp)
2	.02	93	52	.106	.03	.0113	.09	.0309	.0132
2	.041	45	60	.097	.025	.0112	.05	.0271	.0151
2	.082	23	81	.087	.023	.010	.03	.0316	.0128
4	.082	45	50	.106	.025	.0099	.04	.0316	.0128
6	.082	68	55	.137	-	.0135	.07	.0239	.0124

Other conditions: C_o = 1.10 g/l; T = 35°C; C_f = 111 g/l

A = 44.05 cm^2; Klason + UV lignin content of

original pulp = 0.0475 g/g O.D. pulp

Comparison of the two columns in Table 6.4 shows that most of the TOC is accounted for by the decrease in lignin content of the pulp. This suggests that most of the TOC produced after complete breakthrough originates from lignin. The higher calculated TOC_r/HAC_f values could be due to the estimated J ratio being too high. For example, a J value of 0.5 would lead to better agreement between TOC_r and lignin removed from the pulp. Further confirmation was obtained by comparing TOC_f from pulp pads made of fully bleached (i.e. lignin free) pulp and from unbleached pulps. The much higher TOC_f obtained from unbleached pulp in Table 6.5 shows that the largest fraction of TOC_f originates from already reacted lignin.

The production of TOC from lignin after complete chlorine breakthrough could be explained by hydrolysis of chlorinated lignin or by transport limitations of soluble lignin fragments from the fibers. However the latter mechanism seems unlikely since TOC_f is not a function of $\bar{t}_r$ (Table 6.4) and increases with inlet chlorine concentration as will be shown later. Since essentially all the consumed chlorine is accounted for by the carbohydrates reaction, the effect of chlorine in the proposed hydrolysis can only be catalytic in nature. A hydrolysis mechanism was also invoked by Berry and Fleming (17) to account for lignin removal during hot water treatment of pulp.

A plot of TOC_m/C_o versus $\bar{t}_r$ at different pad heights in Figure 6.32 demonstrates that TOC_m/C_o increases with pad height and except for H = 2 cm is hardly influenced by $\bar{t}_r$. This behaviour can be explained by the model proposed earlier when discussing the chlorine breakthrough curves. In this model chlorine reacts rapidly with lignin at the front while upstream of the front chlorinated lignin reacts further with chlorine at a

TABLE 6.5

TOC_f of unbleached and fully bleached pulp

C_o	H	u_o	T	C_f	TOC_f unbleached	TOC_f fully bleached
(g/l)	(cm)	(cm/s)	(°C)	(g/l)	ppm	ppm
1.10	6	.082	34	111	40	13
1.10	6	.164	36	111	30	12
1.10	6	.082	17	111	28	12

Figure 6.32 Effect of mean residence time, $\bar{t}_r$, on TOC_m/C_o.

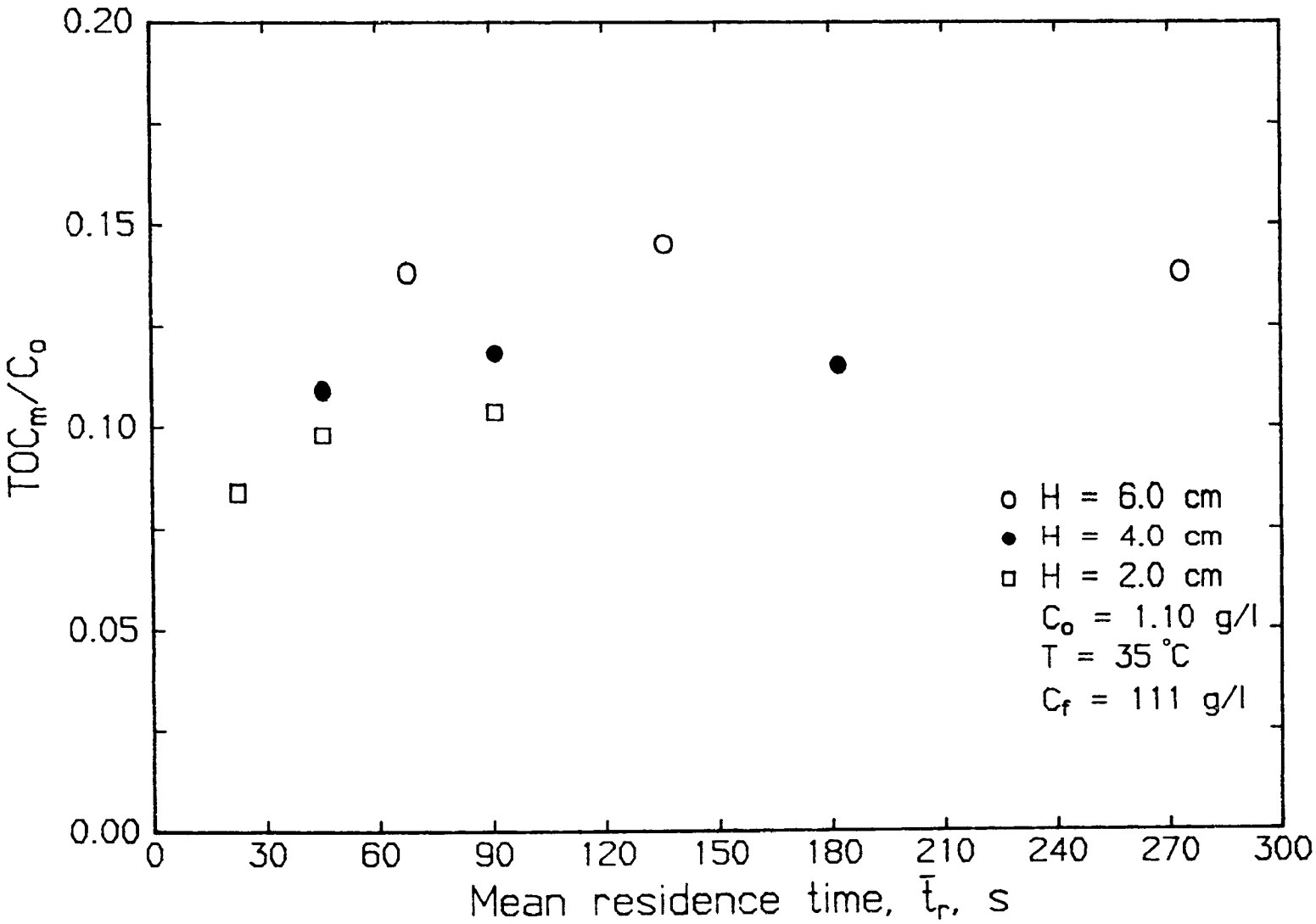
0.20
0.15
0.10
0.05
0.00
TOC$_m$/C$_o$
0
30
60
90
120
150
180
210
240
270
300
Mean residence time, $\bar{t}_r$, s
o H = 6.0 cm
• H = 4.0 cm
□ H = 2.0 cm
C$_o$ = 1.10 g/l
T = 35 °C
C$_f$ = 111 g/l

slow rate. Similarly TOC is also produced at the front and by further reaction (chlorination/hydrolysis) of chlorinated lignin upstream of the front. The TOC concentration generated at the front is proportional to the chlorine concentration at the front, independent of $\bar{t}_r$. The production of TOC upstream of the front is, perhaps, already at a maximum at large $\bar{t}_r$. Thus for the same bed height, TOC_m will only be a function of $\bar{t}_r$ when the degradation reactions before the reaction front are slow and determine the overall release of TOC. This might explain the increase in TOC_m/C_o with $\bar{t}_r$ in Figure 6.31 for H = 2 cm when $\bar{t}_r < 50$ s. For $\bar{t}_r > 50$ s, TOC_m/C_o is relatively insensitive to $\bar{t}_r$ for all bed heights. TOC_m increases with bed height because the thickness of the chlorinated layer before the reaction front increases.

An important conclusion which can be drawn from Figure 6.32 is that the TOC contribution in the effluent can be reduced by employing shallow beds and residence times less than 50 s.

6.5.2.2 Effect of residence time distribution

The effect of residence time distribution on the chlorine breakthrough curves was discussed in section 6.5.1.2. The corresponding total organic carbon breakthrough curves for the poorly and well formed pads of Figure 6.14 are shown in Figure 6.33. The measurement of a significant TOC concentration at negative $(T_c-1)C_o\varepsilon_a/L_oC_f$ for the poorly formed pad confirms the existence of short circuiting flow. The smaller cumulative amount of TOC removed from the poorly formed pad is caused by the reduced quantity of pulp contacted by chlorine. The flat TOC breakthrough curve of the poorly formed pad can also be explained by the non-uniform flow

Figure 6.33 TOC breakthrough curves of poorly formed and well formed pads.

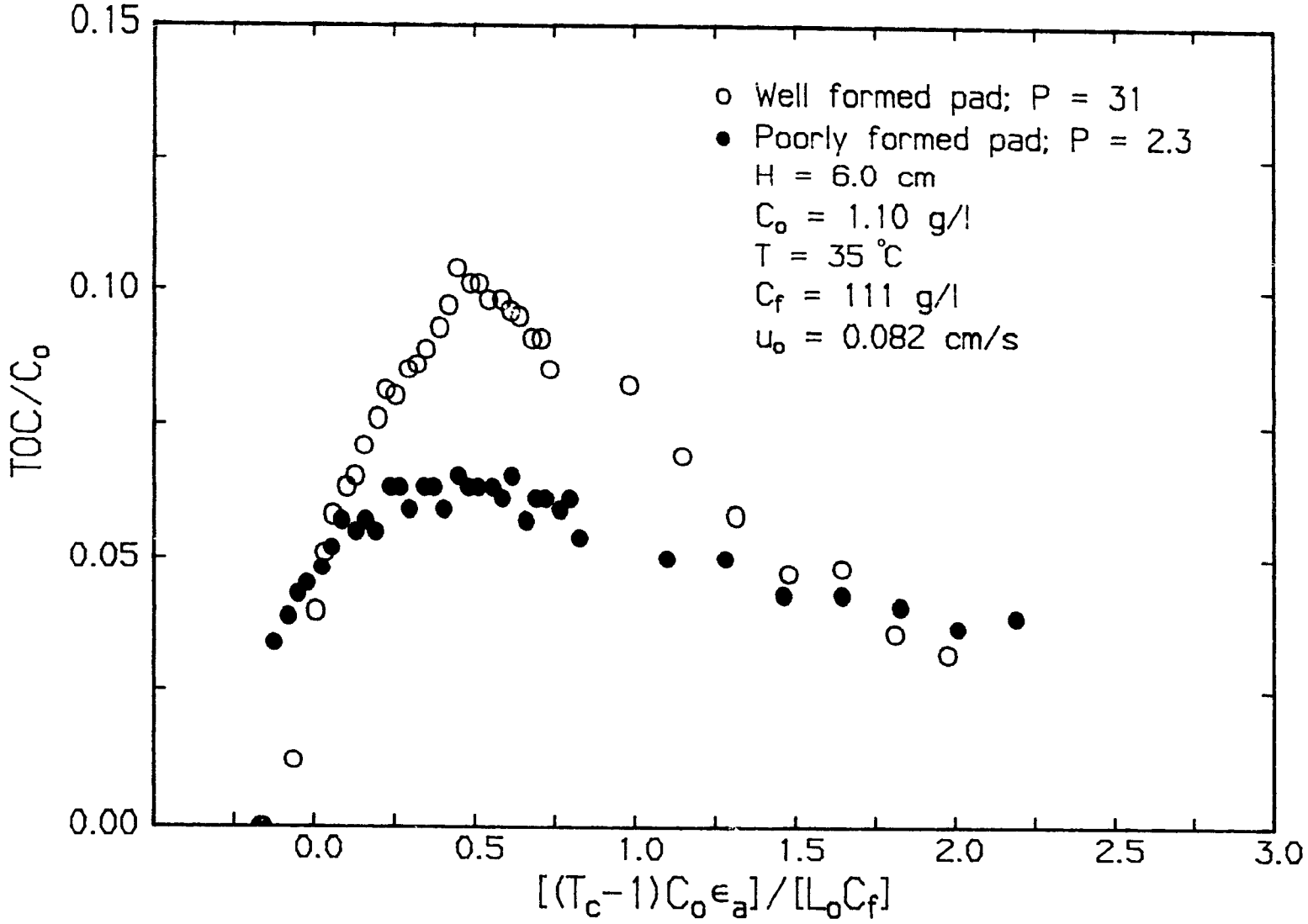
0.15
0.10
0.05
0.00
TOC/C$_o$
o Well formed pad; P = 31
• Poorly formed pad; P = 2.3
H = 6.0 cm
C$_o$ = 1.10 g/l
T = 35 °C
C$_f$ = 111 g/l
u$_o$ = 0.082 cm/s
0.0
0.5
1.0
1.5
2.0
2.5
3.0
[(T$_c$−1)C$_o$ε$_a$]/[L$_o$C$_f$]

distribution which leads to quick breakthrough in certain regions and slow penetration of chlorine in other regions of the pulp pad. The maximum in the TOC curve for the well formed pad occurs when all sections in the pulp pad contribute TOC as a result of the "instantaneous" chlorine-lignin reaction and the degradation of chlorinated lignin before the reaction front.

6.5.2.3 Effect of chlorine concentration

The effect of varying chlorine concentration on the TOC breakthrough curves was investigated at three levels; C_o = 0.55, 1.10 and 2.20 g/l. Dimensionless plots of TOC versus T_c at H = 6 cm, C_p = 10.7% and T = 35°C are shown in Figure 6.34. The larger chlorine supply rates at higher chlorine concentrations lead to the appearance of the TOC peaks at smaller values of T_c. The maximum TOC increases with increasing C_o because the amount of TOC formed by the "instantaneous" reaction between lignin and chlorine is proportional to the chlorine concentration at the reaction front. When the TOC breakthrough curves are replotted as TOC/C_o versus $(T_c-1)C_o\varepsilon_a/L_oC_f$ in Figure 6.35, the magnitude of the maximum, TOC_m/C_o, shows the opposite trend of Figure 6.34, presumably because the TOC contribution from chlorinated lignin before the front does not increase proportionally with C_o. This is further shown in Figure 6.36 where TOC_m shows a somewhat smaller than proportional increase with C_o at three pad heights for the same mean residence times.

Table 6.6 shows that the cumulative total organic carbon removed, TOC_r, decreases when the chlorine concentration increases above 1.10 g/l at a given chlorine application on pulp. This trend could be explained by

Figure 6.34 Effect of chlorine concentration on TOC breakthrough curves.

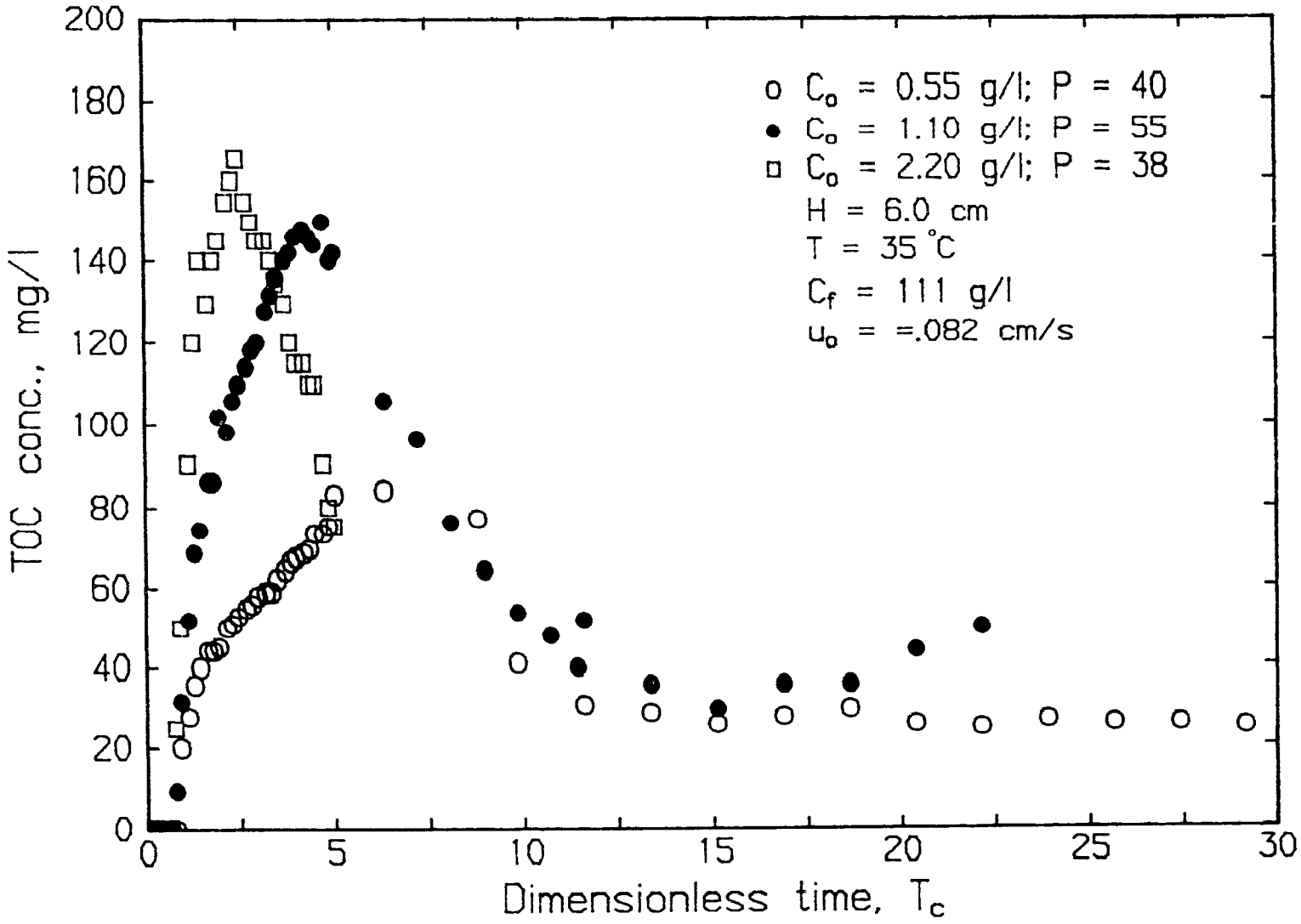
o C_o = 0.55 g/l; P = 40
• C_o = 1.10 g/l; P = 55
□ C_o = 2.20 g/l; P = 38
H = 6.0 cm
T = 35 °C
C_f = 111 g/l
u_o = =.082 cm/s
TOC conc., mg/l
Dimensionless time, T_c
0
20
40
60
80
100
120
140
160
180
200
0
5
10
15
20
25
30

Figure 6.35 Effect of chlorine concentration on generalized TOC breakthrough curves.

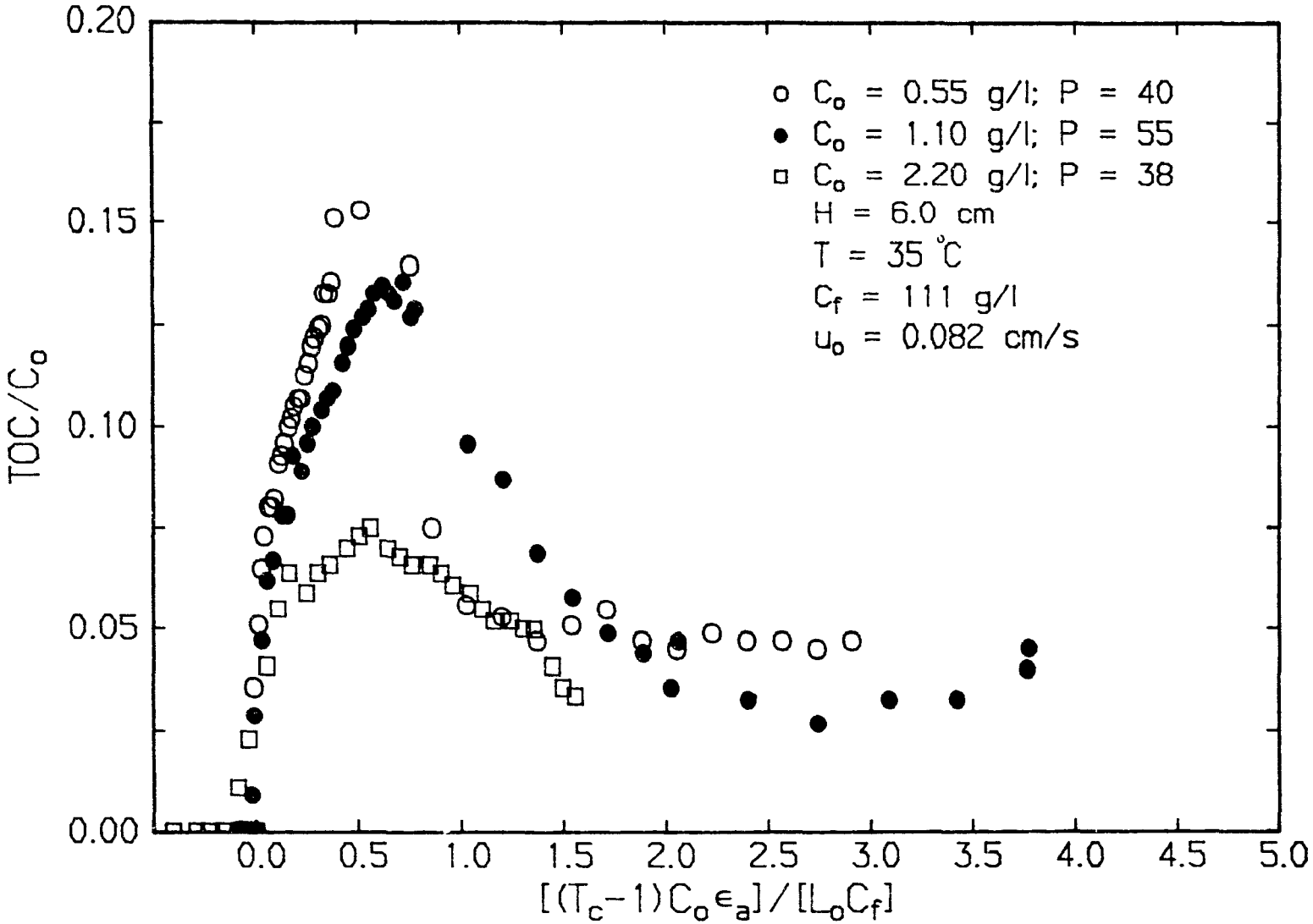
0.20
0.15
0.10
0.05
0.00
TOC/C$_o$
0.0
0.5
1.0
1.5
2.0
2.5
3.0
3.5
4.0
4.5
5.0
[(T$_c$−1)C$_o$∈$_a$]/[L$_o$C$_f$]
o C$_o$ = 0.55 g/l; P = 40
• C$_o$ = 1.10 g/l; P = 55
□ C$_o$ = 2.20 g/l; P = 38
H = 6.0 cm
T = 35 °C
C$_f$ = 111 g/l
u$_o$ = 0.082 cm/s

Figure 6.36 Effect of chlorine concentration on TOC_m.

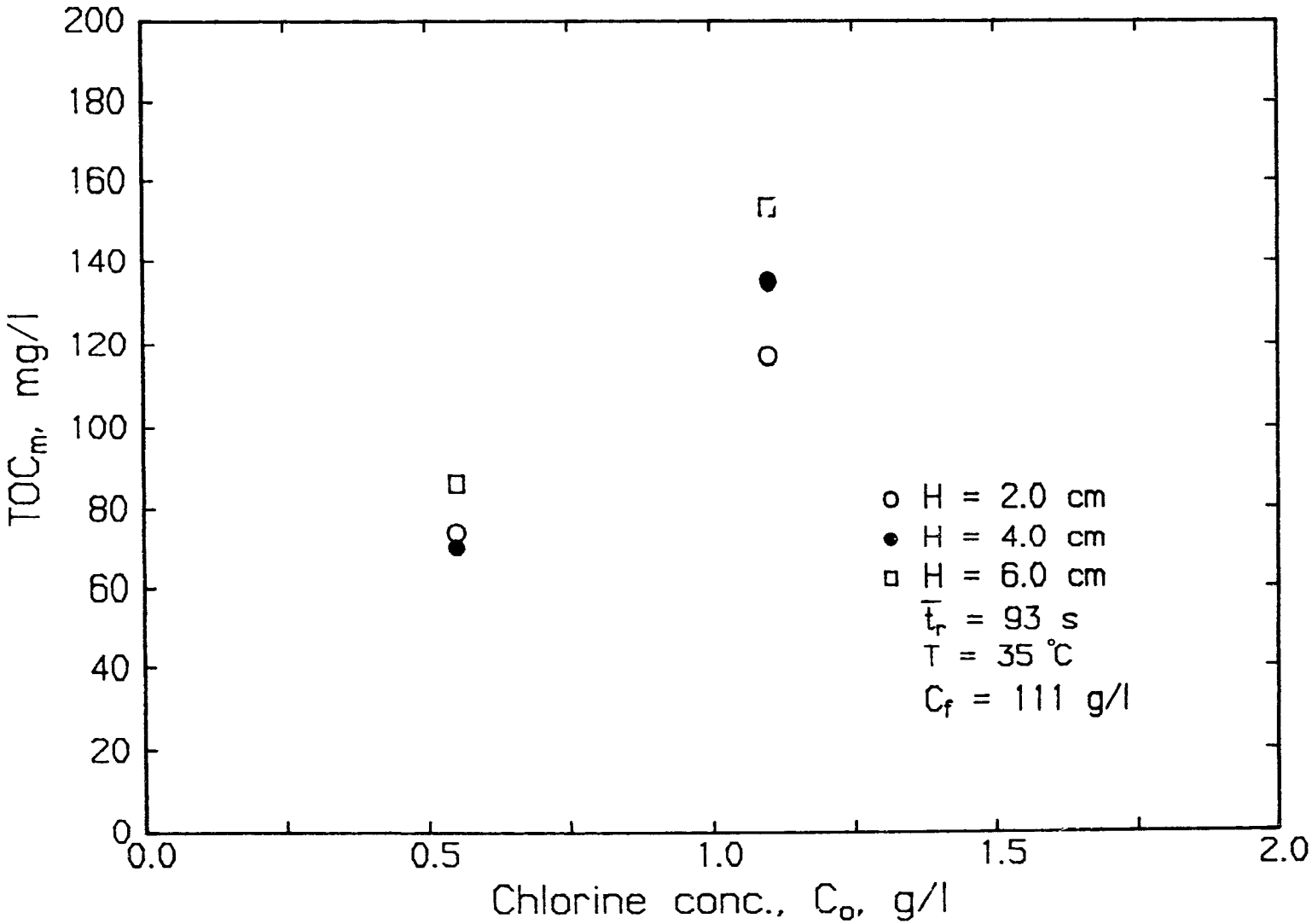
200
180
160
140
120
100
80
60
40
20
0
0.0
0.5
1.0
1.5
2.0
TOC$_m$, mg/l
Chlorine conc., C_o, g/l
o H = 2.0 cm
• H = 4.0 cm
□ H = 6.0 cm
$\bar{t}_r$ = 93 s
T = 35 °C
C_f = 111 g/l

TABLE 6.6

Effect of chlorine concentration on cumulative TOC removal

H (cm)	T (°C)	C_f (g/l)	u_o (cm/s)	C_o (g/l)	$(T_c-1)C_o\varepsilon_a/L_oC_f$ (g/g)	TOC_r (mg)
6	35	111	0.082	0.55	1.84	221
6	35	111	0.082	1.10	1.84	227
6	35	111	0.082	2.20	1.84	128

the fact that less lignin is solubilized and removed by hydrolysis at higher chlorine concentration due to the shorter reaction times. It is interesting to note from Table 6.6 that the cumulative TOC removal at 0.55 and 1.10 g/l are essentially the same.

6.5.2.4 Effect of temperature

The TOC breakthrough curves corresponding to the chlorine breakthrough curves of Figure 6.22 are shown in Figure 6.37. The increase in cumulative TOC removed at higher temperatures is apparent. The increased TOC_r can be explained by increased hydrolysis of chlorinated lignin at higher temperatures. An increase in the extent of oxidation reactions at higher temperatures has been mentioned in a number of reported chlorination studies. This would increase the solubility of chlorinated lignin. Increased TOC from the chlorine- carbohydrates reaction is also expected at higher temperatures. The contribution of the latter reaction at 50°C is difficult to quantify since increasing TOC/C_o is obtained when chlorine water is passed through pulp pads of fully bleached pulps. The increased TOC removal at higher temperatures is supported by lower CW Klason lignin content. This will be addressed in a later section.

Figure 6.38 show plots of TOC_m versus temperature at different fixed chlorine water concentrations and at a fixed mean residence time of 68 seconds. The increased TOC_m at higher temperatures is expected from the above discussions.

6.5.2.5 Effect of consistency

The effect of pulp pad consistency was investigated at three levels; 8.0, 10.7 and 12.8%. The effect of consistency on the chlorine breakthrough curves was previously presented in Figure 6.27. The corresponding TOC breakthrough curves, TOC/C_o versus $(T_c-1)C_o\varepsilon_a/L_oC_f$, are shown

Figure 6.37 Effect of temperature on generalized TOC breakthrough curves.

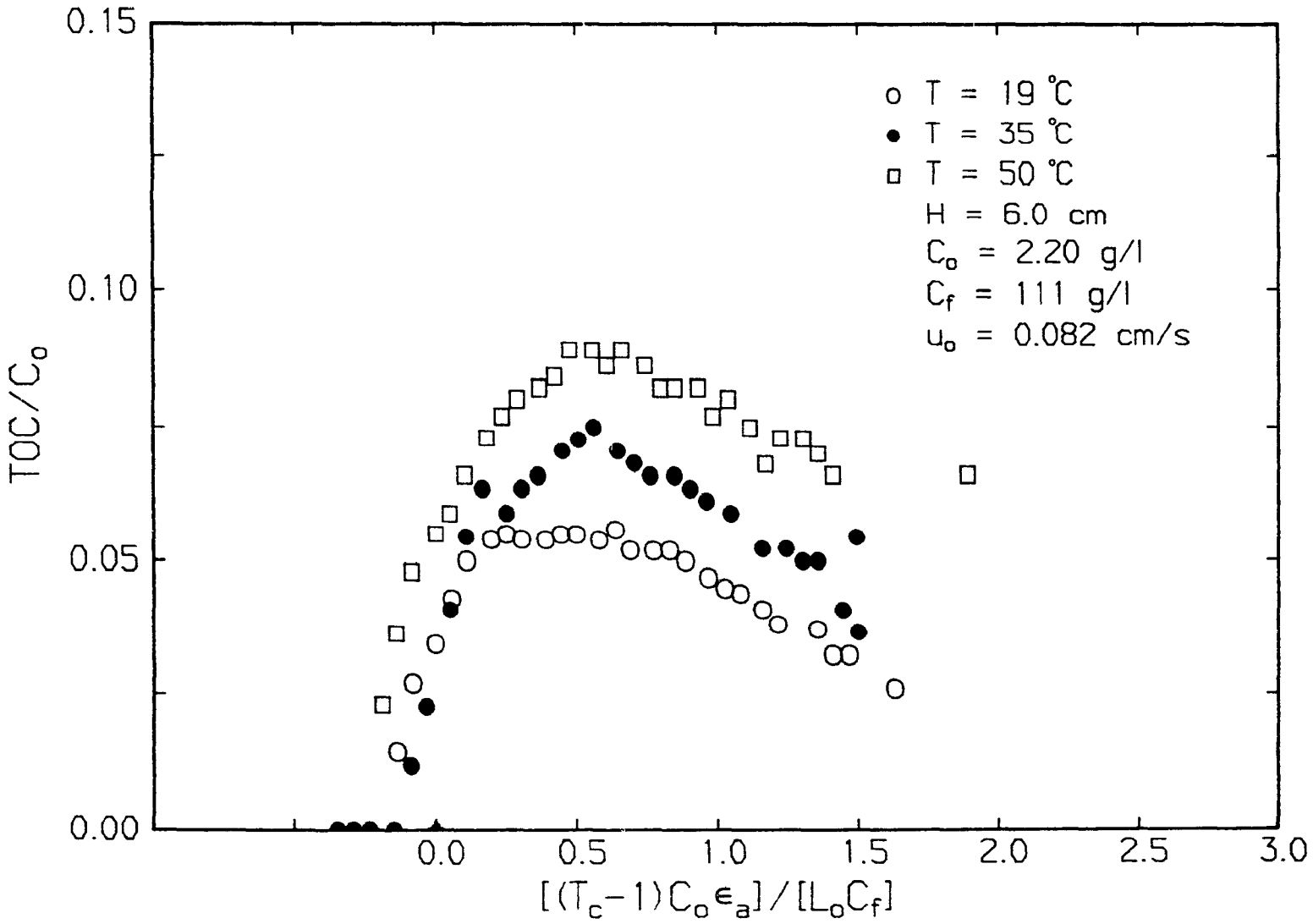
0.15
0.10
0.05
0.00
TOC/C$_o$
0.0
0.5
1.0
1.5
2.0
2.5
3.0
[(T$_c$−1)C$_o$ε$_a$]/[L$_o$C$_f$]
o T = 19 ℃
• T = 35 ℃
□ T = 50 ℃
H = 6.0 cm
C$_o$ = 2.20 g/l
C$_f$ = 111 g/l
u$_o$ = 0.082 cm/s

Figure 6.38 Effect of temperature on TOC_m.

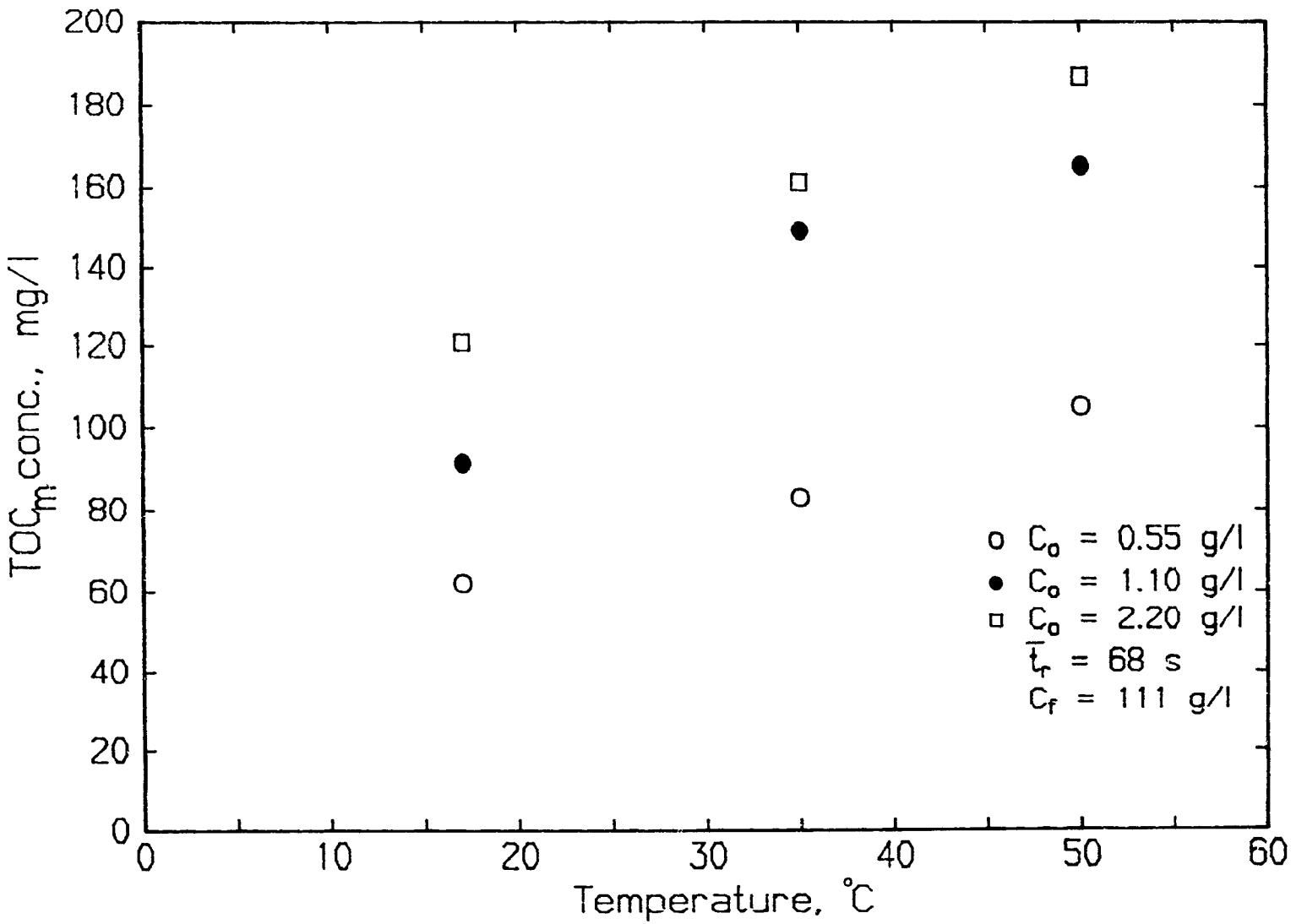
200
180
160
140
120
100
80
60
40
20
0
0
10
20
30
40
50
60
TOC_m conc., mg/l
Temperature, °C
o C_o = 0.55 g/l
● C_o = 1.10 g/l
□ C_o = 2.20 g/l
t̄_r = 68 s
C_f = 111 g/l

in Figure 6.39. The almost identical normalised TOC curves show that the amount of TOC removed per initial weight of lignin is independent of pulp pad consistency. This is surprising since more chlorolignin is present before the reaction front at higher consistencies. This situation is similar to thicker beds at the same consistency and mean residence time, and thus a higher TOC_m and TOC_r is expected for higher consistencies. The possible reason for the independency of TOC_m and TOC_r on consistency might be the decrease in Peclet number with increasing consistency for the experiments in Figure 6.39. A decrease in Peclet number decreases TOC_m and TOC_r which may compensate the expected opposing effect of increasing consistency.

6.5.3 Total inorganic chloride breakthrough curves

6.5.3.1 Effect of mean residence time

The total inorganic chloride breakthrough curves for a 2 cm thick bed at mean residence times of 23, 45 and 93 seconds are shown in Figure 6.40. These breakthrough curves corresponds to the chlorine and TOC breakthrough curves in, respectively, Figure 6.10 and 6.30. The effect of $\bar{t}_r$ produced by varying the bed height H at constant u_a is shown in Figure 6.41. The total inorganic chloride (TICl) breakthrough curves correspond to the TOC breakthrough curves in Figures 6.31. Comparison of the TICl breakthrough curves with the corresponding total organic carbon breakthrough curves shows that chloride appears at the exit simultaneously with TOC. Also the chloride concentration reaches a constant value just after the TOC maximum. Comparison with the corresponding chlorine breakthrough curves shows that the constant TICl concentrations are reached much earlier than complete chlorine breakthrough. In all cases the plateau TICl

Figure 6.39 Effect of consistency on generalized TOC breakthrough curves.

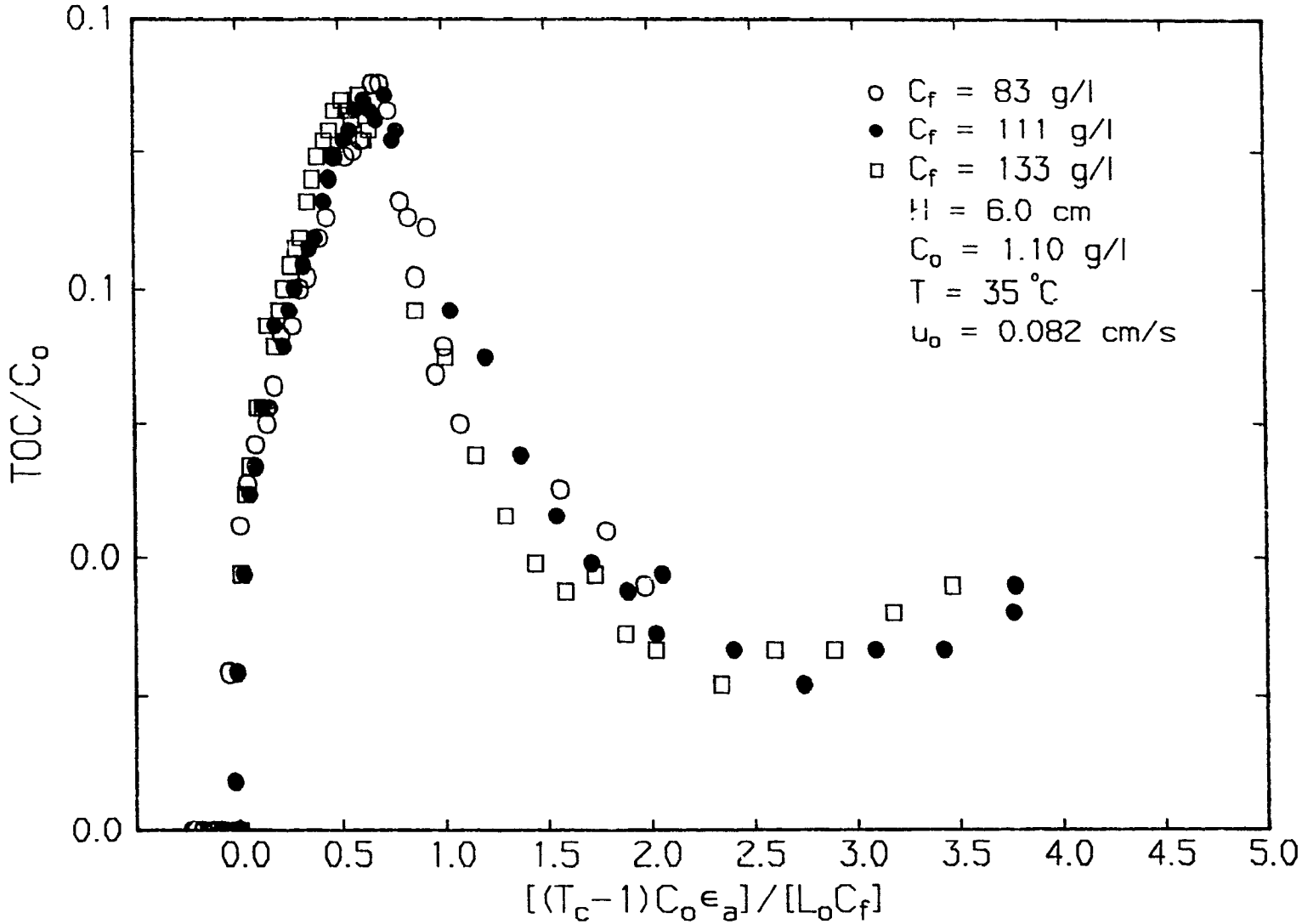
0.1
0.1
0.0
0.0
TOC/C$_o$
0.0
0.5
1.0
1.5
2.0
2.5
3.0
3.5
4.0
4.5
5.0
[(T$_c$−1)C$_o$ε$_a$]/[L$_o$C$_f$]
C$_f$ = 83 g/l
C$_f$ = 111 g/l
C$_f$ = 133 g/l
H = 6.0 cm
C$_o$ = 1.10 g/l
T = 35 °C
u$_o$ = 0.082 cm/s

Figure 6.40 Effect of mean residence time, $\bar{t}_r$, on total inorganic chloride breakthrough curves; variable u_o at fixed H.

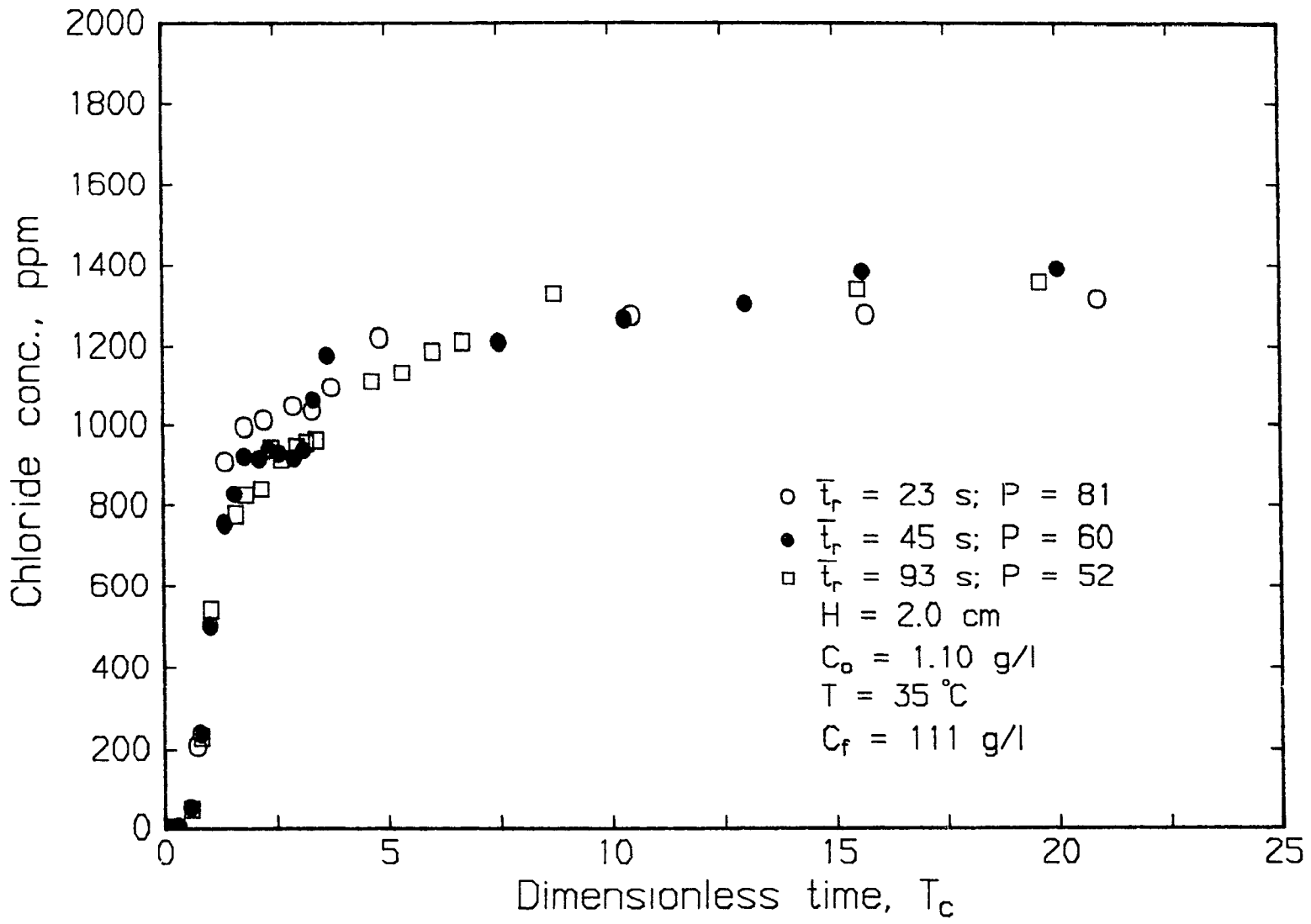
Chloride conc., ppm
2000
1800
1600
1400
1200
1000
800
600
400
200
0
0
5
10
15
20
25
Dimensionless time, T_c
o $\bar{t}_r$ = 23 s; P = 81
● $\bar{t}_r$ = 45 s; P = 60
□ $\bar{t}_r$ = 93 s; P = 52
H = 2.0 cm
C_o = 1.10 g/l
T = 35 °C
C_f = 111 g/l

concentration is greater than the inlet TICl from molecular chlorine. This excess amount is due to additional chloride in the chlorine water tank due to previous degradation of chlorine molecules.

Chenging the mean residence time by changing the flowrate of chlorine water at a fixed pad height does not appear to have much influence on the chloride breakthrough curves (Figure 6.40). There is however some difference when the mean residence times are changed by varying the pad height as shown in Figure 6.41. More TICl appears to be produced at higher pad heights. If substitution and oxidation of lignin only occured at the "instantaneous" reaction front one would expect the TICl BTC to reach a plateau at the same time as the chlorine BTC. Inorganic chloride from the chlorine-carbohydrates reaction also reaches a maximum when chlorine breakthrough is complete. Therefore the present TICl BTC suggests that a significant amount of chloride is also produced by further oxidation of chlorinated lignin between the inlet and reaction front which compensates for the chlorine incorporated in lignin by substitution at the front.

The substitution and oxidation of lignin can be represented by respectively the following overall reactions

$$L + Cl_2 \longrightarrow L\text{-}Cl + HCl \qquad [6.10]$$

and

$$L + Cl_2 \longrightarrow \text{oxidised } L + 2HCl \qquad [6.11]$$

Figure 6.41 Effect of mean residence time, $\bar{t}_r$, on total inorganic chloride breakthrough curves; variable H at fixed u_o.

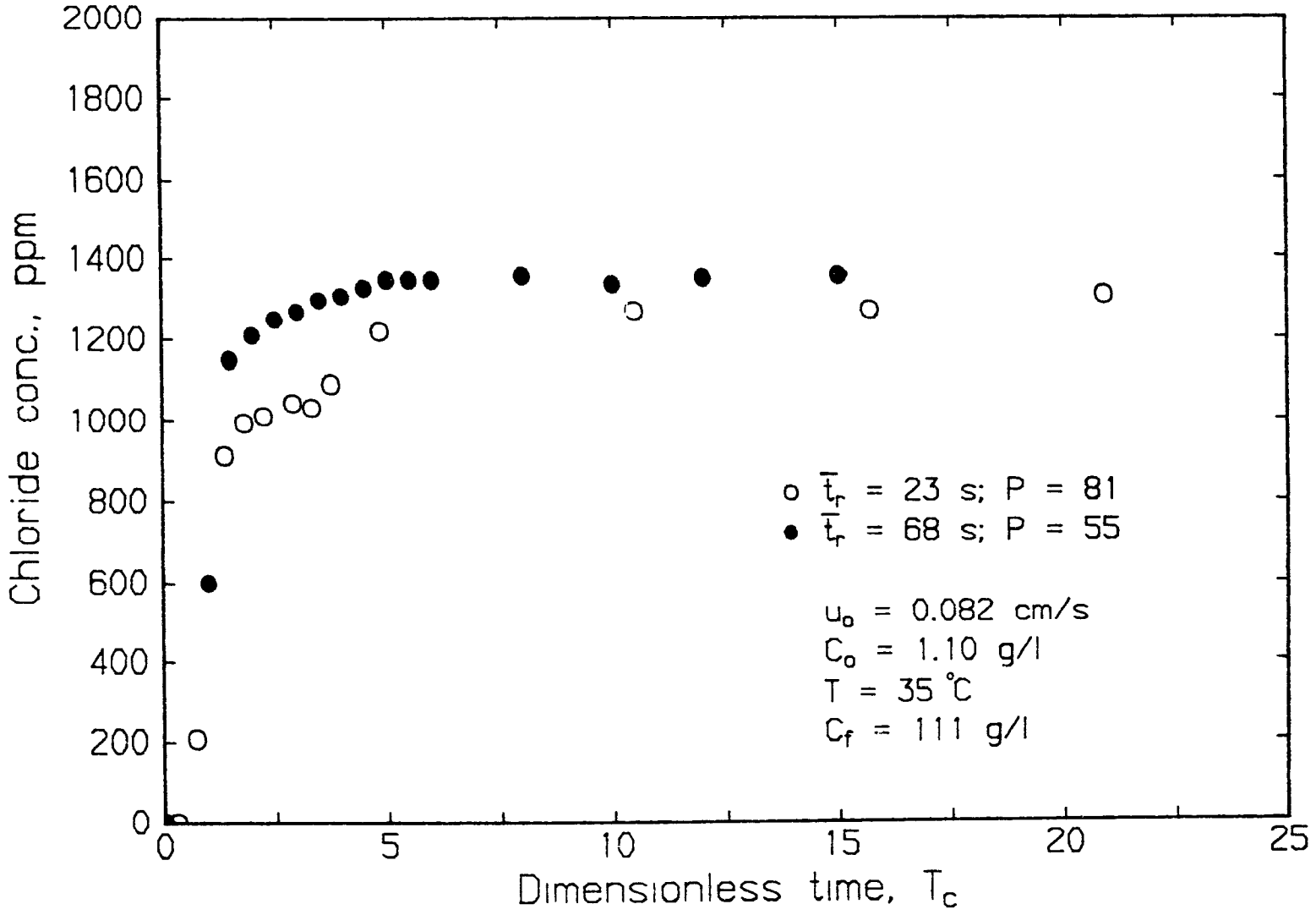
Chloride conc., ppm
2000
1800
1600
1400
1200
1000
800
600
400
200
0
0
5
10
15
20
25
Dimensionless time, T_c
o $\bar{t}_r$ = 23 s; P = 81
● $\bar{t}_r$ = 68 s; P = 55
u_o = 0.082 cm/s
C_o = 1.10 g/l
T = 35 °C
C_f = 111 g/l

Based on these two reactions one can define substitution as a fraction of chlorination, S, as

$$\frac{2[(Cl_2 \text{ consumed by lignin}) - (Cl^- \text{ produced by lignin})]}{(Cl_2 \text{ consumed by lignin})} \qquad [6.12]$$

The substitution fraction, S, therefore also accounts for HCl producing reactions with chlorolignin before the reaction front as if these occur at the front.

S can be calculated with the parallel plug flow model. The total inorganic chloride concentration at the exit of a single channel, $[Cl^-]_{ce}$, is given by:

$$[Cl^-]_{ce} = 0 \text{ when } t < t_r \qquad [6.13]$$

or

$$[Cl^-]_{ce} = [Cl^-]_f + C_o - \frac{SC_o}{2(K(t - t_r) + 1)} \qquad [6.14]$$

$$\text{when } t_r < t < \frac{e^{k_c t_r} - 1}{K} + t_r$$

where $[Cl^-]_f$ is the excess free chloride concentration in the feed and $K = \varepsilon_a C_o k_c / (SL_o L_o C_f)$

or

$$[Cl^-]_{ce} = [Cl^-]_f + C_o \qquad [6.15]$$

$$\text{when } t > t_b > \frac{e^{k_c t_r} - 1}{K} + t_r$$

The total inorganic chloride concentration at the exit of the bed, $[Cl^-]_{ce,t}$, is obtained by summing up the contributions from all channels as

$$[Cl^-]_{ce,t} = \int_0^1 [Cl^-]_{ce}\, dF \qquad [6.16]$$

With the use of equations 6.13 to 6.16 and SL_o determined from the corresponding chlorine BTC, S can be found by trial and error at different reaction times. In this way the chloride BTC's can be transformed into S as a function of time. Because the latter curves give more insight into the phenomena occuring in the bed, all further total inorganic chloride BTC's will be presented as S versus $(T_c-1)C_o\varepsilon_a/(L_oC_f)$. The complete derivation of equations 6.13 to 6.16 are given in Appendix (6-4). It should be noted that because HCl is also produced upstream of the reaction front, negative values for S are expected as longer reaction times.

Different mean residence time at constant pad height shows no consistent influence on S in Figure 6.42. This is in agreement with the observation made when discussing the TOC BTC's, that the oxidation/hydrolysis reactions upstream of the reaction front are not a function of $\bar{t}_r$ at constant H unless $\bar{t}_r$ is very small. The fraction of substitution is, however, distinctly lower at higher $\bar{t}_r$ caused by increasing pad height at the same superficial velocity as shown in Figure 6.43. This again is consistent with the result that more TOC is generated with thicker pulp pads. Thicker pads result in contact of correspondingly larger volumes of

Figure 6.42 Effect of mean residence time, $\bar{t}_r$, on S; variable u_o at fixed H.

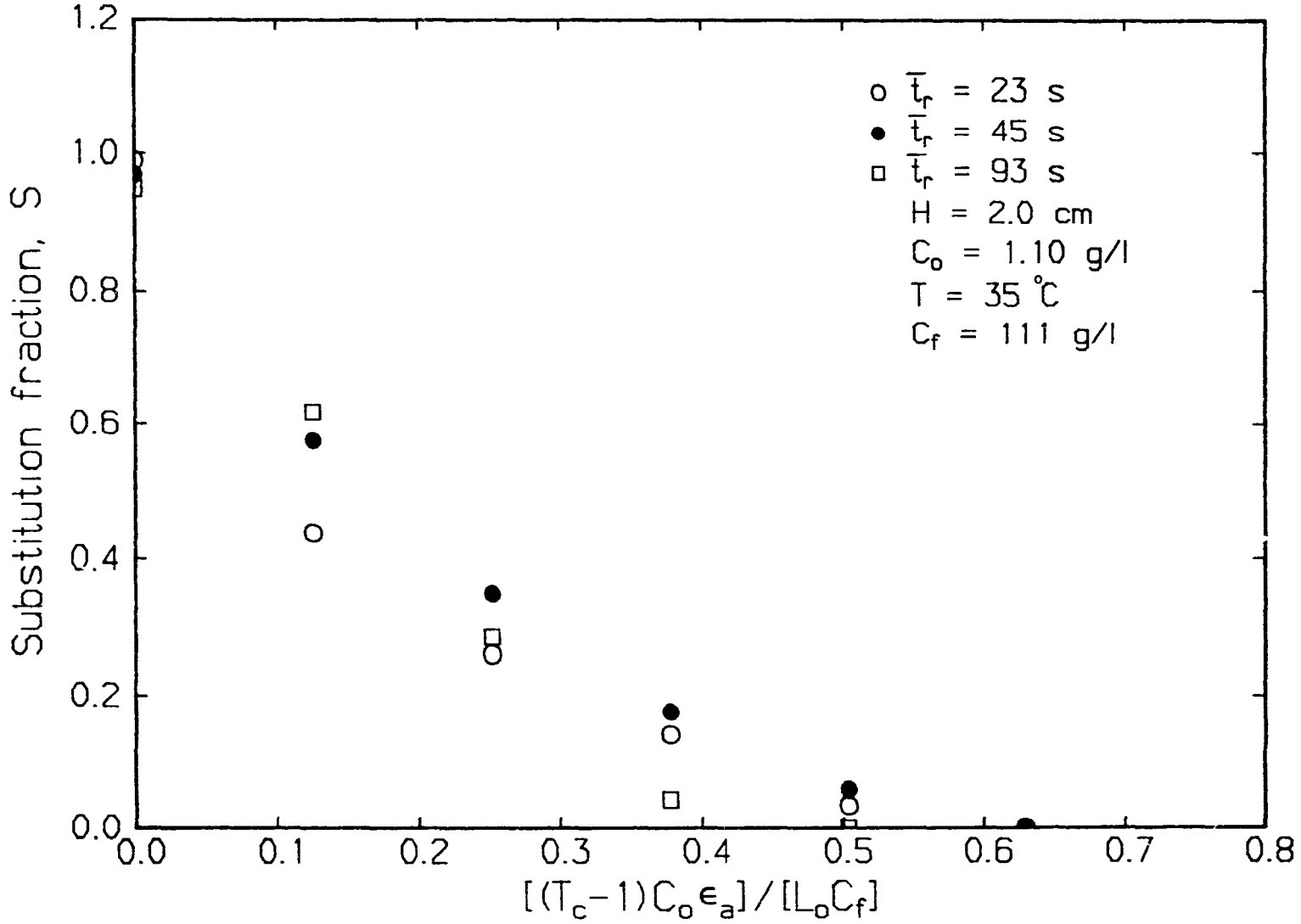
Substitution fraction, S
1.2
1.0
0.8
0.6
0.4
0.2
0.0
0.0
0.1
0.2
0.3
0.4
0.5
0.6
0.7
0.8
[(T_c−1)C_o ε_a]/[L_o C_f]
o t̄_r = 23 s
● t̄_r = 45 s
□ t̄_r = 93 s
H = 2.0 cm
C_o = 1.10 g/l
T = 35 °C
C_f = 111 g/l

Figure 6.43 Effect of mean residence time, $\bar{t}_r$, on S; variable H at fixed u_o.

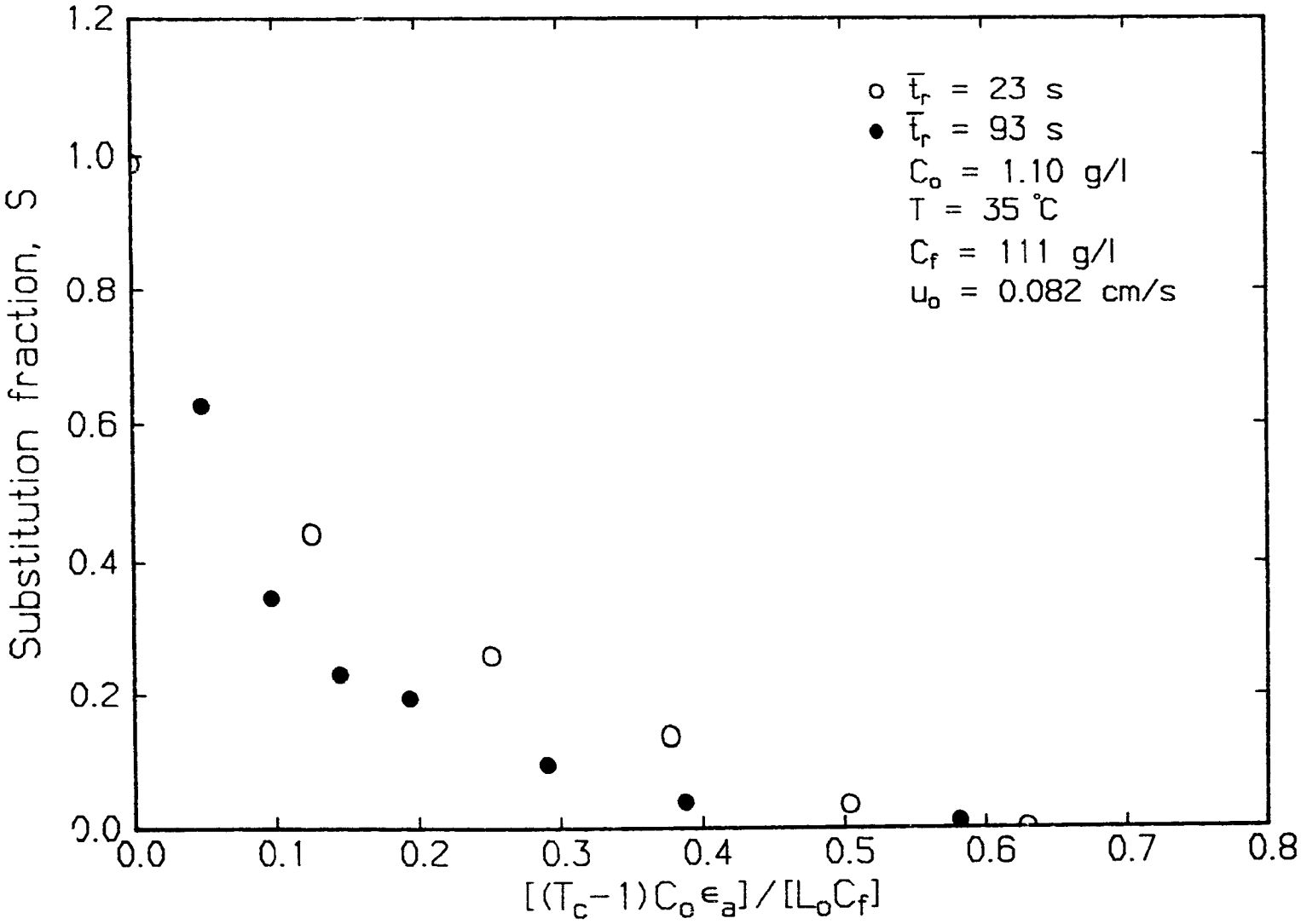
o $\bar{t}_r$ = 23 s
● $\bar{t}_r$ = 93 s
C_o = 1.10 g/l
T = 35 ℃
C_f = 111 g/l
u_o = 0.082 cm/s
Substitution fraction, S
1.2
1.0
0.8
0.6
0.4
0.2
0.0
0.0
0.1
0.2
0.3
0.4
0.5
0.6
0.7
0.8
$[(T_c-1)C_o\epsilon_a]/[L_oC_f]$

chlorine water with reacted lignin upstream of the reaction front. Thus the inorganic chloride contribution upstream of the front increases and consequently substitution as fraction of lignin chlorination decreases.

6.5.3.2 Effect of temperature

The effect of three temperature levels on the substitution fraction is shown in Figure 6.44. The value of S at the same chlorine application on pulp is higher at lower temperatures. This implies that the oxidation reactions as fraction of lignin chlorination increases at higher temperatures. This agrees with previously published work. The decrease in S at higher temperatures can be attributed to increased rate of the oxidation/hydrolysis reactions at higher temperatures upstream of the reaction front.

Comparison of Figure 6.37 and Figure 6.44 shows that S becomes zero at a chlorine application corresponding to the peak of the TOC breakthrough curve.

6.5.3.3 Effect of chlorine concentration

No significant influence of chlorine concentration on S is observed as shown in Figure 6.45. Similar to the other variables discussed S becomes zero at the point corresponding to the maximum of the TOC breakthrough curves for both initial chlorine concentrations.

6.5.4 Methanol breakthrough curves

The TOC breakthrough curves are made up of several organic substances. One of the major reaction products is methanol. Since methanol is formed by removal of the methoxyl group from the guaicyl unit, its breakthrough curve gives more specific information about lignin-chlorine reactions than TOC. This, and its potential use as an easily measured

Figure 6.44 Effect of temperature on S.

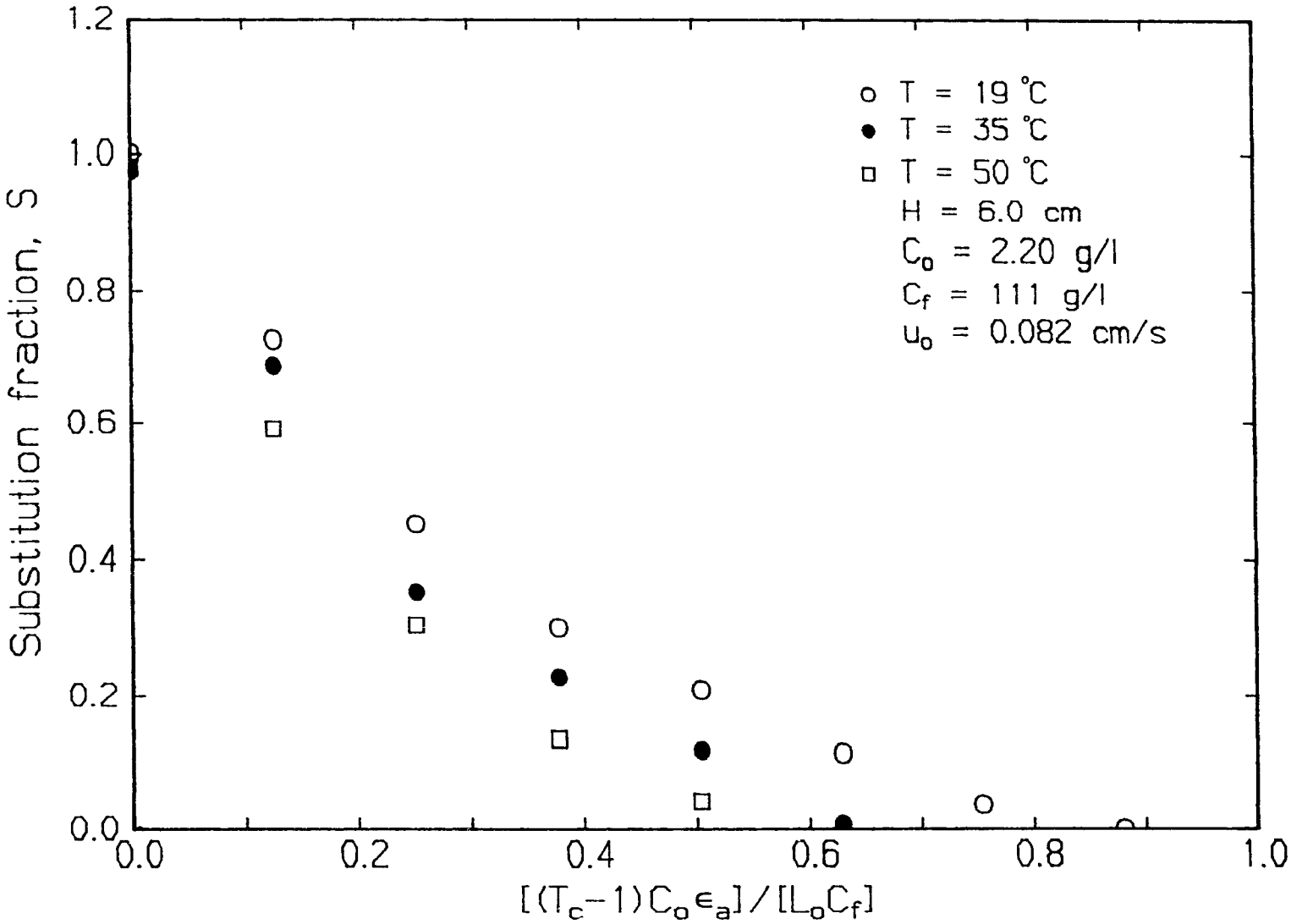
Substitution fraction, S
1.2
1.0
0.8
0.6
0.4
0.2
0.0
0.0
0.2
0.4
0.6
0.8
1.0
[(T_c−1)C_o∈_a]/[L_oC_f]
o T = 19 °C
• T = 35 °C
□ T = 50 °C
H = 6.0 cm
C_o = 2.20 g/l
C_f = 111 g/l
u_o = 0.082 cm/s

Figure 6.45 Effect of chlorine concentration on S.

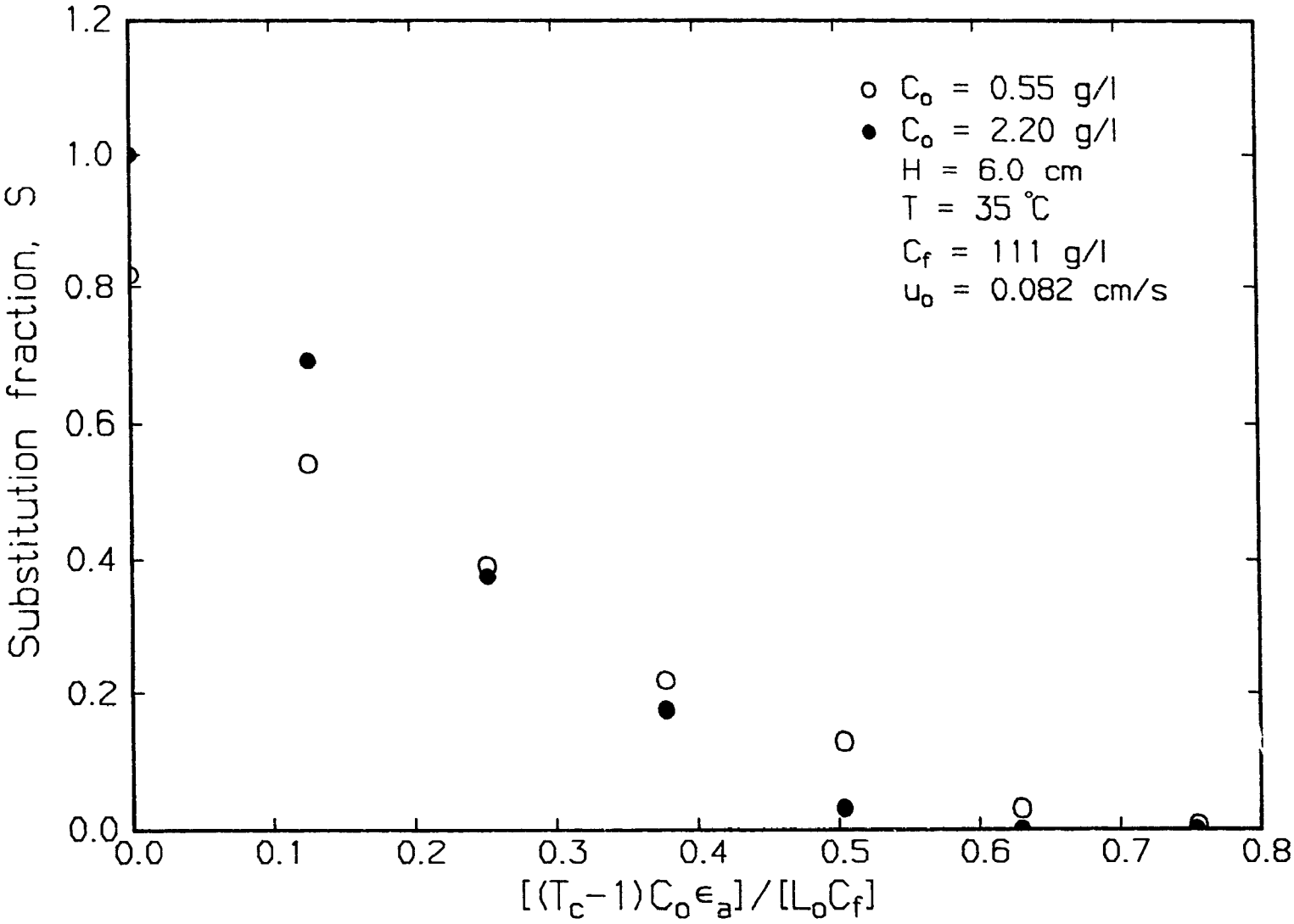
o C_o = 0.55 g/l
● C_o = 2.20 g/l
H = 6.0 cm
T = 35 ℃
C_f = 111 g/l
u_o = 0.082 cm/s
Substitution fraction, S
1.2
1.0
0.8
0.6
0.4
0.2
0.0
0.0
0.1
0.2
0.3
0.4
0.5
0.6
0.7
0.8
$[(T_c-1)C_o\epsilon_a]/[L_oC_f]$

indicator of the lignin degradation reaction, provided the motivation for measuring methanol breakthrough curves.

A typical methanol breakthrough curve is shown in Figure 6.46. After appearance of methanol at the exit, the removal of methoxy groups quickly reaches a maximum followed by a more gradual decrease of the methanol concentration to zero. The methanol breakthrough curve and the corresponding chlorine and total organic carbon breakthrough curves are shown in Figure 6.47. Some interesting observations can be made from Figure 6.47. For example, the methanol concentration decreases shortly before chlorine breakthrough begins and before the TOC maximum is reached. Also before complete chlorine breakthrough and stabilization of TOC at TOC_f, the methanol concentration at the bed exit is equal to zero. This suggests that while chlorine and TOC are both, respectively, consumed and formed at the reaction front and upstream of the front, methanol is only produced at the front.

The contribution of methanol to TOC is more clearly seen when its contribution to TOC, i.e. $(12/32)*CH_3OH$, is subtracted from the total TOC. Shown in Figure 6.48 are the measured TOC breakthrough curve and the TOC breakthrough curve corrected for methanol. It is apparent that the TOC contribution of methanol is only substantial during the initial period. The maximum of the corrected breakthrough curve occurs approximately at the steepest slope of the chlorine breakthrough curve. Also this maximum is only slightly lower than that obtained for the uncorrected TOC breakthrough curve. These results suggest that a major fraction of the TOC originates from chlorinated and/or degraded lignin in the pulp between the reaction front and the bed inlet. The fast formation of methanol at the

Figure 6.46 Typical methanol breakthrough curve.

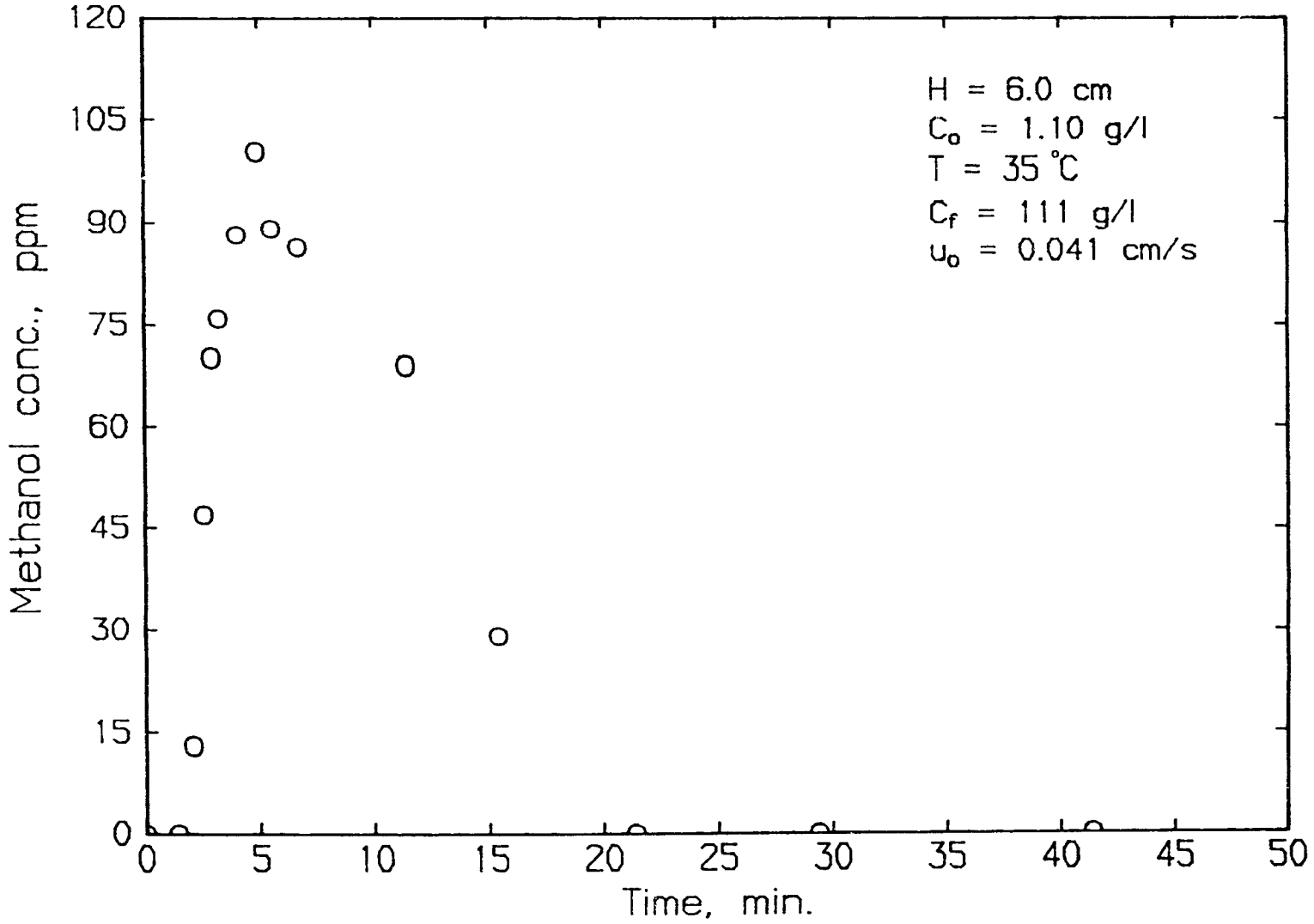
H = 6.0 cm
C_o = 1.10 g/l
T = 35 °C
C_f = 111 g/l
u_o = 0.041 cm/s
Methanol conc., ppm
Time, min.
0
15
30
45
60
75
90
105
120
0
5
10
15
20
25
30
35
40
45
50

Figure 6.47 Comparison of chlorine, TOC and methanol breakthrough curves.

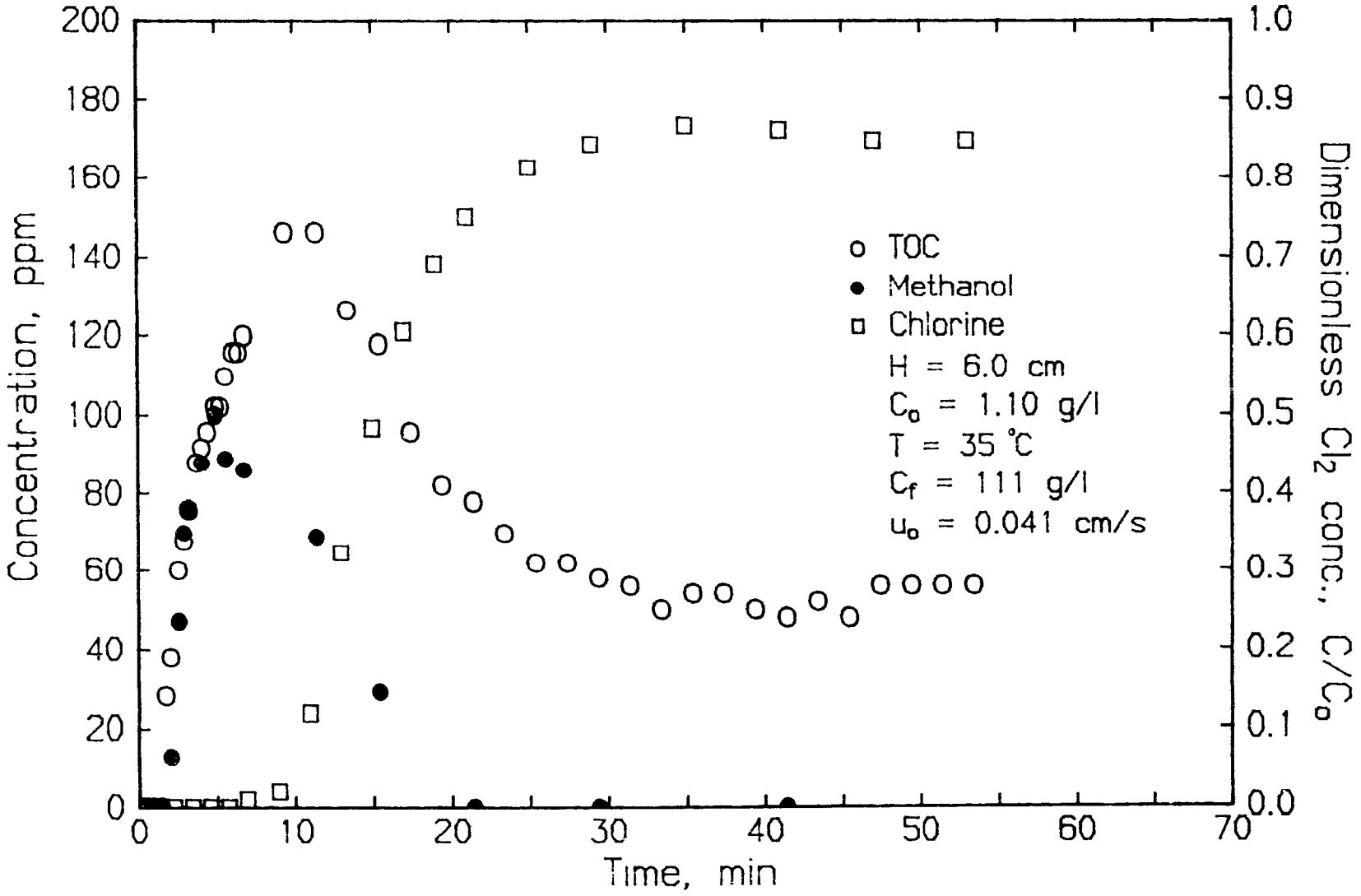
Concentration, ppm
Dimensionless Cl_2 conc., C/C_o
Time, min
TOC
Methanol
Chlorine
H = 6.0 cm
C_o = 1.10 g/l
T = 35 °C
C_f = 111 g/l
u_o = 0.041 cm/s
0
20
40
60
80
100
120
140
160
180
200
0.0
0.1
0.2
0.3
0.4
0.5
0.6
0.7
0.8
0.9
1.0
0
10
20
30
40
50
60
70

Figure 6.48 TOC breakthrough curves with or without correction for methanol.

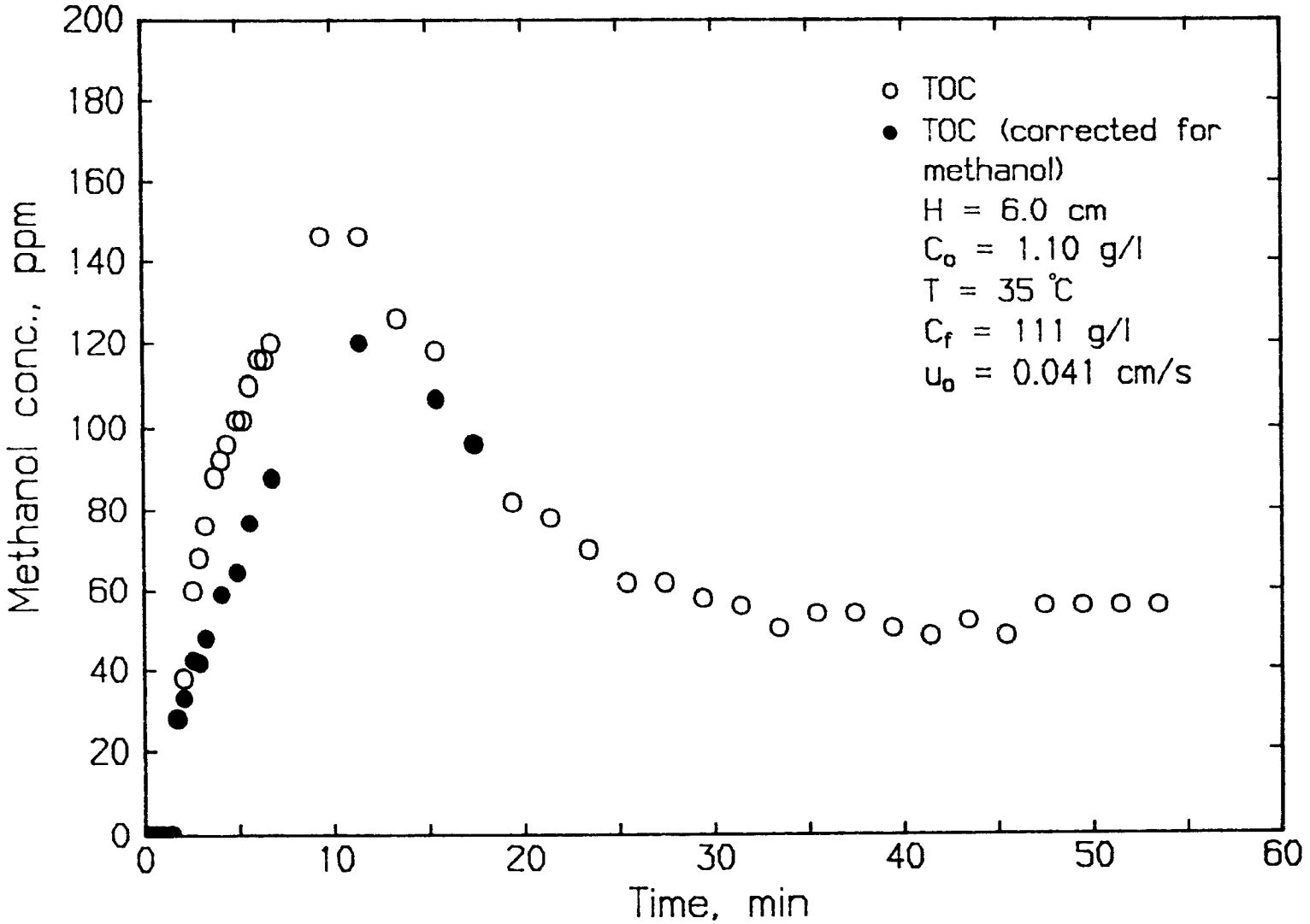
Methanol conc., ppm
Time, min
o TOC
• TOC (corrected for methanol)
H = 6.0 cm
C_o = 1.10 g/l
T = 35 ℃
C_f = 111 g/l
u_o = 0.041 cm/s
0
20
40
60
80
100
120
140
160
180
200
0
10
20
30
40
50
60

reaction front is also consistent with the results of Sarkanen and Strauss (18) who showed that most methanol is liberated within at least 5 minutes during chlorination of softwood kraft lignin.

The influence of temperature on the methanol breakthrough curve is shown in Figure 6.49. Temperatures of 19, 35 and 50°C were used at a pad height, chlorine water concentration and superficial velocity of 6 cm, 1.10 g/l and 0.041 cm/s respectively. The three breakthrough curves are identical within experimental error. This shows that methanol produced per gram of pulp is independent of temperature. This agrees with the "instantaneous" reaction assumption. Integration of the BTC's in Figure 6.49 gives a total amount of methanol removed per original lignin, R, of 0.09 g CH_3OH/g original lignin. This is equivalent to a molar ratio of (OCH_3/lignin C_9 unit) of 0.09*196/32 = 0.55, assuming a molecular weight of 196 for C_9. This value compares favourably with the difference in OCH_3/C_9 ratio between 0.96 and 0.27 for respectively untreated and chlorinated insoluble kraft lignin measured by van Buren and Dence (19). Therefore the major fraction of the OCH_3 group in the guaicyl units are removed during chlorination.

In case of pure plug flow and instantaneous methanol formation, $[CH_3OH]/C_o$ at the bed exit would be R/SL_o for constant R and SL_o during a chlorination experiment. For the conditions of Figure 6.49, R/SL_o is 0.103, 0.082, and 0.070 for, respectively, temperatures of 19, 35 and 50°C. These values agree roughly with the measured maximum $[CH_3OH]/C_o$ of 0.090 in Figure 6.49. This calculation assumes that the chlorine-lignin reaction stoichiometry, SL_o, is constant throughout the experiment. However, previously it was shown that SL_o increases until complete chlorine

Figure 6.49 Effect of temperature on methanol breakthrough curves.

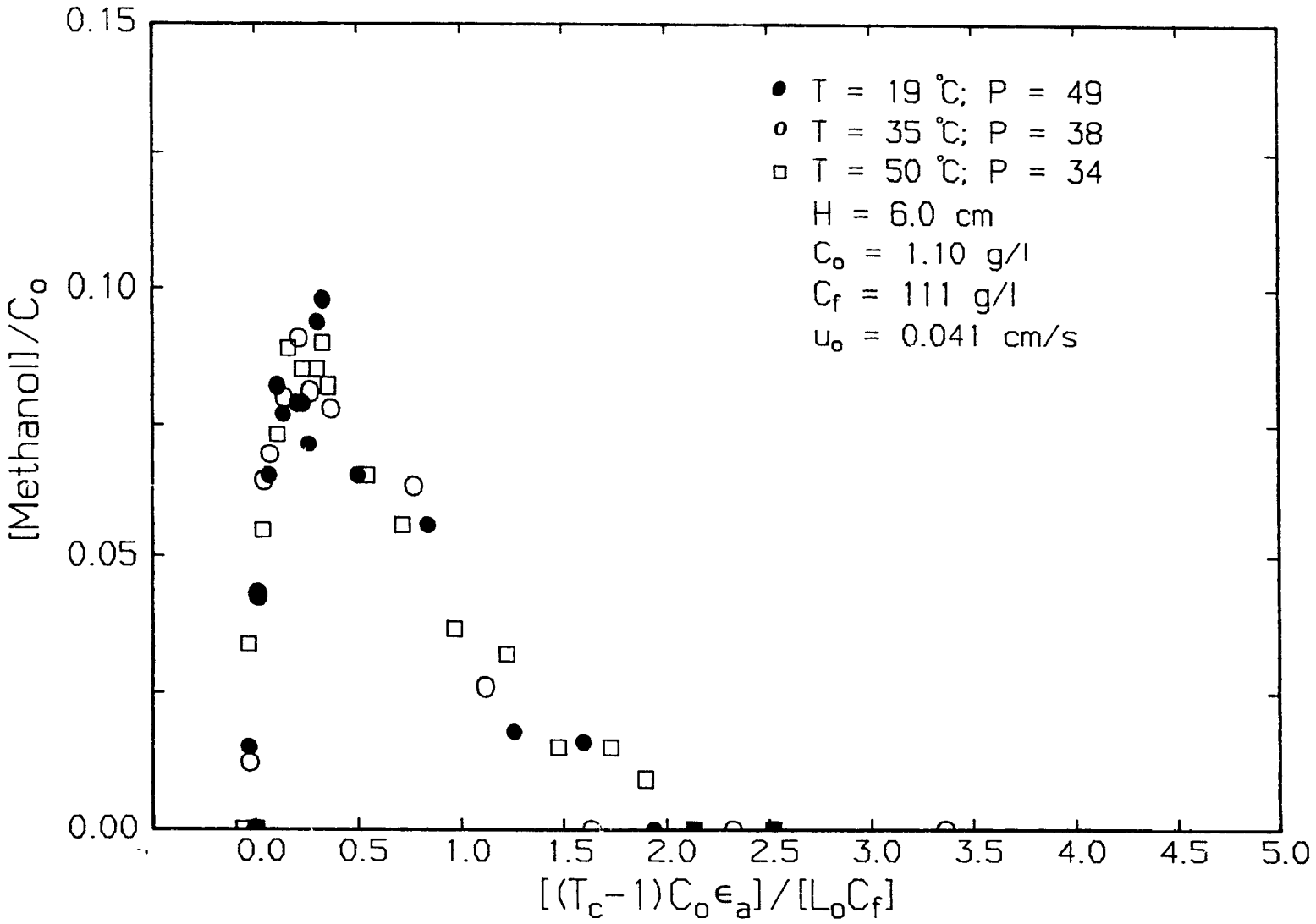
0.15
0.10
0.05
0.00
[Methanol]/C$_o$
0.0
0.5
1.0
1.5
2.0
2.5
3.0
3.5
4.0
4.5
5.0
[(T$_c$−1)C$_o$ϵ$_a$]/[L$_o$C$_f$]
T = 19 °C; P = 49
T = 35 °C; P = 38
T = 50 °C; P = 34
H = 6.0 cm
C$_o$ = 1.10 g/l
C$_f$ = 111 g/l
u$_o$ = 0.041 cm/s

breakthrough is obtained. Therefore the methanol-lignin stoichiometry, R, was calculated over the course of an experiment using the parallel plug flow model.

The net outflow of methanol from the pulp pad can be obtained from the non-dimensional methanol BTC as

$$\varepsilon_a AHC_o \int_o^{T_c} \frac{[\text{Methanol}]_{exit}}{C_o} dT_c \qquad [6.17]$$

It can be shown (Appendix 6-5) that, according to the parallel plug flow model, the net outflow of methanol is represented by

$$\frac{RAHL_o C_f}{k_c \bar{t}_r} \int_o^{F(t_{rc})} [\ell n(K(t_b - t_r) + 1)]\, dF(t_r) + \int_{F(t_{rc})}^{F(t_c)} [\ell n(K(t_c - t_r) + 1)]\, dF(t_r) \qquad [6.18]$$

where

$$K = \frac{\varepsilon_a C_o k_c}{SL_o L_o C_f}$$

with the value of SL_o a function of t_c.

$F(t_{rc})$ is the value of the step-up response function $F(t_r)$ at $t_r = t_{rc}$, where t_{rc} is obtained from the equality

$$t_c = \frac{SL_o L_o C_f}{\varepsilon_a C_o k_c} (e^{k_c t_{rc}} - 1) + t_{rc} \qquad [6.4b]$$

$F(t_c)$ is the value of $F(t_r)$ at $t_r = t_c$.

The first term of 6.18 represents the net outflow of methanol up to time t_c from all the channels for which the lignin-chlorine reaction front has reached the exit. The second term represents the remaining channels for which the front has not yet progressed to the exit at time t_c. By equating 6.17 and 6.18, R can be obtained by trial and error, since SL_o is known from the corresponding chlorine BTC and $F(t_r)$ from the glucose BTC. The profile of R for the methanol breakthrough curve at 35°C is shown in Figure 6.50. R is constant beyond $(T_c - 1)C_o\varepsilon_a/(L_oC_f)$ of 0.5 to 2.5. The fact that R is constant during most of the time when chlorine breakthrough occurs is in agreement with the model which assumes that methanol is only produced at the reaction front.

The combined effect of changing both the chlorine concentration and superficial velocity on the methanol breakthrough curve is shown in Figure 6.51. The more drawn out breakthrough curve at the lower chlorine concentration and superficial velocity is expected because the chlorine supply rate is reduced by a factor 4. The curves collapse to a single curve when the results are plotted as [methanol]/C_o versus $(T_c - 1)C_o\varepsilon_a/L_oC_f)$ in Figure 6.52. This shows that the total amount of methanol produced is neither a function of chlorine concentration nor superficial velocity. Thus in contrast to TOC breakthrough curves which are functions of C_o (Figure 6.35), T (Figure 6.37) and u_o (Figure 6.30) the methanol breakthrough curves are independent of operating conditions. This important result shows that the methanol breakthrough curve can be used as an indicator of whether or not the lignin reaction front has reached the exit of the bed in dynamic chlorination.

Figure 6.50 Profile of R versus $(T_c - 1)C_o\varepsilon_a/[L_oC_f]$.

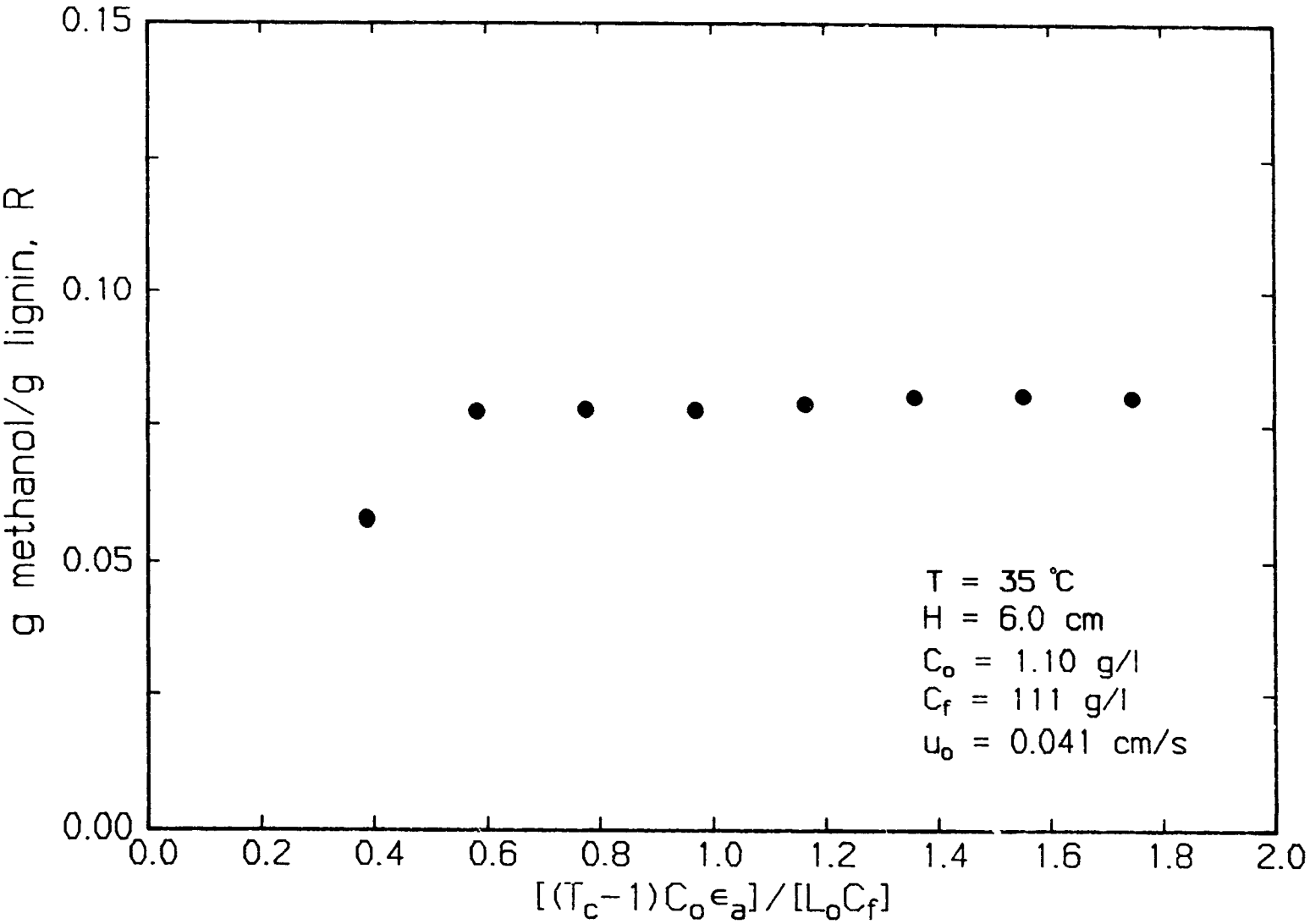
0.15
0.10
0.05
0.00
g methanol/g lignin, R
0.0
0.2
0.4
0.6
0.8
1.0
1.2
1.4
1.6
1.8
2.0
[(T_c − 1) C_o ∈_a] / [L_o C_f]
T = 35 ℃
H = 6.0 cm
C_o = 1.10 g/l
C_f = 111 g/l
u_o = 0.041 cm/s

Figure 6.51 Effect of chlorine concentration and superficial velocity on the methanol breakthrough curves.

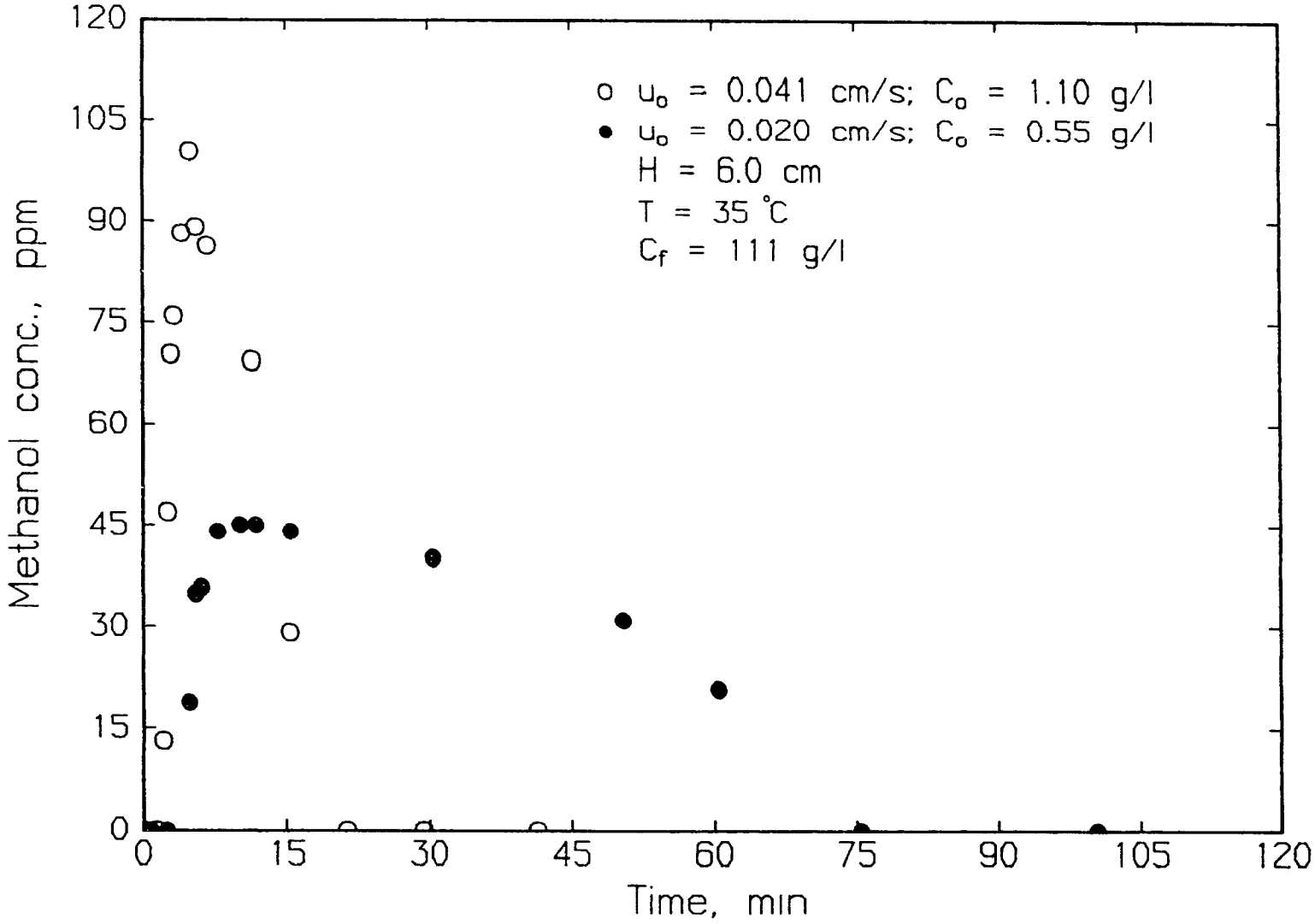
o u_o = 0.041 cm/s; C_o = 1.10 g/l
• u_o = 0.020 cm/s; C_o = 0.55 g/l
H = 6.0 cm
T = 35 °C
C_f = 111 g/l
Methanol conc., ppm
Time, min
0
15
30
45
60
75
90
105
120

Figure 6.52 Effect of chlorine concentration and superficial velocity on generalized methanol breakthrough curves.

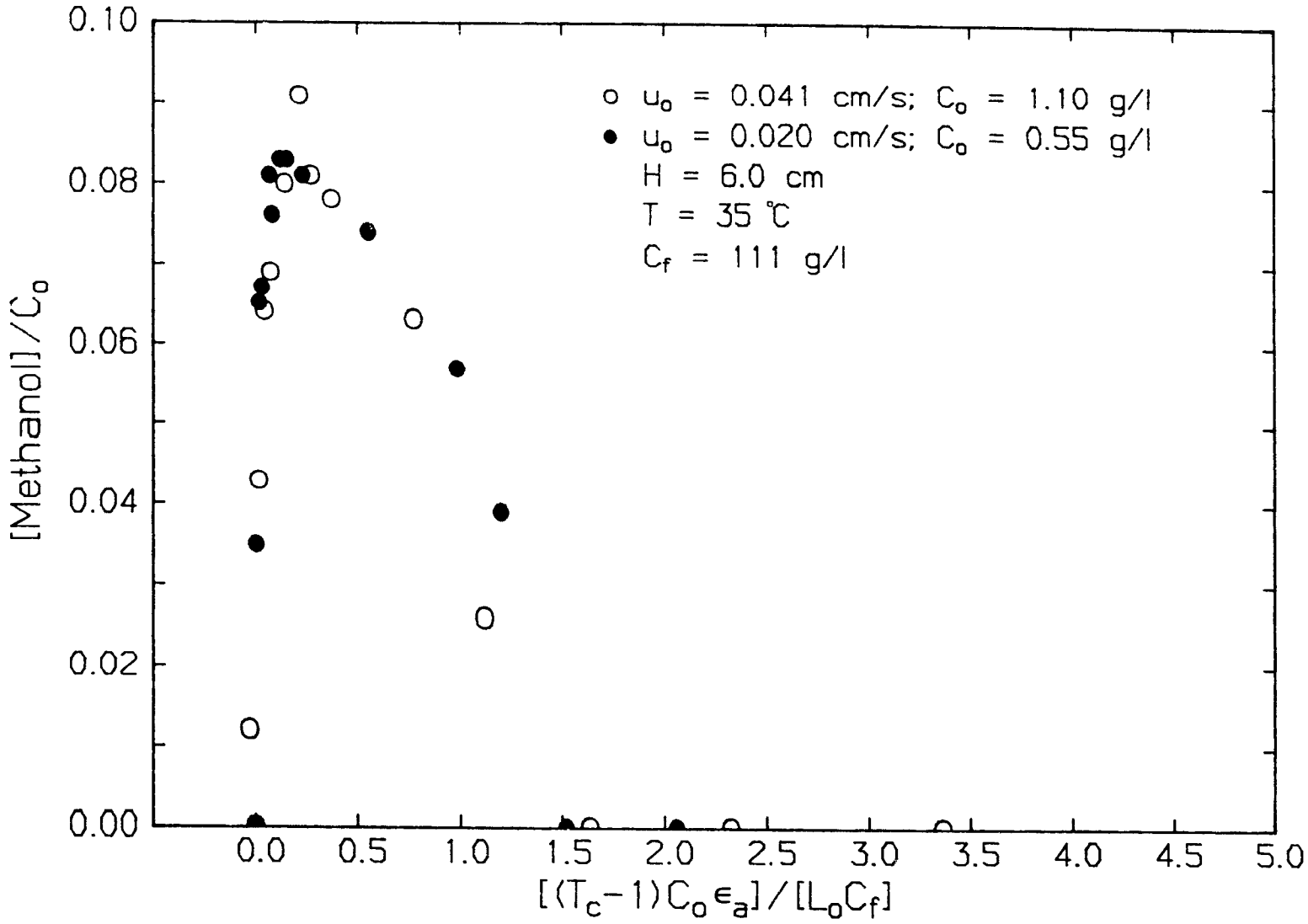
0.10
0.08
0.06
0.04
0.02
0.00
[Methanol]/C$_o$
0.0
0.5
1.0
1.5
2.0
2.5
3.0
3.5
4.0
4.5
5.0
[(T$_c$−1)C$_o$ε$_a$]/[L$_o$C$_f$]
o u$_o$ = 0.041 cm/s; C$_o$ = 1.10 g/l
• u$_o$ = 0.020 cm/s; C$_o$ = 0.55 g/l
H = 6.0 cm
T = 35 ℃
C$_f$ = 111 g/l

6.5.5 Pulp properties

After the dynamic chlorination experiments, the pulps were analysed to determine the degree of de-lignification and cellulose degradation. The former was characterised by the lignin content and kappa number before and after caustic extraction (respectively CW and CWE pulp). The cellulose degradation was measured as CED viscosity after extraction. The pulp properties will be discussed with reference to the BTC's presented in the previous sections. Where possible the de-lignification will be discussed in terms of the fast reaction between chlorine and lignin at the reaction front and of hydrolysis/oxidation of chlorolignin upstream of the reaction front. The degradation of carbohydrates will be related to the consumption of chlorine by carbohydrates as predicted by the parallel plug flow model.

6.5.5.1 Effect of charge factor

The pulp properties are measured after the pulp has been contacted with a certain amount of chlorine water. This means that in contrast to the BTC's which represent a concentration at the bed exit versus time, the pulp properties characterise the condition of the pulp at a fixed time. Therefore before discussing the effect of operating variables like C_o, T and $\bar{t}_r$ it is important to establish the development of pulp properties with the amount of chlorine water contacted with the pulp or with chlorine charge factor. The chlorine charge factor, Q, in grams of chlorine per gram of pulp is defined in equation 6.19.

$$Q = T_c C_o \varepsilon_a / C_f \qquad [6.19]$$

This definition is different from that used in the analysis of the breakthrough curves since T_c instead of (T_c-1) is used. Four experiments were conducted with chlorine charges based on the total pad of 0.034, 0.065, 0.105 and 0.217 g chlorine/g pulp. The pad height, pad consistency, temperature, superficial velocity and chlorine concentration were respectively 6 cm, 10.7%, 35°C, 0.041 cm/s and 1.10 g/l. The dimensionless chlorine concentrations in Figure 6.53 shows when these experiments were stopped. Also shown in Figure 6.53 is the complete chlorine breakthrough curve for the experiment at a charge factor of 0.217 g chlorine/g pulp. Brown spots were observed in the downstream half of the pad at the lowest chlorine charge of 0.034. These brown spots became progressively larger and eventually merge to a completely brown pad. This behaviour is caused by variable permeability of the pulp pad leading to "fingering" flow. In contrast the pulp pad exposed to the highest chlorine charge of 0.217 showed no visible brown spots. These four pulp pads were each split into three equal sized sections and analysed. The CW (Klason + UV) lignin content for each section of the four tests versus chlorine charge based on the entire pad is shown in Figure 6.54. At a fixed chlorine charge the lignin content increases with further downstream position. These differences becomes progressively smaller at higher chlorine charges because a minimum chlorine application is required before the reaction front reaches the downstream sections of the pad. For this reason it is more appropriate to consider the top one third, the top two third sections and also the whole pad as separate beds and thus obtain the average lignin content for each of these three beds. The CW (Klason + UV) lignin content versus chlorine charge based on the bed under consideration is shown in Figure 6.55. A

Figure 6.53 Final dimensionless chlorine concentration at different chlorine charges.

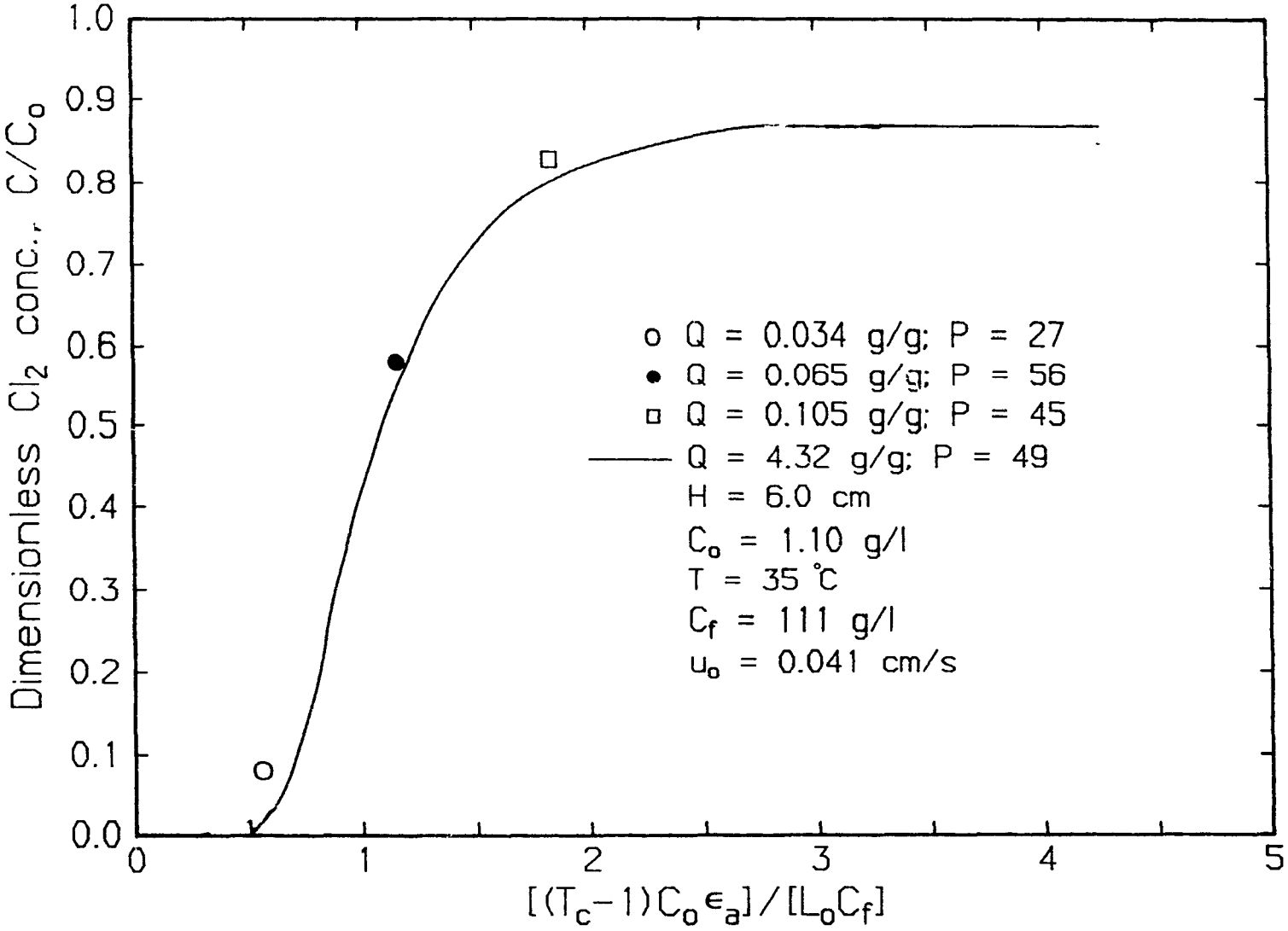
Dimensionless Cl_2 conc., C/C_o
1.0
0.9
0.8
0.7
0.6
0.5
0.4
0.3
0.2
0.1
0.0
0
1
2
3
4
5
$[(T_c-1)C_o\epsilon_a]/[L_oC_f]$
o Q = 0.034 g/g; P = 27
• Q = 0.065 g/g; P = 56
□ Q = 0.105 g/g; P = 45
—— Q = 4.32 g/g; P = 49
H = 6.0 cm
C_o = 1.10 g/l
T = 35 °C
C_f = 111 g/l
u_o = 0.041 cm/s

Figure 6.54 CW (Klason + UV) lignin as a function of chlorine charge based on the whole pad.

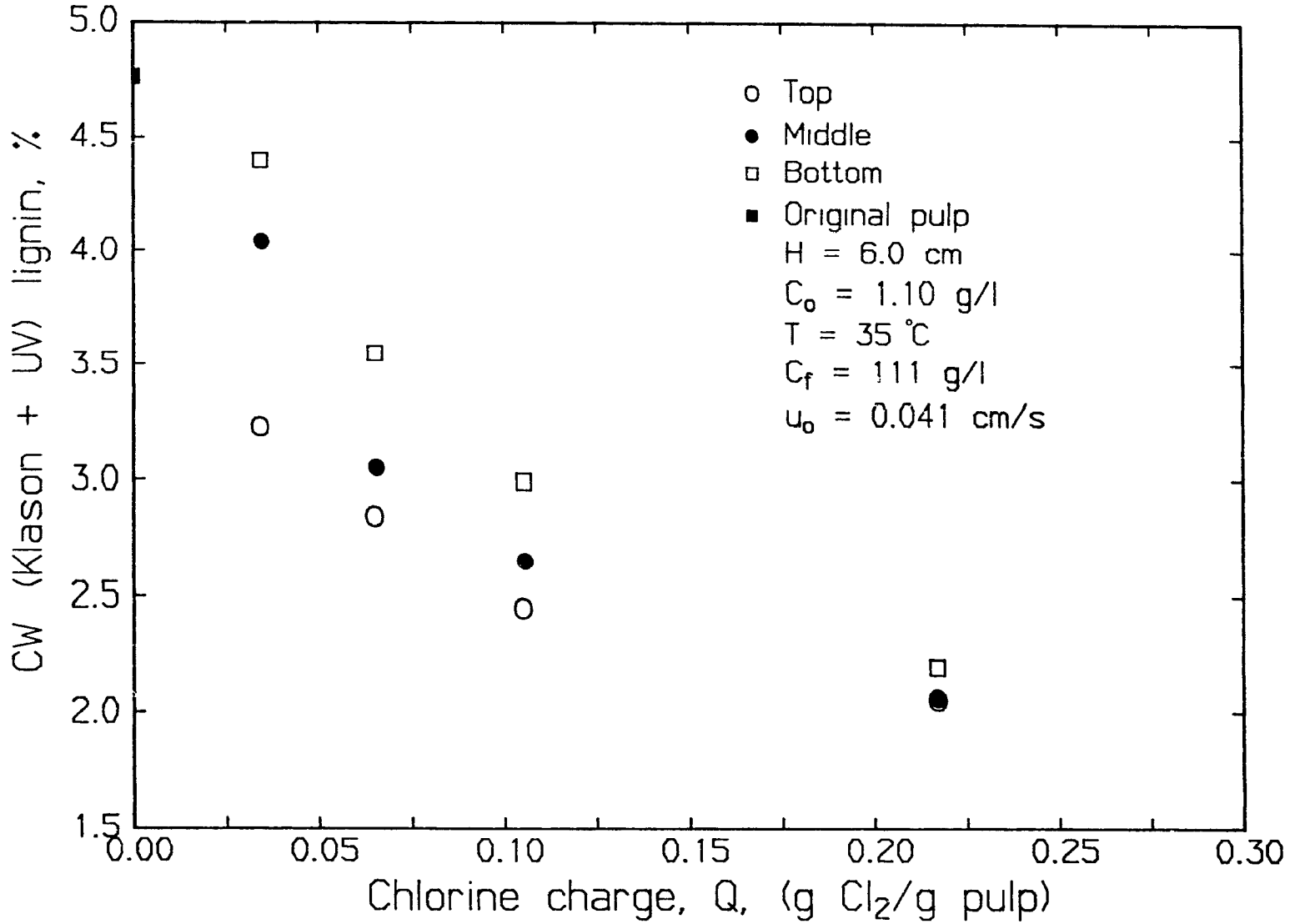
5.0
4.5
4.0
3.5
3.0
2.5
2.0
1.5
CW (Klason + UV) lignin, %
0.00
0.05
0.10
0.15
0.20
0.25
0.30
Chlorine charge, Q, (g Cl2/g pulp)
o Top
● Middle
□ Bottom
■ Original pulp
H = 6.0 cm
Co = 1.10 g/l
T = 35 °C
Cf = 111 g/l
uo = 0.041 cm/s

Figure 6.55 CW (Klason + UV) lignin as a function of chlorine charge based on pulp pad under consideration.

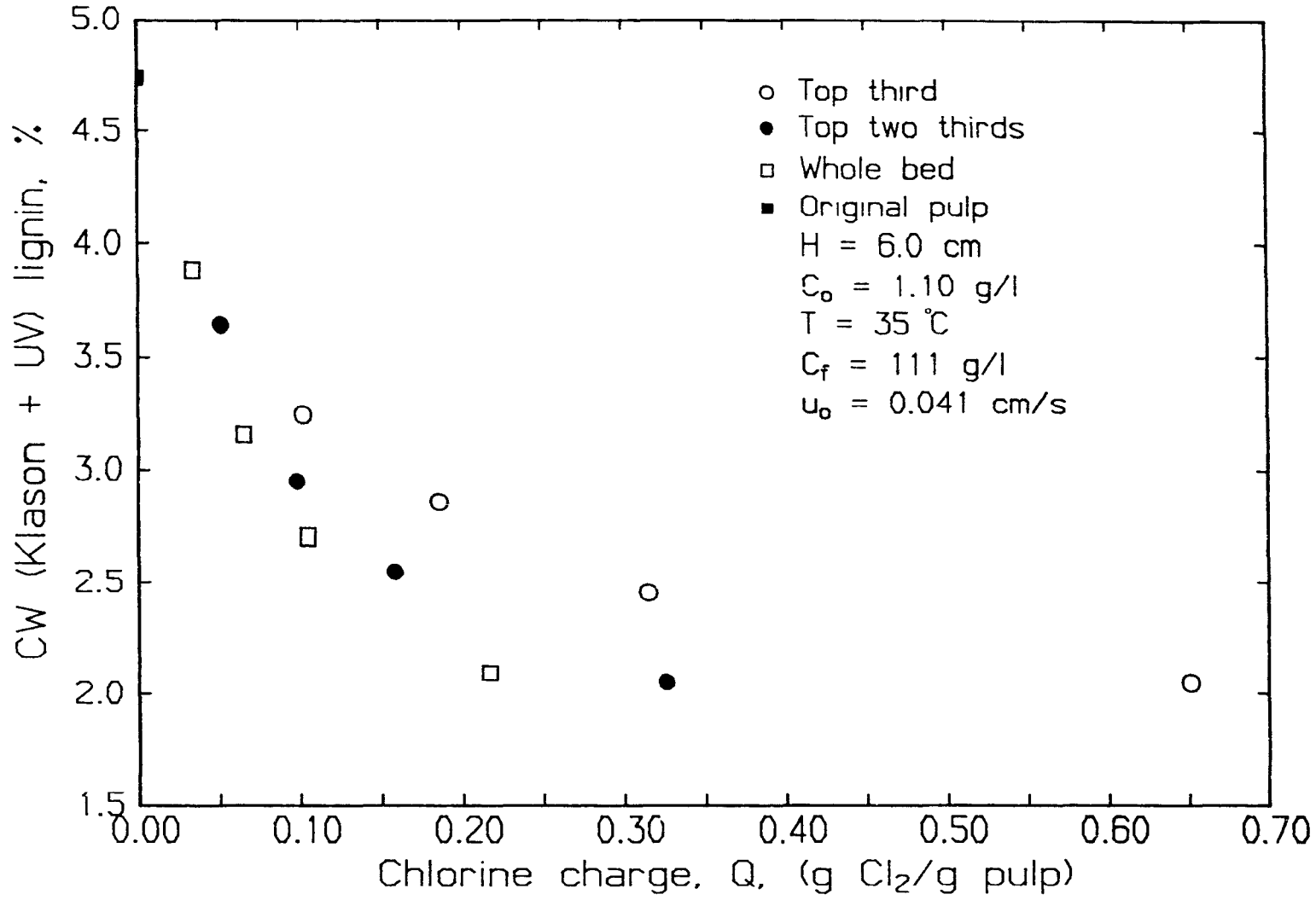
5.0
4.5
4.0
3.5
3.0
2.5
2.0
1.5
CW (Klason + UV) lignin, %
0.00
0.10
0.20
0.30
0.40
0.50
0.60
0.70
Chlorine charge, Q, (g Cl2/g pulp)
Top third
Top two thirds
Whole bed
Original pulp
H = 6.0 cm
Co = 1.10 g/l
T = 35 °C
Cf = 111 g/l
uo = 0.041 cm/s

general trend of decreasing lignin content with increasing chlorine charge is obtained. However the lignin content is slightly lower at the same chlorine charge for thicker beds. This is in agreement with the higher TOC generation for thicker beds because a significant fraction of the lignin is removed (or TOC produced) upstream of the chlorine-lignin reaction front.

A plot of the CWE (Klason + UV) lignin content in the different bed sections as a function of chlorine charge based on the total pulp pad is shown in Figure 6.56. The lignin content decreases rapidly with chlorine charge. The differences between the sections become progressively smaller at higher chlorine application and are negligible at a charge factor of 0.096. The residual lignin content at this point has reached the so-called "floor level" and represents the amount of lignin that cannot be removed further during chlorination and extraction. The CWE (Klason + UV) lignin versus chlorine charge applied to the corresponding combined sections in Figure 6.57 also decreases rapidly up to a chlorine charge of 0.1 after which the "floor level" of about 0.6-0.7% lignin content is reached. Contrary to the (Klason + UV) lignin of the corresponding CW pulp in Figure 6.55 no differences in lignin contents are observed for different pad thicknesses. In Figure 6.58 the CWE Kappa number is plotted versus the chlorine charge based on the section under consideration. A slightly lower kappa number or oxidising power is obtained for thicker pads.

The above results show that at the same chlorine charge the smaller amount of lignin removed during chlorination for thin beds is almost compensated by a larger lignin removal during extraction. It suggests

Figure 6.56 CWE (Klason + UV) lignin as a function of chlorine charge based on the whole pad.

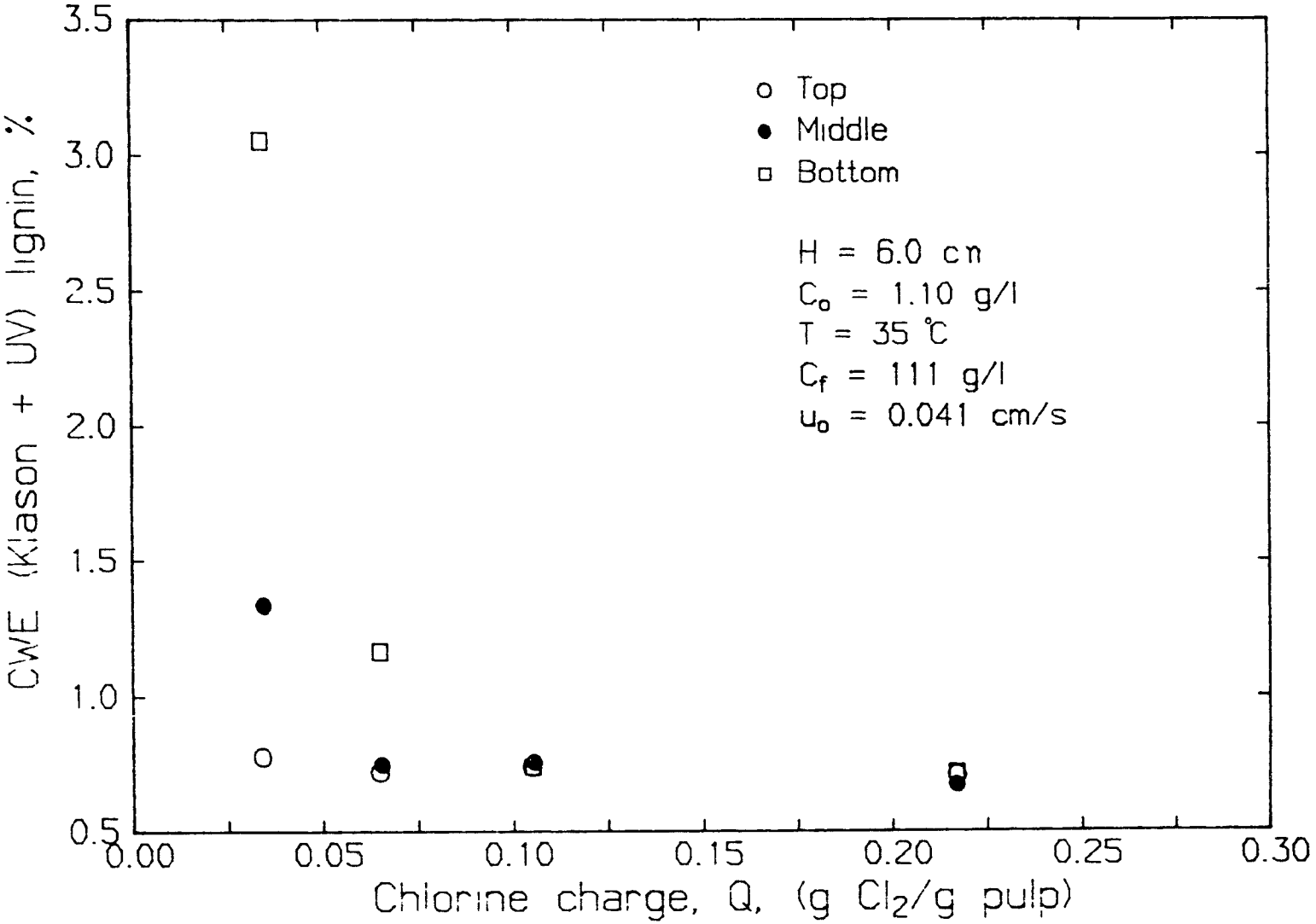
3.5
3.0
2.5
2.0
1.5
1.0
0.5
0.00
0.05
0.10
0.15
0.20
0.25
0.30
CWE (Klason + UV) lignin, %
Chlorine charge, Q, (g Cl2/g pulp)
Top
Middle
Bottom
H = 6.0 cm
Co = 1.10 g/l
T = 35 °C
Cf = 111 g/l
uo = 0.041 cm/s

Figure 6.57 CWE (Klason + UV) lignin as a function of chlorine charge based on sections of the pad.

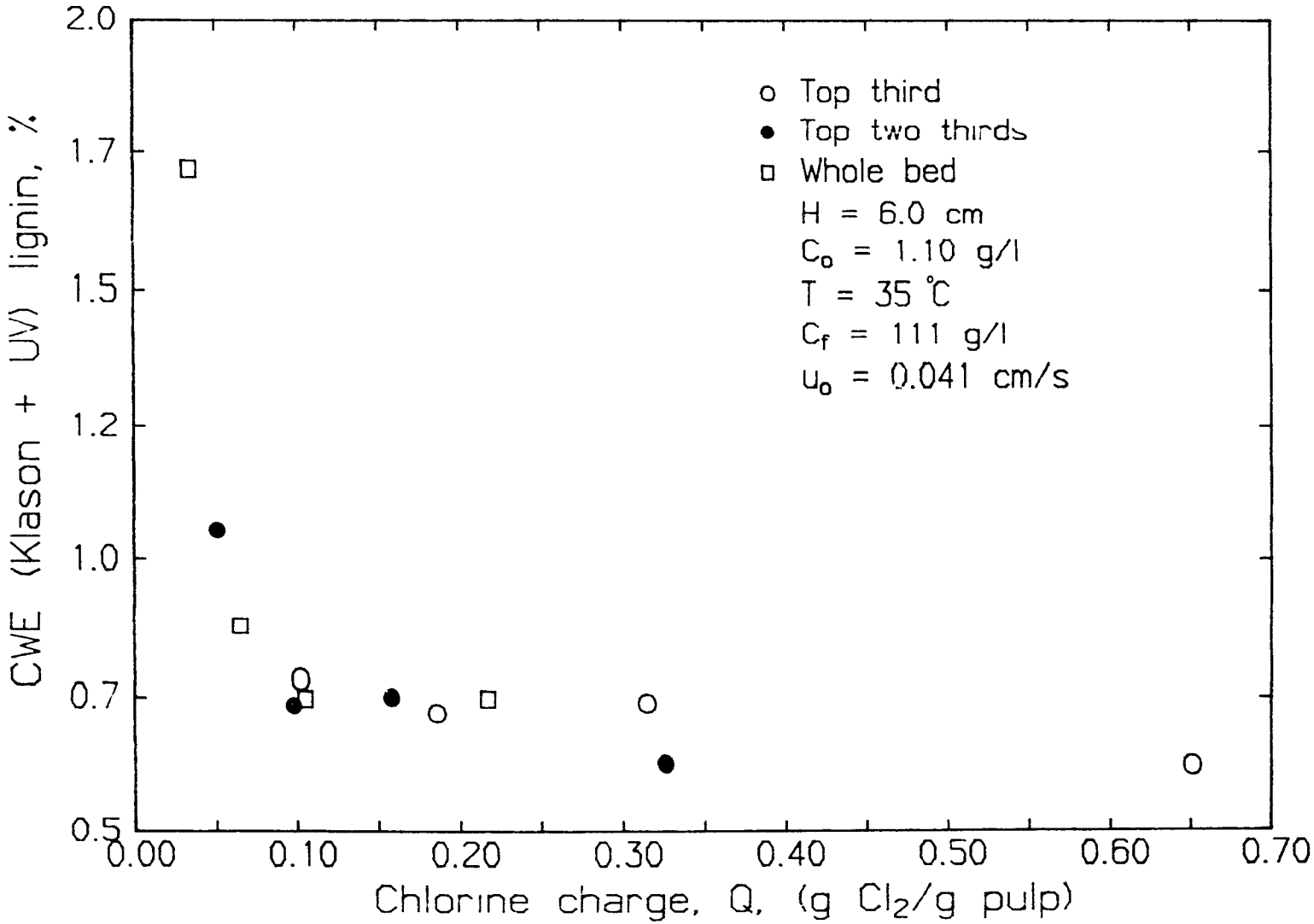
2.0
1.7
1.5
1.2
1.0
0.7
0.5
CWE (Klason + UV) lignin, %
0.00
0.10
0.20
0.30
0.40
0.50
0.60
0.70
Chlorine charge, Q, (g Cl2/g pulp)
o Top third
• Top two thirds
□ Whole bed
H = 6.0 cm
Co = 1.10 g/l
T = 35 °C
Cf = 111 g/l
uo = 0.041 cm/s

Figure 6.58 CWE Kappa number as a function of chlorine charge based on sections of the pad.

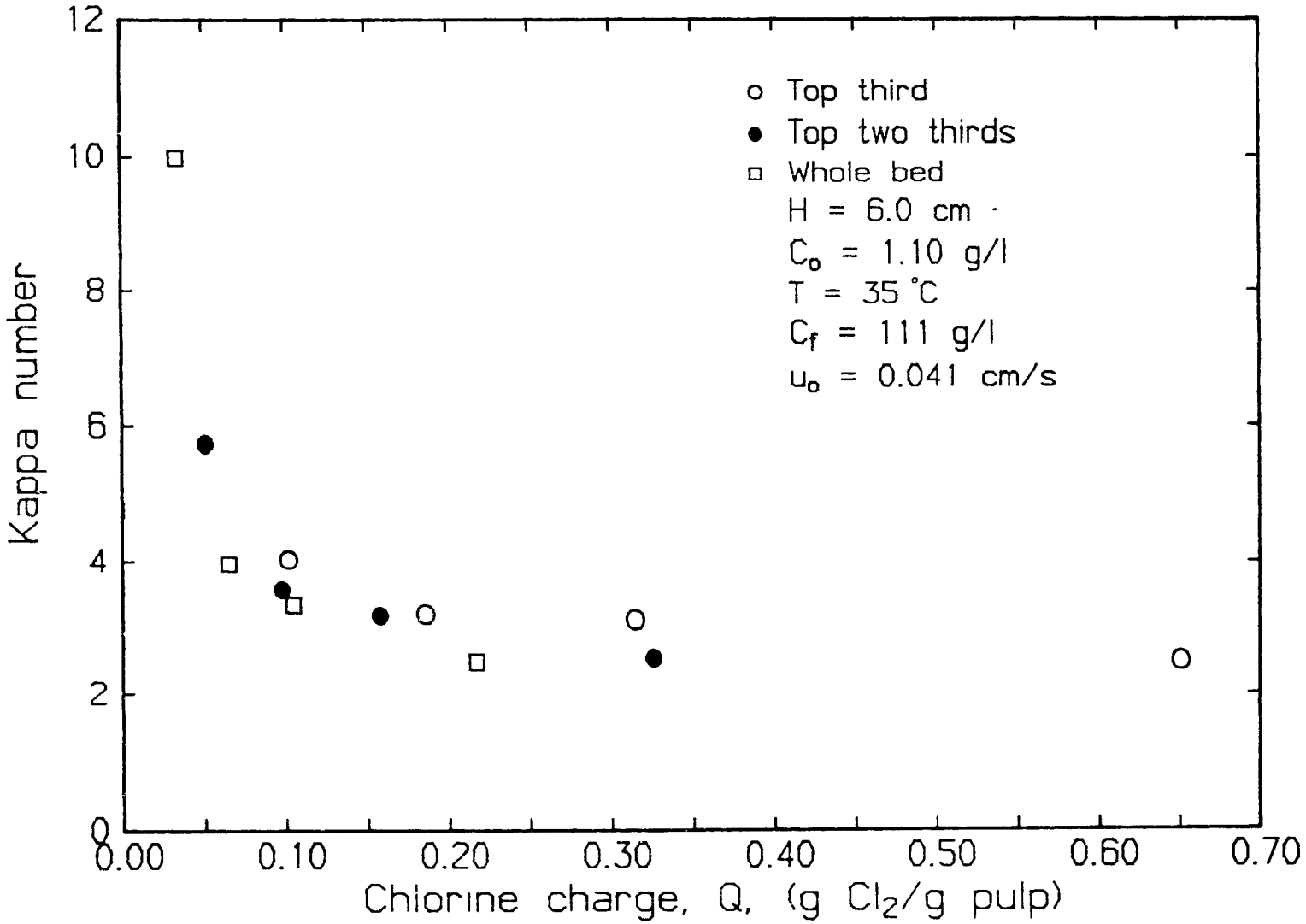
Kappa number
Chlorine charge, Q, (g Cl_2/g pulp)
Top third
Top two thirds
Whole bed
H = 6.0 cm
C_o = 1.10 g/l
T = 35 °C
C_f = 111 g/l
u_o = 0.041 cm/s
0
2
4
6
8
10
12
0.00
0.10
0.20
0.30
0.40
0.50
0.60
0.70

that the chlorinated lignin formed at the reaction front is alkali soluble and that further contact between chlorine and chlorolignin between the reaction front and the inlet is not necessary to obtain a low CWE kappa number. This suggests that the TOC and possibly TOCl generated during dynamic chlorination can be reduced by increasing the speed of the reaction front without a large penalty in CWE kappa number.

The previous results also show that the "floor level" lignin content is approached when the chlorine charge reaches about 0.10 for the present pads. This chlorine application corresponds to almost full chlorine breakthrough. The corresponding optimum chlorine charge in a batch process would be 0.22*(original kappa)/100 = 0.065 g chlorine/g pulp (Liebergott (12)). The reason for the higher chlorine charge in dynamic chlorination is that at complete breakthrough a considerable amount of unreacted chlorine has been removed with the effluent. The net chlorine application on pulp can be reduced by increasing the Peclet number or by recycling the effluent.

The CWE viscosities versus chlorine charge based on the total bed is shown in Figure 6.59. Highest viscosities were obtained in the most downstream sections of the pulp pad because of the time required for the reaction front to reach these positions. Increasing chlorine application decreases the viscosity also because of longer contact between the carbohydrates and chlorine. In order to obtain the viscosity as a function of chlorine charge based on the pulp pad under consideration (as was done for lignin content and kappa number) the average cuene viscosity should be calculated for the different pulp sections. The cuene viscosity is however not additive on a weight fraction basis. Because the intrinsic vis-

Figure 6.59 CWE cuene viscosities as a function of chlorine charge based on the whole pad.

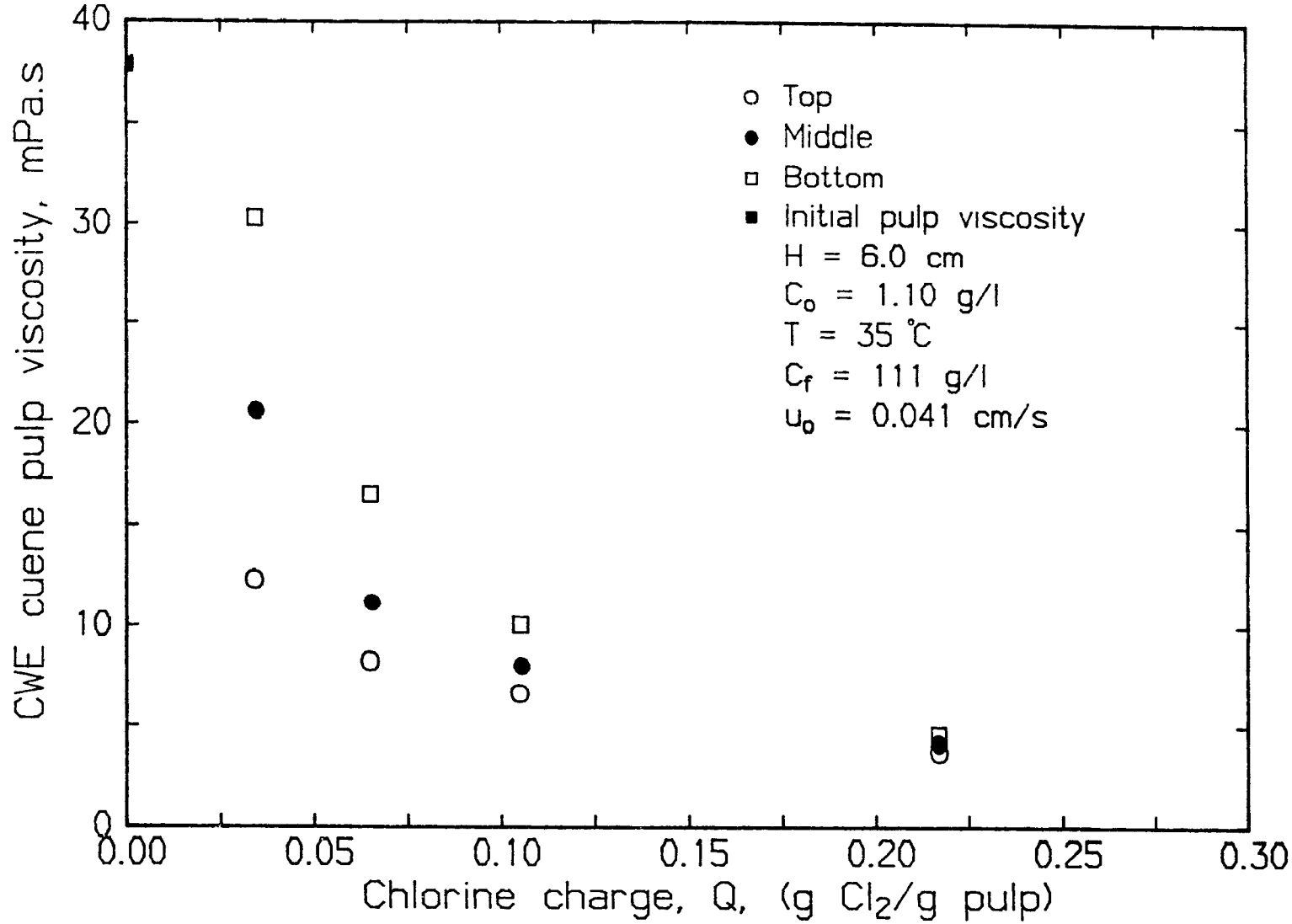
CWE cuene pulp viscosity, mPa.s
40
30
20
10
0
0.00
0.05
0.10
0.15
0.20
0.25
0.30
Chlorine charge, Q, (g Cl_2/g pulp)
Top
Middle
Bottom
Initial pulp viscosity
H = 6.0 cm
C_o = 1.10 g/l
T = 35 °C
C_f = 111 g/l
u_o = 0.041 cm/s

cosity [μ] is additive on a weight fraction basis, the cuene viscosities are converted to intrinsic viscosities with the use of a nomogram in Figure 6.60 reproduced from Gloor and Klug (20). The intrinsic viscosity as a function of chlorine charge based on the pulp pad under consideration is shown in Figure 6.61. A general trend of decreasing intrinsic viscosity with increasing chlorine charge irrespective of the bed section under consideration is apparent. Also at any chlorine charge on pulp lower intrinsic viscosities are obtained for thicker beds.

As a result of the reaction between carbohydrates and chlorine, the weight average degree of polymerization of the polysaccharide, D_{pw}, decreases and thus the concentration of polysaccharide chains, [PS], increases. The relation between D_{pw} and [PS] is

$$1/D_{pw} = \frac{[PS]}{[G]} \qquad [6.20a]$$

where [G] is the concentration of glucose units (mol/l) and [PS] is expressed in (mol/l). When D_{pw} is large, then the concentration of glycosidic bonds, [Gly] is equal to [G] so that

$$1/D_{pw} = \frac{[PS]}{[Gly]} \qquad [6.20b]$$

The relation between the average concentration of carbohydrates chains t_c seconds after chlorine is introduced in the pad, $[PS]_{t_c}$, and the chlorine consumption rate by carbohydrates, $(-\, d[Cl_2]/dt)_c$, is

Figure 6.60 Nomogram relating cuene to intrinsic viscosities, from Gloor and Klug (20).

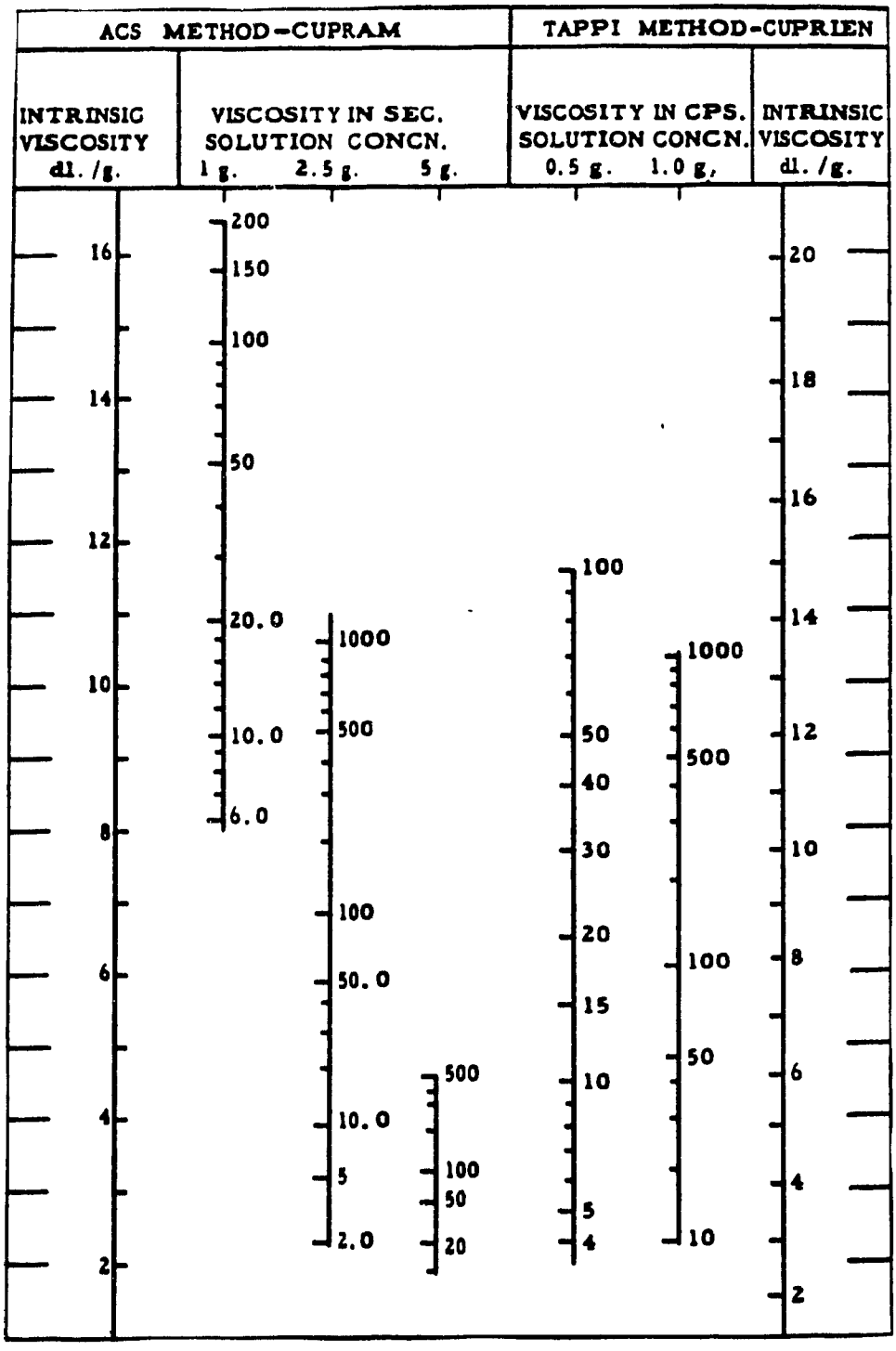
ACS METHOD–CUPRAM
TAPPI METHOD–CUPRIEN
INTRINSIC VISCOSITY dl./g.
VISCOSITY IN SEC. SOLUTION CONCN.
1 g. 2.5 g. 5 g.
VISCOSITY IN CPS. SOLUTION CONCN.
0.5 g. 1.0 g.
INTRINSIC VISCOSITY dl./g.
16
14
12
10
8
6
4
2
200
150
100
50
20.0
10.0
6.0
1000
500
100
50.0
10.0
5
2.0
500
100
50
20
100
50
40
30
20
15
10
5
4
1000
500
100
50
10
20
18
16
14
12
10
8
6
4
2

Figure 6.61 Intrinsic CWE viscosities as a function of chlorine charge based on the pulp pad under consideration.

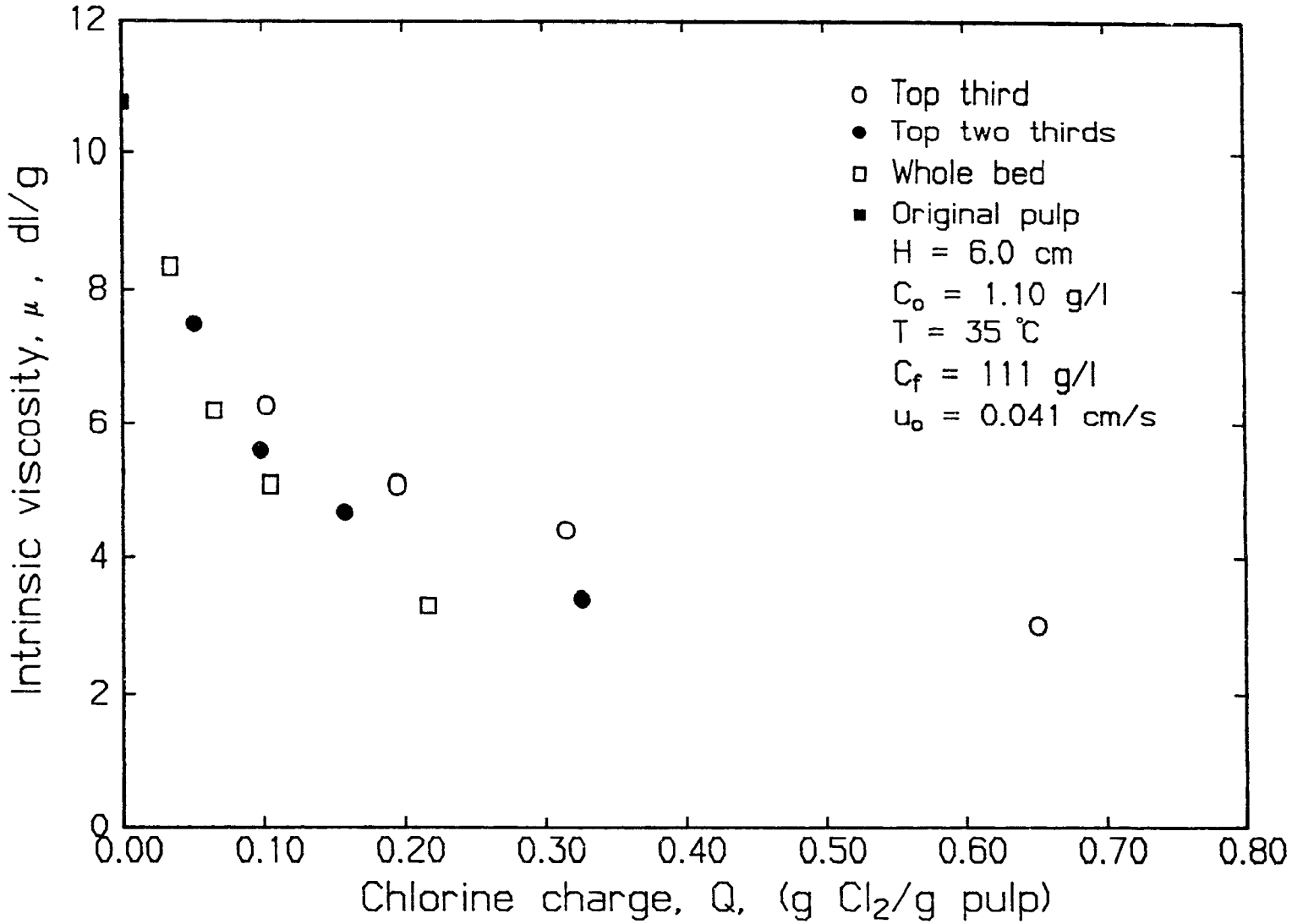
Intrinsic viscosity, μ, dl/g
12
10
8
6
4
2
0
0.00
0.10
0.20
0.30
0.40
0.50
0.60
0.70
0.80
Chlorine charge, Q, (g Cl2/g pulp)
Top third
Top two thirds
Whole bed
Original pulp
H = 6.0 cm
Co = 1.10 g/l
T = 35 ℃
Cf = 111 g/l
uo = 0.041 cm/s

$$[PS]_{t_c} = [PS]_o + \frac{1}{H}\int_o^{t_c}\left[\int_o^{x_f}\frac{1}{M_{Cl_2}}\left(-\frac{d[Cl_2]}{dt}\right)_c\right]dx\ dt_c \qquad [6.21]$$

where $[PS]_o$ is the initial concentration of carbohydrate chains, x_f is the location of the chlorine-lignin reaction front and x is the distance downstream from the bed entrance. This equation is only valid when $t < t_b$ with t_b defined in equation 6.4a. For $t > t_b$, x_f has to be replaced by H. Equation 6.21 is based on the assumption that one chlorine molecule is consumed per cleavage of each glycosidic bond in a hydrocarbon chain.

For $D_{pw} >> 1$, the glycosidic bond concentration is

$$[Gly] = C_f C_h / M_w \qquad [6.22]$$

where C_h is the fraction of carbohydrates in pulp (g/g) and M_w is the molecular weight of an anhydroglycosidic unit $C_6H_{10}O_5$ or $M_w = 162$. Combining equations 6.20, 6.21 and 6.22 gives

$$\frac{1}{[D_{pw}]_{t_c}} - \frac{1}{[D_{pw}]_o} = \frac{M_w}{\varepsilon_a M_{Cl_2} C_h}\cdot\frac{\varepsilon_a A}{HAC_f}\int_o^{t_c}\int_o^{x_f}\left(-\frac{d[Cl_2]}{dt}\right)_c dx dt_c \qquad [6.23]$$

The term between brackets on the right hand side of equation 6.23 is the weight of carbohydrates consumed per weight of pulp (g/g). With the intrinsic viscosity proportional to DP_w equation 6.23 can be written as

$$\frac{1}{[\mu]_{t_c}} - \frac{1}{[\mu_o]} = \frac{K_1 M_w}{\varepsilon_a M_{Cl_2} C_h}\cdot\frac{g\ Cl_2\ \text{consumed by carbohydrates}}{g\ \text{pulp}} \qquad [6.24]$$

where K_1 is a proportionality constant.

It can be shown (Appendix 6-6) that with the parallel plug flow model the weight of chlorine consumed by carbohydrates per weight of pulp is

$$\frac{\varepsilon_a C_o k_c t_c^2 \left(1 - F(t_{rc})\right)}{2\left(\frac{SL_o \cdot L_o C_f}{\varepsilon_a C_o} + 1\right) C_f \bar{t}_r} + \frac{\varepsilon_a C_o k_c}{C_f} \int_o^{F(t_{rc})} (t_c - t_b)\, dF$$

$$+ \frac{\varepsilon_a C_o k_c}{2\left(\frac{SL_o \cdot L_o C_f}{\varepsilon_a C_o} + 1\right) C_f \bar{t}_r} \int_o^{F(t_{rc})} t_b^2\, dF \qquad [6.25]$$

where $F(t_{rc})$ is the value of F at t_{rc} obtained from equation 6.4b and t_b is defined by equation 6.4a for each channel. Equation 6.25 can be re-written with the chlorine charge $Q = \varepsilon_a C_o t_c / (C_f \bar{t}_r)$ as

$$\frac{Q k_c t_c \left(1 - F(t_{rc})\right)}{2\left(\frac{SL_o \cdot L_o C_f}{\varepsilon_a C_o} + 1\right)} + Q k_c \bar{t}_r \int_o^{F(t_{rc})} \left(1 - \frac{t_b}{t_c}\right) dF$$

$$+ \frac{\varepsilon_a C_o k_c}{2\left(\frac{SL_o \cdot L_o C_f}{\varepsilon_a C_o} + 1\right) C_f \bar{t}_r} \int_o^{F(t_{rc})} t_b^2\, dF \qquad [6.26]$$

For large values of t_c, $F(t_{rc}) = 1.0$ so that equation 6.24 reduces to

$$\frac{1}{[\mu]_{t_c}} - \frac{1}{[\mu_o]} = \frac{K_1 M_w}{\varepsilon_a M_{Cl_2} C_h}\left(Qk_c\bar{t}_r - \frac{\varepsilon_a C_o k_c}{C_f}\int_o^1 t_b\, dF + \frac{\varepsilon_a C_o k_c}{2\left(\frac{SL_o L_o C_f}{\varepsilon_a C_o} + 1\right) C_f \bar{t}_r}\int_o^1 t_b^2\, dF\right) \qquad [6.27]$$

where the last two terms are constant, i.e. are not a function of t_c. When $k_c t_r << 1$ and $P >> 1$ then it follows from equation 6.4a that

$$\bar{t}_b \approx \left(\frac{SL_o \cdot L_o C_f}{\varepsilon_a C_o} + 1\right)\bar{t}_r \qquad [6.28]$$

Similarly for these conditions one can approximate the two integrals $\int_o^1 t_b dF$ and $\int_o^1 t_b^2 dF$

by, respectively, $\bar{t}_b$ and $(\bar{t}_b)^2$. With these approximations for the integrals and the use of equation 6.28 one can simplify equation 6.27 to

$$\frac{1}{[\mu]_{t_c}} - \frac{1}{[\mu_o]} = \frac{K_1 M_w k_c}{\varepsilon_a M_{Cl_2} C_h}\left(Q - \left(\frac{1}{2}\ SL_o \cdot L_o + \frac{\varepsilon_a C_o}{C_f}\right)\right)\bar{t}_r \qquad [6.29a]$$

or after replacement of Q by $\varepsilon_a C_o t_c/(C_f \bar{t}_r)$, and use of 6.28 and some rearrangement,

$$\frac{1}{[\mu]_{t_c}} - \frac{1}{[\mu_o]} = \frac{K_1 M_w k_c C_o}{M_{Cl_2} C_h C_f}\left(t_c - \tfrac{1}{2}\bar{t}_b\right) \qquad [6.29b]$$

Equation 6.29b is of interest because it provides a direct description of the influence of experimental variables on the pulp viscosity. Equation 6.29a gives a description of the viscosity in terms of more fundamental operational variables. For small values of t_c, $F(t_{rc}) = 0$ so that equations 6.24 and 6.28 reduce to

$$\frac{1}{[\mu]_{t_c}} - \frac{1}{[\mu_o]} = \frac{Q\, k_c t_c}{2\left(\frac{SL_o L_o C_f}{\varepsilon_a C_o} + 1\right)} \cdot \frac{K_1 M_w}{\varepsilon_a M_{Cl_2} C_h} \qquad [6.30]$$

Based on this analysis, the inverse of the intrinsic viscosities versus chlorine charge Q, with Q based on the bed section under consideration, were plotted in Figure 6.62. It was previously shown in Fig. 6.53 that complete chlorine breakthrough (or $F(t_{rc}) = 1.0$) is obtained when $Q \approx 0.1$. Thus for $Q > 0.1$ one would expect equation 6.29 to hold, which means that $(1/[\mu]_{t_c} - 1/[\mu_o])$ should be proportional to $Qk_c t_r$ since $(SL_o \cdot L_o + \varepsilon_a C_o/C_f))$ in equation 6.29a is constant. Indeed, approximate straight line relationships are obtained for the two smaller bed sections in Figure 6.62 for $Q > 0.1$. Insufficient data is available for the whole bed to claim a linear relationship. Further confirmation of the validity of equation 6.29 is obtained when the slopes of the straight lines for $Q > 0.1$ are compared. The relative slopes of the straight lines for the three bed sections of increasing thickness are 1.0, 2.1, and 3.5, respectively, i.e. approximately proportional to the ratios of $\bar{t}_r$ for the three beds under consideration. The explanation for the fact that the relative slopes are not exactly 1:2:3 is that the three sections were not exactly equal in weight because the pad division was done by eye. Experimental

Figure 6.62 Reciprocal intrinsic CWE viscosities versus chlorine charge based on pulp pad under consideration.

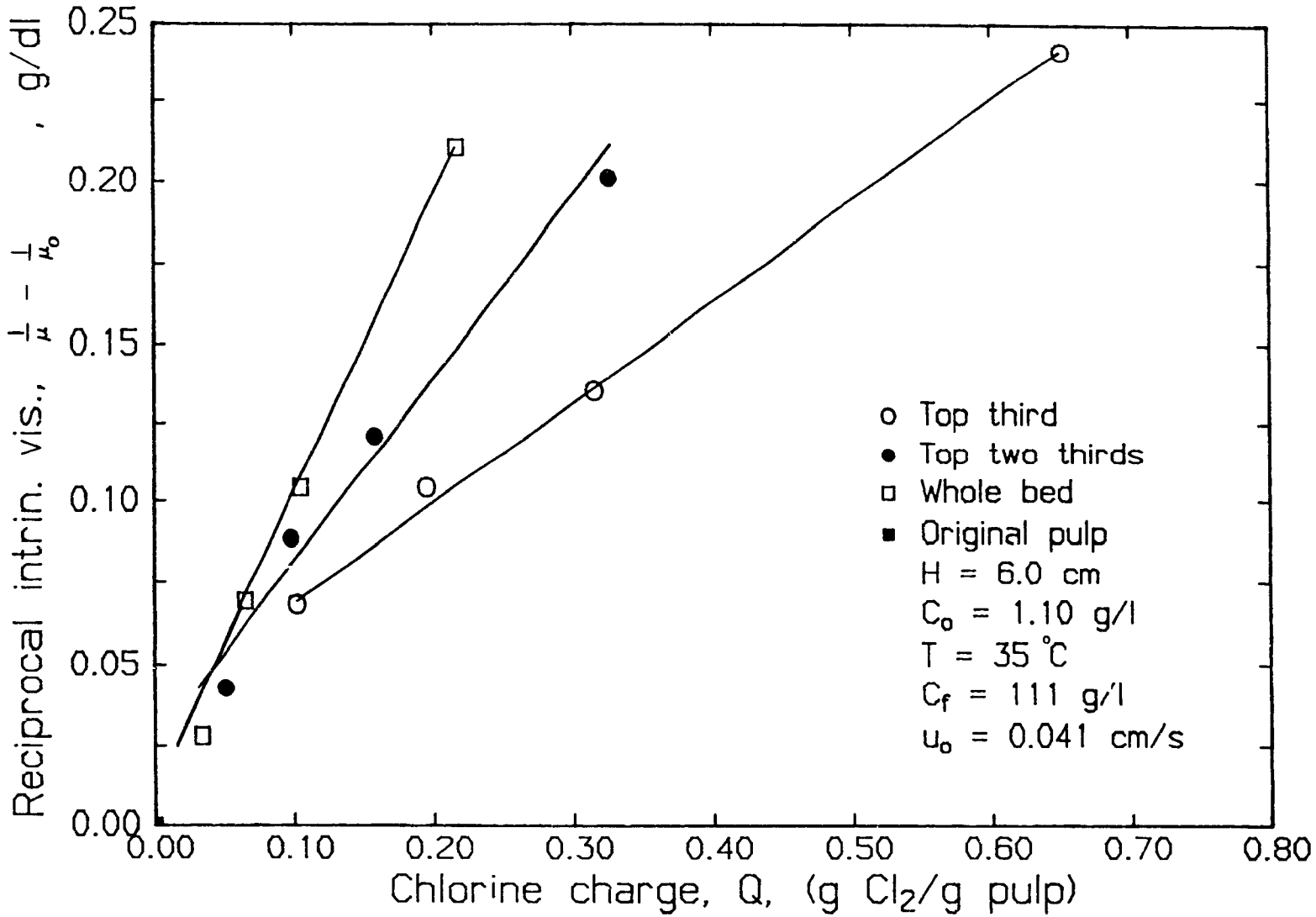
Reciprocal intrin. vis., $\frac{1}{\mu} - \frac{1}{\mu_o}$, g/dl
0.25
0.20
0.15
0.10
0.05
0.00
0.00
0.10
0.20
0.30
0.40
0.50
0.60
0.70
0.80
Chlorine charge, Q, (g Cl_2/g pulp)
Top third
Top two thirds
Whole bed
Original pulp
H = 6.0 cm
C_o = 1.10 g/l
T = 35 °C
C_f = 111 g/l
u_o = 0.041 cm/s

errors, of course, also play a role. Another significant observation which can be made from Figure 6.62 is that $(1/[\mu]_{t_c} - 1/[\mu_o])$ is lower for thinner beds, even at small values of Q. The reason is that at small values of Q (or t_c) equation 6.30 is valid, and for thinner beds the same value of Q is obtained at smaller values of t_c. Thus the results in Figure 6.62 show that the combination of parallel plug flow and chlorine-carbohydrates kinetics can be used to describe the progress of pulp degradation during dynamic chlorination.

6.5.5.2 Effect of chlorine concentration

It was shown previously that increasing chlorine concentration resulted in lower cumulative TOC removal at the same chlorine application. This was attributed to the shorter contact times between chlorine and lignin upstream of the reaction front. Plotted in Figure 6.63 is the CW (Klason + UV) lignin content of various sections of the pulp pad versus chlorine application for the pulp pad (fraction) under consideration. A lower lignin content is obtained at a chlorine concentration of 1.10 g/l compared to 2.20 and 0.55 g/l at the same chlorine application. The lower lignin content at C_o = 1.10 g/l compared to C_o = 2.20 g/l is in agreement with the TOC results shown in Figure 6.35 and Table 6.6, and consistent with the view that more lignin is solubilized upstream of the reaction front due to the longer contact times at lower chlorine concentrations. However the lignin content at C_o = 0.55 g/l is much higher than that at 1.10 g/l, even though the cumulative TOC removal is almost the same (Table 6.6 and Figure 6.35). This suggests that TOC removal alone is not a good measure of the final lignin content of CW pulp.

Figure 6.63 Effect of chlorine concentration on CW (Klason + UV) lignin as a function of chlorine charge based on pulp pad under consideration.

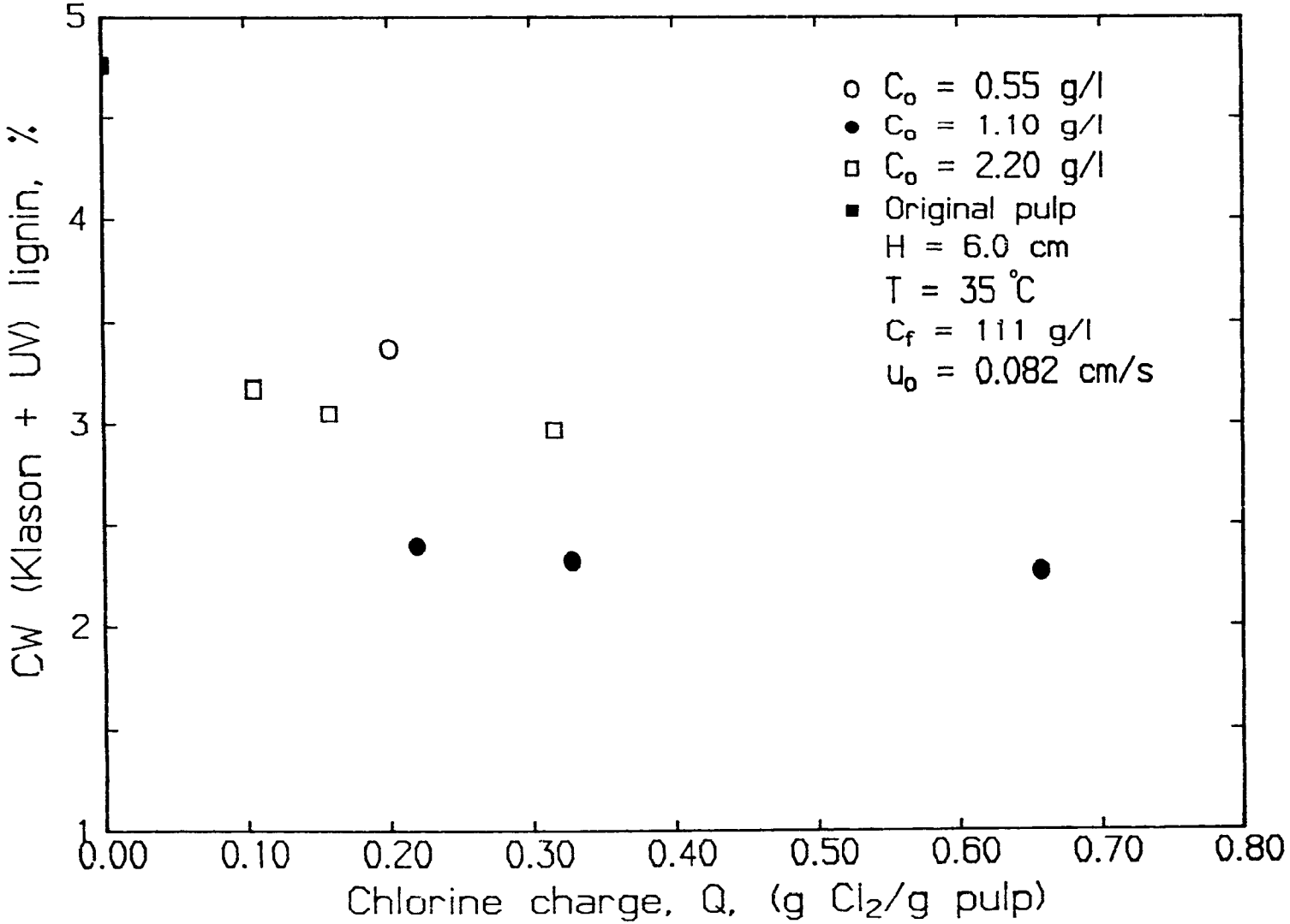
5
4
3
2
1
0.00
0.10
0.20
0.30
0.40
0.50
0.60
0.70
0.80
CW (Klason + UV) lignin, %
Chlorine charge, Q, (g Cl2/g pulp)
o Co = 0.55 g/l
• Co = 1.10 g/l
□ Co = 2.20 g/l
■ Original pulp
H = 6.0 cm
T = 35 °C
Cf = 111 g/l
u0 = 0.082 cm/s

Although the CW (Klason + UV) lignin content versus Q plots are quite different for different chlorine feed concentrations, the CWE (Klason + UV) lignin versus Q are similar. The very small dependence of the lignin content of CWE pulp on Q confirms that chlorination can be stopped when all reaction fronts have reached the bottom of the pulp pad. These results also demonstrate that CW lignin content is not a good indicator of the extent of delignification which can be achieved after extraction.

The CWE cuene viscosities corresponding to the data points shown in Figure 6.63 are converted into reciprocal intrinsic viscosities and plotted versus chlorine charge based on the bed under consideration in Figure 6.64. Lower intrinsic viscosities are obtained at lower chlorine concentrations at the same chlorine charge on pulp. This behavior is not obvious since t_c decreases inversely with C_o at constant Q, while the rate of chlorine-carbohydrates reaction increases proportionally with C_o. Another problem is that $\bar{t}_r$ is a hidden parameter in Figure 6.64, with $Q\bar{t}_r$ being constant for each C_o.

6.5.5.3 Effect of temperature

The effect of three levels of temperature on CW (Klason + UV) lignin contents at the same chlorine charge of 0.105 g chlorine/g pulp is shown in Figure 6.65. Lower CW lignin contents are obtained at higher temperatures and at the top sections of each pulp pad. The lower lignin content at higher temperatures is consistent with larger TOC removal due to increased reaction rates upstream of the reaction front at higher temperatures shown in Figure 6.37. Lower CW lignin contents in the top sections of each pulp pad are due to longer contact times between the pulp

Figure 6.64 Effect of chlorine concentration on reciprocal intrinsic CWE viscosities versus chlorine charge based on pulp pad under consideration.

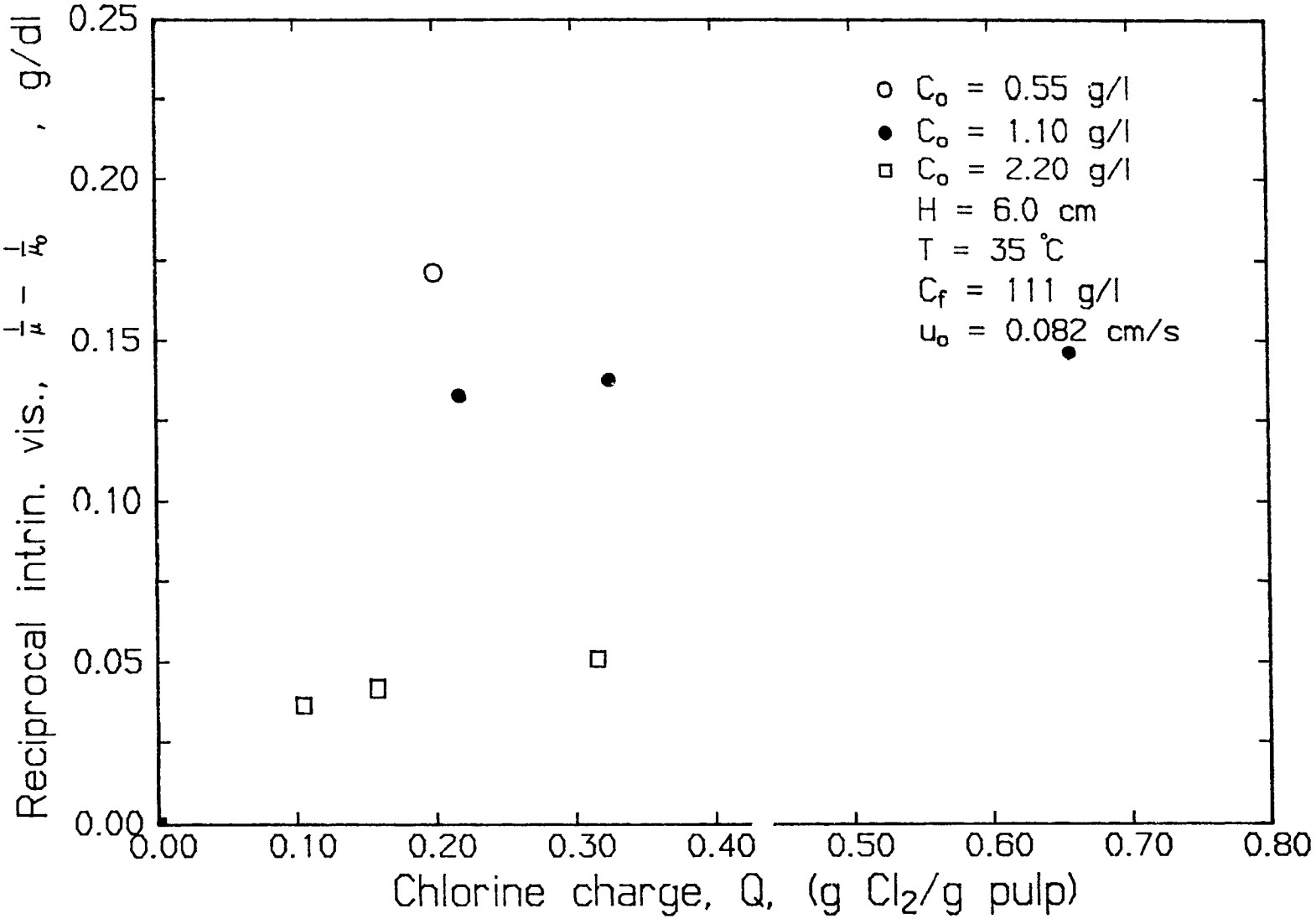
Reciprocal intrin. vis., $\frac{1}{\mu} - \frac{1}{\mu_o}$, g/dl
0.25
0.20
0.15
0.10
0.05
0.00
0.00
0.10
0.20
0.30
0.40
0.50
0.60
0.70
0.80
Chlorine charge, Q, (g Cl_2/g pulp)
o C_o = 0.55 g/l
● C_o = 1.10 g/l
□ C_o = 2.20 g/l
H = 6.0 cm
T = 35 °C
C_f = 111 g/l
u_o = 0.082 cm/s

Figure 6.65 Effect of temperature on CW (Klason + UV) lignin.

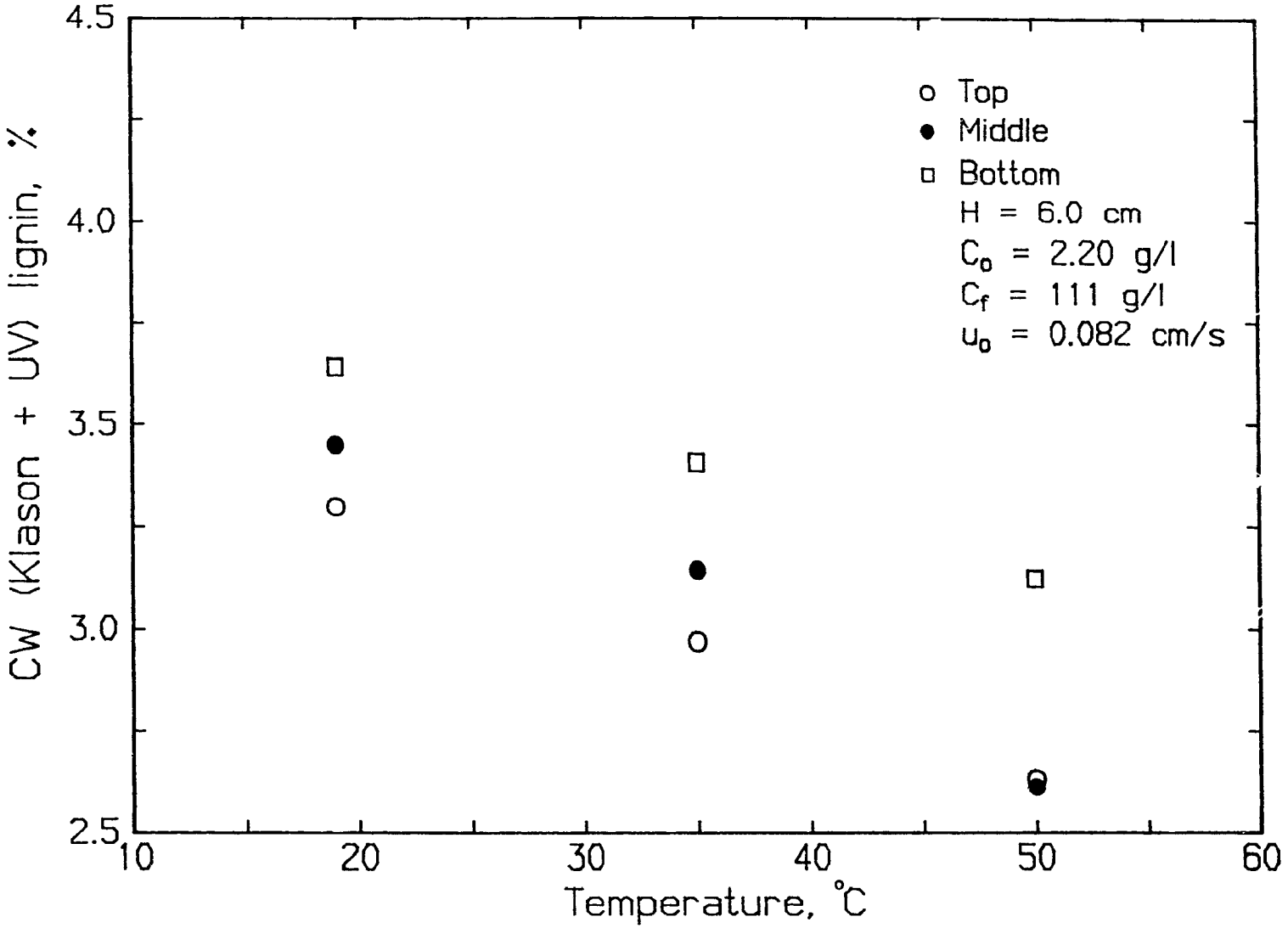
4.5
4.0
3.5
3.0
2.5
10
20
30
40
50
60
CW (Klason + UV) lignin, %
Temperature, °C
Top
Middle
Bottom
H = 6.0 cm
C_o = 2.20 g/l
C_f = 111 g/l
u_o = 0.082 cm/s

and chlorine-water upstream of the reaction front.

The CWE Kappa number versus temperature plots shown in Figure 6.66 also displays similar trends to CW lignin shown in Figure 6.65. The lower kappa number at higher temperatures is possibly due to an increase in the extent of oxidation reactions.

The effect of temperature on viscosity is shown in Figure 6.67 and displays the reciprocal intrinsic viscosities versus chlorine charge on the bed section under consideration. Lower intrinsic viscosities are obtained at higher temperatures at the same chlorine charge on pulp. This follows from equation 6.29 which shows a linear relationship between $(1/[\mu]_{t_c} - 1/]\mu]_o)$ and the temperature dependent chlorine-carbohydrates reaction rate constant, k_c.

6.5.5.4 Effect of consistency

The effect of three levels of pulp pad consistency on CW (Klason + UV) lignin as a function of chlorine charge , Q, based on the portion of the pulp pad under consideration is shown in Figure 6.68. Lower lignin contents are generally obtained at higher consistencies at the same chlorine charge on pulp. This can be explained by the longer reaction times needed at higher pulp pad consistencies to obtain the same chlorine charge on pulp. The similar CWE (Klason + UV) lignin contents of these pulps shown in Figure 6.69 agrees with the conclusion elicited earlier that the CW lignin content is not a good measure of the CWE lignin content. Some of the lignin which is not removed during chlorination is removed during extraction irrespective of the consistency during chlorination.

Figure 6.66 Effect of temperature on CWE kappa number.

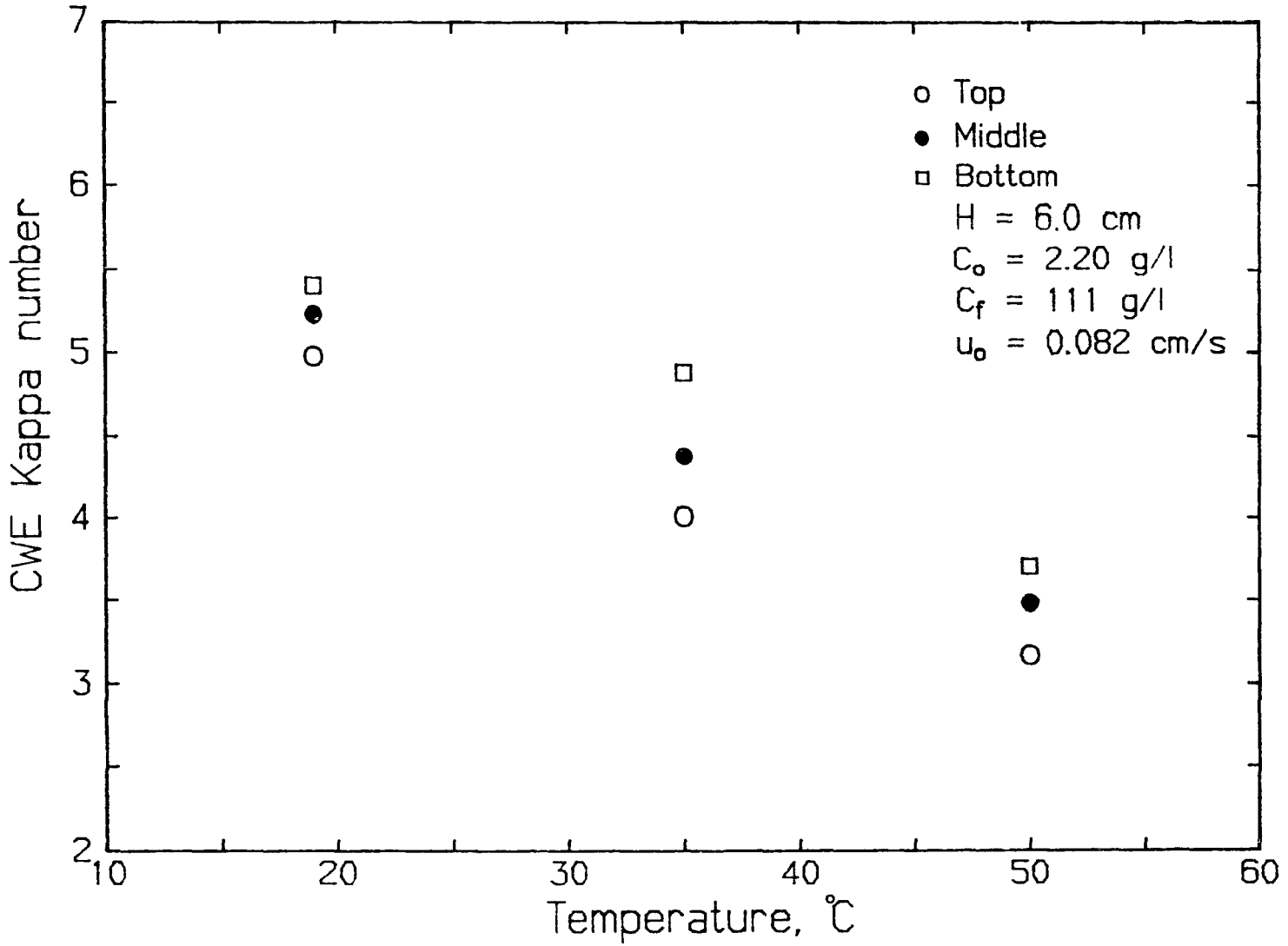
CWE Kappa number
Temperature, °C
o Top
● Middle
□ Bottom
H = 6.0 cm
C_o = 2.20 g/l
C_f = 111 g/l
u_o = 0.082 cm/s
7
6
5
4
3
2
10
20
30
40
50
60

Figure 6.67 Effect of temperature on reciprocal intrinsic viscosities versus chlorine charge based on pulp pad under consideration.

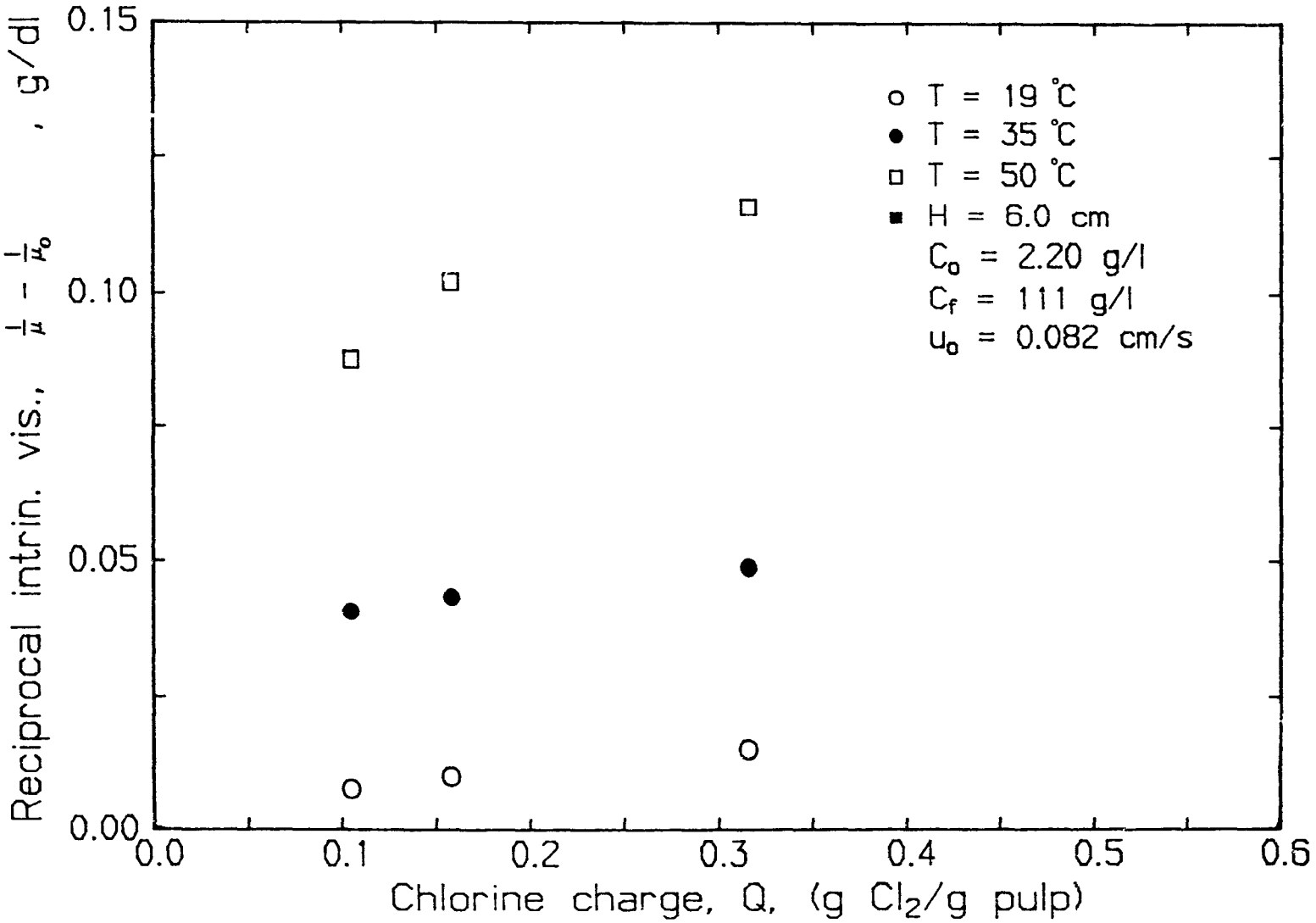
Reciprocal intrin. vis., $\frac{1}{\mu} - \frac{1}{\mu_o}$, g/dl
0.15
0.10
0.05
0.00
0.0
0.1
0.2
0.3
0.4
0.5
0.6
Chlorine charge, Q, (g Cl_2/g pulp)
o T = 19 °C
● T = 35 °C
□ T = 50 °C
■ H = 6.0 cm
C_o = 2.20 g/l
C_f = 111 g/l
u_o = 0.082 cm/s

Figure 6.68 Effect of consistency on CW (Klason + UV) lignin as a function of chlorine charge based on pulp pad under consideration.

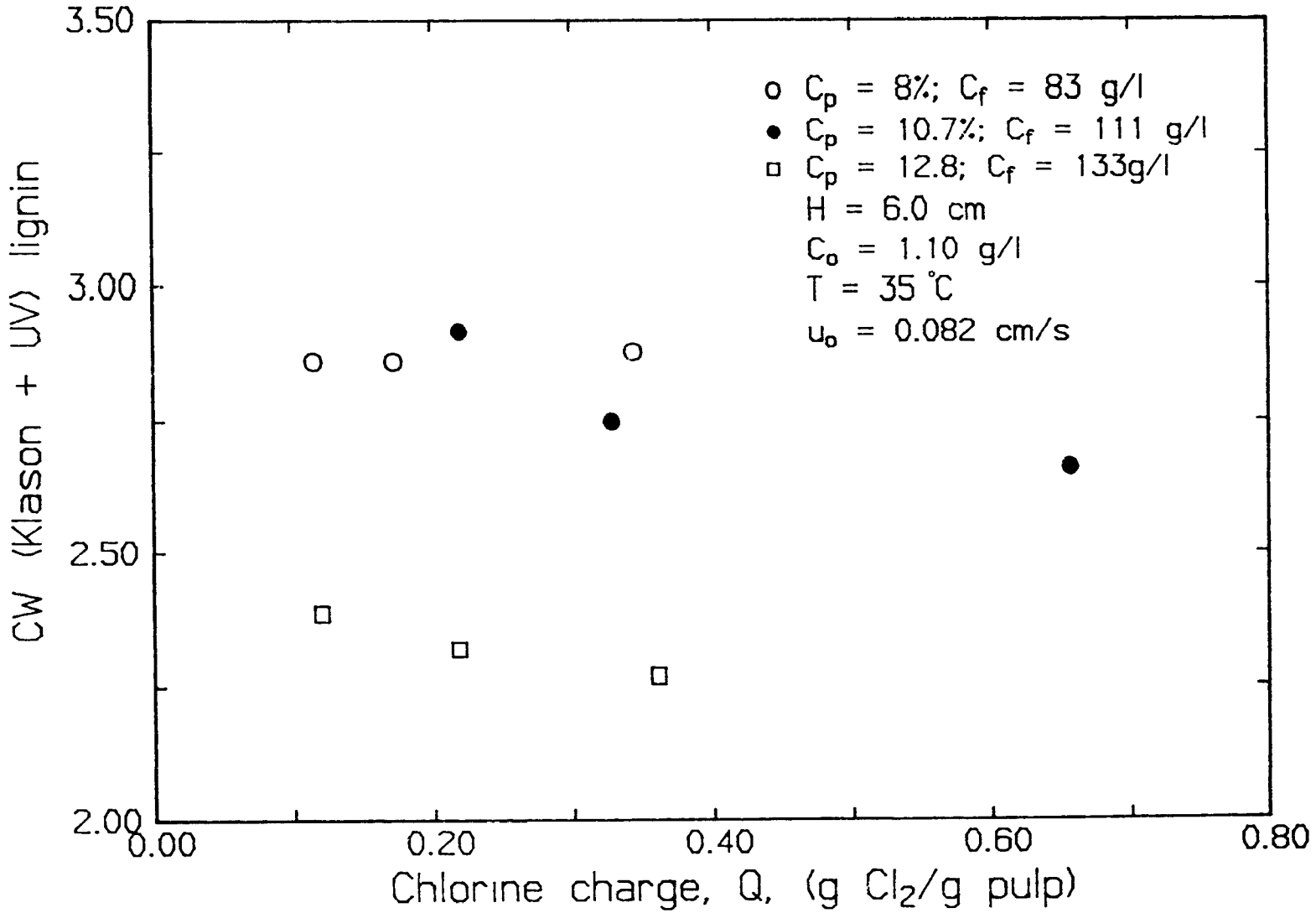
3.50
3.00
2.50
2.00
0.00
0.20
0.40
0.60
0.80
CW (Klason + UV) lignin
Chlorine charge, Q, (g Cl2/g pulp)
o Cp = 8%; Cf = 83 g/l
• Cp = 10.7%; Cf = 111 g/l
□ Cp = 12.8; Cf = 133g/l
H = 6.0 cm
Co = 1.10 g/l
T = 35 °C
uo = 0.082 cm/s

Figure 6.69 Effect of consistency on CWE (Klason + UV) lignin as a function of chlorine charge based on pulp pad under consideration.

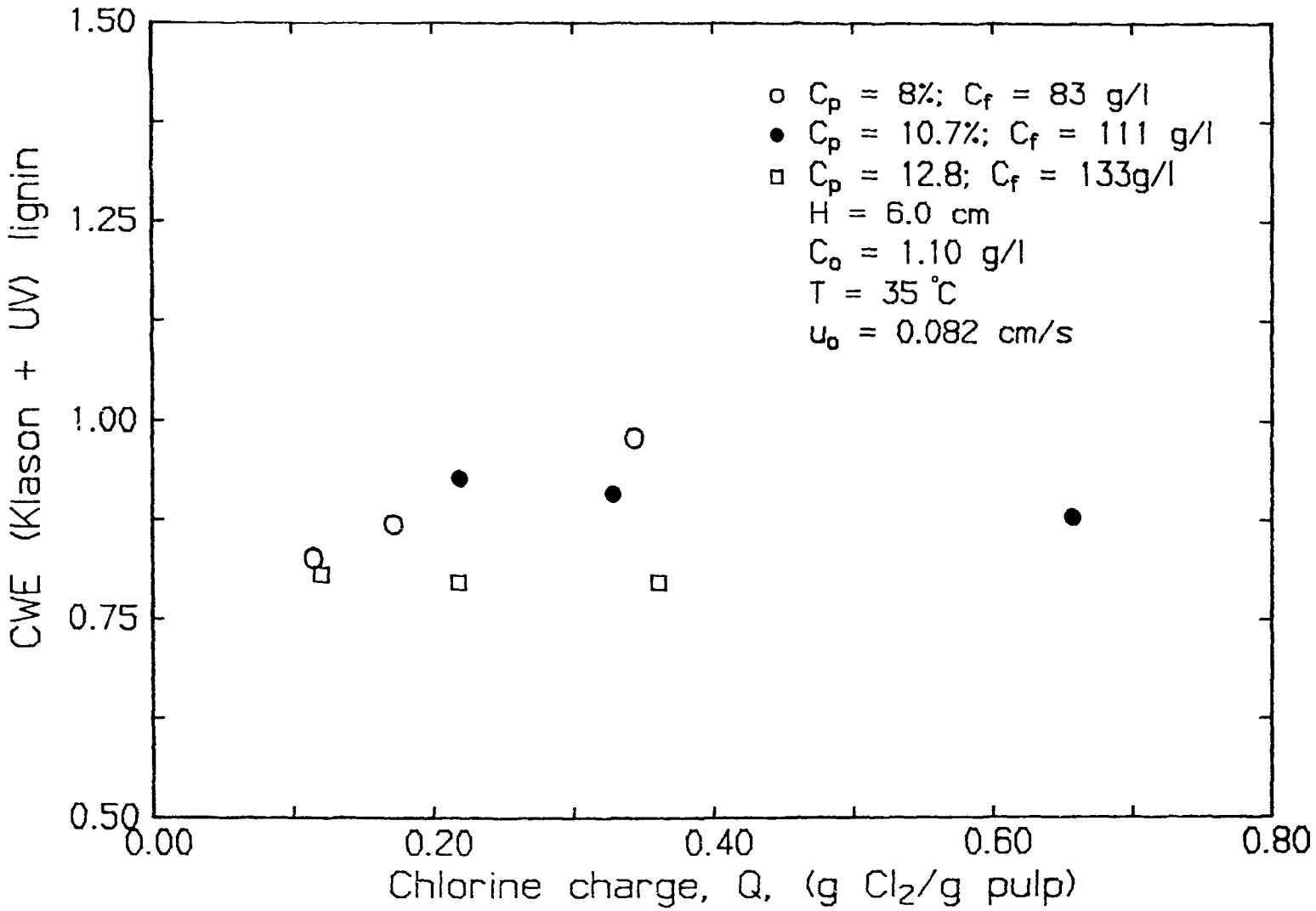
1.50
1.25
1.00
0.75
0.50
0.00
0.20
0.40
0.60
0.80
CWE (Klason + UV) lignin
Chlorine charge, Q, (g Cl_2/g pulp)
o C_p = 8%; C_f = 83 g/l
● C_p = 10.7%; C_f = 111 g/l
□ C_p = 12.8; C_f = 133g/l
H = 6.0 cm
C_o = 1.10 g/l
T = 35 °C
u_o = 0.082 cm/s

Plots of reciprocal intrinsic viscosities versus chlorine charge based on the pulp pad under consideration at three consistencies are shown in Figure 6.70. Lower intrinsic viscosities are obtained at higher consistencies. This can be explained by a proportional increase in k_c with C_f, and the longer contact time at the same Q when C_f is increased.

6.5.5.5 Effect of recycle

The pulp properties of the pulp pads chlorinated with and without spent liquor were very similar. This finding is of importance since the system has the potential to be closed with the consequence of less pollution problems. Further studies are necessary in order to elicit any possible effects on de-lignification rates due to build up of organics and inorganics in the effluent after many recycles.

6.5.5.6 Effect of viscosity protection agents

Chlorination inevitably results in reduction of pulp viscosity. It was shown above that higher mean residence times and temperatures and lower inlet chlorine water concentrations result in increased chlorine consumption by carbohydrates at similar chlorine charges, Q. This increased chlorine consumption leads to decreased cuene and intrinsic viscosities. Decreasing the chlorine consumption by carbohydrates should then lead to higher viscosities at the same chlorine charge on pulp.

Addition of viscosity protection agents like chlorine dioxide are commonly used in bleach plants to serve this purpose. A 10% substitution of chlorine dioxide was then studied in the present experimental system at temperatures of 35 and 50°C under otherwise similar experimental conditions. The pulp pad was divided into three parts in each case and analysed for cuene viscosities. Plots of these cuene viscosities versus

Figure 6.70 Effect of consistency on reciprocal intrinsic viscosities versus chlorine charge based on pulp pad under consideration.

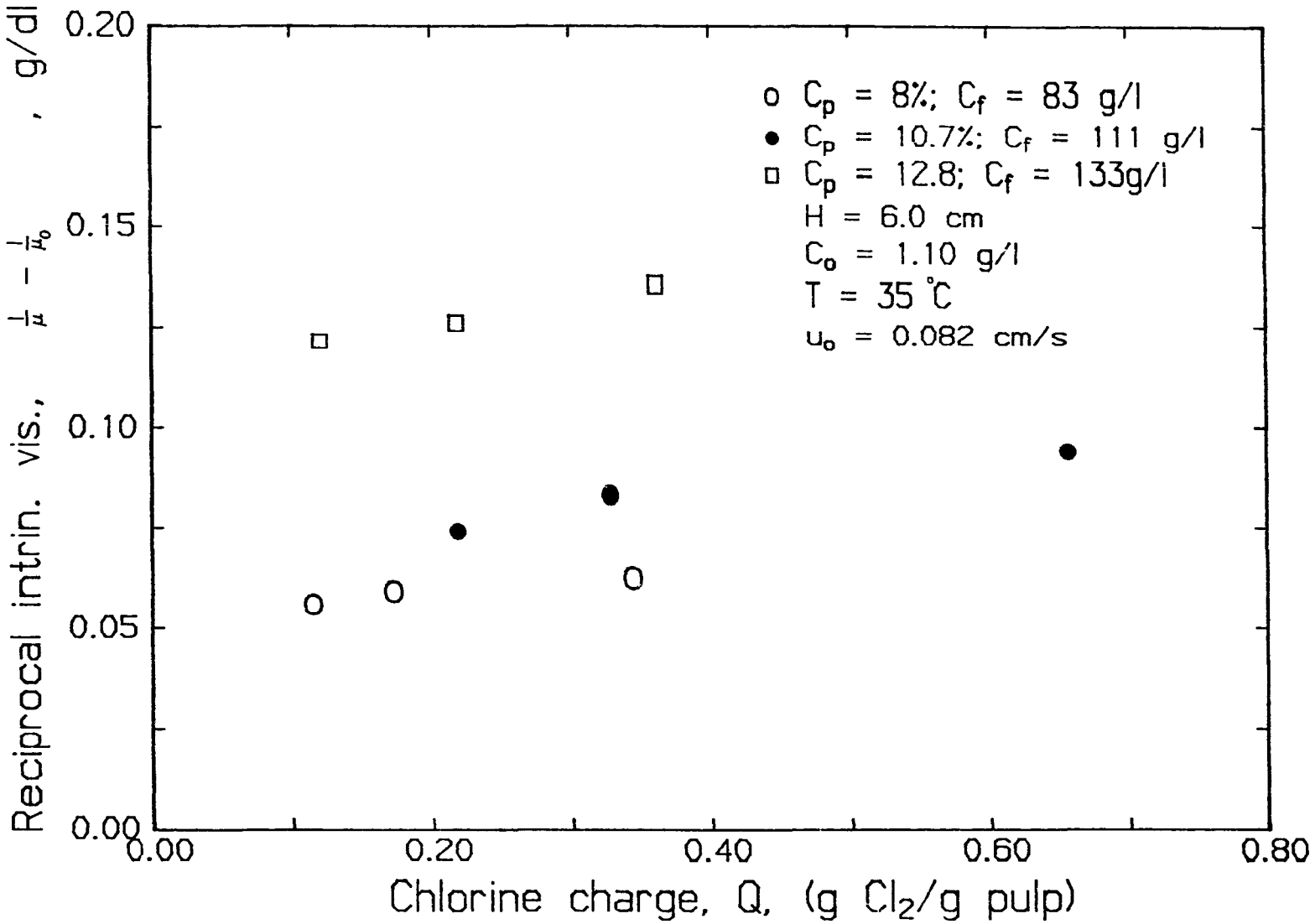
Reciprocal intrin. vis., $\frac{1}{\mu} - \frac{1}{\mu_o}$, g/dl
0.20
0.15
0.10
0.05
0.00
0.00
0.20
0.40
0.60
0.80
Chlorine charge, Q, (g Cl_2/g pulp)
o C_p = 8%; C_f = 83 g/l
• C_p = 10.7%; C_f = 111 g/l
□ C_p = 12.8; C_f = 133g/l
H = 6.0 cm
C_o = 1.10 g/l
T = 35 °C
u_o = 0.082 cm/s

pad position for these two experiments along with two similar experiments conducted in the absence of chlorine dioxide are shown in Figure 6.71. Dramatic increases in pulp viscosities are obtained at either temperatures. Sulfamic acid, another viscosity protector, at five weight percent based on chlorine charge was also studied. Increased viscosities, based on a similar experiment but without sulfamic acid addition, are also obtained as shown in Figure 6.72.

6.6 Conclusions

The effect of several operating variables on the Cl_2, TOC, TIC and methanol breakthrough curves and on pulp properties were presented separately in the preceding sections. The chlorine breakthrough curves were shown to be elongated versions of the corresponding inert glucose tracer curves. Similar to the inert glucose tracer discussed in Chapter 4, the flow behavior of chlorine water through a pulp pad is better represented by channelling flow rather than axial dispersed plug flow. The chlorine breakthrough curves were all explained in terms of the parallel plug flow model with the assumption that an instantaneous delignification reaction occurs at the reaction front of each channel. Delignification is also essentially complete when the Cl_2 breakthrough curves begin to plateau. The effect of operating variables on the chlorine-lignin stoichiometry, SL_o, were shown to be only dependent on temperature and average mean residence time $\bar{t}_r$. These SL_o values are generally smaller than those reported for batch chlorination. This is expected since reacted lignin is continuously washed out in dynamic chlorination and hence do not consume more chlorine. The majority of chlorine consumed in dynamic chlorination is

Figure 6.71 Effect of viscosity protection agent, ClO_2, on cuene viscosities.

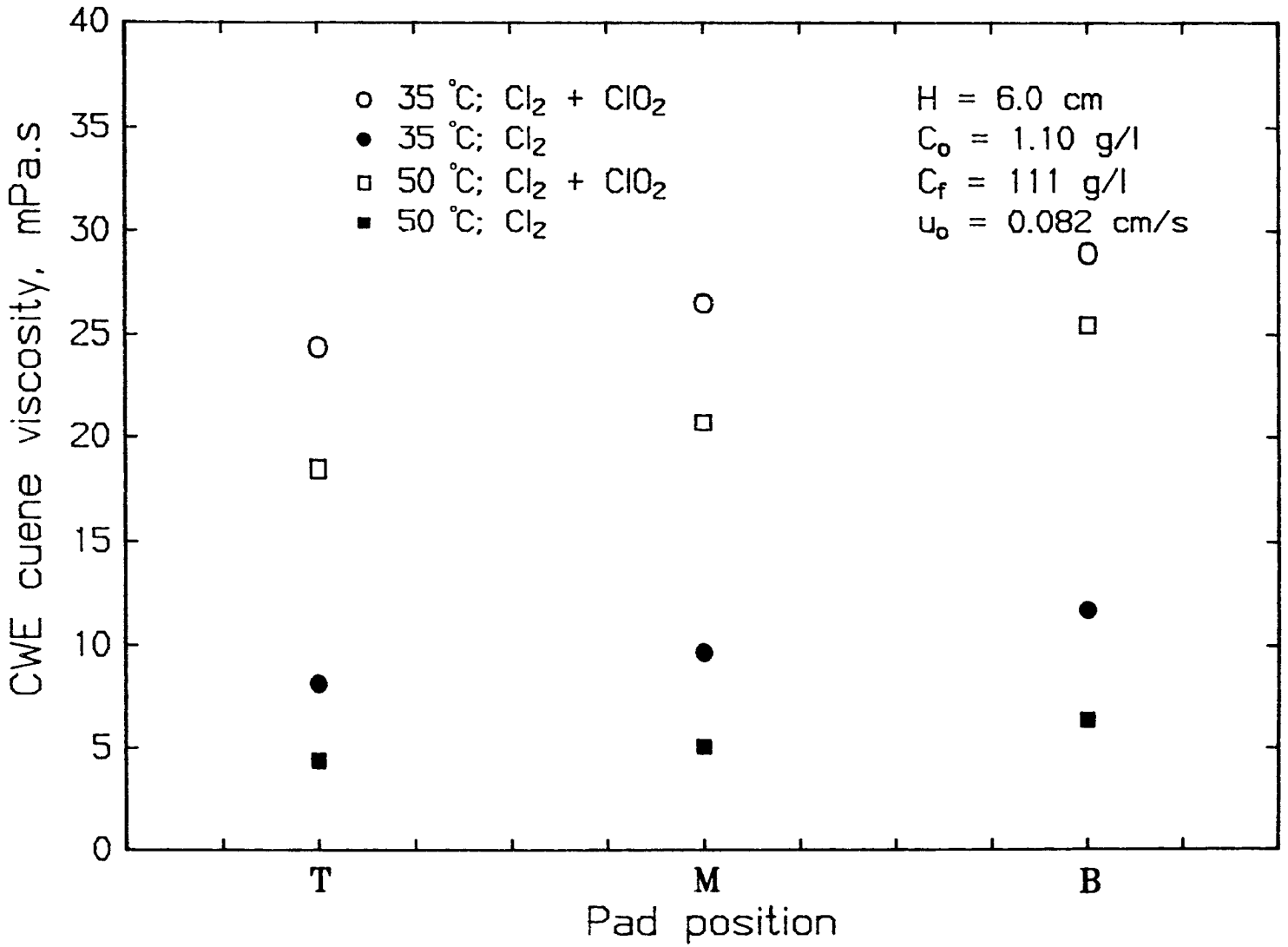
40
35
30
25
20
15
10
5
0
CWE cuene viscosity, mPa.s
o 35 °C; Cl2 + ClO2
• 35 °C; Cl2
□ 50 °C; Cl2 + ClO2
■ 50 °C; Cl2
H = 6.0 cm
Co = 1.10 g/l
Cf = 111 g/l
uo = 0.082 cm/s
T
M
B
Pad position

Figure 6.72 Effect of viscosity protection agent, sulfamic acid, on cuene viscosities.

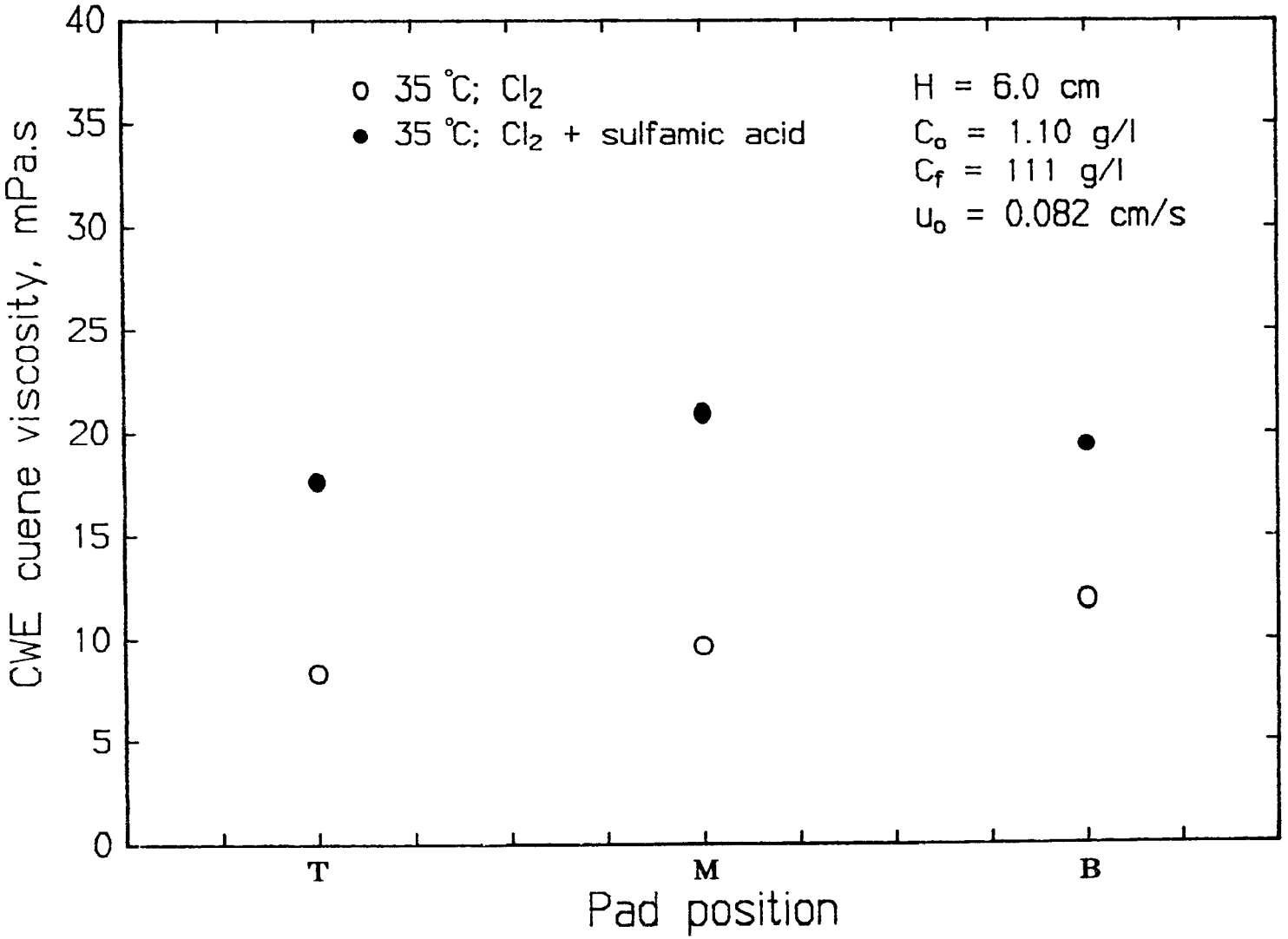
o 35 °C; Cl2
• 35 °C; Cl2 + sulfamic acid
H = 6.0 cm
Co = 1.10 g/l
Cf = 111 g/l
uo = 0.082 cm/s
CWE cuene viscosity, mPa.s
40
35
30
25
20
15
10
5
0
T
M
B
Pad position

consumed upstream of the front by slower delignification reactions.

TOC production during dynamic chlorination is due both to the instantaneous reaction at the reaction front and to oxidation/hydrolysis reactions before the reaction front. It was shown that TOC production after the onset of the plateau region of the TOC breakthrough curve originates mainly from lignin. The chlorine consumption is, however, due mainly to carbohydrates. A catalytic hydrolysis theory was invoked to explain these findings. Less TOC is also removed at higher chlorine concentrations at the same chlorine application on pulp. This was attributed to the shorter chlorination times available for lignin removal by hydrolysis at high chlorine concentrations. Physical limitations, i.e. diffusion, were considered unimportant since the plateau region of the TOC breakthrough curves were independent of chlorine water flow rates. The lower cumulative TOC removal during chlorination at higher chlorine water concentrations was supported by higher CW Klason lignin content. However similar CWE Klason lignin content, irrespective of chlorine water concentrations, indicate that CW Klason lignin is not a good indicator of the possible extent of delignification.

The methanol contribution to the total TOC is small. The production of methanol was explained in terms of the parallel plug flow model with all methanol production occurring at the reaction front from the instantaneous delignification reaction. The end of methanol production was shown to be linked to the end of delignification. This could have important consequences for process control.

The lignin content of the chlorinated pad was shown to be related to the Cl_2, TOC and methanol breakthrough curves. The CWE lignin contents

are at the so-called "floor level" when the Cl_2 and TOC breakthrough curves begin to plateau, and when methanol production has been reduced to zero. Re-cycling of re-concentrated spent liquor has no effect on delignification rates. CWE pulp viscosities were explained in terms of the parallel plug flow model. Linear relationships between reciprocal intrinsic viscosities and chlorine charge on pulp were observed. Addition of viscosity protection agents like chlorine dioxide and sulfamic acid resulted in increased pulp viscosities.

References

1. Rapson, W.H. and Anderson, C.B., "Dynamic bleaching: Continuous movement of liquor through pulp increases bleaching rate", Tappi, vol.49, No.8, 1966.
2. Gullichsen, J., "Pilot plant application of the displacement bleaching process", Tappi, vol.56, No.11, 1973.
3. Gullichsen, J., "Displacement bleaching", 3rd edition, Tappi Press, 1979.
4. Ackert, J.E., Ph.D Thesis, University of Idaho, 1973.
5. Baldus R.F., and Edwards, L.L., Tappi, Vol. 58, No.10, 1975.
6. Pugliese 111, S.C. and McDonough, T.J., "Kraft pulp chlorination: A new mechanistic description", International Pulp Bleaching Conference, Orlando Florida, June 5-9, 1988.
7. Berry, R.M. and Fleming, B.F., 1985 International Symposium on Wood and Pulping Chemistry, August 26-30, 1985.
8. Russel, N.A., Ph.D. Thesis, IPC (1966).
9. Koch, D.D., Ph.D. Thesis, University of Idaho (1971).
10. Levenspiel, O., "Chemical Reaction Engineering", John Wiley & Sons, U.S.A., 1972.
11. Trinh, D.T., "The measurement of lignin in kraft pulping liquors using an automatic colorimetric method", PPR 551, PPRIC internal report, 1985
12. Liebergott, N., Papricourse notes, PPRIC, 1984.
13. Singh, R.P. and Atkinson, E.S., "The bleaching of pulp", 3rd edition, Tappi press, 1979.

14. Patterson, A.H.J. and Kerekes, R.J., "Fundamentals of mixing in pulp suspension: diffusion of reacting chlorine", Tappi, vol.67, No.5, 1984.

15. Kramers, H. and Westerterp, K.R., Elements of Chemical Reactor Design and operation, Netherlands University Press, 1963.

16. Kemf, A.W and Dence, C.W., "Structure and reactivity of chlorolignin; Alkaline hydrolysis of chlorinated Kraft pulp, Tappi, vol.53, No.5, 1970.

17. Berry, R.M. and Fleming, B.I.,"The effect of a hot - water pretreatment on the chemistry of the E stage", PPR 485, PPRIC internal report, 1984.

18. Sarkanen, K.V. and Strauss, R.W., Tappi, vol.44, No.7, 1969.

19. van Buren, J.B. and Dence, C.W., "Chlorination behaviour of pine kraft lignin", Tappi, vol.53, No.12, 1970.

20. Gloor, W.E., and Klug, E.D., "Cellulose and cellulose derivatives", Editors Ott, E., and Spurlin, H.M., Part 3, Interscience publishers, part 3, New York, 1955.

CHAPTER 7

MODELLING OF DYNAMIC PULP CHLORINATION

7.1 Introduction

The shape of the breakthrough curves obtained during dynamic pulp chlorination are governed by the flow residence time distribution, kinetics of the different chlorine-pulp reactions and mass transfer resistances external to and within the pulp fibers. In order to predict the experimental breakthrough curves with a realistic model, these processes have to be quantified in the mathematical description of the model.

Several models (1) are currently available to represent fixed bed reactors. These models are either Fickian or non-Fickian. Fickian models assume a finite diffusion mechanism and the axial dispersion model belongs to this category. Non-Fickian models include the mixing cell (2) and cross-flow (3) models. These models are generally more complex and require specification of several parameters. Most studies of flow through packed beds are restricted to steady state conditions and for regularly shaped packings. It was discussed in Chapter 2 that the axial dispersion model gives a good description of conversion in tubular reactors when radial transport rates are at least twice the reaction rates. Poor prediction of tubular reactor performance were reported (4) at high reaction rates with the axial dispersion model. Considering that the chlorine-lignin reactions are extremely rapid, one should be cautious when applying the axial dispersion model to represent dynamic chlorination.

Modelling of a fiber bed reactor is complicated because pulp fibers are an unusual packing material. They have a small diameter of about 30 microns, a large length/diameter aspect ratio of 100 and are porous, hollow, flexible and compressible. Several fixed bed pulp washing

models based on the axial dispersion model were reported over the last few years (Chapter 2). The most recent study, Poirier's (5), successfully applied the axial dispersion model to represent the sodium and lignin breakthrough curves at high initial concentration of these two solutes. A source term to account for sorption was necessary at low initial solute concentrations.

In the present study the breakthrough curves were predicted using two flow models and appropriate kinetic description of the chlorine-lignin and chlorine-carbohydrates reaction. The two models are the axial dispersed plug flow model and the parallel plug flow model. In the latter it is assumed that the flow is made up of a large number of parallel plug flow channels with no exchange of mass between the channels. The residence time distribution obtained from the glucose tracer experiment (Chapter 4) is used for the specification of both flow models.

The mathematical representation and results of the axial dispersion model will be presented first followed by a similar treatment of the parallel plug flow model. The suitability of these models to predict breakthrough curves in dynamic chlorination will be discussed.

7.2 Axial dispersed plug flow model

7.2.1 Mathematical discription

The unsteady state convection-diffusion equation shown below

$$\varepsilon_i \frac{\partial(C)}{\partial t} + (\varepsilon_a - \varepsilon_i) \frac{\partial(C)}{\partial t} = D_L \varepsilon_i \frac{\partial^2(C)}{\partial x^2} - u_i \varepsilon_i \frac{\partial(C)}{\partial x} \qquad [7.1]$$

with

$$u_o = u_i \varepsilon_i = u_a \varepsilon_a \qquad [7.2]$$

where C is the chlorine water concentration, g/l; ε_a is the accessible porosity, l voids/l bed; ε_i is the interstitial porosity, l external voids/l beds; D_L is the axial dispersion coefficient, cm^2/s; u_o is the liquid velocity based on open area of the reactor, cm/s; u_i is the liquid velocity based on fluid external to fibers, cm/s; u_a is the liquid velocity based on accessible volume, cm/s; and x is the bed depth, cm, forms the basis of the axial dispersed plug flow model. Implicit in equation 7.1 are the assumptions of local equilibrum inside and outside the fibers and the absence of velocity or concentration gradients in the radial direction of the bed. The local equilibrum assumption is supported by calculations by Mackinnon (6) who showed that mass transfer resistances external to and inside the fiber wall can be neglected. Also the tracer experiments, Chapter 4, clearly showed that the local equilibrum assumption is valid for relatively small molecules like glucose. With the addition of a source term which accounts for the chlorine-lignin and chlorine-carbohydrates reactions equation 7.1 becomes

$$\varepsilon_a \frac{\partial(C)}{\partial t} = D_L \varepsilon_i \frac{\partial^2(C)}{\partial x^2} - u_i \varepsilon_i \frac{\partial(C)}{\partial x} - \varepsilon_a \left(\left(C_f \left(SL_{o,1} \cdot (-r_1) \right) + \left(SL_{o,2} \cdot (-r_2) \right) \right) + k_c C \right) \qquad [7.3]$$

where $SL_{o,1}$ is the chlorine-lignin stoichiometry of "fast" reactions, g Cl_2/g original lignin; $SL_{o,2}$ is the chlorine-lignin stoichiometry of

"slow" reaction, g Cl_2/g original lignin; $(-r_1)$ is the "fast" chlorine-lignin reaction rate, g lignin/g pulp·s; $(-r_2)$ is the "slow" chlorine-lignin reaction rate, g lignin/g pulp·s; and k_c is the chlorine-carbohydrates reaction rate constant, s^{-1}. In equation 7.3 it is assumed that chlorine is consumed by the "fast" reacting lignin, L_1, and "slow" reacting lignin, L_2, with the remaining lignin, L_3, being unreactive. These kinetics were first proposed by Ackert (7) and later adopted by Mackinnon (6) as the simplest model to describe the characteristic rapid initial and slow final chlorine consumption rate. The general kinetic equations describing the rate of disappearance of "fast" and "slow" lignin are shown in equations 7.4 and 7.5 respectively.

$$\frac{dL_1}{dt} = -r_1 = k_1[L_1]^e[C]^f \qquad [7.4]$$

$$\frac{dL_2}{dt} = -r_2 = k_2[L_2]^g[C]^h \qquad [7.5]$$

where k_1 is the rate constant of "fast" lignin reaction

$$\frac{1}{s}\left(\frac{\text{g pulp}}{\text{g lignin}}\right)^{e-1}\left(\frac{\text{liters}}{\text{g } Cl_2}\right)^{f},$$

and k_2 is the rate constant of "slow" lignin reaction

$$\frac{1}{s}\left(\frac{\text{g pulp}}{\text{g lignin}}\right)^{g-1}\left(\frac{\text{liters}}{\text{g } Cl_2}\right)^{h}$$

Ackert (7) assumed the reaction orders e, f, g, h to be unity. Mackinnon

(6) obtained as exponents e = 1.51, f = 1.61, g = 1.84 and h = 0.55 from his data base by parameter estimation techniques. Ackert (7) also proposed that the stoichiometry of the fast and slow reaction, $SL_{o,1}$ and $SL_{o,2}$ are both equal to 1.37 (g chlorine/g lignin removed) while Mackinnon employed values of 1.5 and 1.8, respectively. The total amount of lignin, L, at any time is defined as

$$L = L_1 + L_2 + L_3 \qquad [7.6]$$

while the initial lignin content is represented by L_o. The reaction constant suggested by Ackert and Mackinnon are also different i.e. k_1 and k_2 suggested by Ackert is 0.278 exp(- 250/T), ℓ/g Cl_2•s and 0.0056 exp(- 250/T), ℓ/g Cl_2•s while the corresponding values suggested by Mackinnon are 16.1 and $5.89*10^{10}$ exp(- 7670/T), 1/s(g pulp/g lignin)$^{g-1}$ (liters/g Cl_2)^h.

Equations 7.3 to 7.5 were non-dimensionalised by introducing the following dimensionless variables

$$P = \frac{u_i H}{D_L} \qquad [7.7]$$

$$T = \frac{t u_a}{H} \qquad [7.8]$$

$$X = x/H \qquad [7.9]$$

$$L_1^* = L_1/L_o \qquad [7.10]$$

$$L_2^* = L_2/L_o \qquad [7.11]$$

The resulting dimensionless equations are then:

$$\frac{\partial(C/C_o)}{\partial T} = \frac{1}{P}\frac{\partial^2(C/C_o)}{\partial X^2} - \frac{\partial(C/C_o)}{\partial X} - \left[\left(\frac{C_f L_o}{C_o}\cdot \left(\left(SL_{o,1}\cdot(-R_1)\right) + \left(SL_{o,2}\cdot(-R_2)\right)\right)\right) - H\frac{(C/C_o)k_c}{u_a}\right] \qquad [7.12]$$

$$R_1 = \frac{-dL_1^*}{dT} = \frac{k_1 C_o^f L_o^{(e-1)}(C/C_o)^f H}{u_a} L_1^{*e} \qquad [7.13]$$

$$R_2 = \frac{-dL_2^*}{dT} = \frac{k_2 C_o^h L_o^{(g-1)}(C/C_o)^h H}{u_a} L_2^{*g} \qquad [7.14]$$

$$-R = (-R_1) + (-R_2) \qquad [7.15]$$

Equation 7.12 was solved with the following initial condition

$$C/C_o = 0 \text{ for all } X \text{ at } T < 0 \qquad [7.16]$$

and the Danckwerts (8) boundary conditions.

$$C/C_o = 1 + \frac{1}{P}\frac{\partial(C/C_o)}{\partial X} \quad \text{at } X = 0 \text{ for } T > 0 \qquad [7.17]$$

and

$$\frac{\partial(C/C_o)}{\partial X} = 0 \text{ at } X = 1 \text{ for } T > 0 \qquad [7.18]$$

The initial condition used to solve equations 7.13 and 7.14 depend on whether Ackerts' or Mackinnons' kinetics are employed. The following initial conditions were used with Ackerts' kinetics:

$$L_1^* = 0.50 \text{ at } T \leq 0 \qquad [7.19]$$

$$L_2^* = 0.30 \text{ at } T \leq 0 \qquad [7.20]$$

and thus

$$L_3^* = 0.20 \qquad [7.21]$$

The initial conditions used by Mackinnon are

$$L_1^* = 0.65 \text{ at } T \leq 0 \qquad [7.22]$$

$$L_2^* = 0.25 \text{ at } T \leq 0 \qquad [7.23]$$

7.2.2 Numerical solution

The numerical solution used to solve equations 7.12 to 7.15 was based on the control volume formulation of Patankar (9). The pulp pad was divided into control volumes of equal sizes except for the two end control volumes which are half the size of the internal control volume. A schematic representation is shown in Figure 7.1. The differential equations 7.12 to 7.14 were integrated over each control volume from time T to T + dT. For example integration of equation 7.12 over a single internal con-

Figure 7.1 Representation of pulp pad by nodes and control volumes.

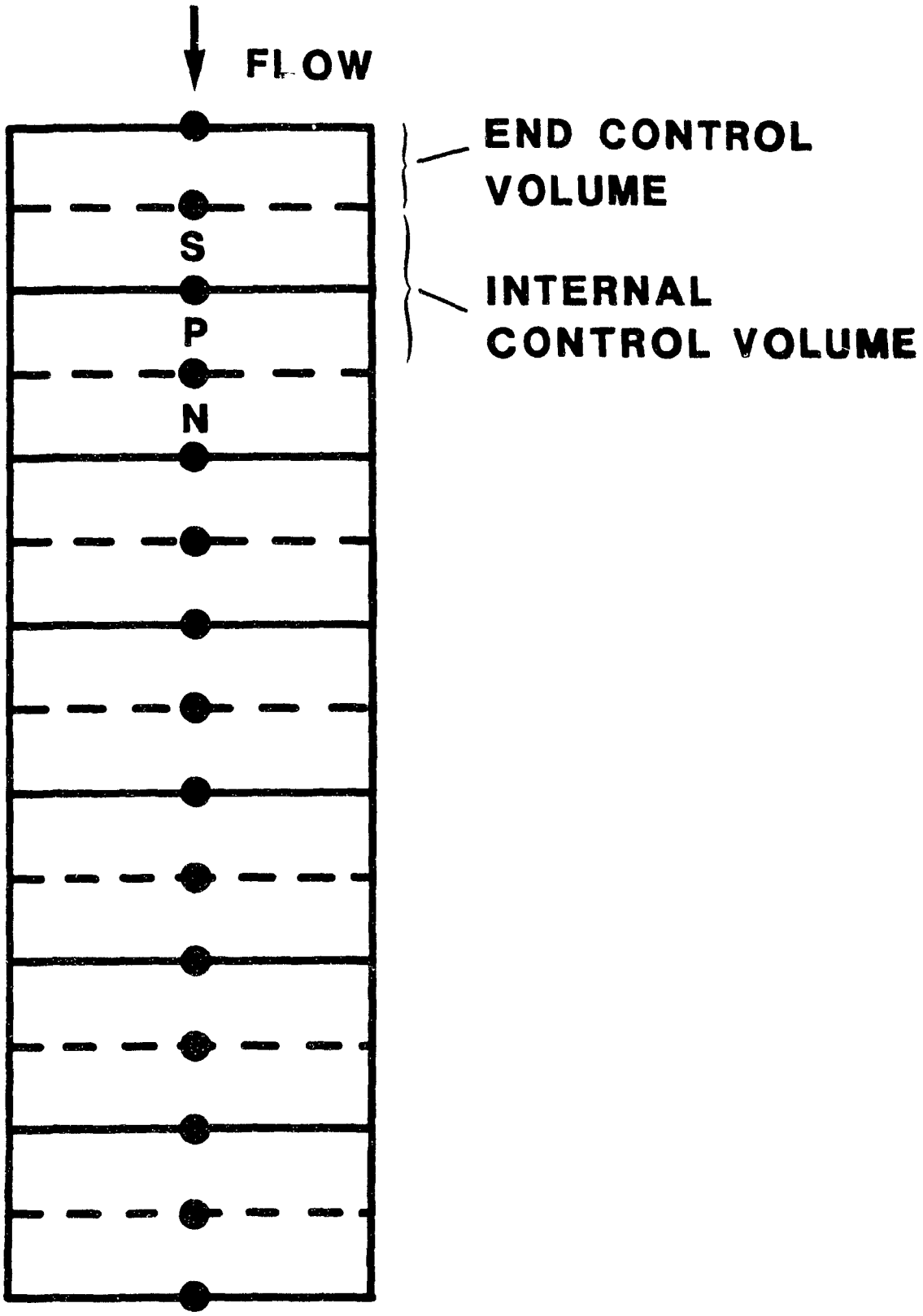
FLOW
END CONTROL VOLUME
INTERNAL CONTROL VOLUME
S
P
N

trol volume gives

$$\int_s^n \int_T^{T+dT} \frac{\partial (C/C_o)}{\partial T}\, dT dX = \int_T^{T+dT} \int_s^n \frac{1}{P} \frac{\partial^2 (C/C_o)}{\partial X^2}\, dX dT - \int_T^{T+dT} \int_s^n \frac{\partial (C/C_o)}{\partial T}\, dX dT - \int_T^{T+dT} \int_s^n S\, dX dT \qquad [7.24]$$

with the source term S representing consumption of chlorine by lignin and carbohydrates. The chlorine-lignin reaction kinetics proposed by Mackinnon was linearized following the method proposed by Patankar (9).

$$S = S^* + \frac{dS^*}{d(C/C_o)} \cdot [(C/C_o)^* - (C/C_o)] \qquad [7.25]$$

The superscript * denotes previous iteration values at time T. Similar linearizations were done for equations 7.13 and 7.14. The source term was rearranged as follows:

$$S = S_c + S_p \qquad [7.26]$$

where S_c is the constant part of the source term and S_p is the coefficient of the dependent variable C/C_o.

Before discretization equations like equation 7.24 can be integrated the variation of C/C_o between grid points must be specified. A

stepwise concentration profile shown in Figure 7.2 is obtained when C/C_o is assumed to be constant over each control volume. The drawback of this assumption is that the slope $d[(C/C_o)/dX]$ is not defined at the control volume faces. The piecewise linear profile shown in Figure 7.3 assumes a linear variation in the dependent variable between grid points and eliminates this difficulty of the stepwise profile.

The stepwise profile was used for the unsteady term and a piecewise linear profile for the diffusion term of equation 7.12 since the latter term requires knowledge of the gradient of C/C_o at the boundaries. Several interpolation schemes i.e. central difference, upwind, hybrid, exponential and power law, were discussed by Patankar (9) for the convection term. The hybrid scheme which reduces to the central difference scheme, i.e. piecewise linear profile, at low grid Peclet numbers was chosen for the present solution. Stepwise profiles were used for both the unsteady and the source terms of equations 7.13 and 7.14.

The variation of C/C_o with time is also needed since the concentration at each node is evaluated at different time steps. The fully implicit scheme, i.e. the new concentration value prevails over the entire time step, was recommended by Patankar and employed here.

The method of solution employed in solving the discretized equations depends on the linearity of the source term. Linearisation of the source term results in the coefficients requiring specification of "old" dependent values i.e. iteration until convergence is needed for each equation. Linear source terms however allow calculation of the dependent variable explicitly. Thus the numerical code employed when Ackerts' linear kinetics are used, version 2, is different from version 1 when

Figure 7.2 Stepwise profile assumption.

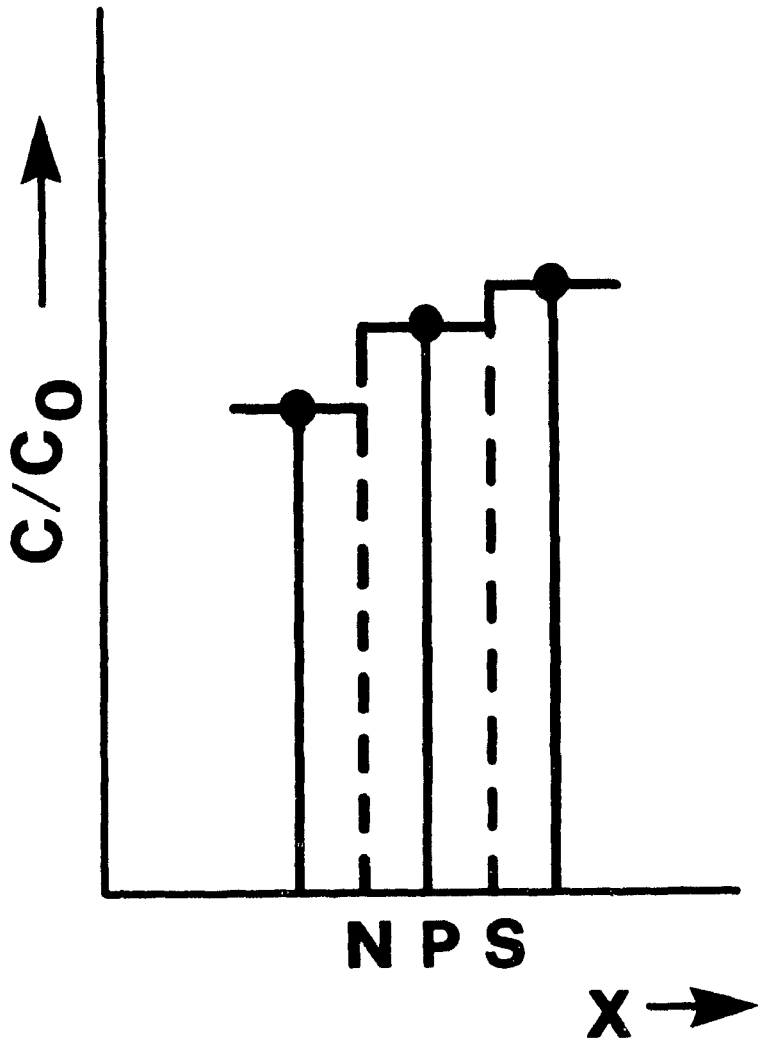
C/C0
N P S
X

Figure 7.3 Piecewise linear profile.

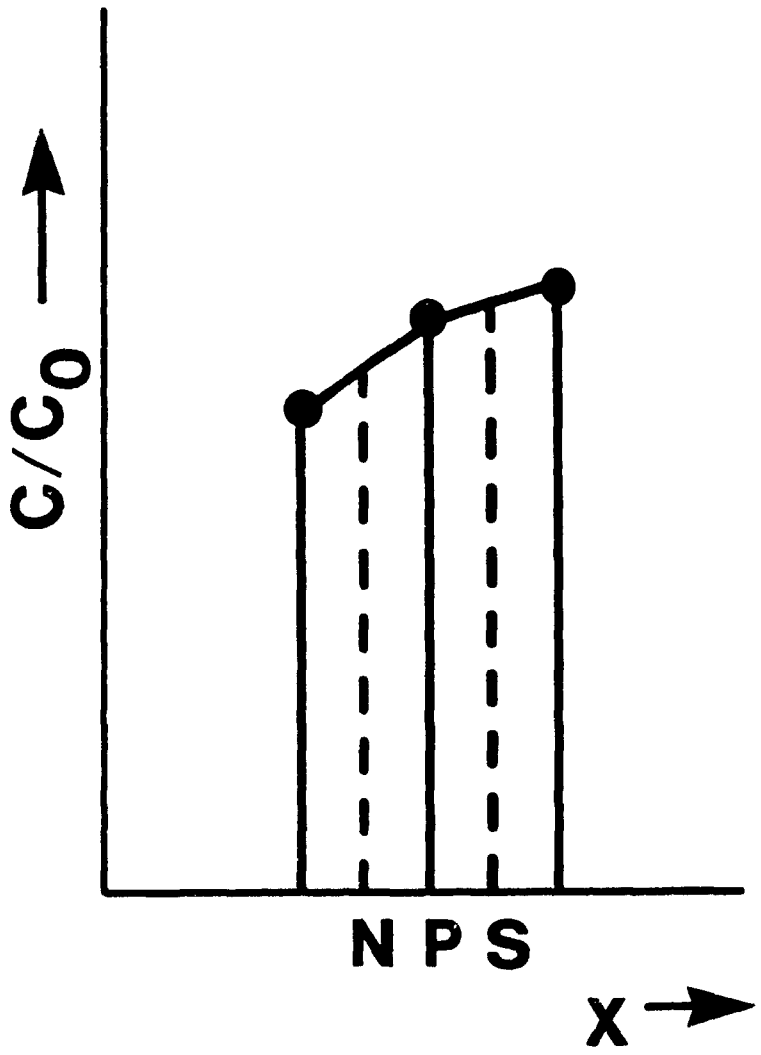
C/C0
N P S
X

Mackinnon's non-linear kinetics are employed. The method of solution of version 1 will be discussed since it is more general. Such an approach is, however, not recommended for actual solution of the equations of version 2 since a separate numerical code for version 2 can take advantage of the explicit evaluation of the discretized equations.

The algorithm used to solve version 1 is shown in Figure 7.4. Three nested loops, corresponding to the main equation 7.12 and two rate equations 7.13 and 7.14 within a main loop are apparent. Iterations occur within each nested loop and within the main loop as shown. Convergence for any time step is obtained when each of the three nested loops is converged. The chlorine and lignin concentration values of the bed exit control volume are printed after a predetermined time. A plot of these chlorine concentrations versus time is the theoretical chlorine breakthrough curve. A copy of the FORTRAN programme developed for this purpose is shown in Appendix (7-1).

The algorithm used to solve version 2 of the axial dispersion model is shown in Figure 7.5. Because of the linearity of the equations and hence explicit solution technique only one loop is required. Convergence for any time step occurs when guessed lignin concentrations agree with the newly calculated ones.

7.2.3 Model verification

7.2.3.1 Effect of number of nodes and time step size

A sound numerical program requires that the solution is independent of node spacing and time step size. Several simulations with different combinations of number of nodes and time step intervals were conducted for both versions 1 and 2 of the axial dispersed plug flow model. The

Figure 7.4 Algorithm for version 1 of axial dispersed plug flow model.

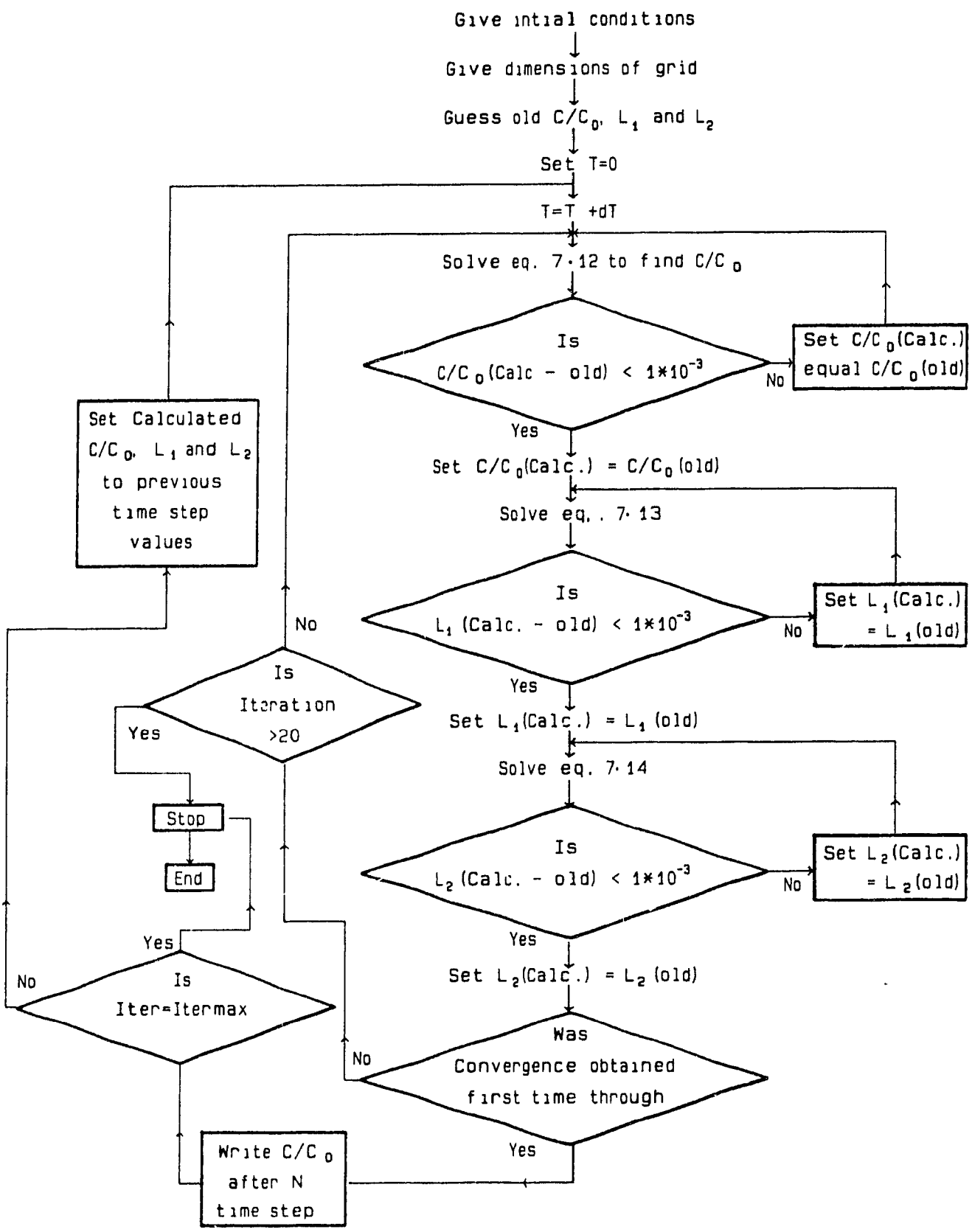
Give intial conditions
Give dimensions of grid
Guess old C/C0, L1 and L2
Set T=0
T=T +dT
Solve eq. 7·12 to find C/C0
Is C/C0(Calc - old) < 1*10-3
No
Set C/C0(Calc.) equal C/C0(old)
Yes
Set C/C0(Calc.) = C/C0(old)
Solve eq. 7·13
Is L1 (Calc. - old) < 1*10-3
No
Set L1(Calc.) = L1(old)
Yes
Set L1(Calc.) = L1 (old)
Solve eq. 7·14
Is L2 (Calc. - old) < 1*10-3
No
Set L2(Calc.) = L2(old)
Yes
Set L2(Calc.) = L2 (old)
Was Convergence obtained first time through
No
Yes
Is Iteration >20
No
Yes
Stop
End
Is Iter=Itermax
No
Yes
Set Calculated C/C0, L1 and L2 to previous time step values
Write C/C0 after N time step

Figure 7.5 Algorithm for version 2 of axial dispersed plug flow model.

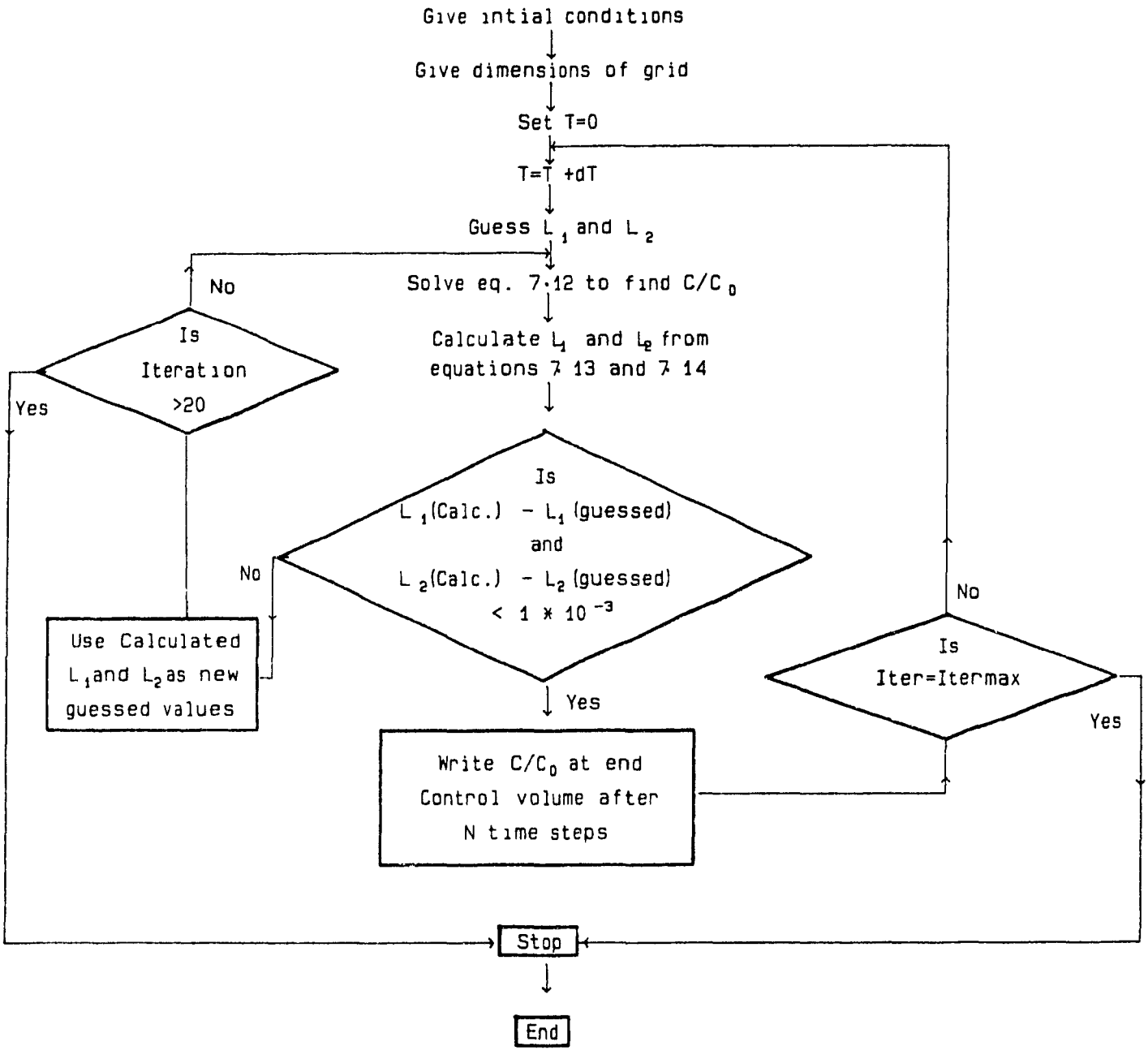
Give intial conditions
Give dimensions of grid
Set T=0
T=T +dT
Guess L_1 and L_2
Solve eq. 7·12 to find C/C_0
Calculate L_1 and L_2 from equations 7 13 and 7 14
Is L_1(Calc.) - L_1 (guessed) and L_2(Calc.) - L_2 (guessed) < $1 * 10^{-3}$
No
Yes
Use Calculated L_1 and L_2 as new guessed values
Is Iteration >20
No
Yes
Is Iter=Itermax
No
Yes
Write C/C_0 at end Control volume after N time steps
Stop
End

effect of number of nodes on the predicted chlorine breakthrough curves for a fixed time step with version 2 is shown in Figure 7.6 for a typical dynamic pulp chlorination experiment. Since the differences are small the steepest region of the breakthrough curves was enlarged and shown in Figure 7.7. The differences between the breakthrough curves are insignificant when the number of nodes were 40 or greater. Forty grid nodes were then used for all further calculations.

The effect of time step size on the shape of the chlorine breakthrough curves for forty grid nodes is shown in Figure 7.8. Considering the small differences between the three chlorine breakthrough curves a value of 0.01 was chosen for the non-dimensional time step. Based on similar calculations for version 1 seventy nodes and a time step of 0.01 was adopted.

7.2.3.2 Comparison with exact solution

A standard way to test numerical codes is to compare the results with analytical solutions. A survey of the literature indicated that the only relevant analytical solutions are those of the unsteady axial dispersion equation derived by Brenner (10). The numerical solutions obtained with appropriate modifications of versions 1 and 2 of the model were then compared against this analytical solution.

The numerical solution without source term was obtained by setting the reaction terms to zero in both versions of the model. The prediction obtained with version 1 are compared with Brenner's (10) exact solution in Figure 7.9. The very good agreement indicates that the numerical code encompassing the main equation is reliable. Similar results were obtained when version 2 was tested. Comparisons with exact solutions of the un-

Figure 7.6 Effect of number of nodes on numerical solution of version 2.

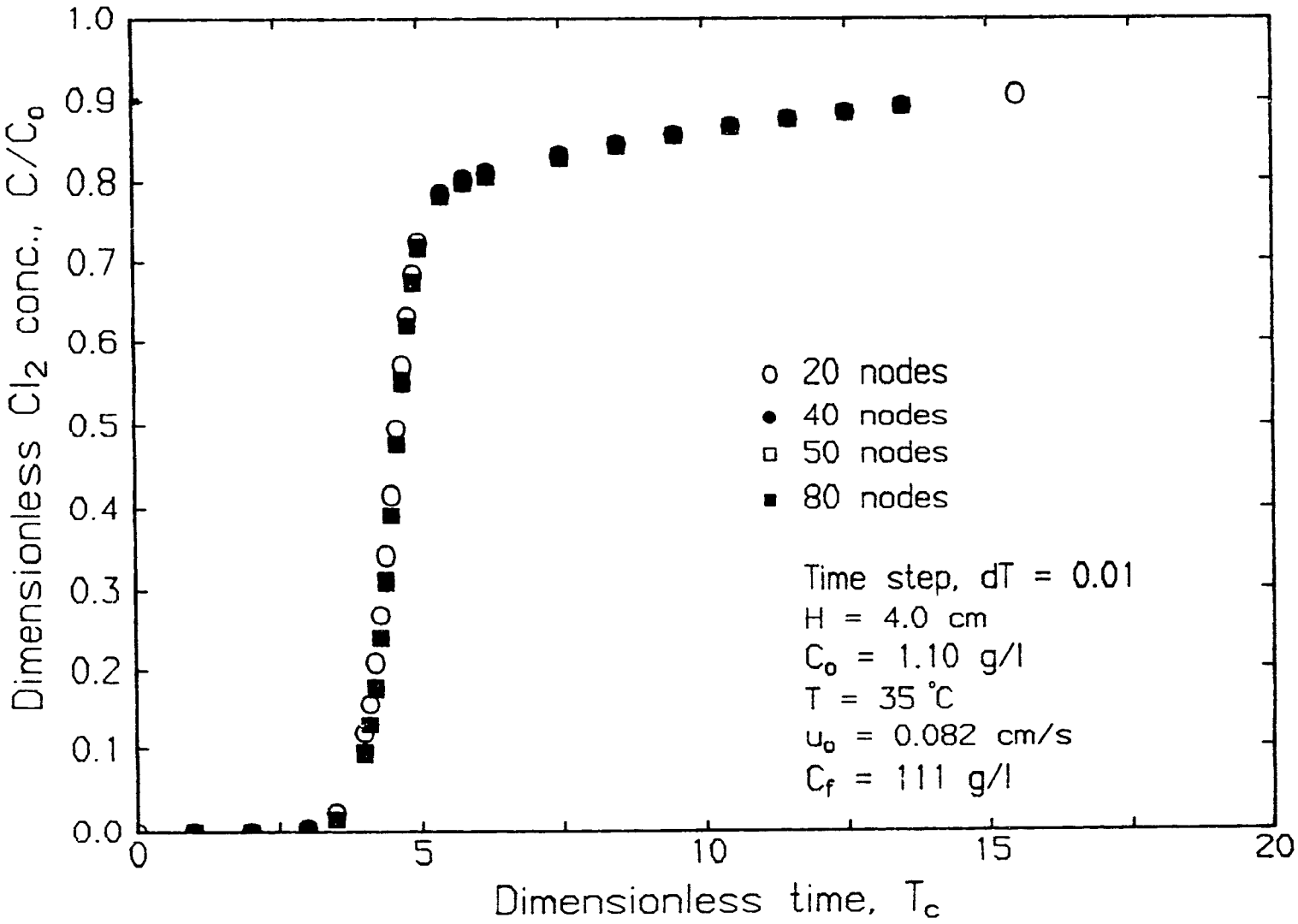
Dimensionless Cl_2 conc., C/C_o
1.0
0.9
0.8
0.7
0.6
0.5
0.4
0.3
0.2
0.1
0.0
0
5
10
15
20
Dimensionless time, T_c
o 20 nodes
• 40 nodes
□ 50 nodes
■ 80 nodes
Time step, dT = 0.01
H = 4.0 cm
C_o = 1.10 g/l
T = 35 °C
u_o = 0.082 cm/s
C_f = 111 g/l

Figure 7.7 Effect of number of nodes on numerical solution of version 2 - expanded scale.

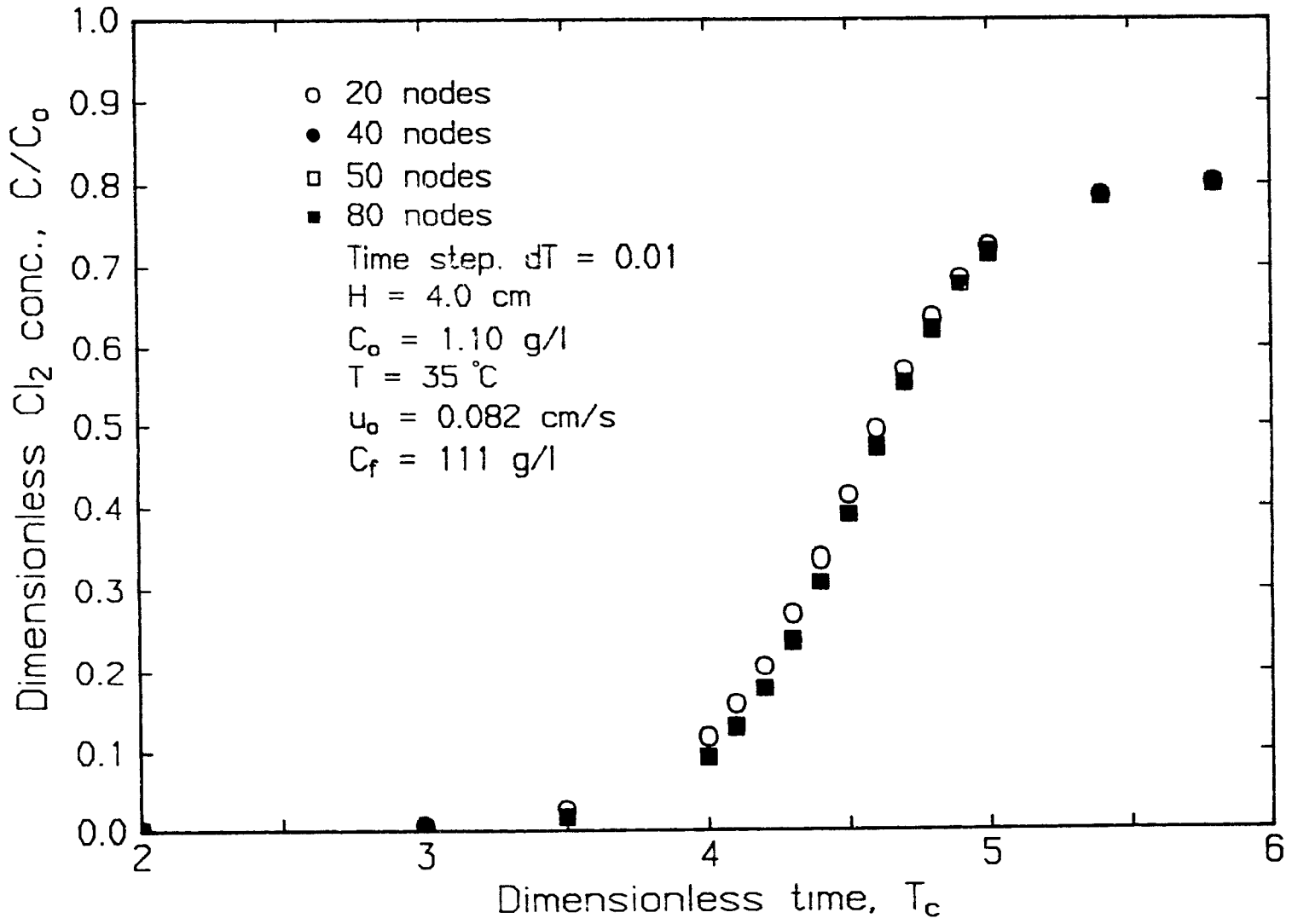
20 nodes
40 nodes
50 nodes
80 nodes
Time step. dT = 0.01
H = 4.0 cm
C_o = 1.10 g/l
T = 35 °C
u_o = 0.082 cm/s
C_f = 111 g/l
Dimensionless Cl_2 conc., C/C_o
Dimensionless time, T_c
0.0
0.1
0.2
0.3
0.4
0.5
0.6
0.7
0.8
0.9
1.0
2
3
4
5
6

Figure 7.8 Effect of time step on numerical solution of version 2.

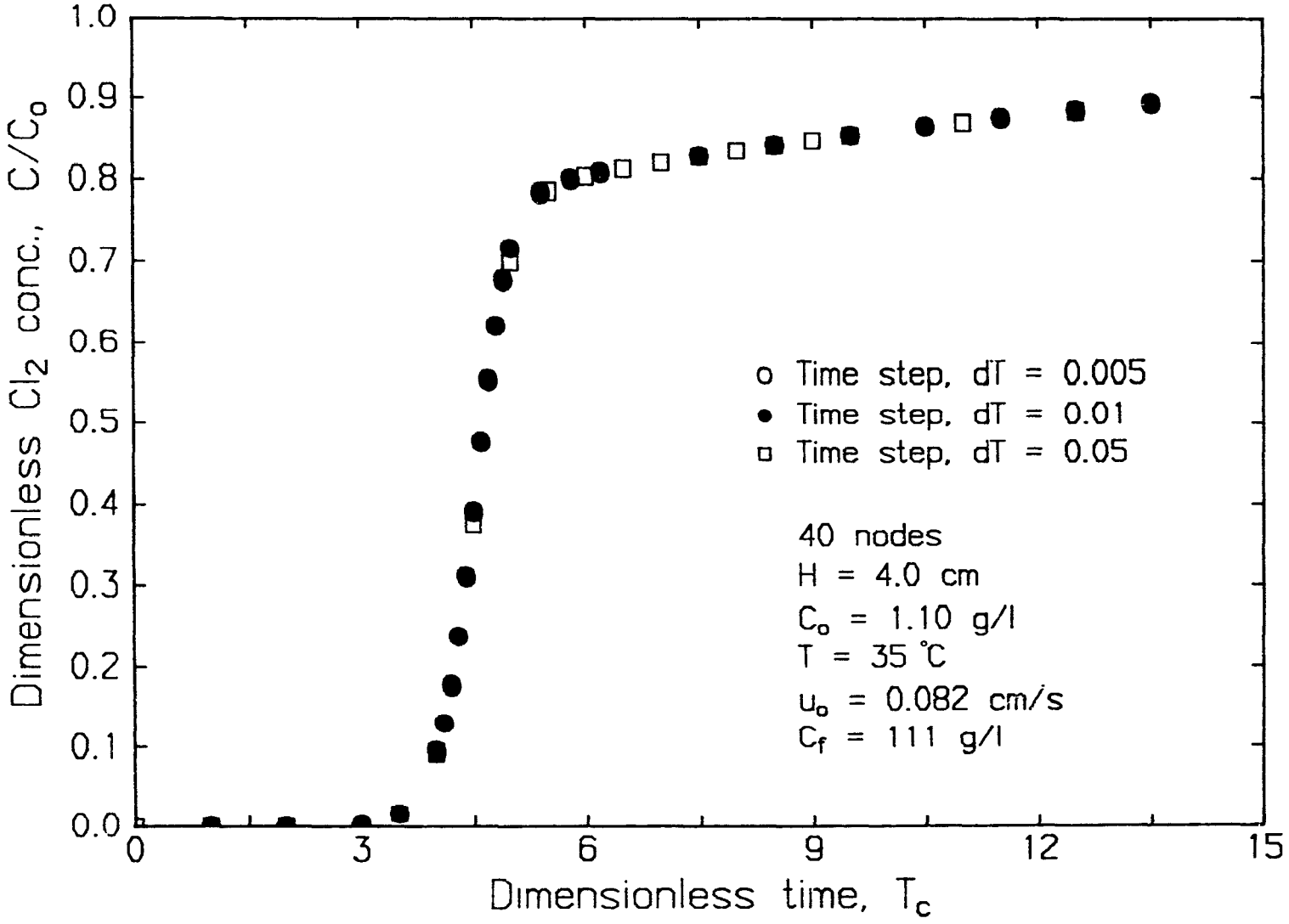
Dimensionless Cl_2 conc., C/C_o
1.0
0.9
0.8
0.7
0.6
0.5
0.4
0.3
0.2
0.1
0.0
0
3
6
9
12
15
Dimensionless time, T_c
o Time step, dT = 0.005
• Time step, dT = 0.01
□ Time step, dT = 0.05
40 nodes
H = 4.0 cm
C_o = 1.10 g/l
T = 35 °C
u_o = 0.082 cm/s
C_f = 111 g/l

Figure 7.9 Comparison of numerical solution, without source terms, to exact analytical solution.

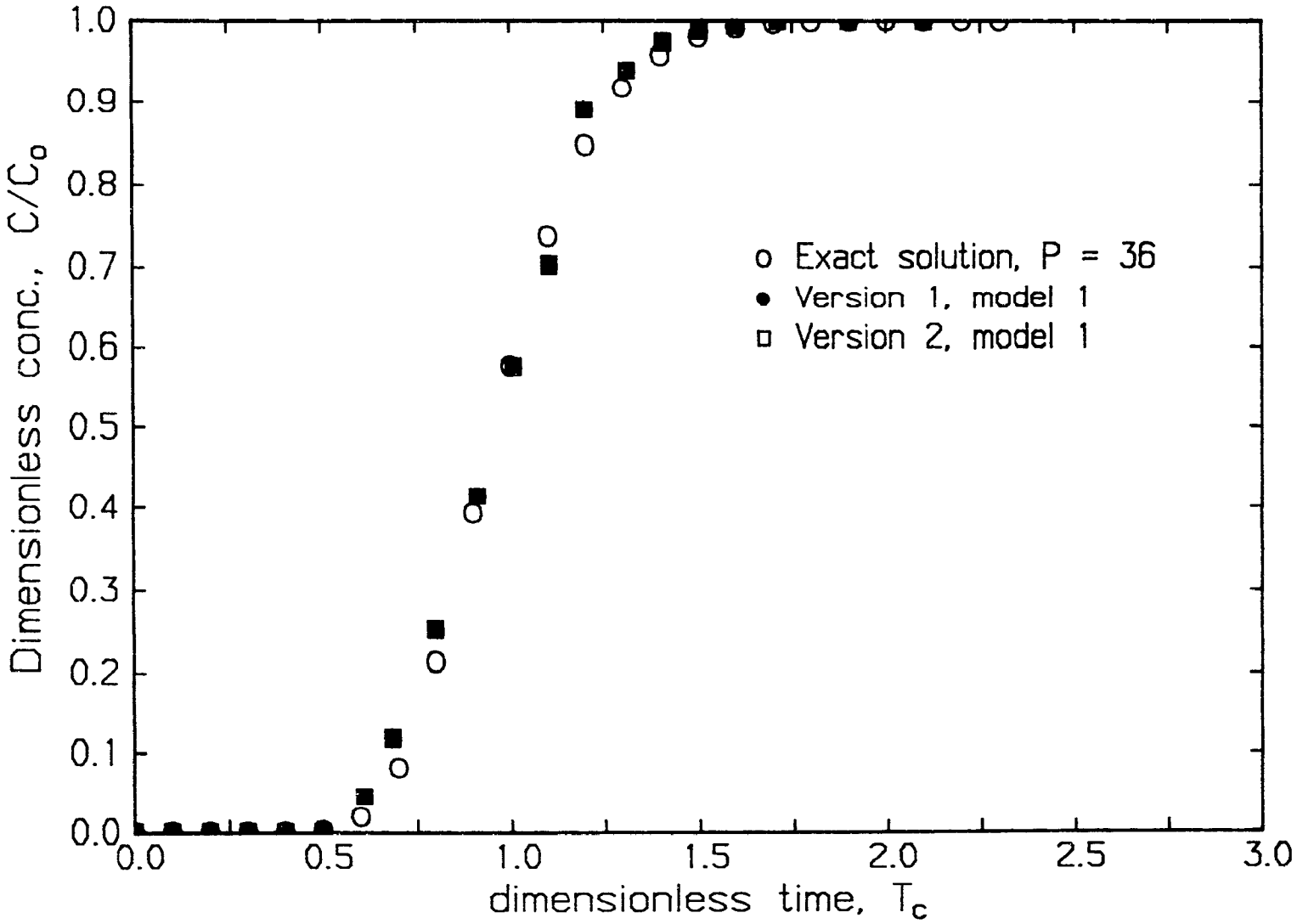
Dimensionless conc., C/C$_o$
dimensionless time, T$_c$
o Exact solution, P = 36
• Version 1, model 1
□ Version 2, model 1
0.0
0.1
0.2
0.3
0.4
0.5
0.6
0.7
0.8
0.9
1.0
0.0
0.5
1.0
1.5
2.0
2.5
3.0

steady state axial dispersion equation with reaction is not possible because of the unavailability or complex nature of these solutions.

7.2.3.4 Prediction of experimental breakthrough curve

The breakthrough curves obtained during dynamic chlorination studies of fully bleached pulp pads were presented in Chapter 5. These breakthrough curves were predicted by setting the chlorine-lignin reaction terms to zero in both versions of the axial dispersed plug flow model. The only reaction term left is the first order chlorine-carbohydrate reaction. The Peclet number of the fully bleached pulp pad determined from the preceeding glucose tracer breakthrough curve was used in the numerical prediction. The agreement between the data and the numerical prediction of the breakthrough curve obtained with version 1 is very good as can be seen in Figure 7.10. The same results were obtained when version 2 was used to generate the theoretical breakthrough curves. Thus the axial dispersion model with first order chlorine-carbohydrates reaction kinetics is adequate to describe dynamic chlorination of a bed of carbohydrate fibers. These results also serve as another test of the numerical codes discussed above.

Simulations with both versions of the axial dispersed plug flow model were done for three typical dynamic pulp chlorination experiments with different initial chlorine concentrations. The results of these three simulations are compared to the experimental breakthrough curves and shown in Figures 7.11 to 7.13. Neither model gives an accurate prediction of experimental data. Version 1 predicts a very steep rise of the exit chlorine concentration from zero to the plateau at full breakthrough. Version 2 is characterised by an earlier breakthrough and an initial fast

Figure 7.10 Prediction of chlorine breakthrough curve for fully bleached pulp; version 1 of axial dispersed plug flow model.

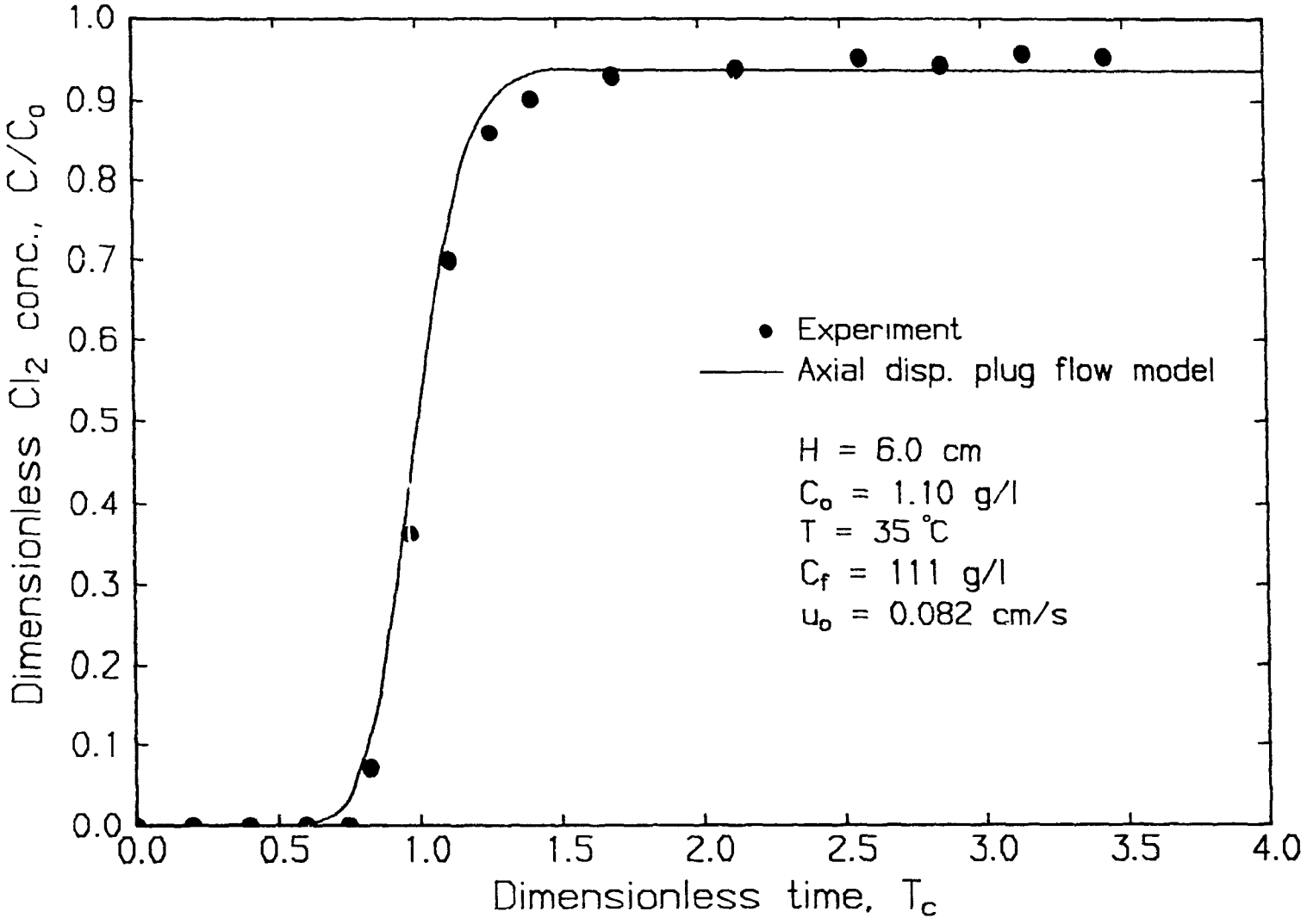
Dimensionless Cl_2 conc., C/C_o
1.0
0.9
0.8
0.7
0.6
0.5
0.4
0.3
0.2
0.1
0.0
0.0
0.5
1.0
1.5
2.0
2.5
3.0
3.5
4.0
Dimensionless time, T_c
Experiment
Axial disp. plug flow model
H = 6.0 cm
C_o = 1.10 g/l
T = 35 °C
C_f = 111 g/l
u_o = 0.082 cm/s

Figure 7.11 Prediction of chlorine breakthrough curve with axial dispersed plug flow model; C_o = 0.55 g/l.

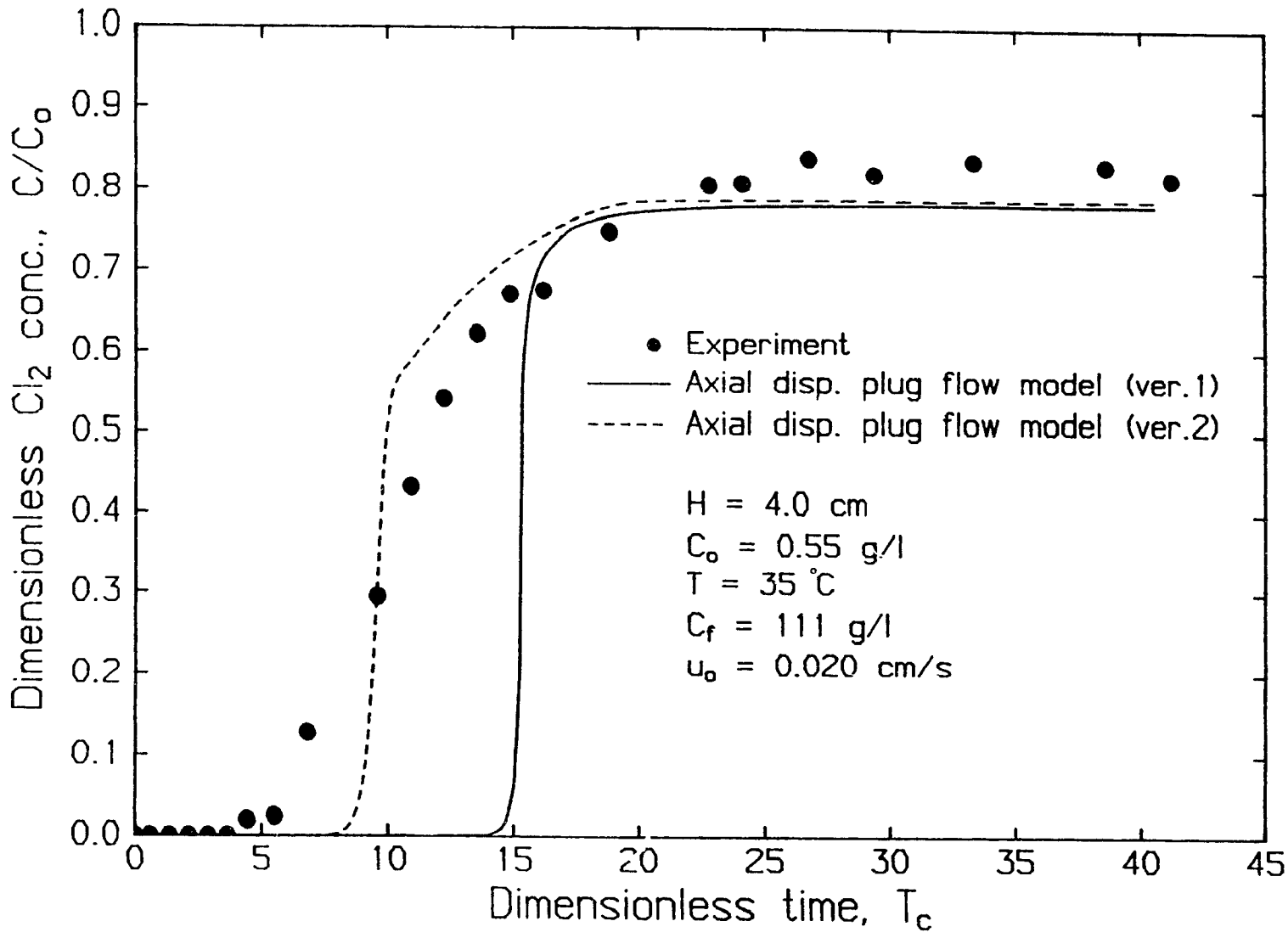
Dimensionless Cl_2 conc., C/C_o
1.0
0.9
0.8
0.7
0.6
0.5
0.4
0.3
0.2
0.1
0.0
0
5
10
15
20
25
30
35
40
45
Dimensionless time, T_c
Experiment
Axial disp. plug flow model (ver.1)
Axial disp. plug flow model (ver.2)
H = 4.0 cm
C_o = 0.55 g/l
T = 35 °C
C_f = 111 g/l
u_o = 0.020 cm/s

Figure 7.12 Prediction of chlorine breakthrough curve with axial dispersed plug flow model; C_o = 1.10 g/l.

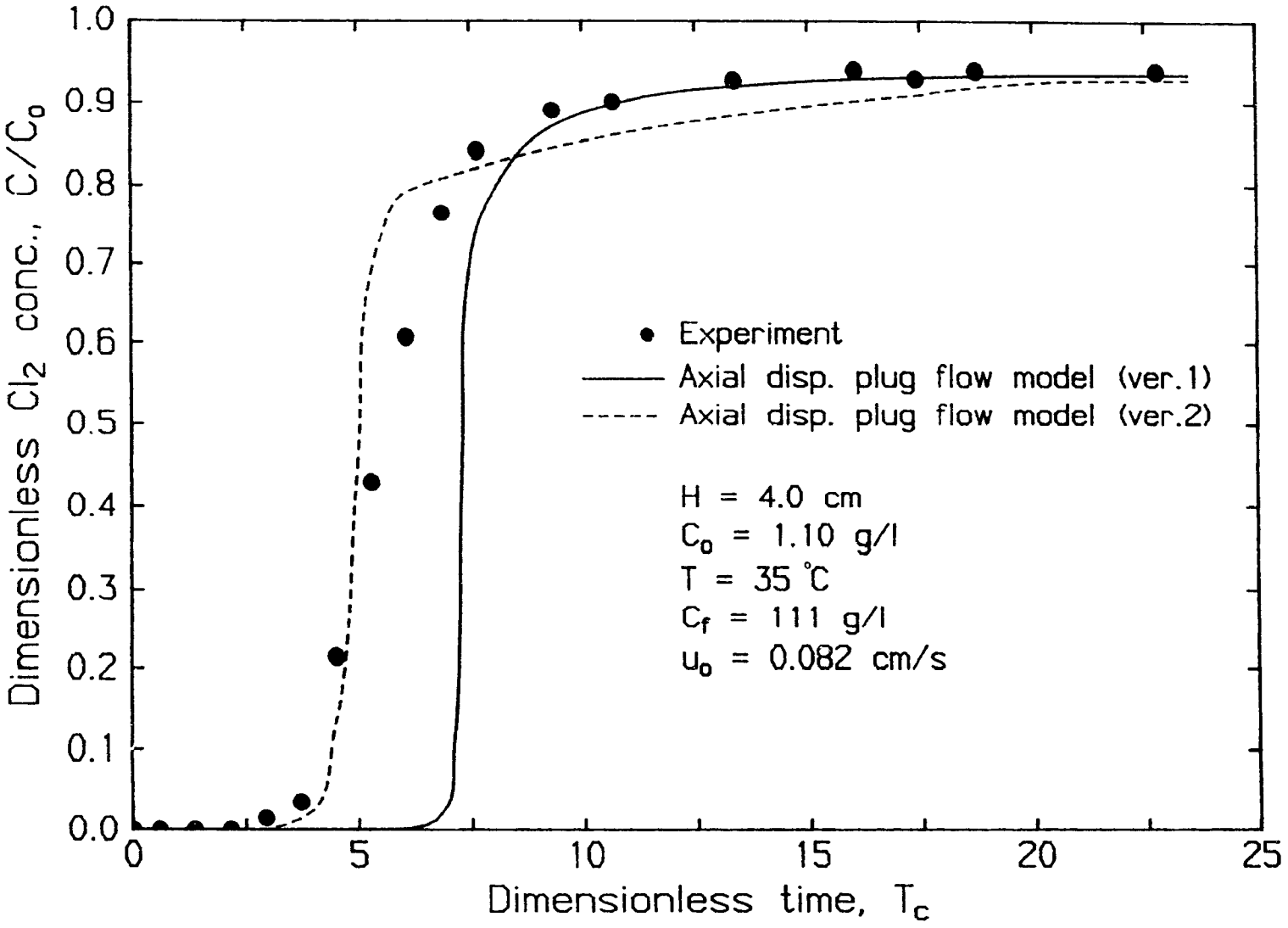
Dimensionless Cl_2 conc., C/C_o
1.0
0.9
0.8
0.7
0.6
0.5
0.4
0.3
0.2
0.1
0.0
0
5
10
15
20
25
Dimensionless time, T_c
Experiment
Axial disp. plug flow model (ver.1)
Axial disp. plug flow model (ver.2)
H = 4.0 cm
C_o = 1.10 g/l
T = 35 ℃
C_f = 111 g/l
u_o = 0.082 cm/s

Figure 7.13 Prediction of chlorine breakthrough curve with axial dispersed plug flow model; C_o = 2.20 g/l.

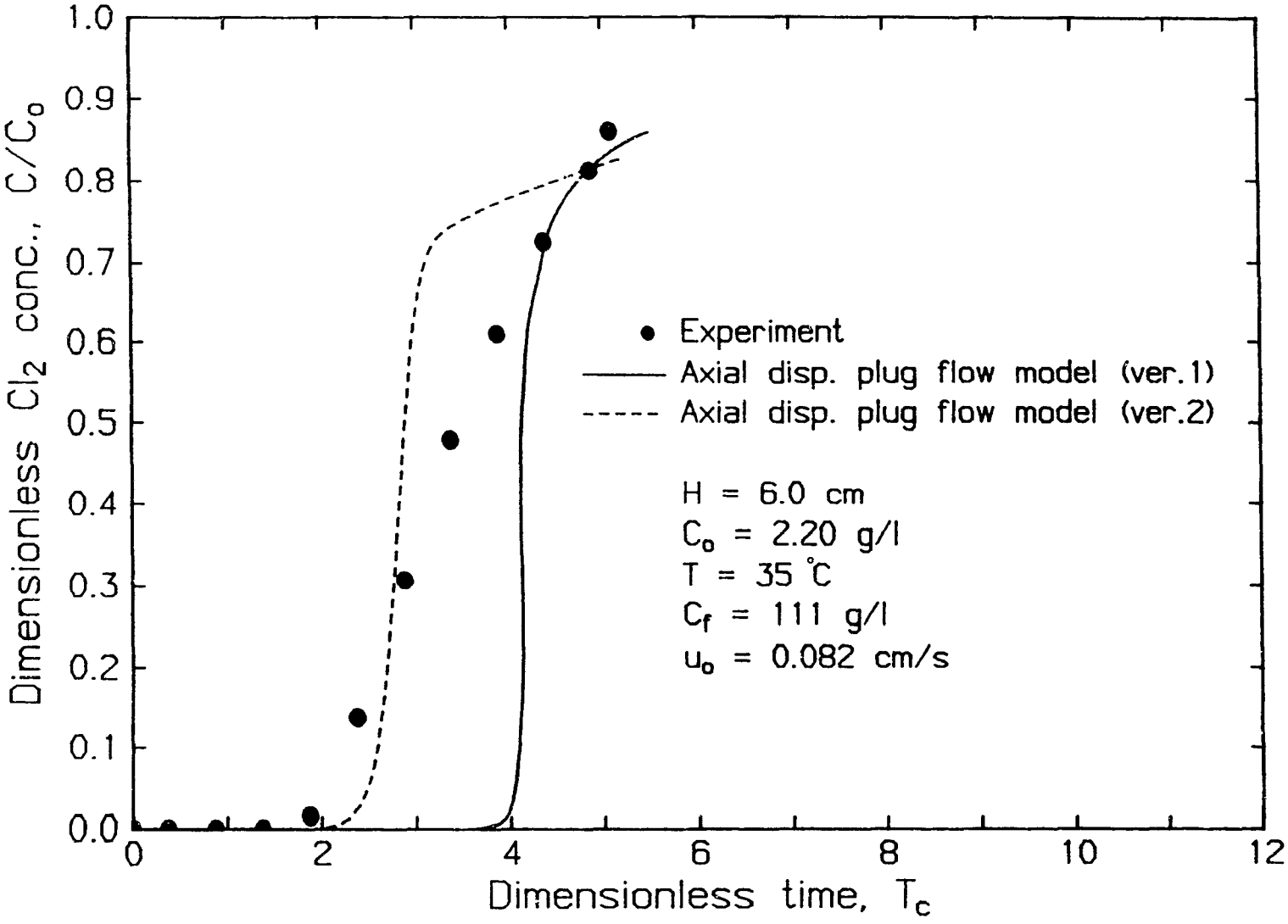
Dimensionless Cl_2 conc., C/C_o
1.0
0.9
0.8
0.7
0.6
0.5
0.4
0.3
0.2
0.1
0.0
0
2
4
6
8
10
12
Dimensionless time, T_c
Experiment
Axial disp. plug flow model (ver.1)
Axial disp. plug flow model (ver.2)
H = 6.0 cm
C_o = 2.20 g/l
T = 35 °C
C_f = 111 g/l
u_o = 0.082 cm/s

rise of the chlorine concentration. The slope changes abruptly near the end of the breakthrough curve before the plateau is reached. These trends are expected since the rate constants of version 1 are much larger than those of version 2. The greater total consumption of chlorine predicted by version 1 is also expected because of the much higher chlorine-lignin stoichiometric values employed. Also the change in shape in version 2 is caused by the much slower chlorine consumption rate when the "fast" lignin is consumed. The reactivity of the "slow" lignin in version 1 is much larger and as a result no change in slope is observed when all "fast" lignin is consumed.

The suitability of both versions of the axial dispersion model to represent the chlorine breakthrough curve was further tested by deliberately altering the source terms. Figure 7.14 reproduces the experimental chlorine breakthrough curve of Figure 7.11 along with theoretical predictions of version 1 with lower chlorine-lignin stoichiometry, SL_o, and reaction rate constants, k_1 and k_2, to better agreement. The unrealistically small values of reaction rate constants needed to obtain a proper representation of the experimental breakthrough curve underlines the weakness of the axial dispersion model.

Thus the axial dispersion model along with either Ackerts' (7) or Mackinnon's (6) chlorine-lignin reaction kinetics is inadequate to represent the dynamic pulp chlorination system. The reason for the inability of this model to represent the breakthrough curves is that the actual flow through the pulp pad is segregated flow through many channels (Chapter 4). This will be discussed subsequently in this chapter.

Figure 7.14 Prediction of chlorine breakthrough curve with version 1 of axial dispersed plug flow model; reaction rate constants artifically changed.

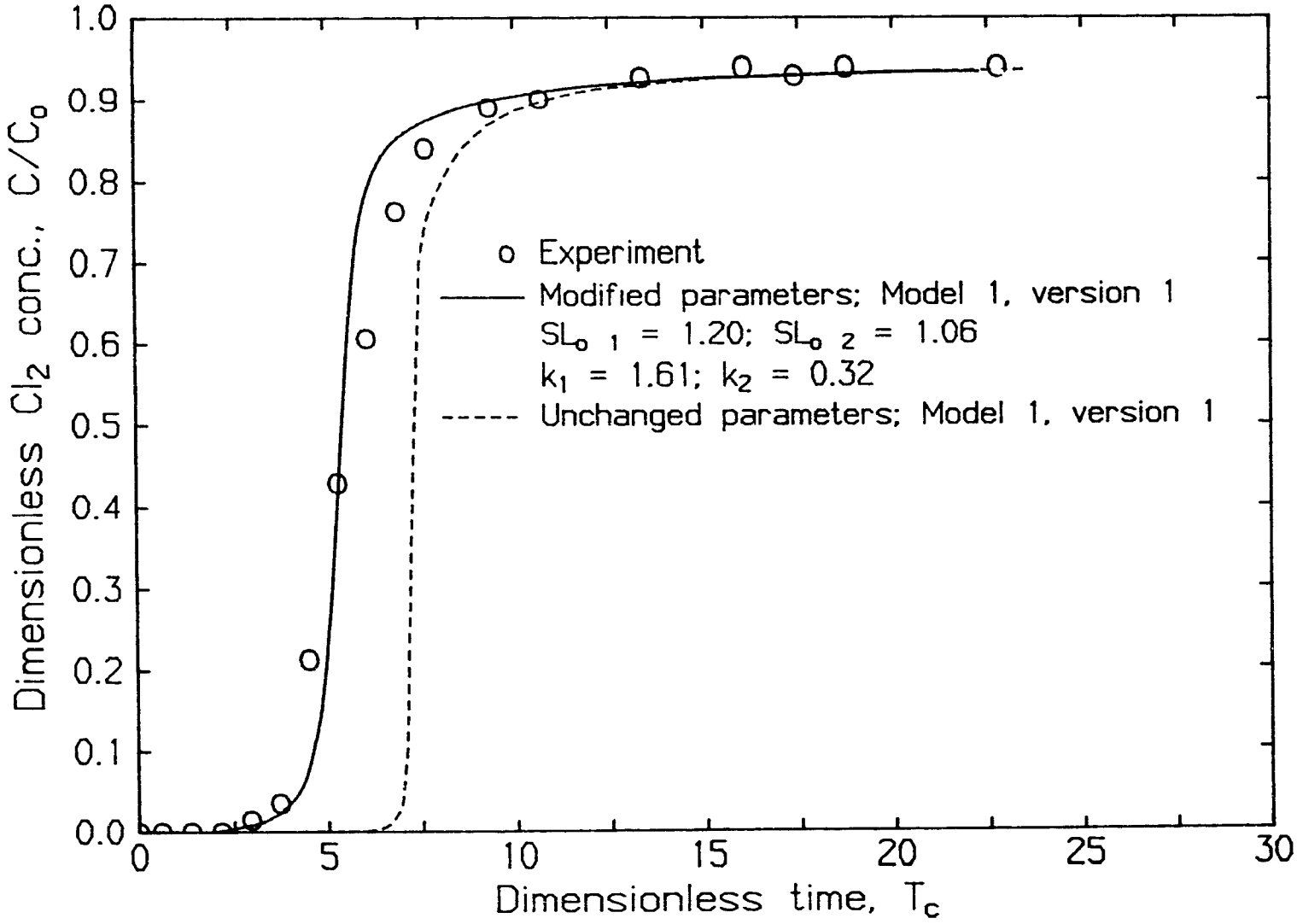
1.0
0.9
0.8
0.7
0.6
0.5
0.4
0.3
0.2
0.1
0.0
Dimensionless Cl_2 conc., C/C_o
0
5
10
15
20
25
30
Dimensionless time, T_c
o Experiment
Modified parameters; Model 1, version 1
$SL_{o\ 1}$ = 1.20; $SL_{o\ 2}$ = 1.06
k_1 = 1.61; k_2 = 0.32
Unchanged parameters; Model 1, version 1

7.3 Parallel plug flow model

7.3.1 Prediction of chlorine breakthrough curve

7.3.1.1 Introduction

The axial dispersed plug flow model with experimentally determined chlorine-lignin and chlorine-carbohydrates kinetics could not describe the experimental chlorine breakthrough curves. The chlorine breakthrough curves for lignin-free pulp on the other hand were well modelled by the axial dispersed plug flow model and chlorine-carbohydrates kinetics. It is known (Levenspiel (1)) that the exit concentration of a homogeneous reaction is completely determined by the RTD for first order kinetics, while for non-linear reactions one also needs to know the degree of micromixing (Zwietering (12)). Since the chlorine-lignin kinetics are highly non-linear and the chlorine-carbohydrates reaction rate is first order in chlorine, the axial dispersed plug flow model results suggest that flow segregation occurs in the pad. Experimental confirmation of the existence of segregated flow are the dark (or unchlorinated) spots when an incompletely chlorinated pulp pad is sectioned in the flow direction. Further evidence of segregated flow was presented in Chapter 4 where it was shown that the Peclet number is independent of bed height and that the difference between step-up and step-down tracer tests can be explained by the mobility ratio of the displaced and displacing fluid. Finally, Lee (12) also showed experimentally that "fingering" flow dominates the flow through a bed of pulp fibers. Theoretical support for "fingering" flow was obtained in Chapter 6 where it was shown that the slope of the chlorine breakthrough curve was proportional to the square root of the Peclet number instead of the Peclet number. In the new model it will be assumed

that dynamic pulp chlorination can be approximated by plug flow and an instantaneous chlorine-lignin reaction in a series of parallel channels. A schematic representation of this concept is shown in Figure 7.15. A flat reaction front then propagates through each channel at different speeds. Downstream of each front is unreacted lignin and no chlorine. Upstream of a front the chlorine concentration increases in the direction of the bed inlet because of consumption of chlorine by carbohydrates. Chlorine appears at the exit when any reaction front reaches the exit of the pulp pad. The chlorine concentration at the exit of the bed is a mass flow weighted average of the concentration from each channel. A mass balance over the lignin reaction front in a single channel can then be written as

$$u_a \varepsilon_a C_{xf} dt = SL_o L_o C_f dx_f + \varepsilon_a C_{xf} dx_f \qquad [7.27]$$

where C_{xf} is the chlorine concentration at the reaction front and x_f is the distance of the front from the inlet of the bed. The value of C_{xf} is determined from the first order chlorine-carbohydrates kinetics as

$$C_{xf} = C_o \, e^{-\left(\frac{k_c x_f}{u_a}\right)} \qquad [7.28]$$

Introduction of equation 7.28 into 7.27 and integration over the entire length of the bed results in

Figure 7.15 Schmematic representation of the pulp pad according to the parallel plug flow model.

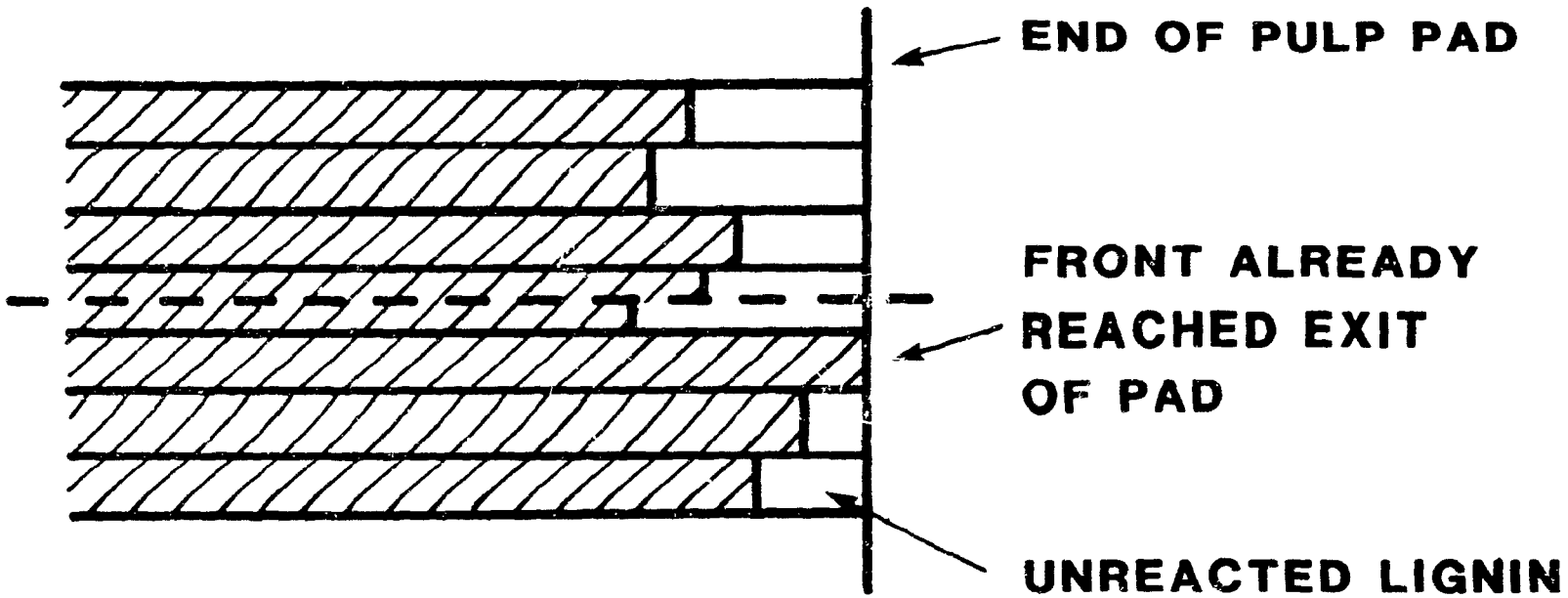
END OF PULP PAD
FRONT ALREADY
REACHED EXIT
OF PAD
UNREACTED LIGNIN

$$\int_{o}^{H} \left(\frac{C_f S L_o L_o}{u_a \epsilon_a C_o} \cdot e^{\frac{k_c x_f}{u_a}} + \frac{1}{u_a} \right) dx_f = t_b \qquad [7.29]$$

where t_b is the chlorine breakthrough time for the channel under consideration. After evaluation of the integral and rearrangement the following relationship is obtained for t_b.

$$t_b = t_r + \frac{C_f S L_o L_o}{\epsilon_a k_c C_o} \left(e^{k_c t_r} - 1 \right) \qquad [7.30]$$

where $t_r = H/u_a$.

After Taylor series expansion of $e^{k_c t_r}$, equation 7.30 becomes

$$t_b = t_r \left[1 + \frac{C_f S L_o L_o}{\epsilon_a C_o} \left(1 + \frac{1}{2} k_c t_r + \frac{1}{6} (k_c t_r)^2 + \ldots \right) \right] \qquad [7.31]$$

If the difference in t_r for the various channels is small (equivalent to $P \gg 1$) and/or $k_c t_r \ll 1$) the term between brackets in equation 7.30 is approximately the same for all channels. Similarly if $P \gg 1$ and/or $k_c t_r \ll 1$ the variation in C_{xf}/C_o between the various channels when the front reaches the bed exit is small. Therefore for pure segregated flow and $P \gg 1$ and/or $k_c t_r \ll 1$ the glucose tracer curve and chlorine breakthrough curve should be similar in shape. Under these conditions the chlorine BTC can be made identical to the non-dimensional glucose tracer curve after normalisation by the chlorine concentration after complete breakthrough

and the average breakthrough time, $\bar{t}_b$. The value of $\bar{t}_b$ is given by equation 7.30 with t_r equal to the average residence time of the entire bed.

The concept of pure segregated flow and instantaneous chlorine-lignin reaction was checked for a typical experiment with the above described normalisation. The agreement between the normalised chlorine BTC and the non-dimensional tracer curve is very good as can be seen from Figure 7.16. Proof that this applies generally to the present dynamic chlorination experiments is shown in Figure 6.28 where it is shown that the slope of the normalised chlorine BTC, $T_c[d(C/C_o)/dT_c]\cdot C_o/C_m$ at $C/C_m = 0.5$ was proportional to $P^{0.5}$ irrespective of the operating conditions. The results in Figure 6.28 show that segregated flow with instantaneous chlorine-lignin reaction provides a good description of dynamic chlorination in a pulp pad. The mathematical description of this parallel plug flow model will be presented in the following section.

7.3.1.2 Mathematical description

The chlorine concentration at the exit of each channel is

$$C/C_o = 0 \qquad \text{when } t < t_b \qquad [7.32]$$

or

$$C/C_o = e^{-k_c t_r} \qquad \text{when } t > t_b \qquad [7.33]$$

where t_b, the chlorine breakthrough time for each channel is given by equation 7.30. The dimensionless chlorine concentration at the exit at any time t is obtained by summing the contributions from all channels as

Figure 7.16 Comparison of normalized chlorine BTC and glucose tracer curve.

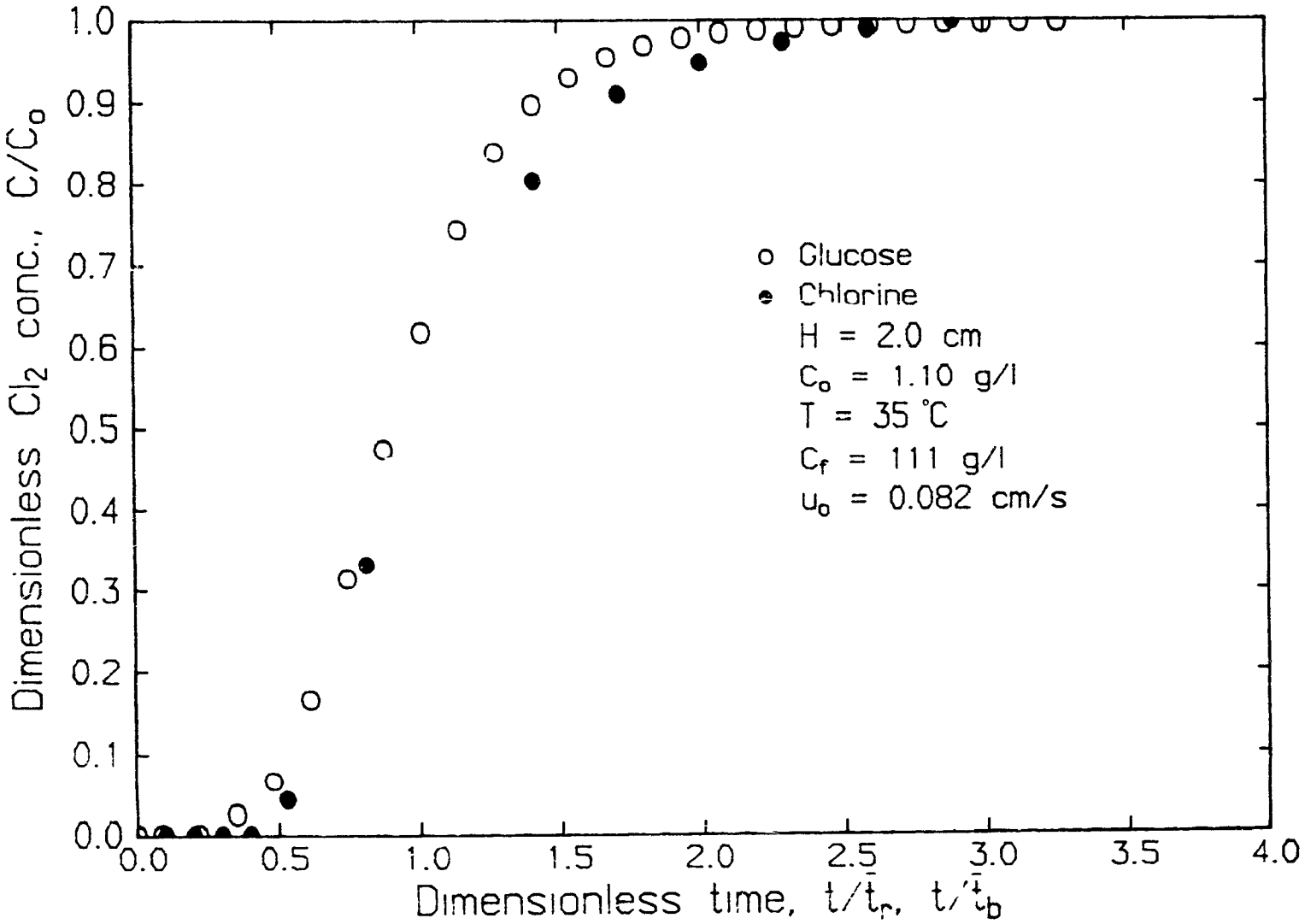
Dimensionless Cl_2 conc., C/C_o
1.0
0.9
0.8
0.7
0.6
0.5
0.4
0.3
0.2
0.1
0.0
0.0
0.5
1.0
1.5
2.0
2.5
3.0
3.5
4.0
Dimensionless time, $t/\bar{t}_r$, $t/\bar{t}_b$
o Glucose
• Chlorine
H = 2.0 cm
C_o = 1.10 g/l
T = 35 °C
C_f = 111 g/l
u_o = 0.082 cm/s

$$C/C_o = \int_0^1 [C/C_o]\, dF(t_r) \qquad [7.34]$$

where $dF(t_r)$ is the fraction of flow with a residence time of t_r and $t_r + dt_r$ and $F(t_r)$ is the residence time distribution of the total flow. The exact solution of the unsteady convection-diffusion equation by Brenner (10), equation 4.6, was used for $F(t_r)$ with the Peclet number obtained by the moments technique from the glucose tracer test preceeding the chlorination experiment. In order to solve equations 7.32-34, the single adjustable parameter of the parallel plug flow model, SL_o, must be specified. The technique for evaluation of SL_o was presented in Chapter 6, section 6.5.1.1. It should be noted that the shape of the experimental breakthrough curve is irrelevant for determination of SL_o.

7.3.1.3 Results

Comparison of the experimental and theoretical chlorine breakthrough curves for the same three cases presented earlier when model 1 was evaluated are shown in Figures 7.17 to 7.19. The very good agreement between the experimental and theoretical breakthrough curves show the superiority of the parallel plug flow model over the axial dispersed plug flow model for high and low chlorine concentrations and flowrates. Further tests of the suitability of the parallel plug flow model under different experimental conditions are shown in Figures 7.20 to 7.22. Figure 7.20 shows the comparison of the theoretical and experimental BTC at 50°C, the highest temperature studied. Figure 7.21 shows the comparison at the highest rate of chlorine application on pulp i.e. u_o = 0.164 cm/s and C_o = 2.20 g/l. Figure 7.22 shows the comparison at the lowest Peclet number of 2.3 i.e. for the poorly formed pad.

Figure 7.17 Prediction of chlorine BTC with parallel plug flow model; C_o = 0.55 g/l, $\bar{t}_r$ = 186 s, T = 35°C, P = 27, SL_o = 0.95.

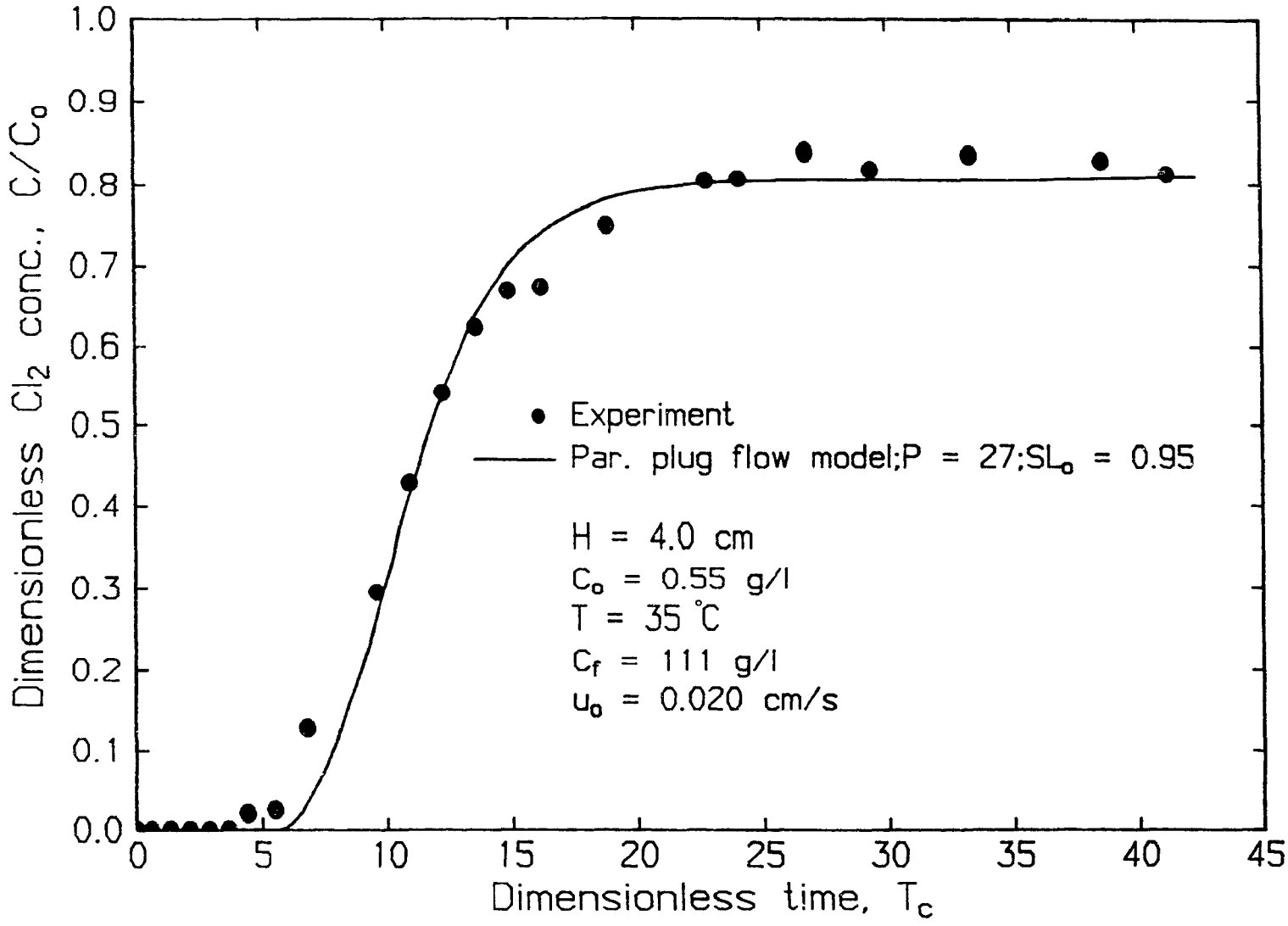
Dimensionless Cl_2 conc., C/C_o
1.0
0.9
0.8
0.7
0.6
0.5
0.4
0.3
0.2
0.1
0.0
0
5
10
15
20
25
30
35
40
45
Dimensionless time, T_c
Experiment
Par. plug flow model;P = 27;SL_o = 0.95
H = 4.0 cm
C_o = 0.55 g/l
T = 35 °C
C_f = 111 g/l
u_o = 0.020 cm/s

Figure 7.18 Prediction of chlorine BTC with parallel plug flow model; C_o = 1.10 g/l, $\bar{t}_r$ = 46 s, T = 35°C, P = 27, SL_o = 0.92.

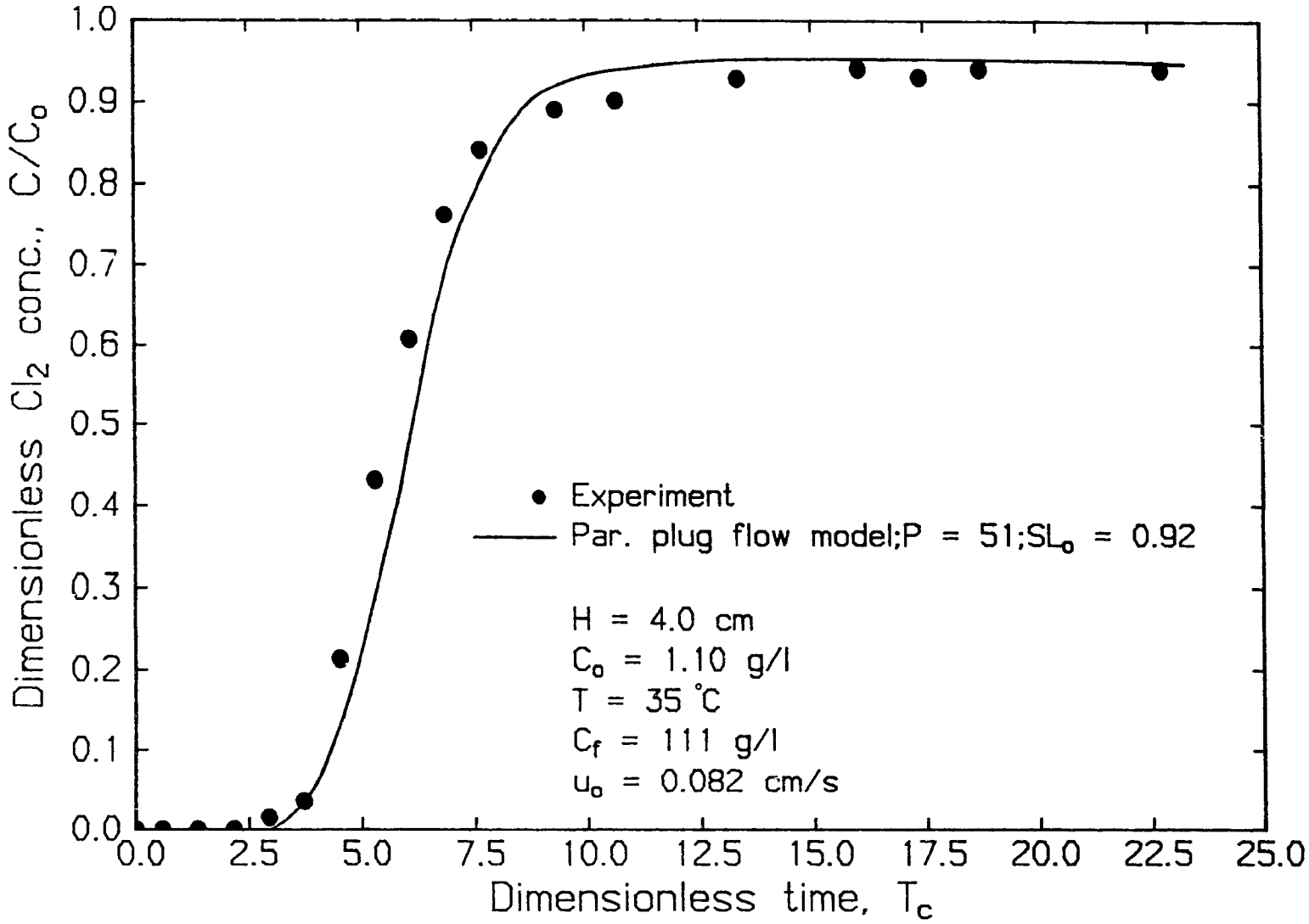
Dimensionless Cl_2 conc., C/C_o
1.0
0.9
0.8
0.7
0.6
0.5
0.4
0.3
0.2
0.1
0.0
0.0
2.5
5.0
7.5
10.0
12.5
15.0
17.5
20.0
22.5
25.0
Dimensionless time, T_c
Experiment
Par. plug flow model;P = 51;SL_o = 0.92
H = 4.0 cm
C_o = 1.10 g/l
T = 35 °C
C_f = 111 g/l
u_o = 0.082 cm/s

Figure 7.19 Prediction of chlorine BTC with parallel plug flow model; C_o = 2.20 g/l, $\bar{t}_r$ = 68 s, T = 35°C, P = 38, SL_o = 0.99.

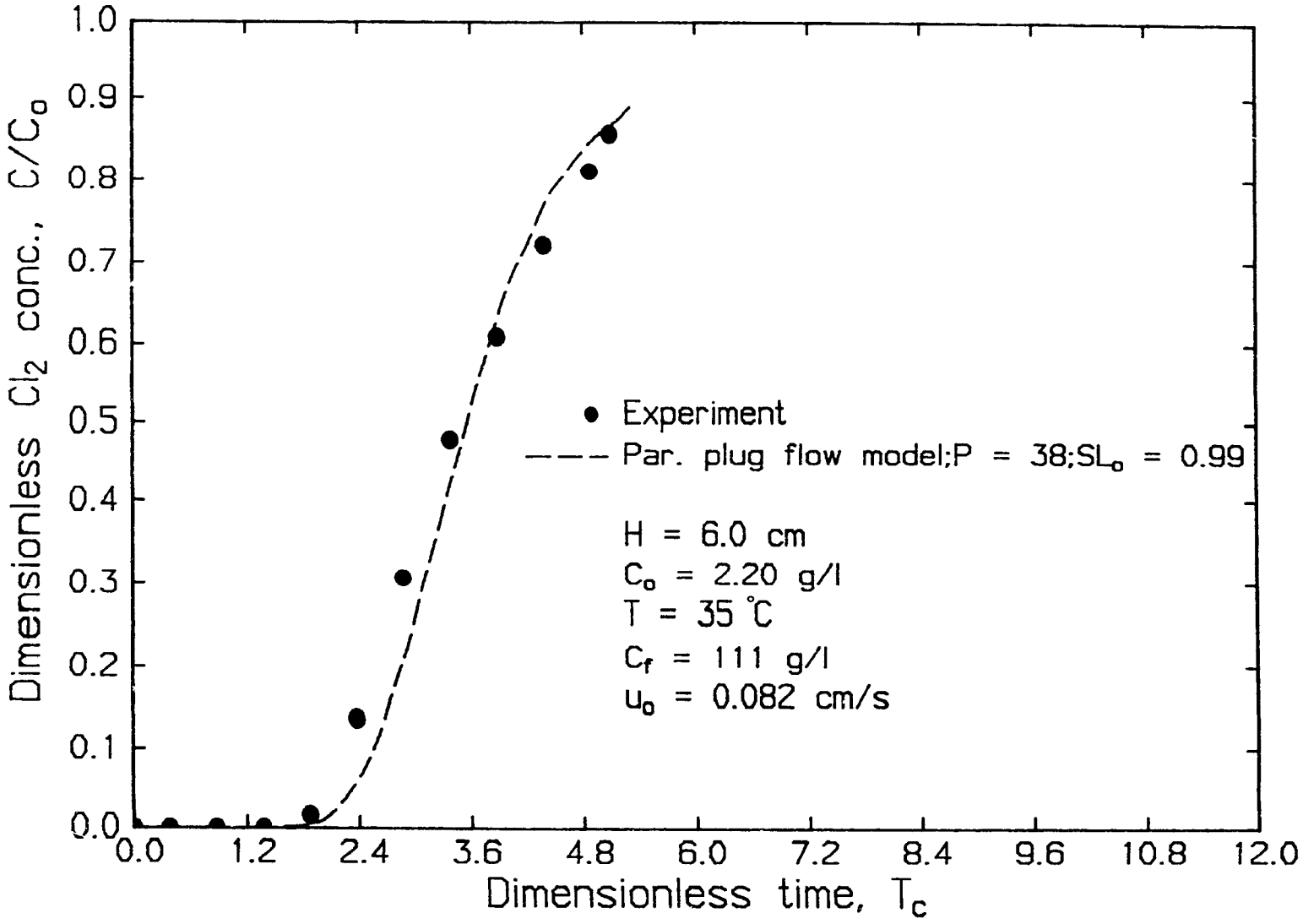
Dimensionless Cl_2 conc., C/C_o
1.0
0.9
0.8
0.7
0.6
0.5
0.4
0.3
0.2
0.1
0.0
0.0
1.2
2.4
3.6
4.8
6.0
7.2
8.4
9.6
10.8
12.0
Dimensionless time, T_c
Experiment
Par. plug flow model;P = 38;SL_o = 0.99
H = 6.0 cm
C_o = 2.20 g/l
T = 35 °C
C_f = 111 g/l
u_o = 0.082 cm/s

Figure 7.20 Prediction of chlorine BTC with parallel plug flow model; C_o = 1.10 g/l, $\bar{t}_r$ = 68 s, T = 50°C, P = 30, SL_o = 1.27.

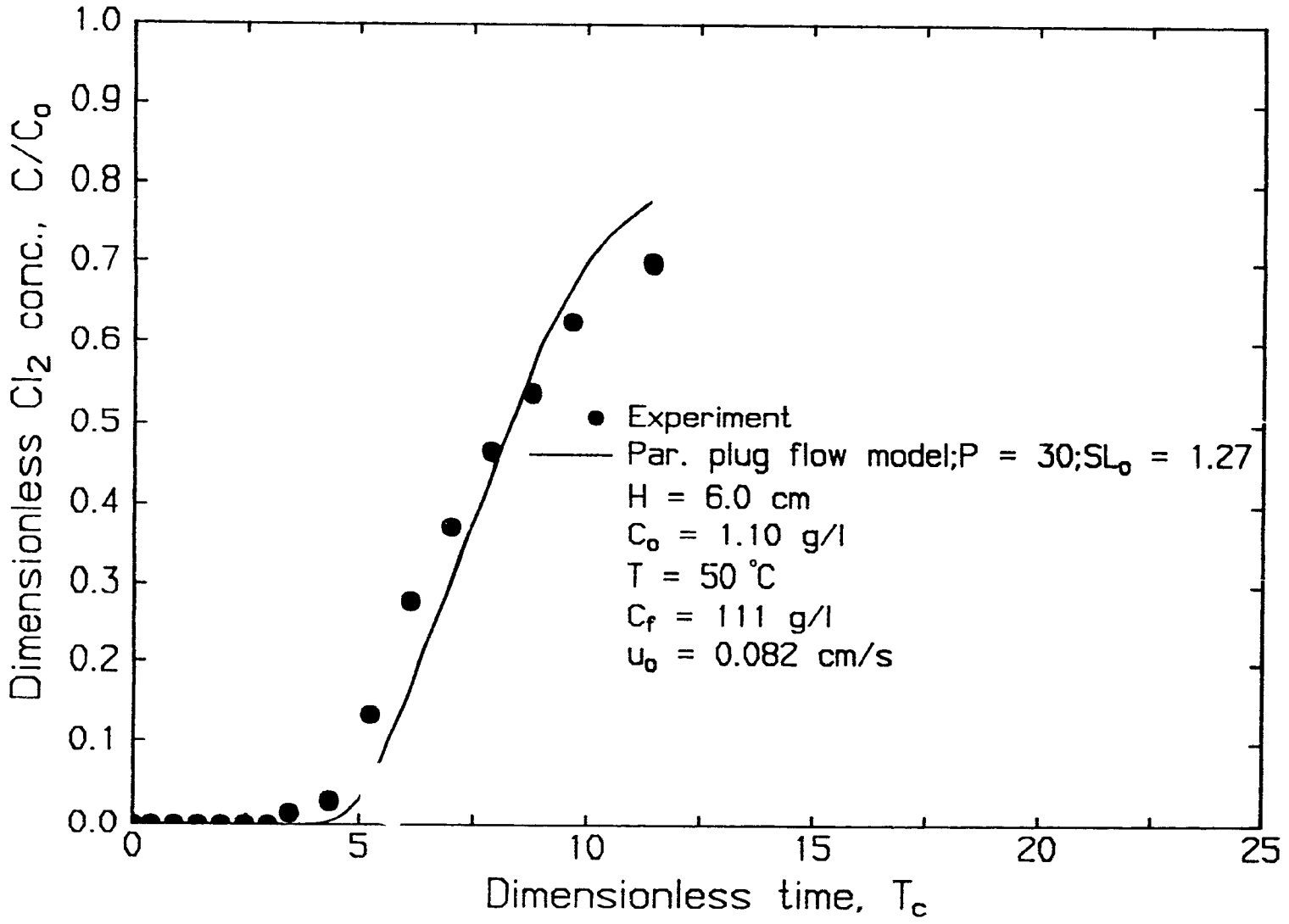
Dimensionless Cl_2 conc., C/C_o
1.0
0.9
0.8
0.7
0.6
0.5
0.4
0.3
0.2
0.1
0.0
0
5
10
15
20
25
Dimensionless time, T_c
Experiment
Par. plug flow model;P = 30;SL_o = 1.27
H = 6.0 cm
C_o = 1.10 g/l
T = 50 °C
C_f = 111 g/l
u_o = 0.082 cm/s

Figure 7.21 Prediction of chlorine BTC with parallel plug flow model; C_o = 2.20 g/l, $\bar{t}_r$ = 34 s, T = 35°C, P = 32, SL_o = 0.80.

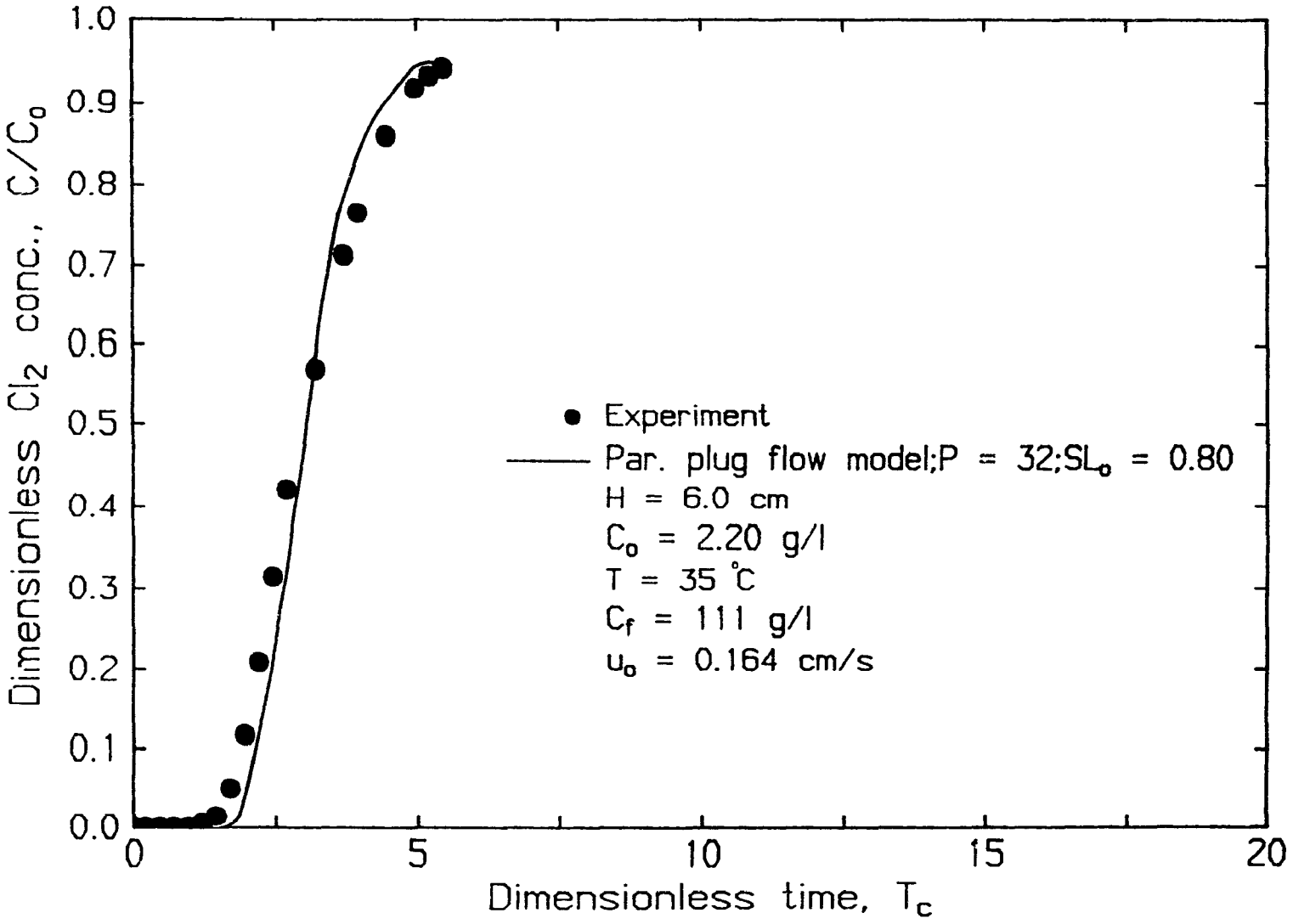
1.0
0.9
0.8
0.7
0.6
0.5
0.4
0.3
0.2
0.1
0.0
Dimensionless Cl_2 conc., C/C_o
0
5
10
15
20
Dimensionless time, T_c
Experiment
Par. plug flow model;P = 32;SL_o = 0.80
H = 6.0 cm
C_o = 2.20 g/l
T = 35 °C
C_f = 111 g/l
u_o = 0.164 cm/s

Figure 7.22 Prediction of chlorine BTC with parallel plug flow model; C_o = 1.10 g/l, $\bar{t}_r$ = 68 s, T = 35°C, P = 2.31 SL_o = 1.02.

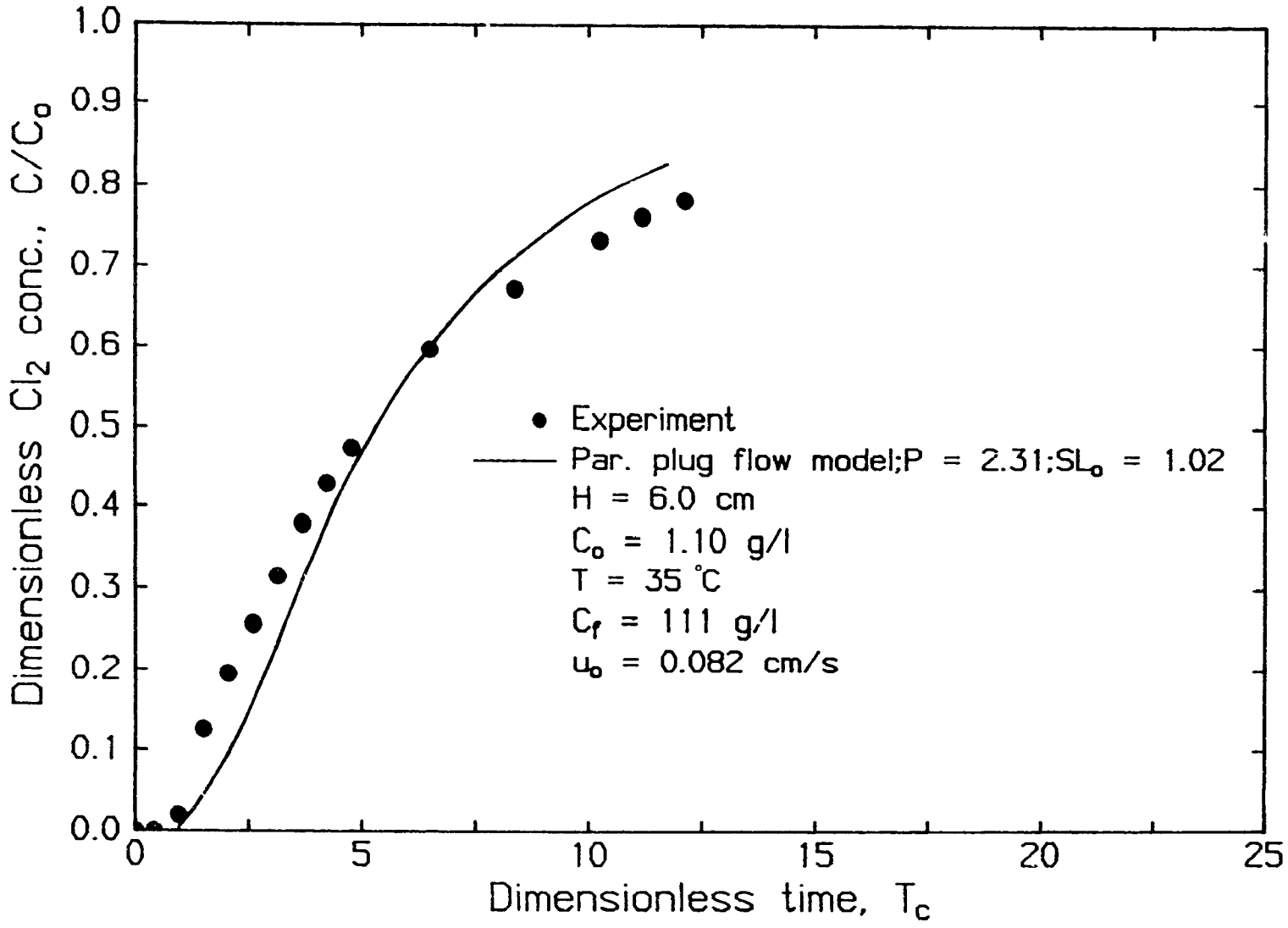
Dimensionless Cl_2 conc., C/C_o
1.0
0.9
0.8
0.7
0.6
0.5
0.4
0.3
0.2
0.1
0.0
0
5
10
15
20
25
Dimensionless time, T_c
Experiment
Par. plug flow model;P = 2.31;SL_o = 1.02
H = 6.0 cm
C_o = 1.10 g/l
T = 35 °C
C_f = 111 g/l
u_o = 0.082 cm/s

The plateau values of the chlorine breakthrough curves are well predicted in all cases. The beginning of breakthrough is well or slightly over predicted and in some cases the steepness of the rising portion of the predicted breakthrough curve is slightly larger than measured. The instantaneous reaction assumption does not allow for diffusion and this could explain the steeper predicted slopes and later breakthrough. However, the generally good representation of these experimental chlorine BTC's further underlines the suitability of the parallel plug flow model for dynamic chlorination of kraft pulp.

7.3.2 Prediction of methanol BTC

7.3.2.1 Mathematical formulation

The general procedure employed for the prediction of the methanol breakthrough curved with the parallel plug flow model is the same as just described for the chlorine breakthrough curves. The main difference arises from the fact that chlorine is a reactant whereas methanol is a product of the chlorine-lignin reaction. Similar to the instantaneous chlorine consumption by lignin it is assumed that methanol is instantaneously produced at the lignin front.

The methanol concentration ,$C_{a,c}$, at the exit of a channel is

$$C_{a,c} = 0 \quad \text{when } t_c < t_r \text{ and } t_c > t_b \qquad [7.35]$$

This means that no methanol appears at the exit of a channel before one channel volume has been displaced by the chlorine water feed or after the reaction front has reached the exit of the channel. During the time when $t_r < t_c < t_b$ methanol is present in the effluent at the exit of a channel.

The concentration $C_{a,c}$ can be derived as follows. When the lignin reaction front has reached a position x_f it can be derived that the time needed to reach this position, t_{cf}, is

$$t_{cf} = \frac{SL_oL_oC_f}{\varepsilon_a C_o k_c}\left(e^{\frac{k_c x_f}{u_a}} - 1\right) + \frac{x_f}{u_a} \qquad [7.36]$$

The product generated at the front x_f, at time t_{cf}, reaches the exit of a channel ($t_r - x_f/u_a$) seconds later or at time t_c with t_c given in equation 7.37.

$$t_c = t_{cf} + t_r - \frac{x_f}{u_a} = \frac{SL_oL_oC_f}{\varepsilon_a C_o k_c}\left(e^{\frac{k_c x_f}{u_a}} - 1\right) + t_r \qquad [7.37]$$

This equation can be rearranged as

$$\frac{x_f}{u_a} = \frac{1}{k_c} \ln\left(\frac{\varepsilon_a C_o k_c}{SL_oL_oC_f} \cdot (t_c - t_r) + 1\right) \qquad [7.38]$$

The concentration of methanol produced at the reaction front is

$$C_{a,c} = \frac{R}{SL_o} C_o \cdot e^{\left(-\frac{k_c x_f}{u_a}\right)} \qquad [7.39]$$

where R is the methanol-lignin stoichiometric ratio (g methanol/g lignin).

After introduction of equation 7.38 in 7.39 one obtains for the methanol concentration at the exit of the channel at time t_c when $t_r < t_c < t_b$

$$C_{a,c} = \frac{R}{SL_o} C_o \frac{1}{\frac{\epsilon_a C_o k_c}{SL_o L_o C_f} (t_c - t_r) + 1} \qquad [7.40]$$

The methanol concentration, C_a, at the exit of the bed at any time t_c is obtained by addition of the contributions from all channels as

$$\frac{C_a}{C_o} = \int_o^1 \frac{C_{a,c}}{C_o} \, dF(t_r) \qquad [7.41]$$

In order to solve equations 7.35, 7.40 and 7.41 together with equation 4.6 and the Peclet number from the glucose tracer curve the overall stoichiometric ratio, R, has to be known. Analogous to the evaluation of SL_o, R is obtained by equating the theoretical and experimental amounts of methanol produced when complete breakthrough is obtained, as shown in section 6.5.4 of Chapter 6. This value of R will automatically satisfy the overall methanol balance when using the parallel plug flow model given by equation 7.41. Again implicit in the derivation is that R is not a function of contact time or residence time distribution.

7.3.2.2 Results

The theoretical prediction of this model is compared against the experimental breakthrough curves in Figure 7.23 to 7.26 under varying experimental conditions. The methanol breakthrough curves are very well predicted. These results further support the validity of the parallel plug flow model and establish that methanol formation is directly related

Figure 7.23 Prediction of methanol BTC with parallel plug flow model; C_o = 1.10 g/l, $\bar{t}_r$ = 136 s, T = 35°C, P = 49 SL_o = 1.20.

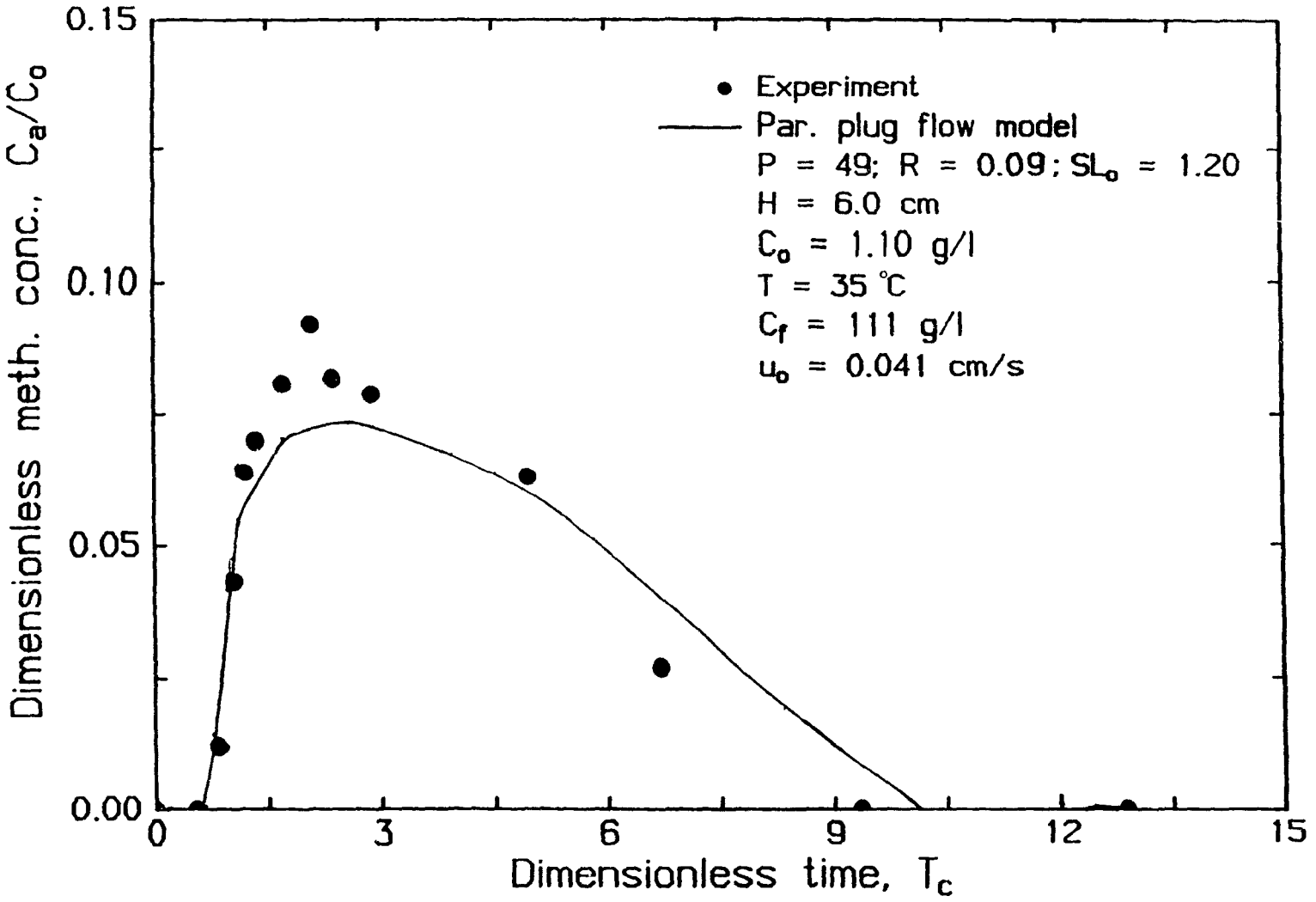
0.15
0.10
0.05
0.00
0
3
6
9
12
15
Dimensionless meth. conc., C_a/C_o
Dimensionless time, T_c
Experiment
Par. plug flow model
P = 49; R = 0.09; SL_o = 1.20
H = 6.0 cm
C_o = 1.10 g/l
T = 35 °C
C_f = 111 g/l
u_o = 0.041 cm/s

Figure 7.24 Prediction of methanol BTC with parallel plug flow model; C_o = 0.55 g/l, $\bar{t}_r$ = 297 s, T = 35°C, P = 61 SL_o = 1.21.

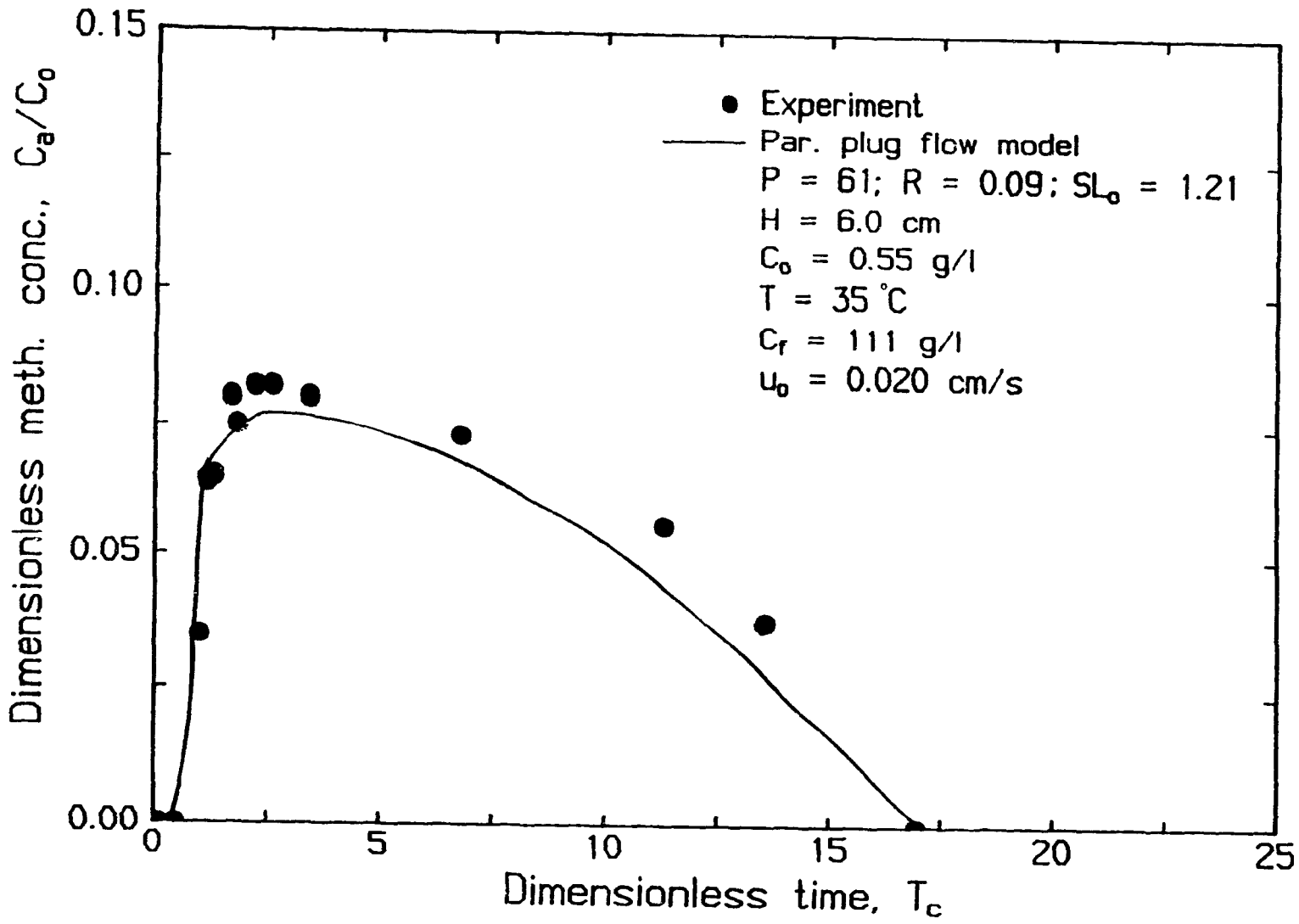
0.15
0.10
0.05
0.00
0
5
10
15
20
25
Dimensionless meth. conc., C_a/C_o
Dimensionless time, T_c
Experiment
Par. plug flow model
P = 61; R = 0.09; SL_o = 1.21
H = 6.0 cm
C_o = 0.55 g/l
T = 35 °C
C_f = 111 g/l
u_o = 0.020 cm/s

Figure 7.25 Prediction of methanol BTC with parallel plug flow model; C_o = 1.10 g/l, $\bar{t}_r$ = 136 s, T = 19°C, P = 38 SL_o = 1.01.

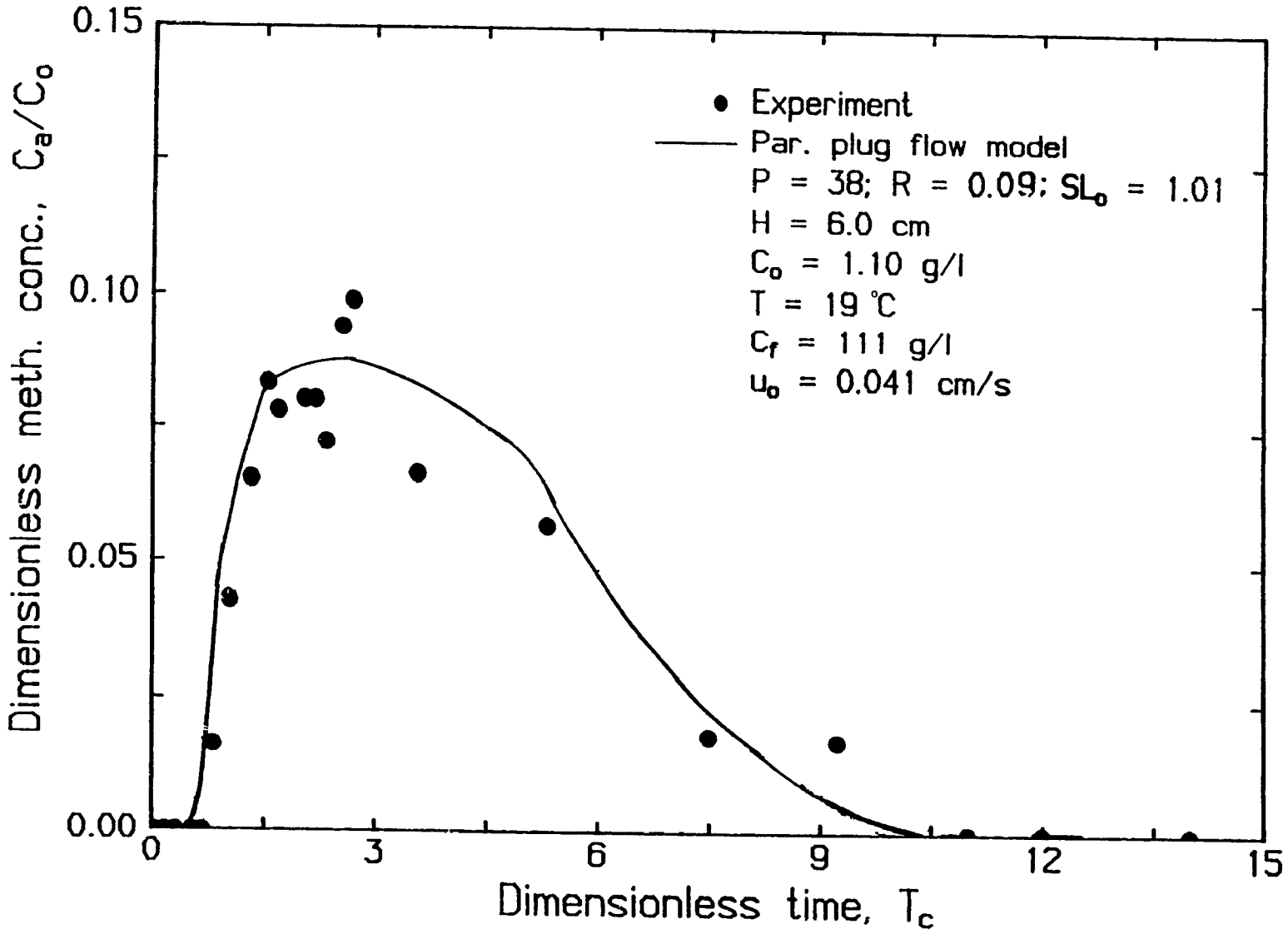
0.15
0.10
0.05
0.00
0
3
6
9
12
15
Dimensionless meth. conc., C_a/C_o
Dimensionless time, T_c
Experiment
Par. plug flow model
P = 38; R = 0.09; SL_o = 1.01
H = 6.0 cm
C_o = 1.10 g/l
T = 19 °C
C_f = 111 g/l
u_o = 0.041 cm/s

Figure 7.26 Prediction of methanol BTC with parallel plug flow model; C_o = 1.10 g/l, $\bar{t}_r$ = 136 s, T = 50°C, P = 34 SL_o = 1.27.

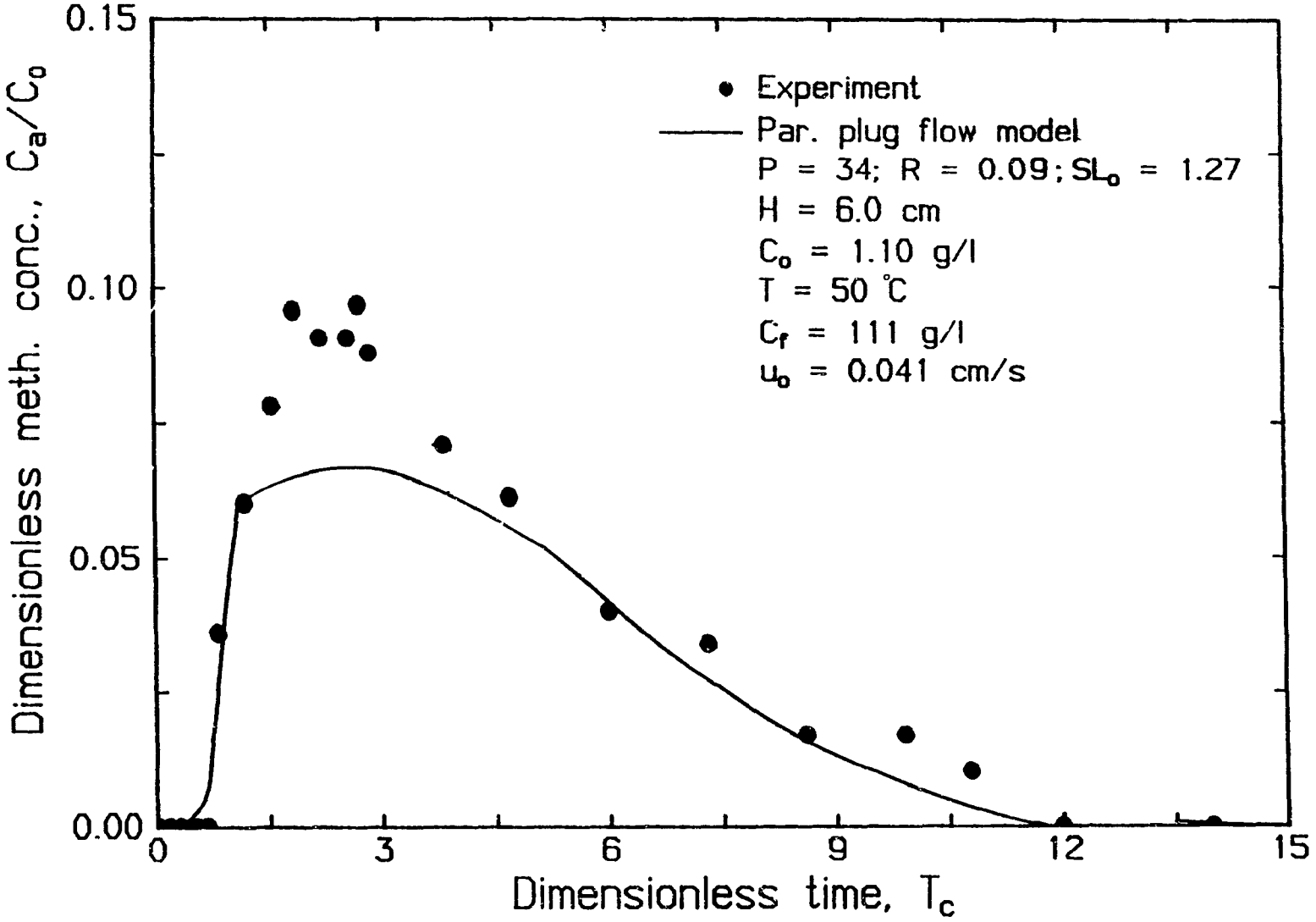
0.15
0.10
0.05
0.00
0
3
6
9
12
15
Dimensionless meth. conc., C_a/C_o
Dimensionless time, T_c
Experiment
Par. plug flow model
P = 34; R = 0.09; SL_o = 1.27
H = 6.0 cm
C_o = 1.10 g/l
T = 50 °C
C_f = 111 g/l
u_o = 0.041 cm/s

to the reaction between chlorine and lignin.

7.4 General Discussion

The axial dispersion model with either Ackert's (7) or Mackinnon's (6) kinetics could not accurately predict the experimental chlorine breakthrough curves. Unrealistic changes in the reaction rate constants were needed in both versions of the axial dispersion model in order to obtain the correct slope for the predicted breakthrough curves. However good predictions of the chlorine-carbohydrates breakthrough curves were obtained. The main difference between these two cases is that the lignin-chlorine kinetics are highly non-linear while the chlorine-carbohydrates kinetics are linear. Since for linear kinetics the breakthrough curves are only dependent on the residence time distribution and not on the actual flow pattern, these results indicate that the "micromixing" (Zwietering (11)) in the bed is not well represented by axial dispersion.

The only comparable study in which the axial dispersed plug flow model was used for pulp fiber beds is the pulp washing study of Poirier (5). For low solute concentrations, Poirier (5) added a source term to the axial dispersed plug flow model to represent the non-linear Langmuir type desorption of sodium ions from the fibers. Good agreement was obtained between the experimental and predicted breakthrough curves by adjusting the Peclet number. No separate measurement of the residence time distributions were made. However for the same conditions, Poirier calculated a Peclet number not significantly different from experiments where sodium sorption could be neglected. The latter Peclet number can be considered to represent the residence time distribution. Since the isotherm is non-linear, Poirier's results are not in agreement with the present

segregated flow model, which predicts that the data would be better modeled with a lower Peclet number for the desorption case and the axial dispersed plug flow model.

The parallel plug flow model, on the other hand, gave very good predictions of the breakthrough curves for both the reactant chlorine and the product methanol of the lignin-chlorine reaction. A single parameter specifying the reaction stoichiometry was used for each of the two types of breakthrough curves. This parameter was independently obtained from the experimentally determined chlorine and methanol breakthrough curves as demonstrated in sections 6.5.1.1 and 6.5.4 for chlorine and methanol, respectively. The shape of the breakthrough curves followed naturally from the parallel plug flow model and the specified residence time distribution. Comparison of the two models confirm the conclusion of Chapters 4 and 6 that flow through a pulp pad is best described by segregated flow through a series of channels. The agreement obtained with the parallel plug flow model also confirms that the assumption of an instantaneous reaction between lignin and chlorine is good enough for the present situation. The slightly steeper predicted breakthrough curves, and the inability to predict the small tailing in some of the breakthrough curves, suggests that the agreement could be further improved by using actual chlorine-lignin kinetics. However, introduction of these kinetics would make the parallel plug flow model considerably more complicated. Besides the high initial reaction rate of the chlorine-lignin reaction, another reason for the success of the instantaneous reaction assumption is related to the form of the chlorine-lignin kinetics. It has been shown by Ackert et al. (13) that the rate of lignin consumption, $- d[L]/dt$, by chlorine

can be described by

$$-\frac{d[L]}{dt} = k[C]^{1.12}\,[L - L_f]^{1.82} \qquad [7.42]$$

where L_f is unreactive lignin (g/g pulp). It should be noted that the reaction order in lignin concentration is much larger than 1.0. With the assumption that the rate of consumption of chlorine is only determined by chemical reaction, i.e. internal and external mass transfer resistances are negligible, the unsteady transport equation for plug flow in a single channel can be written as

$$\frac{\partial C}{\partial T} + \frac{\partial C}{\partial X} + 1000\,\rho_f \left(\frac{1 - \varepsilon_a}{\varepsilon_a}\right) SL_o \left(-\frac{\partial [L]}{\partial T}\right) = 0 \qquad [7.43]$$

This equation is similar in form to the unsteady transport equation for plug flow with adsorption and no diffusion. It is well known (Ruthven (14)) that for the case of desorption, a so-called "constant pattern" behavior is obtained with an unfavourable adsorption isotherm. This means that the concentration front generated by desorption progresses unchanged in shape through the packed bed of the adsorbent. An alternative formulation of the condition to obtain a "constant pattern" behaviour during desorption is that

$$\frac{d^2(-\,dw/dt)}{dC^2} < 0 \qquad [7.44]$$

where (- dw/dt) is the desorption rate of the adsorbate and C the adsorbate concentration in the fluid phase. Similarly for the present reaction

of lignin and chlorine, a "constant pattern" behavior will be obtained when

$$\frac{d^2(-\,d[L]/dt)}{dC^2} < 0 \qquad [7.45]$$

or

$$\frac{d^2(C^{1.12}[L - L_f]^{1.82})}{dC^2} < 0 \qquad [7.46]$$

For "constant pattern" behaviour the relationship

$$\frac{[L - L_f]}{[L_o - L_f]} = \frac{C_o - C}{C_o} \qquad [7.47]$$

is valid (Cooney and Lightfoot (15)). Combining equations 7.46 and 7.47, it follows that constant pattern behaviour is obtained when the sum of the reaction orders of chlorine and lignin is larger than 1.0. Since the sum of the reaction orders of chlorine and lignin in equation 7.46 is almost 3 a narrow "constant pattern" is rapidly achieved in the present case. The formation of a sharp lignin and chlorine concentration front, both remaining unchanged during movement though the fiber bed, also explains why the instantaneous reaction assumption is successful in the parallel plug flow model.

With the inclusion of axial dispersion the constant transport equation in a single channel becomes

$$\frac{\partial C}{\partial T} + 1000\,\rho_f\left(\frac{1 - \varepsilon_a}{\varepsilon_a}\right)SL_o\left(-\frac{\partial [L]}{\partial T}\right) = \frac{1}{P_c}\frac{\partial^2 C}{\partial X^2} - \frac{\partial C}{\partial X} \qquad [7.48]$$

where $P_c = u_1 H/D_{LC}$ is the Peclet number and D_{LC} the axial dispersion coefficient in a single channel. For "constant pattern" behavior this can be written as

$$\frac{\partial C}{\partial T}\left(1 + 1000\,\rho_f\left(\frac{1-\varepsilon_a}{\varepsilon_a}\right) SL_o \frac{[L_o]}{C_o}\right) = \frac{1}{P_c}\frac{\partial^2 C}{\partial X^2} - \frac{\partial C}{\partial X} \qquad [7.49]$$

When the reference frame is moving with the speed of the reaction front the above equation reduces to

$$\frac{\partial C}{\partial T} = \frac{1}{P_c\left(1 + 1000\,\rho_f\left(\frac{1-\varepsilon_a}{\varepsilon_a}\right) SL_o \frac{[L_o]}{C_o}\right)}\frac{\partial^2 C}{\partial Z^2} \qquad [7.50]$$

where $Z = X - T/\left(1 + 1000\,\rho_f\,((1-\varepsilon_a)/\varepsilon_a)\,SL_o\,[L_o]/C_o\right)$.
Since the coefficient of $\partial^2 C/dZ^2$ in equation 7.50 is estimated at approximately $5*10^{-3}$ for a typical experiment (see Appendix 7-2), the spreading of the "constant pattern" concentration front in a single channel due to axial dispersion can be neglected.

Finally an order of magnitude analysis will be presented to provide some theoretical basis as to why the axial dispersion model fails in the present situation and the parallel plug flow model is successful. Implicit in the derivation of the axial dispersion model is the assumption of negligible radial concentration gradients. In order for this assumption to hold it is required that the radial distance covered by the reaction front in the average breakthrough time, $\bar{t}_b$, is large compared to the scale of flow non-uniformity in the radial direction. Alternatively, it follows that the parallel plug flow model holds if the radial distance

travelled by the reaction front, in time $\bar{t}_b$, due to dispersion is small compared to the scale of flow non-uniformity in the radial direction. The radial distance travelled by the reaction front, δ, can be estimated from Danckwerts tarnishing reaction problem (16) for diffusion and instantaneous reaction. Following the simplification presented by Paterson and Kerekes (17) for a pulp suspension one obtains

$$\delta = 2\alpha\sqrt{\frac{\varepsilon_i}{\varepsilon_a} D_R t_b} \qquad [7.51]$$

where D_R is the radial diffusion coefficient and α is obtained from the following relationship

$$\beta = \frac{\varepsilon_a C_o}{SL_o L_o C_f} = \frac{\varepsilon_a}{(1 - \varepsilon_a)} \frac{C_o}{1000\ \rho_f SL_o L_o} = \sqrt{\pi}\ \alpha \exp(\alpha^2)\ \mathrm{erf}(\alpha) \qquad [7.52]$$

Since

$$t_b = t_r\left(1000\left(\frac{1 - \varepsilon_a}{\varepsilon_a}\right)\rho_f \frac{L_o}{C_o} SL_o + 1\right) = t_r(1/\beta + 1) \qquad [7.53]$$

with $t_r = H\varepsilon_a/u_o$ equation 7.51 becomes

$$\delta = 2\alpha\sqrt{\frac{\varepsilon_i D_R H}{u_o}(1/\beta + 1)} \qquad [7.54]$$

For most experiments β varies from 0.1 to 0.5 so that α varies from 0.2 to

0.5 (Appendix 7-3). The radial diffusion coefficient, D_R, is obtained from the radial Peclet number, $Pe_R = d_e u_i / D_R$ in the relationship (Doraiswamy and Sharma (18)),

$$\frac{1}{Pe_R} = \frac{1}{Pe_{t,R}} + \frac{\epsilon_i}{1.5\ Re_e Sc} \qquad [7.55]$$

The equivalent particle diameter, d_e, was calculated from the pressure drop measurements of Chapter 4 as 26.5 microns. The turbulent or flow contribution to the Peclet number, $Pe_{t,R} = d_e u_i / D_R'$ is obtained with the relationship (Doraiswamy and Sharma (18))

$$Pe_{t,R} = \frac{0.09}{1 + 10/(Re_e \cdot Sc)} \qquad [7.56]$$

where $Re_e = d_e u_o / \nu$, $Sc = \nu / D_M$ and D_M = molecular diffusion of chlorine in water. For a typical experiment of u_o = 0.082 cm/s, T = 35°C, H = 6 cm, $Pe_{t,R} = 5.34 * 10^{-2}$ or $D_R = 3.03 \cdot 10^{-9}$ m^2/s (see Appendix 7-3). Insertion of all values in equation 7.54 with $\alpha = 0.2$ and $\beta = 0.1$ give $\delta = 0.60$ mm. This is about one order of magnitude smaller than the minimum dominant floc size of kraft pulps of about 5-10 mm (Kerekes et al. (19)). This analysis clearly shows that the parallel plug flow model gives a much closer representation in a reacting fiber bed than the axial dispersed plug flow model.

Pulp fiber beds are unique among packed beds normally encountered in the process industry because of the long aspect ratio of the fibers.

This leads to flocculation and results in non-uniform permeability of beds on sedimentation of the flocs. In the present situation, as well as in most packed beds used in industry, the radial dispersion is determined by convective mechanisms. As a result the radial Peclet number is around 10 (Doraiswamy and Sharma (18)). Therefore the radial diffusion coefficient is approximately 0.1 $d_e u_i$. The effective particle diameter, d_e, and the interstitial velocity, u_i, for flow through pulp fiber beds are, respectively, 2 and 2-3 orders of magnitude smaller than the corresponding values in typical industrial packed beds. Consequently the radial diffusion coefficient and radial penetration depth in a reacting system (equation 7.51) are, respectively, 4-5 and 2 orders of magnitude smaller than generally found in industrial packed beds. On the other hand, the flow non-uniformities in a packed bed are determined by agglomeration and maldistribution of the bed particles. Softwood pulp fibers have a large aspect ratio of about 100 and this property is responsible for their tendency to form agglomerations called flocs. The floc size is approximately two times the length of the fibers (Kerekes (19)), i.e. 2*2.5 = 5 mm. Therefore the size of the flow non-uniformities in pulp fiber beds is approximately 200 times the fiber diameter or of the order $O(100\ d_e)$. However it is expected that the size of the flow non-uniformities in packed beds of particles with an aspect ratio close to 1 would be of the order of $O(d_e)$. Consequently the ratio of the radial penetration depth and size of flow uniformities is expectd to be two orders of magnitude smaller for softwood pulp fiber beds than for conventional packed beds.

In other words, the aspect ratio of about 100 and a fiber diameter of about 30 microns explain the unique characteristic of a reacting softwood fiber bed that breakthrough curves are well described by a parallel plug flow model and not by an axial dispersion model. The special shape and dimensions of the packing material which are needed for successful application are possibly the reasons why the parallel plug flow model has seen little use in the Chemical Engineering literature to date, Doraiswamy and Sharma (18).

7.5 Conclusions

The axial dispersion model does not represent the actual "micromixing" in a fixed bed of pulp fibers. Poor predictions of the experimental chlorine breakthrough curve were obtained when this model was used with known chlorine-lignin kinetics. Unrealistic changes of the parameters in these kinetics were needed before the predictions improved. The parallel plug flow model, however, gave very good predictions for both the reactant chlorine and the product methanol of the chlorine-lignin reaction. The suitability of the parallel plug flow model and the unsuitability of the axial dispersion model in representing the flow through packed pulp fiber beds is explained by an order of magnitude analysis and the unique flocculation property of fibers of large aspect ratio.

References

1. Levenspiel. O., and Bischoff, K.B., Adv. Chem. Eng., 4, 95-197 (1963).
2. Sundaresean, S., Amundson, N.R., and Ans, R., AIChE, 36 (1980).
3. Hinduja, M.J., Sundaresean, S., and Jackson, R., AIChE. J., 26, (1980).
4. Subramanian, R.S., Gill, E.N., Chem. Eng. Sci., 25, (1970).
5. Poirier, N.A., M.Eng. Thesis, McGill University, 1986.
6. Mackinnon, J., M.Eng. Thesis, McGill University, 1987.
7. Ackert, J.E., Ph.D. Thesis, University of Idaho, 1971.
8. Danckwerts, P.V., Chem. Eng. Sci., 2(1) (1953).
9. Pantankar, S.V., Numerical heat transfer and fluid flow, McGraw Hill, 1980.
10. Brenner, H., Chem. Eng. Sci., 17, 229-243 (1962).
11. Zwietering, T.N., Chem. Eng. Sci., 11, (1959).
12. Lee, P.F., Tappi, 67,11, (1984).
13. Ackert, J.E., Edwards, L.L., and Norström, H., Pulp and Paper Canada, 76,2, TS2, (1975).
14. Ruthven, D.M., Principles of adsorption and Adsorption Processes, John Wiley & Sons, 1984.
15. Cooney, D.O., and Lightfoot, N., Ind. and Eng. Chem. Fund., 4, (1965).
16. Danckwerts, P.V., App. Sci. Res., Sect.A.3, (1953).
17. Paterson, A.H.J., and Kerekes, R.J., Tappi, Vol.67, 5, (1984).

18. Doraiswamy, L.K., and Sharma, M.M., Heterogeneous Reactions: Analysis, Example and Reactor Design, John Wiley & Sons, 1984.

19. Kerekes, R.J., Soszynski, R.M., and Tam Doo, P.A., Transactions of the 8th Fundamental Research Symposium at Oxford, Vol.1, 1985.

CHAPTER 8

CONTRIBUTIONS TO KNOWLEDGE

1. The inter- and intra-fiber voidage in a packed bed of pulp fibers can be quantified by a dynamic version of the solute exclusion technique. The residence time distribution obtained with solutions of sugars of different sizes is representative of the flow of non-adsorbing molecules through a packed bed of pulp fibers.

2. The intra-fiber mass transfer resistance for a relatively small sugar molecule such as glucose can be neglected for flow through a packed bed of pulp fibers when the ratio of diffusion time to the mean residence time, $t_{0.95}/\bar{t}_r$, is small or when

$$t_{0.95}/\bar{t}_r = 0.45\ r\ /D\bar{t}_r = 0.45\ r\ u_a/DH << 1$$

3. For flow through a packed bed of pulp fibers, the intra-fiber transport mechanism for glucose is diffusion through the fiber wall and lumen, while the dominant transport mechanism for dextran T-2000 is convection through the pit openings.

4. Although the residence time distribution (RTD) of flow through a bed of pulp fibers can be represented mathematically by the axial dispersed plug flow model, the actual flow mechanism is shown to be dominated by channelling flow.

5. The long aspect ratio of pulp fibers and the associated formation of fiber flocs result in incomplete radial mixing of a liquid flowing

through a bed of pulp fibers. Incomplete radial mixing is inconsistent with axial dispersed plug flow but consistent with channelling flow. The governing condition for channelling flow is that the extent of transverse mixing is small compared to the periodicity in the transverse direction of the axial velocity fluctuations. The transverse mixing depth, δ_D, obtained from the following equation

$$\delta_D = 1.35\sqrt{D_R \bar{t}_r} = 1.35\sqrt{D_R \epsilon_a H/u_o}$$

is 0.6 mm, while the size of the transverse periodicity in axial velocity is about 200 fiber diameters or 6 mm. Thus, transverse mixing is too small to smoothen radial concentration gradients in pulp fiber beds and channelling is favored.

6. The dispersion in pulp fiber beds is one to two orders of magnitude larger than for beds of regular shaped particles. The smaller dispersion coefficients for packed beds of regular shaped particles are due to similar magnitudes of transverse penetration depths and tranverse concentration gradients. Also, the fiber length rather than the fiber diameter is a better characteristic dimension to unify the Peclet numbers of beds of different fiber types.
7. The effect of operating variables on the dispersion of flow through a packed bed of pulp fibers can only be determined when the structure of the pulp pad is unchanged. Otherwise the dispersion data depend significantly on pad formation, which is an undefined variable.

8. The initial reaction kinetics between chlorine and the carbohydrate fraction of pulp determined by dynamic chlorination of a bed of fully bleached pulp fibers is first order in chlorine. The temperature dependence of the reaction rate constant can be described by an Arrhenius type activation energy.

9. Chlorine consumption by lignin free pulp (carbohydrates) increases with time during dynamic chlorination when the mean residence times and temperatures are above certain values. TOC production increases correspondingly with increasing chlorine consumption.

10. The chlorine-lignin stoichiometry in dynamic chlorination increases with mean residence time and temperature and is independent of chlorine feed concentration. This behavior can be explained by chlorine consumption at a relatively slow rate by chlorinated lignin upstream of the instantaneous chlorine-lignin reaction front.

11. The slopes of the chlorine breakthrough curves were related to the Peclet number, P, obtained from the glucose tracer curve, assuming that axial dispersed plug flow or parallel plug flow is the governing flow mechanism. Axial dispersed plug flow requires a linear relationship between the normalized slope and P according to the following expression:

$$\left(T_c \cdot \frac{d(C/C_o)}{dT_c} \right)_{C/C_m = 0.5} (C_o/C_m) = 0.5\ P$$

The parallel plug flow model, however, requires that the normalized slope be proportional to the square root of P:

$$\left(T_c \cdot \frac{d(C/C_o)}{dT_c}\right)_{C/C_m = 0.5} (C_o/C_m) = 0.282\ (P)^{0.5}$$

The axial dispersed plug flow model significantly over-predicts the experimentally measured normalized slope. The prediction of the parallel plug flow model, however, was very good over the entire range of operating variables. These results demonstrate that channelling flow best represents the mechanism of flow through a bed of pulp fibers.

12. The lignin-methanol stoichiometery in dynamic chlorination is independent of superficial velocity, temperature or chlorine feed concentration. These results are consistent with methanol production only at the instantaneous chlorine-lignin reaction front.
13. The close relationship between methanol production and delignification is demonstrated for dynamic pulp chlorination. This opens the possibility to control dynamic chlorination by measuring the methanol concentration in the bleach effluent.
14. Experimental evidence for the production of TOC and methanol at the instantaneous chlorine-lignin reaction front is presented. Production of TOC due to hydrolysis of already reacted lignin between the inlet of the bed and the reaction front is shown to be significant.
15. The lignin content and kappa number of pulp undergoing dynamic chlorination decreases with increasing chlorine charge. The "floor level" lignin content is approached when the chlorine charge on pulp is about 0.1 The chlorinated lignin formed at the instantaneous

chlorine-lignin reaction front is alkali soluble. Dynamic chlorination can be stopped when all reaction fronts have reached the bottom of the pulp pad. TOC removal is not a good measure of the CW lignin content of pulp. Also the CW lignin content is a poor indicator of the CWE lignin content and kappa number.

16. The much faster carbohydrate degradation in dynamic chlorination compared to standard batch chlorination can be minimized by employing low residence times and high chlorine water concentrations, which lead to short contact times between pulp and chlorine.

17. The chlorine consumption by carbohydrates during dynamic chlorination can be predicted from the chlorine-carbohydrates kinetics. The reciprocal intrinsic pulp viscosity, $[\eta]$, was shown to depend on operating variables according to the following relationship:

$$\frac{1}{[\eta]_{t_c}} - \frac{1}{[\eta]_o} = \frac{K_1 M_w k_c}{\varepsilon_a M_{CL_2} C_h} \left(Q - \frac{1}{2} \left(SL_o L_o + \frac{\varepsilon_a C_o}{C_f} \right) \right) \bar{t}_r$$

18. The axial dispersed plug flow model with appropriate kinetics for the chlorine-lignin and chlorine-carbohydrates reactions gives poor predictions of the chlorine breakthrough curves obtained for dynamic chlorination of a pulp pad. The non-linear character of the chlorine-lignin kinetics and the channelling flow mechanism are responsible for this result.

19. A so-called parallel plug flow model, based on complete segration and instantaneous chlorine-lignin and linear chlorine carbohydrates

reaction kinetics, was formulated for dynamic chlorination of a pulp pad. Good predictions of the chlorine and methanol breakthrough curves are obtained when, respectively, the chlorine-lignin or methanol-lignin stiochiometries in the model are chosen such that the overall chlorine consumption or methanol production agrees with the experimental values.

20. The radial penetration distance travelled by the reaction front during dynamic chlorination is estimated from the Danckwerts' tarnishing reaction problem for diffusion and instantaneous reaction as 0.6 mm. This is about one order of magnitude smaller than the scale of flow non-uniformities of 5-10 mm in the radial direction, and explains why the parallel plug flow model is successful in representing dynamic pulp chlorination of a pad of pulp fibers. The aspect ratio of about 100 and fiber diameter of about 30 microns result in flocculation of pulp fibers and is responsible for the unique characteristics of pulp fiber beds. The assumption of instantaneous reaction kinetics is supported by the observed high initial chlorine-lignin reaction kinetics. The form of these kinetics leads to a "constant pattern" behavior.

APPENDIX 3-1

PHYSICAL AND CHEMICAL PROPERTIES OF PULP USED IN THIS EXPERIMENTAL STUDY.

The pulp used in this experimental work was obtained from pulping black spruce chips by the kraft pulping process. The chemical and physical properties of the pulp are listed in Table 3-1.1. The weighted length distribution as measured by the Kajaani FS-100 instrument is shown in Figure 3-1.1. The weighted length distribution for each size range was obtained as follows:

$$\frac{\sum N l_f^2}{\sum N l_f} \qquad 3\text{-}1.1$$

where N and l_f are, respectively, the number and length of fibers in the size range.

TABLE 3-1.1

Physical and Chemical Properties of Unbleached Pulp.

Chemical	Physical
Kappa number = 29.5	C.S. Freeness = 686 ml
Viscosity = 38 mPa·s	Basis weight = 60.7 g O.D./m^2
	Breaking length = 7.94 km
	Tensile index = 77.84 N·m/g
	Burst index = 5.88 kPa·m^2/g
	Stretch = 2.77%
	Bulk = 1.73 cm^3/g
	Zero span
	breaking length = 20.22 km

Figure 3-1.1 Weighted length distribution of unbleached kraft pulp.

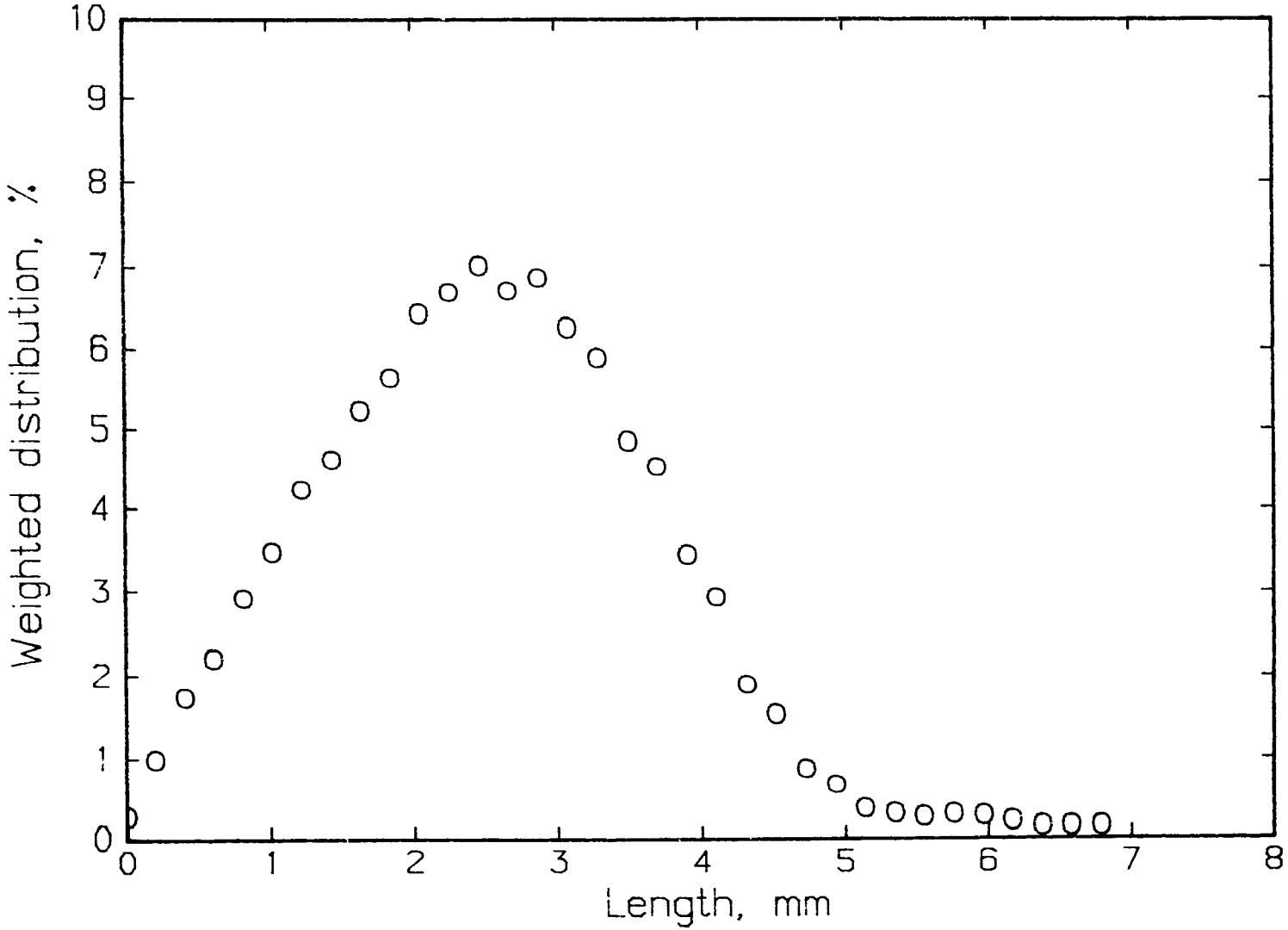
Weighted distribution, %
Length, mm
0
1
2
3
4
5
6
7
8
9
10

APPENDIX 4-1

DERIVATION OF DIMENSIONLESS AXIAL DISPERSION EQUATION

A mass balance for an inert tracer over a section of the pulp pad containing porous fibers with tracer adsorption on the fibers being negligible gives the following dimensional equation:

$$\varepsilon_i D_L \frac{\partial^2 C}{\partial x^2} - \varepsilon_i u_i \frac{\partial C}{\partial x} = \varepsilon_i \frac{\partial C}{\partial t} + (\varepsilon_a - \varepsilon_i) \frac{\partial n}{\partial t} \qquad 4\text{-}1.1$$

The first term on the right hand side represents accumulation in the voids external to the fibers while the second term represents accumulation within the fibers. The second term can be rearranged as follows:

$$(\varepsilon_a - \varepsilon_i) \frac{\partial n}{\partial t} = (\varepsilon_a - \varepsilon_i) \frac{\partial n}{\partial C} \frac{\partial C}{\partial t} \qquad 4\text{-}1.2$$

When local equilibrium is assumed

$$\frac{\partial n}{\partial C} = \frac{\partial C}{\partial C} \qquad 4\text{-}1.3$$

Thus

$$(\varepsilon_a - \varepsilon_i) \frac{\partial n}{\partial t} = (\varepsilon_a - \varepsilon_i) \frac{\partial C}{\partial t} \qquad 4\text{-}1.4$$

The right hand side of equation 4-1.1 can then be written as follows:

$$\varepsilon_i \frac{\partial C}{\partial t} + (\varepsilon_a - \varepsilon_i) \frac{\partial n}{\partial t} = \varepsilon_a \frac{\partial C}{\partial t} \qquad 4\text{-}1.5$$

Equation 4-1.5 can be substituted in 4-1.1 to give equation 4-1.6.

$$\epsilon_a \frac{\partial C}{\partial t} = \epsilon_i D_L \frac{\partial^2 C}{\partial x^2} - \epsilon_i u_i \frac{\partial C}{\partial x} \qquad 4\text{-}1.6$$

Equation 4-1.6 can be non-dimensionalized using the following dimensionless variables

$$X = x/H \qquad 4\text{-}1.7$$

and

$$T = tu_a/H$$

to give

$$\frac{\partial(C/C_o)}{\partial T} = \frac{D_L}{Hu_i} \frac{\partial^2(C/C_o)}{\partial X^2} - \frac{\partial(C/C_o)}{\partial X} \qquad 4\text{-}1.9$$

where

$$\frac{D_L}{Hu_i} = \frac{1}{P} \qquad 4\text{-}1.10$$

APPENDIX 4-2

COMPUTER PROGRAM TO CALCULATE MEAN RESIDENCE TIME AND PECLET NUMBER FROM TRACER BREAKTHROUGH CURVES

```
      INTEGER I,N,TCOUNT,COUNT,M,KCOUNT,ITER
      REAL X(99),Y(99),AREA(99),AREAB,PORATOT,FLO
      REAL AREAA(99),P(99),Q(99),AREAAB,POREXT,SUM(99)
      REAL SUMM,R,PECC,PECC,S,DIFF,CAREAB,CREAAB,CSUMM
      REAL,ADDD,ADD(99),PECCC,DIFFF,DVOL,padht,csarea
      character*11 fname,dname
      character fnameD(11),dnameD(11)
      EQUIVALENCE (FNAME,FNAMED),(DNAME,DNAMED)
      DATA FNAME/'GLUCO1A.ENG'/,DNAME/'DEXTO1A.ENG'/
C
C     DICTIONARY
C
C     DVOL          DEAD VOLUME OF REACTOR
C     X(I)          GLUCOSE DATA POINTS(TIME)
C     Y(I)          GLUCOSE DATA POINTS(C/C_o)
C     P(I)          DEXTRAN DATA POINTS(TIME)
C     Q(I)          DEXTRAN DATA POINTS(C/C_o)
C     AREA(I)       AREA OF INTERVAL(GLUCOSE,C VS T)
C     AREAA(I)      AREA OF INTERVAL(DEXTRAN,C VS T)
C     SUM(I)        AREA OF INTERVAL(DEXTRAN,CT VS T)
C     PORTOT        TOTAL POROSITY
C     POREXT        EXTERNAL POROSITY
```

```
C       FLO             FLOWRATE OF WATER
C       PECC            CALCULATED PECLET NUMBER
C       PECG            GUESSED PECLET NUMBER
C       PADHT           PAD HEIGHT
C       CSAREA          CROSS-SECTIONAL AREA
C       COUNT           COUNTER
C       KCOUNT          COUNTER
C       SUMM            TOTAL AREA OF DEXTRAN (CT VS T)
C       AREAAB          TOTAL AREA OF DEXTRAN (C VS T)
C       AREAB           TOTAL AREA OF DEXTRAN (C VS T)
C       N               NUMBER OF DATA POINTS (GLUCOSE)
C       M               NUMBER OF DATA POINTS (DEXTRAN)
C       CAREAB          CORRECTED AREA(DEAD VOLUME OF REACTOR)
C       CREAAB            SAME
C       CSUMM             SAME
C
        Reading run number
C
        WRITE(*,110)
  110   FORMAT(' RUN NUMBER ?')
        READ (*,114) FNAMED (5),FNAMED (6)
  114   FORMAT(2A1)
        DNAMED(5)=FNAMED(5)
        DNAMED(6)=FNAMAED(6)
C
```

```
C       Reading the flowrate
C
        WRITE(*,111)
  111   FORMAT(' WHAT IS THE FLOW RATE (ML/MIN) ?')
        READ(*,*) FLO
        FLO=FLO/60
C
C       Reading the pad height
C
        WRITE(*,112)
  112   FORMAT(' WHAT IS THE PAD HEIGHT (CM) ?')
        READ (*,*) PADHT
C
C
C       Reading other data
C
        CSAREA=44.05
C       PECC=2.0/R
        AREAB=0.0
        ITER=50
        AREAAB=0.0
        SUMM=0.0
        ADDD=0.0
        DVOL=20.0
C
```

```
C       Reading glucose energraphics file
C
        OPEN(5,FILE=FNAME)
        DO 1 I=1,8
   1    READ(5,*)
        READ(5,*) N
        DO 4 I=1,2
   4    READ(5,*)
C
        TCOUNT=(N-1)/2
        MCOUNT=TCOUNT
C
C       Reading dextran energraphics file
C
        OPEN (6,file=DNAME)
        DO 11 I=1,8
  11    READ (6,*)
        READ (6,*) M
C
        COUNT=(M-1)/2
        KCOUNT=COUNT
C
        DO 10 I=1,N
        READ(5,*) X(I),Y(I)
  10    CONTINUE
```

```
C                          GLUCOSE
C
C
C         Calculation of the zeroth moment from glucose BTC
C
C
C         THE FOLLOWING EXPRESSION TRANSLATES THE CURVE TO STEP
C         DOWN AND THEN CALCULATES THE AREA BELOW THE CURVE
C
C
          DO 20 I=1,TCOUNT
C
C
          AREA(I)=((X((2*I)+1)-X((2*I)-1))/6)*(1-Y((2*I)-1))
          +4*(1-Y+(2*I))+(1-Y((2*I)+1)))
C
C
          AREAB=AREAB+AREA(I)
   20     CONTINUE
          CAREAB=AREAB-(DVOL/FLO)
          WRITE(*,810)
   810    FORMAT('1','GLUCOSE RESULTS')
          WRITE(*,811)
   811    FORMAT(' ','----------------')
          WRITE(*,150)CAREAB
   150    FORMAT(' ','AREA BELOW CURVE= ',F10.4)
          WRITE(*,175)CAREAB
   175    FORMAT(' ','THE MEAN RESIDENCE TIME FOR GLUCOSE IS=
          ',F10.4)
C
```

```
C       CALCULATION OF TOTAL POROSITY FROM ZEROTH
        MOMENT(GLUCOSE)
C
        PORTOT=(CARE^B*FLO)/PADHT*CSAREA)
        WRITE(*,200)PORTOT
  200   FORMAT(' ','THE TOTAL POROSITY IS= ',F10.4)
C
C       Calculation of the first moment from glucose BTC
C
        DO 45 I=1,MCOUNT
        ADD(I)=(((X((2*I)+1)-(DVOL/FLO)))-(X((2*I)-1)
        -(DVOL/FLO)))/6.0*(((1-(Y((2*I)-)))*((X((2*I)-1))
        -(DVOL/FLO)))+(4.0*((1-Y(2*I)))*(X(2*I)-(DVOL/FLO)))
        +(((1-Y((2*I)+1)))*(X((2*I)+1)-(DVOL/FLO))))
C
        ADDD=ADDD+ADD(I)
   45   CONTINUE
        WRITE(*,575) ADDD
  575   FORMAT(' ','THE AREA BELOW THE CT VS T CURVE(GLUCOSE)=
        ',F15.4)
        K=(2.0*ADDD-(CAREAB*CAREAB))/(CAREAB*CAREAB)
        PECCC=2.0/K
        DO 74 I=1,ITER
        DIFFF=(2.0*PECCC**2.0-2.0*PECCC*(1.0-EXP(-PECCC)))
        -K*PECCC**3.0)/(-2.0*PECCC+4.0*(1.0-EXP(-PECCC))-
```

```
      2.0*PECCC**2.0*EXP(-PECCC))
      PECCC=PECCC-DIFFF
      IF (ABS((-DIFFF)/PECCC).LE.1E-6) GO TO 3
   74 CONTINUE
    3 WRITE(*,707) PECCC
  707 FORMAT(' ','PECLET NUMBER FROM GLUCOSE BTC= ',F10.4)
C
C     DEXTRAN
C
C     Calculation of the zeroth moment from dextran BTC
C
      DO 30 I=1,M
      READ(6,*) P(I),Q(I)
   30 CONTINUE
C
C     THE FOLLOWING EXPRESSION TRANSLATES THE CURVE TO STEP
C     DOWN AND TAHEN CALCULATES THE AREA BELOW THE CURVE
C
      DO 40 I=1,COUNT
      AREAA(I)=((P((2*I)+1)-P((2*I)-1))/6)*(1-(Q((2*I)-1))
      +4*(1-Q(2*I))+(1-Q((2*I)+1)))
      AREAAB=AREAAB+AREAA(I)
   40 CONTINUE
      CREAAB=AREAAB-(DVOL/FLO)+0.0
      WRITE(*,824)
```

```
  824   FORMAT(' ')
        WRITE(*,825)

  825   FORMAT(' ','DEXTRAN RESULTS')
        WRITE(*,826)
  826   FORMAT(' ','--------------------')
        WRITE(*,400)CREAAB
  400   FORMAT(' ','AREA BELOW CURVE= ',F10.4)
        WRITE(*450)CREAAB
  450   FORMAT(' ','THE MEAN RESIDENCE TIME FOR DEXTRAN=
        ',F10.4)
C
C       CALCULATION OF EXTERNAL POROSITY
C
        POREXT=(CREAAB*FLO)/(PADHT*CSAREA)
        WRITE(*,500) POREST
  500   FORMAT(' ',(THE EXTERNAL POROSITY OF THE PULP PAD=
        ',F10.4)
C
C       Calculation of the first moment from dextran BTC
C
C       DO 50 I=1,KCOUNT
        SUM(I)=((P((2*I)+1)-(DVOL/FLO)))-(P((2*I)-1)
        -(DVOL/FLO)))/6.0*(((1-(Q((2*I)-1)))*
        ((P((2*I)-1))-(DVOL/FLO)))+(4*((1-Q(2*I))))
        *(P(2*I)-(DVOL/FLO)))+(((1-Q((2*I)+)))
```

```
      *(P((2*I)+1)-(DVOL/FLO))))
C
      SUMM=SUMM+SUM(I)
   50 CONTINUE
      WRITE(*,600)SUMM
  600 FORMAT(' ','THE AREA BELOW THE CT VS T CURVE(DEXTRAN)
      IS= ',F10.4)
      R=(2*SUMM-(CREAAB*CREAAB))/(CREAAB*CREAAB)
      PECC=2.0/R
      DO 72 I=1,ITER
      DIFF=(2.0*PECC**2.0-2.0*PECC*(1.0-EXP(-PECC))
      -R*PECC**3.0)/(-2.0*PECC+4.0*(1.0-EXP(-PECC))
      -2.0*PECC**2.0*EXP(-PECC))
      PECC=PECC-DIFF
      IF(ABS((-DIFF)/PECC).LE.1/-6) GO TO 2
   72 CONTINUE
    2 WRITE(*,700)PECC
  700 FORMAT(' ','PECLET NUMBER FROM DEXTRAN BTC= ',F10.4)
      close(5)
      STOP
      END
```

Glucose Results

Area below curve = 68.43.

The mean residence time for glucose = 68.43.

The total porosity, ε_a = 0.932.

The area below CT vs. T curve = 246.71.

Peclet number, P = 37.1.

Dextran Results

Area below curve = 57.25.

The mean residence time for dextran = 57.25.

The fiber wall and inter-fiber porosity = 0.779.

The Peclet number, P = 23.3.

APPENDIX 4.3

DIMENSIONS OF WATER SWOLLEN FIBER

For dry black spruce fibers, the diameter of the lumen has been measured as 18.4 microns and the fiber coarseness (mass of fiber per unit length) as 0.29 mg/m. Upon pulping these wood fibers, the diameter of the lumen remains essentially unchanged. For the present black spruce of Kappa number 29.5 the pulping yield is 48.5% giving a coarseness of the water swollen fibers of 0.485*0.29 = 0.141 mg/m. Therefore the volume of the lumen per mass of fiber, V_1, can be calculated as:

$$V_1 = (\text{lumen volume/m fiber})/(\text{O.D. mass of fiber/m fiber})$$
$$= [(\pi*18.4*10^{-6}/2)^2/(0.141*10^{-3})] = 1.88 \text{ cm}^3/\text{g O.D. fiber}$$

The pore volume of the fiber wall of the present pulp was determined by the solute exclusion technique as 1.46 cm^3/g O.D. pulp. The volume occupied by the solid wood in the fibers is 0.67 cm^3/g O.D. fibers based on a wood density of 1.50 g/cm^3 independent of wood species for low yield pulp. The present volume of the water swollen fibers is 1.88 + 1.46 + 0.67 = 4.01 cm^3/g O.D. fiber. This corresponds to a fiber diameter in the swollen state of $[4*\text{swollen volume}*\text{coarseness}/\pi]^{0.5} = [4*4.01*10^{-6}*-0.141*10^{-3}/\pi]^{0.5} = 26.8*10^{-6}$ m. The corresponding fiber wall thickness is (26.8-18.4)/2 = 4.2 microns. The fiber wall porosity, ε_w, can be obtained from the wood density (1.50 g/cm^3) and the pore volume of the fiber wall (1.47 cm^3/g) as $\varepsilon_w = 1.46/(1.46 + (1/1.50) = 0.687$.

APPENDIX 4-4

EQUIVALENT DIAMETER OF FIBERS IN PULP PAD

The Carman equation is

$$\frac{2r_e}{H}\frac{\Delta p}{\rho_f(\varepsilon_i u_i)^2} = \frac{(1-\varepsilon_i)^2}{\varepsilon_i^3}\frac{150\,\eta_f}{\rho_f \varepsilon_i u_i \cdot 2r_e} \qquad 4\text{-}4.1$$

and can be simplified to

$$\frac{\Delta P}{H} = \frac{(1-\varepsilon_i)^2}{\varepsilon_i^3} \cdot 150\,\frac{\eta_f \varepsilon_i u_i}{4r_e^2} \qquad 4\text{-}4.2$$

and further to

$$\frac{\Delta P}{H} = \frac{(1-\varepsilon_i)^2}{\varepsilon_i^2}\,\frac{150}{4}\,\frac{\eta_f u_i}{r_e^2} \qquad 4\text{-}4.3$$

or

$$r_e = \frac{1-\varepsilon_i}{\varepsilon_i}\sqrt{\frac{150}{4}\,\frac{\eta_f u_i}{(\Delta P/H)}} \qquad 4\text{-}4.4$$

The external fluid porosity, ε_i, can be calculated from the total pad volume and the swollen fiber volume of 4.01 cm^3/O.D. pulp to be 0.565. Also,

$$\frac{\Delta P/H}{u_i} = \frac{\frac{95\text{ mm Hg}}{6\text{ cm}}}{\frac{250\text{ cm}^3/\text{min}}{44.05\text{ cm}^2 * 0.565}}$$

using the results from Figure 4.21.

or

$$\frac{\Delta P/H}{u_i} = \frac{\frac{95*13.6*9.81 \text{ Pa}}{6*10^{-2}}}{\frac{250*10^{-6} \text{ m}^3/\text{s}}{60*44.05*10^{-4}*0.567 \text{ m}^2}}$$

$$= 12618*10^4 \text{ (Pa}\cdot\text{s/m}^2\text{)}$$

$$= 1.2618*10^8 \text{ kg/m}^3\cdot\text{s}.$$

Noting that the fluid viscosity, η_f, is $1*10^{-3}$ kg/m·s and using the above values in equation 4-4.4 we get

$$r_e = \frac{1-0.565}{0.565}\sqrt{\frac{150}{4}\frac{1*10^{-3}}{1.2618*10^8}}$$

$$r_e = \frac{1-0.565}{0.565}\sqrt{2.97*10^{-10}}$$

$$r_e = 1.327*10^{-5} \text{ m}$$

or d_e the equivalent diameter 26.5 microns. It is interesting to note that this equivalent diameter is similar to the fiber diameter of 26.8 microns (Appendix (4-3)).

APPENDIX 4-5

CALCULATION OF RADIAL DISPERSION COEFFICIENT, D_R

The radial dispersion coefficient, D_R, for glucose can be obtained from

$$\frac{1}{Pe_R} = \frac{1}{Pe_{t,R}} + \frac{\varepsilon_i}{1.5\ Re_e \cdot Sc} \qquad 4\text{-}5.1$$

where

$$\frac{1}{Pe_{t,R}} = \frac{0.09}{1 + 10/Re_e \cdot Sc} \qquad 4\text{-}5.2$$

Now at T = 20°C, $u_o = 0.082$ cm/s and $\varepsilon_i = 0.565$

$$Re_e = \rho d_e u_o/\eta = \frac{1*10^6 \cdot 26.5*10^{-6} \cdot 8.2*10^{-4}}{1}$$

$$= 2.17*10^{-2}$$

$$Sc = \frac{\eta}{\rho D_M} = \frac{1}{10^6 \cdot 6*10^{-10}} = 1667$$

Thus

$$\frac{1}{Pe_R} = \frac{D_R}{\mu_i d_e} = \frac{0.09}{1 + 10/(2.17*10^{-2} \cdot 1667)} + \frac{0.565}{1.5 \cdot 2.17*10^{-2} \cdot 1667} = 0.081$$

or

$$D_R = 0.081 \cdot \frac{8.2*10^{-4}}{0.565} \cdot 25.5*10^{-6} = 3.11*10^{-9}\ m^2/s$$

APPENDIX 6-1

CALCULATION OF HYDRODYNAMIC DIAMETERS OF Cl_2 AND GLUCOSE

According to the Einstein-Stokes equation the molecular diameter is related to the diffusion coefficient according to the following formula:

$$\text{Diameter} = \frac{RT}{3\pi\eta DN} \qquad 6\text{-}1.1$$

where R is the gas constant = 8.314 J/mol K, T is the absolute temperature, η is the viscosity of water = 1.002 g/m•s at 20°C, with D as the diffusivity of glucose = $0.661*10^{-9}$ m^2/s at 20°C or the diffusivity of chlorine = $1.48*10^{-9}$ m^2/s at 20°C.

Substituting these values into the above equation leads to a molecular diameter of about 6.5 Å for glucose and about 2.9 Å for chlorine.

APPENDIX 6-2

DERIVATION OF EQUATIONS TO EVALUATE SL_o

1. The expression for calculating the breakthrough time of each channel, t_b, is shown in Chapter 7 to be

$$t_b = \frac{SL_o L_o C_f}{k_c C_o \varepsilon_a}\left(e^{k_c t_r} - 1\right) + t_r \qquad 6\text{-}2.1$$

The cumulative net inflow of chlorine for a single channel when $t_c > t_b$ (i.e. after the reaction front has reached the exit of the channel) is

$$= C_o(u_a(t_r))\varepsilon_a dA t_c - C_o e^{-k_c t_r} u_a(t_r)\varepsilon_a dA\,(t_c - t_b) \qquad 6\text{-}2.2$$

$$= C_o(u_a(t_r))\varepsilon_a dA\left[t_c - (t_c - t_b)e^{-k_c t_r}\right] \qquad 6\text{-}2.3$$

where t_c is the reaction time.

When $t_c < t_b$ (i.e. before the reaction front has reached the end of the channel) the mass balance is

$$\text{IN-OUT} = C_o(u_a(t_r))\varepsilon_a dA t_c \qquad 6\text{-}2.4$$

The cumulative net inflow for all channels regardless of the location of the reactor front is

$$\text{IN-OUT} = C_o A u_a \varepsilon_a\left[\int_o^1 t_c dF(t_r) - \int_o^{F(t_{rc})} (t_c - t_b)e^{-k_c t_r} dF\right] \qquad 6\text{-}2.5$$

$F(t_{rc})$ is the critical value of F at t_{rc} which is defined as

$$t_c = \frac{SL_o L_o C_f}{k_c C_o \varepsilon_a}\left(e^{k_c t_{rc}} - 1\right) + t_{rc} \qquad 6\text{-}2.6$$

Since

$$T_c = t_c u_a / H \qquad 6\text{-}2.7$$

and

$$T_b = t_b u_a / H \qquad 6\text{-}2.8$$

equation 6-2.5 can be reduced to

$$\text{IN-OUT} = AH\varepsilon_a C_o\left[T_c - \int_o^{F(t_{rc})} (T_c - T_b)\, e^{-k_c t_r}\, dF\right] \qquad 6\text{-}2.9$$

with

$$T_b = \frac{u_a SL_o L_o C_f}{H\varepsilon_a k_c C_o}\left(e^{k_c t_r} - 1\right) + t_r u_a / H \qquad 6\text{-}2.10$$

and $F(t_{rc})$ is the critical value of F at t_{rc} where

$$T_c = \frac{u_a SL_o L_o C_f}{H\varepsilon_a k_c C_o}\left(e^{k_c t_{rc}} - 1\right) + t_{rc} u_a / H \qquad 6\text{-}2.11$$

2. The cumulative net inflow of chlorine determined from the experiment is:

$$IN\text{-}OUT = u_a \varepsilon_a A \int_0^{t_c} (C_o - C)\, dt_c \qquad 6\text{-}2.12$$

Equations 6-2.9 to 6-2.12 can be solved together to yield the chlorine-lignin stoichiometry, SL_o.

APPENDIX 6-3

DERIVATION OF SLOPE OF THE AXIAL DISPERSION MODEL COMBINED WITH A SINGLE INSTANTANEOUS REACTION

If it is assumed that a reference frame moves with the speed of the reaction front in a bed of pulp fibers undergoing chlorination, then the equation describing this situation is

$$(u_o - v)\frac{\partial C}{\partial x} - \varepsilon_i D_L \frac{\partial^2 C}{\partial x^2} = 0 \qquad 6\text{-}3.1$$

where v is the speed of the reaction front.

The boundary conditions are:

(1) $$\frac{\partial C}{\partial x} = 0 \text{ and } C = C_o \text{ at } x = -\infty \qquad 6\text{-}3.2$$

and

(2) $$C = 0 \text{ at } x = x_f \qquad 6\text{-}3.3$$

where x_f is the location of the reaction front in the bed.

Integrating equation 6-3.1,

$$(u_o - v)C - \varepsilon_i D_L \frac{\partial C}{\partial x} = K_1 \qquad 6\text{-}3.4$$

Applying boundary condition 1 (equation 6-3.2)

$$K_1 = (u_o - v)C_o \qquad 6\text{-}3.5$$

Equation 6-3.4 can then be re-written as

$$\varepsilon_i D_L \frac{\partial C}{\partial x} = -(u_o - v)(C_o - C) \qquad 6\text{-}3.6$$

Integrating equation 6-3,6, we get

$$-\int_{(C_o - C)}^{C_o} \frac{d(C_o - C)}{(C_o - C)} = -\frac{(u_o - v)}{\varepsilon_i D_L}\int_{x}^{x_f} dx \qquad 6\text{-}3.7$$

$$-\ln \frac{C_o}{C_o - C} = -\frac{(u_o - v)}{\varepsilon_i D_L}(x_f - x) \qquad 6\text{-}3.8$$

$$\frac{C_o}{C_o - C} = \exp\left[\frac{u_o - v}{\varepsilon_i D_L}(x_f - x)\right] \qquad 6\text{-}3.9$$

or

$$C/C_o = 1 - \exp\left[-\frac{(u_o - v)}{\varepsilon_i D_L}(x_f - x)\right] \qquad 6\text{-}3.10$$

The speed of the reaction front, v, in equation 6-3.10 is needed. From a mass balance, including the reaction front as one boundary, and neglecting the carbohydrate-chlorine reaction:

Inflow-Outflow = Reaction + Accumulation

$$u_a \varepsilon_a A C_o dt - 0 = SL_o L_o C_f A dx_f + \varepsilon_a C_o A dx_f$$

so

$$v = \frac{dx_f}{dt} = \frac{u_a c_a C_o}{SL_o L_o C_f + \varepsilon_a C_o} \qquad 6\text{-}3.12$$

for $k_c x_f / u_a \ll 1$

Integrating equation 6-3.12

$$\int_{x}^{x_f} dx_f = \int_{t}^{t_f} \frac{u_a \varepsilon_a C_o dt}{SL_o L_o C_f + \varepsilon_a C_o} \qquad 6\text{-}3.13$$

where

$$x_f - x = - \frac{u_a \varepsilon_a C_o}{SL_o L_o C_f + \varepsilon_a C_o} (t - t_f) \qquad 6\text{-}3.14$$

Substituting equation 6-3.14 into 6-3.10, we get

$$\frac{C}{C_o} = 1 - \exp\left[\frac{\varepsilon_a (u_o - v) u_a C_o}{\varepsilon_1 D_L (SL_o L_o C_f + \varepsilon_a C_o)} (t - t_f) \right] \qquad 6\text{-}3.15a$$

$$= 1 - \exp\left[\frac{u_1 (u_o - v) C_o}{D_L (SL_o L_o C_f + \varepsilon_a C_o)} (t - t_f) \right] \qquad 6\text{-}3.15b$$

Now

$$\frac{d(C/C_o)}{dt} = \frac{(u_o - v) u_i C_o}{D_L (SL_o L_o C_f + \varepsilon_a C_o)} \exp \left[\frac{(u_o - v) u_1 C_o (t - t_f)}{D_L (SL_o L_o C_f + \varepsilon_a C_o)} \right] \qquad 6\text{-}3.16$$

so

$$\left. \frac{d(C/C_o)}{dt} \right|_{t = t_f} = \frac{(u_o - v) u_1 C_o}{D_L (SL_o L_o C_f + \varepsilon_a C_o)} \qquad 6\text{-}3.17$$

Now,

$$T = t u_a / H \qquad 6\text{-}3.18$$

Substituting equation 6-3.18 into 6-3.17 gives

$$\left.\frac{d(C/C_o)}{dT}\right|_{t = t_f} = \frac{\varepsilon_a(u_o - v)\, HC_o}{\varepsilon_i D_L (SL_o L_o C_f + \varepsilon_a C_o)} \qquad 6\text{-}3.19$$

Since

$$P = u_i H/D_L \qquad 6\text{-}3.20$$

and

$$u_i \varepsilon_i = u_a \varepsilon_a = u_o \qquad 6\text{-}3.21$$

then

$$\left.\frac{d(C/C_o)}{dT}\right|_{t = t_f} = \frac{PC_o}{SL_o L_o C_f + \varepsilon_a C_o}\left(\frac{u_o - v}{u_a}\right) = P(v/u_a)(1 - v/u_o) \qquad 6\text{-}3.22$$

If initial breakthrough occurs at $t = t_{bi}$, then the average breakthrough time, $\bar{t}_b$, can be found as follows from the chlorine breakthrough curve:

$$\bar{t}_b - t_{bi} = \int_{t_{bi}}^{\infty} (1 - C/C_o)\, dt_f \qquad 6\text{-}3.23$$

or

$$\bar{t}_b - t_{bi} = \int_{o}^{\infty} \exp\left[-P\frac{v}{H}\left(1 - \frac{v}{u_o}\right)(t - t_f)\right] d(t - t_f) \qquad 6\text{-}3.24$$

which gives

$$\bar{t}_b - t_{bi} = \frac{1}{P}\frac{u_o}{v}\frac{H}{u_o - v} \qquad 6\text{-}3.25$$

so that

$$\bar{t}_b = t_{bi} + \frac{1}{P}\frac{H}{v}\frac{1}{1 - v/u_o} \qquad 6\text{-}3.26$$

or in non-dimensional form

$$\bar{T}_b = T_{bi} + \frac{1}{P}\frac{1}{(v/u_a)}\cdot\frac{1}{(1 - v/u_a)} \qquad 6\text{-}3.27$$

or

$$\bar{T}_b = T_{bi} + 1\Big/\left[\frac{d(C/C_o)}{dT}\right] t = t_{bi} \qquad 6\text{-}3.28$$

Also valid is

$$A(\bar{t}_b - H/u_a)\, u_a \varepsilon_a C_o = SL_o L_o C_f AH \qquad 6\text{-}3.29$$

or

$$\bar{t}_b = \frac{SL_o L_o HC_f + H\varepsilon_a C_o}{u_a \varepsilon_a C_o} = H/v \qquad 6\text{-}3.30$$

or

$$\bar{T}_b = u_a/v \qquad 6\text{-}3.31$$

Combining 6-3.27 and 6-3.31

$$u_a/v = T_{bi} + \frac{1}{P}\frac{1}{(v/u_a)}\frac{1}{(1 - v/u_o)} \qquad 6\text{-}3.32$$

Now

$$\left.\frac{d(C/C_o)}{dT}\right|_{t = t_{bi}} = P\,\frac{1}{\bar{T}_b}\,(1 - v/u_o) \qquad 6\text{-}3.33$$

or

$$\left.\frac{d(C/C_o)}{dT}\right|_{t = t_{bi}\cdot\bar{T}_b} = P\left(1 - \frac{1}{\varepsilon_a \bar{T}_b}\right) \qquad 6\text{-}3.34$$

when $C/C_o = 0.5$, then from equation 6-3.15 it follows that

$$t - t_{bi} = \frac{0.693}{\left(\frac{v}{u_o}\right) P\left(\frac{u_o - v}{H}\right)} \qquad 6\text{-}3.35$$

Thus

$$\left.\frac{d(C/C_o)}{dt}\right|_{C/C_o = 0.5} = \frac{v}{u_o} P \frac{(u_o - v)}{H} \exp(-0.693) \qquad 6\text{-}3.36$$

$$\left.\frac{d(C/C_o)}{dt}\right|_{C/C_o = 0.5} = \frac{0.5\ P\ (u_o - v)}{H} \frac{v}{u_o} \qquad 6\text{-}3.37$$

$$\left.\frac{d(C/C_o)}{dT}\right|_{C/C_o = 0.5} = 0.5\ P \frac{v}{u_a} \frac{u_o - v}{u_o} = 0.5\ P \frac{v}{u_a}(1 - v/u_o) \qquad 6\text{-}3.38$$

From equation 6-3.31

$$\frac{v}{u_a} = \frac{1}{\bar{T}_b}$$

so

$$\left.\frac{d(C/C_o)}{dT}\right|_{C/C_o = 0.5 \cdot \bar{T}_b} = 0.5\ P\left(1 - \frac{1}{\varepsilon_a \bar{T}_b}\right) \qquad 6\text{-}3.39$$

$T_{(C/C_o = 0.5)}$ has to be determined.

Equation 6-3.35 can be written in non-dimensional form

$$T_{[C/C_o = 0.5]} = T_{bi} + 0.693 \frac{1}{P} \frac{1}{(v/u_a)} \frac{1}{1 - v/u_a} \qquad 6\text{-}3.40$$

Also from equation 6-3.32

$$T_{bi} = u_a/v - \frac{1}{P} \frac{1}{(v/u_a)} \frac{1}{(1 - v/u_o)}$$

Thus

$$T_{(C/C_o = 0.5)} = u_a/v - 0.307 \left(\frac{1}{P} \frac{1}{(v/u_a)} \frac{1}{(1 - v/u_o)} \right) \qquad 6\text{-}3.41$$

From equation 6-3.31, $u_a/v = \bar{T}_b$

Thus

$$T_{(C/C_o = 0.5)} = \bar{T}_b - 0.307 \left(\frac{1}{P} \bar{T}_b \frac{1}{\left(1 - \frac{1}{\varepsilon_a \bar{T}_b}\right)} \right) \qquad 6\text{-}3.42$$

Combining equations 6-3.39 and 6-3.42

$$\left(T_c \frac{d(C/C_o)}{dT_c} \right)_{C/C_o = 0.5} = 0.5 P \left(1 - \frac{1}{\varepsilon_a \bar{T}_b} \right) - 0.1534 \qquad 6\text{-}3.44$$

APPENDIX 6-4

DERIVATION OF EQUATIONS TO EVALUATE S

The chloride concentration at any position x_f along a single plug flow channel in the pulp pad, assuming instantaneous reaction between chlorine and lignin, is the sum of the following contributions: (i) excess free chloride in the feed, $[Cl^-]_f$, (ii) formed by reaction between chlorine and lignin, $[Cl^-]_{RL}$, and (iii) formed by reaction between chlorine and carbohydrates before the reaction front, $[Cl^-]_{RC}$. Both oxidation and substitution reactions are assumed to be taking place at the reaction front. Thus

$$[Cl^-]_{x_f} = [Cl^-]_f + [Cl^-]_{RL} + [Cl^-]_{RC} \qquad 6\text{-}4.1$$

Now,

$$[Cl^-]_{RL} = \left(\frac{1}{2} S + 0\right) \cdot [Cl_2]_{x_f, \text{as } Cl^-} \qquad 6\text{-}4.2$$

where S is the fraction of chlorine used for lignin substitution reactions and 0 the fraction used for lignin oxidation reactions or, since

$$(S + 0) = 1 \qquad 6\text{-}4.3$$

$$[Cl^-]_{RL} = \left(1 - \frac{1}{2} S\right) \cdot [Cl_2]_{x_f, \text{as } Cl^-} \qquad 6\text{-}4.4$$

also

$$[Cl^-]_{RC} = \left(1 - e^{-k_c t_{rf}}\right) \cdot C_{o, \text{as } Cl^-} \qquad 6\text{-}4.5$$

where t_{rf} is a variable residence time in a channel.

Equation 6-4.4 can be expressed in terms of the chlorine concentration at the inlet, $Cl_{o, \text{as } Cl^-}$

$$[Cl^-]_{RL} = \left(1 - \frac{1}{2} S\right) \; e^{- k_c t_{rf}} \; C_{o,as\ Cl^-} \qquad 6\text{-}4.6$$

Substituting 6-4.5 and 6-4.6 into 6-4.1 we get

$$[Cl^-]_{x_f} = [Cl^-]_f + \left(1 - e^{- k_c t_{rf}}\right) \cdot C_{o,as\ Cl^-} + \left(1 - \frac{1}{2} S\right)\left(e^{- k_c t_{rf}}\right) C_{o,as\ Cl^-} \qquad 6\text{-}4.7$$

or

$$[Cl^-]_{x_f} = [Cl^-]_f + \left(1 - \frac{1}{2} S \cdot e^{- k_c t_{rf}}\right) C_{o,as\ Cl^-} \qquad 6\text{-}4.8$$

This chloride concentration reaches the end of the channel $((H - x_f)/u_a)$ seconds later, i.e. the time to travel between the reaction front and the end of the channel. The total time, t_c, for this concentration to reach the bed exit is given by:

$$t_c = \frac{S L_o L_o C_f}{\varepsilon_a C_o k_c}\left(e^{k_c t_{rf}} - 1\right) + t_{rf} + H/u_a - x_f/u_a \qquad 6\text{-}4.9$$

or

$$t_c = \frac{S L_o L_o C_f}{\varepsilon_a C_o k_c}\left(e^{k_c t_{rf}} - 1\right) + t_r \qquad 6\text{-}4.10$$

or

$$e^{k_c t_{rf}} = (t_c - t_r)\left(\frac{\varepsilon_a C_o k_c}{S L_o L_o C_f} + 1\right) \qquad 6\text{-}4.11$$

or

$$t_{rf} = \frac{1}{k_c}\left[\ell n \quad (t_c - t_r)\,\frac{\epsilon_a C_o k_c}{SL_o L_o C_f} + 1\right] \qquad 6\text{-}4.12$$

Substituting equation 6-4.12 into 6-4.8 and defining

$$\frac{\epsilon_a C_o k_c}{SL_o L_o C_f} = K \qquad 6\text{-}4.13$$

so that

$$e^{-k_c t_{rf}} = \frac{1}{[K(t_c - t_r) + 1]}$$

we get

$$[Cl^-]_{exit} = [Cl^-]_f + 1 - [\tfrac{1}{2}S/[K(t - t_r) + 1]] \cdot C_{o,asCl^-} \qquad 6\text{-}4.14$$

Thus for each hannel at any time t

$$[Cl^-]_{ce} = 0 \quad \text{when} \quad t < t_r \qquad 6\text{-}4.15$$

$$[Cl^-]_{ce} = [Cl^-]_f + C_o - [\tfrac{1}{2}SC_o/[K(t - t_r) + 1]] \qquad 6\text{-}4.16$$

$$\text{when } t_c < \frac{e^{k_c t_r} - 1}{K} + t_r$$

and

$$[Cl^-]_{ce} = [Cl^0]_f + C_{o,asCl^-} \qquad 6\text{-}4.17$$

$$\text{when } t_c > \frac{e^{k_c t_r} - 1}{K} + t_r$$

Summing over all channels at any time t

$$[Cl^-]_{ce,t} = \int_0^1 [Cl^-]_{exit,t}\, dF \qquad 6\text{-}4.18$$

By solving equations 6-4.15-18 with knowledge of the experimental chloride breakthrough, the fraction of chlorine used for lignin substitution reactions, S, can be found at different times during the experiment. The division of the pulp pad into channels as needed by equation 6-4.18 is obtained from the preceding glucose tracer curve.

APPENDIX 6-5

DERIVATION OF EQUATIONS TO EVALUATE R

R is defined as

$$\frac{\text{g methanol produced}}{\text{g initial lignin, } L_o} \qquad 6\text{-}5.1$$

The net outflow from a single channel in the pulp pad gives

$$\text{OUT-IN} = \frac{R}{SL_o} u_a(t_r)\varepsilon_a dA \int_{t_r}^{t_c} [C_o]_{x_f} \qquad 6\text{-}5.2$$

where $[C_o]_{x_f}$ is the concentration of chlorine at the reaction front located at x_f.

Since

$$[C_o]_{x_f} = C_o e^{-k_c t_{rf}} \qquad 6\text{-}5.3$$

with $t_{rf} = x_f/u_a$ and from Appendix 6-4

$$e^{-k_c t_{rf}} = 1/(K(t_c - t_r) + 1) \qquad 6\text{-}5.4$$

where $K = \varepsilon_a C_o k_c / SL_o L_o C_f$, equation 6-5.2 becomes

$$\text{IN-OUT} = \frac{R}{SL_o} C_o(u_a(t_r))\ \varepsilon_a dA \int_{t_r}^{t_c} \frac{1}{K(t_c - t_r) + 1}\, dt_c \qquad 6\text{-}5.5$$

when $t_r < t_c < t_b$

Furthermore, OUT-IN = 0 when $t_c < t_r$ and

$$\text{OUT-IN} = \frac{R}{SL_o} C_o(u_a(t_r))\ \varepsilon_a dA \int_{t_r}^{t_b} \frac{1}{K(t_c - t_r) + 1}\, dt_c \qquad 6\text{-}5.6$$

when $t_c > t_b$

The net outflow of methanol for all channels at any time t_c

$$\text{OUT-IN} = \frac{R}{SL_o} C_o u_a \varepsilon_a A \left[\int_o^{F(t_{rc})} \int_{t_r}^{t_b} \frac{1}{(K(t_c - t_r) + 1)}\, dt_c\ dF(t_r) \right. \qquad 6\text{-}5.7$$

$$\left. + \int_{F(t_{rc})}^{F(t_c)} \int_{t_r}^{t_c} \frac{1}{(K(t_c - t_r) + 1)}\, dt_c\ dF(t_r) \right]$$

where $F(t_{rc})$ is the value of F at t_{rc} where t_{rc} is calculated from the equality

$$t_c = \frac{SL_o L_o C_f}{\varepsilon_a C_o k_c} \left(e^{k_c t_{rc}} - 1 \right) + t_{rc} \qquad 6\text{-}5.8$$

After integration

$$\text{OUT-IN} = \frac{RAHL_o C_f}{k_c \bar{t}_r} \left[\int_o^{F(t_{rc})} [\ell n(K(t_b - t_r) + 1)]\ dF(t_r) \right. \qquad 6\text{-}5.9$$

$$\left. + \int_{F(t_{rc})}^{F(t_c)} [\ell n(K(t_c - t_r) + 1)]\ dF(t_r) \right]$$

Experimentally, the net outflow of methanol from the pulp pad is

$$\text{OUT-IN} = u_a \varepsilon_a A \int_o^{t_c} [\text{Methanol}]_{exit}\, dt_c$$

$$= \varepsilon_a AH \int_o^{T_c} [\text{Methanol}]_{exit}\, dT_c \qquad 6\text{-}5.10$$

Equating the experimental (6-5.10) and theoretical (6-5.9) expressions we get

$$\int_o^{T_{cf}} \frac{[\text{Methanol}]_{exit}}{C_o}\, dT_c$$

$$= \frac{R}{SL_o} \frac{u_a}{H} \frac{1}{K} \left[\int_o^{F(t_{rc})} [\ell n(P_{tc}(t_b - t_r) + 1)]\, dF \right.$$

$$\left. + \int_{F(t_{rc})}^{F(t_r)} \ell n(K(t_c - t_r) + 1)\, dF \right] \qquad 6\text{-}5.11$$

R can be found from equation 6-5.11 by a trial and error procedure at any reaction time.

APPENDIX 6-6

CONSUMPTION OF CHLORINE BY CARBOHYDRATES

The total amount of chlorine consumed by carbohydrates in a single plug flow channel of cross-sectional area A is

$$\int_0^t \int_0^{x_f} \varepsilon_a dA \left(- r_{Cl_2}\right) dx_f dt_c \qquad 6\text{-}6.1$$

It was shown in Chapter 5 that $\left(- r_{Cl_2}\right) = k_c C$. Equation 6-6.1 then becomes

$$\int_0^t \int_0^{x_f} \varepsilon_a dA \left(k_c C_{x_f}\right) dx_f dt_c \qquad 6\text{-}6.2$$

For plug flow and first order chlorine-carbohydrates kinetics it follows that $C_{x_f} = C_o e^{(- k_c x_f/u_a)}$ so that equation 6-6.2 becomes

$$\int_0^t \int_0^{x_f} \varepsilon_a dA k_c C_o e^{(- k_c x_f/u_a)} dx_f dt_c \qquad 6\text{-}6.3$$

or

$$- \varepsilon_a dA C_o u_a \int_0^t \int_0^{(k_c x_f u_a)} e^{(- k_c x_f/u_a)} d(- k_c x_f/u_a) dt_c \qquad 6\text{-}6.4$$

and finally

$$\varepsilon_a dA C_o u_a \int_0^t \left(1 - e^{(- k_c x_f/u_a)}\right) dt_c \qquad 6\text{-}6.5$$

Using Taylor expansion and keeping first order terms only, equation 6-6.5 can be approximated by

$$\varepsilon_a dAC_o u_a \int_o^t (k_c x_f/u_a)\, dt_c \qquad 6\text{-}6.6$$

when $k_c x_f/u_a \ll 1$.

This condition is equivalent to assuming that $C_{x_f}/C_o \approx 1$, i.e. the decrease in chlorine concentration due to chlorine-carbohydrates reaction upstream of the reaction front is negligible. It was shown in Chapter 6 that the breakthrough time, t_b, for a single channel is

$$t_b = \frac{SL_o L_o C_f}{\varepsilon_a C_o k_c}\left(e^{(k_c H/u_a)} - 1\right) + \frac{H}{u_a} \qquad 6\text{-}6.7$$

By changing the variables t_b and H to t_c and x_f one obtains

$$t_c = \frac{SL_o L_o C_f}{\varepsilon_a C_o k_c}\left(e^{(k_c x_f/u_a)} - 1\right) + \frac{x_f}{u_a} \qquad 6\text{-}6.8$$

Using the condition that $k_c x_f/u_a \ll 1$, equation 6-6.8 can be re-written as

$$k_c x_f/u_a = \frac{\varepsilon_a C_o k_c t_c/SL_o L_o C_f}{1 + \frac{\varepsilon_a C_o}{SL_o L_o C_f}} \qquad 6\text{-}6.9$$

Substituting equation 6-6.9 into 6-6.6 and integrating, the amount of chlorine consumed by carbohydrates becomes

$$\varepsilon_a C_o u_a dA \frac{\left(\frac{\varepsilon_a C_o}{SL_o L_o C_f}\right)}{\left(1 + \frac{\varepsilon_a C_o}{SL_o L_o C_f}\right)} \frac{k_c t_c^2}{2} \qquad 6\text{-}6.10$$

When breakthrough has taken place or when $t > t_b$, the amount of chlorine consumed is

$$\frac{\varepsilon_a C_o u_a dA k_c t_c^2}{2\left[\frac{SL_o L_o C_f}{\varepsilon_a C_o} + 1\right]} + \varepsilon_a dA k_c C_o H(t_c - t_b) \qquad 6\text{-}6.11$$

The fraction of fluid in the pulp pad effluent which has a residence time between t_r and $(t_r + dt_r)$ is dF, so that

$$dF = \frac{\varepsilon_a u_a dA}{\bar{\varepsilon}_a \bar{u}_a A} \qquad 6\text{-}6.12$$

where $\bar{u}_a$ and $\bar{\varepsilon}_a$ are the average superficial velocity and average accessible bed porosity of the entire pad.

Insertion of equation 6-6.12 into 6-6.11 and 6-6.10 followed by integration over all channels gives

$$\int_{o}^{F(t_{rc})} \frac{\bar{\varepsilon}_a C_o \bar{u}_a A k_c t_b^2}{2\left[\frac{SL_o L_o C_f}{\varepsilon_a C_o} + 1\right]} dF + \int_{F(t_{rc})}^{1} \frac{\bar{\varepsilon}_a C_o \bar{u}_a k_c t_c^2}{2\left[\frac{SL_o L_o C_f}{\varepsilon_a C_o} + 1\right]} dF$$

$$+ \int_{o}^{F(t_{rc})} \frac{\bar{\varepsilon}_a A \bar{u}_a k_c C_o H (t_c - t_b)}{u_a} dF \qquad 6\text{-}6.13$$

where $F(t_{rc})$ is the value of F at t_{rc} where

$$t_c = \frac{SL_o L_o C_f}{k_c C_o \varepsilon_a} \left(e^{k_c t_{rc}} - 1\right) + t_{rc} \qquad 6\text{-}6.14$$

when $P >> 1$ then the variations in ε_a and C_f around the average value $\bar{\varepsilon}_a$ and $\bar{C}_f$ are small so that as a first approximation ε_a and C_f in equation 6-6.13 can be replaced by $\bar{\varepsilon}_a$ and $\bar{C}_f$. The condition $P >> 1$ also assumes that the variation of u_a around $\bar{u}_a$ are relatively small. In addition, since u_a varies approximately linearly with F over the central part of the residence time distribution curve, the error incurred when replacing u_a by $\bar{u}_a$ in equation 6-6.13 is relatively small. With the replacement of u_a, ε_a and C_f by, respectively, $\bar{u}_a$, $\bar{\varepsilon}_a$ and $\bar{C}_f$, equation 6-6.13 can be simplified to

$$\frac{\bar{\varepsilon}_a C_o \bar{u}_a A k_c}{2\left[\frac{SL_o L_o C_f}{\bar{\varepsilon}_a C_o} + 1\right]} \int_{o}^{F(t_{rc})} t_b^2 \, dF \; \frac{\bar{\varepsilon}_a C_o k_c \bar{u}_a A t_c^2}{2\left[\frac{SL_o L_o \bar{C}_f}{\bar{\varepsilon}_a C_o} + 1\right]} \left(1 - F(t_{rc})\right)$$

$$+ \frac{\bar{\varepsilon}_a A \bar{u}_a k_c C_o H}{\bar{u}_a} \int_{o}^{F(t_{rc})} (t_c - t_b) \, dF \qquad 6\text{-}6.15$$

to

When the bars are removed from $\bar{\varepsilon}_a$, $\bar{u}_a$ and $\bar{C}_f$, ε_a, u_a and C_f still represent the average values based on the whole bed. The amount of chlorine consumed by carbohydrates for the entire bed becomes

$$\frac{\varepsilon_a C_o u_a A k_c}{2\left[\frac{SL_o L_o C_f}{\varepsilon_a C_o} + 1\right]} \int_o^{F(t_{rc})} t_b^2 dF + \frac{\varepsilon_a C_o k_c u_a A t_c^2}{2\left[\frac{SL_o L_o C_f}{\varepsilon_a C_o} + 1\right]} (1 - F(t_{rc}))$$

$$+ \varepsilon_a A k_c C_o H \int_o^{F(t_{rc})} (t_c - t_b)\, dF \qquad 6\text{-}6.16$$

Division by the amount of pulp in the bed, AHC_f, and using $\bar{t}_r = H/u_a$ gives as a final expression the weight of chlorine consumed by carbohydrates per weight of pulp in the entire bed.

$$\frac{\varepsilon_a C_o k_c}{2\left[\frac{SL_o L_o C_f}{\varepsilon_a C_o} + 1\right] C_f \bar{t}_r} \int_o^{F(t_{rc})} t_b^2 dF + \frac{\varepsilon_a C_o k_c t_c^2 (1 - F(t\ \ ))}{2\left[\frac{SL_o L_o C_f}{\varepsilon_a C_o} + 1\right] C_f \bar{t}_r}$$

$$+ \frac{\varepsilon_a C_o k_c}{C_f} \int_o^{F(t_{rc})} (t_c - t_b)\, dF \qquad 6\text{-}6.17$$

when $P \gg 1$ and $k_c \bar{t}_r \ll 1$.

APPENDIX 7-1

COMPUTER PROGRAMS FOR BOTH VERSIONS OF MODEL 1

VERSION 1

```
            FORTRAN 77     V10L31              DATE 88.11.20  TIME 11.19.14

000001          IMPLICIT REAL*8(A-H,O-Z)
000002          COMMON/BLOCK1/ Y(100),YCV(100),YDIF(100),CCFLG(100),CCFLC(100),
               CA1G(100.,A1C(100),A2G(100),A2C(100),AP(100),AN(100),
               CAS(100),AC(100),APT(100),PT(100),QT(100),CCPTS(100),
               CA1PTS(100),A2PTS(100),STEP
000003          COMMON/BLOCK2/DIFL1(100),DIFL2(100),CCOLD(100),A1OLD(100),
               CA2OLD(100),T,DT,PEC,DN,DS,FN,FS,DENOM,PE,COUNT,C1,C2,CC,
               CAO,R1 R2,R3,H,VEL,POR,M1,M2,M3,N,ITER,ITRMAX,ITERAT
000004          COMMON/BLOCK3/A11(100),A22(100),DIFL3(100),DEV1,DEV2,DEV3,STO1,
               CSTO2,A,B,C,D,C3,A1,A2,A3,A4,A5,A6,A7,TEM,ITER1,ITER2,ITER5
        C
000005          CALL VALUES
000006          CALL GRID
000007          DO 605 ITER=1,ITRMAX
000008          COUNT=COUNT+1
000009          T=T+DT
000010          CALL CALC
000011          STEP=1.0D0
000012          IF(COUNT.NE.N) GO TO 605
000013          CALL OUTPUT
000014    605   CONTINUE
000015          STOP
000016          END

STATISTICS:     16 STEPS, PROCEDURE SIZE=     150 BYTES, PROGRAM NAME=MAIN
                23 LINES, PROGRAM   SIZE=     542 BYTES, DIAGNOSTICS =    0
                          REMAINING SIZE=    166K BYTES,                    HIGHEST SEVERITY CODE=00
```

```
      C
      C
000017        SUBROUTINE OMAR
      C
      C
000018        IMPLICIT REAL*8(A-H,O-Z)
000019        COMMON/BLOCK1/ Y(100),YCV(100),YDIF(100),CCFLG(100),CCFLC(100),
             CA1G(100),A1C(100),A2G(100),A2C(100),AP(100),AN(100),
             CAS(100),AC(100),APT(100),PT(100),QT(100),CCPTS(100),
             CA1PTS(100),A2PTS(100),STEP
000020        COMMON/BLOCK2/DIFL1(100),DIFL2(100),CCOLD(100),A1OLD(100),
             CA2OLD(100),T,DT,PEC,DN,DS,FN,FS,DENOM,PE,COUNT,C1,C2,CC,
             CAO,R1,R2,R3,H,VEL,POR,M1,M2,M3,N,ITER,ITRMAX,ITERAT
000021        COMMON/BLOCK3/A11(100),A22(100),DIFL3(100),DEV1,DEV2,DEV3,STO1,
             CSTO2,A,B,C,D,C3,A1,A2,A3,A4,A5,A6,A7,TEM,ITER1,ITER2,ITER5
      C
      C
000022        ENTRY VALUES
      C
      C
000023        PEC=35D0
000024        STO1=1.50D0
000025        STO2=1.80D0
000026        POR=0.93D0
000027        CON=111.0D0
000028        AO=0.0430D0
000029        CC=2.20D0
000030        H=6.0D0
000031        VEL=0.082D0
000032        A=1.51D0
000033        B=1.61D0
000034        C=1.84D0
000035        D=0.55D0
000036        TEM=325D0
000037        C1=16.1D0
000038        C2=(5.89*(10**10)*(DEXP(-7670/TEM)))
000039        C3=0 001214D0
000040        A1=((STO1*CON*H*C1)*(AO**A)*(CC**(B-1.0)))
             C/(VEL*POR)
000041        A2=((STO2*CON*H*C2)*(AO**C)*(CC**(D)
             C))/(VEL*POR*CC)
000042        A3=(H*C3)/VEL
000043        A4=((AO**(A-1.0)*(CC**B)*C1*H*(A-1.0)))
             C/VEL
000044        A5=((AO**(C-1.0))*(CC**D)*C2
             C*H*(C-1.0))/VEL
000045        A6=(A*A4)/(A-1.0)
000046        A7=(C*A5)/(C-1.0)
000047        M1=70
000048        M2=M1-1
000049        T=0.0D0
000050        DT=0.01D0
000051        N=50
000052        COUNT=0
000053        ITRMAX=100
000054        STEP=0.0D0
000055        DO 11 J=1,M1
000056   11   CCFLC(J)=0.0D0
```

```
000057          DO 21 J=1,M1
000058    21    CCOLD(J)=0.0D0
000059          DO 31 J=1,M1
000060    31    A1OLD(J)=0.65D0
000061          DO 40 J=1,M1
000062    40    A2OLD(J)=0.25D0
000063          DO 51 J=1,M1
000064    51    A1C(J)=0.0D0
000065          DO 90 J=1,M1
000066    90    A2C(J)=0.0D0
000067          DO 7589 J=1,M1
000068    7589  CCPTS(J)=0.0D0
000069          DO 7590 J=1,M1
000070    7590  A1PTS(J)=0.65D0
000071          DO 7591 J=1,M1
000072    7591  A2PTS(J)=0.252D0
          C
          C
000073          RETURN
          C
000074          ENTRY GRID
          C
          C
000075          Y(1)=0.D0
000076          DY=1.D0/(M1-1)
000077          DO 10 I=1,M2
000078    10    Y(I+1)=Y(I)+DY
000079          DO 20 I=2,M1
000080    20    YDIF(I)=Y(I)-Y(I-1)
000081          YCV(1)=0.5D0*YDIF(2)
000082          DO 30 I=2,M2
000083    30    YCV(I)=0.5D0*(YDIF(I)+YDIF(I+1))
000084          YCV(M1)=0.5D0*YDIF(M1)
          C
          C
000085          RETURN
          C
          C
000086          ENTRY CALC
          C
          C
000087          IF (STEP.EQ.0.0) GO TO 9999
000088          DO 7586 J=1,M1
000089    7586  CCPTS(J)=CCFLC(J)
000090          DO 7587 J=1,M1
000091    7587  A1PTS(J)=A1C(J)
000092          DO 7588 J=1,M1
000093    7588  A2PTS(J)=A2C(J)
000094    9999  ITERAT=0
000095    1     ITERAT=ITERAT+1
000096          IF (ITERAT.GT.20) GO TO 800
000097          DO 296 J=1,M1
000098          IF (A1OLD(J).LT.1E-5) GO TO 6592
000099          A11(J)=(A1*(A1OLD(J)**A))
000100          GO TO 296
000101    6592  A11(J)=0.D0
000102    296   CONTINUE
000103          DO 297 J=1,M1
```

```
000104          IF (A2OLD(J).LT.1E-5) GO TO 6593
000105          A22(J)=(A2*(A2OLD(J)**C))
000106          GO TO 297
000107    6593  A22(J)=0.D0
000108    297   CONTINUE
          C
          C
          C     MAIN EQUATION
          C
          C
000109          ITER5=0.0D0
000110    2     ITER5=ITER5+1.0D0
000111          IF (ITER5.GT.20) GO TO 900
000112          FN=1.0D0
000113          DN=1.D0/PEC/YDIF(M1)
000114          PE=FN/DN
000115          APP=DMAX1(0.D0,(1.D0-0.5D0*DABS(PE)))
000116          AS(1)=0
000117          AN(1)=DN*APP+DMAX1(-FN,0.D0)
000118          APT(1)=YCV(1)/DT
000119          IF (CCOLD(1).GT.1E-4) GO TO 8762
000120          AC(1)=APT(1)*CCPTS(1)+1.0D0
000121          AP(1)=AN(1)+APT(1)+(A3*YCV(1))
000122          GO TO 3139
000123    8762  AC(1)=(APT(1)*CCPTS(1))+((A11(1)*(B-1.0)*(CCOLD(1)
               C**B))*YCV(J))+1.0D0
000124          AP(1)=AN(1)+AS(1)+APT(1)+1.0D0-(((-B*A11(1)*(CCOLD(1)
               C**(B-1.0)))-((D*A22(1)*(CCOLD(1)**(D)))/(CCOLD(1)))-
               C(A22(1)*(1.0D0-D)*(CCOLD(1)**D)/(CCOLD(1)))-A3))
               C*YCV(1)
000125    3139  DO 50 J=2,M2
000126          FN=1.D0
000127          DN=1.D0/PEC/YDIF(J+1)
000128          PE=FN/DN
000129          APP=DMAX1(0.D0,(1.D0-0.5D0*DABS(PE)))
000130          AN(J)=DN*APP+DMAX1(-FN,0.D0)
000131          FS=1.D0
000132          DS=1.D0/PEC/YDIF(J)
000133          PE=FS/DS
000134          APP=DMAX1(0.D0,(1.D0-0.5D0*DABS(PE)))
000135          AS(J)=DS*APP+DMAX1(FS,0.D0)
000136          APT(J)=YCV(J)/DT
000137          IF (CCOLD(J) GT.1E-4) GO TO 2197
000138          AC(J)=APT(J)*CCPTS(J)
000139          AP(J)=AN(J)+AS(J)+APT(J)+(A3*YCV(J))
000140          GO TO 50
000141    2197  AC(J)=(APT(J)*CCPTS(J))+((A11(J)*(B-1.0)*(CCOLD(J)**B))*YCV(J))
000142          AP(J)=AN(J)+AS(J)+APT(J)-(((-B*A11(J)*(CCOLD(J)**(B-1.0)))-
               C((D*A22(J)*(CCOLD(J)**(D)))/(CCOLD(J)))-(A22(J)*
               C(1.0D0-D)*(CCOLD(J)**D)/(CCOLD(J)))-A3))*YCV(J)
000143    50    CONTINUE
000144          FS=1 D0
000145          DS=1.D0/PEC/YDIF(M1)
000146          PE=FS/DS
000147          APP=DMAX1(0.D0,(1.D0-0.5D0*DABS(PE)))
000148          AS(M1)=DS*APP+DMAX1(FS,0.D0)
000149          AN(M1)=0 D0
000150          APT(M1)=YCV(M1)/DT
```

```
000151          IF (CCOLD(M1).GT.1E-4) GO TO 2198
000152          AC(M1)=APT(M1)*CCPTS(M1)
000153          AP(M1)=AN(M1)+AS(M1)+APT(M1)+(A3*YCV(M1))
000154          GO TO 2200
000155    2198 AC(M1)=(APT(M1)*CCPTS(M1))+((A11(M1)*(B-1.0)*(CCOLD(M1)**B))
               C*YCV(J))
000156          AP(M1)=AN(M1)+AS(M1)+APT(M1)-(((-B*A11(M1)*(CCOLD(M1)**(B-1.0)))-
               C((D*A22(M1)*(CCOLD(M1)**(D)))/(CCOLD(M1)))-(A22(M1)*
               C(1.0D0-D)*(CCOLD(M1)**D)/(CCOLD(M1)))-A3))*YCV(M1)
          C
          C
          C     SOLVING MAIN EQUATION
          C
          C
000157    2200 PT(1)=AN(1)/AP(1)
000158          QT(1)=AC(1)/AP(1)
000159          DO 200 J=2,M1
000160          DENOM=AP(J)-AS(J)*PT(J-1)
000161          PT(J)=AN(J)/DENOM
000162     200  QT(J)=(AC(J)+AS(J)*QT(J-1))/DENOM
000163          CCFLC(M1)=QT(M1)
000164          DO 210 JJ=1,M2
000165          J=M2-JJ+1
000166     210  CCFLC(J)=PT(J)*CCFLC(J+1)+QT(J)
          C
          C
          C     TESTING FOR CONVERGENCE IN MAIN EQUATION
          C
          C
000167          DO 233 J=1,M1
000168     233  DIFL1(J)=DABS(CCFLC(J)-CCOLD(J))
000169          DO 234 J=1,M1
000170          DEV1=DIFL1(J)
000171          IF (DEV1.GT.1E-3) GO TO 236
000172     234  CONTINUE
000173          DO 235 J=1,M1
000174     235  CCOLD(J)=CCFLC(J)
000175          GO TO 670
000176     236  DO 237 J=1,M1
000177     237  CCOLD(J)=CCFLC(J)
000178          GO TO 2
          C                              /
          C
          C     FIRST RATE EQUATION
          C
          C
000179      670 ITER1=0.0D0
000180      675 ITER1=ITER1+1.0D0
000181          IF (ITER1.GT.40) GO TO 800
000182          AN(1)=0.D0
000183          AS(1)=0.D0
000184          APT(1)=YCV(1)/DT
000185          IF (CCOLD(1).GT.1E-4) GO TO 7953
000186          GO TO 7989
000187     7953 IF (A1OLD(1).GT.1E-5) GO TO 2201
000188     7989 AC(1)=APT(1)*A1PTS(1)
000189          AP(1)=APT(1)
000190          GO TO 2202
```

```
000191   2201 AC(1)=APT(1)*A1PTS(1)+((A4*(A1OLD(1)**A)*(CCOLD(1)**B))*YCV(1))
000192        AP(1)=APT(1)+YCV(1)*A6*((A1OLD(1)**(A-1.0))*
             C(CCOLD(1)**B))
000193   2202 DO 300 J=2,M2
000194        AN(J)=0.D0
000195        AS(J)=0.D0
000196        APT(J)=YCV(J)/DT
000197        IF (CCOLD(J).GT.1E-4) GO TO 7954
000198        GO TO 7990
000199   7954 IF (A1GLD(J).GT.1E-4) GO TO 2203
000200   7990 AC(J)=APT(J)*A1PTS(J)
000201        AP(J)=APT(J)
000202        GO TO 300
000203   2203 AC(J)=APT(J)*A1PTS(J)+((A4*(A1OLD(J)**(A))*
             C(CCOLD(J)**B))*YCV(J))
000204        AP(J)=APT(J)+YCV(J)*A6*((A1OLD(J)**(A-1.0))*
             C(CCOLD(J)**B))
000205   300  CONTINUE
000206        AN(M1)=0.D0
000207        AS(M1)=0.D0
000208        APT(M1)=YCV(M1)/DT
000209        IF (CCOLD(M1).GT.1E-4) GO TO 7955
000210        GO TO 7991
000211   7955 IF (A1OLD(M1).GT.1E-5) GO TO 2205
000212   7991 AC(M1)=APT(M1)*A1PTS(M1)
000213        AP(M1)=APT(M1)
000214        GO TO 2206
000215   2205 AC(M1)=APT(M1)*A1PTS(M1)+YCV(M1)*(A4*(A1OLD(M1)**A)
             C*(CCOLD(M1)**B))
000216        AP(M1)=APT(M1)+YCV(M1)*A6*((A1OLD(M1)**(A-1.0))*
             C(CCOLD(M1)**B))
             C
             C
             C     SOLVING FIRST RATE EQUATION
             C
             C
000217   2206 PT(1)=AN(1)/AP(1)
000218        QT(1)=AC(1)/AP(1)
000219        DO 400 J=2,M1
000220        DENOM=AP(J)-AS(J)*PT(J-1)
000221        PT(J)=AN(J)/DENOM
000222   400  QT(J)=(AC(J)+AS(J)*QT(J-1))/DENOM
000223        A1C(M1)=QT(M1)
000224        DO 410 JJ=1,M2
000225        J=M2-JJ+1
000226   410  A1C(J)=PT(J)*A1C(J+1)+QT(J)
             C
             C
             C     TESTING FOR CONVERGENCE(FIRST RATE EQUATION)
             C
             C
000227        DO 760 J=1,M1
000228   760  DIFL2(J)=DABS(A1C(J)-A1OLD(J))
000229        DO 761 J=1,M1
000230        DEV2=DIFL2(J)
000231        IF (DEV2.GT.1E-3) GO TO 762
000232   761  CONTINUE
000233        GO TO 764
```

```
                FORTRAN 77     V10L31   OMAR        DATE 88.11.20  TIME 11.19.14

000234    762   DO 763 J=1,M1
         C763   A1OLD(J)=(A1C(J)+A1OLD(J))/2.0
000235    763   A1OLD(J)=A1C(J)
000236          GO TO 675
         C
         C
         C      SECOND RATE EQUATION
         C
         C
000237     764  ITER2=0.0D0
000238          DO 777 J=1,M1
000239     777  A1OLD(J)=A1C(J)
000240     765  ITER2=ITER2+1.0D0
000241          IF (ITER2.GT.40) GO TO 800
000242          AN(1)=0.D0
000243          AS(1)=0.D0
000244          APT(1)=YCV(1)/DT
000245          IF (CCOLD(1).GT.1E-4) GO TO 7956
000246          GO TO 7992
000247    7956  IF (A2OLD(1).GT.1E-5) GO TO 2207
000248    7992  AC(1)=APT(1)*A2PTS(1)
000249          AP(1)=APT(1)
000250          GO TO 2208
000251    2207  AC(1)=APT(1)*A2PTS(1)+((A5*(A2OLD(1)**C)*
              C(CCOLD(1)**D))*YCV(1))
000252          AP(1)=APT(1)+YCV(1)*A7*((A2OLD(1)**(C-1.0))
              C*(CCOLD(1)**D))
000253    2208  DO 500 J=2,M2
000254          AN(J)=0.D(
000255          AS(J)=0.D
000256          APT(J)=YC     /DT
000257          IF (CCOLD(J,.GT.1E-4) GO TO 7957
000258          GO TO 7993
000259    7957  IF (A2OLD(J).GT.1E-5) GO TO 2209
000260    7993  AC(J)=APT(J)*A2PTS(J)
000261          AP(J)=APT(J)
000262          GO TO 500
000263    2209  AC(J)=APT(J)*A2PTS(J)+((A5*(A2OLD(J)**C)*(CCOLD(J)**D))
              C*YCV(J))
000264          AP(J)=APT(J)+YCV(J)*A7*((A2OLD(J)**(C-1.0))*(CCOLD(J)**D))
000265    500   CONTINUE
000266          AN(M1)=0.D0
000267          AS(M1)=0.D0
000268          APT(M1)=YCV(M1)/DT
000269          IF (CCOLD(M1).GT.1E-4) GO TO 7958
000270          GO TO 7994
000271    7958  IF (A2OLD(M1).GT.1E-5) GO TO 2211
000272    7994  AC(M1)=APT(M1)*A2PTS(M1)
000273          AP(M1)=APT(M1)
000274          GO TO 2212
000275    2211  AC(M1)=APT(M1)*A2PTS(M1)+((A5*(A2OLD(M1)**C)*(CCOLD(M1)**D))
              C*YCV(M1))
000276          AP(M1)=APT(M1)+YCV(M1)*A7*((A2OLD(M1)**(C-1.0))*(CCOLD(M1)**D))
         C
         C
         C      SOLVING SECOND RATE EQUATION
         C
         C
```

```
            FORTRAN 77     V10L31   OMAR        DATE 88.11.20  TIME 11.19.14

000277   2212 PT(1)=AN(1)/AP(1)
000278        QT(1)=AC(1)/AP(1)
000279        DO 600 J=2,M1
000280        DENOM=AP(J)-AS(J)*PT(J-1)
000281        PT(J)=AN(J)/DENOM
000282    600 QT(J)=(AC(J)+AS(J)*QT(J-1))/DENOM
000283        A2C(M1)=QT(M1)
000284        DO 610 JJ=1,M2
000285        J=M2-JJ+1
000286    610 A2C(J)=PT(J)*A2C(J+1)+QT(J)
          C
          C
          C     TESTING FOR CONVERGENCE(SECOND RATE EQUATION)
          C
          C
000287        DO 770 J=1,M1
000288    770 DIFL3(J)=DABS(A2C(J)-A2OLD(J))
000289        DO 771 J=1,M1
000290        DEV3=DIFL3(J)
000291        IF (DEV3.GT.1E-3) GO TO 772
000292    771 CONTINUE
000293        GO TO 776
000294    772 DO 773 J=1,M1
000295    773 A2OLD(J)=A2C(J)
000296        GO TO 765
000297    776 DO 778 J=1,M1
000298    778 A2OLD(J)=A2C(J)
000299        IF (ITER1.NE.1) GO TO 1
000300        IF (ITER2.NE.1) GO TO 1
000301        RETURN
000302    800 WRITE(6,900)
000303    900 FORMAT('0',' CONVERGENCE NOT OBTAINED')
000304        STOP
          C
          C
000305        ENTRY OUTPUT
          C
          C
000306        N=N+20
000307        WRITE(6,1000)
000308   1000 FORMAT('0')
000309        WRITE(6,1325)
000310   1325 FORMAT('0')
000311        WRITE(6,2000) T
000312   2000 FORMAT(' AT THE TIME OF   ',F19.6)
000313        WRITE(6,3000) CCFLC(M1)
000314   3000 FORMAT(' THE EXIT CONCENTRATION IS  ',F19.6)
000315        WRITE(6,1875)
000316   1875 FORMAT('0')
000317        WRITE(6,4000) A1C(M1),A2C(M1)
000318   4000 FORMAT(' ','A1C(M1)= ',F19.6,15X,'A2C(M1)= ',F19.6)
000319        RETURN
000320        END

STATISTICS:    304 STEPS, PROCEDURE SIZE=    7182 BYTES, PROGRAM NAME=OMAR
               401 LINES, PROGRAM   SIZE=   10698 BYTES, DIAGNOSTICS =    0
                          REMAINING SIZE=     76K BYTES,                      HIGHEST SEVERITY CODE=00
SPECIFIED OPTIONS: OPTIMIZE(2),OBJECT,LANGLVL(66)
```

VERSION 2

```
FORTRAN IV G1  RELEASE 2.0            MAIN            DATE = 88325        15/35/44

                CWATFIV ,NOEXT,NOWARN,TIME=600
0001                  IMPLICIT REAL*8(A-H,O-Z)
0002                  COMMON Y(100),YCV(100),YDIF(100),CCFLG(100),CCFLC(100),
                     CA1G(100),A1C(100),A2G(100),A2C(100),AP(100),AN(100),
                     CAS(100),AC(100),APT(100),PT(100),QT(100),A1INI(100),
                     CA2INI(100),DIFL1(100),DIFL2(100),CCOLD(100),A1OLD(100),
                     CA2OLD(100),T,DT,TINIT,PEC,DN,DS,FN,FS,DENOM,PE,COUNT,M1,M2,M3,
                     CN,ITER,ITRMAX,ITERAT,C1,C2,CC,AO,R1,R2,R3,L,VEL,POR,
                     DEV1,DEV2,R4,C3
                C
0003                  CALL VALUES
0004                  CALL GRID
0005                  DO 605 ITER=1,ITRMAX
0006                  COUNT=COUNT+1
0007                  T=T+DT
0008                  CALL CALC
0009                  IF(COUNT.NE.N) GO TO 605
0010                  CALL OUTPUT
0011           605    CONTINUE
0012                  STOP
0013                  END
```

```
                C
                C
0001                 SUBROUTINE OMAR
                C
                C
0002                 IMPLICIT REAL*8(A-H,O-Z)
0003                 COMMON Y(100),YCV(100),YDIF(100),CCFLG(100),CCFLC(100),
                    CA1G(100),A1C(100),A2G(100),A2C(100),AP(100),AN(100),
                    CAS(100),AC(100),APT(100),PT(100),QT(100),A1INI(100),
                    CA2INI(100),DIFL1(100),DIFL2(100),CCOLD(100),A1OLD(100),
                    CA2OLD(100),T,DT,TINIT,PEC,DN,DS,FN,FS,DENOM,PE,COUNT,M1,M2,M3,
                    CN,ITER,ITRMAX,ITERAT,C1,C2,CC,AO,R1,R2,R3,L,RHOF,VEL,POR,
                    DEV1,DEV2,R4,C3
                C
0004                 ENTRY VALUES
                C
0005                 M1=40
0006                 T=0.0D0
0007                 TINIT=0.0D0
0008                 COUNT=0
0009                 DT=0.01D0
0010                 N=50
0011                 IF(TINIT.NE.0.D0) GO TO 4
0012                 DO 19 J=1,M1
0013              19 CCOLD(J)=0.0D0
0014                 DO 24 J=1,M1
0015              24 A1OLD(J)=0.50D0
0016                 DO 26 J=1,M1
0017              26 A2OLD(J)=0.30D0
0018              4  ITRMAX=50
0019                 M2=M1-1
0020                 M3=M2-1
0021                 C1=0.1236D0
0022                 C2=0.0025D0
0023                 C3=0.001214D0
0024                 CC=0.55D0
0025                 DO 29 J=1,M1
0026              29 A1INI(J)=0.5000D0
0027                 DO 33 J=1,M1
0028              33 A2INI(J)=0.3000D0
0029                 AO=0.043D0
0030                 L=4.0D0
0031                 VEL=0.020D0
0032                 CON=111.0D0
0033                 POR=0.930D0
0034                 R1=(C1*CC*L/VEL)
0035                 R2=(C2*CC*L/VEL)
0036                 R3=(1.37*AO*CON)/(POR*CC)
0037                 R4=(C3*L/VEL)
0038                 DO 3 J=1,M1
0039               3 A1C(J)=A1INI(J)
0040                 DO 9 J=1,M1
0041               9 A2C(J)=A2INI(J)
0042                 PEC=20.0D0
```

```
0043                  RETURN
                    C
                    C
0044                  ENTRY GRID
                    C
                    C
0045                  Y(1)=0.D0
0046                  DY=1.D0/(M1-1)
0047                  DO 10 I=1,M2
0048                10 Y(I+1)=Y(I)+DY
0049                  DO 20 I=2,M1
0050                20 YDIF(I)=Y(I)-Y(I-1)
0051                  YCV(1)=0.5D0*YDIF(2)
0052                  DO 30 I=2,M2
0053                30 YCV(I)=0.5D0*(YDIF(I)+YDIF(I+1))
0054                  YCV(M1)=0.5D0*YDIF(M1)
0055                  RETURN
                    C
                    C
0056                  ENTRY CALC
                    C
                    C
0057                  IF(ITER.EQ.1) GO TO 25
0058                  DO 38 J=1,M1
0059                38 CCOLD(J)=CCFLC(J)
0060                  DO 39 J=1,M1
0061                39 A1OLD(J)=A1C(J)
0062                  DO 41 J=1,M1
0063                41 A2OLD(J)=A2C(J)
0064                25 ITERAT=0
0065                 1 A1G(1)=A1C(1)
0066                  DO 13 J=2,M1
0067                13 A1G(J)=A1C(J)
0068                  DO 21 J=1,M1
0069                21 A2G(J)=A2C(J)
0070                  ITERAT=ITERAT+1
0071                  IF(ITERAT.GT.20) GO TO 800
0072                  AS(1)=0.D0
0073                  AN(1)=0.D0
0074                  AC(1)=1.D0
0075                  AP(1)=1.D0
0076                  DO 50 J=2,M2
0077                  FN=1.D0
0078                  DN=1.D0/PEC/YDIF(J+1)
0079                  PE=FN/DN
0080                  APP=DMAX1(0.D0,(1.D0-0.5D0*DABS(PE)))
0081                  AN(J)=DN*APP+DMAX1(-FN,0.D0)
0082                  FS=1.D0
0083                  DS=1.D0/PEC/YDIF(J)
0084                  PE=FS/DS
0085                  APP=DMAX1(0.D0,(1.D0-0.5D0*DABS(PE)))
0086                  AS(J)=DS*APP+DMAX1(FS,0.D0)
0087                  APT(J)=YCV(J)/DT
0088                  AC(J)=(APT(J)*CCOLD(J))
```

```
0089              50   AP(J)=AN(J)+AS(J)+APT(J)+(R3*YCV(J)*R1*A1G(J))+(R3*YCV(J)
                      C*R2*A2G(J))+(R4*YCV(J))
0090                   FS=1.D0
0091                   DS=1.D0/PEC/YDIF(M1)
0092                   PE=FS/DS
0093                   APP=DMAX1(0.D0,(1.D0-0.5D0*DABS(PE)))
0094                   AS(M1)=DS*APP+DMAX1(FS,0.D0)
0095                   AN(M1)=0.D0
0096                   APT(M1)=YCV(M1)/DT
0097                   AC(M1)=(APT(M1)*CCOLD(M1))
0098                   AP(M1)=AN(M1)+AS(M1)+APT(M1)+(R3*YCV(M1)*R1*A1G(M1))+(R3*YCV(M1)
                      C*R2*A2G(M1))+(R4*YCV(M1))
                  C
                  C
                  C      SOLVING MAIN EQUATION
                  C
                  C
0099                   PT(1)=AN(1)/AP(1)
0100                   QT(1)=AC(1)/AP(1)
0101                   DO 200 J=2,M1
0102                   DENOM=AP(J)-AS(J)*PT(J-1)
0103                   PT(J)=AN(J)/DENOM
0104              200  QT(J)=(AC(J)+AS(J)*QT(J-1))/DENOM
0105                   CCFLC(M1)=QT(M1)
0106                   DO 210 JJ=1,M2
0107                   J=M2-JJ+1
0108              210  CCFLC(J)=PT(J)*CCFLC(J+1)+QT(J)
                  C
                  C
                  C      FIRST RATE EQUATION
                  C
                  C
0109                   AN(1)=0.D0
0110                   AS(1)=0.D0
0111                   APT(1)=0.5*YCV(1)/DT
0112                   AC(1)=APT(1)*A1OLD(1)
0113                   AP(1)=(YCV(1)/DT)+(R1*CCFLC(1)*YCV(1))
0114                   DO 300 J=2,M2
0115                   AN(J)=0.D0
0116                   AS(J)=0.D0
0117                   APT(J)=YCV(J)/DT
0118                   AC(J)=APT(J)*A1OLD(J)
0119              300  AP(J)=(YCV(J)/DT)+(R1*CCFLC(J)*YCV(J))
0120                   AN(M1)=0.D0
0121                   AS(M1)=0.D0
0122                   APT(M1)=YCV(M1)/DT
0123                   AC(M1)=APT(M1)*A1OLD(M1)
0124                   AP(M1)=(YCV(M1)/DT)+(R1*CCFLC(M1)*YCV(M1))
0125                   PT(1)=AN(1)/AP(1)
0126                   QT(1)=AC(1)/AP(1)
0127                   DO 400 J=2,M1
0128                   DENOM=AP(J)-AS(J)*PT(J-1)
0129                   PT(J)=AN(J)/DENOM
0130              400  QT(J)=(AC(J)+AS(J)*QT(J-1))/DENOM
```

```
0131                A1C(M1)=QT(M1)
0132                DO 410 JJ=1,M2
0133                J=M2-JJ+1
0134             410 A1C(J)=PT(J)*A1C(J+1)+QT(J)
                 C
                 C                  /
                 C
                 C     SECOND RATE EQUATION
                 C
                 C
0135                AN(1)=0.D0
0136                AS(1)=0.D0
0137                APT(1)=YCV(1)/DT
0138                AC(1)=APT(1)*A2OLD(1)
0139                AP(1)=(YCV(1)/DT)+(R2*CCFLC(1)*YCV(1))
0140                DO 500 J=2,M2
0141                AN(J)=0.D0
0142                AS(J)=0.D0
0143                APT(J)=YCV(J)/DT
0144                AC(J)=APT(J)*A2OLD(J)
0145             500 AP(J)=(YCV(J)/DT)+(R2*CCFLC(J)*YCV(J))
0146                AN(M1)=0.D0
0147                AS(M1)=0.D0
0148                APT(M1)=YCV(M1)/DT
0149                AC(M1)=APT(M1)*A2OLD(M1)
0150                AP(M1)=(YCV(M1)/DT)+(R2*CCFLC(M1)*YCV(M1))
0151                PT(1)=AN(1)/AP(1)
0152                QT(1)=AC(1)/AP(1)
0153                DO 600 J=2,M1
0154                DENOM=AP(J)-AS(J)*PT(J-1)
0155                PT(J)=AN(J)/DENOM
0156             600 QT(J)=(AC(J)+AS(J)*QT(J-1))/DENOM
0157                A2C(M1)=QT(M1)
0158                DO 610 JJ=1,M2
0159                J=M2-JJ+1
0160             610 A2C(J)=PT(J)*A2C(J+1)+QT(J)
                 C
                 C
                 C     TESTING FOR CONVERGENCE
                 C
                 C
0161                DO 700 J=1,M1
0162             700 DIFL1(J)=DABS(A1C(J)-A1G(J))
0163                DO 701 J=1,M1
0164             701 DIFL2(J)=DABS(A2C(J)-A2G(J))
0165                DO 702 J=1,M1
0166                DEV1=DIFL1(J)
0167                IF (DEV1.GT.1E-3) GO TO 1
0168             702 CONTINUE
0169                DO 703 J=1,M1
0170                DEV2=DIFL2(J)
0171                IF (DEV2.GT.1E-3) GO TO 1
0172             703 CONTINUE
0173                RETURN
0174             800 WRITE(6,900)
```

```
0175              900  FORMAT('0','CONVERGENCE NOT OBTAINED')
0176                   STOP
                  C
                  C
0177                   ENTRY OUTPUT
                  C
                  C
0178                   N=N+20
0179                   WRITE(6,1000)
0180              1000 FORMAT('0')   /
0181                   WRITE(6,1325)
0182              1325 FORMAT('0')
0183                   WRITE(6,2000) T
0184              2000 FORMAT(' AT THE TIME OF   ',F19.6)
0185                   WRITE(6,3000) CCFLC(M1)
0186              3000 FORMAT(' THE EXIT CONCENTRATION IS  ',F19.6)
0187                   WRITE(6,1875)
0188              1875 FORMAT('0')
0189                   WRITE(6,4000) A1C(M1),A2C(M1)
0190              4000 FORMAT(' ','A1C= ',F19.6,15X,'A2C= ',F19.6)
0191                   RETURN
0192                   END
```

APPENDIX 7-2

APPLICATION OF AXIAL DISPERSION TO "CONSTANT PATTERN" BEHAVIOUR IN FIXED PULP FIBER BEDS.

The transport equation including axial dispersion in a single channel is

$$\frac{\partial C}{\partial T} = \frac{1}{P_c\left[1 + 1000\,\rho_f \frac{1-\varepsilon_a}{\varepsilon_a} SL_o \frac{[L_o]}{C_o}\right]} \frac{\partial^2 C}{\partial Z^2} \qquad 7\text{-}2.1$$

The contribution of axial dispersion to "constant pattern" behavior can be assessed by evaluating the coefficient of the second order term. For the following typical values

$P_c = 35$

$\rho_f = 1.5$ g/cm^3

$\varepsilon_a = 0.93$

$SL_o = 1.0$ g Cl_2/g lignin

$L_o = 0.0475$ g lignin/g pulp

and $C_o = 1.1$ g/l.

The coefficient is $4.86*10^{-3}$ or approximately $5*10^{-3}$. Thus the spreading of the "constant pattern" concentration in a single channel due to axial dispersion can be neglected.

APPENDIX 7-3

DISPERSION CALCULATIONS IN RADIAL DIRECTION FOR FIXED PULP FIBER BEDS

1. Estimation of α in Danckwerts "tarnishing" reaction problem

As shown in equation section 7.4

$$\beta = \frac{\varepsilon_g}{1 - \varepsilon_a} \frac{C_o}{1000 \rho_f SL_o L_o} \sqrt{\pi}\ \alpha\ \exp(\alpha^2)\ \mathrm{erf}(\alpha) \qquad 7\text{-}3.1$$

β can be estimated from the experimental values

$\varepsilon_a = 0.93$

$\rho_f = 1.50\ g/cm^3$

$L_o = 0.0475$ g lignin/g pulp

to be $0.19\ C_o/SL_o$.

Taking $SL_o = 1$ and noting that the range of inlet chlorine water concentrations to be 0.55 to 2.20 g/l, β can be calculated to be 0.10 to 0.42. Allowing for different SL_o values, a range for β of between 0.1 to 0.5 is appropriate for most experiments in this study. From equation 7-3.1 the corresponding range for α is 0.2 to 0.5.

2. Estimation of radial dispersion coefficient, D_R

The radial dispersion coefficient D_R for chlorine can be obtained from

$$\frac{1}{Pe_R} = \frac{1}{Pe_{t,R}} + \frac{\varepsilon_i}{1.5\ Re_e \cdot Sc} \qquad [7.55]$$

where

$$1/Pe_{t,R} = \frac{0.09}{1 + 10/(Re_e \cdot Sc)} \qquad [7.56]$$

with

$$Re_e = d_e u_o/\nu = \frac{26.50*10^{-6}\ m \cdot 8.20*10^{-4}\ m/s}{7.19*10^{-7}\ m^2/s} = 3.02*10^{-2} \qquad 7\text{-}3.2$$

and

$$Sc = \frac{\nu}{D_M} = \frac{7.19*10^{-7}}{1.48*10^{-9}\ m^2/s} = 4.86*10^2 \qquad 7\text{-}3.3$$

Thus

$$1/Pe_{t,R} = \frac{0.09}{1 + 10/(3.02*10^{-2})(4.86*10^2)} = 5.35*10^{-2}$$

From equation [7.55]

$$\frac{1}{Pe_R} = 5.35 \times 10^{-2} + \frac{0.569}{1.5(4.86*10^2)(3.02*10^{-2})} = 7.93 \times 10^{-2}$$

Thus $Pe_R = 12.6$.

Then

$$D_R = \frac{d_e u_i}{Pe_R} = \frac{(26.5*10^{-6}\ m)\cdot(0.082*10^{-2}\ m/s)}{12.6 \times 0.56}$$

or

$$D_R = 3.03*10^{-9}\ m^2/s.$$